Pharmacokinetic interactions of mycophenolic acid: population pharmacokinetics and a translational investigation on *p*-cresol mediated metabolism interaction

by

Yan Rong

A thesis submitted in partial fulfillment of the requirements for the degree of

Doctor of Philosophy

in
Pharmaceutical Sciences

Faculty of Pharmacy and Pharmaceutical Sciences
University of Alberta

Abstract

Background

Mycophenolic acid (MPA) is a frequently used immunosuppressant after organ transplantation to prevent graft rejection. It is almost always prescribed concurrently with tacrolimus and corticosteroids. Despite empiric, fixed dosing regimens, MPA has been associated with significant variations (up to 10-fold) in plasma exposure after kidney transplantation. The therapeutic exposure range of MPA is relatively narrow (30-60 μg×h/mL), and under-exposure could result in organ rejection or graft loss, whereas over-exposure may lead to severe hematological complications such as anemia, leukopenia, and neutropenia. If not mitigated, MPA over-exposure could also result in severe infections and patient death. Understanding the factors contributing to MPA pharmacokinetic/dynamic variabilities could help mitigate the occurrences of MPA associated adverse effects and improve the precision dosing of MPA.

Overall Hypothesis

Large exposure variabilities of MPA can be attributed to extrinsic (i.e., co-administered immunosuppressants such as tacrolimus and corticosteroids) and intrinsic (i.e., endogenous toxins accumulated under uremic conditions such as *p*-cresol species) factors that alter MPA pharmacokinetics in humans.

Methods and Results

Population pharmacokinetic modeling was utilized to characterize the potential clinical variables that may influence MPA pharmacokinetics/dynamics in a variety of patient populations. Using data obtained from adult kidney transplant recipients, a novel population pharmacokinetic model

of MPA was constructed to investigate the effects of corticosteroids and tacrolimus on the pharmacokinetics of MPA. It was found that the overall clearance of MPA was markedly reduced in corticosteroid-free patients, indicating that MPA dose adjustment or therapeutic drug monitoring may be required (e.g., when tapering the dose of corticosteroids) in the clinic to prevent the over-exposure of MPA. On the other hand, tacrolimus dose, trough concentration, and exposure were not identified as significant clinical covariates affecting the pharmacokinetics of MPA, suggesting that dose adjustment may not be warranted when MPA is co-administered with tacrolimus. Furthermore, population pharmacokinetic models of MPA published in the literature were comprehensively, critically summarized with respect to modeling techniques, significant covariates, and clinical utilities. Our analyses indicated that albumin, body weight, creatinine clearance, cyclosporine, and post-transplant time were consistently identified as significant clinical factors affecting MPA pharmacokinetics/dynamics. In addition, Bayesian predictive models are also now available to aid MPA dose-adjustment in a variety of patient (adult and pediatric) populations.

Using a translational investigative approach, the inhibitory effects of *p*-cresol on the glucuronidation of MPA were determined in a metabolically-competent human hepatoma cell line (i.e., HepaRG model), human liver microsomes, and cDNA-expressed human enzymes. The identified inhibitory concentrations of *p*-cresol were physiologically attainable in adult kidney transplant patients, suggesting that fluctuations in *p*-cresol concentrations may be partially responsible for the large variabilities of MPA observed in the clinic. Furthermore, understanding how *p*-cresol is metabolized can help elucidate factors that may affect *p*-cresol disposition and indirectly contribute to MPA variabilities. As *p*-cresol is found in the forms of *p*-cresol sulfate and glucuronide in the human plasma, their enzyme kinetics were also characterized using human

cytosols/microsomes and human recombinant sulfotransferases (SULT)/uridine 5'-diphospho-glucuronosyltransferase (UGT) enzymes. Human SULT1A1 was identified the primary enzyme responsible for the formation of *p*-cresol sulfate (high efficiency/low capacity), whereas human UGT1A6 exhibited the highest catalytic activities toward the generation of *p*-cresol glucuronide (low efficiency/high capacity). These data provided the justification for focusing on *p*-cresol sulfate as the primary metabolite for our clinical investigation, and identified potential druggable targets for mitigating the formation of toxic *p*-cresol metabolites as an approach to reduce the MPA interaction. Finally, the interaction between MPA and *p*-cresol sulfate was investigated in adult kidney transplant recipients within the first year post-transplantation. Significant positive correlations were observed between the total MPA trough concentration and the plasma *p*-cresol sulfate concentration in a prospective, observational study. These clinical findings confirmed a role of *p*-cresol as a significant clinical variable affecting the pharmacokinetics of MPA in patients.

Conclusion

This PhD thesis has identified potential significant extrinsic and intrinsic factors influencing MPA pharmacokinetics. It also systematically characterized a potent metabolism interaction between *p*-cresol and MPA, using the translational approach involving *in vitro* and clinical models. For scientists, this thesis has provided the basis for conducting further mechanistic experiments and for investigating therapeutic approaches for mitigating MPA variability. For clinicians, this thesis has presented a comprehensive overview and critique of potential clinical factors that may contribute to MPA variabilities, as well as identified a novel approach for proactively managing *p*-cresol accumulation and MPA variability. For patients, this thesis may ultimately improve the clinical outcomes and their quality of lives.

Preface

This thesis is an original work by Yan Rong.

Ethics approval:

The research project (Chapter II), of which this thesis is a part, received research ethics approval from the University of British Columbia (and University of Alberta Clinical Research Ethics Boards under reciprocal institutional agreements). Project name: "Population pharmacokinetic modeling of mycophenolic acid and tacrolimus in adult renal transplant recipients on steroid-free regimens"; No. H17-02902; September 7, 2018.

The research project (Chapter IX), of which this thesis is a part, received research ethics approval from the University of Alberta Research Ethics Board. Project name: "Mycophenolic acid and *p*-cresol interaction in adult kidney transplant patients"; No. Pro00105082; December 20, 2021.

The research project (Appendix A. Population pharmacokinetic analysis of immediate-release oral tacrolimus co-administered with mycophenolate mofetil in steroid-free adult kidney transplant recipients), of which this thesis is a part, received research ethics approval from the University of British Columbia (and University of Alberta Clinical Research Ethics Boards under reciprocal institutional agreements). Project name: "Population pharmacokinetic modeling of mycophenolic acid and tacrolimus in adult renal transplant recipients on steroid-free regimens"; No. H17-02902; September 7, 2018.

Published journal articles (all data chapters presented in this thesis have been published in peer-reviewed journals):

Chapter II of this thesis has been published as Rong Y, Mayo P, Ensom MHH, Kiang TKL, "Population pharmacokinetics of mycophenolic acid co-administered with tacrolimus in corticosteroid-free adult kidney transplant patients", *Clin Pharmacokinet*, 2019 Nov;58(11):1483-1495. Rong Y was responsible for data analysis, model construction, and manuscript preparation. Mayo P and Ensom MHH assisted with the data analysis, model construction, and contributed to editing the manuscript. Kiang TKL (corresponding author) was involved in project conception, project management, data analysis, model construction, and final manuscript preparation.

Chapter III of this thesis has been published as Rong Y, Patel V, Kiang TKL, "Recent lessons learned from population pharmacokinetic studies of mycophenolic acid: Physiological, genomic, and drug interactions leading to the prediction of drug effects", *Expert Opinion on Drug Metabolism & Toxicology*, 2022 Jan; 17(12): 1369-1406. Rong Y was responsible for conducting literature search, data extraction, data interpretation, and manuscript preparation. Patel V assisted with the data extraction. Kiang TKL (corresponding author) was involved in project conception, project management, data extraction, data interpretation, and final manuscript preparation.

Chapter IV of this thesis has been published as Rong Y, Jun H, Kiang TKL, "Population pharmacokinetics of mycophenolic acid in paediatric patients", *Br J Clin Pharmacol*, 2021 Apr;87(4):1730-1757. Rong Y was responsible for conducting literature search, data extraction, data interpretation, and manuscript preparation. Jun H assisted with the data extraction and manuscript preparation. Kiang TKL (corresponding author) was involved in project conception, project management, data extraction, data interpretation, and final manuscript preparation.

Chapter V of this thesis has been published as Rong Y, Kiang TKL, "Development and validation of a sensitive liquid-chromatography tandem mass spectrometry assay for mycophenolic acid and

metabolites in HepaRG cell culture: Characterization of metabolism interactions between *p*-cresol and mycophenolic acid", *Biomed Chromatogr*, 2019 Aug;33(8):e4549. Rong Y was responsible for data collection, data analysis, and manuscript preparation. Kiang TKL (corresponding author) was involved in project conception, project management, data analysis, and final manuscript preparation.

Chapter VI of this thesis has been published as Rong Y, Kiang TKL, "Mechanisms of metabolism interaction between *p*-cresol and mycophenolic acid", *Toxicol Sci*, 2020 Feb 1;173(2):267-279. Rong Y was responsible for data collection, data analysis, and manuscript preparation. Kiang TKL (corresponding author) was involved in project conception, project management, data analysis, and final manuscript preparation.

Chapter VII of this thesis has been published as Rong Y, Kiang TKL, "Characterization of human sulfotransferases catalyzing the formation of *p*-cresol sulfate and identification of mefenamic acid as a potent metabolism inhibitor and potential therapeutic agent for detoxification", *Toxicol Appl Pharmacol*, 2021 Aug 15;425:115553. Rong Y was responsible for data collection, data analysis, and manuscript preparation. Kiang TKL (corresponding author) was involved in project conception, project management, data analysis, and final manuscript preparation.

Chapter VIII of this thesis has been published as Rong Y, Kiang TKL, "Characterizations of human UDP-glucuronosyltransferase enzymes in the conjugation of *p*-cresol", *Toxicol Sci*, 2020 Aug 1;176(2):285-296. Rong Y was responsible for data collection, data analysis, and manuscript preparation. Kiang TKL (corresponding author) was involved in project conception, project management, data analysis, and final manuscript preparation.

Chapter IX of this thesis has been published as Rong Y, Colbourne P, Gourishankar S, Kiang TKL, "Significant correlations between *p*-cresol sulfate and mycophenolic acid plasma concentrations in adult kidney transplant recipients", *Clinical Drug investigation*, 2022 Mar;42(3):207-19. All authors contributed to the study conception and design. Material preparation, data collection, analytical measurements, and data analysis were performed by Rong Y and Kiang TKL. The first draft of the manuscript was written by Rong Y. All authors commented on the final version of the manuscript, which was edited/finalized by Kiang TKL.

Appendix A. Population pharmacokinetic analysis of immediate-release oral tacrolimus co-administered with mycophenolate mofetil in steroid-free adult kidney transplant recipientsof this thesis has been published as Rong Y, Mayo P, Ensom MHH, Kiang TKL, "Population pharmacokinetic analysis of immediate-release oral tacrolimus co-administered with mycophenolate mofetil in corticosteroid-free adult kidney transplant recipients", *Eur J Drug Metab Pharmacokinet*, 2019 Jun;44(3):409-422. Rong Y was responsible for data analysis, model construction, and manuscript preparation. Mayo P and Ensom MHH assisted with the data analysis, model construction, and contributed to editing the manuscript. Kiang TKL (corresponding author) was involved in project conception, project management, data analysis, model construction, and final manuscript preparation.

The data/content re-use permissions have been acquired for all of the published papers, please see each section for more details.

Dedication

This thesis is dedicated to my husband and my parents, for your love, support, and encouragement.

Acknowledgments

I would like to express my sincere appreciation to members of my supervisory committee: Dr. Afsaneh Lavasanifar and Dr. Raimar Loebenberg. Thank you for your time and support through each stage of my training process. Special thanks to Dr. Pat Mayo for your valuable suggestions on our population pharmacokinetic model building process. My sincere thanks to my arms-length examiners for your time and expertise, and to Dr. John Seubert for chairing my candidacy and final oral exams. My sincere thanks are also addressed to Dr. Penny Colbourne and Dr. Sita Gourishankar for your participations in our clinical study.

I would also like to thank the past and present lab members: Ms. Sang Zhu, Ms. Yashita Singh, and Ms. Alaa Al Dajani. We have had many happy moments together in the lab.

I would like to thank the Faculty of Pharmacy and Pharmaceutical Sciences and the University of Alberta for providing me various training scholarships.

Lastly, my sincere appreciation goes to my supervisor Dr. Tony KL Kiang. Thank you for giving me the opportunity to join your research group and take part in these research projects. I have gained valuable skills and experiences that will benefit me for the rest of my life. Thank you for always being there to lead me through the tough and good times throughout my PhD training.

Table of Contents

List of Tables

List of Figures

List of Equations

Abbreviations

ABC transporter, ATP-binding cassette transporter

AcMPAG, mycophenolic acid acyl glucuronide

AIC, Akaike information criterion

ALP, alkaline phosphatase

ALT, alanine aminotransferase

ANC, absolute neutrophil count

APE, absolute prediction error

AST, aspartate aminotransferase

AUC, area under the concentration-time curve

BCRP, breast cancer resistance protein

BIC, Bayesian information criterion

BMI, body mass index

BOV, between occasion variability

BSA, bovine serum albumin

BSV, between subject variability

C_0, trough concentration

CI, confidence interval

CKD-EPI equation, chronic kidney disease epidemiology collaboration equation

CL/F, apparent clearance

CL_{int}, intrinsic clearance

CL_{max}, maximum clearance

C_{max}, maximum plasma concentration

CMPF, 3-carboxy-4-methyl-5-propyl-2-furanpropionic acid

CrCL, creatinine clearance

CV, coefficient of variation

CWRES, conditional weighted residuals

CXCL-10, interferon gamma inducible chemokine 10

CYP, cytochrome P450

DBSA, dose per body surface area

DM-MPA, 6-O-desmethyl-mycophenolic acid

DMSO, dimethyl sulfoxide

EC-MPS, enteric-coated mycophenolate sodium

eGFR, estimated glomerular filtration rate

EMA, European Medicines Agency

E_{max}, maximal inhibitory effect

EMIT, enzyme-multiplied immunoassay technique

F, bioavailability

FAIV, the maximum concentration following an intravenous bolus administration of a unit dose

FDA, U.S. Food and Drug Administration

FMO, flavin-containing monooxygenase

FO, first-order algorithm

FOCE, first-order conditional estimation algorithm

FOCE-I, first-order conditional estimation with interaction algorithm

f_u, unbound fraction

GGT, γ-glutamyltransferase

HLA, human leukocyte antigen

HNF1A, hepatic nuclear factor 1 alpha

HPLC-UV DAD, high-performance liquid chromatography with ultraviolet diode-array detector

HPLC-UV, high-performance liquid chromatography with ultraviolet detection

IC_{50}, half maximum inhibitory concentration

IIV, inter-individual variability

IMP, inosine monophosphate

IMPDH, inosine-5'-monophosphate dehydrogenase

IOV, inter-occasion variability

IPRED, individual predicted

IQR, interquartile range

IRES, individual residuals

IV, intravenous

IWRES, individual weighted residuals

k_a, absorption rate constant

K_i, concentration of inhibitor at which under saturating substrate conditions the reaction rate is at half of the maximum rate

K_m, concentration of substrate at which the reaction rate is half of the maximum

K_{si}, the dissociation constant of substrate inhibition

LCMS, liquid chromatography with mass spectrometry

LC-MS/MS, liquid chromatography tandem mass spectrometry

LLOQ, lower limit of quantification

m/z, mass to charge ratio

MDRD equation, modification of diet in renal disease

MMF, mycophenolate mofetil

MPA, mycophenolic acid

MPAG, mycophenolic acid glucuronide

MPE, mean prediction error

MRM, multiple reaction monitoring

MRP2, multidrug resistance associated protein 2

NA, not available

NAD^+, nicotinamide adenine dinucleotide

NPDE, normalized prediction distribution errors

NSAIDs, nonsteroidal anti-inflammatory drugs

OAT3, human renal organic anion transporter 3

OATP1B1/3, organic anion transporting polypeptides 1B1/3

OD, observed data

OFV, objective function value

PAPS, 3'-phosphoadenosine-5'-phosphosulfate

PBMC, peripheral blood mononuclear cell

PE, prediction error

PRED, population predicted

Q/F, apparent inter-compartmental clearance

QC, quality control

R, coefficient of correlation

R^2, coefficient of determination

RMSE, root mean square error

RSE, relative standard error

RUV, residual unexplained variability

RV, residual variability

SAEM, stochastic approximation expectation maximization estimation method

SCr, serum creatinine

SD, standard deviation

SE, standard error

SLC, solute carrier family transporter

SULT, sulfotransferase

Sy.x, root mean square

T_{lag}, absorption lag time

T_{max}, the time to maximum plasma concentration

UGT, uridine 5'-diphospho-glucuronosyltransferase

UPLC-MS/MS, ultra-performance liquid chromatography tandem mass spectrometry

V_1/F or V_c/F, apparent central compartment volume of distribution

V_2/F or V_p/F, apparent peripheral compartment volume of distribution

V_{max}, maximum reaction rate

VPC, visual predictive check

WBC, white blood cell count

WRES, weighted residuals

XMP, xanthosine monophosphate

α, alpha value, the constant that differentiates the specific mechanisms in the mixed inhibition model

Chapter I. Introduction[1]

1. Introduction

1.1. Mycophenolic acid

1.1.1. Discovery and history of development

Mycophenolic acid (MPA), a purified microbial metabolite from *Penicillium* species, was first discovered by an Italian physician, Dr. Bartolomeo Gosio, as an anti-bacterial agent in the year of 1893 and named by Alsberg and Black subsequently in 1913 [1, 2]. Its anti-fungal, anti-viral, and anti-tumor effects had been identified in late 1960s and early 1970s [1]. Around the same time, Franklin et al. reported the inhibitory effects of MPA on the activities of inosine-5'-monophosphate dehydrogenase (IMPDH) in various *in vitro* models, which was associated with decreased synthesis of guanine nucleotides in the "L cell" (i.e., a mouse fibroblast) model [1-3]. These experiments collectively established the mechanisms of immunosuppression for MPA. In 1973, MPA was initially utilized in the treatment of psoriasis [1, 4], but was later discontinued in 1998 due to its serious adverse effects such as carcinogenicity [1, 5]. In the 1990s, as a part of the *Syntex Research Program*, in which novel immunosuppressive agents were tested to replace azathioprine [1], the anti-rejection effects of MPA were further characterized in multiple allograft transplant models [1, 2]. In 1996, the first-in-human study demonstrated the efficacy and safety of MPA in comparison to azathioprine in 503 kidney transplant patients [6]. It was found that patients

[1] This thesis follows the manuscript style; therefore, the thesis introduction chapter is intended to be generalized. Each subsequent data chapters (i.e., published manuscripts) will also provide specific and detailed introductions.

on MPA (either 2 g or 3 g daily dose of mycophenolate mofetil [MMF]) exhibited significant reductions in the occurrence of treatment failure (including *"biopsy-proven rejection, graft loss, and discontinuation of the study drug"* [6]) compared to azathioprine, suggesting MPA was a promising antimetabolite agent. The U.S. Food and Drug Administration (FDA) [7], European Medicines Agency (EMA) [8], and Health Canada [9] officially launched MPA (CellCept®, MMF formulation) on the markets between the years 1995-1996. The original indication approved by the FDA was for the prophylaxis of organ rejection in patients receiving allogeneic renal transplantation, and MPA was widely prescribed as evident by more than 50,000 kidney transplant recipients administered this immunosuppressant from 1995 to 1998 alone [1]. In addition, various other indications for using MPA (e.g., heart transplant and liver transplant) had also been proposed [1].

1.1.2. Formulations

MPA is the active compound in two available formulations: an immediate-release MMF (commercial name: CellCept®, marketed by Hoffmann-La Roche [10, 11] and various generic companies) and a delayed-release enteric-coated mycophenolate sodium (EC-MPS; commercial name: Myfortic®, marketed by Novartis Pharmaceutics and various generic companies) [10, 12]. MMF is the 2, 4-morpholino ethyl ester pro-drug of MPA, and this formulation was devised in 1990 by Lee et al. to improve bioavailability [2, 13]. The commercially available dosage forms of MMF are capsule (250 mg), film-coated tablet (500 mg), oral suspension (powder, 200 mg/mL when reconstituted), and MMF for injection (hydrochloride, lyophilized powder provided, 500 mg/vial, which requires reconstitution prior to intravenous injection) [11]. MMF for intravenous injection should only be given to patients who are not able to consume MMF orally [11], and the

injection should be switched to oral formulations as soon as the patients can tolerate *per os* administration [11]. On the other hand, EC-MPS is the enteric coated formulation of MPA, which was developed in 2005 to mitigate the frequently observed gastrointestinal discomforts of MMF [2, 14, 15]. As per the FDA's prescribing information for MMF, the incidences of diarrhea can be as high as 30.4%, 52.6%, and 51.3% in kidney, heart, and liver transplant patients, respectively [16]. Instead of the acidic environment in the stomach (pH=5), the release of MPA from EC-MPS mainly occurs in the small intestine where the pH is neutral to slightly basic (pH=6-8), which theoretically can increase the tolerance to MPA [2, 10, 14]. EC-MPS is available in 180 mg and 360 mg tablets, which should be swallowed intact to preserve the properties of the enteric coating, and should ideally be administered on an empty stomach [12]. The molecular weights of MMF and mycophenolate sodium are 469.96 g/mol and 342.32 g/mol, respectively [2]; therefore, 720 mg of EC-MPS is approximately equivalent to 1000 mg MMF [2, 10, 14, 15]. The safety and efficacy of EC-MPS have been tested in multiple clinical trials such as Pivotal [17], myPROMS [18-22], and PROGIS [23], indicating that EC-MPS was associated with improved quality-of-life in transplant patients [14]. However, MMF and EC-MPS cannot be administered interchangeably because of their different pharmacokinetic profiles [2, 24] (see further discussion in 1.1.4 Clinical pharmacology). MMF is still considered the most widely used formulation, but increased usage of EC-MPS is becoming evident in some transplant centres (e.g., the University of Alberta Hospital). As such, the majority of our data presented in this thesis are pertaining to the MMF formulation, but EC-MPS data are also discussed as appropriate (i.e., Chapter III [25] of the thesis).

1.1.3. Indications and dosages

MMF or EC-MPS are commonly used in combination with other immunosuppressants such as calcineurin inhibitors and corticosteroids [2]. According to Health Canada, MMF is indicated for the prevention of organ rejection in adult patients receiving allogeneic kidney, heart, or liver transplantation, and in pediatric patients receiving allogeneic kidney transplantation [11]. On the other hand, EC-MPS is only indicated in adult kidney transplant recipients, as its efficacy and safety have not been established in pediatric populations [12]. Typically, adult populations are prescribed a fixed dosing regimen of MMF: 2 g daily in kidney transplants, 3 g daily in heart transplants, and 2 g daily if infused intravenously or 3 g daily if administered orally in liver transplants [11]. MMF administration in pediatric patients with kidney transplantation is commonly based on body surface area: 1200 mg/m^2 body surface area (oral suspension, up to 2 g per day), 1.5 g daily dose (capsules or tablets) for patients with body surface area between 1.25 to 1.5 m^2, and 2 g daily dose (capsules or tablets) for patients whose body surface area exceeded 1.5 m^2 [11]. On the other hand, the recommended dosage for EC-MPS is 1440 mg daily in adult kidney transplant patients [12]. The frequency of administration is usually twice a day for both MMF and EC-MPS [11, 12], and dose adjustment is recommended in patients with severe renal dysfunction (i.e., estimated glomerular filtration rate [eGFR] < 25 mL/min/1.73 m^2) and/or exhibiting neutropenia (i.e., absolute neutrophil count [ANC] < $1.3\times10^3/\mu L$) [11, 12]. In these scenarios, the transplant team will usually reduce the dose of MPA and monitor the patient clinically [11, 12]. Hereafter, unless the intent is to specifically differentiate the effects of formulation, the pharmacokinetic and pharmacodynamic effects will be discussed in relation to the active moiety of both formulations, which is MPA.

Other than the Health Canada-approved indications [11, 12], MPA has been used off-label in various other conditions [2]. The use of MPA in these off-label indications have been supported by clinical trials [26] and can be categorized on an evidence level system, where levels A to C indicates progressively decreased evidence of using MPA in a particular indication [26]. Generally, "level A" (i.e., strongest evidence) indications included lupus nephritis, "level B" indications included allogeneic hematopoietic cell transplantation and lung transplantation, and "level C" indications included autoimmune hepatitis, idiopathic nephrotic syndrome, and myasthenia gravis [26]. In addition, level G is defined as *"Use has been substantiated by inclusion in at least one evidence-based or consensus-based clinical practice guideline"*, such as autoimmune hepatitis, lupus nephritis, myasthenia gravis, and psoriasis [26]. The majority of the data in this thesis are based on the kidney transplant population, but the clinical pharmacology of MPA in non-kidney patients (i.e., other solid organ transplantations, auto-immune conditions) are also discussed in Chapter III [25] and Chapter IV [27] as we anticipate increased usage of MPA in these other indications [2, 24].

1.1.4. Clinical pharmacology

MPA's immunosuppressive effects are mediated through its potent, selective, and uncompetitive inhibition of the IMPDH enzyme (especially the type II IMPDH subtype) [2, 10, 28, 29]. This enzyme is one of the key catalysts involved in the *de novo* biosynthesis of guanosine nucleotide, which converts inosine monophosphate (IMP) to xanthosine monophosphate (XMP) in the presence of nicotinamide adenine dinucleotide (NAD^+, the co-enzyme/co-factor) [2, 28]. T- and B- lymphocytes are important components of the body's adaptive immunity to defend against foreign substances (including the transplanted organs/tissues) and for mediating graft rejections.

The proliferations of T- and B- lymphocytes are reliant on the *de novo* pathway of purine synthesis [2, 10, 29], and MPA reduces their proliferations by inhibiting the IMPDH enzyme as the primary mechanism for suppressing the cell-mediated immune reactions [2, 10, 28, 29]. Furthermore, MPA could also interfere with the maturation of dendritic cells and impede their ability to present antigens, suppress the recruitment of monocytic lineage cells to sites of inflammation and rejection presumably by inducing their differentiation and apoptosis, and prevent the migration of lymphocytes and monocytes to the allografted organs [28, 29]. Despite a clear consensus on the molecular targets of MPA (i.e., pharmacodynamics), the pharmacokinetic-dynamic relationships of MPA remain largely unknown, which will be explored further in our data chapters (Chapter III [25] and Chapter IV [27]) in this thesis.

Large variabilities (as high as 10-fold) in the plasma exposure have been frequently observed for MPA [10, 30], which could be attributed to multiple intrinsic and/or extrinsic factors (e.g., patient biological age, complex (re-)absorption, protein binding displacement, impaired kidney/liver functions, genetic polymorphisms, drug-drug interactions, etc. [2, 10, 31]) affecting its rather complicated pharmacokinetics. After administration, MMF is extensively de-esterified by carboxylesterases-1 and 2 [32] in the stomach and proximal small intestine [2] to release the active MPA, and therefore plasma concentrations of MMF are usually negligible [2, 10]. MPA plasma concentrations from MMF administration can increase rapidly and the peak plasma concentrations (C_{max}) are typically achieved around 0.5-1 hour after dosing [2]. On the other hand, the absorption profile for EC-MPS is different than MMF likely due to the enteric-coating, which releases MPA primarily in the small intestine [2, 10, 14]. This characteristic delays the MPA absorption and increases the time required to reach the maximum plasma concentration (T_{max}, approximately 1.5-6 hours post-EC-MPS dose) in patients [2]. The maximum plasma

concentration after EC-MPS administration is also typically 10-18% lower compared to MMF [2]. Overall, the bioavailability of MMF is approximately 94%, 81%, and 95% in healthy volunteers, kidney transplant patients, and heart transplant patients, respectively [10, 32]. For EC-MPS, oral bioavailability is estimated to be 72% in stable kidney transplant recipients [10, 32].

The majority of MPA in whole blood is found in the plasma compartment (99.99%), with negligible concentrations in blood cells [10]. In plasma, MPA is highly protein bound to albumin with an unbound fraction of ~1-3% as determined in patients with normal kidney and liver functions [10]. Of note, only unbound concentrations of MPA can exert pharmacological activities and be subjected to further metabolism and/or excretion [10, 31]. As the theoretical hepatic extraction of MPA is as low as 0.2 [33], the relationships between total and unbound MPA concentrations could be depicted by the following equations (Equation I-1, Equation I-2) [34]:

Equation I-1

$$Total\ MPA\ concentrations \sim \frac{dose\ rate}{unbound\ fraction\ \times intrinsic\ clearance}$$

Equation I-2

$$Free\ MPA\ concentrations \sim \frac{dose\ rate}{intrinsic\ clearance}$$

Therefore, the total concentrations of MPA may be susceptible to factors influencing the unbound fraction (e.g., protein binding displacement) and/or intrinsic clearance (e.g., drug-drug interactions), whereas the free concentrations of MPA are independent of changes in free fractions and only inversely proportional to intrinsic clearance [10, 31]. The optimal pharmacokinetic models capable of describing MPA pharmacology in consideration of its unique binding

characteristic remain unknown and will be further discussed in Chapter III [25] and Chapter IV [27]. Furthermore, being a hydrophobic drug (please see the chemical structure in Figure I-1), MPA needs to undergo further metabolism to increase its solubility before it can be eliminated from the body. MPA metabolism is primarily catalyzed by the human uridine 5'-diphospho-glucuronosyltransferase (UGT) enzymes [10, 32] in the liver to form mycophenolic acid glucuronide (MPAG, the major metabolite) and mycophenolic acid acyl glucuronide (AcMPAG, the minor metabolite) (Figure I-1), which are pharmacologically inactive and active, respectively [10, 32]. In addition to the liver, the kidneys and small intestines are also capable of conjugating MPA due to the abundant expressions of the responsible UGT enzymes [10, 32]. In humans, UGT1A9 is the primary isoform responsible for the production of MPAG [10, 32, 35], corresponding to 55%, 75%, and 50% of its generation in the liver, kidneys, and intestines, respectively; whereas UGT2B7 is responsible for the generation of AcMPAG [35]. Moreover, UGT1A7, UGT1A8, and UGT1A10 also have documented catalytic activities toward the glucuronidation of MPA, but their relative contributions are minor [10, 32]. In addition to phase II conjugation, phase I oxidation has also been reported for MPA [36], and the oxidative metabolite, 6-O-desmethyl-mycophenolic acid (DM-MPA) (Figure I-1), is considered a product of the cytochrome P450 (CYP)3A4 and CYP3A5 enzymes [36]. Parts of this thesis address the effects of genetic polymorphisms of these metabolism enzymes on the pharmacokinetics of MPA (Chapter III [25] and Chapter IV [27]).

The most abundant metabolite, MPAG, is primarily excreted in the urine [10, 37]. This was demonstrated in 4 healthy male subjects administered a single oral dose of 1 g radiolabeled MMF ([mycophenolate-14 C] mofetil) under fasting conditions, whose urine, fecal, and blood samples were collected for 7 days post dosing [37]. The recovered radio-activities indicated that 90.4% of

the administered MMF dose was detected within the first 3 days after administration, of which 96.3% was recovered in the urine as "almost exclusively" MPAG [37], indicating that approximately 87% of the MPA dose was renally excreted as the predominant metabolite [10]. In contrast, the urinary recoveries of MPA and AcMPAG were negligible in healthy human volunteers (i.e., 0.6% and 0.3%, respectively) [37]. The excretion of MPAG into the urine is believed to be facilitated by human renal organic anion transporter 3 (OAT3, located on the basolateral membrane and responsible for the uptake of MPAG from the systemic circulation into the renal proximal tubular cells) [30, 32, 38] and multidrug resistance associated protein 2 (MRP2, located on the apical membrane and responsible for the efflux of MPAG from the renal proximal tubular cells into the urine tubules) [30, 32, 39].

In addition to renal elimination, MPAG could also be excreted into the bile [10, 30, 32], where MPAG is deconjugated by β-glucuronidases produced from intestinal microflora and the liberated MPA can be re-absorbed in the colon [10, 32], leading to secondary peaks which are typically observed at 6-12 hours post-dose in its plasma concentration-time profiles [10]. This entero-hepatic recirculation process can account for up to 40% of the total MPA exposure [10, 30] and may involve multiple transporters: the organic anion transporting polypeptides 1B1/3 (OATP1B1/3) are possibly responsible for the uptake of MPAG into the hepatocytes from the sinusoidal membrane [40-43], while the MRP2 [41, 44-49] and breast cancer resistance protein (BCRP) transporters [42] are responsible for excreting MPAG into the bile at the canalicular membrane [10, 30, 32]. Likewise, the optimal pharmacokinetic models capable of describing MPA entero-hepatic recirculation in consideration of contributory clinical covariates (e.g., intrinsic, extrinsic factors, including genetic polymorphisms of involved transporters) remain unknown, and

will be further discussed in Chapter III [25] and Chapter IV [27]. The general pharmacokinetic behaviors of MPA are summarized in Figure I-1.

The aforementioned MPA pharmacokinetic characteristics were mainly derived from healthy subjects, and kinetic parameters can be further altered in different disease states [10]. For example, hypoalbuminemia (i.e., decreased plasma albumin due to impaired liver/kidney functions) is one of the common manifestations of liver and/or kidney transplantation, which may increase the free fraction of MPA leading to decreased total (but not free) MPA concentrations [10]. Evidently, a study in adult kidney transplant patients has determined a "threshold" albumin value of 31 g/L below which the MPA free fraction would be significantly increased [50]. Furthermore, MPAG is primarily excreted renally, and impairments in renal function may hinder its elimination and thereby lead to the accumulation of its plasma concentrations [10]. As MPAG is also highly protein bound to serum albumin (~82%), it can also displace the protein binding of MPA in the plasma [10]. Unfortunately, the specific patient factors leading to the overall MPA pharmacokinetic variability remain largely unknown, with often inconsistent findings reported in the literature (e.g., [31, 51]). Therefore, a part of this thesis will critically summarize the available literature in order to identify key clinical variables (from the distinctive perspectives of adult and pediatric patients, due known differences in pharmacokinetic behaviors) likely to influence MPA pharmacology in various diseased conditions (Chapter III [25] and Chapter IV [27]). In addition, renal dysfunction itself may lead to the accumulation of uremic toxins, some of which could also displace the protein binding of MPA [10] and/or directly reduce its intrinsic clearance by inhibiting the hepatic UGT enzymes [52, 53]. As reported by Barnes et al., *p*-cresol (i.e., a protein-bound uremic toxin) was capable of inhibiting the catalytic activities of UGT1A1, UGT1A4, UGT1A6, UGT1A9 (exhibiting the most potent effects), UGT2B4, and UGT2B7 by 78%, 33%, 8%, 93%,

20%, and 48%, respectively, in human liver microsomes [52], and can theoretically affect the disposition of MPA. A major part of this thesis (i.e., Chapter V [54], Chapter VI [55], Chapter VII [56], Chapter VIII [57], and Chapter IX [58]) will present our systematic and mechanistic investigations to elucidate the metabolism interaction between *p*-cresol and MPA using a variety of complementary human *in vitro* and clinical models.

In addition, certain drugs are known to cause pharmacokinetic/dynamic interactions with MPA and are not recommended to be co-administered simultaneously: acyclovir/valacyclovir (competes with the tubular secretion of MPAG), antibiotics (affect the entero-hepatic recirculation of MPA by altering the bacterial flora), azathioprine (exhibits a similar mechanism of immunosuppression), cholestyramine (binds physically to MPAG and interferes with the enterohepatic recirculation), cyclosporine (inhibits biliary transporters and reduces the enterohepatic recirculation of MPA), magnesium and aluminum hydroxide containing antacids (chelate with MPA and decrease its absorption), proton pump inhibitors (increase gastric pH and reduce the bioavailability of MPA), rifampicin (enhances the intrinsic clearance of MPA by inducing the expression of UGT enzymes and/or MRP2 transporter proteins), and telmisartan (potentially increases the intrinsic clearance by enhancing UGT1A9 expression) [10, 11, 32]. In addition to these documented MPA drug interactions provided in the monograph, additional potential drug-drug interactions are also evident in peer-reviewed literature, which will be discussed in Chapter III [25] and Chapter IV [27] of this thesis. Furthermore, the data supporting the interacting effects of the commonly co-administered immunosuppressants (i.e., tacrolimus and corticosteroids) with MPA are still contradictory, which will be discussed in section 2. Hypothesis and further addressed in thesis Chapter II [59] and Appendix A. Population pharmacokinetic

analysis of immediate-release oral tacrolimus co-administered with mycophenolate mofetil in steroid-free adult kidney transplant recipients [60].

MPA exerts its immunosuppression effects by inhibiting the IMPDH enzyme [2, 10, 28, 29], and the relationships between MPA exposure and efficacy or toxicity have been investigated in multiple patient populations [2, 29, 61]. The efficacy of MPA in solid organ transplantation patients is mainly assessed by the incidence of graft rejection, graft loss, and patient survival [2, 10, 29]. Unfortunately, MPA is also frequently associated with toxicities including gastrointestinal adverse effects (e.g., constipation, diarrhea, dyspepsia, nausea, and vomiting), hematological disorders (e.g., anemia, leukopenia, neutropenia, and thrombocytopenia), and infections (e.g., cytomegalovirus infection and *pneumocystis* pneumonia) [29]. Based on a controlled study in *de novo* adult renal transplant recipients, more than 20% of patients were reported to have experienced the following adverse reactions: abdominal pain (22.4%), diarrhea (30.4%), anemia (20.0%), leukopenia (28.6%), and bacterial infections (39.9%) [16]. Overall, there are many approaches to the therapeutic drug monitoring of MPA [24]. The most common approach is to monitor plasma concentrations [10], where the relatively cost-effective, easy-to-obtain, and the most convenient marker would be the trough concentration. However, trough concentrations are not considered a suitable surrogate marker for MPA exposure [2, 10] due to the relatively weak relationships observed with the risks of rejection [10]. Instead, area under the concentration-time curve $(AUC)_{0\text{-}12}$ is generally agreed upon to be a better indicator for predicting clinical efficacy and adverse effects [2, 10, 24, 51, 61, 62], and therefore the current available target therapeutic ranges of MPA are generally defined based on $AUC_{0\text{-}12}$ (or sometimes $AUC_{0\text{-}24}$) values [2, 10, 24, 62].

In 1999, van Gelder et al. first determined the relationship between MPA exposure (i.e., $AUC_{0\text{-}12}$) and biopsy-proven acute rejection or the occurrence of the adverse reactions in adult

kidney transplant patients taking MMF, cyclosporine, and prednisone within 6-months after transplantation [63]. Their results indicated that the incidences of biopsy-proven acute rejections were significantly reduced in patients with elevated MPA AUC_{0-12} [63], but higher MPA AUC_{0-12} was also correlated with the manifestation of adverse outcomes including abdominal pain, diarrhea, leukopenia, pneumonia, and vomiting [63]. Based on their findings, the currently utilized target therapeutic range for MPA AUC_{0-12} was established as 30-60 μg×h/mL in this specific patient population [63]. Subsequently, this therapeutic range was further extended to adult kidney transplant patients taking MMF, tacrolimus, in the presence or absence of steroids; adult kidney transplant patients after 6-month post-transplantation; and pediatric kidney transplant recipients [2].

The target therapeutic range for MPA AUC_{0-12} can also vary depending on the patient population or indication [2]. For example, MPA AUC_{0-12} targets in liver transplant recipients are dependent on the co-administered immunosuppressants (e.g., 15-30 μg×h/mL with glucocorticoids vs. 30-60 μg×h/mL without glucocorticoids, with concomitant tacrolimus). In heart transplant recipients, MPA AUC_{0-12} was recommended to be maintained at > 36 μg×h/mL in patients co-administered MMF, a calcineurin inhibitor (cyclosporine or tacrolimus), and steroids [2]. In adult stem cell transplant recipients, AUC_{0-24} is utilized instead of AUC_{0-12}, and exposure values > 30 μg×h/mL or < 30 μg×h/mL have been recommended for allogeneic bone marrow transplantation or cord blood transplantation, respectively [2]. On the other hand, the target exposure ranges for MPA have not been identified from exposure-effect or concentration-controlled studies in patients administered the EC-MPS formulation or in patients receiving lung transplantation or lupus nephritis [2]. Likewise, the guidance on MPA therapeutic targets in pediatric subjects is generally lacking and debated in the literature [2]. However, despite the availability of therapeutic exposure

targets, the necessity for conducting MPA clinical concentration monitoring is still equivocal. Conflicting opinions are still evident from various regulatory agencies regarding the designation of MPA being a "narrow therapeutic index drug" [2]. For example, while the FDA and Health Canada classify MPA as a narrow therapeutic index drug [2], the EMA does not consider MPA to have a narrow therapeutic index, but at the same time cautions that its administration should still be monitored closely[8, 24, 64]. Nevertheless, the general consensus in the scientific community, which is still a subject of occasional debate, is that therapeutic drug monitoring of MPA should be conducted because of its considerable pharmacokinetic variabilities and the strong correlations between exposure and clinical outcomes [10, 24].

To estimate MPA AUC, the following approaches can be utilized: i) the conventional trapezoidal method by collecting plasma samples frequently over the entire dosing period, which usually requires 10-12 sampling points; ii) limited sampling strategies using multiple linear regression equations, e.g., Equation I-3,

Equation I-3

$$AUC = a \times C_i + b \times C_j + c \times C_k$$

where "*a*", "*b*", and "*c*" are constant coefficients, and "C_i", "C_j" and "C_k" are plasma concentrations of MPA collected at clinically convenient sampling time points i, j, and k; and iii) limited sampling strategies derived from maximum *a-posteriori* Bayesian estimation, where the AUC is estimated using a complex mathematical algorithm constructed from population pharmacokinetic (i.e., non-linear mixed-effects) models [2, 10, 24, 62]. Limited sampling strategies are more suitable for the clinic because only a few concentration-time points are usually

sufficient, rather than the full concentration-time profiles [2, 10, 62]. In addition, MPA pharmacodynamic monitoring may also be utilized for the precision dosing MPA [2, 10, 62]. In particular, IMPDH gene expression and/or activities could be measured as a direct surrogate of MPA's biological effects [2, 10, 62]; however, the clinical utility of this approach is still limited because of the technical challenges in the routine quantification of the IMPDH marker in the clinic [2, 10, 62]. The majority of limited sampling strategy exposure models have been published strictly in the adult patient populations [2, 51, 62], and currently, there is a general lack of understanding of how MPA pharmacokinetic variability can affect the therapeutic drug monitoring of MPA in pediatrics, which will be addressed in Chapter IV [27] of this thesis.

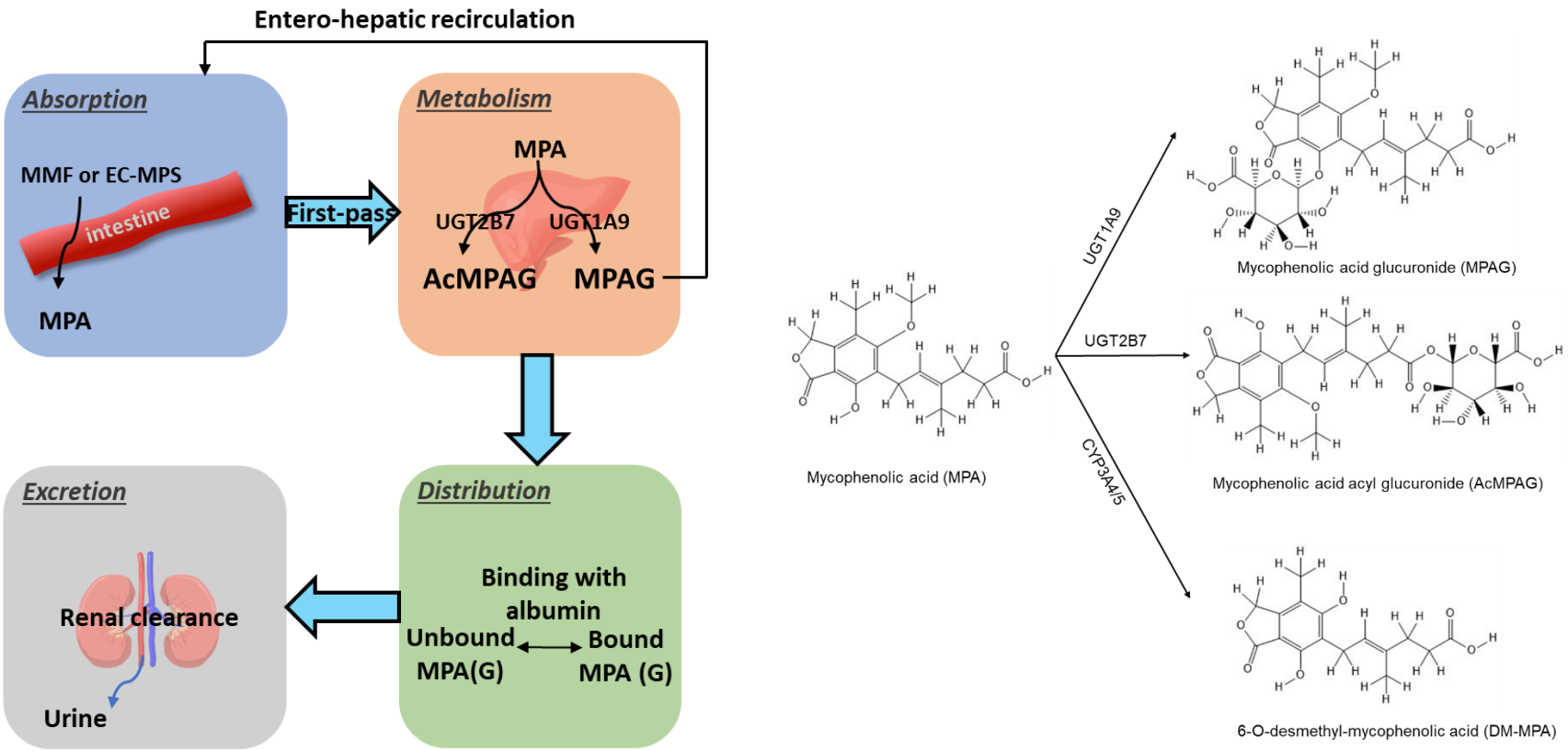

Figure I-1 The chemical structures and the pharmacokinetics of mycophenolic acid and its metabolites

Upon administration, MMF or EC-MPS is extensively dissolved in the gastrointestinal tract to release the active MPA. MPA undergoes metabolism primarily by the human UGT enzymes in the liver, to form MPAG (the pharmacologically inactive major metabolite, through UGT1A9) and AcMPAG (the pharmacologically active minor metabolite, via UGT2B7). A small portion of MPA may also be metabolized by CYP3A4/5 in the production of DM-MPA. Both MPA and MPAG are bound to albumin, and the unbound fractions (which can exert pharmacological activities) are approximately 1-3% and 18%, respectively. MPAG is also excreted in the bile and can

be deconjugated by β-glucuronidases to release MPA. Once liberated, MPA can be re-absorbed in the colon in a process called entero-hepatic recirculation, leading to the occasionally observed secondary peaks. In addition to biliary excretion, the majority of MPAG and AcMPAG are excreted through the kidneys.

1.2. Population pharmacokinetic modeling

1.2.1. Background

The concept of population pharmacokinetics was originated in 1972 by Sheiner et al., when it was utilized as a statistical tool to connect patients' clinical characteristics with drug concentrations or effects [65]. The main feature of population pharmacokinetics is the estimation of kinetic parameters representing the whole population [65, 66] and its ability to characterize various sources of (explainable) pharmacokinetic variabilities from intrinsic (e.g., demographic variables such as age, sex, race; pathophysiological attributes such as albumin level, liver impairment, kidney impairment; and genetic polymorphisms with gain or loss of enzymatic functions) or extrinsic factors (e.g., environmental exposures such as cigarette smoke, pollution, and co-administered drugs) [66]. In addition, population pharmacokinetics modeling is also capable of estimating the unexplained (i.e., random) variabilities within the population [66], which is a feature not found in conventional kinetic modeling. Collectively, these attributes make population pharmacokinetic modeling a very powerful statistical approach in clinical research, where heterogeneity and inter-subject variabilities are the norm.

Various approaches of population pharmacokinetic modeling have evolved overtime, represented by the following general stages: i) naïve average approach, ii) naïve pooled data analysis, iii) two-stage approach (including standard two-stage, global two-stage, iterative two-stage, and the Bayesian two-stage), and iv) nonlinear mixed-effects modelling [67]. Currently, the nonlinear mixed-effects modelling has become the most commonly used method for population pharmacokinetics, with several sub-variations based on the utilized statistical algorithms (e.g., first order, first order conditional estimation, nonparametric adaptive grid, and stochastic approximation expectation maximization) [68]. "Mixed-effects" represents the combination of

both “fixed” and “random” effects [67, 69], where fixed effects (parameterized by θ [theta]) are most commonly used to describe population estimates of pharmacokinetic parameters such as volume of distribution and systemic clearance [67, 69]. On the other hand, random effects describe the differences in parameter values between individuals or between occasions, representing inter-individual (or between-subject) and inter-occasion (between-study) variabilities, respectively. These random variabilities are usually associated with patient characteristics (i.e., covariates) which are commonly parameterized by η (eta) [67, 69]. The distribution of η values is assumed to be normally distributed which is typically represented by the symbol ω (omega) [67, 69]. In addition, residual errors ε (epsilon) are also categorized as a form of random error [67, 69] and can be generated from, as examples, analytical errors in drug concentration measurement, mis-recording of sampling time points, and/or model misspecification [67, 69]. In general, the typical population pharmacokinetic model is consisted of a structural model (e.g., the number of compartments and the specific absorption or elimination behaviors), covariate models (e.g., effects of body weight on the systemic clearance; effects of sex on the absorption…etc.), and statistical models (e.g., for quantifying inter-individual variabilities and the residual error) [67, 69].

Compared to conventional pharmacokinetic studies, a clear advantage of population pharmacokinetic modeling is the allowance of both intensive and sparse sampling [65, 66, 70], the latter attribute making this approach particularly useful for general clinical use and also in populations where repetitive blood sampling could be difficult (e.g., pediatrics, geriatrics, and patients in critical care [65, 66, 70]). Furthermore, population pharmacokinetics allows the combination of heterogenous data from different sources / multiple studies, which can help expand the power of analysis. When population pharmacokinetic models are used in maximum *a posteriori* Bayesian forecasting, a limited number of patient plasma concentration data can be

leveraged to accurately predict their pharmacokinetic parameters and the expected drug exposures, while considering variabilities from multiple sources [62]. Overall, population pharmacokinetics is considered a powerful approach, which is now widely used for estimating population pharmacokinetic estimates, calculating population variabilities, optimizing dosing, and improving therapeutic drug monitoring [65, 66, 70]. In the context of MPA, population pharmacokinetic modeling is the optimal approach for studying the sources and correlates of its pharmacokinetic/pharmacodynamic variability in a variety of patient populations as evident by the large number of models published in the past few decades [10, 30, 31, 62, 71-74]. However, this approach is rapidly evolving, and it is still not clear what is the optimal population modeling methodology for MPA, where a critical analysis of the collective literature in the most recent 5 years is still lacking [31]. Chapter III [25] and Chapter IV [27] of this thesis will provide detailed analyses on the current state of MPA population pharmacokinetic modeling (i.e., the optimal model, the clinically significant covariates, utilities in therapeutic drug monitoring) and Chapter II [59] and Appendix A. Population pharmacokinetic analysis of immediate-release oral tacrolimus co-administered with mycophenolate mofetil in steroid-free adult kidney transplant recipients [60] will provide 2 novel population pharmacokinetic models constructed for the purpose of characterizing MPA drug interactions with the co-administered immunosuppressants.

1.3. Uremic toxins

1.3.1 Background

Uremic toxins (or uremic retention solutes that exhibit negative effects on human health) are a group of compounds produced by the intestinal microbiome that are accumulated under

impaired renal function [53, 75]. Uremic toxins can cause toxicities in various organs and/or tissues including the kidneys, heart, liver, vascular system, and the immune system [53, 75]. Research on uremic toxins is rapidly expanding as evident by the large number of published papers in recent years [75]. A classification system for uremic toxins was originally proposed by Vanholder et al. [76] based on the molecular weight and physio-chemical properties of these compounds: i) freely water-soluble low molecular weight toxins have molecular weights < 500 Dalton and are usually not protein bound (e.g., creatinine); ii) protein-bound uremic toxins are extensively bound to plasma proteins and typically exhibit molecular weights < 500 Dalton (e.g., *p*-cresol), and iii) middle molecule uremic toxins usually have molecular weights > 500 Dalton (e.g., β2-microglobulin) [75, 76]. Of these, protein-bound uremic toxins are generally considered more pathogenic as their dialysis removal efficiency is relatively poor compared to small water-soluble molecules and middle molecules [75]. As only the unbound (i.e., free) compounds can be excreted renally, protein-bound toxins could be accumulated to dangerously high concentrations in the plasma of uremic patients. Moreover, protein-bound uremic toxins can be further classified based on their chemical structures, where the presence of specific functional groups may be associated with select biological effects [77]. For example, advanced glycation end products are associated with "arterial stiffness, diabetic nephropathy, endothelial dysfunctions, and immune system dysregulations"; hippurates are known to induce "endothelial dysfunction and renal tubule damage"; indoles have been documented to cause "bone disease, cardiovascular disease, endothelial dysfunction, inflammation, muscle weakness/atrophy, neurotoxicity, and oxidative stress"; phenols are associated with "all-cause mortality, cardiovascular disease, inflammation, oxidative stress, renal fibrosis, and vascular remodeling"; and the polyamines are known to cause "anemia" [77]. In addition to biological effects, protein-bound uremic toxins are also known to

affect the expressions and activities of metabolism enzymes (e.g., CYPs, sulfotransferases [SULTs], and UGTs) and transporters (e.g., BCRPs, MRPs, OATs, and OATPs) [53]. As such, uremic toxins can also potentially alter the pharmacokinetics of xenobiotics, although very little data are yet available documenting toxin-drug pharmacokinetic interactions. To address the critical literature gap, this thesis provides a systematic translational investigation, from *in vitro* (Chapter V [54], Chapter VI [55], Chapter VII [56], and Chapter VIII [57]) to human clinical models (Chapter IX [58]), to elucidate the mechanism(s) and clinical relevance of the pharmacokinetic interaction between *p*-cresol and MPA.

1.3.2 *p*-Cresol and metabolites

p-Cresol is a prototypical protein-bound uremic toxin [76] with a simple phenol chemical structure as shown in Figure I-2. The major sources of *p*-cresol are dietary amino acids [78, 79], where *p*-cresol is mainly metabolized from tyrosine and phenylalanine by aerobic and anaerobic bacteria in the large intestine [78, 79]. Examples of bacterial families involved in the generation of *p*-cresol are *Bacteroidaceae, Bifidobacteriaceae, Clostridiaceae, Enterobacteriaceae, Enterococcaceae, Eubacteriaceae, Fusobacteriaceae, Lachnospiraceae, Lactobacillaceae, Porphyromonadaceae, Staphylococcaceae, Ruminococcaceae, and Veillonellaceae* [78], and additional species are also likely involved. In addition to diet, other sources such as environmental contaminants (e.g., coal and smoke), industrial chemicals (e.g., antiseptics and disinfectants), food products (e.g., edible oil and preservatives), and pharmaceuticals (e.g., herbal substances and traditional medicine) can also contribute to the total human exposure of *p*-cresol [79]. Once produced, *p*-cresol is further metabolized in the human intestine and the liver, being subjected to the extensive first pass extraction process [78]. The primary metabolites of *p*-cresol in humans are

p-cresol sulfate and *p*-cresol glucuronide [78] (chemical structures shown in Figure I-2), which constitute the main forms of *p*-cresol in the human plasma. As the result, the plasma *p*-cresol concentrations are usually negligible [78, 80-82], and *p*-cresol sulfate and *p*-cresol glucuronide are typically quantified, instead of *p*-cresol, to represent the overall plasma exposure of this uremic toxin [83, 84]. Moreover, *p*-cresol sulfate is extensively bound to plasma albumin, with the unbound fraction of ~8.6% [85], whereas *p*-cresol glucuronide is mainly found in the unbound form in human plasma, exhibiting only ~9.3% protein binding [86]. Little is known of the relative contributions of metabolism enzymes involved in the conjugations of *p*-cresol or how *p*-cresol sulfate and glucuronide are cleared from the body. The different kinetic behaviors of sulfotransferases and UDP-glucuronosyltransferases involved in the conjugation of *p*-cresol, and the different contributions of glomerular filtration or tubular secretion (with distinctive passive and active transporters) involved in the clearance of these conjugated metabolites likely translate to completely unique kinetic behaviors of individual *p*-cresol metabolites in humans. In order to study the pharmacokinetic interaction between *p*-cresol and MPA in our clinical experiment (Chapter IX [58]), the enzyme kinetics behaviors of *p*-cresol sulfate and *p*-cresol glucuronide have also been systematically characterized (Chapter VII [56] and Chapter VIII [57]).

The biological effects (i.e., toxicities) of *p*-cresol metabolites have been well documented in multiple review articles (e.g., [75, 78, 87-89]). Using *in vitro*/*ex vivo* models, it has been reported that *p*-cresol sulfate is capable of inducing cell death in human kidney proximal tubular epithelial cells [90, 91], primary human hepatocytes [92], and HepaRG cells [93]); causing morphological changes to human umbilical vein endothelial cells [94]; generating inflammation in human kidney proximal tubular epithelial cells [91]; inducing insulin resistance in isolated human adipocytes [95]; and producing oxidative stress in non-stimulated human leukocytes [96], human umbilical vein

endothelial or human vascular smooth muscle cells [97], and human kidney proximal tubular epithelial cells [91]). Similarly, *p*-cresol glucuronide also has deleterious effects on various cell types, as evident by its ability to affect the cellular morphology, induce endothelial-to-mesenchymal transition, and decrease the activities of mitochondrial succinate dehydrogenase in human kidney proximal tubular epithelial cells [98, 99]; reduce the cell viability in primary human hepatocytes [92] and HepaRG cells [93]; and alter the mitochondrial membrane potential in primary cultures of human hepatocytes [92]. In addition, the overall effects on cardiovascular and renal toxicities and/or overall mortality of *p*-cresol sulfate and glucuronide have been demonstrated in many clinical investigations, the majority of which have been observed in chronic kidney disease patients [84-86, 98, 100-102]. These cellular damaging effects of *p*-cresol sulfate or *p*-cresol glucuronide may also indirectly affect the distributions of MPA by potentially altering the tissue permeability and/or tissue uptake processes of drugs. As such, Chapter VII [56] of this thesis provides our novel findings on a potentially potent and selective approach to detoxify *p*-cresol sulfate as a means to mitigate its deleterious pharmacokinetic interacting effects.

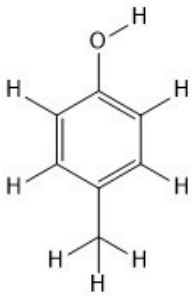

(a) *p*-Cresol

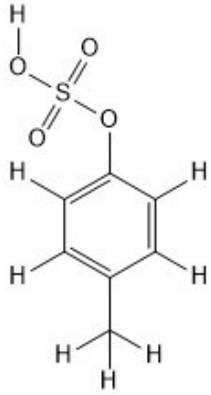

(b) *p*-Cresol sulfate

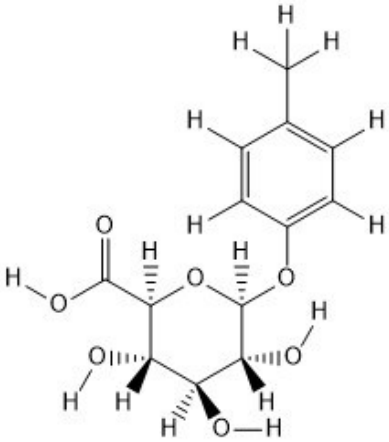

(c) *p*-Cresol glucuronide

Figure I-2 The chemical structures of (a) p-cresol, (b) p-cresol sulfate, and (c) p-cresol glucuronide

2. Hypothesis

MPA is an immunosuppressant frequently used lifelong in preventing graft rejection after organ transplantation and is almost always prescribed concurrently with tacrolimus and corticosteroids. As the therapeutic exposure range of MPA is relatively narrow in kidney transplant patients (i.e., 30-60 μg×h/mL) [63], gastrointestinal adverse effects such as constipation, diarrhea, dyspepsia, nausea, and vomiting are commonly experienced [29], which could affect the patients' quality-of-life. More importantly, the over-exposure of MPA could lead to severe hematological complications (e.g., anemia, leukopenia, and neutropenia) in over ~25% of the kidney transplant patients, which may result in infections that can further threaten the survival of the graft [61]. If not mitigated, MPA over exposure-associated toxicities could lead to patient death [61]. On the other hand, the under-exposure of MPA could also result in organ rejection and graft loss [29]. Based on the data provided by the Kidney Foundation of Canada, over 3500 Canadians are waiting for kidney transplantation in the year of 2019, and this number is significantly greater than the currently available donors [103], pointing to the need to further optimize MPA therapy to minimize graft loss. As such, understanding factors that can contribute to the pharmacokinetic/dynamic variability of MPA (i.e., **this thesis's overarching hypothesis**) can ultimately reduce the incidences of its over- and under-exposure, and thus optimize the health of the transplanted organ and the patient.

As discussed in section 1.1.4. Clinical pharmacology, the pharmacokinetics of MPA are complex and large variabilities in MPA exposure (up to 10-fold) are commonly observed in the clinic despite standardized, empiric dosing. The large pharmacokinetic variability may be attributed to extrinsic (e.g., drug-drug interactions) and/or intrinsic (e.g., hepatic/renal dysfunctions, genetic polymorphisms, or disease states) factors, but unfortunately, little is known

of which factors are clinically relevant. The un-controlled variations in MPA exposure can likely lead to graft rejection, severe infections, and hematological toxicities, resulting in significant morbidities and mortalities to this already fragile patient population. Therefore, understanding the sources or factors contributing to MPA pharmacokinetic variability is critical to improving the precision dosing of MPA.

Due to the fact that MPA is almost always used in combination with tacrolimus and corticosteroids, these co-administered drugs should be considered the most common extrinsic factors influencing the pharmacokinetics of MPA. Based on literature data, tacrolimus is known to inhibit the glucuronidation of MPA in human liver microsomes [104], and MPA is shown to decrease tacrolimus intrinsic clearance through CYP3A4 inhibition under specific *in vitro* experimental conditions [36]. Similarly, corticosteroids are known to induce the expressions of enzymes responsible for the intrinsic clearance of MPA in primary cultures of human hepatocytes [105]. However, direct evidence supporting these molecular interactions are still limited, and clinical data often show inconsistent findings of these co-administered immunosuppressants on MPA pharmacokinetics in transplant patients [106-125].

In addition to interacting drugs, endogenous substances (i.e., intrinsic factors) could also affect the pharmacokinetics of MPA. More specifically, *p*-cresol (and metabolites), which are deemed of significant toxicological interest [75], are found at relatively high concentrations in the plasma of patients with impaired renal function (e.g., kidney transplant recipients [83, 126-130]). In addition, *p*-cresol can theoretically reduce the catalytic activities of UGT1A9 [52] and lead to significantly decreased clearance of MPA in transplant recipients. However, direct evidence supporting the interaction between *p*-cresol and MPA is still lacking, the mechanisms of the

interactions also remain to be characterized, and the clinical relevance of this interaction warrants a human investigation.

The **overall hypothesis** of my PhD project is that large exposure variabilities of MPA can be attributed to extrinsic (i.e., co-administered immunosuppressants) and intrinsic (i.e., *p*-cresol species accumulated under uremic conditions) factors that alter MPA pharmacokinetics in humans.

3. Objectives

The specific objectives of my research program are summarized in Figure I-3:

1) To characterize, critically evaluate, and construct *de novo* population pharmacokinetic-dynamic models of MPA for determining the pharmacokinetic-dynamic interactions between MPA and clinical covariates using original data obtained from adult kidney transplant recipients (Chapter II of this thesis [59]) and literature data from a variety of patient populations (Chapter III [25] and Chapter IV [27] of this thesis).
2) To develop and validate liquid-chromatography tandem mass spectrometry (LC-MS/MS) and ultra-high performance liquid chromatography analytical assays for the quantification of MPA, MPAG, AcMPAG, *p*-cresol, *p*-cresol sulfate, and *p*-cresol glucuronide in a variety of biological matrices utilized in this thesis (Chapter V [54], Chapter VI [55], Chapter VII [56], Chapter VIII [57]).
3) To characterize the metabolism interaction between MPA and *p*-cresol using a metabolically competent human hepatoma cell line, *in vitro* human microsomes, and cDNA-expressed human enzymes (Chapter V [54] and Chapter VI [55] of this thesis).
4) To determine the enzyme kinetics of *p*-cresol sulfate and *p*-cresol glucuronide formation using *in vitro* human cytosolic/microsomal preparations and cDNA-expressed human enzymes; and to systematically identify potent and selective inhibitors of *p*-cresol sulfate formation as a potential approach to detoxify this metabolite (Chapter VII [56] and Chapter VIII [57] of this thesis).
5) To characterize the pharmacokinetic interactions between MPA and *p*-cresol (metabolites) in adult kidney transplant recipients within the first-year post-transplantation (Chapter IX [58] of this thesis).

An overall summary of the individual objectives in this thesis is illustrated in Figure I-3.

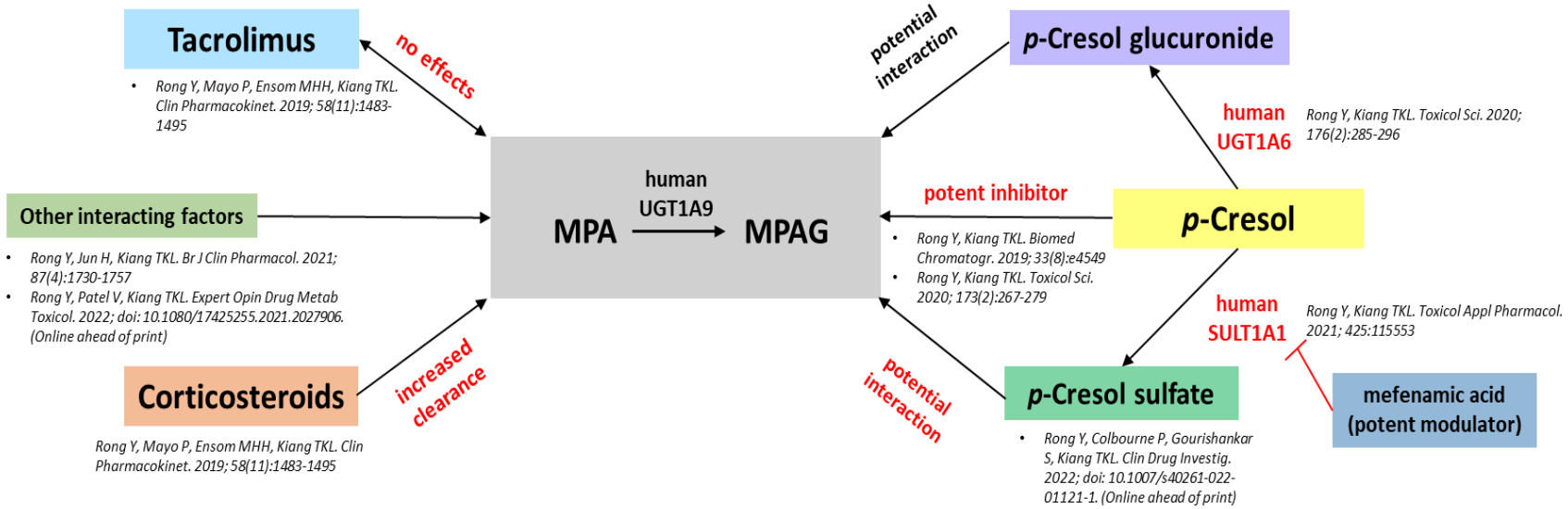

Figure I-3 Overall summary of thesis objectives and the associated publications

Chapter II. Population pharmacokinetics of mycophenolic acid co-administered with tacrolimus in corticosteroid-free adult kidney transplant patients[2]

Prologue:

MPA is almost always used in combination with tacrolimus and corticosteroids, and these co-administered drugs are considered the most common extrinsic factors influencing the pharmacokinetics of MPA. However, the significance of their interacting effects is still debatable, with inconsistent findings reported in the literature. The aim of this chapter was to construct an MPA population pharmacokinetic model to identify the clinical and/or biochemical variables ***(including the co-administrations of tacrolimus and corticosteroids)*** *influencing the pharmacokinetics of MPA in adult kidney transplant patients. As drug interactions can be bi-directional, a tacrolimus population model has also been constructed (please see Appendix A*. Population pharmacokinetic analysis of immediate-release oral tacrolimus co-administered with

[2] This chapter is already published in a peer-reviewed journal. **Rong Y**, Mayo P, Ensom MHH, Kiang TKL. Population pharmacokinetics of mycophenolic acid co-administered with tacrolimus in corticosteroid-free adult kidney transplant patients. *Clinical Pharmacokinetics*. 2019 Nov;58(11):1483-1495. doi: 10.1007/s40262-019-00771-3.

Acknowledgement: Reprinted by permission from Springer Nature: Springer Nature, Clinical Pharmacokinetics. Population pharmacokinetics of mycophenolic acid co-administered with tacrolimus in corticosteroid-free adult kidney transplant patients. **Rong Y**, Mayo P, Ensom MHH, Kiang TKL. License number: 5222091464982 (2019).

mycophenolate mofetil in steroid-free adult kidney transplant recipients *[60]) to characterize the effects of MPA on the pharmacokinetics of tacrolimus.*

Abstract

Background and Objective: Mycophenolic acid (MPA) is commonly prescribed to adult kidney transplant recipients. MPA is extensively metabolized to MPA-glucuronide (MPAG, major metabolite) and MPA-acyl-glucuronide (AcMPAG, minor metabolite). We hypothesized that i) adult kidney transplant patients on corticosteroid-free regimens exhibit unique MPA population pharmacokinetics (PK) compared to patients on corticosteroid-based therapy, and ii) MPA clearance is directly dependent on glucuronide metabolite formation.

Methods: Non-linear mixed-effects modeling was conducted with MonolixSuite-2018R1 (n=27). Optimal PK models were selected based on objective function values, standard errors, and biological plausibility.

Results: Clinical demographic data were: gender (female, 16), age (47±13years, mean±SD), weight (70±16 kg), height (165±9 cm), albumin (43±4 g/L), serum creatinine (102±27 μmol/L), estimated glomerular filtration rate (61±16 mL/min/1.73m^2), MPA dosage (1.4±0.5 g/day, as mycophenolate mofetil), and tacrolimus dosage (5±3 mg/day, immediate release). The population PK of MPA can be described by a two-compartment, first-order absorption with lag-time, and linear elimination structural model. The apparent oral clearance (CL/F) estimate in the final model (population mean, relative standard error) was 2.87 L/h, 42.3%, which is lower than that reported for similar patients on steroid-based regimens (11.9-26.3 L/h). Other PK parameters were comparable to historical data obtained in steroid-based patients. Both AcMPAG trough concentration and area-under the concentration-time curve ratio (AUC_{MPAG}/AUC_{MPA}) were significant covariates that reduced MPA CL/F from 16.5 (base model) to 2.87 L/h. The model was evaluated based on bootstrapping, visual-predictive check, and diagnostic plots.

Conclusions: Our novel findings suggest the potential need to reduce MPA dosage in subjects on steroid-free regimens. Steroid-free subjects may also be potentially more sensitive to drug/gene interactions.

1. Introduction

Mycophenolate mofetil (MMF) is an immunosuppressant that is commonly used in kidney transplant patients [31, 51, 131, 132]. MMF is quickly and extensively de-esterified upon oral absorption to form mycophenolic acid (MPA), the pharmacologically active moiety [29]. MPA exerts its therapeutic action by inhibiting inosine-5'-monophosphate dehydrogenase, thereby decreasing the production of T- and B- lymphocytes. Although MPA is frequently prescribed in conjunction with a calcineurin inhibitor (e.g. tacrolimus) and a corticosteroid, an increasing trend of *corticosteroid avoidance* has been observed in practice (e.g. [133]) due to clinical evidence supporting the minimization of long-term steroid adverse effects while maintaining adequate immunosuppression [134-136].

The clinical pharmacokinetics of MPA have been summarized extensively in the literature by our group and others [10, 29, 31, 51]. MMF is extensively absorbed (bioavailability 70-90%) and quickly converted to MPA, which is extensively bound to plasma albumin (free fraction ~3%). MPA undergoes extensive hepatic biotransformation that is primarily mediated by UDP-glucuronosyltransferase (UGT) enzymes in the formation of the major, but pharmacologically inert MPA-glucuronide (MPAG) and the minor, but putatively active MPA-acyl-glucuronide (AcMPAG). The glucuronide metabolites can be excreted renally, which is the primary route of MPA clearance from the body. Alternatively, the glucuronide metabolites undergo de-conjugation and enterohepatic recirculation via the biliary pathways to re-enter the systemic circulation. The entero-hepatic recirculation of MPA has been attributed by some investigators to be the cause of the secondary peak(s) sometimes observed in the concentration-time profiles of MMF [31]. As MPA is considered a low hepatic extraction drug, its systematic clearance is theoretically dependent on free fraction and hepatic intrinsic clearance.

The effects of corticosteroids on MPA pharmacokinetics have not been well characterized. On the molecular level, corticosteroids can theoretically increase the hepatic intrinsic clearance of MPA by UGT enzyme induction [105] and enhance biliary excretion by hepatocyte transporter up-regulation [137]. In the clinic, steroid-withdrawal has been associated with elevated MPA exposure and decreased clearance [106], but definitive evidence supporting the interaction is still lacking. The pharmacokinetics of MPA in the absence of corticosteroids have only been characterized using non-compartmental pharmacokinetic analysis [138], which lacks sufficient analytical rigor compared to non-linear mixed-effects modeling. The population pharmacokinetics of MPA have been summarized recently by our group [31] and others [30, 62, 72]. The rapidly expanding literature body on the subject matter attests to the significant clinical and scientific interests in this topic [139-141]. Recent population pharmacokinetic models have become more sophisticated [31], incorporating metabolite [114, 140, 142-146], free concentration [140, 143], and multi-compartmental models capable of describing the entero-hepatic recirculation process [30]. However, based on our investigation of all population pharmacokinetic models on mycophenolic acid in kidney transplant recipients published from 1999 to 2018 (n=25 [114, 139-162]) and the major recent review articles [30, 31, 62, 72], a population pharmacokinetic model of MPA (from the MMF formulation) in the *corticosteroid-free* population is still lacking in adult kidney transplant patients.

We hypothesized that adult kidney transplant patients taking MMF and tacrolimus would exhibit unique population pharmacokinetic characteristics of MPA compared to patients on corticosteroid-based therapy. Our objective was to develop and validate a novel population pharmacokinetic model of MPA in this patient population. Our modeling process included a comprehensive panel of clinical and biochemical variables as covariates and mechanistically

assessed factors (e.g., intrinsic clearance, free fraction, and renal clearance) known to affect MPA disposition. This novel population pharmacokinetic model establishes a solid foundation for further clinical applications with the potential to significantly impact patient care in this population.

2. Patients and methods

2.1. Study population and sampling protocol

The study was approved by the University of British Columbia and University of Alberta Research Ethics Boards (H17-02902). This study was a retrospective non-linear mixed-effects modeling of data obtained from *corticosteroid-free* adult kidney transplant recipients in an independent single-center, open-label, non-randomized, observational clinical study [138]. Adult (older than 18 years old) kidney transplant patients (N=28) on *corticosteroid-free* regimen including oral MMF (twice daily formulation) and immediate-release oral tacrolimus (twice daily formulation) satisfying the inclusion criteria were enrolled. Subjects on steady-state (i.e., at least five days of the same dosing regimen) MMF and tacrolimus with stable graft function (estimated glomerular filtration rate [eGFR] >40 mL/min/1.73m^2 on two consecutive clinic readings) were included. The exclusion criteria were: evidence of organ rejection or gastrointestinal disease; cytomegalovirus (CMV)-seronegative patients receiving organ from a CMV-seropositive donor; and/or subjects receiving co-medications which could potentially affect the pharmacokinetics of MPA. The following data were collected from clinical charts: sex, age, weight, height, albumin, serum creatinine (SCr), eGFR, and post-transplant time. Patients were identified as "*corticosteroid-free*" if they had received two doses or less of intravenous methylprednisolone in the perioperative period and no subsequent oral corticosteroids.

Blood samples (at steady-state conditions) were collected prior to, and at 0.5, 1, 2, 3, 4, 6, 8, 10, and 12 hours after oral administration of MMF and tacrolimus [138]. One subject was removed from the dataset due to their atypical concentration-time profile (i.e., maximum concentration appearing before the administered extravascular MMF dose), reducing the sample size to 27. The plasma concentrations of MPA, MPAG, AcMPAG, and whole blood concentrations of tacrolimus were determined by validated high-performance liquid chromatography (with ultraviolet-light detection) and liquid chromatography mass-spectrometry assays, respectively [138]. Area-under the concentration-time curves (AUCs) of MPA, MPAG, and tacrolimus were calculated by linear trapezoidal rule. The free fraction of MPA was determined as described previously [138, 163, 164].

2.2. Development of population pharmacokinetic models

2.2.1. Software for non-linear mixed-effects modeling

The natural log-transformed MPA concentration data were fitted using the stochastic approximation expectation-maximization (SAEM) algorithm in MonolixSuite-2018R1 (Lixoft SAS, 8 rue de la Renaissance, Batiment D, Antony, France [165]). Reductions in objective function values (OFV, expressed as minus two logarithms of the likelihood) greater than 3.84 corresponded to significant improvements (i.e., $p<0.05$ in chi squared distribution when degree of freedom=1) in model fitting [65, 68, 166]. The base/final model containing 27 patients was constructed under steady-state conditions (i.e. setting the administration dose to “11”, or “5 dosing days”, in the Monolix software).

2.2.2. Population pharmacokinetic base model selection

The pro-drug MMF is rapidly and completely de-esterified to the active MPA moiety after oral administration [10, 29]; therefore, consistent with other reports [30, 31, 62, 72], the rate of conversion from MMF to MPA was not considered in our modeling process. An extravascular input characterized by zero/first-order (with/without lag-time) or transit compartmental process was initially tested to describe the absorption of MMF. Subsequently, one- to three- compartments with linear elimination were investigated to describe the best structural model. Constant, proportional, or combined residual error models using either normal, lognormal, or logitnormal transformations were assessed. The selection of the suitable model was based on changes in OFV, graphic analyses (goodness-of-fit plots and visual predictive checks (VPC)), assessment of biological plausibility of population mean estimates and their relative standard errors (RSE), and determination of model shrinkage values, as described previously by our group and others [60, 65, 68, 166].

2.2.3. Population pharmacokinetic covariate model selection

The effects of the following covariates on the individual MPA population pharmacokinetic parameters were investigated: “age”, “sex”, “weight”, “height”, “albumin”, “serum creatinine” (SCr), “eGFR’, “post-transplant time”, “oral tacrolimus study dose”, “tacrolimus trough concentration”, “tacrolimus AUC”, “AcMPAG trough concentration”, “MPAG AUC”, “AUC_{MPAG} /AUC_{MPA}”, and “free fraction of MPA”. All variables except for sex were utilized as continuous independent covariates (being natural log-transformed).

The effects of individual continuous covariates on the population pharmacokinetics of MPA can be characterized by the following equation (Equation II-1, using age as an example):

Equation II-1

$$\theta_i = \theta_{pop} \times age_i^{\beta} \times e^{\eta_{i\prime}}$$

Where, "θ_i" is the pharmacokinetic parameter θ for the ith individual, "θ_{pop}" is the population pharmacokinetic parameter θ estimates, "age_i"is the age of the ith individual, "β" is a scaling exponent, and "$\eta^{i\prime}$" is the random effect of the ith individual from the population estimate. Potentially significant covariates were identified by three independent approaches: i) Pearson's correlation test, ii) the Wald test, and iii) a forward inclusion covariate identification program in Rsmlx package (Rsmlx, version 1.1.0, Xpop Inria Team) with R software v3.4.2 (R Core Team, Vienna, Australia [167]) as described by our group previously [60]. The threshold for significance in Pearson's correlation and the Wald test was $p<0.05$. All covariates obtained from these independent approaches were included in the population pharmacokinetic base model and subjected to removal using stepwise backward elimination based on the following criteria: i) when the elimination of covariates significantly impacted the pharmacokinetic parameters based on Pearson's correlation and the Wald test (i.e. $p<0.05$), ii) when the increase in overall model OFV was more than 3.84 (i.e. significant), and iii) when the exclusion of covariates in the model was pharmacologically plausible.

2.3. Population pharmacokinetic model evaluation

Plots of observed and predicted concentration-time curves for each individual subject were initially assessed to ensure optimal model fitting. Goodness-of-fit plot of each model was further

determined using the following: observed concentration vs. population predicted concentration (PRED) or individual predicted concentration (IPRED); population-weighted residuals (PWRES) or individual weighted residuals (IWRES) vs. time or predicted concentration. Moreover, the central trend and variability were graphically illustrated by prediction-corrected VPC, using multiple simulations (N=1000) designating the 5^{th} and 95^{th} percentile (i.e., a 95% prediction interval). These approaches have been described by our group and others previously [60, 68, 166]. Bootstrap resampling (N=500 replicates) was conducted using Rsmlx package in R software to estimate the model-simulated population mean and confidence intervals (95% CI).

3. Results

3.1. Sample population

A total of 27 (16 female) subjects were included in the pharmacokinetic population model building process. The average (± standard deviation [SD]) age and weight were 47 (±13) years old and 70 (±16) kg, respectively (Table II-1). Demographic and biochemistry data (N=27) are summarized in Table II-1. The sampled population (collected in Vancouver, Canada) consisted of ~50% Caucasian and ~50% Asian. We did not include "ethnicity" in our model building process because the genealogies of each subject were not systematically characterized.

3.2. Population pharmacokinetic base model selection

The process of selecting the optimal population pharmacokinetic base model is shown in Table II-2. Various combinations of absorption, multi-compartmental, and residual models with different transformation processes were systematically tested. Ultimately, a two-compartment,

first-order absorption with lag-time, linear elimination structural model with combined error model was selected to depict the population pharmacokinetics of MPA (Figure II-1; model 5 in Table II-2). This model can be described by six parameters: 1) lag time in the absorption phase (Tlag, h), 2) absorption rate constant (ka, h^{-1}), 3) apparent clearance of MPA from the central compartment (CL/F, L/h), 4) apparent inter-compartmental clearance (Q/F, L/h), 5) apparent volume of distribution of the central compartment (V_1/F, L), and 6) apparent volume of distribution of the peripheral compartment (V_2/F, L). The initial estimates of Tlag were fixed to a range (0.31±1.0 h) in order to improve model fitting. Table II-3 summarizes the population pharmacokinetic parameter estimates. An example of model fitting as illustrated by concentration-time profiles of an individual (subject #19) is provided (Figure II-2).

3.3. Population pharmacokinetic covariates modeling

The initial analysis identified multiple potential covariates (i.e., "age", "sex", "weight", "height", "SCr", "eGFR", "oral tacrolimus study dose", "tacrolimus trough concentration", "tacrolimus AUC", and "post-transplant time" that were subsequently eliminated based on the criteria defined in 2.2.3 Population Pharmacokinetic Covariates Model Selection. On the other hand, AcMPAG trough concentration (negative relationship) and AUC_{MPAG} / AUC_{MPA} ratio (positive relationship) were found to significantly affect MPA CL/F (Table II-3), as their inclusion decreased the OFV by 22.59 and was pharmacologically reasonable. As a result, the final model consisted of "AcMPAG trough concentration" and "AUC_{MPAG} / AUC_{MPA}" ratio as significant covariates of CL/F, which can be characterized by Equation II-2 (please see Equation II-1 for symbol abbreviations):

Equation II-2

$$CL/F_i = 2.87 \times (\text{AcMPAG trough concentration})_i^{-0.0929} \times (\text{AUC}_{MPAG}/\ \text{AUC}_{MPA})_i^{0.678} \times e^{\eta_{i\prime}}$$

The η-shrinkage values in the distribution of individual parameters were generally <15% (data not shown), indicating the lack of misspecification in the final model [168].

3.4. Model evaluation

Initial diagnosis of the final model was conducted using correlational plots (Figure II-3, Figure II-4), where the observation vs. population or individual predictions (Figure II-3) were generally evenly-distributed around the line of identity, indicating reasonably good model fitting. Likewise, except for some positive bias in the PWRES vs. time or predicted concentration plots (Figure II-4 (a) and (b)), the scattered residuals were generally symmetrically distributed around the y=0 line, confirming acceptable accuracy and precision of the structural (Figure II-4 (a) and 4(c)) and error (Figure II-4 (b) and 4(d)) models. Furthermore, the prediction-corrected VPC indicated that the majority of MPA plasma concentrations were within the areas of predicted theoretical percentiles (Figure II-5), confirming the lack of significant model-misspecifications. Consistently, parameter estimates from bootstrapping (Table II-3) closely matched the mean estimates from the population model, confirming model stability.

4. Discussion

MPA has been widely prescribed in combination with tacrolimus and corticosteroids in adult kidney transplant patients [31, 51, 131, 132]. There is a growing trend of corticosteroid avoidance based on the clinical observation that corticosteroid-tapering does not increase the risk

of graft loss but can mitigate the associated adverse effects [134-136]. To our knowledge, we have developed and evaluated a novel population pharmacokinetic model in *corticosteroid-free* adult kidney transplant patients. Similar to other published MPA models in adult kidney-transplant patients (but with corticosteroid co-administration) (summarized in Table II-4) [114, 147-149, 154, 158], a two-compartment, first-order absorption with lag-time, and linear elimination structural model best described our data. This suggests that the exclusion of corticosteroids does not drastically alter the fundamental pharmacokinetic characteristics of MPA. On the other hand, an attempt was made to construct a model with individual MPAG and gallbladder compartments in order to better mimic the physiological process of entero-hepatic recirculation (data not shown). However, this particular multi-compartmental model ultimately failed, possibly due to over-parameterization in the setting of relatively small sample size. Consistent with others [114, 143, 147, 148], we did not observe a prominent secondary peak that is typically associated with entero-hepatic recirculation in our dataset (Figure II-5). Ultimately, our simpler 2-compartment model is consistent with the principle of parsimony and may be better suited for clinical use.

With the exception of CL/F and Tlag (the latter was fixed in our model to improve fitting and was close to the reported range), the population pharmacokinetic parameter estimates obtained from our model (Table II-3) are in general agreement with population estimates reported in other studies in adult kidney transplant patients on MMF and immediate-release tacrolimus (but co-administered with corticosteroid) [114, 147-149, 154, 158] (Table II-4). Comparisons were made only with patients on MMF and tacrolimus because it is well documented that MPA formulation [169] and type of calcineurin inhibitor co-administration [29] can significantly affect the pharmacokinetics of MPA. More specifically, our data on drug absorption (reflected by ka, 1.98 h^{-1} [mean]), volumes of distribution, and inter-compartment clearance (V_1/F=25 L, V_2/F=607 L,

and Q/F=36.7 L/h) all agreed with the findings from other corticosteroid-based studies (ka=0.64-3.9 h^{-1}, V_1/F=10.3-75.9 L, V_2/F=183-4910 L, and Q/F=11.2-38 L/h) [114, 147-149, 154, 158]. These findings indicate little effect of corticosteroids on these pharmacokinetic processes. On the other hand, the population CL/F estimate in our final model (2.87 L/h) was significantly lower than the reported CL/F ranges (11.9-26.3 L/h) in similar patients who were co-administered corticosteroids (Table II-4). This CL/F value in our final model represents the true MPA clearance (without the effects of metabolites) which is lower than the value generated by Cremer et al [114] (11.9 L/h) that has also obtained a MPA clearance without metabolite influence. As well, the CL values illustrated in Table II-4 are all likely representing the true clearance of MPA, because (as discussed further below), little changes in MPA clearance are evident in steroid-based patients with or without the incorporation of MPA metabolites into the various models. This *novel* finding confirms the significant effects of corticosteroids on the clearance of MPA, as inferred by other clinical studies using steroid minimization regimens [106].

The mechanism by which corticosteroids affects MPA clearance is likely mediated by the alteration of MPA hepatic intrinsic clearance; or more specifically, the induction of MPA glucuronidation. Although corticosteroids are known to induce UGT enzymes [106, 170, 171], their direct effects on MPA conjugation, hence clearance, still remain to be characterized. This molecular interaction can be studied using established *in vitro* models such as primary human hepatocytes or metabolically competent liver cells [105, 172], which are suitable for characterizing induction-mediated drug interactions. Clinically, the finding of a significant reduction in MPA clearance in patients on corticosteroid-free regimens would suggest that empiric MPA dose adjustment (i.e., using a less aggressive dosing approach) or therapeutic drug monitoring may be needed to mitigate the potential for over-exposure and the development of severe toxicities (e.g.,

neutropenia) [133]. Ideally, future pharmacokinetic studies should either incorporate a matched control group (on corticosteroid-based therapy) or a cross-over arm (where each patient can serve as their control) and also collect pharmacodynamic data in order to verify our findings in a single experimental setting and to establish exposure-response relationships in this specific population.

The identified significant covariates affecting MPA CL/F were AUC_{MPAG} / AUC_{MPA} ratio (positive correlation) and AcMPAG trough concentration (negative correlation). The positive relationship observed with AUC_{MPAG} / AUC_{MPA} is a direct reflection on the predominant role of UGT1A9 in the production of MPAG [35, 173-175]. In human liver microsomes, UGT1A9 is responsible for ~ 55% of MPAG formation [35] and hence acts as a quantitatively important pathway for MPA intrinsic clearance. On the other hand, the negative relationship between AcMPAG trough concentration and MPA CL/F observed in our model is less consistent with known data, given that AcMPAG, or the UGT2B7 enzyme responsible for its formation [35, 176], is not considered a major metabolite/metabolic pathway of MPA metabolism and should not contribute significantly to the overall MPA clearance [29]. It may be possible that AcMPAG directly inhibits the formation of MPAG and reduces the clearance of MPA, but data supporting this molecular interaction are not available to our knowledge. Alternatively, our observation may point to the scenario where elevated AcMPAG concentration may be a surrogate of compromised MPAG production, therefore indirectly explaining the inverse relationship observed with MPA clearance. In essence, it may be hypothesized that elevated AcMPAG concentrations are the results of reduced MPAG formation due to the shunting of MPA conjugation toward the minor UGT2B7 pathway; the latter does not affect MPA clearance itself. This hypothesis requires further mechanistic investigation. Furthermore, a limitation in our modeling was the use of AcMPAG trough concentration due to quantification challenges preventing accurate AUC determination

[138]; therefore, it also remains to be determined if the same relationship with MPA CL/F could be observed with AcMPAG exposure.

Our findings of significant covariate relationships between MPA glucuronides and MPA clearance in corticosteroid-free patients are being reported, to our knowledge, for the first time. Most existing MPA population pharmacokinetic models in kidney transplant patients do not have MPA metabolite data [139, 141, 147-162]; whereas the few studies that do have metabolite data [114, 140, 142-146] have not identified MPAG or AcMPAG as significant covariates in the corticosteroid-based cohorts [140, 146]. Furthermore, in those population models that have incorporated MPA metabolites directly in their structural model in corticosteroid-based subjects [114, 142-146], little changes in MPA clearance were generally identified in comparison to data obtained from models without metabolite data [139, 141, 147-162]. These are in contrast to the large reduction of MPA CL/F (from 16.5 L/h in the base to 2.87 L/h in the final model) observed in our population model in corticosteroid-free subjects (Table II-3). This apparent discrepancy on the ability of metabolite (or metabolism) to influence MPA clearance in corticosteroid-based vs. corticosteroid-free patients could indicate that patients on corticosteroid-free regimens may be *more sensitive* to fluctuations in MPA metabolism, an observation that may be clinically important as these individuals could more likely be subjected to significant drug/gene interactions mediated by UGT1A9 modulation. Mechanistically, it can be hypothesized that subjects taking corticosteroids (in the induced state) may already have maximized/saturated the catalytic activities of UGT1A9 enzyme; therefore, further changes in this metabolism pathway would have little effects on the clearance of MPA. On the other hand, in corticosteroid-free subjects, the catalytic activities of UGT1A9 (in the un-induced state) can still be modulated where changes in metabolism have more contributions to the fluctuations in MPA clearance. The concept of

differential sensitivity to drug/gene interactions based on different states of metabolic activity has already been reported for patients on MPA (e.g. [177]) and other agents (e.g. [178]). Our laboratory is in the process of investigating the novel hypothesis that corticosteroid treatment can influence the sensitivity of gene or drug interactions involving MPA.

Various published models have reported "body weight" and "albumin" as common significant covariates of MPA pharmacokinetics [30, 31, 62, 72]. However, none of these clinical variables were significant predictors of MPA CL/F in our population pharmacokinetic model, which could be explained by the relatively small variabilities in these factors observed in our dataset (weight range 70±16 kg, N=22, with 82% of the patients weighing between 50- 90 kg; albumin 43±4 g/L, with 96% of the patients having albumin levels between 35-50 g/L). Furthermore, the clearance of MPA, being a low hepatic extraction drug, should also be affected by its "free fraction" which would be altered in the clinical scenarios of reduced protein binding [29, 51]. Atcheson et al [50] indicated that the free instead of total concentration of MPA should be monitored clinically when the plasma albumin is ≤31 g/L; however, our data set also exhibited very little fluctuations in free fraction (1.04% - 2.7%) and only one patient (albumin=28 g/L) in our study population would fit their albumin criteria, possibly explaining the negative findings with these covariates. Direct measurement of free MPA (and metabolite) concentrations would be a more elegant approach than estimating free fraction in population pharmacokinetic analysis (e.g., [140, 143]). Further population pharmacokinetic models in this study population should also characterize free MPA clearance values which are considered more pharmacologically/physiologically important (e.g., [140]).

Despite being successfully developed and validated, this model can be further improved in future studies: 1) we were only able to evaluate our model internally, which is consistent with the

many other MPA population pharmacokinetic models presented in the literature (e.g. [30, 31, 62, 72]), primarily due to the limited sample size. A pharmacokinetic model should be ideally evaluated externally in a separate cohort of patients [65, 68, 166]. Nevertheless, our model is still proven to be robust and stable based on the extensive validation criteria implemented following guidelines from published protocols [65, 68, 166]. 2) The relatively small sample has also translated to some evidence of variability, as measured by RSE values, in certain fixed and random effect estimates. However, large variability has also been reported by other MPA pharmacokinetic population models [30, 31, 62, 72] and is commonly observed in the clinic [29]. Despite the documented variability, however, little evidence of model mis-specification was observed, confirming the accuracy of our findings. 3) As suggested by Li et al [179], kidney transplant patients of Asian ethnicity can exhibit elevated dose-normalized MPA exposure compared to Caucasian patients (up to 1.8 fold). Given that ~half of our data were obtained from Asian subjects, a reduced clearance value observed in our dataset may also be partially attributed to ethnicity. 4) Emerging pharmacogenomic data have indicated significant effects of single nucleotide polymorphisms (SNPs) in UGT enzymes (e.g. UGT1A9, UGT2B7) in altering the pharmacokinetics of MPA [29]. Given our finding of MPA glucuronidation being a significant covariate affecting CL/F and the appearance of higher sensitivity toward metabolism fluctuation in this corticosteroid-free population, it remains to be tested whether these patients are also likely subject to the effects of UGT polymorphism. 5) The pharmacokinetics of MPA can be modulated by other processes (e.g., entero-hepatic recirculation) involving a variety of transporter proteins (e.g., multidrug resistance-associated protein, organic anion transporting polypeptide) which were not characterized in our model. Further mechanistic modeling incorporating additional compartments representing MPA enterohepatic recirculation (e.g. [30]) and genomic analyses of

transporter enzymes are warranted. Nonetheless, our model serves as a solid foundation for these additional experiments involving a larger cohort of patients.

5. Conclusion

Our finding of a significant reduction in MPA clearance in corticosteroid-free subjects in comparison to corticosteroid-based patients would suggest that clinical dose adjustment or therapeutic drug monitoring may be warranted in this specific patient population. Moreover, the identification of MPA glucuronide metabolites (surrogates for MPA metabolism) as significant covariates affecting MPA clearance might indicate that molecular interactions (i.e., enzyme inhibition or induction) or genetic polymorphisms affecting UGT enzymes are more likely to lead to clinically significant interactions in corticosteroid-free subjects.

Table II-1 Demographic and biochemistry data

Parameter	***Values (N=27)***
Sex (Female/Male)	16/11
Age (yrs)	47 ± 13
Weight (kg)	70 ± 16
Height (cm)	165.1 ± 9.2
Albumin (g/L)	42.8 ± 3.9
SCr (μmol/L)	102.4 ± 27.0
eGFR (mL/min/1.73m^2)	61.0 ± 15.7
Post-transplant time (days)	916 ± 709
Tacrolimus dose (mg/day)	4.8 ± 2.9
MMF dose (mg/day)	1352 ± 492
Tacrolimus C_0 (μg/L)	5.9 ± 1.61
Tacrolimus $AUC_{0\text{-}12}$ (μg·h/L)	115.3 ± 31.3
MPA $AUC_{0\text{-}12}$ (mg·h/L)	32.1 ± 11.2
Tacrolimus $AUC_{0\text{-}12}$/dose (μg·h/L/mg)	53.3 ± 24.9
MPA $AUC_{0\text{-}12}$/dose (mg·h/L/g)	53.0 ± 27.1
MPAG $AUC_{0\text{-}12}$/dose (mg·h/L/g)	588.8 ± 216.4
AcMPAG C_0 (mg/L)	0.54 ± 0.66
Free fraction of MPA (%)	1.7± 0.6

Continuous data are presented as mean ± standard deviation (SD); categorical data are presented as counts.

Abbreviation(s): *AUC* area-under the concentration-time curve; *AcMPAG* mycophenolic acid acyl-glucuronide; *C_0* trough concentration; *eGFR* estimated glomerular filtration rate; *MMF* mycophenolate mofetil; *MPA* mycophenolic acid; *MPAG* mycophenolic acid glucuronide; *NA* not available; *SCr* serum creatinine.

Table II-2 The population pharmacokinetic base model building process (N=27)

Model	*Structural model description*	*Error model*	*OFV*	*AIC*	*BIC*
1	One-compartment model, first-order absorption with no delay, linear elimination	Combined 1	933.71	957.71	973.69
2	One-compartment model, first-order absorption with lag time, linear elimination	Combined 1	921.21	999.21	1051.15
3	One-compartment model, first-order transit absorption, linear elimination	Combined 1	971.47[n]	997.47[n]	1014.79[n]
4	Two-compartment model, first-order absorption with no delay, linear elimination	Combined 1	907.67	935.67	954.32
[*]5	**Two-compartment model, first-order absorption with lag time, linear elimination**	Combined 1	855.80	883.80	901.95
6	Two-compartment model, first-order transit absorption, linear elimination	Combined 1	857.59[n]	885.59[n]	903.74[n]
7	Three-compartment model, first-order absorption with no delay, linear elimination	Combined 1	1041.49	1067.49	1084.8
8	Three-compartment model, first-order absorption with lag time, linear elimination	Combined 1	908.58	936.58	955.23
9	Three-compartment model, first-order transit absorption, linear elimination	Combined 1	910.74[n]	938.74[n]	957.39[n]
10	Two-compartment model, first-order absorption with lag time, linear elimination	Constant	893.71	921.71	940.36
11	Two-compartment model, first-order absorption with lag time, linear elimination	Proportional	892.59[n]	918.59[n]	935.91[n]
12	Two-compartment model, first-order absorption with lag time, linear elimination	Combined 2	892.19	920.19	938.84

*5 is the population pharmacokinetic base model; ^{n} when the fisher matrix was not estimated correctly

Abbreviation(s): *AIC* Akaike information criterion; *BIC* Bayesian information criterion; *OFV* objective function value.

Constant error model: $y = f + a\varepsilon$; Proportional error model: $y = f + bf^{c}\varepsilon$; Combined 1 error model: $y = f + (a + bf^{c})\varepsilon$; Combined 2 error model: $y = f + \sqrt{a^2 + b^2(f^{c})^2}\varepsilon$;

a, *b* additive components of residual error; *c* proportional component of residual error; ε residual errors; *f* function of structural models.

Table II-3 Pharmacokinetic parameter estimates and bootstrapping analysis

Parameters	***Base model***		***Final model (covariates)***	
	Estimated mean value (RSE %)	***Bootstrap mean (95% CI)***	***Estimated mean value (RSE %)***	***Bootstrap mean (95% CI)***
Tlag (h)[f]	0.166 (fixed)	0.166 (0.073-0.379)	0.162 (fixed)	0.162 (0.073-0.364)
ka (h^{-1})	1.21 (22.8)	1.21 (0.77-3.91)	1.98 (41.5)	1.98 (0.79-2.96)
CL/F (L/h)	16.5 (14.4)	16.5 (6.2-20.9)	2.87 (42.3)	2.87 (0.58-6.59)
$\beta^{AcMPAG_through}$CL/F		NA	-0.09 (45)	-0.09 (-0.28 to -0.04)
β^{MPAG_AUC/MPA_AUC}CL/F		NA	0.68 (23.2)	0.68 (0.27-1.23)
V_1/F (L)	13.6 (55)	13.6 (1.4-71.3)	25 (28.5)	25 (1.3-75.7)
Q/F (L/h)	37.5 (11.7)	37.5 (28.3-48.7)	36.7 (12.6)	36.7 (24.3-46.3)
V_2/F (L)	897 (39.8)	897 (449-3603)	607 (35.4)	607 (376-2284)
ω_Tlag	1.09 (30.3)	1.09 (0.30-1.69)	1.08 (29.8)	1.08 (0.32-1.70)
ω_ka	0.73 (26.7)	0.73 (0.12-2.24)	0.99 (26.9)	0.99 (0.10-2.35)
ω_CL/F	0.45 (18)	0.45 (0.32-0.73)	0.23 (27.6)	0.23 (0.03-0.30)
ω_V_1/F	0.48 (62.6)	0.48 (0.11-1.60)	0.18 (127)	0.18 (0.09-1.81)
ω_Q/F	0.31 (33)	0.30 (0.10-0.49)	0.27 (94.8)	0.27 (0.11-0.52)
ω_V_2/F	1.12 (20.7)	1.12 (0.49-1.35)	1.08 (19.8)	1.08 (0.34-1.36)
a (mg/L)	0.11 (62.2)	0.11 (0.01-0.23)	0.08 (82.1)	0.08 (0-0.24)
b (mg/L)	0.29 (13.1)	0.29 (0.21-0.38)	0.32 (12.6)	0.32 (0.21-0.38)
-2 log-likelihood		855.80		833.21[*]

AIC	883.80	865.21*
BIC	901.95	885.94*

All pharmacokinetic parameters are apparent values; *p<0.05, significant reduction in OFV (final model with covariate effects vs. base model); ∫ initial estimate of paramter was fixed to a range.

Abbreviation(s): *AUC* area-under the concentration-time curve; *AcMPAG* mycophenolic acid acyl-glucuronide; *AIC* Akaike information criterion; *BIC* Bayesian information criterion; *β*- covariate parameter estimate; *CI* confidence interval; *CL/F* clearance of tacrolimus from central compartment; *MPA* mycophenolic acid; *MPAG* mycophenolic acid glucuronide; *NA* not applicable; *OFV* objective function value; *Q/F* inter-compartment clearance; *RSE* relative standard error; *Tlag* lag time of first-order absorption; V_1/F, volume of distribution of the central compartment; V_2/F volume distribution of the peripheral compartment; ω inter-individual variability.

Table II-4 Previously reported population pharmacokinetic models on mycophenolate mofetil administered with tacrolimus and corticosteroid in adult kidney transplant patients

References	***Cremers et al, 2005 [114]***	***Staatz et al, 2005 [158]***	***Lamba et al, 2010 [154]***	***de Winter et al, 2010 [147]***	***de Winter et al, 2011 [148]***	***de Winter et al, 2012 [149]***
Sample size	N=31 (tacrolimus)	N=117 (tacrolimus/cyclosporine)	N=17 (tacrolimus)	N=17 (tacrolimus)	N=101 (tacrolimus)	N=32 (tacrolimus)
Age (yrs)	44.9 ± 12.5	50 (19-72)	44.6 ± 10.8	50 (19-75)	53 (19-76)	54 (20-71)
Post-transplant time	During the first year	During the first week	Day 1 to 3.5 years	Day 3 to day 8	Day 3 to day 168	Week 1 to month 6
Structure model	Four-compartment model	Two-compartment, first order absorption, bi-exponential elimination models	Two-compartment, first order absorption	Two-compartment model with lag time, first-order absorption and first-order elimination	Two-compartment model with lag time, first-order elimination	Two-compartment model with lag time, first-order absorption and first-order elimination
Tlag (h)	0.567 (~ 24% RSE)	NA	NA	0.294 (3% RSE)	0.21 (2% RSE)	0.24 (1.2% RSE)
ka (h^{-1})	NA	0.64	Fixed (value not provided)	Fixed to 4	3.9 (10% RSE)	1.9 (7.8% RSE)
CL/F (L/h)	11.9 (~15% RSE)	25.4 (tacrolimus co-therapy)	13.6 (8.53% RSE)	26.3	17.0 (9% RSE)	13.0 (5.5% RSE)
V_1/F (L)	10.3 (~163% RSE)	65	61.8 (23.3% RSE)	75.9 (9 % RSE)	68 (14% RSE)	34.9 (7.4% RSE)
Q/F (L/h)	11.2 (~37% RSE)	30	Fixed (value not provided)	26.3 (9 % RSE)	38 (7% RSE)	24.7 (6.5% RSE)
V_2/F (L)	183 (~41% RSE)	496	Fixed (value not provided)	255 (44 % RSE)	229 (9% RSE)	4910 (403% RSE)

Abbreviation(s): *CL/F* clearance of tacrolimus from central compartment; *NA* not applicable; *Q/F* inter-compartment clearance; *RSE* relative standard error; *Tlag* lag time of first-order absorption;

V_1/F, volume of distribution of central compartment; V_2/F volume distribution of peripheral compartment.

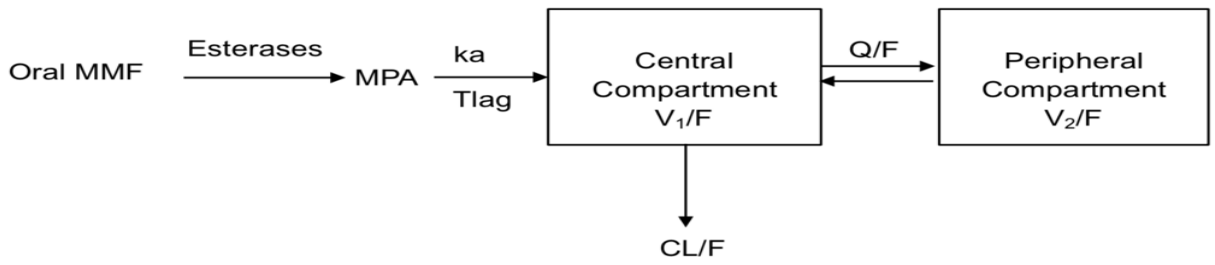

Figure II-1 Population pharmacokinetic structural model of mycophenolic acid in adult kidney transplant patients on a corticosteroid-free regimen

Abbreviation(s): *CL/F*, apparent clearance; *MMF*, mycophenolate mofetil; *MPA*, mycophenolic acid; k_a, absorption rate constant; *Q/F*, apparent inter-compartmental clearance; T_{lag}, absorption lag time; V_1/F, apparent central compartment volume of distribution, V_2/F, apparent peripheral compartment volume of distribution.

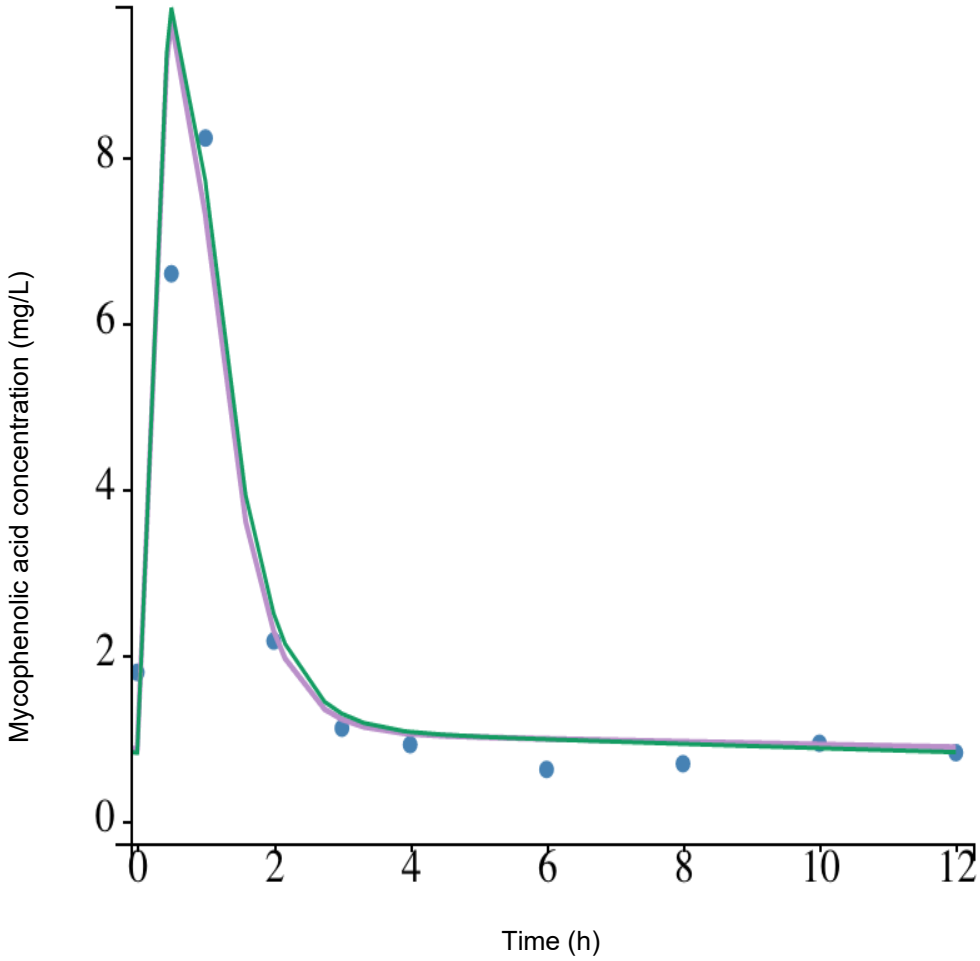

Figure II-2 An example of individual concentration-time profile fitting for subject #19 in the population pharmacokinetic final model

Blue dots: observed plasma concentration of mycophenolic acid; purple line: fitting using individual predicted pharmacokinetic parameters; green line: fitting using population predicted pharmacokinetic parameters, including the effects of covariates.

(a)

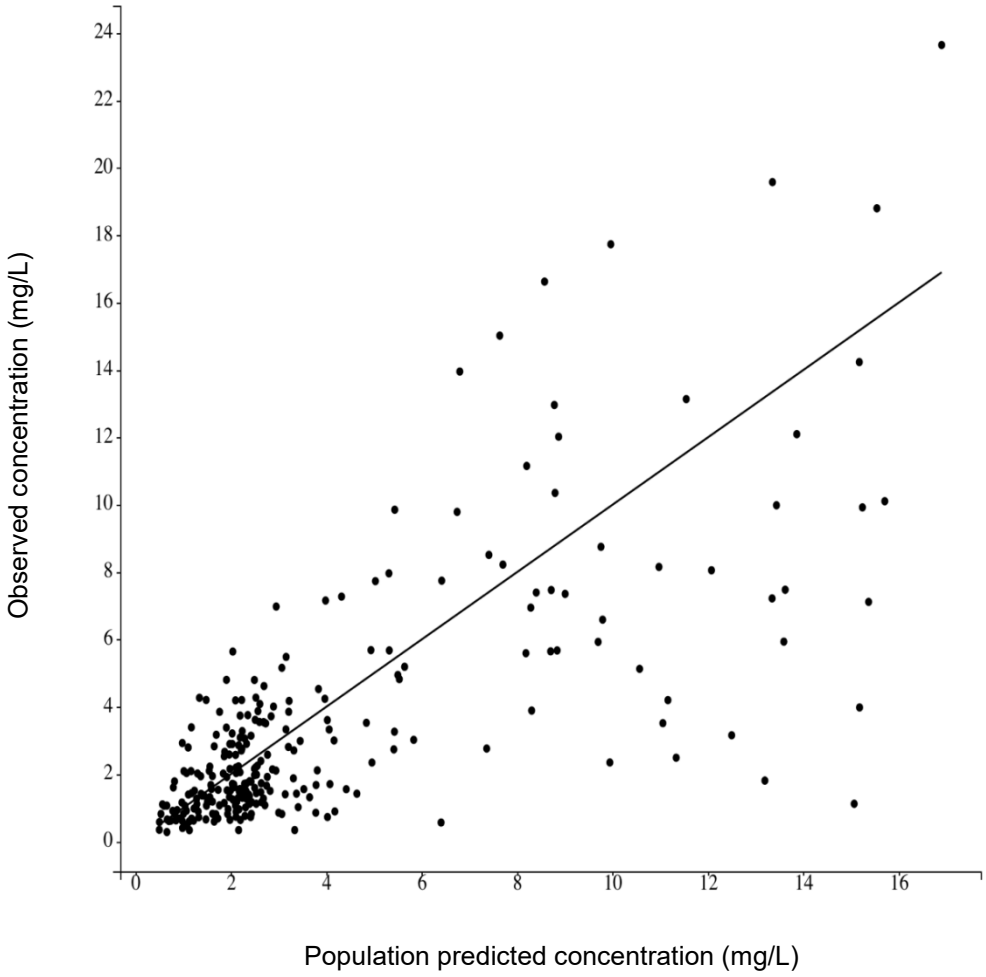
Observed concentration (mg/L)
Population predicted concentration (mg/L)
0
2
4
6
8
10
12
14
16
18
20
22
24

(b)

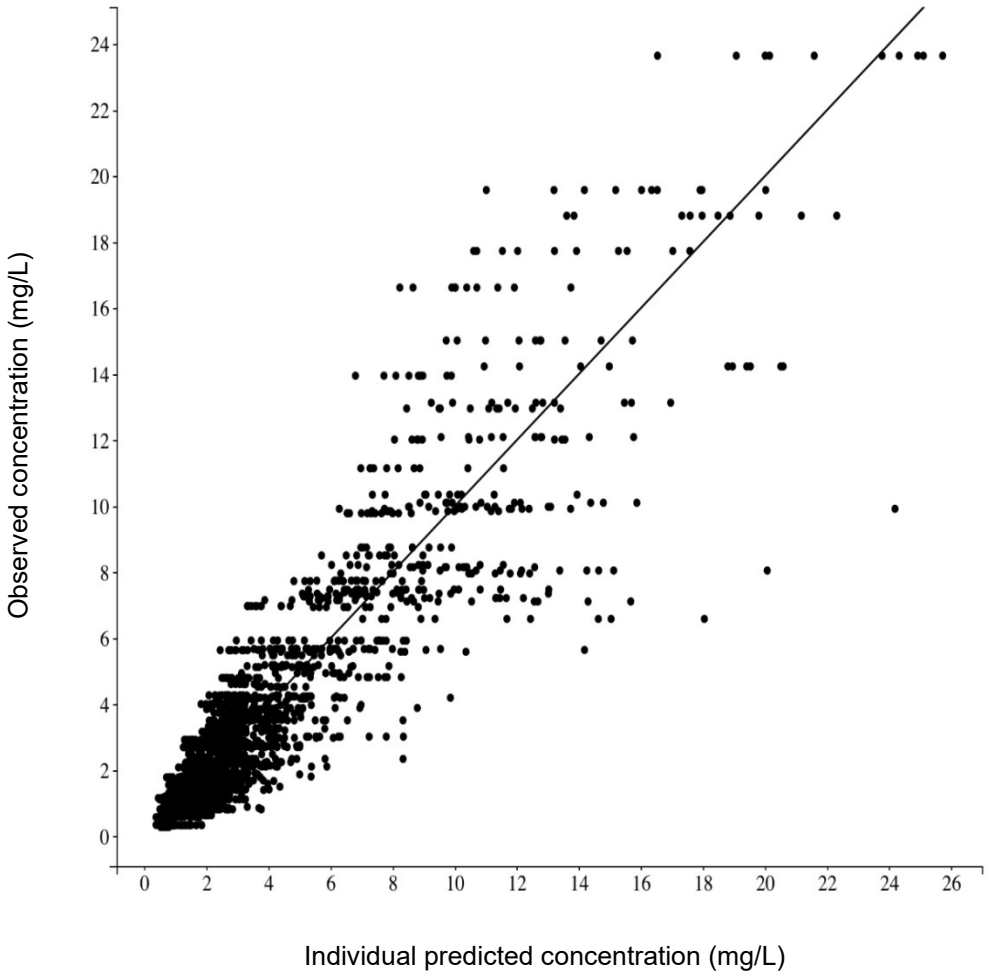

Figure II-3 (a) Observed plasma concentration of mycophenolic acid vs. population predicted concentration (PRED); (b) observed plasma concentration of mycophenolic acid vs. individual predicted concentration (IPRED) for the final population pharmacokinetic model of mycophenolic acid in adult kidney transplant recipients on corticosteroid-free regimens

(a)

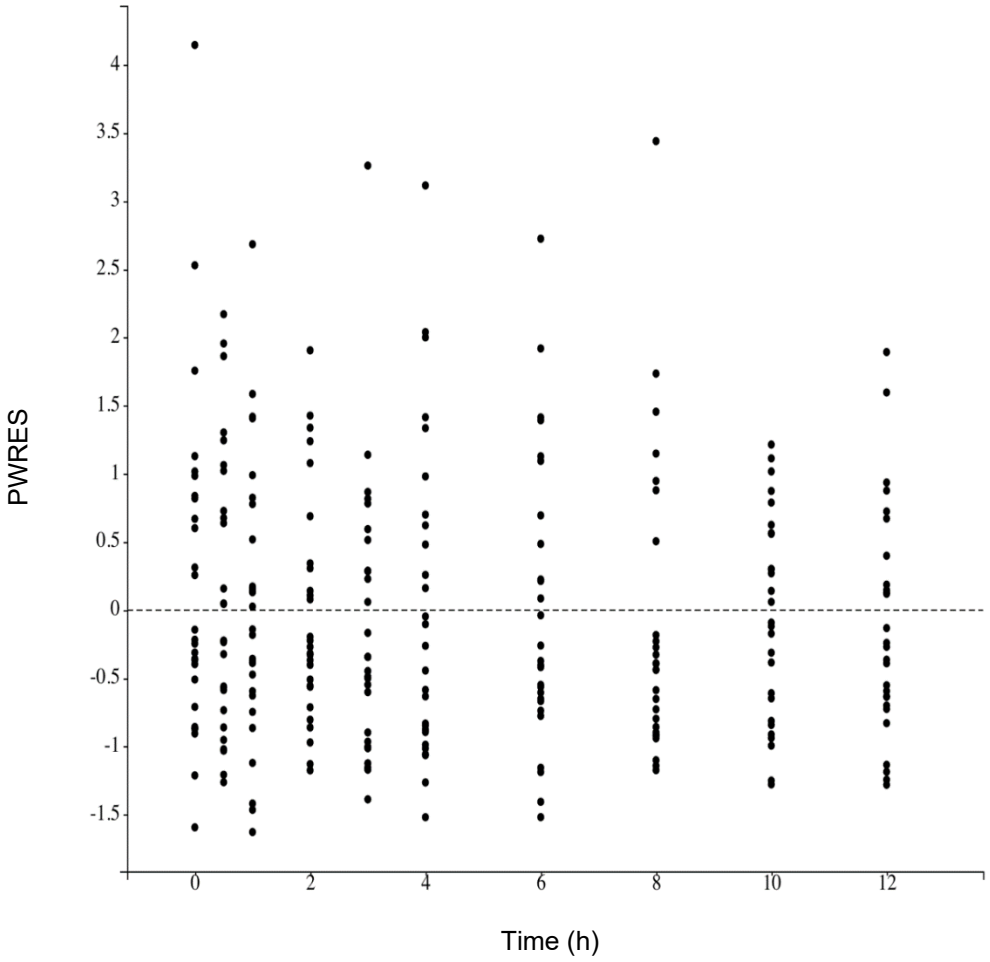

(b)

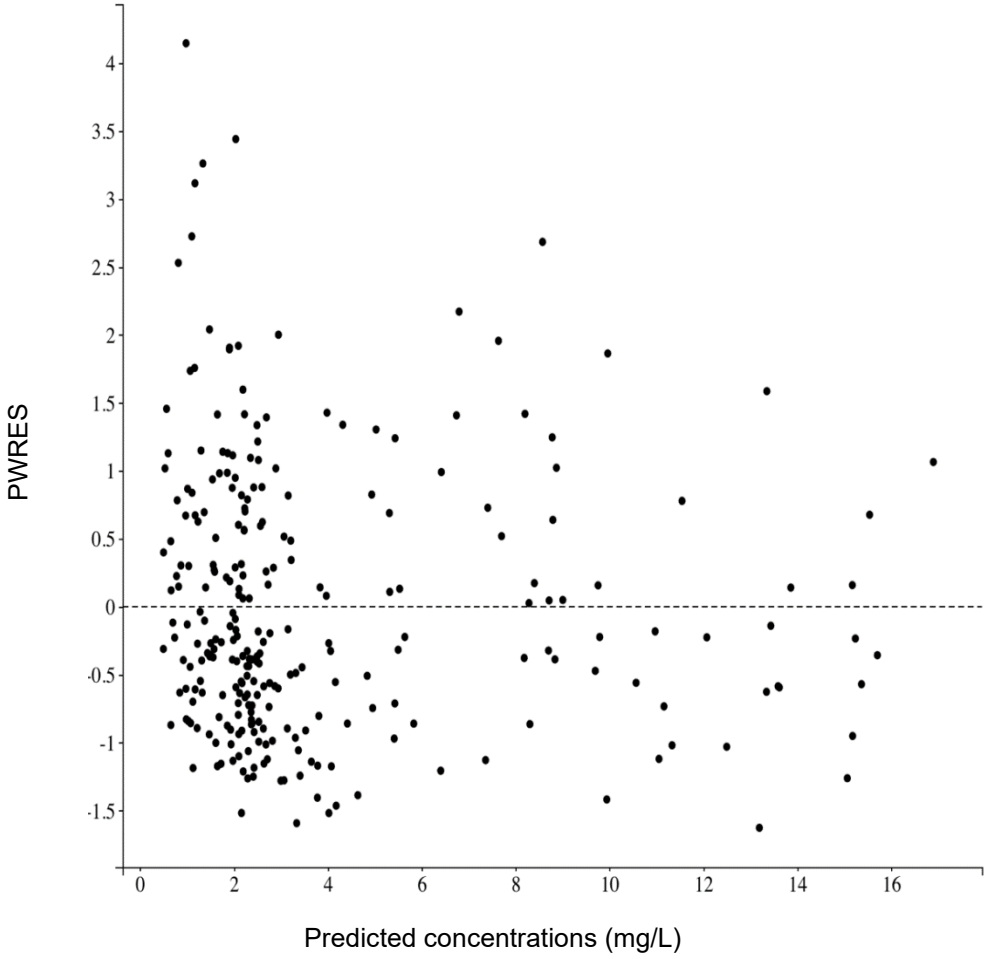
PWRES
4
3.5
3
2.5
2
1.5
1
0.5
0
-0.5
-1
-1.5
0
2
4
6
8
10
12
14
16
Predicted concentrations (mg/L)

(c)

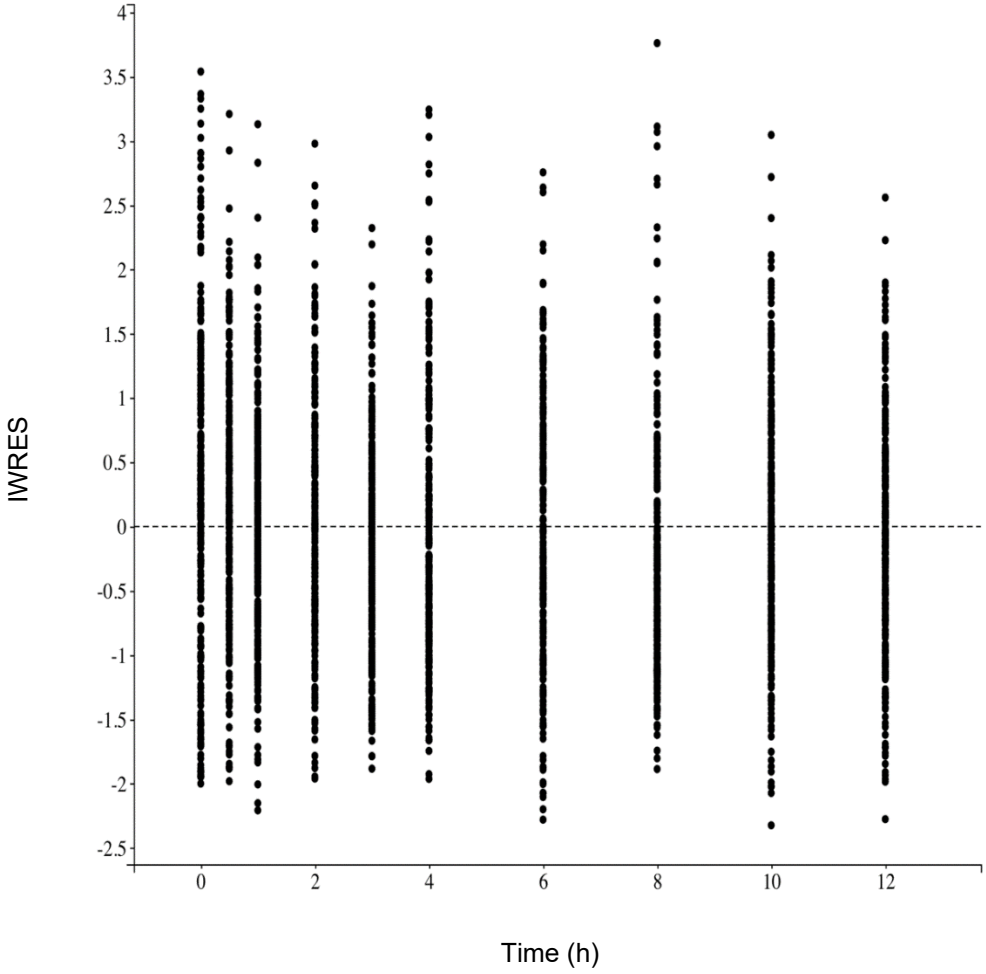

(d)

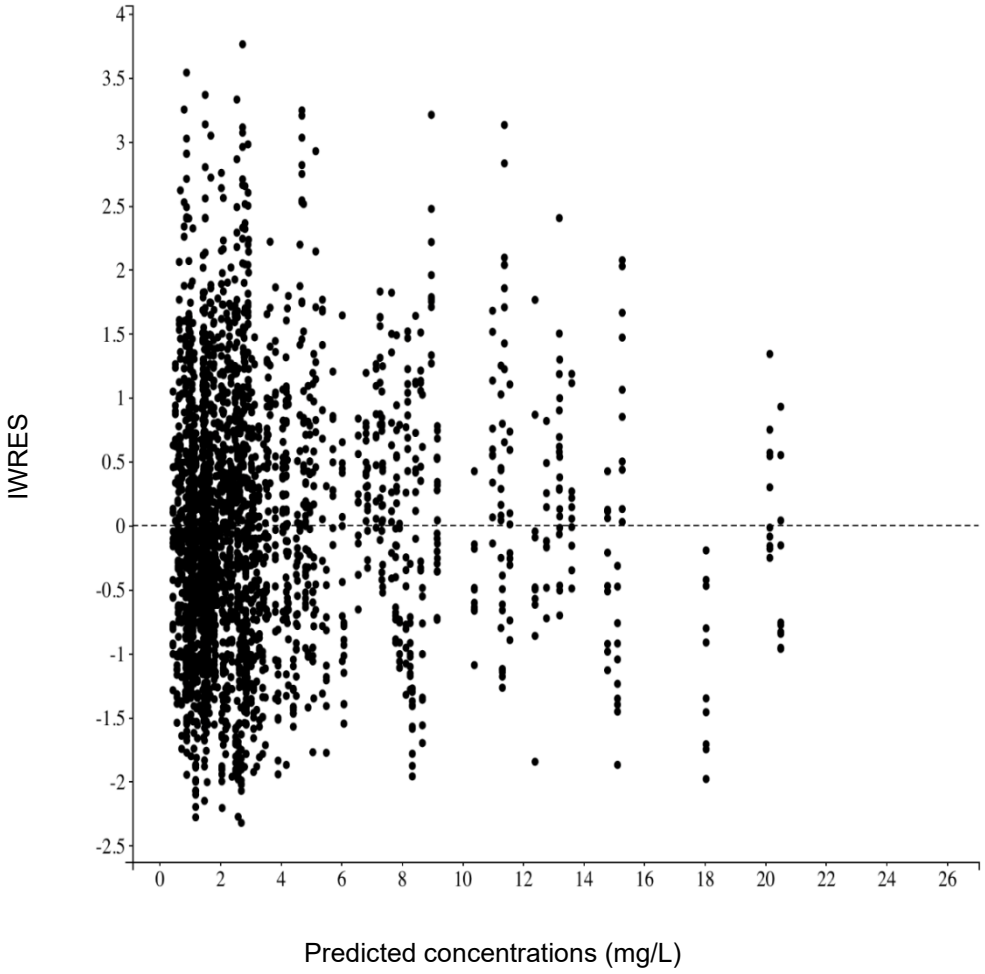

Figure II-4 (a) Population-weighted residuals (PWRES) vs. time; (b) PWRES versus predicted mycophenolic acid plasma concentration; (c) individual-weighted residuals (IWRES) vs. time; (d) IWRES versus predicted mycophenolic acid plasma concentration for the final population pharmacokinetic model of mycophenolic acid in adult kidney transplant recipients on corticosteroid-free regimens

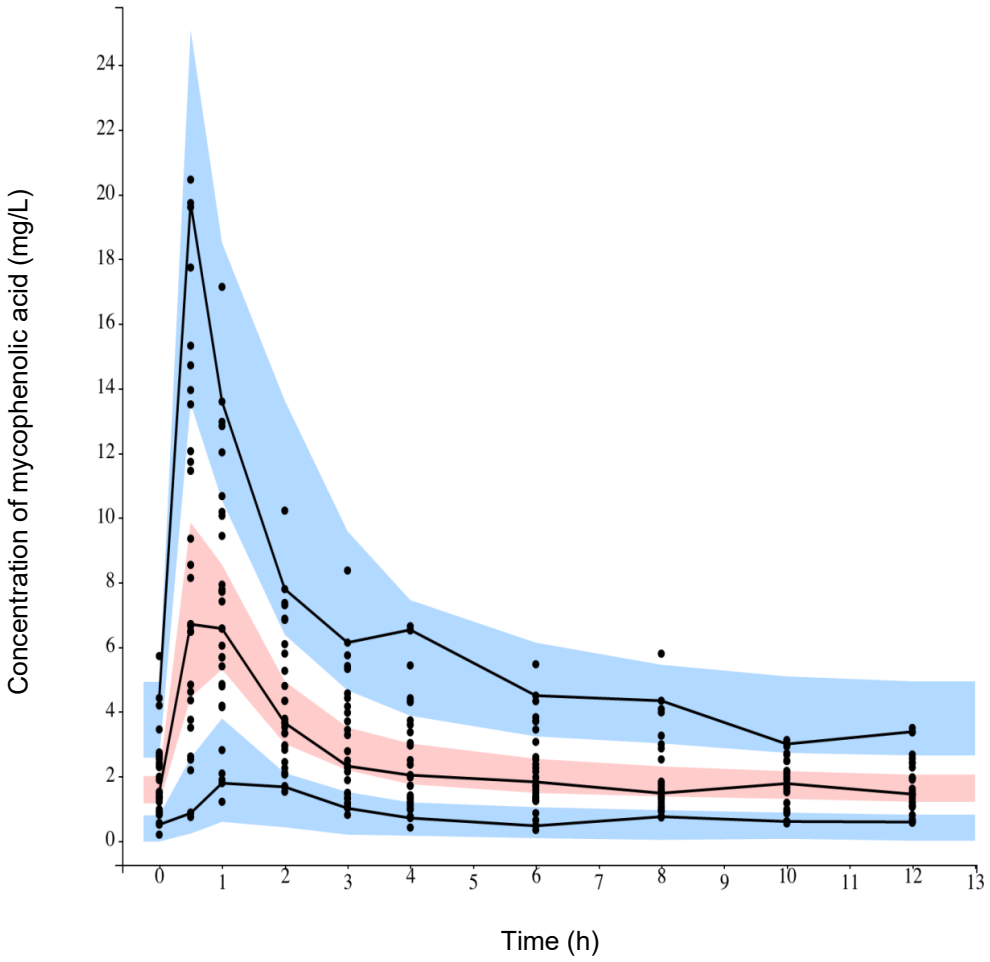

Figure II-5 Prediction-corrected visual predictive check for mycophenolic acid plasma concentration-time response in adult kidney transplant recipients on corticosteroid-free regimens

Solid black lines represent the 5th, median, and 95th empirical percentiles of the observed concentrations; black dots represent individual concentrations of mycophenolic acid. The prediction intervals are displayed as blue (5th and 95th percentiles) or pink (median) areas based on 1000 simulations.

Chapter III. Recent lessons learned from population pharmacokinetic studies of mycophenolic acid: Physiological, genomic, and drug interactions leading to the prediction of drug effects[3]

Prologue:

Numerous MPA population pharmacokinetic models have been published in the literature in the past 5 years, but these data have not been collectively, critically evaluated. The aims of this chapter were i) to summarize the most recent MPA population pharmacokinetic models in a variety of patient populations, ii) to identify novel approaches for MPA population pharmacokinetic-dynamic modeling, and iii) to determine the significant clinical interactions affecting MPA pharmacokinetics/dynamics. The primary focus of this chapter was on adult populations, and the complementary pediatric data are presented in the next Chapter (Chapter IV [27]).

[3] This chapter is already published in a peer-reviewed journal. **Rong Y**, Patel V, Kiang TKL. Recent lessons learned from population pharmacokinetic studies of mycophenolic acid: Physiological, genomic, and drug interactions leading to the prediction of drug effects. *Expert Opinion on Drug Metabolism & Toxicology*. 2022 Jan 24; 17(12): 1369-1406. doi: 10.1080/17425255.2021.2027906.

Acknowledgement: This is an 'Accepted/Original Manuscript' of an article published by Taylor & Francis Group in Expert Opinion on Drug Metabolism & Toxicology on Janurary 24, 2022, available online: https://wwww.tandfonline.com / doi: 10.1080/17425255.2021.2027906.

Abstract

Introduction: Mycophenolic acid (MPA) is a widely used immunosuppressant in transplantation and autoimmune disease. Highly variable pharmacokinetics have been observed with MPA, but the exact mechanisms remain largely unknown.

Areas covered: The current review provided a critical, comprehensive update of recently published population pharmacokinetic/dynamic models of MPA (n=16 papers identified from PubMed and Embase, inclusive from January 2017 to August 2021), with specific emphases on the intrinsic and extrinsic factors influencing the pharmacology of MPA. The significance of the identified covariates, potential mechanisms, and comparisons to historical literature have been provided.

Expert opinion: While select covariates affecting the population pharmacokinetics of MPA are consistently observed and mechanistically supported (e.g., cyclosporine and post-transplant time on MPA clearance), some variables have not been regularly reported and/or lacked mechanistic explanation (e.g., diarrhea and several genetic polymorphisms). Very few pharmacodynamic models were available, pointing to the need to extrapolate pharmacokinetic findings. Ideal models of MPA should consist of: i) utilizing optimal sampling points to allow the characterizations of absorption, re-absorption, and elimination phases; ii) characterizing unbound/total MPA, MPA metabolites, plasma/urinary concentrations, and genetic polymorphisms to facilitate mechanistic interpretations; and iii) incorporating actual outcomes (e.g., rejection, leukopenia, infections) and pharmacodynamic data (e.g., inosine-5′-monophosphate dehydrogenase activities) to establish clinical relevance. We anticipate the field will continue to expand in the next 5 to 10 years.

1. Introduction

Mycophenolic acid (MPA) is a widely used immunosuppressant for the prevention of organ rejection in both adult and pediatric patients [10, 24, 29, 31]. Two common oral formulations of MPA are the immediate-release mycophenolate mofetil (MMF) and the enteric-coated mycophenolate sodium (EC-MPS), which exhibit different pharmacokinetic characteristics [10, 24, 29, 31]. MPA reversibly inhibits inosine-5′-monophosphate dehydrogenase (IMPDH), thereby decreasing the synthesis of guanine nucleotide and eventually reducing the proliferation of T- and B-lymphocytes [180]. The pharmacokinetic variability of MPA is relatively large [10, 24, 29, 31], where up to 10-fold differences in dose-normalized exposure have been observed in solid organ transplant patients [181]. MPA over-exposure has been associated with severe, and sometimes life-threatening gastrointestinal, infectious, and hematological adverse effects [29, 61]. On the other hand, increased risks of biopsy-proven acute rejection have been associated with low MPA exposures [10, 24, 29, 31]. Given the complexity of MPA pharmacokinetics/dynamics, non-linear mixed-effects modeling has been widely used over the past ~20 years to characterize population estimates, inter-individual variabilities, inter-occasional variabilities, and/or pharmacological effects in various populations [114, 143-146, 148, 150, 152-162, 182-210]. As the population models of MPA are evolving [10, 27, 30, 31, 62, 71-74], the primary purpose of this review was to provide a critical, comprehensive update of recently published population pharmacokinetic/dynamic models, with specific emphases on the intrinsic (e.g., physiological variables and genetic polymorphisms) and extrinsic (e.g., drug-drug interactions) factors influencing the pharmacology of MPA.

2. Methods

This review focused on studies published after the most recent comprehensive, critical review articles summarizing the population pharmacokinetics of MPA [10, 27, 30, 31, 62, 71-74]. Critical review is defined as having provided a thorough analysis/interpretation of the included studies. PubMed and Embase were searched using the following keyword combinations: *"entero-hepatic recirculation (or circulation), gastrointestinal, infection, iterative two-stage*, mycophenolate, mycophenolic acid, neutropenia, non-linear mixed-effects model*, NONMEM, pharmacodynamic*, pharmacogenomic*, pharmacokinetic*, population pharmacokinetic*, rejection, stochastic approximation expectation maximization (SAEM), and toxicity"*. The search was limited to English articles published between January 2017 to August 2021 (i.e., since the publications of the most recent comprehensive articles). Original research articles reporting the population pharmacokinetics of both MPA formulations were included. Duplicate publications between the two databases, review articles, conference abstracts, studies without population pharmacokinetic models, and papers that were already thoroughly and critically reviewed were excluded (Figure III-1). The primary focus of this review paper is on adult populations because pediatric models have been recently reviewed [27], except for one new study [211] (see sections 4.3 and 5.3). The article selection procedures are provided in Figure III-1.

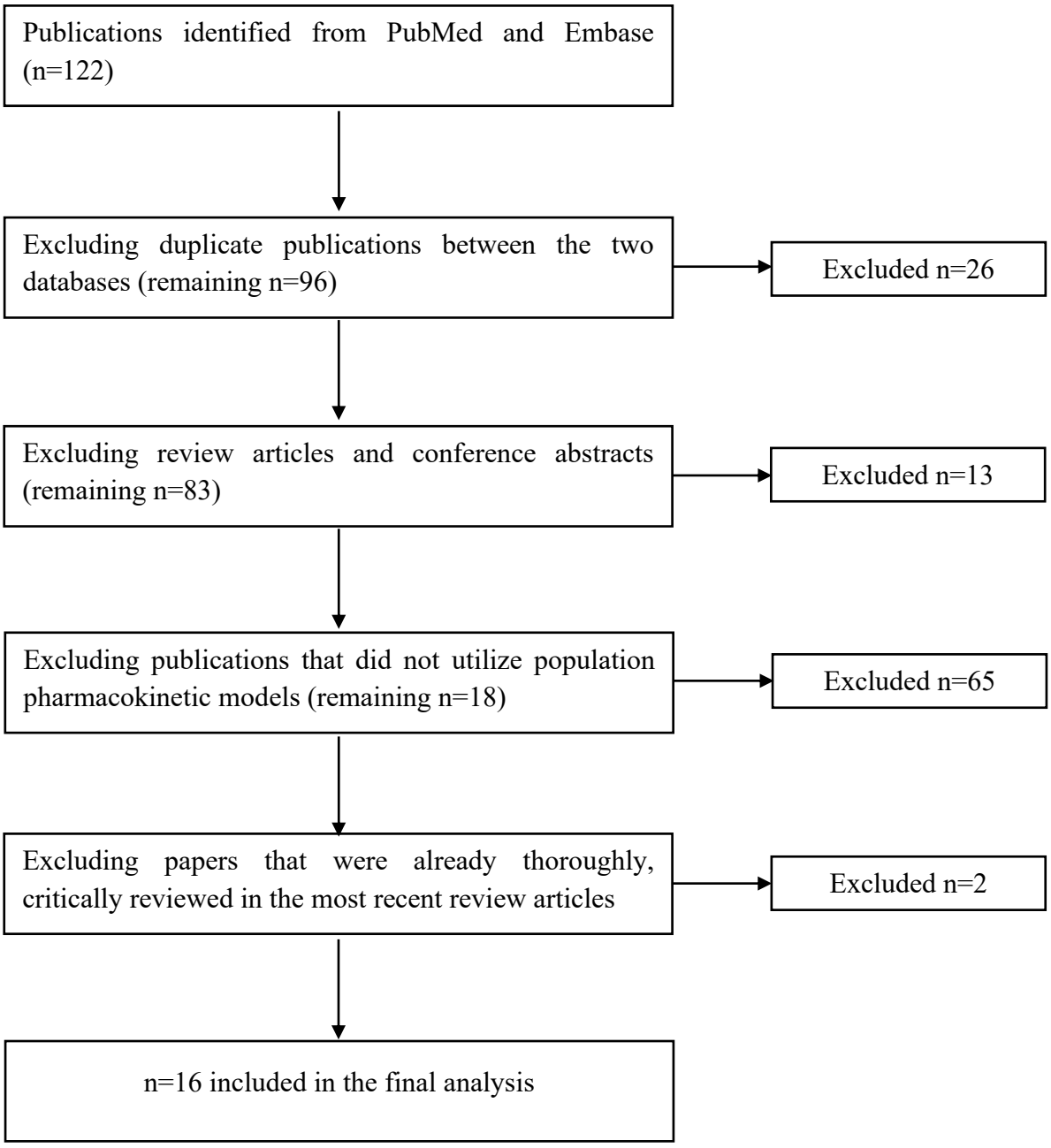

Figure III-1 Article identification, exclusion, and selection process

3. Overall characteristics of recent, novel population pharmacokinetic/dynamic studies

The 16 papers included in our analysis (Figure III-1, Table III-1, Table III-2) are hereafter designated as the "current dataset" [59, 117, 118, 139-141, 211-220], whereas the "historical dataset" refers to all MPA population pharmacokinetic models published prior to these papers [114, 143-146, 148, 150, 152-162, 182-210]. The current data were mostly derived from the adult population (n=15 [59, 117, 118, 139-141, 212-220]), with only one pediatric paper identified ([211]) (Table III-1, Table III-2). Approximately 2/3 of the studies enrolled renal transplant recipients, where one study included kidney-pancreas transplant patients [59, 117, 139-141, 213-216, 218, 219]. The remaining 1/3, hereafter designated as "non-renal transplant", enrolled adult hematopoietic stem cell transplant patients (n=2 [212, 220]), adult lupus nephritis patients (n=1 [217]), adult healthy male volunteers (n=1 [118]), and juvenile dermatomyositis patients (n=1 [211]). The types of indications in the current dataset were consistent with historical data that we could identify (i.e., n=26 in strictly renal transplant populations (i.e., ~51%) [114, 143-146, 148, 150, 152-162, 185, 187, 195-198, 204, 210], n=4 in combined populations containing renal transplant patients (i.e., ~8%) [147, 149, 151, 221], and n=21 in non-renal transplant populations (i.e., ~41%) [182-184, 186, 188-194, 199-203, 205-209]). The current dataset represented a wide range of ethnicities (listed alphabetically): Caucasian (n=1 [214]), Chinese (n=5 [139, 141, 211, 218, 219]), Japanese (n=1 [220]), Korean (n=2 [117, 118]), Mexican (n=2 [215, 217]), and multiple or unspecified (n=5 [59, 140, 212, 213, 216]). Only one study utilized the EC-MPS [141].

With respect to modeling techniques, 12 studies were constructed with NOMEM software [117, 118, 139-141, 213-215, 217-220], 3 using Monolix [59, 211, 216], and 1 employing ITSIM (in house software) and Pmetrics [212]. More diversity was evident in the modeling algorithm, where stochastic approximation expectation maximization estimation (n=6 [59, 140, 211, 214, 216,

218]) and first-order conditional estimation with interaction (n=6 [117, 118, 213, 215, 217, 219]) have been used more frequently than first-order conditional estimation/first-order (n=2 [139, 141]), iterative two-stage Bayesian parametric and nonparametric approaches (n=1 [212]), or unspecified algorithm (n=1 [220]). Similar to data reviewed previously (e.g., [27, 31, 62, 71, 72]), simple structural models (i.e., one or two-compartmental models with various combinations of absorption and elimination) were employed by most studies in the current dataset (Table III-1, Table III-2); however, complex, mechanistic models with unique features were also utilized (e.g., using unbound concentrations of MPA [140, 213, 216, 218], metabolites of MPA [117, 118, 213, 218-220], intracellular drug concentrations [216], and entero-hepatic recirculation [117, 118, 140, 213, 218, 220]). It is worth the while noting that a variety of entero-hepatic recirculation models have been utilized in the current dataset (i.e., using total or free concentrations, presence or absence of specific compartments, and with or without MPA metabolites) [117, 118, 140, 213, 218, 220], but it was not clear if these models were systematically derived and if head-to-head comparisons were conducted between models. Therefore, it was not possible to designate an optimal entero-hepatic recirculation model or optimal sampling times from these data. Three of the identified papers collected clinical outcomes (e.g., risks of acute rejection in adult kidney transplant patients [214] and occurrence of rejection in adult kidney transplant patients [216]) and pharmacodynamic data (e.g., IMPDH activities in adult hematopoietic stem cell transplant patients [220]).

In subsequent sections, discussions are organized on the basis of "intrinsic or extrinsic factors", and sub-categorized into "adult renal transplant recipients", "adult non-renal transplant recipients", or "pediatric patients". Under each sub-category, data were analyzed as *"absorption"*, *"distribution"*, and *"metabolism and excretion"*. Metabolism and excretion were discussed as a single process as urinary excretion data were not available in the current dataset.

4. Intrinsic factors influencing the population pharmacokinetics of MPA

The large variabilities observed in the pharmacokinetics of MPA are known to be attributed to intrinsic patient- and disease-specific variables [10, 31]. In this current dataset, data pertaining to physiological (e.g., body weight, type of transplantation/indication, co-morbidities) and genetic variations in metabolism enzymes or transporters were analyzed (Table III-1, Table III-2).

4.1. Adult renal transplant recipients

All renal transplant studies included in this review were conducted in the adult population and have attempted to incorporate physiological factors to explain the pharmacokinetic variabilities of MPA [59, 117, 139-141, 213-216, 218, 219]. Overall, 8 studies have successfully identified significant physiological covariates [59, 139, 140, 213, 215, 216, 218, 219], and amongst the 7 papers that have collected pharmacogenomic data [117, 139, 140, 213, 215, 216, 219], 5 have successfully incorporated genetic polymorphisms into their final models [117, 139, 213, 215, 216] (Table III-1, Table III-2).

4.1.1. Absorption

For the purpose of this manuscript, “MPA” is utilized when discussing the general absorption process; however, the absorption process may differ by formulation. MMF requires hydrolysis to form MPA as the initial step in the absorption process [10], and both MPA and MMF may undergo absorption [30]. MPA absorption in the current dataset was most commonly described by linear processes with [59, 140, 141, 214, 218] or without delay [117, 139, 213, 215,

219], parameterized using first-order absorption rate constant (k_a) with/without lag time (t_{lag}) (Table III-1, Table III-2), which are consistent with the historical data [10, 31, 62]. On the other hand, zero-order absorption (depicted by rate constant, Tk0) was only used in one study [216], possibility due to the limited number of data points collected, which may have resulted in large variabilities in their absorption phase (according to the authors) [216] (Table III-1, Table III-2). Zero-order absorption models had also been used in historical studies in adult kidney transplant patients (e.g., [152, 155]), as Sherwin et al. had proposed that MPA absorption is likely a time-dependent process which cannot be simply described by either first- or zero-order rate constants [30]. However, other absorption models evident in the historical dataset (i.e., gamma distributions, Erlang absorption, and/or transit models [10, 27, 30, 31, 62, 71, 72, 74]) were not observed in the current dataset.

Physiological variables affecting MPA absorption were not identified in the current dataset. This could be due to insufficient data collected during absorption leading to studies having to fix k_a or t_{lag} (e.g., [59, 117]) or the lack of covariate screening in relation to MPA absorption (e.g., effects of covariates were not determined against Tk0 [216]; race and donor type were excluded from covariate modeling [213]). Okour et al. reported increased entero-hepatic recirculation of mycophenolic acid glucuronide (MPAG; %EHC) in patients carrying the polymorphic allele of nuclear factor 1 alpha (HNF1A) (rs2393791), which was hypothesized by the authors to be involved in the expression of bile acid transporters [213]. However, the effects of HNF1A on MPA kinetics had not been reported historically, warranting further mechanistic studies.

Historically, race had been identified as a covariate of k_a in a combined population of kidney transplant and rheumatoid arthritis patients [151]. Japanese and Caucasian patients tended to exhibit similar k_a values (eliminating outliers), which were generally lower than k_a from fasted

African Americans subjects [151]. The lack of effects of "race" in the current dataset might be explained by the limited number of studies with more than one ethnicity or the lack of investigation of race as a covariate (Table III-1, Table III-2). As an example, although recipient/donor race were reported by Okour et al., these data were excluded from covariate modeling as Caucasians made up of >90% of their study population [213]. Moreover, it was previously determined by Han et al. [153] that uridine 5'-diphospho-glucuronosyltransferase (UGT) 1A9-118delT 9/10 or 10/10 carriers (rs3832043) exhibited significantly decreased k_a values compared to UGT1A9-118delT 9/9 (i.e., wild type) carriers in adult Korean patients [153]. Although the same polymorphism was examined by Kim et al. (Table III-1, Table III-2), it was not determined as a significant covariate of k_a or any other parameters [117]. This discrepancy may be due to an interacting effect by MPA formulation, where patients in Kim et al. were given MMF [117], while Han et al. had utilized EC-MPS [153]. It may be possible that MPA absorption is more sensitive to variations in intestinal metabolism in patients administered the enteric-coated formulation, as the result of the slower absorption reported by Han et al. [153]. However, although enteric-coated formulation was used by Chen et al. in the current dataset, significant variables on MPA absorption was not reported [141]. Taken together, the effects of physiological and genomic variables on the absorption of MPA have not been extensively investigated in adult renal transplant populations.

4.1.2. Distribution

MPA and MPAG are highly protein bound to serum albumin, with unbound fractions approximated at 1-3% (for MPA) in patients with normal liver and kidney functions [10] and 18% (for MPAG) in stable kidney transplant recipients [37]. Only the unbound concentrations of MPA are biologically active [10, 31]; therefore, characterizing factors influencing MPA/MPAG binding

and the kinetics of unbound MPA are pharmacologically more relevant [31]. Of the 11 studies identified in adult renal transplant patients [59, 117, 139-141, 213-216, 218, 219], 4 incorporated unbound plasma concentrations of MPA [140, 213, 216, 218], and Riglet et al. also measured MPA concentrations in peripheral blood mononuclear cells [216] (Table III-1, Table III-2). In these studies, only the linear protein binding model, parameterized with the binding rate constant (k_B, also representing the number of binding sites) [140, 216, 218] and/or the unbound fraction of MPA [213, 216], were utilized.

The current dataset have attempted to characterize the effects of physiological (n=10 [59, 117, 139-141, 213-216, 218]) and genomic (n=6 [117, 139, 140, 213, 215, 216]) variables on MPA distribution, parameterized with apparent volume of distribution (V/F), apparent intercompartmental clearance (Q/F), and k_B. However, significant physiological [140, 215, 216, 218] and genomic effects [117, 139, 215] were only identified in some studies. In Reséndiz-Galván et al., a positive correlation between the apparent volume of distribution of the central compartment (V_c/F) of MPA and blood urea nitrogen was observed [215]. A possible mechanism is that impaired renal function, as evident by elevated blood urea nitrogen, can potentially reduce the urinary excretion of MPAG [10, 215]. The accumulated MPAG could then compete with the protein binding and increase the unbound fractions of MPA [10, 215]. Because MPA is considered a low hepatic extraction drug, its total concentrations are inversely proportional to its unbound fraction [10]; therefore, elevated unbound fractions of MPA could theoretically lead to reduced total MPA concentrations and increased total V_c/F. Another possible hypothesis is uremic toxins (accumulated due to renal dysfunction) displacing MPA binding [215] or inhibiting the uptake/efflux transporters mediating the urinary excretion of MPAG [38, 53]. Measuring concentrations of unbound MPA (independent of protein binding), MPAG, and uremic toxins

would provide further mechanistic insights into the observed interaction by Reséndiz-Galván et al. [215]. Furthermore, uremic toxin accumulation due to kidney impairment could also explain the inverse relationship, in our opinion, between creatinine clearance and the apparent volume of distribution of the peripheral compartment (V_p/F) of the unbound MPA [216]. According to the authors, decreased creatinine clearance would increase the unbound fractions of MPA. However, it may not be apparent how increased unbound fraction would lead to increased V_p/F, as this mechanism alone should not have impacted the unbound concentrations of MPA [10]. An alternative hypothesis could be the inhibitory effects of accumulated uremic toxins on MPA metabolism [52-55] leading to increased unbound concentrations of MPA, hence enhanced distribution into the peripheral compartment. However, uremic toxins can potentially elicit multiple pharmacokinetic interactions simultaneously (i.e., protein binding displacement, intrinsic clearance inhibition, and transporter inhibition) [10, 53-55, 222, 223], and one would need to characterize both bound and unbound concentrations of MPA in both the plasma and urine to clearly elucidate the responsible interacting mechanism(s).

In the current dataset, body weight was positively associated with the Q/F of unbound MPA [218] (Table III-1, Table III-2), which could be hypothesized to be due to increased adipose tissue mass facilitating the distribution of lipophilic MPA from the central to peripheral compartments. Moreover, in studies utilizing protein binding equations [140, 213, 216, 218] (Table III-1, Table III-2), albumin was identified as a significant positive covariate on k_B [216, 218]. This observation is consistent with the nature of the proposed linear protein binding model (i.e., Equation III-1),

Equation III-1

$$MPA_t = (1 + k_B) \times MPA_u$$

MPA_t=MPA total concentration, MPA_u=MPA unbound concentration, where increased albumin could be interpreted as increased number of MPA binding sites [216, 218]. Furthermore, the positive association between creatinine clearance and k_B reported in Colom et al. [140] was possibly attributed, in our opinion, to reduced concentrations of MPAG and/or uremic toxins in patients with healthier kidneys, with minimal protein binding displacement effects. Although albumin was not directly correlated with any protein binding parameters in this particular study, its effects should not be completely ruled out due to its collinearity with creatinine clearance and the small range of albumin observed, according to the authors [140].

The effects of creatinine clearance [153, 204], but not body weight, observed in the current dataset had been documented historically. The effects of albumin had been reported previously to correlate with the maximum number of binding sites (B_{max}), but in a completely different, mechanistic model [143]. Although non-linear binding equations have been tested in the current dataset (e.g., [140, 218]), they were not included in the final population pharmacokinetic models. In addition, albumin had been identified as one of the significant covariates on V_c/F historically [160, 161]; however, this (inverse) association was not observed in the current dataset possibly because only a few studies have tested albumin in the covariate model (i.e., [59, 139-141, 213, 218]) (Table III-1, Table III-2), and the reported albumin ranges were relatively narrow or above the critical threshold [50]. Likewise, van Hest et al. had reported a negative association between total MPAG concentrations and k_B, which was consistent with the competing effects of MPAG towards the albumin-MPA binding complex [204], but this relationship was not tested/reported in the current dataset. The previously determined relationship between race and V/F [151] was also not observed in the current dataset, possibly as a consequence of limited ethnicity data (discussed above).

The effects of genetic polymorphism on MPA distribution had not been characterized, to our knowledge, historically in population pharmacokinetic studies. In the current dataset, heterozygotes of the UGT1A9 -275 T>A (rs6714486) mutation were shown to have increased MPA V_c/F compared to TT carriers [215]. The mechanism was hypothesized to be increased formation of MPAG [215] and increased unbound fraction (hence decreased total concentrations) of MPA. Similarly, the UGT2B7 211 G>T (rs number not reported) genotype had a significant association on MPA V_c/F, and the authors attributed this observation to increased MPA exposure [139] (Table III-1, Table III-2). However, concentrations of MPAG, acyl mycophenolic acid glucuronide (AcMPAG), and unbound MPA are required to confirm these hypotheses in both studies [139, 215]. Furthermore, MPAG V/F was positively associated (~ a 1.2-fold increase) with wild type carriers of the solute carrier organic anion transporter family member 1B3 (SLCO1B3) 334 gene (rs4149117) [117]. According to Kim and Picard et al. [43, 117], the SLCO1B3 transporter is involved in the hepatic uptake of MPAG, and T carriers of SLCO1B3 334T>G should have increased activities [43], leading to larger volume of distribution.

Overall, significant physiological and genetic covariates influencing the distribution of MPA have been identified. In particular, the contributions of creatinine clearance and albumin have been characterized in both the historical and current datasets, suggesting the likely significance of these variables.

4.1.3. Metabolism and excretion

The hepatic metabolism and renal excretion of MPA were commonly characterized as single, first order processes (parametrized by the apparent oral clearance, CL/F) in all adult kidney

transplant patients in the current dataset [59, 117, 139-141, 213-216, 218, 219] (Table III-1, Table III-2). Theoretically, unbound concentrations of MPA are only affected by intrinsic clearance, but total concentrations can be dependent on both the unbound fraction and intrinsic clearance; therefore, changes in total MPA concentrations may not always be consistent with the unbound concentrations [10, 31]. As only the unbound MPA is subjected to metabolism and excretion, characterizing the CL/F of unbound MPA is more biologically and clinically relevant. In the current dataset, total MPA CL/F was reported in 7 studies [59, 117, 139, 141, 214, 215, 219], while 4 studies characterized the unbound CL/F [140, 213, 216, 218]. Moreover, total MPAG CL/F [219], total MPAG and AcMPAG CL/F [213], elimination rate constants of total MPAG (k_{70}) and total AcMPAG (k_{90}) [117], and unbound MPAG CL/F [218] were also utilized in some models to characterize the clearance of MPA (Table III-1, Table III-2).

Being the most important population parameter estimate, the majority of studies in the current dataset have attempted to characterize the effects of physiological factors [59, 117, 139-141, 213-216, 218, 219] and genetic polymorphisms [117, 139, 140, 213, 215, 216, 219] on MPA CL/F. Body weight was positively associated with total MPA CL/F [139], and it may be hypothesized that increased body mass could be associated with enhanced hepatic UGT protein expression [27, 224], leading to elevated intrinsic clearance of MPA. In support of this, Quintairos et al. reported a population estimate of CL/F scaled based on body weight [214] (Table III-1, Table III-2), and the effects of body weight had also been observed historically in adult kidney transplant patients (e.g., [155]). In addition, positive relationships between serum creatinine [139, 215] with total MPA CL/F have been reported, which, according to the authors, may be attributed to “low plasma albumin concentration, metabolic acidosis, and uremia” [139, 215]. To expand on these observations, it may be possible that elevated levels of serum creatinine simply reflected impaired

kidney functions, which could lead to the accumulation of MPAG and/or uremic toxins [139, 215]. In addition, certain uremic toxins (e.g., indoxyl sulfate or *p*-cresol sulfate [53]) are also inhibitors of hepatic (multidrug resistance-associated protein 2 transporter [MRP-2] and/or organic-anion-transporting polypeptides 1B1/3 [OATP1B1/3]) or renal (MRP-2 and/or organic anion transporter-3 [OAT-3]) transporters which are responsible for the biliary or renal excretion of MPAG [32, 38, 39, 43, 53]. Collectively, these mechanisms can potentially explain the relationship between serum creatinine and MPA CL/F. The same mechanisms could also explain the negative associations observed between post-transplant time and the CL/F of total MPA [219], where kidney functions are gradually improved with increasing time post-transplant. This can be further confirmed by the negative relationships observed between total MPA CL/F and albumin [219].

In the current dataset, total MPA CL/F was positively correlated with "MPAG to MPA area under the concentration-time curve (AUC) ratio" (an indicator of intrinsic clearance, Table III-1, Table III-2), which could be explained by the fact that MPAG is the primary metabolic product of MPA [59]. On the other hand, a negative association between AcMPAG trough concentration and total MPA CL/F was reported by Rong et al., where it remains to be proven if an inhibitory effect of AcMPAG on the production of MPAG was a contributory mechanism [59]. It is worth noting that uremic toxins could also reduce the intrinsic clearance of MPA [52, 54, 55], which could oppose their effects on protein binding displacement and transporter inhibition, thereby cancelling the overall effects on total MPA CL/F. On the contrary, the inhibitory effects of uremic toxins on unbound MPA clearance are independent of protein binding displacement, and these effects were potentially demonstrated by the positive relationship observed between creatinine clearance and the unbound CL/F of MPA [213, 216]. Overall, these data further support

the notion that MPA pharmacokinetics should ideally be characterized with unbound concentrations to minimize the confounding effects of protein binding displacement.

Donor sex and diabetes at time of transplant significantly affected the CL/F of total MPAG in the current dataset [213] (Table III-1, Table III-2). Okour et al. reported male donors being more likely to exhibit increased total MPAG CL/F, and this may be attributed, according to the authors, to these individuals having "larger kidneys" [213]. On the other hand, patients with diabetes at time of transplant exhibited reduced total MPAG CL/F, and the authors attributed this observation to reduced MPAG biliary and renal excretion via impaired transporters [213]. While the effects of diabetes on the expressions/activities of breast cancer resistance protein (BCRP, involved in the biliary excretion of MPAG [42]) and MRP-2 transporters have been documented in animal models [225], further systematic investigations in humans are warranted. In addition, the positive associations between creatinine clearance with total MPAG CL/F [219] and between estimated glomerular filtration rate with unbound MPAG CL/F [218] are consistent with the established role of renal excretion in MPAG clearance [10, 218, 219]. Specifically, decreased creatinine clearance and estimated glomerular filtration rates may be indicative of impaired kidney function, which could be associated with reduced active tubular secretion of MPAG [10].

In the current dataset, CT and TT carriers of UGT2B7 802 C>T (rs7439366) exhibited reduced metabolism rate constant (i.e., k_{59}) from MPA to AcMPAG compared to wild type controls [117]. This observation is consistent with the reduction of MPA intrinsic clearance in the formation of AcMPAG in *in vitro* human liver microsomes obtained from UGT2B7 802 CT and TT donors [109, 117] and the notion that UGT2B7 is the predominant enzyme responsible for the production of AcMPAG [10]. Moreover, TT carriers of the ATP-binding cassette sub-family B member 1 (ABCB1, encoding p-glycoprotein) 3435 C>T (rs1045642) polymorphism exhibited decreased

apparent clearance of MPA from the peripheral blood mononuclear cell compartment (CL_{out}/F) compared to CC and CT carriers [216]. It was hypothesized by the authors that p-glycoprotein is an efflux transporter facilitating the movement of MPA out of these cells [216], but these observations should be further verified using human *ex-vivo* or *in vitro* models. In addition, heterozygotes of IMPDH-1 (rs2288553) exhibited elevated total MPAG CL/F [213], but the mechanism(s) may still warrant further investigation as no prior data, to our knowledge, have documented this "pharmacodynamically driven-pharmacokinetic" interaction.

The effects of body weight [152, 155], post-transplant time [148, 152, 154], and albumin [160, 161] on total MPA clearance had been extensively reported historically. Instead of serum creatinine identified in the current dataset (Table III-1, Table III-2), the negative associations between creatinine clearance and total MPA CL/F had been reported historically [160, 161]. On the contrary, the effects of age [162], sex [161], hemoglobin [160], race [151], and the ratio of aspartate aminotransferase to alanine aminotransferase [144] on MPA total clearance (or elimination rate constant), which had been reported historically, have not been replicated in the current dataset (Table III-1, Table III-2). Although age has been tested as a covariate in many studies [59, 117, 139, 140, 213-216, 218], it was not included in the final models (Table III-1, Table III-2) possibly because all studies were conducted in adults in whom the metabolism enzymes (e.g., UGT1A9) and transporters (e.g., MRP-2) associated with MPA are already fully expressed [226, 227]. Likewise, the influence of sex on total MPA CL/F has rarely been identified (e.g., [161]) and should be further tested given the limited amount of data in the literature. On the contrary, increased levels of hemoglobin had been correlated with reduced MPA clearance [160], but this association was not observed in the current dataset because hemoglobin was only examined as a covariate in a few studies [140, 215, 218]. Although Asians had been proposed to

have reduced MPA clearance compared to Caucasians in various models (e.g., [151, 179]), this effect has not been conclusively proven in a strictly controlled experiment, to our knowledge. As well, the ratio of aspartate to alanine aminotransferase had been positively linked to MPA clearance in a single study previously [144], but it was not tested as a covariate in the current dataset (Table III-1, Table III-2). Moreover, the relationships observed between kidney functions (e.g., creatinine clearance and estimated glomerular filtration rate) and the clearances of MPAG or AcMPAG had also been identified in the historical dataset [143-146], but more confirmatory studies are warranted given the scarcity of these data.

In the historical dataset, single nucleotide polymorphism in the solute carrier organic anion transporter family member 1B1 (SLCO1B1) 388A>G (rs2306283) gene had been correlated with reduced CL/F of total MPA in adult Korean patients [153]. As SLCO1B1 gene encodes OATP1B1, a transporter responsible for the uptake of MPAG [43] into hepatocytes, Han et al. suggested this genetic polymorphism may contribute to the oral bioavailability of MPA. This polymorphism has also been tested in Kim et al. (Korean population) in the current dataset, but significant relationships were not identified [117]. These observations are consistent with the previous findings by Picard et al., where SLCO1B1 388A>G was not associated with alterations of MPA pharmacokinetics, in general, in kidney transplant patients [43]. The inconsistent findings with respect to this specific genetic polymorphism would warrant further investigations.

Overall, the effects of intrinsic factors on MPA CL/F have been extensively investigated in the current dataset, where body weight, albumin concentration, and kidney function have been identified as significant variables (Table III-1, Table III-2). However, the biological mechanisms leading to these interactions still require more investigations, perhaps employing more mechanistic models incorporating unbound concentrations, metabolites, and genetic polymorphisms.

4.2. Adult non-renal transplant recipients

4.2.1. Absorption

The effects of physiological and genetic variables have been investigated in 3 studies [118, 217, 220], but significant physiological findings were only reported by 1 paper [220] and no effects on genetic polymorphism were identified (Table III-1, Table III-2). MPA absorption in non-renal patients was most commonly described by a first-order function [118, 217, 220], similar to the kidney transplant data [59, 117, 139-141, 213-216, 218, 219]. Labriffe et al. utilized the sum of two gamma distributions to characterize the occasionally observed secondary peaks possibly due to syringe purging in adult hematopoietic stem cell transplant patients [212]. Similar absorption models were used in adult kidney transplant [197] and reduced-intensity adult hematopoietic stem cell transplant patients [201] to describe the complex absorption processes. The only significant physiological variable affecting MPA absorption in the current dataset was diarrhea on the first-order rate constant describing the entero-hepatic recirculation of MPAG (i.e., the movement of MPAG from the central compartment to the gastrointestinal track, k_{EHC}) in adult hematopoietic stem cell transplant patients [220]. According to the authors, diarrhea-associated reduction in k_{EHC} can be explained by the "destruction of intestinal flora" leading to the inhibition of MPA reabsorption [220]. Based on this, it may be further hypothesized that the disturbed intestinal microbiota could lead to abnormal uremic toxin milieu, which can have inhibitory effects on first-pass metabolism and transport of MPA [53-55, 222, 223]. Another possible mechanism is that diarrhea may have shortened the gastrointestinal retention time of MPA, leading to a reduction in the extent of absorption. As the effects of diarrhea are novel and only identified in a single study [220], further investigations (e.g., characterizing changes to the microbiome or evaluating the

effects on MPA first-pass metabolism and transporter expressions/activities) are required to support these hypotheses. In the historical data, reductions in MPA k_a values had also been evident in adult lung transplant compared to kidney transplant recipients [149]. This was potentially attributed, according to the study authors, to surgery-related gastroparesis in lung transplant patients [149]. However, neither lung transplantation nor gastroparesis were investigated in the current dataset to confirm these findings (Table III-1, Table III-2). Overall, there is a general lack of data pertaining to the intrinsic factors affecting the absorption of MPA.

4.2.2. Distribution

The effects of physiological and pharmacogenomic variables on MPA distribution were screened in 3 studies in the current dataset [118, 217, 220] (Table III-1, Table III-2). A negative relationship between albumin and volume of distribution of MPA (V, based on a single compartmental model) in Japanese adult hematopoietic stem cell transplant patients [220] and a positive relationship between body weight and V_c/F in Mexican lupus nephritis adult patients [217] were identified. The underlying mechanisms are possibly similar to that discussed in section 4.1 (i.e., decreased free fraction with higher albumin and increased fat mass with higher weight, respectively). On the other hand, genetic polymorphisms were not identified to affect MPA distribution in both current and historical datasets in non-renal transplant populations.

4.2.3. Metabolism and excretion

A limited number of intrinsic factors influencing MPA clearance have been identified in adult non-kidney transplant patients in the current dataset (Table III-1, Table III-2). According to Yoshimura et al., elevated albumin levels were associated with decreased total MPA CL/F in adult

hematopoietic stem cell transplant patients [220]. This is not surprising as increased albumin can lead to both decreased unbound fraction and the total CL/F of MPA. Total MPA CL/F was reportedly lower in lupus nephritis patients exhibiting reduced creatinine clearance [217], and the authors attributed this relationship to "reduced hepatic metabolism" caused by chronic renal failure [217], which is consistent with the inhibitory effects of uremic toxins or endogenous compounds [217] discussed in section 4.1.3. In addition, creatinine clearance was identified a significant covariate of both total MPAG CL/F and total AcMPAG CL/F in adult hematopoietic cell transplant patients [220]. These observations support the notion that the clearances of these metabolites are primarily dependent on renal excretion [10, 220]. On the other hand, although genetic polymorphisms were examined in 3 papers [118, 217, 220], significant effects were not identified (Table III-1, Table III-2).

The influence of albumin and creatinine clearance on total MPA clearance had been reported historically in various adult populations [147, 184, 192, 202]. On the contrary, the previously reported effects of body weight [205], cystic fibrosis [205, 206], and type of transplant [149] on total MPA CL/F were not observed in the current dataset (Table III-1, Table III-2). The discrepancy on body weight might be attributed to the multiple mechanisms (e.g., liver/kidney dysfunctions, drug interactions, and genetic polymorphisms) contributing to the intrinsic clearance of MPA, some of which may be more influential than body weight alone. Lung transplant patients with cystic fibrosis had been associated with higher total MPA CL/F compared to non-cystic fibrosis patients [205, 206], and de Winter et al. reported increased total MPA CL/F in lung transplant patients compared to patients receiving kidney transplantation [149]. However, the effects of cystic fibrosis and type of transplantation could not be reproduced in the current dataset due to the lack of patient representation (Table III-1, Table III-2). With respect to the clearance of

MPA metabolites, the positive relationship between renal function and the clearance of MPAG and/or AcMPAG have been consistently described in both the current (Table III-1, Table III-2) and historical datasets [182, 193, 202]. On the contrary, the effects of race on MPAG CL/F (i.e., clearance in Caucasians being higher than the Chinese [194]) were not observed in the current dataset (Table III-1, Table III-2), possibly due to limited available data as discussed in section 4.1.1. Moreover, no data are available, to our knowledge, regarding the effects of genetic polymorphisms on MPA clearance in non-renal transplant patients, including the current dataset (Table III-1, Table III-2).

Taken together, the effects of physiological variables (i.e., albumin and creatinine clearance) on the metabolism and excretion of MPA (and its metabolites) have been well characterized in the current dataset. The influence of genetic polymorphisms, however, would require further characterization.

4.3. Pediatric patients

Wang et al. constructed a population pharmacokinetic model using total MPA concentrations in juvenile dermatomyositis patients as the only pediatric study in the current dataset [211] (Table III-1, Table III-2). A two-compartmental model with first-order absorption (with lag time) and elimination was used. A variety of physiological covariates were tested (Table III-1, Table III-2), and only height was identified as a significant covariate affecting MPA clearance. However, the positive relationship between height and total MPA CL/F was likely attributed, according to the authors, to its collinearity with body weight [211], but the latter variable was not included in their final model [211]. Although albumin had been known to affect MPA pharmacokinetics historically in the pediatric population [27, 209], it was not identified a

significant covariate in the current study probably because the albumin levels were above the critical threshold according to the authors [211]. In our opinion, the limited number of sampling points and the lack of pharmacogenomic data possibly made it challenging to characterize the complex pharmacokinetics of MPA.

5. Extrinsic factors influencing the population pharmacokinetics of MPA

Extrinsic factors have been known to influence the population pharmacokinetic variabilities of MPA [10, 29, 31]. The most common extrinsic factors are co-administered medications, but the effects of food and formulation (i.e., MMF vs. EC-MPS) have also been reported.

5.1. Adult renal transplant recipients

5.1.1. Absorption

The effects of co-administered medications (e.g., antacids, corticosteroids, cyclosporine, proton pump inhibitors, sirolimus, and tacrolimus) have been tested in 7 adult kidney transplant studies in the current dataset [59, 139-141, 213, 215, 218] (Table III-1, Table III-2). However, only cyclosporine was presumed a significant variable, where patients co-administered this specific calcineurin inhibitor were fixed (based on previous population estimates) to a significantly lower transport rate constant of unbound MPA from the central compartment to gallbladder (k_{CG}) compared to patients receiving tacrolimus or sirolimus [140]. Although the effects of cyclosporine on entero-hepatic recirculation had already been documented extensively in the literature (as recently reviewed by [228]), this process is more often modeled with MPAG instead of MPA (e.g.,

[30]). As such, it was not apparent if the documented effects of cyclosporine [140] were mediated by the inhibition of MRP-2 [228] or based on an entirely different mechanism. To expand on the latter possibility, other transporters such as OATP1B1/3 [43] have also been known to mediate the entero-hepatic recirculation of MPA and may be involved in the cyclosporine interaction [229]. Moreover, studies in the current dataset have not attempted to characterize the effects of food on the absorption of MPA, possibly because the study subjects were either all under fasting conditions [139, 215] or data regarding patients' diets have not been clearly reported (Table III-1, Table III-2). On the effects of MPA formulation, the majority of studies in the current dataset had utilized MMF (Table III-1, Table III-2), and only Chen et al. characterized the population pharmacokinetics of EC-MPS, but it was not a significant covariate of MPA absorption [141].

In the historical dataset, co-administration of antacids (composition unknown) was identified a significant covariate for MPA absorption [151]. Adult kidney transplant recipients and rheumatoid arthritis patients who were not administered antacids exhibited increased t_{lag} values compared to patients in whom the co-administration status was not clear [151]. Unfortunately, the only study attempting to characterize these interacting effects in the current dataset had a small number of patients (i.e., <20%) administered antacids and could not reproduce the observation [218] (Table III-1, Table III-2). In addition, it was reported previously that the k_a values of MPA had been positively associated with the dose of the co-administered cyclosporine [160], which was not observed in the current dataset (Table III-1, Table III-2). However, the exact mechanism behind the cyclosporine and MPA absorption interaction reported by van Hest et al. might warrant further investigation. Moreover, significant effects of food on the absorption of MPA had been identified previously by Funaki et al. [151], but not observed in the current literature due to limited data availability as discussed above. In addition, Musuamba et al. had evaluated the absorption of

both MMF and EC-MPS within the same study utilizing the transit compartment model, and MPA formulation was identified as a significant covariate influencing the number of transit compartments [156].

Overall, population pharmacokinetic models evaluating the effects of concurrent medications (except for cyclosporine), food, and/or formulation on MPA absorption are still limited.

5.1.2. Distribution

The effects of antacids, cyclosporine, proton pump inhibitors, sirolimus, steroids, and tacrolimus on the distribution of MPA have been tested in the current dataset, but significant variables were not identified (Table III-1, Table III-2). A positive correlation had been documented between antacids and V or V_c/F historically [151, 160], but the mechanism remains unknown, and this relationship was not observed in the current dataset possibly because of unbalanced comparison groups [213, 218] (Table III-1, Table III-2). The effects of food and formulation were not screened in the current dataset (Table III-1, Table III-2).

5.1.3. Metabolism and excretion

The co-administration of cyclosporine was a significant extrinsic factor influencing the metabolism and excretion of MPA in the current dataset (Table III-1, Table III-2). Increases in both total [141] and unbound MPA CL/F [140, 213] were observed in patients co-administered cyclosporine, which could be attributed to its inhibitory effects on the entero-hepatic recirculation of MPA [140, 141] (discussed in section 5.1.1). On the other hand, corticosteroid co-administration

was not directly identified a significant covariate in the current dataset, as the dosage information were not documented by some authors, and its covariate effects were only tested in 2 studies [139, 213]) (Table III-1, Table III-2). However, Rong et al. reported significantly reduced total MPA CL/F in kidney transplant recipients who were steroid-free compared to the literature control. According to the authors, the reduction in MPA CL/F could be due to the lack of corticosteroid-mediated induction in MPA glucuronidation [59], but direct evidence supporting this hypothesis is still limited. Although nifedipine co-administration had been reported to increase the clearance of total MPA historically [162], this effect could not be verified in the current dataset as nifedipine was only administered to <16% of the study subjects in a single study [218] (Table III-1, Table III-2). The effects of nifedipine toward UGT1A9, the primary enzyme responsible for MPA conjugation, would also require further characterization.

In summary, the extrinsic factors influencing the metabolism and excretion of MPA have not been thoroughly studied, with cyclosporine being identified as the only extrinsic covariate in the current dataset (Table III-1, Table III-2). Collectively, the effects of cyclosporine on the process of MPA clearance (through entero-hepatic recirculation) have been well described in both current and historical datasets; therefore, MPA dose adjustment should be considered when cyclosporine is co-administered or discontinued to minimize adverse outcomes [228].

5.2. Adult non-renal transplant recipients

5.2.1. Absorption

Of the 4 studies characterizing MPA population pharmacokinetics in non-renal transplant patients (Table III-1, Table III-2), only Romano-Aguilar et al. tested the effects of co-administered

drugs on the absorption of MPA, in adult Mexican lupus nephritis patients [217] (Table III-1, Table III-2). However, none of the concurrent medications were identified as significant variables in their final model, possibly because the study sample size may not be sufficient to capture the effects of a large number of covariates (i.e., 33 variables in 40 subjects) [217]. Consistently, little data were available historically to describe the effects of extrinsic factors on MPA absorption. Abd Rahman et al. reported cyclosporine's inhibitory effects toward MPA entero-hepatic recirculation in adult lupus nephritis patients [182], and this interaction has been thoroughly discussed in this paper and elsewhere [228].

5.2.2. Distribution

Co-medications were tested as covariates in Mexican lupus nephritis patients [217] (Table III-1, Table III-2), but significant relationships were not identified (Table III-1, Table III-2). The lack of data is generally consistent with that observed historically.

5.2.3. Metabolism and excretion

In the only observed significant covariate in the current dataset, Romano-Aguilar et al. reported increased CL/F of total MPA in prednisone co-administered lupus nephritis patients [217]. The authors attributed this observation to corticosteroid-mediated induction of hepatic glucuronidation of MPA [217], consistent with the effects observed in Rong et al. in kidney transplant recipients [59]. Cyclosporine was not identified as a significant factor influencing MPA clearance in the current dataset possibly because it is not the preferred calcineurin inhibitor today. Only one study in adult hematopoietic stem cell transplant patients had utilized cyclosporine in the

current dataset [212] (Table III-1, Table III-2), but the secondary peaks were likely attributed, according to the authors, to syringe purging, and not entero-hepatic recirculation. Moreover, hematopoietic stem cell transplant patients may also be subjected to conditioning regimens which may mask the effects of cyclosporine on MPA entero-hepatic recirculation (e.g. reviewed previously [27]). Overall, the effects of cyclosporine are likely dependent on the type of transplant, and the associated dose adjustment of MPA should take into consideration the specific patient population.

5.3. Pediatric patients

The effects of intravenous immune globulin and cotrimoxazole have been tested in juvenile dermatomyositis patients taking MMF in the current dataset [211], but only cotrimoxazole was retained in the final model. According to the authors, decreased MPA V_p/F might be due to the large volume of distribution of cotrimoxazole which interfered with the distribution of MPA [211]. However, in our opinion, the effects of cotrimoxazole might warrant further confirmation as only 2 patients (out of 15) were administered the drug [211], and the mechanism of the interaction also remains to be tested.

6. Clinical outcomes/population pharmacodynamic studies

Most of the models in the current dataset focused on the population pharmacokinetics of MPA (Table III-1, Table III-2), and only 3 studies have characterized the clinical outcomes or pharmacodynamics of MPA in relation to pharmacokinetics [214, 216, 220]. Riglet et al. evaluated the associations between various clinical covariates (including albumin, age, body weight, and

creatinine clearance at baseline; and total, unbound, and peripheral blood mononuclear cell intracellular MPA exposures on day 15) and the occurrence of rejection in kidney transplant recipients [216]. However, no associations were identified using a logistic regression model, which were likely attributed, according to the authors, to relatively low rejection rates and large pharmacokinetic variabilities [216]. In addition, Quintairos et al. described a population logistic regression model capable of predicting the probabilities of acute rejection using urinary miR155-5p pellet expression in adult kidney transplant patients [214]. In that particular study, interferon gamma inducible chemokine 10, total MPA exposure, tacrolimus exposure, and other covariates (listed in Table III-1, Table III-2) did not correlate with acute rejection. These negative findings were probably attributed, according to the authors, to the effectiveness of the concurrent therapeutic drug monitoring and the limited numbers of acute rejection events identified [214]. The inconsistencies between Riglet et al. or Quintairos et al. and the widely accepted MPA exposure-rejection relationship [61, 63] could also be attributed to limitations of the regression (i.e., association by nature) models. Furthermore, a direct sigmoid inhibitory maximum effect model was utilized to characterize the relationship between total MPA concentration and IMPDH activity in adult hematopoietic stem cell transplant recipients in the current dataset [220] (Table III-1, Table III-2). Despite a variety of tested covariates, only C-reactive protein was identified to have a significant relationship with IMPDH activity via the half-maximal inhibitory concentrations of MPA (IC_{50}) [220]. The observed positive association between C-reactive protein and the IC_{50} of MPA could be attributed, according to the authors, to the presence of infection or inflammatory cytokines [220]. To our knowledge, these reported clinical outcomes/pharmacodynamic effects are novel observations that would warrant further investigations to determine their clinical significance.

7. Conclusion

The intrinsic and extrinsic factors influencing the population pharmacokinetics/dynamics of MPA observed in recent publications have been comprehensively and critically reviewed. Mechanisms of the covariate effects, novelty, and comparisons to historical literature have been discussed in a format suitable for both researchers and clinicians.

8. Expert opinion

Non-linear mixed-effects modeling is a powerful approach for characterizing the complex pharmacokinetics of MPA, especially the sources of its variabilities via covariate modeling [31, 66, 166, 230]. This is evident by the large body of literature documenting MPA population models in various patient populations (e.g., as reviewed by [10, 27, 30, 31, 62, 71-74]) and the popular service provided by the Limoges group (https://pharmaco.chu-limoges.fr) to improve the therapeutic drug monitoring and/or precision dosing of MPA. Despite the very limited availability of population pharmacokinetic-pharmacodynamic models, we have identified the following variables to have consistent, significant effects on MPA pharmacokinetics in both current and historical datasets: albumin, body weight, creatinine clearance, co-administration of cyclosporine, and post-transplant time (Table III-1, Table III-2). In our opinion, cyclosporine co-administration and post-transplant time are more likely to be significant predictors of MPA pharmacodynamic effects, because the mechanisms of their relationships with MPA exposure have been well characterized. These covariates are likely to be (or have already been) incorporated into the precision dosing of MPA in the clinic. On the contrary, the effects of albumin, body weight, and creatinine clearance on the therapeutic effects/toxicities of MPA would still warrant further

verification, before the incorporation into clinical practice, due to multiple potential interacting mechanisms. Likewise, due to the lack of reproducibility or contradictory findings reported of the following covariates on MPA population pharmacokinetics, further confirmatory studies are required: age, blood urea nitrogen, co-administration of nifedipine, co-administration of prednisone, diet, disease states (such as diabetes, and diarrhea), several genetic polymorphisms identified in this review (Table III-1, Table III-2), height, hemoglobin, race, ratio of aspartate to alanine aminotransferases, sex, and type of transplantation. We foresee continued characterizations of these variables on both MPA pharmacokinetics and pharmacodynamics over the next few years.

The following features are, in our opinion, the necessary components of an ideal MPA population pharmacokinetic/pharmacodynamic model for identifying significant covariates. 1) In our review, several covariates identified historically could not be reproduced in the current dataset (and vice versa), possibly due to inadequate sampling points. Therefore, optimal design of sample collection protocols is necessary to capture the effects of potential covariates (i.e., using early [0.5-3 hours] and late [4-8 hours post-administration] collections to successfully capture all possible complex absorption, entero-hepatic recirculation, and elimination phases which may vary between patient populations, using well-established empiric or mechanistic modeling techniques, e.g., [197]). 2) Some studies have attempted to examine large amounts of covariates in relatively small sample populations, which may have attributed to false-negative effects. Therefore, the selection of covariates should be strategic and based on biological plausibility, while considering the likely collinearity of various variables. 3) Certain significant relationships could be interpreted by multiple, sometimes contradictory mechanisms. For example, impaired kidney function could be associated with decreased albumin synthesis, protein binding displacement, reduced intrinsic clearance, and transporter inhibition. In order to elucidate the real mechanism(s) behind a covariate

effect, population pharmacokinetic models should incorporate unbound/total MPA, MPA metabolites, plasma/urinary concentrations, and genomic data. 4) In order to properly assess the effects of genotypes, future studies should be adequately powered and controlled in consideration of the typically low minor allele-frequencies to minimize the chance of false-negative findings and maximize the probability of detecting a real genomic effect. 5) In the current and historical datasets, several patient populations other than kidney transplantation (e.g., other solid organ transplantations, autoimmune disease, stem cell transplant…etc.,) and subjects taking EC-MPS formulations are still under-represented. More emphases should be placed on these indications as MPA is increasingly used in these settings. 6) As discussed above, population models incorporating actual clinical outcomes (e.g., graft rejection, neutropenia, and infections) and/or characterizing MPA pharmacodynamics (e.g., IMPDH activities) are of limited availability. Although much more complicated and costly to construct, these population pharmacokinetic-pharmacodynamic models are ultimately more clinically relevant.

Despite its potential powers, population pharmacokinetic/dynamic modeling is not yet widely implemented in the dosing of MPA in many transplant centers. This could be due to the lack of understanding of the nature of population modeling (i.e., sometimes referred to as a black box approach) and the relative complexity of implementing this type of service, with the requirement of complicated software models, in the clinic. Therefore, in addition to advancing the science of MPA population pharmacokinetic/dynamic modeling as described above, user education and the simplification of user interfaces are required to popularize this approach and truly unlock its clinical benefits. Taken together, we foresee the field to continue to evolve quickly over the next 5-10 years to the point where it will be routinely used by clinicians for MPA precision dosing.

Table III-1 Summary information of patient demographic and biochemical parameters, concurrent medication, and genomic data in MPA population pharmacokinetic models

Patient population	Patient demographic and biochemical parameters	Concurrent medication	Patient genomic data	Reference
Adult renal transplant patients				
Study design: prospective, observational study **Population**: Chinese adult kidney transplant patients (n=102)	**Sex** (male/female): 64/38 **Age** (median or mean [range]): 41 (20-66) years **Body weight**: 59.5 (40.0-92.0) kg **Albumin**: 3.5 (2.5-4.9) g/dL **Red blood cells**: 3.04 (2.05-4.06)×10^9/mL **Hematocrit**: 27.9 (19.0-35.5) % **Hemoglobin**: 9.3 (5.1-15.4) g/dL **SCr**: 1.2 (0.7-12.9) mg/dL **CrCL** (calculated by Cockcroft-Gault equation): 65.3 (2.2-114.3) mL/min **Uric acid**: 4.9 (1.9-10.5) mg/dL **Blood urea nitrogen**: 20.7 (7.6-90.7) mg/dL **ALT**: 2.1 (0.9-8.6) U/dL **AST**: 1.6 (0.8-5.4) U/dL **Total bilirubin**: 0.8 (0.1-1.7) mg/dL **Post-transplant time**: 12.3 (4-126 or 148) days	**Induction treatment**: not specified **Documented medications**: EC-MPS; tacrolimus or cyclosporine; and corticosteroids **EC-MPS dose** (oral administration; median or mean [range]): 720 (360-900) mg; 720 mg every 12 hours (adjusted based on concentration and clinical assessment) **Plasma total MPA concentration** (nature of estimate±variability not specified):6.24±8.73 μg/mL (enzyme-multiplied immunoassay) **Plasma total MPA AUC_{0-12}**: 86.6±44.3 μg×h/mL in tacrolimus co-administered patients; 52.7±25.1 μg×h/mL in cyclosporine co-administered patients **Tacrolimus dose** (immediate release formulation): 0.1 mg/kg/day given twice daily at the initial stage, then adjusted based on C_0 **Cyclosporine dose**: 7 mg/kg/day given twice daily at the initial stage, then adjusted based on C_0 after day 3 post-transplant **Methylprednisolone or prednisone dose**: intravenous administration during surgery (500 mg), then oral administration of prednisone at a tapered maintenance dose (5-10 mg per day) after 1 month post-transplant	Not specified	Chen et al. [141]
Study design: prospective, randomized, multicenter, open-label,	**Sex** (male/female): 34/22 **Age** (global median [range]): 50 (23-63) years	**Induction treatment**: daclizumab	**ABCC2 -24 C>T**(CC/CT/TT) (n, number of subjects): 36/19/1	Colom et al. [140]

Patient population	Patient demographic and biochemical parameters	Concurrent medication	Patient genomic data	Reference
a part of the Symphony study [231, 232] **Population**: adult kidney transplant patients (within the first year post-transplant, n=56)	**Body weight**: 71 (35-100) kg **Albumin**: 42 (28-67) g/L **Hemoglobin**: 12.1 (7.3-16.9) g/dL **CrCL** (calculated by Cockcroft-Gault equation): 59.51 (8.43-134.90) mL/min **ALT**: 24 (6-318) U/L **AST**: 20.0 (6.6-104.0) U/L **Total bilirubin**: 0.50 (0.17-8.60) mg/dL **Low graft function (**as defined as "CrCL<25 mL/min"; n, number of subjects): 4 **Post-transplant time**: within 12 months post-transplant (data collected at 5 visits: "day 7, 1st month, 3rd month, 6th month, 1st year")	**Documented medications**: MMF (1 or 1.5 g, twice-daily, fixed dose); corticosteroids; with cyclosporine, tacrolimus, or sirolimus **MMF dose** (oral administration; median [range]**)**: 1000 (250-1000) mg, twice daily **Plasma MPAG C_0** (global): 96.88 (4.64-604.71) µmol/L (HPLC-UV) **Plasma MPAG C_0** (in patients on cyclosporine): 111.43 (6.49-422.92) µmol/L **Plasma MPAG C_0** (in patients on tacrolimus or sirolimus): 87.66 (4.64-604.17) µmol/L **Cyclosporine dose**: 100 (50-300) mg/day **Cyclosporine C_0**: 124 (26-500) ng/mL (assay not specified) Plasma total MPA, unbound MPA, and total MPAG concentrations were quantified by HPLC-UV	**ABCC2 3972 C>T** (CC/CT/TT): 21/28/6	
Study design: prospective, observational study **Population**: Korean adult stable kidney transplant patients (post-transplant time ≥ 6 months, n=32)	**Sex** (male/female): 20/12 **Age** (median [range]): 52 (20-70) years **Body weight**: 62.7 (43.9-102.4) kg **Height**: 165.8 (151-180) cm **Albumin**: 4.4 (3.8-5.0) g/dL **Hematocrit**: 43.6 (32.3-53.8) % **Hemoglobin**: 14.1 (10.6- 17.5) g/dL **SCr**: 1.22 (0.69-1.66) mg/dL **eGFR** (calculated by MDRD equation): 59.5 (35.0-85.7) mL/min/1.73 m^2 **Total bilirubin**: 0.7 (0.5-2.4) mg/dL **Post-transplant time**: 5.7 (0.6-10.4) years	**Induction treatment**: not specified **Documented medications**: MMF (≥2 weeks, at steady-state); tacrolimus; and prednisone **MMF dose** (oral administration; median [range]**)**: 1000 (500-2000) mg/day **Tacrolimus dose** (immediate release formulation): 2 (1-6) mg/day **Prednisone dose**: 5 (2.5-5) mg/day Plasma total MPA, MPAG, and AcMPAG concentrations were quantified by LC-MS/MS	**CYP3A5 (rs776746) expressers*** (n [percentage to the total number of patients]): 13 (40.6%) **SLCO1B3 334 T>G** (rs4149117) **T carrier**: 15 (46.9%) **UGT2B7 802 C>T** (rs7439366) **T carrier**: 15 (46.9%) *expressers are defined as patients carrying CYP3A5*1/*1 or CYP3A5*1/*3 genotypes CYP3A4*1G (rs2242480), SLCO1B1*1B (rs2306283), SLCO1B1*5 (rs4149056), SLCO1B3 699 G>A (rs7311358), ABCC2 -24 C>T (rs717620),	Kim et al. [117]

Patient population	Patient demographic and biochemical parameters	Concurrent medication	Patient genomic data	Reference
			ABCC2 1249 G>A (rs2273697), ABCC2 3972 C>T (rs3740066), and UGT1A9*1b (rs3832043) were also determined, however, data were not reported	
Study design: multicenter, observational, Deterioration of Kidney Allograft Function (DeKAF) Genomics study **Population**: adult kidney or kidney-pancreas transplant patients (n=89)	**Sex** (male/female): 62/27 **Donor sex** (male/female): 52/37 **Race** ("white"/"black"/ "Asian"): 83/5/1 **Donor race** ("white"/ "black"): 28/2 **Age** (mean±SD): 51±12 years **Donor age**: 42±12 years **Body weight**: 82.3±17 kg **Height**:173±8.3 cm **BMI**: 28±5.7 kg/m^2 **Albumin**: 3.94±0.5 g/dL (from n=91) **SCr**: 1.2±0.3 mg/dL **CrCL**: 82.8±24.9 mL/min **ALT**: 27±19.4 IU/L **ALP**: 93.6±95.8 IU/L **Serum bilirubin**: 0.5±0.3 mg/dL **Post-transplant time**: 36±15 days **Donor type** (deceased/living): 1/88 **Preemptive transplantation without undergoing dialysis** (yes/no): 42/47 **Diabetes** (yes/no): 26/63 **Number of HLA mismatches** (1/2/3/4/5/other): 9/12/27/9/18/13 **Prior kidney transplantation** (none/1-prior): 73/16 **Primary causes of kidney disease** (diabetes/glomerular disease/hypertension/other/polycystic kidney disease/unknown: 19/21/6/17/21/5)	**Induction treatment** (IL2/ monoclonal/polyclonal): 32/19/38 **Documented medications**: MMF (≥2 days, at steady-state); *Calcineurin inhibitor* (tacrolimus/cyclosporine: 58/31 *Steriod* (yes/no): 57/32 *Proton pump inhibitor* (yes/no): 66/23 **MMF dose** (oral administration): 500-1500 mg/day, twice daily Plasma unbound MPA, total MPA, MPAG, and AcMPAG concentrations were quantified by LC-MS/MS	n=133 single nucleotide polymorphisms (related to pharmacokinetics or pharmacodynamics of MPA; see Table S1 in [213]	Okour et al. [213]
Study design: "European multicenter prospective observational" study **Population**: Caucasian adult kidney transplant patients (n=58)	**Sex** (male/female): 38/20 **Age** (median [IQR]): 48 (38-58) years **Donor age**: 52 (45-60) years **Albumin**: N/A **Body weight**: 73 (62.9-86.8) kg	**Induction treatment**: basiliximab 20 mg for 2 doses **Documented medications**: MMF; tacrolimus; and methylprednisolone	Not specified	Quintairos et al. [214]

Patient population	Patient demographic and biochemical parameters	Concurrent medication	Patient genomic data	Reference
	Height: 170 (163-177) cm **BMI**: 24 (22-29) kg/m^2 **GFR** (calculated by MDRD equation): 44 (15-55) mL/min **Donor type** (deceased/living): 28/30 **Post-transplant time**: within 6 months post-transplant (data collected at 5 visits: "1st week [1-11days], 1st month, 2nd month, 3rd month, 6th month") **The occurrence of infection** (n [percentage to the total number of patients]): 34 (59%) **The occurrence of acute rejection**: 8 (14%) **Cytomegalovirus**: 14 (24%) **BK virus**: 9 (15%) **Diabetes mellitus**: 5 (9%) **miR155-5p** (mean [IQR]): 0.39 (0.03-0.55) ΔCt **CXCL-10**: 81.63 (22.26-107.55) pg/mL	**MMF dose** (oral administration; mean [IQR]): 1547 (1250-2000) mg per day **Plasma total MPA C$_0$**: 2.64 (1.76-3.90) µg/mL (HPLC-UV) **Tacrolimus dose** (immediate release formulation): 8.7 (6-10) mg **Whole blood tacrolimus C$_0$**: 9.3 (7.4-12.0) ng/mL (LC-MS/MS) **Methylprednisolone dose**: 500 mg daily dose before surgery, then tapered to 40 mg by day 5, 20 mg by 2 weeks, and 5 mg by 2 months post-transplant [233]		
Study design: prospective, observational study **Population**: Mexican adult kidney transplant patients (n=77, n=42 *de novo* patients)	**Sex** (male/female): 46/31 **Age** (median [range]): 32 (18-68) years **Body weight**: 64 (41-101) kg **Height**: 1.6 (1.4-1.8) m **BMI**: 23.4 (18.2-35.4) kg/m^2 **Glucose**: 101.2 (44.4-244.3) mg/dL **Hematocrit**: 29.6 (20.4-60.1) % **Hemoglobin**: 9.9 (6.3- 19.7) g/dL **SCr**: 1.9 (0.6-15.4) mg/dL **CrCL** (calculated by Cockcroft-Gault equation): 49.7 (7.2-138.1) mL/min **Urea**: 63.3 (11.8-230.1) mg/dL **Uric acid**: 5.8 (2.4-9.5) mg/dL **Blood urea nitrogen**: 29.6 (5.5-107.5) mg/dL **Post-transplant time**: 5 (3-4219) days **Donor type** (deceased/living): 59/18	**Induction treatment**: not specified **Documented medications**: MMF (at steady-state); tacrolimus; and prednisone **MMF dose** (oral administration): 500 mg every 12 hours **Plasma total MPA concentration** (mean [range]): 3.6 (0.2-18.1 mg/L) (UPLC-MS/MS) **Tacrolimus concentration** (median [range]): 5.9 (0.5-17.3) ng/mL (assay not specified) **Prednisone dose**: not specified	**UGT1A8 518 C>G** (rs1042597) (CC/CG/GG) (frequency): 52%/39%/9% **UGT1A9 -275 T>A** (rs6714486) (TT/TA/AA): 95%/5%/0% **UGT2B7 802 C>T** (hCV32449742) (CC/CT/TT): 56%/34%/10% **ABCC2 -24 C>T** (rs717620) (CC/CT/TT): 77%/23%/0% **SLCO1B3 334 T>G** (rs4149117) (TT/TG/GG): 1%/42%/57%	Reséndiz-Galván et al. [215]

Patient population	Patient demographic and biochemical parameters	Concurrent medication	Patient genomic data	Reference
Study design: CIMTRE (a prospective, observational) study **Population**: adult kidney transplant patients (n=78)	**Sex** (male/female): 45/33 **Age** (median [range]): 50 (21-78) years **Body weight**: 66.5 (36-125) kg **Albumin**: 30.3 (20.4-43.6) g/L (15 days post-transplant, n=71); 34.5 (21.8-43.1) g/L (1 month post-transplant, n=73); 36.4 (21.7-63.1) g/L (2 months post-transplant, n=70); 36.4 (23.7-48.5) g/L (6 months post-transplant, n=57) **CrCL** (calculated by Cockcroft-Gault equation): 47.4 (7.3-132.4) mL/min (15 days post-transplant, n=71); 54.6 (10.9-122.2) mL/min (1 month post-transplant, n=73); 59.0 (18.2-133.4) mL/min (2 months post-transplant, n=70); 60.7 (17.4-110.3) mL/min (6 months post-transplant, n=57) **Post-transplant time**: within 6 months post-transplant (data collected at 5 visits: transplant day, 15th day, 1st month, 2nd month, 6th month) **Graft rejection event** (n [percentage to the total number of patients]): 11 yes (14.1%)/67 no (85.9%)	**Induction treatment**: not specified **Documented medications**: MMF; tacrolimus; and prednisone **MMF dose** (oral administration): 1000 mg twice daily and adjusted based on clinical effects **Plasma MPA_t AUC_{0-12}** (median [range]): 47.9 (13.6-113.7) mg×h/L (15 days post-transplant, n=71); 48.9 (10.4-124.7) mg×h/L (1 month post-transplant, n=73); 54.6 (12.9-121.5) mg×h/L (2 months post-transplant, n=70); 40.2 (6.7-81.7) mg×h/L (6 months post-transplant, n=57) (HPLC-UV) **Plasma MPA_u AUC_{0-12}**: 0.9 (0.2-1.8) mg×h/L (15 days post-transplant, n=71); 0.9 (0.3-2.8) mg×h/L (1 month post-transplant, n=73); 1.0 (0.4-1.8) mg×h/L (2 months post-transplant, n=70); 0.7 (0.2-1.4) mg×h/L (6 months post-transplant, n=57) (HPLC-UV) **PBMC MPA_{cell} AUC_{0-12}**: 27.33 (3.1-444.8) mg×h/L (15 days post-transplant, n=71); 19.7 (1.5-191.0) mg×h/L (1 month post-transplant, n=73); 24.2 (3.4-407.2) mg×h/L (2 months post-transplant, n=70); 18.9 (2.7-319.9) mg×h/L (6 months post-transplant, n=57) (LC-MS/MS) **Tacrolimus dose** (immediate release formulation): 0.2 mg/kg per day (adjusted based on C_0 target of 5-15 ng/mL) **Prednisone dose**: not specified	**ABCB1 3435 C>T** (rs1045642) (CC/CT/TT)* (n [percentage to the total number of patients]): 30 (43.5%)/28 (40.6%)/11 (15.9%) **ABCC2 -24 C>T** (rs717620) (CC/CT/TT)*: 40 (58.0%)/23 (33.3%)/6 (8.7%) **SLCO1B3 334 T>G** (rs4149117) (AA/AG/GG)**: 50 (71.4%)/17 (24.3%)/3 (4.3%) Data were not available from *n=8 or **9 patients, where the most common genotypes were assumed by the authors	Riglet et al. [216]
Study design: single-center, open-label, non-randomized, observational	**Sex** (male/female): 11/16 **Age** (mean±SD): 47±13 years **Body weight**: 70±16 kg	**Induction treatment**: not specified	Not specified	Rong et al. [59]

Patient population	Patient demographic and biochemical parameters	Concurrent medication	Patient genomic data	Reference
study (with retrospective population pharmacokinetic analysis) **Population**: adult stable kidney transplant patients on *"corticosteroid-free"* regimes (n=27; *"corticosteroid-free"* defined as patients who *"had received two doses or fewer of intravenous methylprednisolone in the perioperative period and no subsequent oral corticosteroids"*).	**Height**: 165.1±9.2 cm **Albumin**: 42.8±3.9 g/L **SCr**: 102.4±27.0 µmol/L **eGFR**: 61.0±15.7 mL/min/1.73 m^2 **Post-transplant time**: 916±709 days	**Documented medications**: MMF (twice-daily formulation, ≥5 days, at steady-state); and tacrolimus (immediate-release, twice-daily formulation) **MMF dose** (oral administration; mean±SD**)**: 1352±492 mg/day **Plasma total MPA AUC_{0-12}**: 32.1±11.2 mg×h/L (HPLC-UV) **Plasma total MPA AUC_{0-12}/dose**: 53.0±27.1 mg×h/L/g **Plasma total MPAG AUC_{0-12}/dose**: 588.8±216.4 mg×h/L/g (HPLC-UV) **Plasma total AcMPAG C_0**: 0.54±0.66 mg/L (HPLC-UV) $f_{u,MPA}$: 1.7±0.6% **Tacrolimus dose** (immediate release formulation): 4.8±2.9 mg/day **Whole blood tacrolimus C_0**: 5.9±1.61 µg/L (LCMS) **Whole blood tacrolimus AUC_{0-12}**: 115.3±31.3 µg×h/L **Whole blood tacrolimus AUC_{0-12}/dose**: 53.3±24.9 µg×h/L/mg		
Study design: combination of *Study 1* (prospective observational study) [234] and *Study 2* (open-label, two-phase, sequential, bioequivalence study) [40] **Population**: Chinese adult kidney transplant patients (n=58; n=20 in *Study 1*, n=38 in *Study 2*)	<u>*Study 1*</u> **Sex** (male/female): 11/9 **Age** (median [range]): 36 (19-61) years **Body weight**: 55 (40-71) kg **Albumin**: 31 (20-43) g/L **Hemoglobin**: 86 (72-134) g/L **SCr**: 96 (50-443) µmol/L **GFR**: 76.12 (calculated by CKD-EPI equation) (11.17-123.8) mL/min **ALT**: 24 (10-390) U/L **AST**: 20 (7-139) U/L **Post-transplant time**: 10 (3-148) days <u>*Study 2*</u> **Sex** (male/female): 34/4	**Induction treatment**: not specified **Documented medications**: MMF; cyclosporine; and corticosteroids <u>*Study 1*</u> **MMF dose** (oral administration; median [range]): 1500 (750-2000) mg/day **Cyclosporine dose**: 300 (0-400) mg/day **Corticosteroid dose**: 20 (5-675) mg/day **Proton pump inhibitors** (n [percentage to the total number of *Study 1* patients): 6 (22%) **Aspirin**: 0 (0%) **Nifedipine**: 4 (15%)	Not specified	Sheng et al. [218]

Patient population	Patient demographic and biochemical parameters	Concurrent medication	Patient genomic data	Reference
	Age (median [range]): 38 (18-62) years **Body weight**: 65 (42-82.5) kg **Albumin**: 44.9 (32.3-50) g/L **Hemoglobin**: 139 (103-181) g/L **SCr**: 104.5 (76-152.9) µmol/L **GFR** (calculated by CKD-EPI equation): 74.42 (45.14-102.3) mL/min **ALT**: 18 (7-64) U/L **AST**: 24 (8.6-86) U/L **Post-transplant time**: 298 (70-3084) days	**Diltiazem**: 0 (0%) *Study 2* **MMF dose** (oral administration; median [range]): 1000 (1000-2000) mg/day **Cyclosporine dose**: 220 (100-400) mg/day **Corticosteroid dose**: 10 (3-20) mg/day **Aluminum hydroxide / sodium hydrogen carbonate** (n [percentage to the total number of *Study 2* patients): 5 (13%) **Aspirin**: 6 (16%) **Nifedipine**: 5 (13%) **Diltiazem**: 7 (18%) Plasma total MPA, unbound MPA, and total MPAG concentrations were quantified by HPLC		
Study design: prospective observational study **Population**: Chinese adult kidney transplant patients (n=191)	**Sex** (male/female): 142/49 **Age** (median [range]): 35 (18-64) years **Body weight**: 63 (35-91) kg **Albumin**: 44.6 (21.2-60.3) g/L **Platelet count**: 184 (28-492)×10^9/L **Hemoglobin**: 125 (58-205) g/L **CrCL** (calculated by Cockcroft-Gault equation): 68.5 (7.7-190.3) mL/min **Blood urea nitrogen**: 7.9 (2.9-61.8) mmol/L **ALT**: 19 (6-307) U/L **AST**: 20 (3-505) U/L **ALP**: 80 (9-633) U/L **GGT**: 29 (2-593) U/L **Total bilirubin**: 10.5 (1.7-45.9) µmol/L **Serum total bilirubin**: 109 (18-1007.3) µmol/L **Post-transplant time**: 136 (7-3204) days	**Induction treatment**: not specified **Documented medication**: MMF; tacrolimus; and methylprednisolone/prednisone **MMF dose** (oral administration; median [range]): 1000 (500-1500) mg/day **Tacrolimus dose** (immediate release formulation): 0.1 mg/kg per day (adjusted based on C_0 target of 10-15 ng/mL, ≤1-month post-transplant; and 5-10 ng/mL, >1-month post-transplant) **Tacrolimus C_0** (median [range]): 8.95 (1.30-40.80) ng/mL (assay not specified) **Methylprednisolone dose**: intravenous administration during surgery (500 mg), then oral	n=31 single nucleotide polymorphisms associated with UGT1A8, UGT1A9, UGT2B7, ABCB1, ABCC2, ABCG2, SLCO1B1, SLCO1B3, and HNF1A; see Table 2 in [219]	Yang et al. [219]

Patient population	Patient demographic and biochemical parameters	Concurrent medication	Patient genomic data	Reference
		prednisone at 10 mg per day after a rapid taper Plasma total MPA and MPAG concentrations were quantified by HPLC		
Study design: retrospective study **Population**: Chinese adult kidney transplant patients (n=118; n=79 in model development group, n=39 in model validation group) Data were extracted for model development group (n=79)	**Sex** (male/female): 47/32 **Age** (mean±SD [range]): 41.4±11.2 (18-68) years **Body weight**: 58.0±9.33 (39-82) kg **Albumin**: 33.5±5.9 (4.8-49) g/L **Hematocrit**: 0.256±0.057 (0.13-0.42) g/L **SCr**: 141.2±128.5 (61-915) μmol/L **Uric acid**: 286.1±103.3 (120-599) μmol/L **Blood urea nitrogen**: 9.84±9.36 (3.4-75.8) mmol/L **ALT**: 31.3±27.9 (8-114) IU/L **AST**: 22.1±10.9 (9-62) IU/L **ALP**: 62.7±102.3 (24-938) IU/L **GGT**: 38.9±28.8 (9-147) IU/L **Total bilirubin**: 14.6±6.55 (3.6-36) μmol/L **Post-transplant time**: 26.9±44.0 (2-209) days	**Induction treatment**: not specified **Documented medications**: MMF (1 g twice daily); cyclosporine or tacrolimus (n=72 and 7 in model development group, respectively); and corticosteroids **MMF dose** (oral administration; mean±SD [range]**)**: 900.1±177.0 (250-1250) mg every 12 hours (adjusted based on clinical assessment) **Plasma total MPA concentration**: 5.79±6.35 (0.25-47.46) mg/L (HPLC) **Cyclosporine dose**: 7 mg/kg/day given twice daily at the initial stage, then adjusted based on C_0 after 3 days post-transplant; 164.4±36.5 (25-250) mg every 12 hours **Cyclosporine C_0**: 212.3±102.0 (19.9-511.5) μg/L (assay not specified) **Tacrolimus dose** (immediate release formulation): 0.1 mg/kg/day at the initial stage, then adjusted based on C_0; 3.34±0.80 (2-4) mg every 12 hours **Tacrolimus C_0**: 8.17±3.50 (3.9-13.8) μg/L (assay not specified) **Methylprednisolone or prednisone dose**: intravenous administration during surgery (500 mg), then oral administration of prednisone at a tapered maintenance dose (5-20 mg per day); 23.4±26.9 (5-200) mg/day	**UGT2B7 211 G>T** (GG/GT/TT) (n, number of subjects): 32/40/7 **UGT1A9*22**: not specified	Yu et al. [139]

Patient population	Patient demographic and biochemical parameters	Concurrent medication	Patient genomic data	Reference
Adult non-renal transplant patients				
Study design: open label, single dose, three-period, fixed sequence study **Population**: Korean healthy adult male volunteers (n=17)	**Sex** (male/female): 17/0 **Age** (median [range]): 25 (20-42) years **Body weight**: 69.7 (57.4-88.3) kg **Height**: 173.4 (167.7-192.8) cm **Albumin**: 4.6 (4.2-4.9) g/dL **Hematocrit**: 44.6 (41.0-47.4) % **Hemoglobin**: 15.0 (13.6- 16.2) g/dL **SCr**: 0.86 (0.79-1.20) mg/dL **eGFR** (calculated by MDRD equation): 104.8 (74.1-122.3) mL/min/1.73 m^2 **Total bilirubin**: 0.8 (0.5-1.2) mg/dL **Absolute neutrophil count**: 3022 (1553-5858) /μL	**Induction treatment**: N/A **Dosage regimen**: first period-- MMF (1000 mg); second period--tacrolimus (5 mg, immediate release formulation); third period--the combination of MMF and tacrolimus (1000 mg and 5 mg, respectively); all treatments were single dose, oral administration with 240 mL water; one-week washout time between each period Plasma total MPA, MPAG, and AcMPAG concentrations were quantified by LC-MS/MS	**CYP3A4** (rs2242480, GG/GA/AA) (n, number of subjects): 13/3/1 **CYP3A5** (rs776746, GG/GA/AA): 13/3/1 **SLCO1B1** (rs2306283 GG/GA/AA): 10/6/1 **SLCO1B1** (rs4149056, TT/TC/CC): 11/6/0 **SLCO1B3** (rs4149117, GG/GT/TT): 8/5/4 **SLCO1B3** (rs7311358, AA/AG/GG): 8/5/4 **ABCC2** (rs717620, CC/CT/TT): 11/6/0 **ABCC2** (rs2273697, GG/GA/AA): 15/2/0 **ABCC2** (rs3740066, CC/CT/TT): 9/6/2 **UGT1A9** (rs3832043, TT/T-/--): 8/8/1 **UGT2B7** (rs7439366, CC/CT/TT): 7/9/1	Kim et al. [118]
Study design: prospective, observational study **Population**: adult hematopoietic stem cell transplant patients (n=34; n=26 in development dataset, n=8 in validation dataset [for Bayesian estimation])	*Development dataset* **Sex** (male/female): 20/6 **Age** (median [range]): 60 (41-70) years **Post-transplant time**: 14 (1-45) days *Validation dataset* **Sex** (male/female): 4/4 **Age** (median [range]): 50 (38-62) years **Post-transplant time**: 14 (1-27) days	**Conditioning treatment**: Not specified **Documented medications**: MMF; and cyclosporine *Development dataset* **MMF dose** (2-hour intravenous infusion administration, every 8 hourly; median [range]): 1000 (750-1250) mg *Validation dataset* **MMF dose** (2-hour intravenous infusion administration, every 8 hourly; median [range]): 1000 (1000-1250) mg	Not specified	Labriffe et al. [212]

Patient population	Patient demographic and biochemical parameters	Concurrent medication	Patient genomic data	Reference
		Plasma total MPA concentrations were quantified by HPLC-UV DAD		
Study design: prospective, observational study **Population**: Mexican lupus nephritis adult patients (n=40)	**Sex** (male/female): 7/33 **Age** (median [range]): 31 (18-59) years **Body weight**: 61.2 (41-97) kg **Height**: 1.60 (1.48-1.72) m **BMI**: 24.72 (16.9-37.3) kg/m^2 **Albumin**: N/A **Glucose**: 86 (69-117) mg/dL **Duration of disease**: 6.5 (0.16-30) years **SCr**: 0.86 (0.4-5.06) mg/dL **CrCL** (calculated by CKD-EPI equation, mean±SD): 88.7±45.5 mL/min **Hemoglobin**: 12.61±2.36 g/dL **Class of lupus nephritis** (n [percentage to the total number of patients]): 16 (40%) (Class I); 1 (2.5%) (Class II); 1 (2.5%) (Class III); 13 (32.5%) (Class IV); 6 (15%) (Class V); 3 (7.5%) (Class IV/V)	**Induction treatment**: N/A **Documented medications**: MMF (≥4 weeks, at steady-state); tacrolimus (n=9); calcitriol; chloroquine; and prednisone (n=32) **MMF dose** (oral administration; median [range]**)**: 1000 (500-2500) mg/day **Prednisone dose**: not specified Plasma total MPA concentrations were quantified by UPLC-MS/MS	**UGT1A8 518 C>G** (rs1042597) (CC/CG/GG) (frequency [%]): 16 (40%)/19 (47.5%)/5 (12.5%) **UGT1A9 -275 T>A** (rs6714486) (TT/TA/AA): 34 (85%)/5 (12.5%)/1 (2.5%) **UGT2B7 802 C>T** (rs7439366) (CC/CT/TT): 25 (62.5%)/14 (35%)/1 (2.5%) **ABCC2 -24 C>T** (rs717620) (CC/CT/TT): 29 (72.5%)/10 (25%)/1 (2.5%) **SLCO1B3 334 T>G** (rs4149117) (TT/TG/GG): 2 (5%)/10 (25%)/28 (70%)	Romano-Aguilar et al. [217]
Study design: prospective, observational study **Population**: Japanese adult hematopoietic stem cell (cord blood, bone marrow, or peripheral blood stem cell) transplant patients (n=49)	**Sex** (male/female): 34/15 **Stem cell source for transplantation** (cord blood/bone marrow stem cell/peripheral blood stem cell): 34/13/2 **Diarrhea post MPA administration** (1 week/3 weeks): 29/25 **Age** (median [range]): 49 (21-66) years **Body weight**: 61.9 (33.5-84.2) kg **Albumin**: 3.2 (1.6-4.1) mg/dL **CrCL**: 112 (20-262) mL/min **AST**: 18 (6-206) U/L **Total bilirubin**: 0.5 (0.2-2.1) mg/dL	**Conditioning treatment**: reduced intensity (n=23); myeloablative conditioning (n=26) **Documented medications**: MMF (30 mg/day/kg, given every 8 or 12 hourly); tacrolimus (immediate release formulation); and methotrexate (for bone marrow and peripheral blood stem cell transplant patients) **MMF dose** (oral administration; median [range]**)**: 1750 (1000-3000) mg/day	**UGT2B7 -842 G>A**(rs7439366) (wildtype/heterozygote/homozygote) (n, number of subjects): 20/21/6 **ABCC2 -24 C>T** (rs717620) (wildtype/heterozygote/homozygote) : 35/12/0 **IMPDH-1 -106 G>A** (rs2278294) (pre-transplant; wildtype/heterozygote/homozygote): 12/23/12 **IMPDH-1 -106 G>A** (rs2278294) (5-week post-transplant; wildtype/heterozygote/homozygote): 11/23/15 **IMPDH-1 125 G>A** (rs2278293) (pre-transplant;	Yoshimura et al. [220]

Patient population	Patient demographic and biochemical parameters	Concurrent medication	Patient genomic data	Reference
	C-reactive protein: 1.2 (0-25.1) mg/dL **Post-transplant time**: approximately 1 week and 3 weeks	**Body weight normalized MMF dose**: 30.3 (21.3-57.7) mg/day/kg Plasma total MPA, MPAG, and AcMPAG concentrations were quantified by LC-MS/MS	wildtype/heterozygote/homozygote): 18/20/9 **IMPDH-1 125 G>A** (rs2278293) (5-week post-transplant; wildtype/heterozygote/homozygote): 20/18/11 **IMPDH-2 3757 T>C** (rs11706052) (pre-transplant; wildtype/heterozygote/homozygote): 44/2/1 **IMPDH-2 3757 T>C** (rs11706052) (5-week post-transplant; wildtype/heterozygote/homozygote): 41/8/0	
Pediatric juvenile dermatomyositis				
Study design: retrospective study of routinely collected clinical data **Population**: pediatric patients with juvenile dermatomyositis (n=15, assumed Chinese ethnicity as the data collection was conducted in China)	**Sex** (male/female): 8/7 **Age** (median [range]): 7.4 (3.1-16.1) years **Body weight**: 22.3 (11.0-70.0) kg **Height**: 119 (94-168) cm **Albumin**: 41.4 (32.4-45.4) g/L **Globulin**: 30.1 (23.8-42.5) g/L **Hemoglobin**: 130 (110-147) g/L **CrCL** (calculated by Schwartz equation): 124 (91.0-177) mL/min/1.73 m^2 **Blood urea nitrogen**: 4.40 (2.70-7.40) mmol/L **Total bilirubin**: 5.05 (3.20-10.8) µmol/L **Direct bilirubin**: 1.60 (0.800-3.50) µmol/L	**Induction treatment**: N/A **Documented medications**: MMF dispersible tablet (≥10 days, at steady-state); intravenous immune globulin (n=7; dose not specified); cotrimoxazole (n=2; dose not specified) **MMF dose** (oral administration; median [range]**)**: 10.4 (5.44-22.7) mg/kg/dose or 21.8 (10.9-38.5) mg/kg/day Plasma total MPA concentrations were quantified by enzyme-multiplied immunoassay	Not specified	Wang et al. [211]

Abbreviation(s) [59, 117, 118, 139-141, 211-220]: *ABC transporter*, ATP-binding cassette transporter; *AcMPAG*, mycophenolic acid acyl glucuronide; *ALP*, alkaline phosphatase; *ALT*, alanine aminotransferase; *AST*, aspartate aminotransferase; *AUC*, area under the concentration-time curve; *BMI*, body mass index; C_0, trough concentration; *CKD-EPI equation*, chronic kidney disease epidemiology collaboration equation; *CrCL*, creatinine clearance; *CXCL-10*, interferon gamma inducible chemokine 10; *EC-MPS*, enteric-coated mycophenolate sodium; *eGFR*, estimated glomerular filtration rate; $f_{u,MPA}$, unbound fraction of mycophenolic

acid; *GFR*, glomerular filtration rate; *GGT*, γ-glutamyltransferase; *HLA*, human leukocyte antigen; *HNF1A*, hepatic nuclear factor 1 alpha; *HPLC-UV DAD*, high-performance liquid chromatography with ultraviolet diode-array detector; *HPLC-UV*, high-performance liquid chromatography with ultraviolet detection; *IMPDH*, inosine-5'-monophosphate dehydrogenase; *IQR*, interquartile range; *LCMS*, liquid chromatography with mass spectrometry; *LC-MS/MS*, liquid chromatography tandem mass spectrometry; *MDRD equation*, modification of diet in renal disease; *MMF*, mycophenolate mofetil; *MPA*, mycophenolic acid; MPA_{cell}, peripheral blood mononuclear cell intracellular mycophenolic acid; MPA_t, total mycophenolic acid; MPA_u, unbound mycophenolic acid; *N/A*, not applicable; *PBMC*, peripheral blood mononuclear cell; *SCr*, serum creatinine; *SD*, standard deviation; SLC, solute carrier family transporter; *UPLC-MS/MS*, ultra-performance liquid chromatography tandem mass spectrometry.

Table III-2 Summary information of model construction procedures, estimated parameters, and evaluation/validation approaches in MPA population pharmacokinetic models

Patient population	Population PK model construction procedures and estimated parameters	Evaluation/validation	Reference
Adult renal transplant patients			
Study design: prospective, observational study **Population**: Chinese adult kidney transplant patients (n=102)	**Sampling protocol**: 0, 0.5, 1, 1.5, 2, 4, 6, 8, 10, and 12 hours post dose (intense sampling protocol); 0, 1.5, 2 hours post dose (sparse sampling protocol 1); or 0, 1.5, 2, and 4 hours post dose (sparse sampling protocol 2); or 1.5, 2, and 4 hours post dose (sparse sampling protocol 3) **Software**: NONMEM version 6 **Algorithm**: FOCE **Screened covariates**: not specified ("pathophysiologic characteristics were evaluated", including albumin, body weight, cyclosporine co-administration, and others) **Significant covariates identification approach(es)**: forward inclusion and backward elimination Various covariate models were investigated as follow: $\theta=\theta_{pop}\times$(covariate); $\theta=\theta_{pop}+\beta\times$(covariate); $\theta=\theta_{pop}\times e^{(\beta\times[covariate])}$; $\theta=\theta_{pop}\times$(covariate/mean value of covariate)$^{\beta}$ **Structural model**: two-compartment, first-order absorption with lag time, and first-order elimination (built from 892 sample concentrations) **IIV model**: exponential **RUV model**: additive **Fixed effects parameter estimation** (parameter estimate [SE]): k_a (h^{-1}): 0.70 (0.121) t_{lag} (h): 0.91 (0.028) V_c/F (L): 26.3 (5.7) Q/F (L/h): 24.5 (3.97) V_p/F (L): 532 (351) CL/F (L/h): 11 (0.95) Calcineurin inhibitor (increased CL/F in cyclosporine co-administrated patients versus tacrolimus): 0.21 (coefficient for a covariate model; exact model not specified) (0.076)	**Internal evaluation**: goodness-of-fit plots, VPC plot, and bootstrap analysis	Chen et al. [141]

Patient population	Population PK model construction procedures and estimated parameters	Evaluation/validation	Reference
	IIV (parameter estimate, assumed to be %CV based on the utilized software [SE]): ω_k_a (%): 72.5 (not specified) ω_t_{lag} (%): 21.7 (not specified) ω_V_c/F (%): 120 (106) ω_Q/F (%): 82.6 (66.7) ω_V_p/F (%): 263 (362) ω_CL/F (%): 41.8 (21.3) **RUV** (parameter estimate [SE]): $\sigma_{additive}$ (%): 51.6 (20.8)		
Study design: prospective, randomized, multicenter, open-label, a part of the Symphony study [231, 232] **Population**: adult kidney transplant patients (within the first year post-transplant, n=56)	**Sampling protocol**: 0, 0.33, 0.67, 1.25, 2, 3, 4, 6, 8, 10, and 12 hours post dose **Software**: NONMEM version 7.3 and subroutine ADVAN13 **Algorithm**: SAEM/importance sampling **Screened covariates**: age, albumin, ALT, AST, body weight, bilirubin, comedications (i.e. cyclosporine vs. tacrolimus or sirolimus), CrCL, cyclosporine C_0, cyclosporine daily dose, genetic polymorphisms, hemoglobin, "low graft function" (as defined as CrCL<25 mL/min), MPAG C_0, post-transplant time, sex **Significant covariates identification approach(es)**: univariate regression analysis, forward inclusion and backward elimination (allometric, linear, exponential, or power relationships were tested) **Structural model**: five-compartment (1-MPA_u central; 2-MPA_b central; 3-MPA_u peripheral; 4-gallbaldder; 5-gut), 2046 MPA_u sample concentrations; and 2038 MPA_t sample concentrations, first-order absorption with lag time, and first-order elimination $MPA_t=(1+k_B)\times MPA_u$ **IIV model**: exponential **IOV model**: exponential **RUV model**: proportional **Fixed effects parameter estimation** (parameter estimate [RSE%]) (for MPA_u): k_a (h^{-1}): 1.41 (4.32) t_{lag} (h): 0.293 (1.51) V_c/F (L): 18.3 (19.18) Q/F (L/h): 749 (3.14) V_p/F (L): 29100 (8.59) CL/F (L/h):	**Internal evaluation**: goodness-of-fit plots, shrinkage values, prediction-corrected VPC plot, and posterior predictive check plot **External evaluation:** bias and imprecision of trough and AUC using external set	Colom et al. [140]

Patient population	Population PK model construction procedures and estimated parameters	Evaluation/validation	Reference
	θ_1×(1+cyclosporine×$\beta_{CL/F,cyclosporine}$) θ_1 (L/h): 410 (3.00) $\beta_{CL/F,cyclosporine}$: 0.594 (22.39) if co-administered with cyclosporine, "cyclosporine"=1; if co-administered with sirolimus or tacrolimus, "cyclosporine"=0; k_B: θ_2×(CrCL/59.51)^$\beta_{kB,CrCL}$ θ_2: 43.1 (3.13) $\beta_{kB,CrCL}$: 0.394 (10.66) k_{CG} (h^{-1}): 0.03 (fixed, if cyclosporine); 0.224 (fixed, if sirolimus or tacrolimus) k_{GB} (h^{-1}): 10 (fixed) T_{GB} (h): 1.5 (fixed) **IIV** (parameter estimate, %CV [RSE%]): ω_V_c/F (%): 99.45 (36.91) ω_CL/F (%): 26.81 (69.82) ω_k_B (%): 24.10 (29.95) **IOV** (parameter estimate, %CV [RSE%]): γ_V_c/F (%): 137.6 (22.00) γ_CL/F (%): 40.9 (52.10) **RUV** (parameter estimate [RSE%]): $\sigma_{unbound,MPA,proportional}$ (%): 58.30 (47.35) $\sigma_{total,MPA,proportional}$ (%): 46.90 (4.18)		
Study design: prospective, observational study **Population**: Korean adult stable kidney transplant patients (post-transplant time ≥ 6 months, n=32)	**Sampling protocol**: pre dose, 1, 2, 3, and 4 hours post dose **Software**: NONMEM version 7.3 and user defined subroutine ADVAN6 **Algorithm**: Laplacian with interaction and FOCE-I [118] **Screened covariates**: age, body weight, genetic polymorphisms, eGFR, hematocrit, and SCr **Significant covariates identification approach(es)**: stepwise covariate modeling, forward inclusion and backward elimination **Structural model**: six-compartment (1-gut; 2- MPA central; 3-MPA peripheral; 4-MPAG; 5-gallbladder/bile; 6-AcMPAG), first-order absorption, and first-order elimination of MPAG and AcMPAG (consisting of interaction effects between MPA and tacrolimus characterized by an inverse exponential equation) $CL_{Tacrolimus}$/F (L/h) =21.9×(e^[0.06×MPA concentration])$^{-1}$×1.49^CYP3A5	**Internal evaluation**: goodness-of-fit plots, shrinkage values, and prediction-corrected VPC plot	Kim et al. [117]

Patient population	Population PK model construction procedures and estimated parameters	Evaluation/validation	Reference
	if CYP3A5 expresser, "CYP3A5"=1; if not CYP3A5 expresser, "CYP3A5"=0 **IIV model**: exponential [118] **RUV model**: proportional (MPA and MPAG); combined (AcMPAG) **Fixed effects parameter estimation** (parameter estimate [RSE%]): k_a (h^{-1}): 2.29 (fixed) $V_{c,MPA}/F$ (L): 23.2 (33) k_{56} (h^{-1}): 1.75 (23) k_{65} (h^{-1}): 0.0089 (18) (k_{56} and k_{65}: intercompartment rate constants of MPA) CL_{MPA}/F (L/h): 3.27 (10) f_{MPA}: 0.85 (fixed) V_{MPAG}/F (L): 1.76 (15) SLCO1B3 334T>G (T carriers) on V_{MPAG}/F (fold increase): 1.2 (10) k_{70} (elimination rate constant of MPAG, h^{-1}): 0.103 (18) %EHC: 0.367 (fixed) V_{AcMPAG}/F (L): 13.9 (fixed) k_{90} (elimination rate constant of AcMPAG, h^{-1}): 0.407 (fixed) UGT2B7 802 C>T (CT and TT) on k_{59} (metabolism rate constant of MPA to AcMPAG, fold decrease): 0.812 (10) MTIME1 (h): 7.96 (fixed) MTIME2 (h): 1 (fixed) k_{84} (gallbladder emptying rate constant, h^{-1}): 18.4 (fixed) Interaction constant between MPA and tacrolimus: 0.06 (35) **IIV** (parameter estimate, %CV [RSE%]): $\omega\_V_{c,MPA}/F$ (%): 42.9 (19) ω_CL_{MPA}/F (%): 25.8 (17) **RUV** (parameter estimate [RSE%]): $\sigma_{MPA,proportional}$: 0.515 (7) $\sigma_{MPAG,proportional}$: 0.216 (8) $\sigma_{AcMPAG,additive}$: 0.0647 (23) $\sigma_{AcMPAG,proportional}$: 0.268 (8)		
Study design: multicenter, observational, Deterioration of Kidney Allograft Function (DeKAF) Genomics study **Population**: adult kidney or kidney-pancreas transplant patients (n=89)	**Sampling protocol**: 1, 2, 4, 6, 8, and 12 hours post dose **Software**: NONMEM version 7.2 **Algorithm**: FOCE-I **Screened covariates**: age, albumin, ALP, ALT, BMI, body weight, co-administration of calcineurin inhibitor (tacrolimus or cyclosporine), co-administration of proton pump inhibitor, co-administration of steroids, CrCL,	**Internal evaluation**: goodness-of-fit plots, shrinkage values, and VPC plot	Okour et al. [213]

Patient population	Population PK model construction procedures and estimated parameters	Evaluation/validation	Reference
	diabetes, donor age, donor sex, genetic polymorphisms with minor allele frequency ≥5%, height, number of HLA mismatch, post-transplant time, preemptive transplantation (without undergoing dialysis), primary cause of kidney disease, prior kidney transplant, SCr, sex, and serum bilirubin **Significant covariates identification approach(es)**: univariate regression analysis, stepwise backward elimination Co-administration of calcineurin inhibitor (tacrolimus or cyclosporine) was incorporated in the base model on CL_{uMPA}/F **Structural model**: five-compartment (1-gut; 2- MPA_u/MPA_t; 3-MPAG; 4-AcMPAG; 5-gallbladder), first-order absorption, and first-order elimination $MPA_t=MPA_u/f_{u,MPA}$ $\%EHC=k_{DG}/(k_{DG}+k_{30}) \times 100$ (k_{DG}-biliary circulation of MPAG into bile or gut; k_{30}- elimination rate constant of MPAG) **IIV model**: exponential **RUV model**: proportional **Fixed effects parameter estimation** (parameter estimate [RSE%]): k_a (h^{-1}): 2 (18.4) V_{uMPA}/F (L): 5630 (7.9) CL_{uMPA}/F (L/h): $\theta_1 \times (1+\beta_{CL,uMPA/F,CrCL} \times [CrCL-77.37]) \times 1.148$ [if on cyclosporine] θ_1 (L/h): 1450 (6.5) $\beta_{CL,uMPA/F,CrCL}$: 0.008 (30.5) $\beta_{CL,uMPA/F,cyclosporine}$: 0.15 (61.1) $f_{u,MPA}$: 0.024 (5.2) V_{MPAG}/F (L): 5.7 (4.9) CL_{MPAG}/F (L/h): $\theta_2 \times (1+\beta_{CL,MPAG/F,diabetes} \times$ "diabetes") $\times (1+\beta_{CL,MPAG/F,female} \times$ "female") $\times (1+\beta_{CL,MPAG/F,IMPDH-1,rs2288553,heterozygous} \times$ "IMPDH-1,rs2288553,heterozygous") θ_2 (L/h): 0.96 (4.8) $\beta_{CL,MPAG/F,diabetes}$: -0.19 (31.6) $\beta_{CL,MPAG/F,female}$: -0.18 (34.4) $\beta_{CL,MPAG/F,IMPDH-1,rs2288553,heterozygous}$: 0.33 (37.0) %EHC: $\theta_3 \times (1+\beta_{\%EHC,HNF1A,rs2393791,heterozygous\ or\ homozygous} \times$ "HNF1A,rs2393791,heterozygous or homozygous") θ_3: 0.37 (5.9) $\beta_{\%EHC,HNF1A,rs2393791,heterozygous\ or\ homozygous}$: 0.16 (55.0) V_{AcMPAG}/F (L): 17.9 (9.4) CL_{AcMPAG}/F (L/h): 32.3 (7.6)		

Patient population	Population PK model construction procedures and estimated parameters	Evaluation/validation	Reference
	MTIME1 (h): 7.7 (0.1) **IIV** (parameter estimate, assumed to be %CV based on the utilized software [RSE%]): ω_k_a (%): 108.6 (29.3) ω_V_{uMPA}/F (%): 35.5 (33.6) ω_CL_{uMPA}/F (%): 30.1 (25.4) $\omega\_f_{u,MPA}$ (%): 24 (24.3) ω_CL_{MPAG}/F (%): 27.2 (20.6) ω_%EHC (%): 27.8 (29.4) ω_CL_{AcMPAG}/F (%): 46.3 (19.8) **RUV** (parameter estimate [RSE%]): $\sigma_{unbound,MPA,proportional}$: 40.5 (9) $\sigma_{total,MPA,proportional}$: 35.8 (10.9) $\sigma_{MPAG,proportional}$: 12.2 (6) $\sigma_{AcMPAG,proportional}$: 24.8 (7.8)		
Study design: "European multicenter prospective observational" study **Population**: Caucasian adult kidney transplant patients (n=58)	**Sampling protocol**: 0, 0.5, 1, 1.5, 2, 3, 4, 6, 8, and 12 hours post dose (1st week); 0, 1.5, 2, and 4 hours post dose (1st month, 2nd month, 3rd month, 6th month) **Software**: NONMEM version 7.4.1 **Algorithm**: SAEM **Screened covariates**: age, cold ischemia time, diabetes mellitus, donor age, donor type (deceased or living), GFR, lymphocyte count, sex, and time of dialysis Dose was tested on CL/F and V_c/F **Significant covariates identification approach(es)**: linear, exponential, or power relationships were first tested utilizing stepwise forward inclusion and backward elimination approaches **Structural model**: two-compartment, first-order absorption with lag time, and first-order elimination (built from 1071 sample concentrations) **IIV model**: exponential **IOV model**: exponential **RUV model**: proportional **Fixed effects parameter estimation** (parameter estimate [RSE%]): k_a (h^{-1}): 1.79 (16) t_{lag} (h): 0.243 (29)	**Internal evaluation**: goodness-of-fit plots, shrinkage values, prediction-corrected VPC plot, bootstrap analysis, and NPDE plots	Quintairos et al. [214]

Patient population	Population PK model construction procedures and estimated parameters	Evaluation/validation	Reference
	V_c/F (L/70 kg): 106 (22) Q/F (L/h/70 kg): 37.1 (9) V_p/F (L/70 kg): 800 (fixed) CL/F (L/h/70 kg): 11.8 (5) **IIV** (parameter estimate, assumed to be %CV based on the utilized software [RSE%]): ω_V_c/F (%): 133.8 (15) ω_V_p/F (%): 164.6 (14) ω_CL/F (%): 34.9 (11) **RUV** (parameter estimate [RSE%]): $\sigma_{proportional}$: 55.3 (6) Allometric exponent of 0.75 was applied to CL/F and Q/F Allometric exponent of 1 was applied to V_c/F and V_p/F No significant covariates were included		
Study design: prospective, observational study **Population**: Mexican adult kidney transplant patients (n=77, n=42 *de novo* patients)	**Sampling protocol**: pre dose, up to 11 hours post dose (number of samples collected varied between patients) **Software**: NONMEM version 7.4 **Algorithm**: FOCE-I **Screened covariates**: age, blood urea nitrogen, BMI, body weight, CrCL, donor type (deceased or living), genetic polymorphisms, glucose, height, hematocrit, hemoglobin, post-transplant time, SCr, sex, tacrolimus level, urea, and uric acid **Significant covariates identification approach(es)**: stepwise forward inclusion and backward elimination **Structural model**: two-compartment model, first-order absorption, and first-order elimination (built from 343 sample concentrations) **IIV model**: exponential **RUV model**: proportional **Fixed effects parameter estimation** (parameter estimate [RSE%]): k_a (h^{-1}): 1.67 (16) V_c/F (L): θ_1×blood urea nitrogen×$\beta_{Vc/F,UGT1A9}$ θ_1 (L): 1.54 (9) if UGT1A9-TT, $\beta_{Vc/F,UGT1A9}$=1;	**Internal evaluation**: goodness-of-fit plots, shrinkage values, prediction-corrected VPC plot, and bootstrap analysis	Reséndiz-Galván et al. [215]

Patient population	Population PK model construction procedures and estimated parameters	Evaluation/validation	Reference
	if UGT1A9-TA, $\beta_{Vc/F,UGT1A9}$=8.89 (21); Q/F (L/h): 29.9 (14) V_p/F (L): 658 (18) CL/F (L/h): $\theta_2 \times e^{(\beta_{CL/F,SCr} \times SCr) \times (1+\beta_{CL/F,uric\ acid} \times uric\ acid)}$ θ_2 (L/h): 2.17 (16) $\beta_{CL/F,SCr}$: 0.09 (23) $\beta_{CL/F,uric\ acid}$: 0.66 (12) **IIV** (parameter estimate, assumed to be %CV based on the utilized software [RSE%]): ω_V_c/F (%): 137.5 (105.8) ω_CL/F (%): 71.1 (56.5) **RUV** (parameter estimate [RSE%]): $\sigma_{proportional}$ (%): 41.8 (41.8)		
Study design: CIMTRE (a prospective, observational) study **Population**: adult kidney transplant patients (n=78)	**Sampling protocol**: pre dose, 0.5, and 2 hours post dose (transplant day, 15th day, 2nd month, 6th month); pre dose, 0.5, 1, 2, 4, 6, and 8 hours post dose (1st month) **Software**: Monolix version 2016 **Algorithm**: SAEM **Screened covariates**: age and body weight on CL_u/F, Q_u/F, CL_{in}/F, $V_{c,u}$/F, and $V_{p,u}$/F; CrCL on CL_u/F and $V_{p,u}$/F; albumin on k_B; genetic polymorphism on $V_{c,u}$/F, CL_u/F, CL_{out}/F and V_{cell}/F **Significant covariates identification approach(es)**: univariate regression analyses, stepwise backward elimination approach **Structural model**: three-compartment (1-MPA_u central; 2-MPA_u peripheral; 3-MPA_{cell}), zero-order absorption, first-order elimination (built from 1931 sample concentrations) $MPA_t=(1+k_B) \times MPA_u$ **IIV model**: exponential **IOV model**: exponential **RUV model**: proportional **Fixed effects parameter estimation** (parameter estimate [RSE%]): Tk0 (h): 1.29 (8) $V_{c,u}$/F (L): 1620 (9) Q_u/F (L/h): 2040 (15) $V_{p,u}$/F (L): $\theta_1 \times$(CrCL/median value based on post-transplant period)$^{\beta_{Vpu/F,CrCL}} \times e^{IIV} \times e^{IOV}$	**Internal evaluation**: goodness-of-fit plots, shrinkage values, and prediction-corrected VPC plot	Riglet et al. [216]

Patient population	Population PK model construction procedures and estimated parameters	Evaluation/validation	Reference
	θ_1 (L): 19,400 (29) $\beta_{Vpu/F,CrCL}$: -1.03 (40) CL_u/F (L/h): $\theta_2 \times (CrCL/54.81)^{\beta_{CLu/F,CrCL}} \times e^{IIV} \times e^{IOV}$ θ_2 (L/h): 900 (4) $\beta_{CLu/F,CrCL}$: 0.38 (19) k_B: $\theta_3 \times$(albumin/median value based on post-transplant period)$^{\beta_{kB,albumin}} \times e^{IIV} \times e^{IOV}$ θ_3: 56.5 (3) $\beta_{kB,albumin}$: 1.46 (15) $f_{u,MPA}$ (%): 1.8 (3) CL_{in}/F (L/h): 1200 (12) CL_{out}/F (L/h): $\theta_4 \times$("ABCB1")$^{\beta_{CLout/F,ABCB1}} \times e^{IIV} \times e^{IOV}$ θ_4 (L/h): 43.8 (16) $\beta_{CLout/F,ABCB1}$: -0.64 (44) ABCB1 *TT3435* with lower estimate compared to *CT3435* and *CC3435* V_{cell}/F (L): 1980 (18) **IIV** (parameter estimate, %CV [RSE%]): ω_Tk0 (%): 44 (15) ω_$V_{p,u}/F$ (%): 70 (15) ω_CL_u/F (%): 30 (11) ω_kB (%): 16 (53) ω_CLout/F (%): 70 (12) **IOV** (parameter estimate, %CV [RSE%]): γ_Tk0 (%): 60 (7) γ_Q_u/F (%): 153 (9) γ_$V_{p,u}/F$ (%): 89 (20) γ_CL_u/F (%): 23 (9) γ_CL_{out}/F (%): 91 (6) γ_V_{cell}/F (%): 33 (11) **RUV** (parameter estimate [RSE%]): $\sigma_{unbound\ MPA,proportional}$ (%): 28 (6) $\sigma_{total\ MPA,proportional}$ (%): 29 (4) $\sigma_{PBMC\ intracellular\ MPA,proportional}$ (%): 39 (16)		
Study design: single-center, open-label, non-randomized, observational study (with retrospective population pharmacokinetic analysis) **Population**: adult stable kidney transplant patients on *"corticosteroid-free"* regimes (n=27;	**Sampling protocol**: pre dose, 0.5, 1, 2, 3, 4, 6, 8, 10, and 12 hours post dose **Software**: Monolix version 2018R1 **Algorithm**: SAEM **Screened covariates**: AcMPAG C_0, age, albumin, body weight, $f_{u,MPA}$, eGFR, height, MPAG AUC_{0-12}, post-transplant time, SCr, sex, tacrolimus AUC_{0-12},	**Internal evaluation**: goodness-of-fit plots, shrinkage values, prediction-corrected VPC plot, and bootstrap analysis	Rong et al. [59]

Patient population	Population PK model construction procedures and estimated parameters	Evaluation/validation	Reference
"corticosteroid-free" defined as patients who *"had received two doses or fewer of intravenous methylprednisolone in the perioperative period and no subsequent oral corticosteroids"*).	tacrolimus C_0, tacrolimus dose, and the ratio of MPAG AUC_{0-12} to MPA AUC_{0-12} **Significant covariates identification approach(es)**: Pearson's correlation test, the Wald test, forward inclusion and backward elimination **Structural model**: two-compartment, first-order absorption with lag time, and first-order elimination **IIV model**: exponential **RUV model**: combined **Fixed effects parameter estimation** (parameter estimate [RSE%]): k_a (h^{-1}): 1.98 (41.5) t_{lag} (h): 0.162 (fixed) V_c/F (L): 25 (28.5) Q/F (L/h): 36.7 (12.6) V_p/F (L): 607 (35.4) CL/F (L/h): $\theta_1 \times (\text{AcMPAG } C_0)^{\beta_{CL/F,AcMPAG\ C0}} \times (AUC_{MPAG}/AUC_{MPA})^{\beta_{CL/F,AUC\ ratio}} \times e^{IIV}$ θ_1 (L/h): 2.87 (42.3) $\beta_{CL/F,AcMPAG\ C0}$: -0.09 (45) $\beta_{CL/F,AUC\ ratio}$: 0.68 (23.2) **IIV** (parameter estimate, SD [RSE%]): ω_k_a: 0.99 (26.9) ω_t_{lag}: 1.08 (29.8) ω_V_c/F: 0.18 (127) ω_Q/F: 0.27 (94.8) ω_V_p/F: 1.08 (19.8) ω_CL/F: 0.23 (27.6) **RUV** (parameter estimate [RSE%]): $\sigma_{additive}$ (mg/L): 0.08 (82.1) $\sigma_{proportional}$: 0.32 (12.6)		
Study design: combination of *Study 1* (prospective observational study) [234] and *Study 2* (open-label, two-phase, sequential, bioequivalence study) [40] **Population**: Chinese adult kidney transplant patients (n=58; n=20 in *Study 1*, n=38 in *Study 2*)	**Sampling protocol**: 0, 0.5, 1, 1.5, 2, 3, 4, 6, 8, 10, and 12 hours post dose *[Study 1]*; 0, 0.5, 1, 1.5, 2, 2.5, 3, 4, 6, 9, 10, and 12 hours post dose *[Study 2]* **Software**: NONMEM version 7.4 **Algorithm**: SAEM	**Internal evaluation**: goodness-of-fit plots, shrinkage values, prediction-corrected VPC plot, bootstrap analysis, and posterior predictive check	Sheng et al. [218]

Patient population	Population PK model construction procedures and estimated parameters	Evaluation/validation	Reference
	Screened covariates: age, albumin, ALT, AST, body weight, co-administration of antacids, cyclosporine daily dose, GFR, hemoglobin, post-transplant time, SCr, and sex **Significant covariates identification approach(es)**: stepwise forward inclusion and backward elimination **Structural model**: five-compartment (1-gut; 2-MPA_u central; 3-MPA_u peripheral; 4-$MPAG_u$; 5-gallbladder; 740 MPA_u sample concentrations, 741 MPA_t sample concentrations; and 734 $MPAG_t$ sample concentrations), first-order absorption with lag time, and first-order elimination $MPA_t=(1+k_B)\times MPA_u$ The unbound fraction of MPAG was fixed at 18% $\%EHC=k_{GG}/(k_{GG}+k_{e0}) \times 100$ **IIV model**: exponential **RUV model**: exponential **Fixed effects parameter estimation** (parameter estimate [RSE%]): k_a (h^{-1}): 1.35 (11.1) t_{lag} (h): 0.447 (16.8) $V_{c,uMPA}/F$ (L): 718 (18.5) Q_{uMPA}/F (L/h): $\theta_1\times(\text{body weight}/70)^{\wedge}\beta_{Q,uMPA/F,body\ weight}$ θ_1 (L/h): 857 (11) $\beta_{Q,uMPA/F,body\ weight}$: 2.11 (24.2) $V_{p,uMPA}/F$ (L): 34300 (fixed) CL_{uMPA}/F (L/h): 851 (7.1) k_B (h^{-1}): $\theta_2\times(\text{albumin}/40)$ θ_2 (h^{-1}): 53.4 (2.3) $V_{c,uMPAG}/F$ (L): 29.9 (7.7) CL_{uMPAG}/F (L/h): $\theta_3\times(GFR/80)^{\wedge}\beta_{CL,uMPAG/F,GFR}$ θ_3 (L/h): 5.71 (4.4) $\beta_{CL,uMPAG/F,GFR}$: 0.865 (11.6) %EHC: 5.53 (26.2) **Fixed effects parameter estimation for total MPA and MPAG** (parameter estimate *generated by multiplying unbound concentration parameters by 1.84% and 18% for MPA and MPAG, respectively)*: $V_{c,tMPA}/F$ (L): 13.21 Q_{tMPA}/F (L/h): 15.77 $V_{p,tMPA}/F$ (L): 631.12 CL_{tMPA}/F (L/h): 15.66		

Patient population	Population PK model construction procedures and estimated parameters	Evaluation/validation	Reference
	$V_{c,tMPAG}$/F (L): 5.38 CL_{tMPAG}/F (L/h): 1.03 **IIV** (parameter estimate, %CV [RSE%]): ω_k_a (%): 46.5 (20.4) ω_t_{lag} (%): 107.7 (15.8) ω_$V_{c,uMPA}$/F (%): 80.0 (25.2) ω_Q_{uMPA}/F (%): 45.5 (16.2) ω_CL_{uMPA}/F (%): 51.0 (11.0) ω_k_B (%): 10.0 (fixed) ω_$V_{c,uMPAG}$/F (%): 48.4 (25.0) ω_CL_{uMPAG}/F (%): 31.8 (13.3) ω_%EHC (%): 61.6 (55.9) **RUV** (parameter estimate [RSE%]): $\sigma_{unbound\ MPA,exponential}$ (%): 47.0 (3.5) $\sigma_{total\ MPA,exponential}$ (%): 45.9 (3.7) $\sigma_{unbound\ MPAG,exponential}$ (%): 22.0 (3.1)		
Study design: prospective observational study **Population**: Chinese adult kidney transplant patients (n=191)	**Sampling protocol**: 0, 0.5, 1, 2, 4, 6, 8, and 12 hours post morning dose (dense sampling); 10 hours post dose (sparse sampling) **Software**: NONMEM version 7.4.0 **Algorithm**: FOCE-I **Screened covariates**: albumin, body weight, CrCL, post-transplant time, UGT1A9 I399 T>C (rs2741049), UGT2B7 1059 C>G (rs4292394), UGT2B7 1062 C>T (rs4348159), and UGT2B7 735 A>G (rs28365062) on CL/F of MPA; body weight, CrCL, SLCO1B1 571 T>C (rs4149057), and UGT1A9 855+9535 T>A (rs17868323) on CL/F of MPAG **Significant covariates identification approach(es)**: stepwise forward inclusion and backward elimination (linear and power relationships were tested for continuous covariates; scale models were tested for categorical covariates) **Structural model**: four-compartment (1-gut; 2-MPA central; 3-MPA peripheral; 4-MPAG central; 917 MPA sample concentrations, 740 MPAG sample concentrations), first-order absorption, and first-order elimination **IIV model**: exponential **RUV model**: proportional **Fixed effects parameter estimation** (parameter estimate [RSE%]): k_a (h^{-1}): 1.22 (8.9)	**Internal evaluation**: goodness-of-fit plots, shrinkage values, prediction-corrected VPC plot, and bootstrap analysis	Yang et al. [219]

Patient population	Population PK model construction procedures and estimated parameters	Evaluation/validation	Reference

	$V_{c,MPA}$/F (L): 30.8 (10.6)
	Q_{MPA}/F (L/h): 18.1 (fixed)
	$V_{p,MPA}$/F (L): 114 (11.5)
	CL_{MPA}/F (L/h):
	$\theta_1 \times (\beta_{CL,MPA/F,post\text{-}transplant\ time})$^"post-transplant time"×(albumin/42)^$\beta_{CL,MPA/F,albumin}$
	θ_1 (L/h): 10.9 (3.6)
	$\beta_{CL,MPA/F,post\text{-}transplant\ time}$: 0.83 (2.6)
	if post-transplant time > 1 month, "post-transplant time"=1;
	if post-transplant time < 1 month, "post-transplant time"=0;
	$\beta_{CL,MPA/F,albumin}$: -0.362 (22)
	$V_{c,MPAG}$/F (L): 6.06 (21.3)
	CL_{MPAG}/F (L/h):
	$\theta_2 \times (CrCL/72)^{\beta_{CL,MPAG/F,CrCL}}$
	θ_2 (L/h): 1.09 (3.8)
	$\beta_{CL,MPAG/F,CrCL}$: 0.374 (5.7)
	
	IIV (parameter estimate, assumed to be %CV based on the utilized software [RSE%]):
	ω_CL_{MPA}/F (%): 28.2 (8)
	ω_CL_{MPAG}/F (%): 31.9 (7)
	
	RUV (%CV, [RSE%]):
	$\sigma_{MPA,proportional}$ (%): 46.9 (3.1)
	$\sigma_{MPAG,proportional}$ (%): 39.2 (2.8)		

Study design: retrospective study **Population**: Chinese adult kidney transplant patients (n=118; n=79 in model development group, n=39 in model validation group) Data were extracted for model development group (n=79)	**Sampling protocol**: pre dose, 0.5, 1, 1.5, 2, 4, 6, 8, 10, and 12 hours post dose (intense sampling protocol); 0, 0.5, 2 hours post dose (sparse sampling protocol 1); or 0, 0.5, 2, and 8 hours post dose (sparse sampling protocol 2) **Software**: NONMEM version 5.1.1 and subroutine ADVAN4 or 6 **Algorithm**: FO and FOCE **Screened covariates**: age, albumin, ALP, ALT, AST, blood urea nitrogen, body weight, co-administration of corticosteroids, cyclosporine or tacrolimus concentrations, genetic polymorphisms, GGT, hematocrit, SCr, sex, total bilirubin, and uric acid **Significant covariates identification approach(es)**: stepwise forward inclusion and backward elimination **Structural model**: two-compartment, first-order absorption, and first-order elimination (built from 783 sample concentrations) **IIV model**: exponential	**Internal evaluation**: goodness-of-fit plots	Yu et al. [139]

Patient population	Population PK model construction procedures and estimated parameters	Evaluation/validation	Reference
	RUV model: combined **Fixed effects parameter estimation** (parameter estimate [SE%]): k_a (h^{-1}): 1.89 (22.7) V_c/F (L): $\theta_1+\beta_{Vc/F,UGT2B7}\times$UGT2B7 genotype θ_1 (L): 14.7 (15.3) $\beta_{Vc/F,UGT2B7}$: 7.72 (6.85) k_{12} (h^{-1}): 0.915 (23.7) k_{21} (h^{-1}): 0.059 (15.8) V_p/F (L): not specified CL/F (L/h): $\theta_2+\beta_{CL/F,body\ weight}\times$body weight$+\beta_{CL/F,SCr}\times$SCr θ_2 (L/h): 7.98 (7.51) $\beta_{CL/F,body\ weight}$: 0.0916 (12.7) $\beta_{CL/F,SCr}$: 0.0417 (34.3) **IIV** (parameter estimate, %CV): ω_k_a (%): 51.3 ω_V_c/F (%): 21.3 ω_k_{12} (%): 31.2 ω_k_{21} (%): 138 ω_CL/F (%): 34.2 **IOV** (parameter estimate, %CV): γ_V_c/F (%): 13.7 γ_CL/F (%): 13.7 **RUV** (parameter estimate): $\sigma_{additive}$ (mg/L): 0.15 $\sigma_{proportional}$ (%): 15.8		
Adult non-renal transplant patients			
Study design: open label, single dose, three-period, fixed sequence study **Population**: Korean healthy adult male volunteers (n=17)	**Sampling protocol**: pre dose, 1, 2, 4, 6, 8, 12, 24, 48, 72, and 168 hours post dose **Software**: NONMEM version 7.3 and user defined subroutine ADVAN6 **Algorithm**: Laplacian with interaction or FOCE-I **Screened covariates**: absolute neutrophil count, age, albumin, body weight, genetic polymorphisms, GFR, height, hematocrit, hemoglobin, SCr, and total bilirubin were tested on V/F and CL/F	**Internal evaluation**: goodness-of-fit plots, shrinkage values, and prediction-corrected VPC plot	Kim et al. [118]

Patient population	Population PK model construction procedures and estimated parameters	Evaluation/validation	Reference
	Significant covariates identification approach(es): stepwise covariate modeling, forward inclusion and backward elimination **Structural model**: six-compartment (1-gut; 2-MPA central; 3-MPA peripheral; 4-MPAG; 5-gallbladder/bile; 6-AcMPAG), first-order absorption, and first-order elimination (consisting of an interaction effect from MPA to tacrolimus characterized by an inverse exponential equation) $CL_{Tacrolimus}$/F (L/h) =13.8×(e^[0.0294×MPA concentration])$^{-1}$×1.48^CYP3A5 if CYP3A5 expresser, "CYP3A5"=1; if not CYP3A5 expresser, "CYP3A5"=0 %EHC=$k_{78}/(k_{78}+k_{70})$ ×100 (k_{78}-biliary circulation of MPAG into bile; k_{70}- elimination rate constant of MPAG) **IIV model**: exponential **RUV model**: proportional (MPA and AcMPAG); combined (MPAG) **Fixed effects parameter estimation in the "integrated model"** (parameter estimate [RSE%]): k_a (h^{-1}): 2.29 (9) $V_{c,MPA}$/F (L): 19.7 (11) k_{56} (h^{-1}): 1.12 (10) k_{65} (h^{-1}): 0.131 (7) (k_{56} and k_{65}: intercompartment rate constants of MPA) CL_{MPA}/F (L/h): 16.3 (7) f_{MPA}: 0.85 (fixed) V_{MPAG}/F (L): 5.83 (7) k_{70} (elimination rate constant of MPAG, h^{-1}): 0.251 (13) %EHC: 0.367 (15) V_{AcMPAG}/F (L): 23 (fixed) k_{90} (elimination rate constant of AcMPAG, h^{-1}): 2.15 (fixed) MTIME1 (h): 7.96 (1) MTIME2 (h): 1 (fixed) k_{84} (gallbladder emptying rate constant, h^{-1}): 18.4 (160) Interaction constant between MPA and tacrolimus: 0.0294 (154) **IIV** (parameter estimate, %CV [RSE%]): ω_ka (%): 56.6 (28) ω_$V_{c,MPA}$/F (%): 18.2 (27) ω_CL_{MPA}/F (%): 18.7 (32) ω_%EHC (%): 35.5 (18) **RUV** (parameter estimate [RSE%]): $\sigma_{MPA,proportional}$: 0.524 (7)		

Patient population	Population PK model construction procedures and estimated parameters	Evaluation/validation	Reference
	$\sigma_{MPAG,additive}$: 0.104 (31) $\sigma_{MPAG,proportional}$: 0.237 (12) $\sigma_{AcMPAG,proportional}$: 0.651 (22)		
Study design: prospective, observational study **Population**: adult hematopoietic stem cell transplant patients (n=34; n=26 in development dataset, n=8 in validation dataset [for Bayesian estimation])	**Sampling protocol**: pre dose, 0, 0.33, 1, 2, 3, and 4 hours post dose **Software**: ITSIM and Pmetrics **Algorithm**: iterative two-stage Bayesian parametric method (ITSIM) and non-parametric approach (Pmetrics) **Covariate analysis**: no covariates analyses were conducted **Structural model**: one-compartment, sum of two gamma distributions, and first-order elimination (built from 48 concentration-time profiles) **RUV model**: combined **Double gamma absorption model** [197]: $V_{abs}(t)=F\times D\times[r\times f_1(t)+(1-r)\times f_2(t)]$ $f(t)=\frac{{b_i}^{a_i}}{\Gamma(a_i)}\times t^{a_i-1}\exp(-b_i t)$ $V_{abs}(t)$-the absorption rate at time t; F-bioavailability; D-dose administered; r-the dose fraction absorbed from the faster (i.e. 1st) gamma function; f(t)-absorption time profile; a_i-the shape of the gamma function; b_i-the scale of the gamma function; Γ-the gamma function **Population PK parameter estimation** (parameter estimate median [range]): <u>*Parametric approach (ITSIM)*</u> Estimated C_0 after a theoretical 100 mg dose administration (mg/L): 0.06 (0.01-0.15) FAIV (mg/L): 2.80 (1.02-5.90) a_1: 12.3 (3.2-25.2) a_2: 16.6 (1.0-25.1) b_1 (h^{-1}): 25.1 (11.7-47.9) b_2 (h^{-1}): 10.2 (3.1-15.2) r: 0.37 (0.01-0.60) α (h^{-1}): 1.93 (0.91-3.27) <u>*Nonparametric approach (Pmetrics)*</u>	**Internal evaluation**: goodness-of-fit plots, VPC plot, and Bayesian estimation utilizing an internally-split dataset	Labriffe et al. [212]

Patient population	Population PK model construction procedures and estimated parameters	Evaluation/validation	Reference
	Estimated C_0 after a theoretical 100 mg dose administration (mg/L): 0.06 (0.01-0.18) FAIV (mg/L): 3.33 (0.80-9.95) a_1: 23.3 (1.3-52.7) a_2: 25.7 (3.2-49.3) b_1 (h^{-1}): 43.1 (0.5-98.5) b_2 (h^{-1}): 19.8 (4.8-49.8) r: 0.45 (0.02-1.00) α (h^{-1}): 1.93 (0.87-4.98) **RUV** (parameter estimate): $\sigma_{additive}$: 0.25 $\sigma_{proportional}$: 0.03 $\sigma_{additive,Pmetrics}$: 0.02		
Study design: prospective, observational study **Population**: Mexican lupus nephritis adult patients (n=40)	**Sampling protocol**: pre dose, 0.3, 0.6, 1, 1.5, 2, 4, 6 hours post dose **Software**: NONMEM version 7.3, subroutines ADVAN1, TRANS2, ADVAN3, TRANS4 **Algorithm**: FOCE-I **Screened covariates**: age, ALP, ALT, AST, blood urea nitrogen, BMI, body weight, co-administrations (e.g. calcitriol, chloroquine, folic acid, losartan, omeprazole, paracetamol, prednisone, and tacrolimus), co-morbidities (e.g. diabetes, epilepsy, hypertension, and hypothyroidism), CrCL, genetic polymorphisms, glucose, height, hematocrit, hemoglobin, lupus nephritis class, SCr, sex, and urea **approach(es)**: stepwise forward selection (via allometric, linear, or exponential models) and backward elimination **Structural model**: two-compartment model, first-order absorption, and first-order elimination (built from 294 sample concentrations) **IIV model**: exponential **RUV model**: proportional **Fixed effects parameter estimation** (parameter estimate [RSE%]): k_a (h^{-1}): 1.28 (8) V_c/F (L/kg): 0.381×body weight (14) Q/F (L/h): 20.3 (18) V_p/F (L): 768 (13) CL/F (L/h): $\theta_1 \times (CrCL/80)^{\beta_{CL/F,CrCL}} \times (1+\beta_{CL/F,prednisone})$ θ_1 (L/h): 15.4 (11) $\beta_{CL/F,CrCL}$: 0.633 (18)	**Internal evaluation**: goodness-of-fit plots, shrinkage values, VPC plot, and bootstrap analysis	Romano-Aguilar et al. [217]

Patient population	Population PK model construction procedures and estimated parameters	Evaluation/validation	Reference
	$\beta_{CL/F,prednisone}$: 0.583 (35) **IIV** (parameter estimate, assumed to be %CV based on the utilized software [RSE%]): ω_V_c/F (%): 71.7 (19) ω_Q/F (%): 86.6 (18) ω_CL/F (%): 33.6 (13) **RUV** (parameter estimate [RSE%]): $\sigma_{proportional}$ (%): 42.89 (9)		
Study design: prospective, observational study **Population**: Japanese adult hematopoietic stem cell (cord blood, bone marrow, or peripheral blood stem cell) transplant patients (n=49)	**Sampling protocol**: 1, 2, 4, and 8 hours post dose (and 12 hours post dose for only one patient) **Software**: NONMEM (version not specified) **Algorithm**: not specified **Screened covariates**: age, albumin, AST, body weight, diarrhea, genetic polymorphisms, MMF dose, sex, stem cell source, total bilirubin, and CrCL **Significant covariates identification approach(es)**: stepwise forward inclusion and backward elimination **Structural model**: four-compartment (1-gut; 2- MPA; 3-MPAG; 4-AcMPAG; 522 sample concentrations for MPA, MPAG, and AcMPAG), first-order absorption, and first-order elimination **IIV model**: exponential **IOV model**: exponential **RUV model**: proportional **Fixed effects parameter estimation** (parameter estimate [RSE%]): k_a (h^{-1}): 1.18 (39.5) F: 1 (fixed) V_{MPA} (L): $\theta_1 \times (albumin/3.2)^{\wedge}\beta_{V,MPA,albumin}$ θ_1 (L): 41.5 (17.3) $\beta_{V,MPA,albumin}$: -3.71 (29.4) CL_{MPA} (L/h): $\theta_2 \times (albumin/3.2)^{\wedge}\beta_{CL,MPA,albumin}$ θ_2 (L/h): 44.5 (17.0) $\beta_{CL,MPA,albumin}$: -1.02 (43.2) V_{MPAG} (L): 17.3 (17.1) CL_{MPAG} (L/h): $\theta_3 \times (CrCL/112)^{\wedge}\beta_{CL,MPAG,CrCL}$	**Internal evaluation**: goodness-of-fit plots, shrinkage values, and prediction-corrected VPC plot	Yoshimura et al. [220]

Patient population	Population PK model construction procedures and estimated parameters	Evaluation/validation	Reference
	θ_3 (L/h): 2.46 (14.8) $\beta_{CL,MPAG,CrCL}$: 0.730 (69.7) V_{AcMPAG} (L): 5.50 (15.7) CL_{AcMPAG} (L/h): $\theta_4 \times (CrCL/112)^{\wedge}\beta_{CL,AcMPAG,CrCL}$ θ_4 (L/h): 3.17 (16.7) $\beta_{CL,AcMPAG,CrCL}$: 0.537 (17.0) k_{EHC} (h^{-1}): $\theta_5 \times (\beta_{k,EHC,diarrhea})^{\wedge}$"diarrhea" θ_5 (h^{-1}): 0.0635 (23.8) $\beta_{k,EHC,diarrhea}$: 0.375 (30.7) if patients with diarrhea, "diarrhea"=1; if patients without diarrhea, "diarrhea"=0 **IIV** (parameter estimate, assumed to be %CV based on the utilized software [RSE%]): ω_F (%): 84.9 (6.06) ω_V_{MPA} (%): 56.9 (38.3) **IOV** (parameter estimate, assumed to be %CV based on the utilized software [RSE%]): γ_k_a (%): 97.9 (24.6) γ_F (%): 19.1 (47.7) γ_CL_{MPAG} (%): 33.0 (22.7) γ_CL_{AcMPAG} (%): 42.0 (23.8) γ_k_{EHC} (%): 91.2 (21.9) **RUV** (parameter estimate [RSE%]): $\sigma_{MPA,proportional}$ (%): 40.9 (12.4) $\sigma_{MPAG,proportional}$ (%): 18.8 (10.5) $\sigma_{AcMPAG,proportional}$ (%): 31.4 (6.53)		
Pediatric juvenile dermatomyositis			
Study design: retrospective study of routinely collected clinical data **Population**: pediatric patients with juvenile dermatomyositis (n=15, assumed Chinese ethnicity as the data collection was conducted in China)	**Sampling protocol**: 0.5 hour pre dose, 0.33, 1 and 2 hours post dose **Software**: Monolix version 2019R1 **Algorithm**: not specified (assumed SAEM as the only option in Monolix) **Screened covariates**: age, albumin, blood urea nitrogen, body weight, co-administered cotrimoxazole, co-administered intravenous immune globulin, direct bilirubin, globulin, height, hemoglobin, sex, and total bilirubin	**Internal evaluation**: goodness-of-fit plots, shrinkage values, NPDE plots, VPC plot, and bootstrap analysis	Wang et al. [211]

Patient population	Population PK model construction procedures and estimated parameters	Evaluation/validation	Reference
	Significant covariates identification approach(es): Correlational analysis (Pearson's test and Wald's test), stepwise forward inclusion and backward elimination **Structural model**: two-compartment, first-order absorption with lag time, and first-order elimination (built from 80 sample concentrations) **IIV model**: exponential **RUV model**: combined **Fixed effects parameter estimation** (parameter estimate [RSE%]): k_a (h^{-1}): 4.10 (fixed) t_{lag} (h): 0.303 (18.1) V_c/F (L): 13.6 (30.7) Q/F (L/h): 19.5 (12.3) V_p/F (L): $\theta_1 \times e^{\wedge}$("cotrimoxazole"$\times \beta_{Vp/F,cotrimoxazole}$) θ_1 (L): 978 (8.42) $\beta_{Vp/F,cotrimoxazole}$: -0.709 (22.9) if co-administered with cotrimoxazole, "cotrimoxazole"=1; if not co-administered, "cotrimoxazole"=0 CL/F (L/h): $\theta_2 \times (height/123)^{\wedge}\beta_{CL/F,height}$ θ_2 (L/h): 1.27 (9.73) $\beta_{CL/F,height}$: 7.52 (6.18) **IIV** (parameter estimate, SD [RSE%]): ω_t_{lag}: 0.598 (37.3) ω_V_c/F: 1.11 (22.7) ω_Q/F: 0.366 (38.4) ω_V_p/F: 0.0928 (63.1) ω_CL/F: 0.0772 (75.7) **RUV** (parameter estimate [RSE%]): $\sigma_{additive}$: 0.348 (48.8) $\sigma_{proportional}$: 0.216 (41.3)		

Abbreviation(s) [59, 117, 118, 139-141, 211-220]: *%EHC*, percentage of mycophenolic acid glucuronide recycled into the systemic circulation (represents the process of enterohepatic circulation); a_1 *and* a_2, the shape of the gamma function; *ABC transporter*, ATP-binding cassette transporter; *AcMPAG*, mycophenolic acid acyl glucuronide; *ALP*, alkaline phosphatase; *ALT*, alanine aminotransferase; *AST*, aspartate aminotransferase; *AUC*, area under the concentration-time curve; b_1 *and* b_2, the scale of the gamma function; *BMI*, body mass index; C_0, trough concentration; *CL/F*, apparent total clearance; CL_{in}/F, apparent clearance of unbound mycophenolic acid distributed from central compartment into peripheral blood mononuclear cell compartment; CL_{out}/F, apparent clearance of mycophenolic acid

eliminated from peripheral blood mononuclear cell compartment; *CrCL*, creatinine clearance; *CV*, coefficient of variation; *eGFR*, estimated glomerular filtration rate; *EHC*, enterohepatic circulation; *F*, bioavailability; *FAIV*, the maximum concentration following an intravenous bolus administration of a unit dose; f_{MPA}, metabolism fraction from mycophenolic acid to mycophenolic acid glucuronide; *FO*, first-order algorithm; *FOCE*, first-order conditional estimation algorithm; *FOCE-I*, first-order conditional estimation with interaction algorithm; $f_{u,MPA}$, unbound fraction of mycophenolic acid; *GFR*, glomerular filtration rate; *GGT*, γ-glutamyltransferase; *HLA*, human leukocyte antigen; *HNF1A*, hepatic nuclear factor 1 alpha; *IIV*, inter-individual variability; *IMPDH*, inosine-5'-monophosphate dehydrogenase; *IOV*, inter-occasion variability; k_{12} *and* k_{21}, rate constants of intercompartment distribution; k_a, absorption rate constant; k_B, rate constant of protein binding (represents number of binding sites); k_{CG}, transport rate constant from mycophenolic acid central compartment to gallbladder; k_{e0}, elimination rate constant from unbound mycophenolic acid glucuronide central compartment; k_{EHC}, first-order rate constant of enterohepatic circulation; k_{GB}, rate constant of gallbladder emptying; k_{GG}, transport rate constant from unbound mycophenolic acid glucuronide central compartment to gallbladder; *MMF*, mycophenolate mofetil; *MPA*, mycophenolic acid; MPA_{cell}, peripheral blood mononuclear cell intracellular mycophenolic acid; $MPAG_u$, unbound mycophenolic acid glucuronide; MPA_t, total mycophenolic acid; MPA_u, unbound mycophenolic acid; *MTIME1*, meal time; *MTIME2 or* T_{GB}, gallbladder emptying duration; *NPDE*, normalized prediction distribution errors; *PBMC*, peripheral blood mononuclear cell; *PK*, pharmacokinetic; *Q/F*, apparent intercompartmental clearance; *r*, the dose fraction absorbed from the first gamma function; *RSE*, relative standard error; *RUV*, residual unexplained variability; *SAEM*, stochastic approximation expectation maximization estimation method, *SCr*, serum creatinine; *SD*, standard deviation; *SE*, standard error; SLC, solute carrier family transporter; *Tk0*, zero-order absorption rate constant; t_{lag}, lag time; *UGT*, uridine 5'-diphospho-glucuronosyltransferase; V_c/F, apparent volume of distribution in the central compartment; V_p/F, apparent volume of distribution in the peripheral compartment; *VPC*, visual predictive check; α, elimination parameter; β, covariate effect; θ, population pharmacokinetic fixed-effect parameter estimate.

Chapter IV. Population pharmacokinetics of mycophenolic acid in paediatric patients[4]

Prologue:

In addition to adult populations (Chapter III [25]), MPA is also widely used in pediatric kidney transplant patients and sometimes prescribed for additional indications. Compared to adults, pediatric patients may exhibit unique clinical pharmacology of MPA. The aim of this chapter was to provide an up-to-date critique of the currently available pediatric MPA population pharmacokinetic models, focusing on the clinical factors influencing the pharmacokinetics/dynamics of MPA. In addition, the optimal modeling approaches and the clinical utility of population kinetic models in the precision dosing of MPA were also discussed.

[4] This chapter is already published in a peer-reviewed journal. **Rong Y**, Jun H, Kiang TKL. Population pharmacokinetics of mycophenolic acid in paediatric patients. *British Journal of Clinical Pharmacology*. 2021 Apr;87(4):1730-1757. doi: 10.1111/bcp.14590.

Acknowledgement: Reprinted by permission from John Wiley and Sons: British Journal of Clinical Pharmacology. Population pharmacokinetics of mycophenolic acid in paediatric patients. **Rong Y**, Jun H, Kiang TKL. License number: 5222171041671 (2021).

Abstract

Mycophenolic acid (MPA) is widely used in paediatric kidney transplant patients and sometimes prescribed for additional indications. Population pharmacokinetic or pharmacodynamic modelling has been frequently used to characterize the fixed, random, and covariate effects of MPA in adult patients. However, MPA population pharmacokinetic data in the paediatric population have not been systematically summarized. The objective of this narrative review was to provide an up-to-date critique of currently available paediatric MPA population pharmacokinetic models, with emphases on modelling techniques, pharmacological findings, and clinical relevance. PubMed and EMBASE were searched from inception of database to May, 2020, where a total of 11 studies have been identified representing kidney transplant (n=4), liver transplant (n=1), haematopoietic stem cell transplant (n=1), idiopathic nephrotic syndrome (n=2), systemic lupus erythematosus (n=2), and a combined population consisted of kidney, liver, and haematopoietic stem cell transplant patients (n=1). Critical analyses were provided in the context of MPA absorption, distribution, metabolism, excretion, and bioavailability in this paediatric database. Comparisons to adult patients were also provided. With respect to clinical utility, Bayesian estimation models (n=6) with acceptable accuracy and precision for MPA exposure determination have also been identified and systematically evaluated. Overall, our analyses have identified unique features of MPA clinical pharmacology in the paediatric population, while recognizing several gaps that still warrant further investigations. This review can be used by pharmacologists and clinicians for improving MPA pharmacokinetic-pharmacodynamic modelling and patient care.

1. Introduction

Mycophenolic acid (MPA) is widely used in paediatric kidney transplant patients [235-237], and sometimes prescribed for glomerulonephritis [238], lupus nephritis [239], nephrotic syndrome [240], heart transplantation, liver transplantation, haematopoietic stem cell transplantation, rheumatic disease, and autoimmune disorders [241]. MPA is a reversible inhibitor of inosine monophosphate dehydrogenase (IMPDH), reducing the synthesis of guanine nucleotide and the proliferation of T- and B-lymphocytes [180]. The gastrointestinal, infectious, and haematological adverse effects of MPA are severe and frequently occurring, where associations to the exposure of MPA have been documented [61]. Population pharmacokinetic or pharmacodynamic modelling has been frequently used to characterize the fixed, random, and covariate effects of MPA. To our knowledge, more than 40 MPA population-based models are available in the adult population to date (e.g. [59, 114, 118, 139-141, 143-162, 182, 186, 188, 190-194, 199, 201, 202, 204, 206, 212, 220]), which have been reviewed by various investigators (e.g. [10, 30, 31, 62, 71-73]). However, the population pharmacokinetic data of MPA in the paediatric population have yet to be systematically summarized. The objective of this narrative review was to provide an up-to-date critique of currently available paediatric MPA population pharmacokinetic models, with specific emphases on modelling techniques, pharmacological findings, and clinical relevancies.

2. Methodology

PubMed and EMBASE were searched using combinations of the following terms: *mycophenolate, mycophenolic acid, paediatric, child, population pharmacokinetics, non-linear*

mixed-effect modelling, iterative two-stage, and *NONMEM.* No search limits were implemented other than the exclusion of non-English articles. Results up to May 24th, 2020 were included for assessment. The title, abstract, and the reference list of the identified papers were manually screened. Papers were only included for evaluation if i) they were peer reviewed, ii) they reported population pharmacokinetic data of MPA, and iii) the majority of enrolled-subjects were classified as paediatric patients (i.e. mean or median age in the study population < 18 years old). The exclusion criteria are presented in Figure IV-1, which summarizes the process for obtaining the final list of papers included in this review.

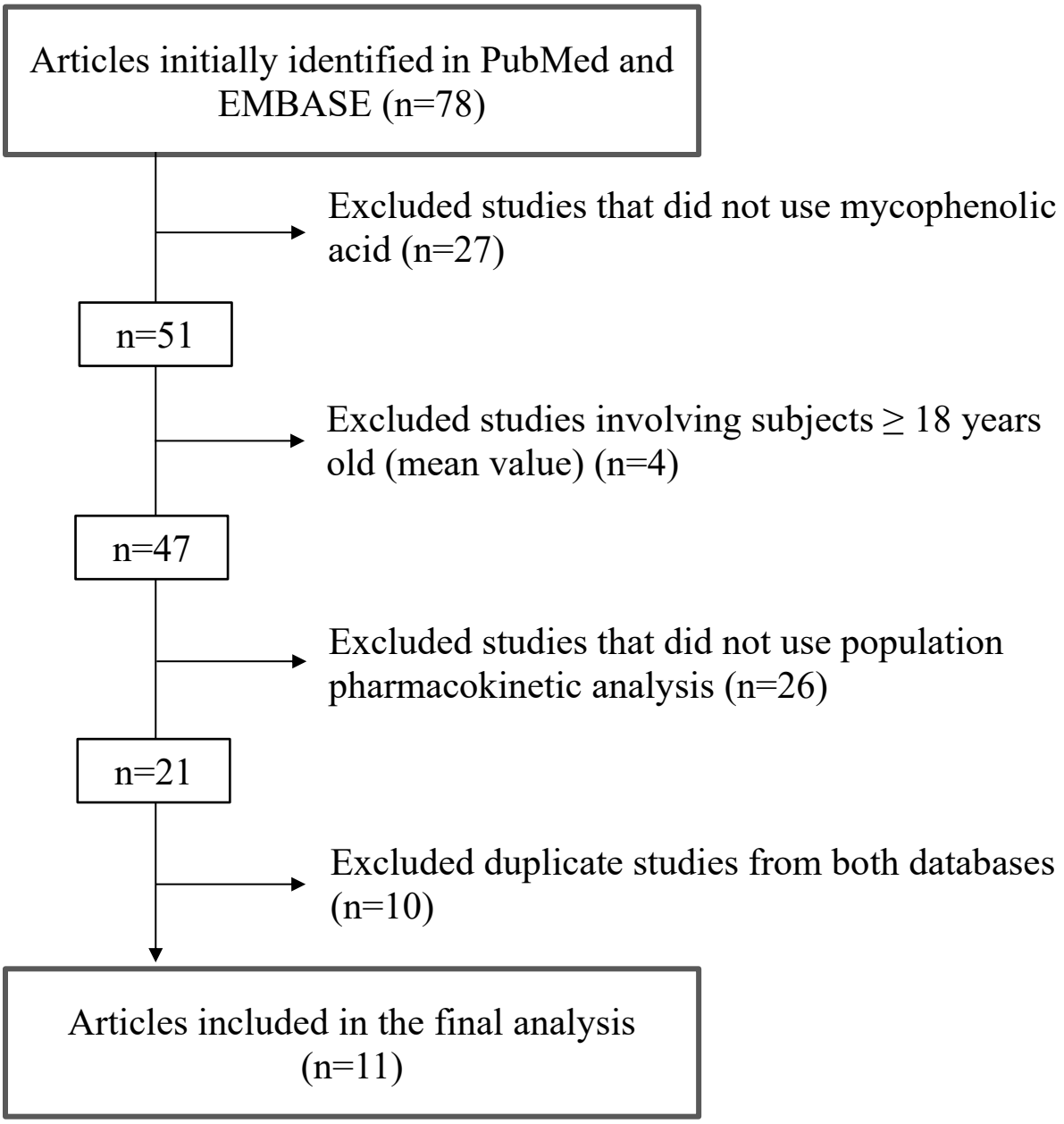

Figure IV-1 Article selection, inclusion/exclusion flow chart

3. Results

Table IV-1 summarizes the 11 studies included in this review based on chronological order [183, 185, 189, 196, 198, 200, 203, 207, 209, 210, 221]. The data are discussed in the context of the fundamental pharmacokinetic processes (i.e. absorption, distribution, metabolism, excretion, and bioavailability). Specifically, the modelling approaches, the biological relevancies of the population estimates, and comparisons to the adult population are critically evaluated. The clinical utilities of Bayesian-predictive models for MPA exposure are also discussed (summarized in Table IV-2). The overall limitations and literature gaps are summarized in Table IV-3. Overall, the majority (i.e. ~73%) of the included studies utilized NONMEM software, and the remaining used BigWinPops [198], WinNonMix [183], or in-house programs [200, 207]. First-order conditional estimation with interaction was the most common algorithm [185, 189, 198, 209, 221], but first-order estimation, which can occasionally generate inaccurate estimates of random effects [68], has also been utilized [196]. Although the majority of the studies used parametric modelling, the nonparametric adaptive grid algorithm was implemented by Prémaud et al. [198], which was evidently more suitable for studies containing outlier data. None of the studies used stochastic approximation expectation-maximization algorithm, which has been demonstrated to be equally accurate as first-order conditional estimation with interaction in some simulations (e.g. [242]). Furthermore, various combinations of standard evaluation/validation approaches had been utilized (i.e. goodness-of-fit plots, visual predictive checks, and bootstrapping analyses) [183, 185, 189, 196, 198, 203, 207, 209, 210, 221]. External or simulated-external validation of the predictability of the developed models using Bayesian estimation was conducted in a select number of studies, which will be discussed in a separate section below [183, 196, 198, 200, 207, 209].

3.1. Absorption

MPA is the active moiety of mycophenolate mofetil (MMF, immediate-release formulation) or enteric-coated mycophenolate sodium (EC-MPS, delayed-release formulation), but different pharmacokinetic characteristics are exhibited by the two formulations [10]. As only MMF was administered in the included studies [183, 185, 189, 196, 198, 200, 203, 207, 209, 210, 221], this formulation will be the focus of our discussion. MMF can be administered orally or intravenously [16] and is fully hydrolysed by carboxylesterases to MPA [243]. MPA is rapidly and extensively absorbed from the intestine into the portal circulation, where it is transported to the liver and subjected to first pass hepatic metabolism [30, 51]. There is also the possibility of complex, double absorption due to pH variations along the gastrointestinal tract [244]. In addition, MPA can undergo entero-hepatic recirculation whereby its conjugated metabolites (i.e. MPA glucuronide [MPAG] or MPA acyl glucuronide [AcMPAG]) are subjected to biliary-intestinal recycling mediated by the multidrug resistance-associated protein 2 (MRP-2) transporter [47] and intestinal microflora [245]. The entero-hepatic recirculation process and/or double absorption are responsible for the secondary peaks sometimes observed in the MPA concentration-time profiles in the clinic [30, 244]. To characterize the complex absorption of MPA, various population pharmacokinetic models with entero-hepatic recirculation or double absorption have been summarized by Sherwin et al. [30].

Of the 11 papers reviewed, six studies utilized a simple absorption model (i.e. first order without/with lag time) [183, 189, 196, 198, 209, 221], while complex absorption models were applied in five papers (i.e. multiple transit compartment absorption [185, 203], Erlang distribution [210], and gamma absorption with two parallel routes [200, 207]) (Table IV-1). In addition, one study included genetic polymorphism data on the MRP-2 transporter known to be involved in the

entero-hepatic recirculation process [209]. The most commonly used pharmacokinetic parameter to describe the absorption process was the absorption rate constant (k_a), where the reported values showed significant between subject variability (BSV) ranging from 43.1-308.4% [183, 185, 196, 198, 210, 221]. In studies with evident secondary peaks (e.g. [200, 203, 207]), complex mechanistic or empiric absorption models incorporating entero-hepatic recirculation and/or double absorption appeared to have provided better physiological fitting. In addition, Prémaud et al. compared parametric and nonparametric adaptive grid modelling approaches to estimate the absorption parameters, where higher k_a estimates were obtained from the nonparametric method [198]. This observation, according to the authors, was possibly attributed to the better ability of the non-parametric model to capture outliers typically associated with the large variability known to be observed with MPA [10, 29]. Furthermore, some studies have fixed k_a values based on previously published estimates [189, 203] possibly due to insufficient sampling at the early post-dose periods. This observation is similar to various adult models (e.g. reviewed in [10, 30, 31, 62, 71-73]) that have also taken the absorption process "out of the modelling" (i.e. by fixing) due to insufficient sample collection or complexity of MPA absorption.

The k_a values reported in the current dataset of paediatric population pharmacokinetic studies were highly variable ranging from 0.39-5.21 h^{-1} (Table IV-1) [183, 185, 189, 196, 198, 203, 209, 221]. Specifically, the lowest k_a (i.e. 0.39 h^{-1}) reported by Zeng et al. might be explained, according to the authors [221], by the majority of the sample population (i.e. 60.5%) receiving bone marrow transplantation, which may have required conditioning regimens that can potentially lead to gastrointestinal toxicities [221, 246]. On the contrary, Prémaud et al. reported the highest k_a (i.e. 5.21 h^{-1}) using nonparametric adaptive grid modelling in a population prescribed the capsule or suspension formulations of MMF [198]. As MMF oral suspension is known to be absorbed

faster compared to the capsules [64], formulation could possibly explain the increased k_a estimate in this study [198]. However, neither the effects of transplant type or formulation on MPA absorption could be verified in the entire paediatric dataset, because k_a was fixed in the only other study conducted in allogenic haematopoietic stem transplant patients [189], no other study used the suspension formulation (Table IV-1), and covariate analyses were not conducted on these parameters (Table IV-1) [183, 185, 189, 196, 198, 200, 203, 207, 209, 210, 221]. Other pharmacokinetic estimates describing the absorption process, including mean transit time, lag time, constant transfer rate between absorption compartments, mean absorption time of the absorption phase i, and standard deviation of absorption time, were not comparable across our dataset due to the limited sample size (Table IV-1) [185, 196, 198, 200, 207, 209, 210].

The ~13-fold variability of BSV associated with the k_a of MPA in this dataset might be explained by covariate effects. The only statistically significant covariate identified affecting k_a in the current paediatric dataset was the negative association between age and k_a in Barau et al. [183], which may be related to the ontogeny of intestinal MRP-2 where younger patients are more likely to exhibit relatively immature expression of the efflux transporter [226]. However, polymorphisms in MRP-2 (i.e. -24C>T, 1249G>A, 3563T>A, and 3972C>T) were not identified as significant covariates affecting the pharmacokinetic parameters of MPA in paediatric renal transplant recipients [210], although this could be a false negative finding attributed to the low minor allele frequencies reported in the study. Other than Barau et al., no obvious trends of the effects of age on k_a were observed in our dataset (Table IV-1) [183, 185, 189, 196, 198, 200, 203, 207, 209, 210, 221]. In addition, the k_a values were generally comparable between paediatric and adult patients (~0.92-6.28 h^{-1}) (e.g. reviewed in [10, 30, 31, 62, 71-73]), but this could be attributed to the large BSV and between occasion variability (BOV) observed in the pharmacokinetics of MPA in both

populations [10, 30, 31, 62, 71-73, 183, 185, 189, 196, 198, 200, 203, 207, 209, 210, 221], potentially masking a quantitative difference. These findings indicate that further characterizations are needed to determine the effects of age on MPA absorption.

Furthermore, the variability of k_a in this dataset could also be explained by concurrent medications. As examples, cyclosporine is known to inhibit the hepato-biliary MRP-2 transporter [45, 46, 48] and reduce the entero-hepatic recirculation, hence indirectly affecting the absorption of MPA; concomitant antibiotics can affect MPA entero-hepatic recirculation by changing the intestinal microbiota [10]; co-administration of gastric acid suppression agents (e.g. aluminium/magnesium hydroxide [247] or proton pump inhibitors [248]) can affect MPA (double/re) absorption by chelation [247] or alkalization [248]; and food intake can delay gastric emptying and influence the (double/re) absorption rate of MPA (e.g. [247]). With respect to entero-hepatic recirculation and double absorption, no clear trends were observed in our dataset on these variables because secondary peaks were only modelled in three of the 11 studies [200, 203, 207]. Additional studies had either shown secondary peaks in concentration-time profiles or commented in the text [183, 185, 196, 198, 210], but it was not possible to assess covariate effects on the entero-hepatic recirculation or double absorption process because these secondary peaks were not incorporated in their structural models. As well, information on antibiotics, gastrointestinal medications, or food consumption were relatively limited (Table IV-1) [183, 185, 189, 196, 198, 200, 203, 207, 209, 210, 221].

In summary, large variabilities in the population k_a estimates were observed in paediatric patients. A variety of approaches were utilized to model MPA absorption in this population, where complex models were more suitable for datasets illustrating evidence of secondary peaks (Table IV-1) [183, 185, 189, 196, 198, 200, 203, 207, 209, 210, 221]. Only age was identified as a

significant covariate on absorption [183], whereas factors such as transplant type and formulation would require further systematic analyses (e.g. rigorous covariate modelling) to determine their effects on the absorption of MPA in paediatric populations.

3.2. Distribution

After absorption, MPA is primarily distributed into the plasma compartment and extensively bound to serum albumin [249]. MPAG, the primary metabolite of MPA, is also highly bound (i.e. 82%) to serum albumin in stable kidney transplant patients [37], which could displace the binding of MPA [250]. In general, the distribution of MPA can be controlled by factors affecting serum albumin concentrations or binding characteristics.

Total MPA distribution was modelled in 10 out of 11 studies, with only Kim et al. characterizing unbound MPA concentrations (Table IV-1) [183, 185, 189, 196, 198, 200, 203, 207, 209, 210, 221]. Similar to the adult data (e.g. reviewed in [10, 30, 31, 62, 71-73]), the best approach for modelling distribution was using the two-compartmental model, which was iteratively derived in many studies in this dataset [185, 196, 198, 221]. In those papers that utilized a one-compartmental model [183, 200, 207], it was also not apparent if other compartmental models had been considered. In contrast to empiric models, Sherwin et al. utilized a multi-compartmental mechanistic model to characterize the distribution of MPAG (discussed above in the section on Absorption), but MPA distribution was still based on a two-compartmental configuration [203]. Both parametric and nonparametric approaches generated comparable volume of distribution values [198], suggesting no apparent advantage of particular modelling methodologies. Moreover, only one study in this dataset had attempted to incorporate serum albumin directly into the structural model, in comparison to treating albumin as a covariate (i.e. similar to the approach

utilized in some adult studies, e.g. [140]), but that particular model by Zeng et al. was not usable due to large standard errors [221].

The apparent volumes of distribution in the central compartment (V_c/F, equivalent to V_d/F in one-compartmental models) and peripheral compartment (V_p/F) are commonly used to describe the distribution of MPA. The reported range of V_c/F (or V_d/F) in this paediatric dataset was 4.75-64.7 l (Table IV-1) [183, 185, 189, 196, 198, 200, 203, 207, 209, 210, 221]. The lowest reported value (i.e. 4.75 l) was documented in a kidney transplant study, where body weight was found to be linearly associated with V_c/F [196]. However, the relationship between body weight and V_c/F was identified to be exponential in nature in another paediatric kidney transplant study [210], indicating a non-linear relationship. The generally positive correlation between V_c/F (or V_d/F) and body weight was also observed in healthy adult volunteers (e.g. [194]) or adult patients (e.g. [151]), and may hypothesized to be related to increased fat tissue [251] facilitating distribution of the lipophilic MPA. On the other hand, the highest estimate of V_c/F (or V_d/F) reported in Barau et al. (i.e. 64.7 l) was inversely correlated with post-transplant time in paediatric liver transplant recipients [183]. According to the authors, increased free fraction of MPA immediately post-liver transplant as a result of low albumin and high bilirubin may have led to elevated V_c/F [183]. However, post-transplant time (or disease duration) was not found a significant covariate in other studies reviewed in this paper (Table IV-1) [189, 203, 207, 209, 210, 221].

Population estimates for V_p/F (ranging from 35-411 l [185, 221]) were available in six studies utilizing two-compartmental models [185, 189, 203, 209, 210, 221]. In general, V_p/F values were directly proportional to V_c/F, but significant covariates were not identified on V_p/F in this dataset (Table IV-1) [183, 185, 189, 196, 198, 200, 203, 207, 209, 210, 221]. Overall, V_c/F and V_p/F values in paediatric patients were lower than adults (V_c/F: 0.653-90 l, V_p/F: 60.3-4910 l [10,

30, 31, 62, 71-73]), which may be explained by the potential influence of body weight as discussed above. This is evident by the lack of significant difference between weight-normalized V_c/F (V_d/F) or V_p/F in this paediatric dataset compared to the adult control data in the literature [10, 30, 31, 62, 71-73]. Furthermore, in models utilizing two-compartmental models, rates of MPA transfer between central and peripheral compartments were characterized by apparent inter-compartmental clearance (Q/F, e.g. [185, 189, 203, 209, 210, 221]) or inter-compartment transfer constants (i.e. k_{12} and k_{21}, e.g. [196, 198]). Similar to other distribution parameters reported in this review, these fixed estimates were highly variable (BSV: 26.6-207.83%, Table IV-1), and covariate modelling have not been conducted to explain the variabilities (Table IV-1) [183, 185, 189, 196, 198, 200, 203, 207, 209, 210, 221].

Serum albumin has been known to affect the distribution and free fraction of MPA (e.g. [10, 161, 183, 220]), but albumin was not incorporated into the final structural or covariate models in the reviewed paediatric studies (Table IV-1) [183, 185, 189, 196, 198, 200, 203, 207, 209, 210, 221]. The apparent lack of albumin effect on MPA distribution in this dataset might be explained by the relatively narrow distribution of albumin concentrations, the majority of studies reporting normal albumin levels, and the possibility that there could be an albumin threshold value below which the probability of increased MPA free fraction is higher as observed in an adult kidney transplant population with hypoalbuminemia (e.g. [50]). Theoretically, MPA distribution could also be affected by co-medications, metabolites (e.g. MPAG), or endogenous uremic toxins that displace the protein binding of MPA [10], but no apparent relationships on these variables were observed in this dataset (Table IV-1) [183, 185, 189, 196, 198, 200, 203, 207, 209, 210, 221]. In general, the limited free MPA fraction data available in the two paediatric studies [183, 221] were

comparable to the adult data [10], but further experimental values are required for a more robust qualitative analysis.

In summary, MPA distribution is best modelled by two-compartmental models. The estimated V_c/F (or V_d/F) and V_p/F values were highly variable across different studies in this paediatric dataset, which may potentially be explained by body weight and post-transplantation time [183, 196, 210]. Further population pharmacokinetic analyses incorporating the effects of serum albumin (i.e. directly into the structural model, e.g. [140]) and MPA metabolites could better improve the characterization of MPA distribution in paediatric patients.

3.3. Metabolism and excretion

The metabolism of MPA is primarily mediated by hepatic uridine 5'-diphospho-glucuronosyltransferase (UGT) enzymes in the formation of two conjugated metabolites: i) MPAG, the major (i.e. exhibiting up to 100 fold higher concentration in plasma than MPA) but pharmacologically inactive; and ii) AcMPAG, the minor but potentially active metabolites [10, 29, 51]. MPAG and AcMPAG formations are primarily mediated by UGT1A9 and UGT2B7, respectively, whereas UGT1A1, UGT1A7, UGT1A8, UGT1A10, and UGT2B4 can have additional minor contributions [35, 173-175, 252, 253]. The majority of MPA is excreted in the urine as MPAG (~87% of the administered MPA dose), while MPA and AcMPAG contribute to less than 1% in healthy adults administered oral MMF [37]. The urinary excretion of MPAG is mediated by MRP-2 and organic anion transporters [38, 39]. Alternatively, the glucuronide metabolites can also be excreted into the bile and recycled into the systemic recirculation via the entero-hepatic recirculation process (discussed above). As MPAG is the major metabolite of MPA,

plasma and urinary concentrations of MPAG or the MPAG-to-MPA ratio can be utilized as surrogate markers for UGT1A9-mediated MPA metabolism.

In this dataset (Table IV-1) [183, 185, 189, 196, 198, 200, 203, 207, 209, 210, 221], two papers reported MPAG concentrations [183, 203] and only one incorporated MPAG into their structural model where the proportion of MPAG formation was fixed at 85% [203]. However, urinary excretion data were not available in this dataset to allow the assessment of renal elimination (Table IV-1) [183, 185, 189, 196, 198, 200, 203, 207, 209, 210, 221]. As such, the metabolism and excretion processes are discussed as a combined "elimination" process, which is characterized by the overall MPA clearance. In general, clearance was characterized as a first-order elimination process in all papers in this dataset, which is consistent with the adult models (e.g. reviewed in [10, 30, 31, 62, 71-73]). Utilizing both parametric and nonparametric methods, Prémaud et al. did not report drastically different elimination rate constant (k) values, supporting consistency between the two modelling approaches for estimating MPA clearance [198]. Moreover, Zhao et al. assessed the effects of single nucleotide polymorphisms in UGT1A8, UGT1A9, and UGT2B7 on the pharmacokinetics of MPA, but the findings were primarily negative and control MPAG data were not available [210]. The total (i.e. sum of bound and unbound) MPA clearance reported by the majority of studies (10/11, Table IV-1) [183, 185, 189, 196, 198, 200, 203, 207, 209, 210, 221] might not be the best marker characterizing MPA elimination because it is affected by both intrinsic clearance and free fraction [10, 181]. On the other hand, free (i.e. unbound) MPA clearance, as reported by Kim et al. [189], is a better surrogate characterizing MPA metabolism as it is not dependent on MPA protein binding. The elimination of MPA is also impacted by entero-hepatic recirculation, and this process has been described above in the Absorption section.

The elimination of MPA is parameterized by apparent clearance (CL/F) in the majority of the studies (Table IV-1) [183, 185, 189, 196, 198, 200, 203, 207, 209, 210, 221]. For Prémaud et al., the reported k values were converted to CL/F (i.e. $CL/F = k \times V_d/F$) to allow comparison to the dataset. The reported range in total CL/F (i.e. the absolute population estimate without considering the effects of covariates) in this paediatric dataset was 12.7-25.3 $l \cdot h^{-1}$ (Table IV-1) [183, 185, 196, 198, 200, 203, 207, 209, 210, 221], where the lowest CL/F was observed in liver transplant paediatric recipients [183]. The relatively reduced CL/F in Barau et al. might be explained by the relatively lower average total body weight and compromised liver metabolism as evident by elevated serum aspartate aminotransferase and serum alanine aminotransferase values [183]. The highest CL/F was reported in paediatric patients with systemic lupus erythematosus, which might also be attributable to the relatively higher average total body weight [203]. The findings on weight were consistent with the trend toward a positive association (i.e. using regression analysis) between CL/F and total body weight in Saint-Marcoux et al. [200] and in five other papers in this dataset where body weight was identified as a significant covariate on CL/F using population modelling [185, 189, 209, 210, 221]. It may be possible that body weight is just an indirect marker for other variables such as hepatic UGT protein content or overall clearance (e.g. [224]), but this hypothesis requires further investigation. Moreover, the relationship between body weight and CL/F can be described by either a positive exponential association, where a wide range of exponents have been documented, or a simple linear association [185, 189, 209, 210, 221]. Based on the identified exponential coefficients, body weight was more influential on CL/F in patients with haematopoietic stem cell transplants (i.e. 0.75, exponential coefficient, a fixed parameter) [189] and idiopathic nephrotic syndrome (0.75) [209] than kidney transplants (0.31-0.42) [185, 210].

However, systematic evaluations on type of transplant (i.e. using covariate modelling) are still needed to confirm this observation.

MPA is a low hepatic extraction drug [31] and its overall clearance can be affected by other intrinsic factors known to influence free fraction and/or intrinsic clearance in paediatric patients (e.g. serum albumin, creatine clearance, total bilirubin, and polymorphism to MPA metabolism enzymes). The inverse correlation between serum albumin concentration and total MPA CL/F identified in several studies in this dataset [200, 209, 221] may be explained indirectly by increased free fraction of MPA. Moreover, impaired renal function as evident by decreased creatinine clearance can lead to the accumulation of uremic toxins that directly inhibit MPA metabolism [55], thereby decreasing CL/F. The uremic toxin effect was suggested by Kim et al. [189] but was not further verified with MPAG or toxin control data. Another hypothesis is that renal impairment might reduce the urinary excretion of MPAG, thereby increasing its bile excretion and the reabsorption of MPA through entero-hepatic recirculation, thus indirectly decreasing MPA CL/F. On the other hand, accumulation of MPAG due to renal dysfunction could also displace the albumin binding of MPA, which could lead to increased free fraction (and CL/F) as suggested by Zeng et al. [221]. These opposing effects from renal impairment (i.e. indirect inhibition of MPA metabolism, indirect increase in MPA bioavailability, and increase in free fraction) might explain the lack of overall association between renal function and MPA CL/F in this paediatric dataset (Table IV-1) [183, 185, 189, 196, 198, 200, 203, 207, 209, 210, 221].

The relatively low *free* MPA CL/F in Kim et al. [189] might be associated with increased total bilirubin concentration which is reflective of compromised hepatic UGT activities (according to the authors). However, this association was not evident in another liver transplant study that utilized *total* MPA concentration [183] possibly because bilirubin was also likely to have displaced

MPA and MPAG from albumin, therefore providing opposing effects to reduced hepatic UGT function. Furthermore, single nucleotide polymorphism (SNP) to UGT2B7 (802C>T) was demonstrated to decrease MPA CL/F in Zhao et al. [210], but UGT1A9 SNPs (e.g. -275T>A, -2152C>T) that are known to increase MPA clearance in adult kidney transplant patients [254] was not found to alter the pharmacokinetics of total MPA in their study. It can be hypothesized that the discrepancy could be that hepatic mRNA expression of UGT2B7 is relatively higher than UGT1A9 in children [227], which alters the relative contributions of these enzymes in the conjugation of MPA. However, MPAG and AcMPAG concentration data were not available to support this hypothesis, and mRNA expression is not always known to correlate with protein expression/activity (e.g. [255]). Moreover, the lack of significant finding on UGT1A9 polymorphism could also be attributed to the low minor allele frequencies, per Zhao et al. [210], and their relatively small sample size. With respect to extrinsic factors affecting MPA clearance, concurrent cyclosporine administration, compared to tacrolimus, resulted in significantly higher MPA CL/F based on covariate modelling in Zhao et al. and Zeng et al. [210, 221]. The underlying mechanism associated with the cyclosporine interaction has already been extensively explained in the literature, where cyclosporine is known to increase MPA clearance by inhibiting biliary MRP-2 [45, 46, 48] and possibly organic anion-transporting polypeptide 1B3 transporters [43], thereby decreasing the reabsorption of MPA through entero-hepatic recirculation.

In contrast to the significant covariates discussed above, other factors which have been known to influence MPA elimination were not identified in this paediatric dataset. For example, post-transplantation time has been determined to affect MPA clearance [10], but it was not identified a significant variable in the majority of papers in this dataset using population modelling [183, 189, 203, 207, 209, 210, 221]. The lack of significant effects might be explained by the

limited number of longitudinal studies spanning both acute (i.e. <9 months) and stabilized (i.e. >9 months) post-transplant periods which have been identified to be important time-markers affecting MPA CL/F [236]. Furthermore, an inverse association between age and MPA CL/F has been reported in paediatric kidney [256] or liver [257] transplant recipients using traditional, non-compartmental pharmacokinetic approaches. However, similar associations were not observed in this dataset possibly due to limited sample sizes or the lack of sufficiently wide age distribution in many studies (Table IV-1) [183, 185, 189, 196, 198, 200, 203, 207, 209, 210, 221]. Although corticosteroids are known to induce hepatic UGT enzymes [105] and increase the intrinsic clearance of MPA [59], it was difficult to elucidate their effects in this dataset because the doses and tapering regimens have not always been clearly documented. Overall, the total and free CL/F of MPA reported in this paediatric dataset and the MPAG CL/F documented by Sherwin et al. (i.e. 2.5 $l \cdot h^{-1}$ [203]) were in agreement with adult data (0.847-2.12 $l \cdot h^{-1}$) [10, 30, 31, 62, 71-73]. However, these comparisons might be difficult to interpret due to the large variabilities observed in both adult and paediatric populations [10, 30, 31, 62, 71-73, 183, 185, 189, 196, 198, 200, 203, 207, 209, 210, 221].

In summary, the elimination of MPA is commonly described by a first-order process (Table IV-1) [183, 185, 189, 196, 198, 200, 203, 207, 209, 210, 221]. Total or free MPA CL/F is associated with total body weight ([185, 209, 210, 221] for total CL/F; [189] for free CL/F), serum albumin ([209] for total CL/F), kidney function (e.g. creatine clearance [189] for free CL/F), liver function (e.g. total bilirubin [189] for free CL/F), genetic polymorphism to UGT2B7 (802C>T) ([210] for total CL/F), and concomitant cyclosporine ([210, 221] for total CL/F) in this paediatric population. With the exception of one study [203], MPA metabolites have not been characterized to confirm the effects of these covariates on the metabolism of MPA. Future studies would also

benefit from the determination of free MPA CL/F, which would effectively remove the confounding effects of protein binding and improve the interpretation of MPA clearance.

3.4. Bioavailability

The bioavailability of MPA can be influenced by absorption and metabolism. The majority of studies in this review (Table IV-1) [183, 185, 189, 196, 198, 200, 203, 207, 209, 210, 221] did not provide concurrent oral and intravenous data which are required to estimate the absolute bioavailability of MPA. Instead, apparent values of pharmacokinetic parameters (e.g. V_d/F, Q/F, and CL/F) were reported (Table IV-1) [183, 185, 196, 198, 200, 203, 207, 209, 210]. Only Kim et al. and Zeng et al. collected data on orally and intravenously administered MMF [189, 221], but Kim et al. had to fix MPA bioavailability to "1" due to insufficient number of samples from oral administration (only n=2 profiles) [189]. The MPA bioavailability value reported in Zeng et al. using population-based modelling was 48% (34.6% BSV) [221], which is lower than the typical value (i.e. 94%) reported in healthy adult volunteers [10]. The reduced bioavailability in Zeng et al. could be attributed, according to the authors, to the preparative regimens required of their blood or marrow transplant recipients that may have induced gastrointestinal toxicity and thus reduced MPA absorption [221, 246]. Moreover, Dong et al. reported a non-proportional relationship between oral bioavailability and dose of MMF in paediatric kidney transplant recipients, using a power function that was consistent with data demonstrated in adult populations (i.e. -0.43 vs. -0.41, respectively) [148, 185]. Although decreased bioavailability with increasing MMF dose has been attributed to saturations in absorption and/or entero-hepatic recirculation [148, 185], further modelling (e.g. using physiologically-based approaches) are required to confirm this hypothesis in the paediatric population. Overall, the data on MPA bioavailability were fairly scarce in this

dataset, and covariate analysis were not conducted to explain the observed variabilities. Further studies might consider incorporating MPA intravenous data (if available) into the population pharmacokinetic structural model to calculate the absolute bioavailability variable in order to improve the estimations of other pharmacokinetic parameters.

3.5. Population pharmacokinetic-pharmacodynamic modelling

The majority of population models in this paediatric dataset have focused on pharmacokinetic data and only a limited number of studies have reported pharmacodynamic effects. Dong et al. constructed a population pharmacokinetic-pharmacodynamic model utilizing IMPDH enzyme activity [185], which has been utilized as a pharmacodynamic marker for MPA activity in some studies [29, 258, 259] despite conflicting findings on its usefulness in predicting efficacy or toxicity [29]. Consistent with other non-population based studies in paediatric patients [260, 261] and population-based studies in adult haematopoietic cell transplant patients [193, 220], the relationship between MPA concentration and IMPDH activity was best described by an inhibitory maximum effect (E_{max}) model [185]. The MPA concentration associated with half maximal IMPDH inhibition (EC_{50}) by Dong et al. (i.e. 1.73 $mg \cdot l^{-1}$) was similar to other (non-population-based) paediatric kidney transplant studies (i.e. 0.97-9.6 $mg \cdot l^{-1}$) [260, 261], but lower than the data reported in adult haematopoietic cell transplant recipients (i.e. 3.23-3.59 $mg \cdot l^{-1}$) [193, 220]. This discrepancy might be hypothesized to be attributed to large variabilities associated with both MPA concentration and IMPDH measurements; however, direct comparisons of EC_{50} values between studies might be confounded by differences in baseline IMPDH activities and/or maximal inhibitory effects reported in different experimental settings [193, 220, 260, 261]. Moreover, two additional studies assessed the pharmacokinetic-pharmacodynamic outcomes of MPA using a

regression approach, where MPA exposure was associated with clinical status/disease activity in patients with idiopathic nephrotic syndrome [200] and systemic lupus erythematosus [207]. Overall, MPA pharmacokinetic-pharmacodynamic models in the paediatric population have not directly considered adverse outcomes such as infectious and haematological complications [61]. Future kinetic-dynamic models would also benefit from the utilization of additional predictive biomarkers (e.g. donor-specific antibodies [262]), consideration of free MPA concentrations that are representative of the active pharmacological effects (e.g. [193, 237]), and the evaluation of covariate effects (e.g. [220]).

3.6. Bayesian estimation of mycophenolic acid area under the concentration-time curve

Six studies have utilized Bayesian analysis to predict the area under the concentration-time curve (AUC) of MPA in this paediatric dataset [183, 185, 189, 196, 198, 200, 203, 207, 209, 210, 221] (summarized in Table IV-2 [183, 196, 198, 200, 207, 209]). With respect to modelling in general, NONMEM was the most commonly used software [196, 198, 209], but other programs such as Adapt II [183, 198] and in-house programs [200, 207] have also been utilized. As Bayesian estimation requires robust baseline parameters generated from population pharmacokinetic models, the predictive performance and clinical utility of these models are directly associated with (and only as good as) their underlying non-linear mixed-effects models [62]. In the six studies that have generated Bayesian estimators, similar predictive performances based on bias and precision evaluations have been observed in one- [183, 200, 207] or two-compartment-based models [196, 198, 221]. On the other hand, Bayesian estimators are lacking in studies with more complex mechanistic models (e.g. the six-compartmental model developed by Sherwin et al. incorporating MPAG and entero-hepatic recirculation [203]), which might be attributed to drastically elevated

computational requirements and complex input variables (e.g. MPAG data) that may not always be available in the typical clinical setting. Based on the findings of Prémaud et al., Bayesian analysis from non-parametric models also appeared more accurate and precise in estimating MPA AUC compared to the parametric approach [198]. Overall, all six studies have utilized $AUC_{(0\text{-}12)}$ as the model output as this pharmacokinetic parameter has been widely used in the therapeutic drug monitoring of MPA [10, 62]. Although Prémaud et al. evaluated the predictive performance of individual plasma concentrations, it was not clear which concentrations were utilized [198].

In this dataset, the reference $AUC_{(0\text{-}12)}$ values used for model validation have all been determined using conventional trapezoidal calculations with intense sampling (i.e. 7 to 17 time points per subject). Sampling times typically spanned from 0 to 12 hours with the exception of Barau et al. where the last time point was 8 hours post dose, which may lead to inaccurate estimation of $AUC_{(0\text{-}12)}$ (Table IV-2) [183, 196, 198, 200, 207, 209]. To ensure clinical utility, combinations of a maximum of *four time points* no longer than *six hours* post-dose were generally implemented in the final Bayesian models. Only Saint-Marcoux et al. applied D-optimality criterion to determine the best sampling times, while others had selected input time points based on empirically-designed protocols (Table IV-2) [183, 196, 198, 200, 207, 209]. However, it was not clear if D-optimal design had improved the accuracy and precision of AUC prediction, as no direct comparisons were made in the predictive performance by different approaches in the same setting. Moreover, three of the reviewed studies performed external validation (i.e. the gold standard approach) by enrolling separate sets of patients [183, 198, 200], whereas the others utilized the same or simulated/circular permutated dataset to evaluate the performance of their Bayesian models. The latter approach appeared to have generated relatively lower bias and imprecision possibly due to the validation of the dataset in a quasi-internal manner [196, 207, 209].

Mean prediction error (MPE, represents bias) and root mean squared prediction error (RMSE, represents precision) [263], the most widely accepted approach for prediction-error analysis, were calculated in most studies [196, 198, 200, 207, 209]. However, others had utilized secondary approaches such as scatter plots, Pearson correlation tests, Bland-Altman plots, or regression analysis (Table IV-2) [183, 196, 198, 200, 207, 209], which may not have fully illustrated the bias and imprecision of their models. In general, the methods used for developing and validating Bayesian estimators in predicting MPA exposure in this paediatric population were similar to adults [62].

Bayesian estimators can only be applied to the specific population in which the models were originally derived in [62]. In this regard, the predictive performance of Bayesian models is expected to be affected by specific population characteristics such as transplant type, post-transplant time, co-medication, and significant covariates, etc. [62] which are summarized for quick reference in Table IV-2 [183, 196, 198, 200, 207, 209]. Unfortunately, in this paediatric dataset, Bayesian models were only available in kidney transplant [196, 198], liver transplant [183], idiopathic nephrotic syndrome [200, 209], and systemic lupus erythematosus [207] patients, which were all administered the MMF formulation. This is a limitation in comparison to the adult population where a larger variety of models representative of a diversity of patient populations are currently available [62]. Based on bias and precision evaluations, the optimal sampling time combinations in this paediatric dataset appeared to be “1 and 4 hours” [196], “pre-dose, 1, and 4 hours” [183, 209], and “20 minutes, 1, and 3 hours” [200, 207] (Table IV-2). These sampling times were selected based on the process of iteration in some studies [183, 196, 207, 209], whereas others had only utilized a single time combination empirically (e.g. [200]). Moreover, these optimal sampling times would appear to have physiological relevance: the pre-dose, 20 minute, and 1 hour

samples likely reflected the absorption phase of MPA as the peak concentration typically occurs at 1.3±0.6 hours after administration in stable paediatric renal transplant patients [264], and the 3 or 4 hour samples likely captured the MPA distribution, double absorption/ entero-hepatic recirculation, and the elimination processes [10]. Although the incorporation of additional sampling times (e.g. > 6 hours) may better predict the entero-hepatic recirculation and MPA clearance, they are not considered clinically feasible. Moreover, the reported bias, where available, were within ±4% and the imprecision no higher than 16% (Table IV-2) [183, 196, 198, 200, 207, 209], indicating most models had acceptable predictive performance. The relatively large imprecision might be the result of generally small sample sizes utilized in both model development and validation (Table IV-2) [183, 196, 198, 200, 207, 209], and may potentially affect the clinical utility of these Bayesian estimators as the therapeutic range of MPA is relatively narrow (i.e. 30-60 $mg \cdot h \cdot l^{-1}$ [63]). Unfortunately, the effects of covariates on accuracy and precision were not reported in this paediatric dataset to account for the observed variability (Table IV-2) [183, 196, 198, 200, 207, 209]. In general, the reported optimal sampling times and predictive performances were similar to that documented in adult populations [62].

In summary, a limited number of Bayesian estimators have been established to forecast MPA $AUC_{(0-12)}$ after MMF administration in select paediatric patient populations (Table IV-2) [183, 196, 198, 200, 207, 209]. The utilities of these Bayesian estimators, however, in improving actual clinical outcomes (i.e. reduction of graft rejection or minimization of toxicities) in the paediatric population would still remain to be investigated.

4. Summary, future perspectives, and conclusion

This review provided an up-to-date critique of the published MPA population pharmacokinetic models in paediatric patients (Table IV-1, Table IV-2) [183, 185, 189, 196, 198, 200, 203, 207, 209, 210, 221]. With respect to modelling, the majority of the studies have utilized empiric approaches, but mechanistic models incorporating free MPA concentrations ([189]), bioavailability data ([221]), MPAG concentrations ([203]), secondary peaks (entero-hepatic recirculation or double absorption) ([200, 203, 207]), pharmacogenetics ([210]), and pharmacokinetic-pharmacodynamic relationships ([185]) are also available (Table IV-3) [183, 185, 189, 196, 198, 200, 203, 207, 209, 210, 221]. The utilization of free (pharmacologically-active) MPA concentration can improve the interpretation of MPA clearance because the confounding effects of protein binding are removed. The modelling of absolute bioavailability parameter in datasets containing both oral and intravenous MPA data may improve the estimations of other pharmacokinetic parameters. The inclusion of MPAG and AcMPAG data allows the quantification of MPA metabolism as concentration ratios of these metabolites can directly reflect UGT1A9 and UGT2B7 enzyme activities, respectively [10]. The modelling of entero-hepatic recirculation and/or double absorption may improve the fitting of data exhibiting secondary peaks to allow more accurate and precise estimation of MPA clearance. The inclusion of single nucleotide polymorphism data (e.g. UGT or MRP-2) can also improve the estimation of MPA clearance based on emerging pharmacogenomic data reported of MPA (e.g. [265, 266]). Furthermore, the modelling of pharmacodynamic markers (e.g. IMPDH) can provide a more direct means to characterize MPA's desired pharmacological or toxicity effects. However, to our knowledge, no single model in the paediatric population has yet incorporated all of these ideal modelling attributes (Table IV-3) [183, 185, 189, 196, 198, 200, 203, 207, 209, 210, 221]. Such a comprehensive

mechanistic model could improve the understanding of MPA pharmacology in the paediatric population. However, it would also require significantly increased sample size, analytical costs, and frequency/volume of blood draw, which may prove challenging both physiologically and ethically in the paediatric population.

With respect to biological attributes and clinical applications, this review has provided a detailed summary on MPA population pharmacokinetic parameter estimates, variabilities, and covariates in specific paediatric populations (Table IV-1) [183, 185, 189, 196, 198, 200, 203, 207, 209, 210, 221]. Our assessment found differences and similarities compared to the adult data, although mechanistic investigations with properly controlled experiments are often lacking to explain the underling pharmacology. Furthermore, Bayesian forecasting models are also now available in select paediatric patient groups with acceptable accuracy and precision for estimating MPA exposure (Table IV-2) [183, 196, 198, 200, 207, 209]; however, the represented patient populations are very limited and the clinical utilities of the developed Bayesian models have not yet been investigated. In addition, the lack of data in additional indications in which MPA may be prescribed (e.g. paediatric thoracic and/or heart transplantations) and on alternative formulations (e.g. EC-MPS, which is experiencing increasing usage [235]) may limit the generalizability of these findings. In order to conduct a more systematic comparison to the adult data, a larger body of paediatric literature is also warranted. In conclusion, this review has comprehensively summarized the currently available MPA population pharmacokinetic data in paediatric patients. This review can be used by pharmacologists and clinicians to improve MPA modelling and patient care.

Table IV-1 Summary of population pharmacokinetic studies for mycophenolic acid in paediatric populations

Patient population	Dosing regimen	Assay	Model	Population PK (or PD) parameters	Validation	References
Kidney transplant						
Study design: prospective, multi-centre clinical study *PK model* **Sample size:** 24 subjects, 214 samples **Race:** 20 Caucasians, 4 African Americans **Age (years):** 12.1 (2.1-20.2) (mean [range]) **Gender:** 15 males, 9 females **Weight (kg):** 39.8 (10.3-106.4) **Renal function:** CrCl ($ml \cdot min^{-1} \cdot 1.73\ m^{-2}$) 118.1 (20.5-228.3) (Schwartz formula) **Liver function:** NA **Serum albumin ($g \cdot dl^{-1}$):** 3.5 (2.1-4.7) **Post-transplant time (days):** 4-9 *PK-PD model* **Sample size:** 17 subjects, 97 samples	**Induction:** basiliximab or rabbit antithymocyte globulin **Maintenance MMF/day:** 450 or 600 $mg \cdot m^{-2}$ orally twice daily (adjusted based on clinical status); steady-state not specified. **Co-medication:** cyclosporine was excluded; tacrolimus (twice daily; titrated based on target trough concentrations); prednisone (1.0-1.5 $mg \cdot kg^{-1}$ twice daily, subsequently tapered)	HPLC; total MPA	**Software/algorithm:** NONMEM version 7.2.0; non-linear mixed effect modelling; FOCE-I *PK model* **Structural model:** 8-transit compartment absorption, two-compartment (type of elimination not specified) **BSV:** exponential model **BOV:** fixed to 0 **RV:** log transformed, additive model **Screened covariates:** age, CrCl, gender, height, induction therapy (basiliximab, thymoglobulin), race, serum albumin, weight **Included covariates:** weight on CL/F *PK-PD model*	*PK model* **Fixed effects (mean [95% CI from bootstrapping]):** k_a (h^{-1}), 2.5 [1.45, 4.93] **MTT** (h), 0.25 [0.12, 0.50] V_c/F (l), 45.4 [29.6, 55.6] V_p/F (l), 411 [152.6, 1472.6] **Q/F** ($l \cdot h^{-1}$), 22.4 [16.0, 32.5] **CL/F** ($l \cdot h^{-1} \cdot 70\ kg^{-1}$), $CL/F=\theta_1 \times (body\ weight/70)^{\theta 2}$ θ_1, 22.0 $l \cdot h^{-1}$ [14.8, 25.2] θ_2, 0.31 [0.03, 0.63] **Relative bioavailability**, $Bioavailability=\theta_3 \times (D\ BSA/450)^{\theta 4}$ θ_3, 1, fixed θ_4, -0.43 [-1.00, -0.06] **BSV CV%:**	**Validation:** goodness-of-fit plots (OD-PRED, OD-IPRED, CWRES-PRED, CWRES-time after dose); prediction corrected VPC plot; bootstrapping; shrinkage values (η, ε)	Dong et al. 2014 [185]

Patient population	Dosing regimen	Assay	Model	Population PK (or PD) parameters	Validation	References
Race: 15 Caucasians, 2 African Americans **Age (years):** 13.4 (4.1-20.2) (mean [range]) **Gender:** 10 males, 7 females **Weight (kg):** 43.5 (10.3-106.0) **Renal function:** CrCl ($ml \cdot min^{-1} \cdot 1.73\ m^{-2}$) 114.6 (20.5-228.0) (Schwartz formula) **Liver function:** NA **Serum albumin ($g \cdot dl^{-1}$):** 3.4 (2.1-4.4) **Post-transplant time (days):** 4-9	**Additional concurrent medications:** NA		**Structural model:** inhibitory E_{max} model **BSV:** exponential model **BOV:** fixed to 0 **RV:** proportional model **Screened covariates:** Same as PK model **Included covariates:** None (trends observed with race and serum albumin)	**ω (k_a)**, 299.6 [123.6, 910.8] **ω (MTT)**, 144.8 [69.4, 414.1] **ω (V_c/F)**, 0 fixed **ω (V_p/F)**, 0 fixed **ω (Q/F)**, 0 fixed **ω (CL/F)**, 25.9 [8.1, 38.5] shrinkage, 10-34% **RV CV%:** **$\sigma_{additive}$**, 51.0 [43.5, 57.1] *PK-PD model (PD marker: IMPDH activity)* **Fixed effects (mean [95% CI from bootstrapping]):** **E_0** ($nmol \cdot h^{-1} \cdot mg\ protein^{-1}$), 3.45 [2.61, 4.56] **$EC_{50}$** ($mg \cdot l^{-1}$), 1.73 [1.16, 3.01] **$E_{max}$** ($nmol \cdot h^{-1} \cdot mg\ protein^{-1}$), 0 fixed **BSV CV%:** **ω (E_0)**, 39.6 [9.6, 56.2] **ω (EC_{50})**, 72.5 [18.1, 152.5]		

Patient population	Dosing regimen	Assay	Model	Population PK (or PD) parameters	Validation	References
				ω (E_{max}), 0 fixed **shrinkage, 8-26%** **RV CV%:** **$\sigma_{proportional}$**, 42.2 [34.6, 48.3]		
Study design: German Study Group on MMF therapy (open-label, prospective) and Tricontinental MMF suspension trial (open-label, prospective, multi-centre) [267] **Sample size:** patients combined from 2 studies (German [44 subjects] and Tricontinental [22 subjects]) were randomly assigned to 2 groups (34 subjects [development group; 73 profiles] and 32 subjects [Bayesian validation group; 56 profiles]). **Race:** 44 Caucasians, 22 not specified (based on data provided in Weber et al. [267]) **Age (years):** 11.2±3.2 (mean±SD,	**Induction:** NA **Maintenance MMF/day:** 600 mg·m^{-2} orally twice daily (maximum of 2 g·day^{-1}); 625±178 mg (development set), 569±213 mg (Bayesian validation set); steady-state not verified. n=22 from the Tricontinental cohort started with oral suspension but switched to capsule 9 months after transplantation. **Co-medication:**	HPLC-UV; total MPA	*Parametric approach* **Software/algorithm:** NONMEM version VI and Wings for NONMEN version 614; non-linear mixed effect modelling; FOCE-I **Structural model:** first-order absorption with lag time, two-compartment, first-order elimination **BSV:** exponential model **BOV:** exponential model **RV:** combined model **Screened covariates:** age, gender, weight **Included covariates:** None (trends observed with post-transplant time)	*Parametric approach* **Fixed effects (mean [SE]):** **k_a** (h^{-1}), 2.28 [0.51] **t_{lag}** (h), 0.26 [0.01] **V_c/F** (l), 17.7 [1.84] **k_{12}** (h^{-1}), 0.58 [0.10] **k_{21}** (h^{-1}), 0.007 [0.001] **k** (h^{-1}), 0.78 [0.07] **BSV CV%** (mean [95% CI]): **ω (t_{lag})**, 15 [0, 23] **ω (k_{12})**, 62 [11, 87] **ω (k)**, 20 [0, 31] **BOV CV%** (mean [95% CI]): **ω (k_a)**, 109 [68, 139] **ω (V_c/F)**, 53 [39, 63] **RV:** **$\sigma_{1,\ proportional}$ (%),** 38.7 **$\sigma_{2,\ additive}$ (mg·l^{-1}),** 0.08 *Nonparametric approach*	*Parametric approach* **Validation:** conditional number and extreme eigenvalues; goodness-of-fit plots (OD-PRED, OD-IPRED, CWRES-PRED, CWRES-time); VPC plot; bootstrapping; shrinkage values (η, ε) *Nonparametric approach* **Validation:** goodness-of-fit plots (OD-PRED, OD-IPRED)	Prémaud et al. 2011 [198]

Patient population	Dosing regimen	Assay	Model	Population PK (or PD) parameters	Validation	References
development), 8.9±4.9 (Bayesian validation) **Gender:** 23 males/11 females (development), 19/13 (Bayesian validation) **Weight (kg):** 32.2±11.5 (development), 30.5±16.1 (Bayesian validation) **Renal function:** NA **Liver function:** NA **Serum albumin (g·dl^{-1}):** NA **Post-transplant time:** day 21; month 3, 6, 9	German study cohort, cyclosporine microemulsion formulation (300 mg·m^{-2}·day^{-1}, dose-adjusted based on trough levels); methylprednisolone (300 mg·m^{-2} to start, then rapidly tapered to 4 mg·m^{-2} after 6 weeks) Tricontinental study cohort, cyclosporine and prednisone based on individual centre's protocols **Additional concurrent medications:** NA		Bayesian model: see Table IV-2 *Nonparametric approach* **Software/algorithm:** BigWinPops version 0.03; nonparametric expectation maximization **Structural model:** first-order absorption with lag time, two-compartment, first-order elimination Bayesian model: see Table IV-2	(mean, median, BSV CV%, range) **k_a** (h^{-1}), 5.21, 2.87, 92.20, [0.10-20.10] **t_{lag}** (h), 0.40, 0.28, 98.54, [0.0001-1.85] **V_c/F** (l), 16.11, 12.13, 74.80, [1.80-56.92] **k_{12}** (h^{-1}), 1.30, 1.05, 82.16, [0.002-5.00] **k_{21}** (h^{-1}), 0.69, 0.03, 207.83, [0.005-4.99] **k** (h^{-1}), 1.16, 1.05, 56.40, [0.26-4.33]		
Study design: prospective, multi-centre **Sample size:** 89 subjects, 18 full profiles and 71 sparse profiles, 497 samples **Race:** NA	**Induction:** thymoglobulin or basiliximab **Maintenance MMF/day:**	HPLC-UV (25% samples) or EMIT (75%	**Software/algorithm:** NONMEM; non-linear mixed effect modelling; FOCE **Structural model:**	**Fixed effects (estimate [RSE%]):** **k_r** (h^{-1}), 6.2 [10] **V_c/F** (l), $V_c/F=\theta_1\times(\text{body weight}/30.3)^{\theta 2}$ θ_1, 23.0 l [19]	**Validation:** goodness-of-fit plots (OD-IPRED, IWRES-IPRED, IRES-time); VPC plot;	Zhao et al. 2010 [210]

Patient population	Dosing regimen	Assay	Model	Population PK (or PD) parameters	Validation	References
Age (years): 10.1±5.3 **Gender:** 53 males, 36 females **Weight (kg):** 32.7±16.2 (mean±SD) **Renal function:** CrCl ($ml \cdot min^{-1}$) 95.8±25.7 (Swartz formula) **Liver function:** NA **Serum albumin ($g \cdot dl^{-1}$):** NA **Post-transplant time (days):** 23.0±11.9 (<60 days)	1078.0±511.8 $mg \cdot day^{-1}$; adjusted to maintain MPA AUC 30-60 $mg \cdot h \cdot l^{-1}$; steady-state not specified. **Co-medication:** Cyclosporine microemulsion formulation (n=41; target trough concentration 150-250 $ng \cdot ml^{-1}$; 252.7±115.7 $mg \cdot day^{-1}$); or tacrolimus (n=47; target trough concentration 5-15 $ng \cdot ml^{-1}$; 7.6±3.7 $mg \cdot day^{-1}$); and prednisone (60 $mg \cdot m^{-2}$ daily; tapered to 7.5 $mg \cdot m^{-2}$ over 6 months). **Additional concurrent medications:** NA	samples) (applied scaling factors); total MPA	Erlang distribution (numbers of serial compartments, n=4), two-compartment, first-order elimination **BSV:** exponential model **BOV:** NA **RV:** combined model **Screened covariates:** MRP-2 (-24C>T, 1249G>A, 3563T>A, 3972C>T), age, co-medication of immunosuppressants, CrCl, gender, post-transplant time, UGT1A8 (830G>A), UGT1A9 (-2152C>T, -275T>A, 98T>C), UGT2B7 (802C>T), weight **Included covariates:** weight on V_c/F, co-medication (tacrolimus vs. cyclosporine), UGT2B7 variation (802C>T), weight on CL/F	θ_2, 1.35 [21] **V_p/F** (l), 158 [19] **Q/F** ($l \cdot h^{-1}$), 25.6 [23] **CL/F** ($l \cdot h^{-1}$), $CL/F=\theta_3 \times (\text{body weight}/30.3)^{\theta 4} \times (\theta_5^{\text{comedication}}) \times (\theta_6^{\text{heterozygous}}) \times (\theta_7^{\text{homozygous}})$ θ_3, 12.9 $l \cdot h^{-1}$ [16] θ_4, 0.424 [32] θ_5, 0.778 [16] if cyclosporine=0; if tacrolimus=1 θ_6, 1.29 [15] if UGT2B7-802 C/T heterozygous=1 and homozygous=0 θ_7, 1.51 [21] if UGT2B7-802 T/T homozygous=1 and heterozygous=0 **BSV CV%:** **ω (k_r)**, 74.9 [24.8] **ω (V_c/F)**, 61.6 [46.0] **ω (Q/F)**, 115.3 [31.9] **ω (CL/F)**, 53.5 [23.4] **RV:** **$\sigma_{proportional,EMIT}$ (%)**, 8.9 [62.1] **$\sigma_{additive,EMIT}$**, 1.27 [7.9]	bootstrapping	

Patient population	Dosing regimen	Assay	Model	Population PK (or PD) parameters	Validation	References
			Analytical bias between HPLC and EMIT was included.	$\sigma_{additive,HPLC}$, 0.69 [44.8]		
Study design: NA **Sample size:** 41 subjects (total), development group (32 subjects) and Bayesian validation group (13 subjects: 9 independent subjects and 4 from development group) **Race:** NA **Age (years):** 12.9 (2.0-21.0) (mean [range], total), 12.5 (2.0-21.0) (development), 12.2 (2.0-19.0) (Bayesian validation) **Gender:** 29 males/12 females (total), 24/8 (development), 9/6 (Bayesian validation) **Weight (kg):** 39.4 (12.0-68.6) (total), 39.5 (12.0-61.9) (development), 37.0 (11.4-68.6) (Bayesian validation) **Renal function:** CrCl ($ml \cdot min^{-1}$) 128 (32-248) (total), 139 (45-248) (development), 105 (32-214) (Bayesian validation)	**Induction:** NA **Maintenance MMF/day:** 600 $mg \cdot m^{-2}$ orally twice daily; adjusted based on efficacy and toxicity; target trough concentration 1-5 $\mu g \cdot ml^{-1}$; on empty stomach; steady-state not specified ("on long term oral MMF continuous therapy". **Co-medication:** cyclosporine (n=38, dose not specified); or tacrolimus (n=3, dose not specified); and corticosteroids (60 $mg \cdot m^{-2}$ daily;	HPLC; total MPA	**Software/algorithm:** NONMEM version 5.1.1; non-linear mixed effect modelling; FO and FOCE **Structural model:** first-order absorption with lag time, two-compartment, first-order elimination **BSV:** exponential model **BOV:** combined model **RV:** combined model **Screened covariates:** age, BSA, co-medication, CrCl, weight **Included covariates:** weight on V_c/F Bayesian model: see Table IV-2	**Fixed effects (estimate [CV%]):** **α** (h^{-1}), 7.50 [-] **β** (h^{-1}), 0.00746 [28.9] $\mathbf{k_a}$ (h^{-1}), 0.61 [20.5] $\mathbf{t_{lag}}$ (h), 0.65 [5.1] $\mathbf{V_c/F}$ (l), $Vc/F=\theta_4 \times weight$ (4.75 l) θ_4, 0.121 $l \cdot kg^{-1}$ [13.0] $\mathbf{k_{21}}$ (h^{-1}), 0.0172 [32.2] **CL/F** ($l \cdot h^{-1}$), 16.0; $CL=(\alpha \times \beta)/k_{21} \times V_C/F$ **BSV CV%:** **ω (α)**, 0 fixed **ω (β)**, 23.2 **ω (k_a)**, 43.1 **ω (t_{lag})**, 97.5 **ω (V_c/F)**, 29.7 **ω (k_{21})**, 26.6 **ω (CL/F)**, 50.8 **BOV:** 18.5%; 0.56	**Validation:** goodness-of-fit plots (OD-PRED, OD-IPRED, WRES-PRED, WRES-time)	Payen et al. 2005 [196]

Patient population	Dosing regimen	Assay	Model	Population PK (or PD) parameters	Validation	References
Liver function: NA ("normal", per authors) **Serum albumin ($g \cdot dl^{-1}$):** NA **Post-transplant time (days):** first kinetic profiles at 12-3754 days	tapered to 5 $mg \cdot m^{-2}$ over 6 months). **Additional concurrent medications:** NA					
Liver transplant						
Study design: NA **Sample size:** 28 subjects (total), development group (16 subjects, 16 profiles) and Bayesian/external validation group (12 subjects, 26 profiles) **Race:** NA **Age (years):** 8.65 (1.1-18.0) (median [range], total), 8.7 (1.1-15.2) (development), 11.1 (2.2-18.0) (Bayesian/external validation) **Gender:** 14 males, 14 females **Weight (kg):** 23.8 (9.3-49.2) (development), 36 (13.5-63.2) (Bayesian/external validation) **Renal function:**	**Induction:** NA **Maintenance MMF/day:** median dose 380 (186-594) $mg \cdot m^{-2}$ orally twice daily; dose adjusted to MPA $AUC_{(0-12)}$ 30-60 $mg \cdot h \cdot l^{-1}$; steady-state assumed. **Co-medication:** cyclosporine (n=5; with trough concentration target within 1st month of 150-250 $ng \cdot ml^{-1}$; median dose 3.1 [2.0-6.5] $mg \cdot kg^{-1} \cdot day^{-1}$); or	HPLC; total and unbound MPA; total MPA G	**Software/algorithm:** WinNonMix, version 2.0.1; non-linear mixed effect modelling **Structural model:** first-order absorption, one-compartment, first-order elimination **BSV:** exponential model **BOV:** NA **RV:** proportional model **Screened covariates:** acute or chronic rejection, age, ALT, AST, bilirubin, blood cell counts, BSA, BUN, co-medication (cyclosporine/tacrolimus, prednisone), CrCl, donor's age, factor V, gender, haematocrit,	**Fixed effects for total MPA (mean [RSE%]):** **k_a** (h^{-1}), $k_a=(k_{aTV}-[age/8.65]\times\theta_{age})\times exp(BSV)$ k_a, 3.9 [3.8] θ_{age}, 2.2 [3.7] **V_d/F** (l), $V_d/F=V_d/F_{TV}\times(\theta_{post\text{-}transplant\ time}^{post\text{-}transplant\ time})\times exp(BSV)$ V_d/F, 64.7 [13.2] $\theta_{post\text{-}transplant\ time}$, 2.3 [26.3], 0 for period >6 months and 1 for period ≤6 months **CL/F** ($l \cdot h^{-1}$), 12.7 [10.8] **BSV CV% for total MPA:** **ω (k_a)**, 308.4 [68.7]	**Validation:** goodness-of-fit plots (OD-PRED, OD-IPRED, WRES-PRED, WRES-time); VPC plot	Barau et al. 2012 [183]

Patient population	Dosing regimen	Assay	Model	Population PK (or PD) parameters	Validation	References
CrCl (ml·min^{-1}) 155 (17-296) (development), 118 (46-175) (Bayesian/external validation) (Schwartz formula); SCr (µmol·l^{-1})[a] 37 (18-364) (development), 57 (30-89) (validation) **Liver function:** ALT (IU·l^{-1}) 93 (24-495) (development), 100 (4-578) (Bayesian/external validation); AST (IU·l^{-1}) 64 (28-310) (development), 70 (15-708) (Bayesian/external validation); total bilirubin (µmol·l^{-1})[b] 20 (4-263) (development), 11 (6-599) (Bayesian/external validation) **Serum albumin (g·dl^{-1}):** 3.17 (1.72-3.50) (development), 3.43 (3.90-5.47) (Bayesian/external validation) **Free fraction:** 2.8% (1.2%-8.5%) (≤6 months,	tacrolimus (n=23; with trough concentration target within 1st month of 10-15 ng·ml^{-1}; median dose 0.09 [0.01-0.21] mg·kg^{-1}·day^{-1}); and prednisone (n=14; median 0.50 [0.08-1.20] mg·kg^{-1}·day^{-1}). **Additional concurrent medications:** NA		haemoglobin, MMF dosage, neutrophils, platelets, post-transplant time, SCr, serum albumin, time after start of MMF, weight **Included covariates:** age on k_a; post-transplant time (≤ and > 6 months) on V_d/F Bayesian model: see Table IV-2	**ω (V_d/F)**, 41.8 [81.1] **ω (CL/F)**, 28.4 [96.8] **RV CV% for total MPA:** 59.6 [36.9]		

Patient population	Dosing regimen	Assay	Model	Population PK (or PD) parameters	Validation	References
n=7), 1.0% (0.3%-3.8%) (>6 months, n=9) **Post-transplant time (months):** 17.2 (0.2-188.5) (total); immediate period (≤6 months, n=7) and stable period (>6 months, n=9) (development) **Indications:** biliary atresia (n=14), fulminant hepatitis (n=8), progressive familial intrahepatic cholestasis (n=3), Alagille syndrome (n=1), cystic fibrosis (n=1), Wilson disease (n=1)						
Allogenic haematopoietic stem cell transplant						
Study design: NA **Sample size:** 36 subjects, 87 profiles (85 IV, 2 oral), 417 samples **Race:** NA **Age (years):** 5 (0.17-36) (median [range]) **Gender:** 69% male **Weight (kg):** 19.1 (4.4-99.5) **Renal function:** BUN ($mg \cdot dl^{-1}$) 38 (7-161); CrCl ($ml \cdot min^{-1}$) 80 (24-336) $ml \cdot min^{-1}$ (≤17 years,	**Induction/preparative regimens:** alemtuzumab, busulfan and cyclophosphamide; or alemtuzumab, clofarabine and melphalan; or anti-thymocyte globulin, cyclophosphamide and fludarabine	HPLC-MS/MS; unbound MPA	**Software/algorithm:** NONMEM version VII; non-linear mixed effect modelling; FOCE-I **Structural model:** first-order absorption, two-compartment, linear elimination **BSV:** exponential model **BOV:** NA **RV:** proportional model	**Fixed effects for free MPA (median [RSE%]):** $\mathbf{k_a}$ (h^{-1}), 4 fixed [-] $\mathbf{V_c}$ (l), 367 [17.9] $\mathbf{V_p}$ (l), 795 [18.4] **Q** ($l \cdot h^{-1}$), 113 [25.3] **CL** ($l \cdot h^{-1}$), $CL=\theta_{CL} \times (\text{body weight}/20)^{0.75} \times (CrCl/80)^{\theta CrCl} \times (\theta_{TBIL}{}^{TBIL}) \times \exp(BSV)$ θ_{CL}, 711 [11.7] θ_{CrCl}, 0.677 [23.2]	**Validation:** goodness-of-fit plots; VPC plot; bootstrapping	Kim et al. 2012 [189]

Patient population	Dosing regimen	Assay	Model	Population PK (or PD) parameters	Validation	References
Schwartz formula; >17 years, Cockcroft-Gault equation); SCr ($mg \cdot dl^{-1}$) 0.6 (0.17-3.39); renal impairment (mild n=11, moderate n=9, severe n=1) **Liver function:** ALP ($IU \cdot l^{-1}$) 18 (4-359), ALT ($IU \cdot l^{-1}$) 126 (10-711); total bilirubin ($mg \cdot dl^{-1}$) 1.1 (0.1-26.8) (>10 $mg \cdot dl^{-1}$, n=6) **Serum albumin ($g \cdot dl^{-1}$):** 2.3 (1.9-4.1) **Post-transplant time (days):** 13 (2-100+); >100 (n=3), fixed to 100 **Indications:** X-linked adrenoleukodystrophy (n=15), Hurler's syndrome (n=5), Wolman's disease (n=2), hemoglobinopathy (n=7), hematologic malignancy (n=2), other (n=5)	**Maintenance MMF/day:** IV (infused over 2 hours) from day-3 to day+7, then converted to oral; steady-state; <45 kg, 15 $mg \cdot kg^{-1}$ (maximum 1 g) every 8h; ≥45 kg, 1500 mg every 12h; adjusted to maintain $AUC_{(0-8)}$ 200-250 $ng \cdot h \cdot ml^{-1}$ and $AUC_{(0-12h)}$ 300-350 $ng \cdot h \cdot ml^{-1}$. **Co-medication:** cyclosporine (IV 2.5 $mg \cdot kg^{-1}$ every 12h from day-3; converted to oral when tolerated; adjusted to maintain trough concentration 200-400 $ng \cdot ml^{-1}$);		**Screened covariates:** age, ALP, ALT, BUN, CrCl, SCr, post-stem cell infusion time, serum albumin, total bilirubin **Included covariates:** CrCl, total bilirubin, weight on unbound MPA CL Total bilirubin was treated as a categorical covariate (>10 $mg \cdot dl^{-1}$ or ≤10 $mg \cdot dl^{-1}$) Clearance was allometrically scaled to weight (fixed exponent of 0.75).	θ_{TBIL}, 0.543 [9.9] if total bilirubin ≤10 $mg \cdot dl^{-1}$ TBIL=0; if total bilirubin >10 $mg \cdot dl^{-1}$ TBIL=1 **BSV CV% for free MPA:** **ω (V_c)**, 51.6 [48.9] **ω (V_p)**, 31.3 [80.3] **ω (CL)**, 37.0 [24.7] **RV CV% for free MPA:** 56.1 [13.8] Bioavailability was fixed to 1.		

Patient population	Dosing regimen	Assay	Model	Population PK (or PD) parameters	Validation	References
	Additional concurrent medications: NA fluoroquinolone for antibiotic prophylaxis and gut decontamination					
Combined kidney, liver, and haematopoietic stem cell transplant						
Study design: prospective, single-centre, observational **Sample size:** 38 subjects (13 intensive, 7 sparse, 18 random sampling), 859 samples **Race:** NA **Age (years):** 8.4 (0.4-19.9) (median [range]) **Gender:** 20 males, 18 females **Weight (kg):** 27.9 (3.4-87.7) **Renal function:** CrCl ($l \cdot h^{-1} \cdot kg^{-1}$) 0.12 (0.01-0.31) (Counahan formula) **Liver function:** NA **Serum albumin ($g \cdot dl^{-1}$):** 3.1 (2.2-4.4)	**Induction:** NA **Maintenance MMF/day:** oral (n=18), IV (2 hour infusion, n=13), both oral and IV (n=7); 10-15 $mg \cdot kg^{-1}$ twice or three times daily; steady-state. **Co-medication:** cyclosporine (n=23) or tacrolimus (n=15), doses not specified; corticosteroids not specified.	HPLC; total MPA	**Software/algorithm:** NONMEM, version V, level 1.1; non-linear mixed effect modelling; FOCE-I **Structural model:** first-order absorption, two-compartment, first-order elimination **BSV:** exponential model **BOV:** exponential model **RV:** exponential model **Screened covariates:** age, BMI, BSA, co-medication (cyclosporine, acyclovir), CrCl, days of therapy, gender, GFR, height, MPA unbound	**Fixed effects for total MPA (estimate [RSE%]):** k_a (h^{-1}), 0.39 [20] V_c (l), 7.24 [55] V_p (l), 16.80 [52] **Q** ($l \cdot h^{-1}$), 3.74 [46] **CL** ($l \cdot h^{-1}$), $CL=\theta_1 \times (1+\theta_7 \times [\text{body weight}/27.9]) \times (1+\theta_8 \times CYTA) \times \exp(BSV+BOV)$ CL, 6.42 $l \cdot h^{-1}$ [34]; 14.74 $l \cdot h^{-1}$ (cyclosporine); 5.51 $l \cdot h^{-1}$ (tacrolimus) θ_7, 1.09 [30] θ_8, -0.60 [10] if cyclosporine CYTA=0; if tacrolimus CYTA=1	**Validation:** goodness-of-fit plot (OD-PRED); bootstrapping	Zeng et al. 2010 [221]

Patient population	Dosing regimen	Assay	Model	Population PK (or PD) parameters	Validation	References
Free fraction: 1.16% (0.49%-6%) **Type of transplantation:** blood or marrow transplant (n=23), kidney transplant (n=5), liver transplant (n=10) **Post-transplant time:** NA	**Additional concurrent medications:** acyclovir (n=9), dose not specified.		fraction, post-transplant time, serum albumin, type of transplantation, weight, allometrically scaled weight (exponent of 0.75) **Included covariates:** co-medication (cyclosporine), weight on CL Negative trend with CrCl and CL (p>0.05) Negative trend with albumin and CL (p>0.05) Covariate analysis was not conducted on V_c. Albumin-dependent scaling of total MPA concentration was not included in the model.	**F**, 0.48 [32] **BSV CV% for total MPA:** **ω (k_a)**, 59.1 [79] **ω (CL)**, 31.6 [26] **ω (F)**, 34.6 [59] ω not estimated for Q, V_c, V_p **BOV CV% for total MPA:** **ω (CL)**, 5.8 [105] **RV for total MPA:** 0.48 [14]		
Idiopathic nephrotic syndrome						
Study design: retrospective **Sample size:** 60 subjects (total), 45 subjects (development) and 15 subjects (Bayesian/external validation) **Race:** NA	**Induction:** NA **Maintenance MMF/day:** 605±150 (development), 564±150 (Bayesian/external validation) $mg \cdot m^{-}$	"in-house liquid chromatography method";	**Software/algorithm:** in-house software; iterative two-stage method **Structural model:** gamma absorption with 2 parallel routes, one-	**Fixed effects (mean±SD):** **MAT_1** (h), 0.35±0.14 **$SDAT_1$** (h), 0.10±0.03 **MAT_2** (h), 1.23±0.70 **$SDAT_2$** (h), 0.33±0.28 **V_c/F** (l), 14.66±9.09	**Validation:** regression and individual goodness-of-fit plots	Saint-Marcoux et al. 2011 [200]

Patient population	Dosing regimen	Assay	Model	Population PK (or PD) parameters	Validation	References
Age (years): 10.6±4.6 (mean or median [not specified] ±SD, development), 13.5±4.3 (Bayesian/external validation) **Gender:** NA **Weight (kg):** 34.5±15.8 (development), 41.7±11.2 (Bayesian/external validation) **Renal function:** NA **Liver function:** NA **Patient classification based on disease stages:** 1) remission ("urine protein/creatinine ratio<0.03 g·mmol^{-1} and serum albumin>3 g·dl^{-1}") 75.6% (development), 66.7% (Bayesian/external validation) 2) recent remission ("urine protein/creatinine ratio<0.03 g·mmol^{-1} and serum albumin<3 g·dl^{-1}") 8.9% (development), 6.7% (Bayesian/external validation) 3) partial remission ("urine protein/creatinine ratio<0.2	^{2}·day^{-1}; steady-state not specified. **Co-medication:** cyclosporine or tacrolimus were excluded; with or without corticosteroids (regimen not specified). **Additional concurrent medications:** NA	total MPA	compartment, first-order elimination **Screened covariates on CL/F (regression and principal component analyses):** age, co-medication (corticosteroids), height, MMF dose, serum albumin, serum proteins, time after initiation of treatment, urine creatinine, urine proteins, weight **(Identified) covariates:** weight on CL/F CL/F=7.82+0.17x weight Negative association between albumin and CL/F (for albumin < 3.0 g·dl^{-1}) Bayesian model: see Table IV-2 *PK-PD relationship:* Regression of AUC vs. clinical status (i.e. "Relapse", "Partial	**CL/F** (l·h^{-1}), 14.01±6.67 **BSV (reported as DF50):** **MAT$_1$**, 0.11 **SDAT$_1$**, 0.04 **MAT$_2$**, 0.61 **SDAT$_2$**, 0.18 **V$_c$/F**, 8.58 **CL/F**, 6.36 *PK-PD relationship:* "Remission" group exhibited significantly higher AUC than other groups.		

Patient population	Dosing regimen	Assay	Model	Population PK (or PD) parameters	Validation	References
and >0.03 g·mmol^{-1} and serum albumin>3 g·dl^{-1}") NA (development and Bayesian/external validation) 4) recent relapse ("urine protein/creatinine ratio>0.2 g·mmol^{-1} and serum albumin>3 g·dl^{-1}") 11.1% (development), 13.3% (Bayesian/external validation) 5) full relapse ("urine protein/creatinine ratio>0.2 g·mmol^{-1} and serum albumin<3 g·dl^{-1}") 4.4% (development), 13.3% (Bayesian/external validation) **Time after start of MMF (days):** NA			relapse", "Remission", and "Partial remission").			
Study design: prospective, multi-centre for children with relapsed steroid-dependent nephrotic syndrome **Sample size:** 23 subjects (total; 41 profiles, 285 samples), 21/23 subjects had kinetic profile at 1month after inclusion	**Induction:** NA **Maintenance MMF/day:**1200 mg·m^{-2}·day^{-1} in two divided doses; 563±212 (M1), 540±209 (M6) mg·day^{-1}, steady-state not specified.	HPLC-UV; total MPA	**Software/algorithm:** NONMEM version 6.1.1; non-linear mixed effect modelling; FOCE-I **Structural model:** first-order absorption with lag time, two-	**Fixed effects (estimate [SE%]):** k_a (h^{-1}), 5.16 [43.4] t_{lag} (h), 0.215 [37.9] V_c/F (l), 22.3 [22.6] V_p/F (l), 250 fixed [-] **Q/F** (l·h^{-1}), 18.8 [14.8] **CL/F** (l·h^{-1}),	**Validation:** goodness-of-fit plots (WRES-PRED, WRES-time); VPC plot	Zhao et al. 2010 [209]

Patient population	Dosing regimen	Assay	Model	Population PK (or PD) parameters	Validation	References
("M1"), and 20/23 subjects had kinetic profiles 6 months after inclusion ("M6") **Race:** NA **Age (years):** 7.4±3.8 (mean±SD**,** total), 7.5±4.1 (M1), 7.3±3.8 (M6) **Gender:** 18 males/5 females (total), 17/4 (M1), 15/5 (M6) **Weight (kg):** 29.9±18.0 (total), 30.3±17.1 (M1), 29.6±18.0 (M6) **Renal function:** CrCl ($ml \cdot min^{-1}$) 125.6±26.2 (M1), 130.4±37.1 (M6) (Schwartz formula) **Liver function:** ALP ($IU \cdot l^{-1}$) 152±59 (M1), 193±73 (M6); ALT ($IU \cdot l^{-1}$) 15±5 (M1), 15±4 (M6); AST ($IU \cdot l^{-1}$) 22±7 (M1), 25±13 (M6) **Serum albumin ($g \cdot dl^{-1}$):** 3.6±0.5 (M1), 3.96±0.42 (M6) **Time after start of MMF (days):** 33±7 (M1), 176±14 (M6)	**Co-medication:** prednisone (initial 60 $mg \cdot m^{-2} \cdot day^{-1}$ and tapered over 6 months; 47±14 (M1), 13±8 (M6) mg per 2 days **Additional concurrent medications:** NA		compartment, first-order elimination **BSV:** exponential model **BOV:** not assessed **RV:** proportional model **Screened covariates:** age, ALP, ALT, AST, BSA, cholesterol, CrCl, gender, height, haemoglobin, prednisone dose, serum albumin, time after start of therapy, urine protein, weight **Included covariates:** serum albumin, weight on CL/F Bayesian model: see Table IV-2	$CL=\theta_1 \times (\text{body weight}/23.5)^{\theta 2} \times (1-\theta_3 \times [\text{albumin}/38.6])$ θ_1, 22.5 $l \cdot h^{-1}$ [16.9] θ_2, 0.753 [11.2] θ_3, 0.570 [12.9] **BSV CV%:** **ω (t_{lag})**, 54.0 [100.3] **ω (V_c/F)**, 79.9 [67.6] **ω (Q/F)**, 57.6 [35.2] **ω (CL/F)**, 22.0 [42.6] **RV CV%:** **$\sigma_{proportional}$**, 44.6 [9.4]		

Patient population	Dosing regimen	Assay	Model	Population PK (or PD) parameters	Validation	References
Systemic lupus erythematosus						
Study design: retrospective **Sample size:** 36 subjects (16 subjects having active disease), 295 samples; development set based on 1000 simulated profiles; Bayesian external validation set based on 500 simulated profiles **Race:** NA **Age (years):** 12.9±2.6 (mean±SD) **Gender:** 10 male, 26 females **Weight (kg):** 45.8±16.1 **Renal function:** NA **Liver function:** NA **Serum albumin ($g \cdot dl^{-1}$):** 3.69±0.41 **Time after start of MMF (days):** 274 (6-2680) (median [range])	**Maintenance MMF/day:** 728±255 (mean±SD) mg MMF morning dose, 544±175 $mg \cdot m^{-2}$ MMF morning dose/BSA, total daily dose not specified; steady-state not specified. **Co-medication:** NA **Additional concurrent medications:** NA	HPLC; total MPA	**Software/algorithm:** in-house software; iterative two stage Bayesian approach **Structural model:** gamma absorption with 2 parallel routes, one-compartment, first-order elimination **BSV:** NA **BOV:** NA **RV:** logistic model **Screened covariates (logistic regression model):** age, gender, serum albumin, time after start of MMF **Included covariates:** none Bayesian model: see Table IV-2 *PK-PD relationship:* Logistic regression of C_0 or AUC (with/without	**Fixed effects (mean±SD):** **Real samples (n=36)** **a1**, 21.2±6.9 **b1**, 47.9±14.1 **a2**, 30.2±12.5 **b2**, 27.6±10.7 **FA-IV**, 5.0±2.1 **r**, 0.3±0.2 **V_c/F** (l), 24.8±13.5 **CL/F** ($l \cdot h^{-1}$), 19.2±13.2 "a"= shape "b"=scale of the two gamma laws; "r"= fraction of dose absorbed from the first gamma function. *PK-PD relationship:* AUC < 44 $mg \cdot h \cdot l^{-1}$: 21 times higher chance of active disease AUC/dose < 0.06: 59 times higher chance of active disease	**Validation:** goodness-of-fit plot (WRES-PRED); regression plots; individual goodness-of-fit plots	Woillard et al. 2014 [207]

Patient population	Dosing regimen	Assay	Model	Population PK (or PD) parameters	Validation	References
			dose-normalization) vs. SLEDAI (≥6)			
Study design: open-label, prospective, outpatient study **Sample size:** 19 (186 MPA concentrations, 186 MPAG concentrations) **Race:** 11 African American, 8 Caucasian **Ethnicity:** 4 Hispanic, 15 Non-Hispanic **Age (years):** 16.9±4 (mean±SD); 2-12 (n=2), 12-21 (n=14), >21 (n=3). Diagnosis made on/before 16 yrs old. **Gender:** 1 male, 18 females **Weight (kg):** 66.6±15 **Renal function:** SCr ($mg \cdot dl^{-1}$) 0.69±0.17 (n=17) **Liver function:** ALT ($U \cdot l^{-1}$) 28±29 (n=13); AST ($U \cdot l^{-1}$) 47±59 (n=13) **Serum albumin ($g \cdot dl^{-1}$):** 3.5±0.26 (n=17) **Time after start of MMF (years):** 1.5±1.3	**Maintenance MMF/day:** 600 $mg \cdot m^{-2}$ orally twice daily (1973±634 $mg \cdot day^{-1}$); same MMF dose for >3 weeks. **Co-medication:** oral prednisone (n=18; 17.2±10.4 $mg \cdot day^{-1}$), n=3 were on "high dose" IV methylprednisolone (dose NA). **Additional concurrent medications:** hydroxychloroquine (n=17), NSAIDs (n=11), antihypertensives (n=8), antacids were excluded.	HPLC; total MPA and MPAG	**Software/algorithm:** NONMEM, version 7.1; non-linear mixed effect modelling **Structural model:** first-order absorption and single series of transit compartments; multi-compartment (gut, central MPA, peripheral MPA, central MPAG, gallbladder); gallbladder release triggered by meal times (1 & 4 hours post dose) **BSV:** exponential model **BOV:** NA **RV:** combined model **Screened covariates:** age, disease duration, ethnicity, gender, race, weight ALT, AST, high dose IV methylprednisolone, SCr, or serum albumin not evaluated due to non-	**Fixed effects (Estimate [95% CI] from bootstrapping):** EHC (%), 35 fixed [-] FM (%), 85 fixed [-] k_a (h^{-1}), 1.5 fixed [-] **$V3_{MPA}$** (l), 20.9 [13.7, 31.2] **$V4_{MPA}$** (l), 234 [230.2, 247.8] **$CL1_{MPA}$** ($l \cdot h^{-1}$), 25.3 [17.2, 32.4] **$CL2_{MPA}$** ($l \cdot h^{-1}$), 19.8 [19.2, 31.6] **CLM_{MPAG}** ($l \cdot h^{-1}$), 2.5 [0.3, 4.9] **BSV CV%:** **ω ($V3_{MPA}$)**, 59.2 [49.8, 65.4] **ω ($V4_{MPA}$)**, 60.0 [52.4, 67.6] **ω ($CL1_{MPA}$)**, 48.6 [33.9, 59.1] **ω ($CL2_{MPA}$)**, 42.9 [30.1, 52.1] **ω (CLM_{MPAG})**, 55.9 [42.2, 65.9] **RV CV%:** **$σ_{MPA}$,** 41.2 [35.8, 43.2]	**Validation:** goodness-of-fit plots on both MPA and MPAG (OD-PRED, OD-IPRED, CWRES-PRED, CWRES-time); VPC plot; bootstrapping	Sherwin et al. 2012 [203]

Patient population	Dosing regimen	Assay	Model	Population PK (or PD) parameters	Validation	References
			concurrent collection time vs. kinetic data **Included covariates:** none	**σMPAG,** 45.4 [35.7, 48.9]		

[a], SCr unit conversion, 1 μmol·l^{-1}=0.0113 mg·dl^{-1}. [b], bilirubin unit conversion, 1 μmol·l^{-1}=0.0585 mg·dl^{-1}.

Abbreviation(s): *ALP*, serum alkaline phosphatase; *ALT*, serum alanine aminotransferase; *AST*, serum aspartate aminotransferase; *AUC*, area under the concentration-time curve; *BMI*, body mass index; BSA, body surface area; *BUN*, blood urea nitrogen; *CI*, confidence interval; *CL*, clearance; *CL/F*, apparent clearance; $CL1_{MPA}$, apparent oral CL/F for MPA in the central compartment; $CL2_{MPA}$, apparent intercompartmental CL/F in the peripheral compartment; CLM_{MPAG}, apparent renal CL/F of MPAG; *CrCl*, creatinine clearance; *CV*, coefficient of variation; *CWRES*, conditional weighted residuals; *DBSA*, dose per body surface area; *DF50*, 50% dispersion factor; E_0, baseline inosine monophosphate dehydrogenase activity; EC_{50}, MPA concentration at half E_{max}; E_{max}, maximal inhibitory effect; *EMIT*, enzyme-multiplied immunoassay technique; *FA-IV* is the "disposition coefficient following an intravenous bolus administration of a unit dose"; *FM*, fraction metabolite (MPAG); *FO*, first-order; *FOCE*, first-order conditional estimation; *FOCE-I*, first-order conditional estimation with interaction; *GFR*, glomerular filtration rate; *HPLC*, high-performance liquid chromatography; *BSV*, between subject variability; *IMPDH*, inosine monophosphate dehydrogenase; *BOV*, between occasion variability; *IPRED*, individual predicted; *IRES*, individual residuals; *IV*, intravenous; *IWRES*, individual weighted residuals; k_{12} *and* k_{21}, inter-compartment transfer constant; k_a, absorption rate constant; k, elimination rate constant; k_r, constant transfer rate between absorption compartments; MAT_i, mean absorption time of the absorption phase i; *MMF*, mycophenolate mofetil; *MPA*, mycophenolic acid; *MPAG*, MPA glucuronide; *MRP-2*, multidrug

resistance-associated protein 2 transporter; *MS/MS*, tandem mass spectrometry; *MTT*, mean transit time; *NA*, not available or not specified; *NSAIDs*, nonsteroidal anti-inflammatory drugs; *OD*, observed data; *PD*, pharmacodynamic; *PK*, pharmacokinetic; *PRED*, population predicted, *Q*, inter-compartmental clearance; *Q/F*, apparent inter-compartmental clearance; *RSE*, relative standard error; *RV*, residual variability; *SCr*, serum creatinine; *SD*, standard deviation; $SDAT_i$, standard deviation of absorption time; *SE*, standard error; *SLEDAI*, "systemic lupus erythematosus disease activity index"; t_{lag}, absorption lag time; *TV*, typical value of the PK parameter in the population; *UV*, ultra-violet spectrometry; $V3_{MPA}$, apparent volume of distribution of MPA in the central compartment; $V4_{MPA}$, apparent volume of distribution of MPA in the peripheral compartment; V_c, central volume of distribution; V_c/F, apparent central volume of distribution; V_d/F, apparent volume of distribution; V_p, peripheral volume of distribution; V_p/F, apparent peripheral volume of distribution; *VPC*, visual predictive check; *WRES*, weighted residuals; α, apparent rate constant of distribution; β, apparent rate constant of elimination; θ, covariate effect; σ, residual variability; ω, between subject variability or between occasion variability.

Table IV-2 Summary of Bayesian models in population pharmacokinetic studies for mycophenolic acid in paediatric populations

Validation population	Sample size	Pharmacokinetic model	PK parameters validated	Bias and precision	Reference
Type of transplantation: kidney **Age (years):** 8.9±4.9 (mean±SD) **Weight (kg):** 30.5±16.1 **Renal function:** NA **Serum albumin ($g \cdot dl^{-1}$):** NA **Post-transplant time:** day 21; month 3, 6, 9[a] **Co-immunosuppressants:** cyclosporine; methylprednisolone or prednisone	32	**Structural model:** first-order absorption with lag time, two-compartment, first-order elimination **Covariate model:** None **Sampling time points:** 8 points (pre-dose, 30min, 1h, 1.5h, 2h, 4h, 8h, 12h post-dose) or 9 points (pre-dose, 20min, 40min, 75 min, 2h, 4h, 6h, 8h, 12h post-dose)	Estimated $AUC_{(0-12)}$ or plasma concentrations	**Estimated $AUC_{(0-12)}$:** *Sampling time, h* / *Approaches* / *Bias, MPE%* / *Precision, RMSE%* NA / Parametric / -9.53* / 14.51 NA / Nonparametric (normal model) / 1.40 / 12.10 NA / Nonparametric (lognormal model) / -1.68 / 6.87 *p<0.05 **Plasma concentrations:** *Sampling time, h* / *Approaches* / *Bias, MPE%* / *Precision, RMRE%* NA / Parametric / 13.67* / 77 NA / Nonparametric (normal model) / 11.53 / 44.71 NA / Nonparametric (lognormal model) / 13.6 / 50.02 *p<0.05 **Additional validation methods:** scatter plots (observed vs. predicted plasma concentrations)	Prémaud et al. 2011 [198]

Type of transplantation: kidney **Age (years):** 12.2 (2.0-19.0) (mean [range]) **Weight (kg):** 37.0 (11.4-68.6) **Renal function:** CrCl (ml·min^{-1}) 105 (32-214) **Serum albumin (g·dl^{-1}):** NA **Post-transplant time (days):** first kinetic profile at 12-3754[a] **Co-immunosuppressants:** cyclosporine or tacrolimus; corticosteroids	13	**Structural model:** first-order absorption with lag time, two-compartment, first-order elimination **Covariate model:** weight on V_c/F **Sampling time points:** 8 points (pre-dose, 1h, 2h, 4h, 6h, 8h, 10h, 12h post-dose)	Estimated $AUC_{(0-12)}$	**Estimated $AUC_{(0-12)}$:** *Sampling time, h* / *Bias, MPE%* / *Precision, RMSE%* / *95% CI of bias, %* 1-2-6[b,c] / -1.98 / 9.21 / -6.74, -2.79 1-2-4 / -1.48 / 7.10 / -5.16, -2.21 1-2-6 / -0.51 / 9.48 / -5.53, 4.51 1-4-6 / -0.045 / 5.18 / -2.70, 2.79 1-2 / 0.021 / 12.4 / -6.90, 6.94 1-4[d] / -0.90 / 6.02 / -3.72, 2.91 4 / -1.28 / 11.9 / -5.42, 6.98 **Additional validation methods:** scatter plot (reference vs. predicted $AUC_{(0-12)}$)	Payen et al. 2005 [196]
Type of transplantation: liver **Age (years):** 11.1 (2.2-18.0) (median [range]) **Weight (kg):** 36 (13.5-63.2) **Renal function:** CrCl (ml·min^{-1}) 118 (46-175)	12	**Structural model:** first-order absorption, one-compartment, first-order elimination **Covariate model:** age on k_a;	MPA estimated $AUC_{(0-12)}$	**Estimated $AUC_{(0-12)}$:** *Sampling time, h* / *Bias, %* / *Precision, %* 0-0.5-2 0-1-2 0-2-4 1-2-4 0-1-4[d] 0-0.5-1-2 0-1-2-4 NA		Barau et al. 2012 [183]

(Bayesian/external validation) (Schwartz formula); SCr (μmol·l^{-1})[e] 57 (30-89) (validation) **Serum albumin (g·dl^{-1}):** 3.43 (3.90-5.47) **Post-transplant time (months):** 17.2 (0.2-188.5)[a] **Co-immunosuppressants:** cyclosporine or tacrolimus; prednisone		post-transplant time (≤ and >6 months) on V_d/F **Sampling time points:** 7 points (pre-dose, 0.5h, 1h, 2h, 4h, 6h, 8h post-dose)		0-0.5-2-4 **Additional validation methods:** Scatter plot (reference vs. predicted $AUC_{(0-12)}$; Pearson's correlation test (r^2=0.9041, p<0.0001, reference vs. predicted $AUC_{(0-12)}$); Bland-Altman plot (slight negative bias observed)	
Indication: idiopathic nephrotic syndrome **Age (years):** 13.5±4.3 (mean or median±SD) **Weight (kg):** 41.7±11.2 **Renal function:** NA **Serum albumin (g·dl^{-1}):** <3.0 (20.0%); >3.0 (80.0%) **Co-immunosuppressants:** with or without corticosteroids	15	**Structural model:** gamma absorption with 2 parallel routes, one-compartment, first-order elimination **Covariate model:** None **Sampling time points:** 10 points (pre-dose, 20min,	MPA estimated $AUC_{(0-12)}$	**Estimated $AUC_{(0-12)}$:** *Sampling time, min* / *Bias, MPE% (mean±SD)* / *Precision, RMSE%* 20-60-180[d] / -3.6±14.5 / 14 Other sampling time combinations not specified. **Additional validation methods:** regression analysis (r^2=0.88, reference vs. predicted concentrations)	Saint-Marcoux et al. 2011 [200]

Patient classification based on disease stages: 1) remission ("urine protein/creatinine ratio<0.03 g·mmol^{-1} and serum albumin>3 g·dl^{-1}") 66.7% 2) recent remission ("urine protein/creatinine ratio<0.03 g·mmol^{-1} and serum albumin<3 g·dl^{-1}") 6.7% 3) partial remission ("urine protein/creatinine ratio<0.2 and >0.03 g·mmol^{-1} and serum albumin>3 g·dl^{-1}") NA 4) recent relapse ("urine protein/creatinine ratio>0.2 g·mmol^{-1} and serum albumin>3 g·dl^{-1}") 13.3% 5) full relapse ("urine protein/creatinine	40min, 1h, 2h, 3h, 4h, 6h, 8h, 12h post-dose)

ratio>0.2 g·mmol^{-1} and serum albumin<3 g·dl^{-1}") 13.3%					
Indication: idiopathic nephrotic syndrome **Age (years):** 7.4±3.8[a] (mean±SD) **Weight (kg):** 29.9±18.0[a] **Renal function:** CrCl (ml·min^{-1}) 125.6±26.2[a] (21 patients at month 1, M1), 130.4±37.1[a] (20 patients at month 6, M6) (Schwartz formula) **Serum albumin (g·dl^{-1}):** 3.60±0.50[a] (M1), 3.96±0.42[a] (M6) **Co-immunosuppressants:** prednisone	23 (divided into four subsets for circular permutation validation)	**Structural model:** first-order absorption with lag time, two-compartment, first-order elimination **Covariate model:** serum albumin, weight on CL/F **Sampling time points:** 7 points (pre-dose, 0.5h, 1h, 2h, 4h, 8h, 12h post-dose)	MPA estimated $AUC_{(0-12)}$	**Estimated $AUC_{(0-12)}$:** *Sampling time, h* / *Bias, PE % (mean±SD)* / *Precision, APE% (mean±SD)* *Estimated using original data* 0-1-4[d]: 1.7±12.0 / 9.5±7.4 0-0.5-4: 2.5±14.4 / 11.5±8.8 0-0.5-2: 5.6±9.6 / 9.2±6.1 0.5-1-4: -7.3±12.8 / 12.3±7.9 0.5-1-2: 1.5±11.3 / 7.8±8.2 *Estimated using circular permutation data* 0-1-4[d]: 0.3±15.6 / 12.0±9.8 0.5-1-2: 2.6±22.2 / 17.0±14.3 **Additional validation methods:** Bland-Altman plot	Zhao et al. 2010 [209]
Indication: systemic lupus erythematosus **Age (years):** 12.9±2.6 (mean±SD)	500 simulated patients based on a model developed from 36	**Structural model:** gamma absorption with 2 parallel routes, one-compartment, first-order elimination	MPA estimated $AUC_{(0-12)}$	**Estimated $AUC_{(0-12)}$:** *Sampling time, h* / *Bias, mg·h·l^{-1} (mean)* / *Precision, RMSE%* 0.33-1-3[d]: -0.002 / 15.8 0.33-1-4: 7.45 / 22.02	Woillard et al. 2014 [207]

Weight (kg): 45.8±16.1 **Renal function:** NA **Serum albumin (g·dl^{-1}):** 3.69±0.41 **Time after start of MMF (days):** 274 (6-2680) (median [range]) **Co-immunosuppressants:** NA	subjects with 1000 simulations	**Covariate model:** NA **Sampling time points:** 17 points (pre-dose, 20min, 40min, 1h, 1.5h, 2h, 2.5h, 3h, 4h, 5h, 6h, 7h, 8h, 9h, 10h, 11h, 12h)	0.33-3-4 0.66-1-3 0.66-2-3 0.66-3-4	8.53 0.66 -1.90 3.71	25.79 17.67 19.45 22.59
			Additional validation methods: regression analysis (r^2=0.97, reference vs. predicted $AUC_{(0-12)}$; r^2=0.99, reference vs. predicted concentrations)		

[a], reported based on original total population group; [b], in comparison to noncompartmental approach (reference AUC); [c], calculated from multiple-linear regression equation; [d], best combination of sampling time points selected by the investigators; [e], SCr unit conversion, 1 μmol·l^{-1}=0.0113 mg·dl^{-1}.

Abbreviation(s): *APE*, absolute prediction error; *AUC*, area under the concentration-time curve; *CI*, confidence interval; *CL/F*, apparent clearance; *CV*, coefficient of variation; k_a, absorption rate constant; *MLR*, multiple-linear regression; *MPE*, mean prediction error; *NA*, not available or not specified; *PE*; prediction error; *RMSE*, root mean squared prediction error; *SD*, standard deviation; V_c/F, apparent central volume of distribution; V_d/F, apparent volume of distribution.

Table IV-3 Summary of modelling features in population pharmacokinetic studies for mycophenolic acid in paediatric populations

Total/free MPA concentration	Metabolites	Secondary peaks	Bayesian AUC prediction	Population pharmacokinetic-pharmacogenetic model	Population pharmacokinetic-pharmacodynamic model	References
Kidney transplant						
Total	×	×	×	×	✓ Inhibitory E_{max} model	Dong et al. 2014 [185]
Total	×	×	✓ Optimal sampling time not specified	×	×	Prémaud et al. 2011 [198]
Total	×	×	×	✓ Single nucleotide polymorphism to UGT2B7 (802C>T) affected MPA clearance	×	Zhao et al. 2010 [210]
Total	×	×	✓ Optimal sampling time: 1 hour and 4 hours	×	×	Payen et al. 2005 [196]
Liver transplant						
Total	×	×	✓ Optimal sampling time: pre-dose, 1 hour, and 4 hours	×	×	Barau et al. 2012 [183]

Haematopoietic stem cell transplant						
Free	×	×	×	×	×	Kim et al. 2012 [189]
Combined kidney, liver, and haematopoietic stem cell transplant						
Total	×	×	×	×	×	Zeng et al. 2010 [221]
Idiopathic nephrotic syndrome						
Total	×	✓ Gamma absorption with two parallel routes	✓ Optimal sampling time: 20 minutes, 1 hour, and 3 hours	×	×	Saint-Marcoux et al. 2011 [200]
Total	×	No	✓ Optimal sampling time: pre-dose, 1 hour, and 4 hours	×	×	Zhao et al. 2010 [209]
Systemic lupus erythematosus						
Total	×	✓ Gamma absorption with two parallel routes	✓ Optimal sampling time: 20 minutes, 1 hour, and 3 hours	×	×	Woillard et al. 2014 [207]
Total	✓ Total MPAG	✓ Gallbladder compartment	×	×	×	Sherwin et al. 2012 [203]

Abbreviation(s): *AUC*, area under the concentration-time curve; E_{max}, maximal inhibitory effect; *MPA*, mycophenolic acid; *MPAG*, MPA glucuronide.

Chapter V. Development and validation of a sensitive liquid-chromatography tandem mass-spectrometry assay for mycophenolic acid and metabolites in HepaRG cell culture: characterization of metabolism interactions between *p*-cresol and mycophenolic acid[5]

Prologue:

This is the first of five chapters demonstrating our mechanistic investigations into the novel inhibitory effects of p-cresol toward MPA metabolism. The aim of this chapter was to develop and validate a highly sensitive liquid chromatography tandem mass spectrometry assay for the quantification of MPA, MPAG, and AcMPAG, and to characterize the metabolism interaction, for the first time, between MPA and p-cresol using a metabolically competent human hepatoma cell line (HepaRG).

---

[5] This chapter is already published in a peer-reviewed journal. **Rong Y** and Kiang TKL. Development and validation of a sensitive liquid-chromatography tandem mass spectrometry assay for mycophenolic acid and metabolites in HepaRG cell culture: Characterization of metabolism interactions between *p*-cresol and mycophenolic acid. *Biomedical Chromatography*. 2019 Aug;33(8):e4549. doi: 10.1002/bmc.4549.

Acknowledgement: Reprinted by permission from John Wiley and Sons: Biomedical Chromatography. Development and validation of a sensitive liquid-chromatography tandem mass spectrometry assay for mycophenolic acid and metabolites in HepaRG cell culture: Characterization of metabolism interactions between *p*-cresol and mycophenolic acid. **Rong Y** and Kiang TKL. License number: 5222100819834 (2019).

Abstract

Mycophenolic acid (MPA), a frequently used immunosuppressant, exhibits large inter-patient pharmacokinetic variability. This study 1) developed and validated a sensitive liquid chromatography-tandem mass spectrometry (LC-MS/MS) assay for MPA and metabolites (MPA glucuronide [MPAG] and acyl-glucuronide [AcMPAG]) in the culture medium of HepaRG cells; and 2) characterized the metabolism interaction between mycophenolic acid and *p*-cresol (common uremic toxin) in this *in vitro* model as a potential mechanism of pharmacokinetic variability. Chromatographic separation was achieved with a C18 column (4.6×250 mm, 5 µm) using a gradient elution with water and methanol (with 0.1% formic acid and 2 mM ammonium acetate). A dual ion source ionization mode with positive multiple reaction monitoring (MRM) was utilized. MRM mass transitions (m/z) were: MPA (320.95→207.05), MPAG (514.10→303.20), and AcMPAG (514.10→207.05). MPA-d_3 (323.95→210.15) and MPAG-d_3 (517.00→306.10) were utilized as internal standards. The calibration curves were linear from 0.00467-3.2 µg/mL for MPA/MPAG and 0.00467-0.2 µg/mL for AcMPAG. The assay was validated based on industry standards. *p*-Cresol inhibited MPA glucuronidation (IC_{50} ~ 55 µM) and increased MPA concentration (up to >2 folds) at physiologically-relevant substrate-inhibitor concentrations (n=3). Our findings suggested that fluctuations in p-cresol concentrations might be in-part responsible for the large pharmacokinetic variability observed for MPA in the clinic.

1. Introduction

Mycophenolate mofetil (MMF) is an immunosuppressant frequently used for the prevention of graft rejection following solid organ transplantation [131, 132]. As a pro-drug, MMF is rapidly absorbed after oral administration and hydrolyzed to its active form, mycophenolic acid (MPA, structure shown in Figure V-1). MPA's pharmacological action is mediated by its ability to reduce *de novo* guanosine nucleotide synthesis thereby decreasing the proliferation of T- and B-lymphocytes [131, 132]. MPA is primarily metabolized in the liver by uridine diphosphate glucuronosyltransferase (UGT) 1A9 enzyme in the production of the quantitatively major MPA glucuronide (MPAG, Figure V-1), and by UGT2B7 in the generation of the minor MPA acyl-glucuronide (AcMPAG, Figure V-1) [31]. The glucuronide metabolites can be excreted in the urine or converted back to MPA via enterohepatic recirculation [31]. The entero-hepatic recirculation of MPAG produces the secondary MPA peaks sometimes observed in its plasma concentration-time profiles [29]. Because MPA is highly bound to plasma albumin (97-99 %), its pharmacological effects should ideally be assessed in relation to its free concentrations [10].

Large between- and within- patient variabilities in MPA pharmacokinetics have been observed in the clinic [31]. These variabilities can be attributed to both extrinsic (e.g. concurrently administered medications) and/or intrinsic (e.g. altered hepatic and renal functions, disease states) factors that affect MPA clearance [29]. An important extrinsic factor is drug-drug interaction modulating the catalytic activities of UGT enzymes. For example, corticosteroids are known to induce the expression of UGT enzymes and potentially enhance the clearance of MPA [106, 268]; whereas select non-steroidal anti-inflammatory drugs (e.g. niflumic acid) are potent UGT inhibitors that can significantly reduce MPA glucuronidation [269]. In addition to interacting drugs, the hepatic clearance of MPA can also be affected by endogenous substances such as uremic toxins

that accumulate in patients with reduced renal function (e.g. chronic renal failure) which are capable of reducing the catalytic activities of UGT enzymes [52, 99].

p-Cresol is an example of a protein-bound toxin of toxicological interest due to its significant plasma accumulation under uremic conditions [53]. In human liver microsomes, *p*-cresol is an inhibitor of both UGT1A9 and UGT2B7, as evident by significant reductions in probe substrate activities for these enzyme pathways [52]. Because *p*-cresol is a potent inhibitor of UGT1A9, the primary enzyme responsible for MPA glucuronidation, a clinically significant uremic toxin-drug interaction is possible but this has yet been characterized. Based on these observations, we hypothesized that physiological concentrations of *p*-cresol can reduce the hepatic clearance of MPA and that this molecular interaction is one of the mechanisms for the observed variability in MPA pharmacokinetics in humans.

To test the "*p*-cresol and MPA" interaction hypothesis, the inhibitory effects of *p*-cresol toward MPA metabolism were characterized using the metabolically-competent HepaRG cell line, which has become a popular model for the assessment of drug metabolism and drug-drug interactions [172]. HepaRG cells exhibit hepatocyte- and biliary-like morphology after differentiation in culture. The cell line also expresses multiple liver-specific functions, including the expression of drug metabolism enzymes that are comparable to primary human hepatocytes [172, 270]. In order to characterize the interaction between *p*-cresol and MPA in this *in vitro* model, an analytical assay that can quantify MPA and its metabolites in cell culture needed to be developed and validated. The objectives of this study were 1) to develop and validate a sensitive liquid chromatography-tandem mass spectrometry (LC-MS/MS) assay for the quantification of MPA and its glucuronidated metabolites (i.e. MPAG and AcMPAG) in the culture medium of

HepaRG cells, and 2) to characterize the inhibitory effects of *p*-cresol toward the metabolism of MPA.

2. Experimental

2.1. Materials and reagents

MPA (≥98% purity), high performance liquid chromatography (HPLC) plus grade methanol, dimethyl sulfoxide (DMSO) (≥99.5% purity, for cell culture use), triton-X, niflumic acid (≤100%), and *p*-cresol (99% purity) were purchased from Sigma-Aldrich (Oakville, Ontario, Canada). MPA-d_3 (100 µg/mL in acetonitrile) was purchased from Cerilliant (Round Rock, Texas, USA). MPAG (catalog no. M831520), MPAG-d_3 (catalog no. M831522), and AcMPAG (catalog no. M831522) were obtained from Toronto Research Chemicals (North York, Ontario, Canada). HPLC grade water and acetonitrile were obtained from VWR (Mississauga, Ontario, Canada). Ammonium acetate (97% purity) was purchased from Caledon Laboratories Ltd (Georgetown, Ontario, Canada), and further filtered using the Millex® 0.45 µM filters (Cork, Ireland) for the preparation of the mobile phases. Liquid chromatography-mass spectrometry (LC-MS) grade formic acid and acetic acid (>99.7% purity) were purchased from Fisher Scientific (Ottawa, Ontario, Canada). Ethylenediaminetetraacetic acid (EDTA) was purchased from Truin Science (Edmonton, Alberta, Canada).

Undifferentiated HepaRG cells, growth additives (ADD711C), and differentiation additives (ADD721C) were obtained from Biopredic International (Rennes, France). William's E basal medium and 24-well tissue culture plates were purchased from Fisher Scientific (Ottawa, Ontario, Canada). Tissue culture flasks (25 cm^2 and 75 cm^2) were purchased from Corning (New

York, USA). The cytotoxicity test kit (i.e. lactate dehydrogenase [LDH] assay kit) was purchased from Roche (Mississauga, Ontario, Canada). The SpectraMax M2 microplate reader was purchased from Molecular Devices (San Jose, California, USA).

2.2. Instrumentation and LC-MS/MS conditions

The LC-MS/MS system (Shimadzu, Kyoto, Japan) consisting of a system controller (CBM-20A), a degasser unit (DGU-20A 5R), a binary pump (LC-30AD), an autosampler (SIL-30AC), a column oven (CTO-20AC), and a triple quadrupole mass spectrometry (MS) detector with unit resolution of 0.7 μ (LCMS-8050) was used for sample analysis. Chromatographic separation was achieved with Zorbax Eclipse XDB-C18 analytical column, 4.6×250 mm, 5 μm particle size, from Agilent Technologies (Mississauga, Ontario, Canada) fitted to a Zorbax Eclipse XDB-C18 guard column (4.6×12.5 mm, 5 μm particle size). The mobile phases consisted of two solutions, (A) water and (B) methanol, each containing 0.1% formic acid and 2 mM ammonium acetate. Separation was achieved with a gradient elution which consisted of 30% solution (B) (0-2 min); linear increase from 30% to 90% solution (B) (2-6 min); 100% solution (B) (6-8 min); linear decrease from 100% to 30% solution (B) (8-8.5 min); and 30% solution (B) (8.5-15 min). The flow rate was kept at 1 mL/min except from 7-10 min where it was increased to 1.5 mL/min. Autosampler injection volume was 5 μL. The autosampler temperature and column oven temperature were maintained at 4°C and 40°C, respectively. MPA-d_3 was used as the internal standard for quantifying MPA, whereas MPAG-d_3 was utilized as the internal standard for both MPAG and AcMPAG. Dual ion source (DUIS), a combination of electrospray ionization (ESI) and atmospheric pressure chemical ionization (APCI), along with positive multiple reaction monitoring (MRM), was performed to analyze the samples. The MRM mass transitions (m/z) were

320.95→207.05 for MPA; 323.95→210.15 for MPA-d_3; 514.10→303.20 for MPAG; 514.10→207.05 for AcMPAG, and 517.00→306.10 for MPAG-d_3. Data acquisition and chromatography integration were performed with LabSolutions software (version 5.91) [271].

2.3. Optimization of compound-specific and source parameters

Compound-specific parameters including MRM mass transitions, Q_1/Q_3 pre-bias, and collision energy (CE) were initially optimized automatically using LabSolutions software by flow injecting a mixture of MPA, MPAG, AcMPAG, MPA-d_3, and MPAG-d_3. Subsequently, the instrument conditions were further optimized manually using two separate mixtures: 1) MPA with MPA-d_3 and 2) MPAG, AcMPAG, with MPAG-d_3, grouping together analytes with similar physiochemical properties. The final MS conditions corresponded with instrument parameters associated with the highest sensitivity for all analytes.

2.4. Preparation of calibration standards and quality control samples

Stock solutions of MPA (1 mg/mL), MPAG (100 µg/mL), AcMPAG (100 µg/mL), MPA-d_3 (20 µg/mL), and MPAG-d_3 (100 µg/mL) were prepared in methanol and stored at -80°C. Working solutions of all analytes (MPA, MPAG, AcMPAG, 10 µg/mL) and internal standards (MPA-d_3 [0.4 µg/mL] and MPAG-d_3 [2 µg/mL]) were further diluted in methanol for each assay. Standard calibrators (0.00467, 0.00778, 0.01296, 0.0216, 0.036, 0.06, 0.1, 0.2, 0.4, 0.8, 1.6, and 3.2 µg/mL for MPA and MPAG; 0.00467, 0.00778, 0.01296, 0.0216, 0.036, 0.06, 0.1, and 0.2 µg/mL for AcMPAG) and four concentrations of quality control (QC) samples (lower limit of quantification [LLOQ], low QC, medium QC, and high QC [0.00467, 0.01296, 0.1, and 1.6 for

MPA and MPAG; 0.00467, 0.01296, 0.036, and 0.1 µg/mL for AcMPAG, respectively]) were prepared by diluting working solutions in HepaRG differentiation cell culture medium. The QC samples were prepared independently at the same time as the calibrators.

2.5. Sample preparation

To each 100 µL of calibrators, QC samples, or actual samples, 50 µL of each internal standard (MPA-d_3 [0.4 µg/mL] and MPAG-d_3 [2 µg/mL]) were spiked, followed by 52 µL of the protein precipitation solution (PPS). The PPS is composed of 25 µL acetonitrile, 25 µL methanol, and 2 µL 10% (v/v) acetic acid, the latter used to stabilize AcMPAG [163]. Subsequently, 200 µL of the assay mixture was vortexed at a fixed speed using vortex mixer from Fisher Scientific (Ottawa, Ontario, Canada) for 30 seconds. The mixture was then centrifuged at 18600 × g for 4 minutes with Eppendorf centrifuge (Mississauga, Ontario, Canada) to condense the precipitated proteins. Clear supernatant (180 µL) was then transferred to pre-labeled glass vials and 5 µL was injected into the LC-MS/MS. For the determination of free concentrations, a 200 µL mixture of analytes, internal standards, and PPS were centrifuged via Amicon® ultra-centrifugal filters (MW cut-off 30 kDa) purchased from Sigma-Aldrich (Oakville, Ontario, Canada) at 14000 × g for 10 minutes instead of general-purpose tubes, using the same protocol as that described previously [272].

2.6. Method validation

The developed assay was validated as per FDA Guidance for Industry: Bioanalytical Method Validation [273].

2.6.1. Calibration curves

A blank calibrator (HepaRG cell culture medium without internal standards), a zero calibrator (culture medium with internal standards), and eight (AcMPAG) to twelve (MPA and MPAG) individual concentrations were prepared according section 2.4. Calibration curves were constructed by plotting the peak area ratios (analyte : internal standard) versus nominal concentrations for each analyte. A weighted ($1/x^2$) least-squares linear regression model was utilized to obtain the intercepts, slopes, and coefficients of determination (R^2) for each standard curve.

2.6.2. Selectivity and sensitivity

Six individual sources of HepaRG cell culture medium were prepared independently as blank calibrators. The absence of chromatographic peaks at the same retention times of authentic standards in the zero calibrators (defined as response < 5% of the LLOQ samples) was the criteria for assay selectivity [273]. LLOQ, corresponding to assay sensitivity, was defined as lowest, but non-zero, concentration on the calibration curve with acceptable precision and accuracy (i.e. ± 20%). The analyte responses at LLOQ were at least five fold than the background responses obtained in the zero calibrators [273].

2.6.3. Carryover effects and recovery

Carryover effects were assessed by the presence of chromatographic peaks in blank samples injected immediately after a highest calibrator sample. By convention, a lack of carryover is evident only when the blank sample exhibited less than 20% of the response of an LLOQ sample (e.g. [274]). Recovery was assessed by comparing peak areas from extracted samples at low, medium, and high QC concentrations to that obtained from the same analytes in reference samples that were spiked with authentic standards only after extraction.

2.6.4. Precision and accuracy

Six replicates of QC samples at 4 designated concentrations (as stated in section 2.4) were assayed on three individual days with freshly prepared calibration curves. Intra- and inter-day precision were assessed based on coefficient of variation (CV %), whereas bias (%) calculation was used to denote accuracy [273]. By convention, the % precision and accuracy were acceptable if ≤15% for the low, medium, and high QC concentrations. For the LLOQ, ≤ 20% was acceptable.

2.6.5. Stability

The stability of analytes in HepaRG cell culture medium was evaluated under various processing/storage conditions including i) autosampler stability (up to 24 hours on autosampler racks at 4°C), ii) bench-top stability (6 hours at controlled-ambient temperature, 23.5 °C), iii) long-term stability (-80°C for 30 days), and iv) freeze-thaw stability (3 cycles of free-thawing from -80°C). Four replicates of low and high QC samples were subjected to the above processings, in

comparison to freshly prepared samples as controls. A bias determination of ≤15% was deemed acceptable [273].

2.7. Application to the in vitro interaction between MPA and p-cresol

2.7.1. HepaRG maintenance and differentiation

Undifferentiated, cryopreserved HepaRG cells were cultured based on Biopredic International's protocols [275]. Briefly, cells were seeded at a density of 0.5×10^6 cells in 25 cm^2 flasks and maintained for 2 weeks (per passage) to reach confluency (doubling time ~24 hours) in William's E basal medium supplemented with growth additives. Based on Gripon et al [270], the growth additive consisted of fetal bovine serum (10%), antibiotics (e.g. penicillin [100 units/mL] /streptomycin [100 µg/mL]), insulin (5 µg/mL), hydrocortisone hemisuccinate (5×10^{-5} M), and glutamine (1%, v/v). At selected passage (i.e. passage 16 for our experiments), cells were differentiated in basal medium supplemented with differentiation additives for an additional 2 weeks. Based on Gripon et al [270], the differentiation additives consisted of additional DMSO (2%) to growth additives. Differentiated cells were plated at a density of 0.4×10^6 cells/well in 24-well tissue culture plates. Experiments were performed after 12 days of plating to allow cell acclimatization. The growth medium or differentiation medium was renewed every 2 or 3 days after microscopic observation.

2.7.2. Treatment of HepaRG cells

When cells were ready for treatment, the cell culture medium was aspirated and replaced with fresh differentiation medium containing 1.25 µM of MPA (i.e. 0.4 µg/mL, in 0.4% v/v

methanol). This MPA concentration corresponded to the average *free* maximum concentration that can be attained in human subjects administered therapeutic doses of MMF [138]. In order to determine MPAG and AcMPAG formation in relation to incubation time, cell supernatant was collected at 1) 0, 3, 6, 12, 18, 20, 24 hours, and 2), 36, 48, 60, and 72 hours following MPA (1.25 μM) treatment. Samples were snap-frozen on dry ice and transferred immediately to -80°C freezer for storage. MPA and metabolite concentrations were quantified using the above validated method.

The effects of niflumic acid (0, 2, 4, 8, and 10 μM, known positive control inhibitor for UGT1A9 [269]) and *p*-cresol (0, 5, 10, 30, 60, 100, and 200 μM, physiological range in uremic conditions [52, 276]) on MPA, MPAG, and AcMPAG concentrations in culture supernatant were accessed in cells treated with MPA (1.25 μM). Reactions were stopped at 6 hours for niflumic acid experiments and 3 hours for *p*-cresol experiments, respectively. These represented linear enzymatic conditions based on results from time-course experiments (Discussed further below).

As a control experiment to determine cell viability in all treatment groups, LDH release was tested using a cytotoxicity kit based on the manufacture's protocol [277]. Briefly, cell supernatant was first collected. Then the lysis buffer (composed of 2% v/v triton X-100 and 20mM EDTA in cell culture medium) was used to detach the cells. Subsequently, cell suspensions were homogenized by vortex-mixing 30 seconds and debris removed by centrifugation (20,000 × g for 10 minutes at 4°C). Absorbance of the reaction mixture (a mixture of catalyst, dye solution, and samples) was measured at a wavelength of 490 nm after 7 minutes incubation at room temperature (linear enzymatic conditions determined in preliminary experiments, data not shown). The degree of cytotoxicity was calculated as the percentage of LDH release into the culture supernatant (i.e. indicating membrane disruption and cell death) and was calculated as follows (Equation V-1):

Equation V-1

$$\text{Cytotoxicity \%} = \frac{\text{LDH activity in cell supernatant}}{\text{LDH activity in cell supernatant} + \text{LDH activity in cell lysate}} \times 100\ \%$$

2.8. Statistical analyses

Statistical analyses were performed in SigmaStat 3.5 (Systat Software Inc., San Jose, California, USA). Differences between multiple groups were determined by Kruskal-Wallis one-way analysis of variance on ranks where $p<0.05$ was deemed significant. Curve fitting was performed with SigmaPlot 14 (Systat Software Inc., San Jose, California, USA).

3. Results and discussion

3.1. Method development

We have developed a sensitive LC-MS/MS assay for the simultaneous quantification of MPA, MPAG, and AcMPAG in HepaRG cell culture medium, using MPA-d_3 and MPAG-d_3 as internal standards. LC-MS/MS assays for MPA and/or metabolites have been described in human plasma [272, 278-281], urine [282, 283], dried blood spots [284], and human liver microsomes [285]. In contrast to other biological fluids (i.e. plasma, urine, and dried blood samples), cell culture medium contains distinct components such as basal medium (e.g. William's E), fetal bovine serum, antibiotics (e.g. penicillin/streptomycin), insulin, hydrocortisone hemisuccinate, glutamine, and DMSO [270]. Because HepaRG cell culture medium consists of proteins and growth factors, a sample preparation procedure requiring protein precipitation was also required.

A variety of columns were tested initially. Although an ultra-high performance LC column would be ideal for enhanced throughput, the current column was selected based on the best balance between separation and efficiency tailored to this biological matrix. The compositions of the two mobile phase solutions and the gradient conditions were initially based on previous reports for MPA (e.g. [272, 278]) but fine-tuned experimentally to achieve excellent separation with sharp, symmetrical peak shapes on our LC-MS/MS. Representative chromatograms of MPA, MPAG, AcMPAG (based on LLOQs), MPA-d_3, and MPAG-d_3 are illustrated in Figure V-2. We were able to achieve clean separations of MPA, MPAG, and AcMPAG, allowing accurate simultaneous quantifications of these analytes (Figure V-2). As hypothesized by Figurski et al [279], poor chromatographic separation of AcMPAG and MPAG may have resulted in reduced precision at the LLOQ for AcMPAG in their assay. Our chromatographic conditions were devoid of this limitation due to sufficient resolution of the respective peaks.

In contrast to the frequently used ESI for the quantification of MPA and metabolites [272, 278-284], a DUIS approach combining both ESI and APCI ionizations was utilized in our assay. The ESI probe and the APCI corona needle are positioned in a 90-degree angle in the ion source and have distinctive ionization zones. DUIS is suitable for simultaneously ionizing compound mixtures with a wide range of physiochemical characteristics (i.e. ESI for highly polar compounds and APCI for lower polarity compounds, such as the analyte mixture utilized in this manuscript) (e.g. [286, 287]). Based on our preliminary experiments, DUIS exhibited increased sensitivity, compared to ESI or APCI alone. During assay development, the absolute ion counts from DUIS (vs. ESI or APCI, respectively) were 4% and 12,990% higher for MPA; 5% and 10,874% higher for MPAG; and 824% and 8,090% higher for AcMPAG. These suggested that DUIS offered improved sensitivity for these analytes. Three product ions for MPA at m/z 207.05, 303.20, and

159.30 were identified after collision-induced dissociation, and only m/z 207.05 was utilized due to its highest intensity. The same procedure for the selection of product ions was applied to MPAG and AcMPAG. These mass transitions are comparable to previously published literature [272, 284], indicating common fragmentation patterns of MPA and its metabolites under various experimental conditions. Similar to other studies [288], the ammonium adduct precursor ions were also identified but ultimately not utilized in our method due to their relatively weak responses in our experimental conditions. The glucuronide moieties can be subjected to in-source fragmentation as a result of high temperature or collision energy [281]; therefore, ion source temperature and voltage were further optimized manually to minimize this effect. The final conditions and mass transitions are presented as follows: The Q_1 pre-bias, collision energy, and Q_3 pre-bias were -12 V, -23 V, -14 V (MPA); -24 V, -18 V, -21 V (MPAG); -26 V, -20 V, -11 V (AcMPAG); -11 V, -21 V, -13 V (MPA-d_3); and -36 V, -21 V, -26 V (MPAG-d_3), respectively. Collision-induced dissociation gas was 270 kPa. Conversion dynode voltage and DUIS corona needle voltage were 10 and 2 kV, respectively. Desolvation line temperature, heat block temperature, and interface temperature were 250, 200, and 100 °C, respectively. Drying gas flow, heating gas flow, and nebulizing gas flow were 15, 5, and 2 L/min, respectively. MPA is highly bound (97%-99%) to albumin in plasma, therefore free drug concentration measurements should be conducted to reflect the biologically active concentrations in any biological matrix. In order to determine the free fraction of MPA and metabolites in our culture model, we extracted unbound MPA (and metabolites) by ultra-filtering cell culture medium samples using an already established protocol [272]. In comparison to total MPA (and metabolites) concentrations, the free concentrations in our culture medium were determined to be 106 ± 9% (mean ± standard deviation) for MPA, 105 ± 9% for MPAG, and 103 ± 6% for AcMPAG, indicating negligible binding of MPA (and metabolites)

in this model. This was not suprising because the albumin content in culture medium (2.3 g/L, primarily consisting of fetal bovine serum) is considered much lower than that in plasma (35-55 g/L [289]), leading to minimal binding. Essentially, we were mesausring free (pharmacologically active) concentrations in the culture medium; therefore futher ultra-filtration of samples for the determination of free concentrations were not necessary. This finding cuts down the costs and increases the overall throughput associated with our assay.

3.2. Method validation

The assay was comprehensively validated according to FDA Guidance for industry: Bioanalytical method validation [273]. Calibration curves were prepared using a weighting factor of $1/x^2$ and proven to be linear ($R^2 > 0.99$) over the concentrations ranging from 0.00467-3.2 μg/mL (MPA and MPAG) and 0.00467-0.1 μg/mL (AcMPAG) (Figure V-3). The equations for MPA, MPAG, and AcMPAG were y=6.0395x+0.1258, y=3.0525x+0.0559, and y=4.0896x+0.0127, respectively. To our knowledge, in comparison to other published methods that have simultaneously quantified MPA, MPAG, and AcMPAG [272, 278-284], no other assays have obtained better sensitivity for MPA and MPAG. On the other hand, only Figurski et al [279] reported a lower LLOQ (0.0002 μg/mL) for free AcMPAG concentration in plasma compared to 0.00467 μg/mL obtained in our assay. However, their LLOQ for AcMPAG was associated with larger imprecision and reduced accuracy, with the reported test/re-test coefficient of variation (28%) exceeding the acceptable limits. As suggested by Figuriski et al [279], this may be attributed to insufficient baseline separation of AcMPAG and MPAG and the associated increase in variability. Considering these limitations in Figurski et al's AcMPAG data, our assay could be considered one of, if not the, most sensitive assays available for AcMPAG as well.

No interfering peaks were observed at the retention times of MPA, MPAG, and AcMPAG in our assay. Carryover effects were within acceptable limits (6.86-14.59% of LLOQ). The intra- and inter-day precision and accuracy data are summarized in Table V-1. The inter-day precision was 6.47 to 9.72% for MPA, 4.49 to 7.12% for MPAG, and 7.00 to 9.73% for AcMPAG. The inter-day accuracy was -8.50 to 0.95% for MPA, -7.88 to-13.07% for MPAG, and -5.44 to 12.05% for AcMPAG. Both intra- and inter- day precision and accuracy fulfilled the acceptance criteria set by the FDA [273]. The extraction efficiency of MPA, MPAG, and AcMPAG were no less than 90% (data not shown) which is comparable to that described by others (e.g. [279]), indicating high sample recovery. The stabilities of analytes under various processing or storage conditions (i.e. autosampler, bench-top, freeze-thaw, long-term) were all within acceptable limits (i.e. ≤15% of nominal concentrations, N=4, Table V-2), satisfying the requirements set by the FDA.

3.3. Application to the in vitro interaction between MPA and p-cresol

In cells exposed to a fixed physiological free concentration of MPA (1.25 μM, i.e. 0.4 μg/mL), the concentrations of MPA and MPAG determined in the culture medium as a function of incubation time are presented in Figure V-4. Because the rates of MPA depletion and MPAG formation were linear between 0 to 12 hours, 3 or 6 (suitable for modulatory experiments) hours were selected as the optimum incubation times in subsequent experiments. Only concentrations in the culture medium were determined because the majority of analytes were found in the medium (vs. cell lysates) in similar cellular systems [290]. Additionally, the sum of concentrations of MPA and MPAG detected in the cell culture supernatant in our model (at various incubation times, Figure V-4) was close to the original substrate (i.e. MPA) concentration exposed to the cells at time zero, indicating little accumulation of drugs/metabolites within the cells after exposure and

further confirming the suitability of only quantifying MPA and metabolite concentrations in the culture medium. The presence of MPAG in our model confirmed that MPA did gain entry into the cells, where metabolism took place in the endoplasmic reticulum. Our first discovery was that the concentrations of MPAG generated in this *in vitro* system (i.e. up to 1.05 µg/mL per million cells) were comparable to that observed in human plasma [138], indicating the physiological relevance and the suitability for *in vitro-in vivo* extrapolation of our model. Because MPA is known to be primarily metabolized by UGT1A9 in the formation of MPAG [10], another discovery was the confirmation of functional expression of UGT1A9 in HepaRG cell line. Based on these findings, we have established that the HepaRG cell line could be utilized for the characterization of drug-drug interactions mediated by the UGT1A9 enzyme, using MPA as a probe substrate.

On the other hand, AcMPAG was not detected in this culture model, despite 1) extending the incubation time to 72 hours, 2) increasing substrate concentration to 750 µM, and 3) pre-exposing the HepaRG cells with UGT inducers (e.g. rifampin, beta-naphthoflavone) (data not shown). This finding is consistent with the very low concentrations of AcMPAG typically observed in plasma which are sometimes not detected [291] and/or the fact that UGT2B subfamily is generally under-expressed in HepaRG cells compared to primary human hepatocytes [292]. In human plasma, the typical MPAG to AcMPAG ratios are 75 and 90 for MMF formulation and enteric-coated mycophenolate sodium (EC-MPS) formulation, respectively [169], therefore determining the formation of the quantitatively major MPAG from MPA (and not AcMPAG) is ultimately more practical for the purpose of characterizing MPA drug interactions. Further experiments are on-going to determine culture conditions that can produce adequate concentrations of AcMPAG (e.g. enzyme over-expression) and characterize the expression (gene and protein) of UGT2B7 in this *in vitro* system. In any case, the lack of detection of AcMPAG under the tested

culture conditions did not discount our discoveries and the primary utility of this model: the suitability for studying the primary MPA metabolic pathway (MPAG formation), which is quantitatively important in elucidating MPA-associated drug interactions.

In order to determine the suitability of this *in vitro* system for drug inhibition studies, initial positive control experiments confirmed the potent and concentration-dependent inhibitory effects of niflumic acid toward the formation of MPAG, using a free MPA substrate concentration (1.25 μM, i.e. 0.4 μg/mL) that is attainable in transplant patients taking MMF. Niflumic acid has been demonstrated, in various experimental conditions, to be a selective and potent inhibitor of UGT1A9 and MPA glucuronidation [269]. In order to characterize the inhibitory effects of *p*-cresol, cells were exposed to increasing concentrations of *p*-cresol (0 – 200 μM, which is physiologically attainable in humans under uremic conditions [52]) at a fixed physiological MPA concentration (1.25 μM). None of these experimental conditions caused cell death, as evident by similar LDH release profiles compared to the vehicle control (data not shown).

Our results indicated that *p*-cresol (at ≥ 60 μM) significantly decreased the formation of MPAG while increasing the concentration of MPA in a concentration-dependent manner (Figure V-5). Maximum inhibition of MPAG formation (96.6 ± 0.2%, N=3) was obtained at a *p*-cresol concentration ≥ 100 μM, which corresponded to a > 2 fold increase in MPA concentration (part of the increase may have been attributed to other pathways of MPA metabolism inhibited by *p*-cresol). The IC_{50} value characterizing *p*-cresol's inhibitory effects was ~55 μM (Figure V-6). These findings are potentially clinically relevant because we have demonstrated that uremic concentrations of *p*-cresol were capable of significantly reducing MPA metabolism and increasing MPA concentration. These observations provided direct evidence supporting our hypothesis that fluctuations in *p*-cresol concentration may influence MPA exposure; therefore potentially

explaining the observed wide pharmacokinetic variabilities of MPA in the clinic. Further confirmatory experiments in humans are needed to verify our *in vitro* observation.

One might hypothesize that the primary mechanism by which *p*-cresol inhibited MPAG formation was the reduction of UGT1A9 catalytic activity because this specific enzyme has been demonstrated to be responsible for ~ 55% of MPAG formation in human liver microsomes [35]. However, *p*-cresol was able to reduce MPAG production by > 95% in our model, suggesting that additional putative pathways of MPAG formation (e.g. UGT2B4 [253] which is expressed in HepaRG cells [292]) may also have been affected by *p*-cresol, making up the balance of the inhibitory activities in our model. Furthermore, because the HepaRG cell line is derived from a single individual [172], the effects of genetic variations or inter-individual variabilities in UGT expression on the extent of *p*-cresol – MPA interaction remained unknown. Additional investigations using a variety of *in vitro* models (e.g. human liver microsomes with documented single nucleotide polymorphisms and recombinant UGT enzymes) are being conducted to support these primary observations.

4. Conclusions

We have successfully developed and validated a sensitive LC-MS/MS assay for the simultaneous quantifications of MPA, MPAG, and AcMPAG in HepaRG cell culture medium. Our *in vitro* experiments have provided the following discoveries: 1) the ability to generate physiologically relevant MPAG concentrations in this HepaRG cell culture system, 2) the ability to study UGT1A9-mediated drug-drug interactions using MPA as probe substrate in this culture model, and 3) the inhibitory effects of *p*-cresol (IC_{50} ~ 55 μM) toward MPA metabolism under

substrate – inhibitor concentrations that are attainable under uremic, physiological conditions. In our opinion, these findings are potentially clinically relevant and serve as a piece of evidence supporting further *in vitro* and *in vivo* mechanistic studies to elucidate the mechanism and clinical relevance of the identified interaction.

Table V-1 Intra- and inter-run precision and accuracy of MPA, MPAG, and AcMPAG

	Nominal concentration, ng/mL	Intra-day (1) (n=6)		Intra-day (2) (n=6)		Intra-day (3) (n=6)		Inter-day (n=18)	
		CV (%)	Accuracy (%)	CV (%)	Accuracy (%)	CV (%)	Accuracy (%)	CV (%)	Accuracy (%)
MPA	4.67	8.58	104.57	14.10	104.88	5.10	90.73	9.72	100.06
	12.96	6.78	98.34	9.25	107.04	3.61	89.12	6.91	100.95
	100	8.71	103.97	9.83	102.68	3.87	87.78	7.89	98.15
	1600	6.17	93.42	10.44	95.26	1.40	85.83	6.47	91.50
MPAG	4.67	5.38	114.10	14.86	105.36	2.02	119.73	6.54	113.07
	12.96	6.56	108.36	1.99	113.78	4.65	105.73	4.49	108.39
	100	10.84	109.78	4.25	111.52	1.59	105.67	5.54	108.99
	1600	8.62	85.83	10.76	104.01	2.49	86.52	7.12	92.12
AcMPAG	4.67	4.35	110.54	16.81	107.89	1.80	117.70	7.04	112.05
	12.96	11.19	101.73	12.40	104.62	5.94	110.30	9.73	105.55
	36	9.47	98.90	7.79	100.38	3.46	97.52	7.00	98.93
	100	12.19	98.33	4.95	93.02	6.12	92.33	8.12	94.56

Abbreviation(s): AcMPAG, mycophenolic acid acyl-glucuronide; CV, coefficient of variation; MPA, mycophenolic acid; MPAG, mycophenolic acid glucuronide; QC, quality control.

Table V-2 Stability of MPA, MPAG, and AcMPAG under various collection and storage conditions

	MPA		MPAG		AcMPAG	
	Low QC	High QC	Low QC	High QC	Low QC	High QC
Nominal concentration, ng/mL	12.96	1600	12.96	1600	12.96	100
Autosampler stability (%)	114.76	87.58	100.55	88.87	97.58	85.81
Bench-top stability (%)	105.36	94.67	111.86	104.97	95.51	99.60
Freeze-thaw stability (%)	103.14	109.18	111.99	104.97	96.50	100.64
Long-term stability (%)	102.24	97.30	105.07	90.73	112.09	106.82

Abbreviation(s): AcMPAG, mycophenolic acid acyl-glucuronide; MPA, mycophenolic acid; MPAG, mycophenolic acid glucuronide; QC, quality control.

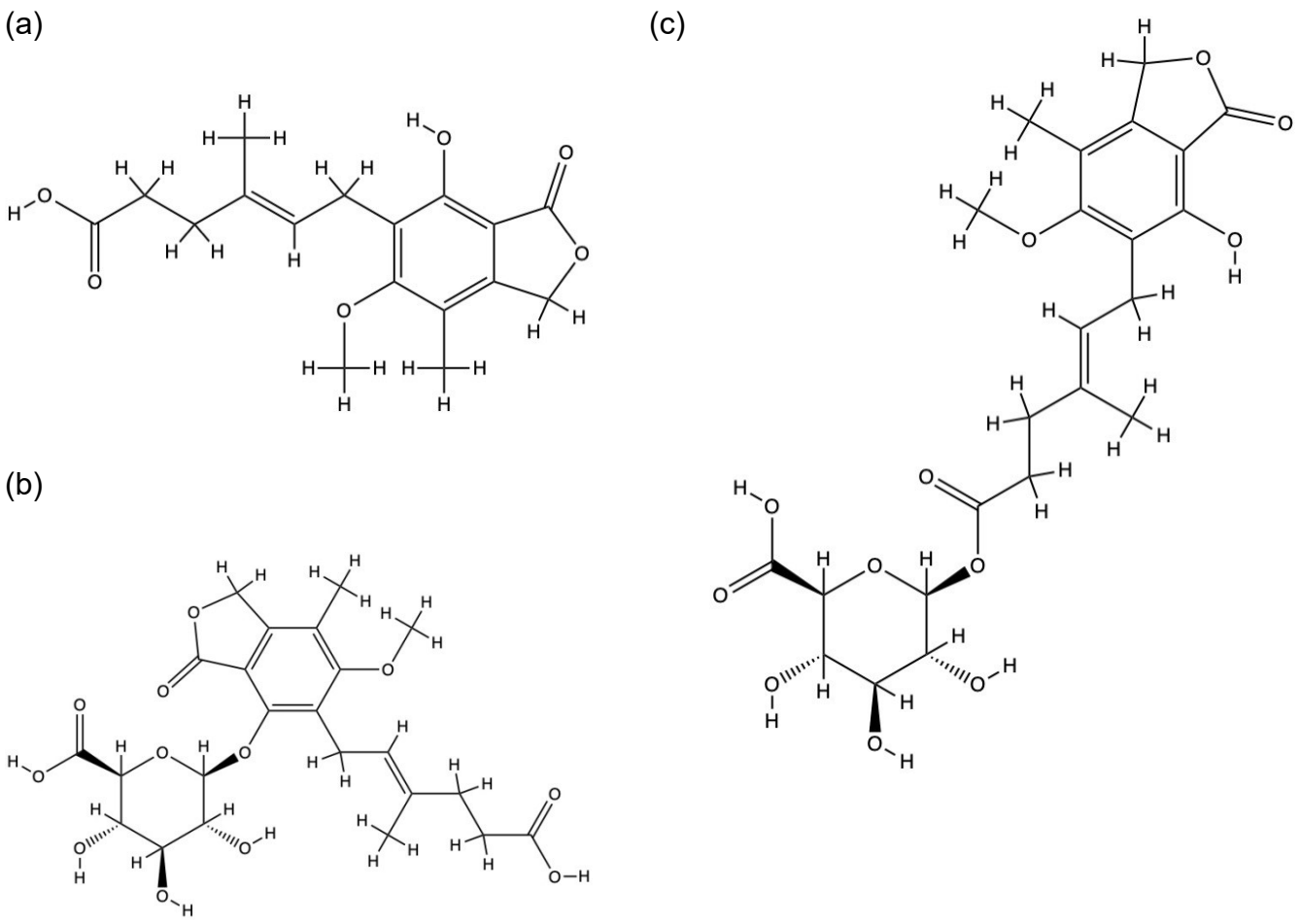

Figure V-1 Chemical structures of (a) mycophenolic acid (MPA), (b) mycophenolic acid glucuronide (MPAG), and (c) mycophenolic acid acyl-glucuronide (AcMPAG)

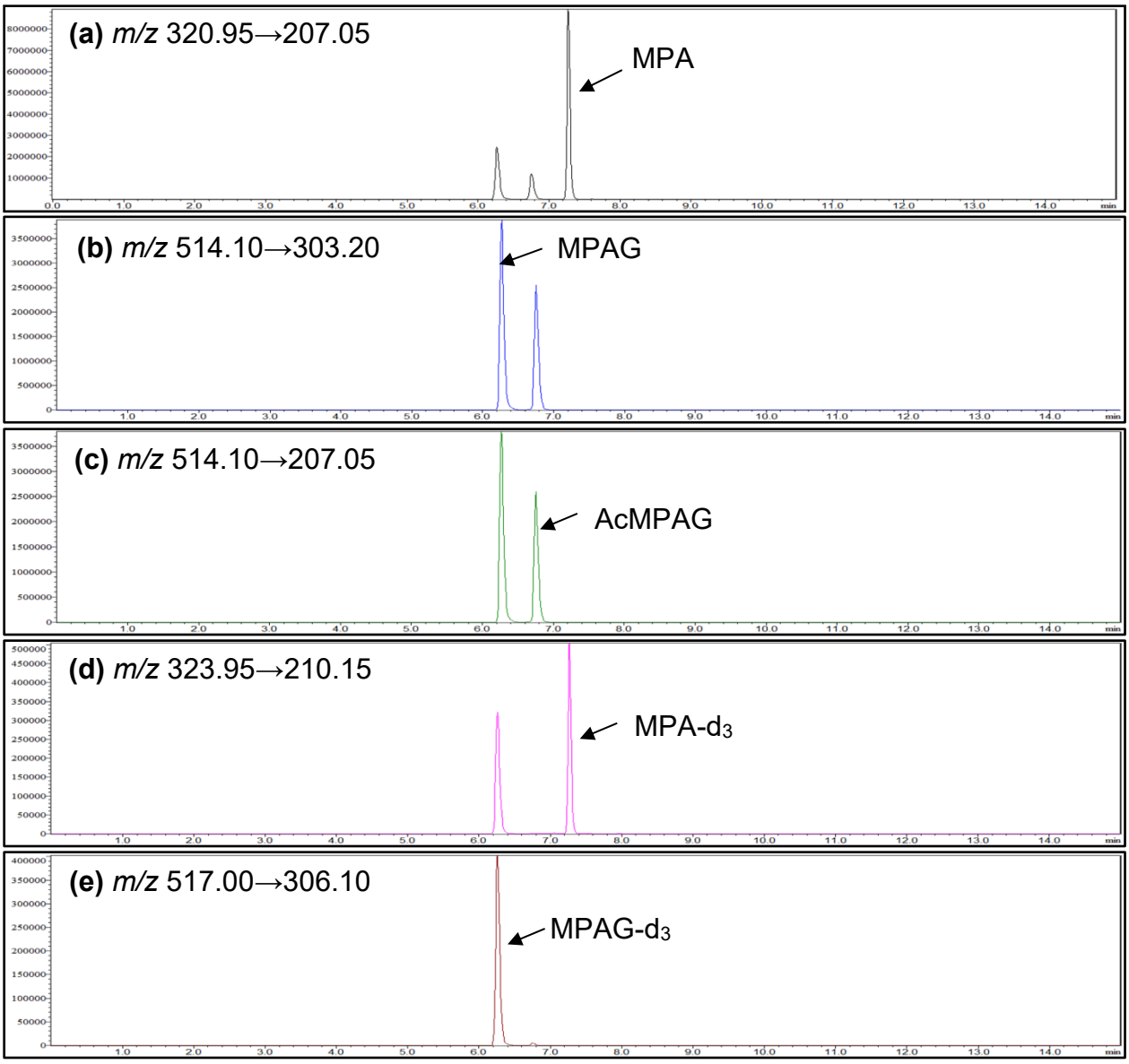

Figure V-2 Representative MRM chromatograms of: (a) mycophenolic acid (MPA) at lower limit of quantification (LLOQ), (b) mycophenolic acid glucuronide (MPAG) at LLOQ, (c) mycophenolic acid acyl-glucuronide (AcMPAG) at LLOQ, (d) deuterated mycophenolic acid (MPA-d_3), and (e) deuterated mycophenolic acid glucuronide (MPAG-d_3)

The two extra small peaks in MPA channel were generated from in-source fragmentation of MPAG and AcMPAG; the extra peaks in the MPAG and AcMPAG channels were due to

overlapping MRM transitions between these two channels. The extra peak in the MPA-d_3 channel is due to in-source fragmentation of MPAG-d_3.

(a)

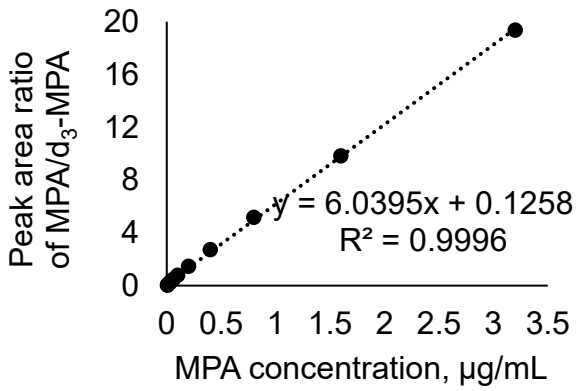
Peak area ratio of MPA/d3-MPA
20
16
12
8
4
0
y = 6.0395x + 0.1258
R² = 0.9996
0 0.5 1 1.5 2 2.5 3 3.5
MPA concentration, µg/mL

(b)

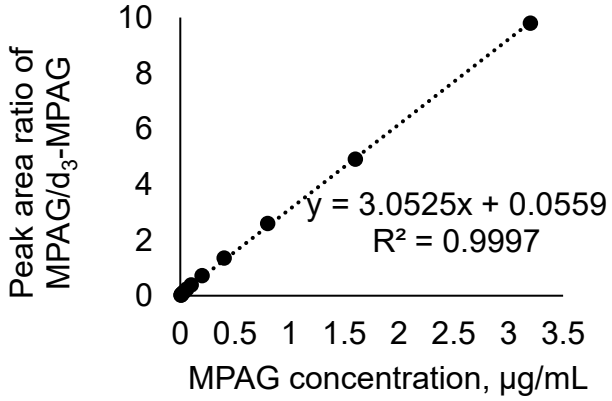
Peak area ratio of MPAG/d3-MPAG
10
8
6
4
2
0
y = 3.0525x + 0.0559
R² = 0.9997
0 0.5 1 1.5 2 2.5 3 3.5
MPAG concentration, µg/mL

(c)

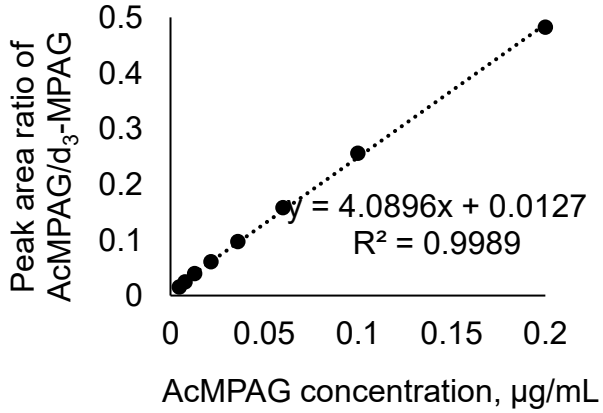
Peak area ratio of AcMPAG/d3-MPAG
0.5
0.4
0.3
0.2
0.1
0
y = 4.0896x + 0.0127
R² = 0.9989
0 0.05 0.1 0.15 0.2
AcMPAG concentration, µg/mL

Figure V-3 Representative calibration curves for (a) mycophenolic acid (MPA), (b) mycophenolic acid glucuronide (MPAG), and (c) mycophenolic acid acyl-glucuronide (AcMPAG)

A weighted ($1/x^2$) least-squares linear regression model was utilized.

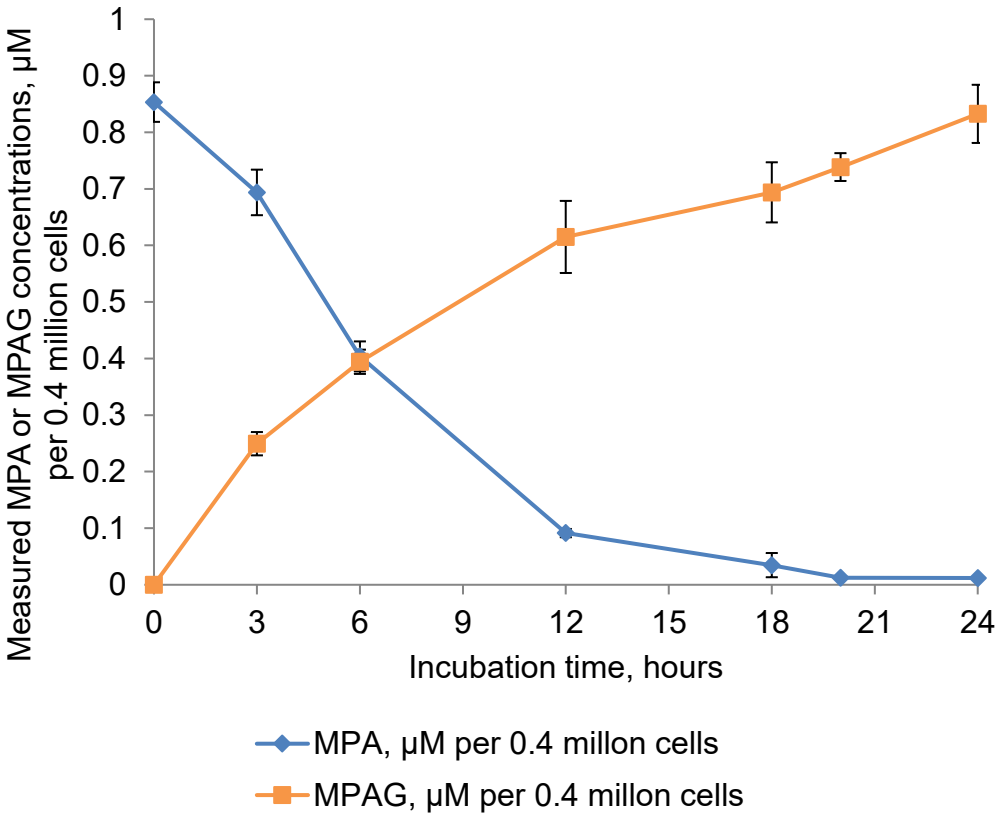

Figure V-4 Mycophenolic acid (MPA) depletion and mycophenolic acid glucuronide (MPAG) formation in HepaRG culture medium as a function of time

MPA was exposed at 1.25 µM, using a cell density of 0.4×10^6 cells/well, in 24-well tissue culture plates (n=3). The incubation time was 0-24 hours. Time zero concentration was the measured concentration after treatment (with a lag of ~3-5 minutes).

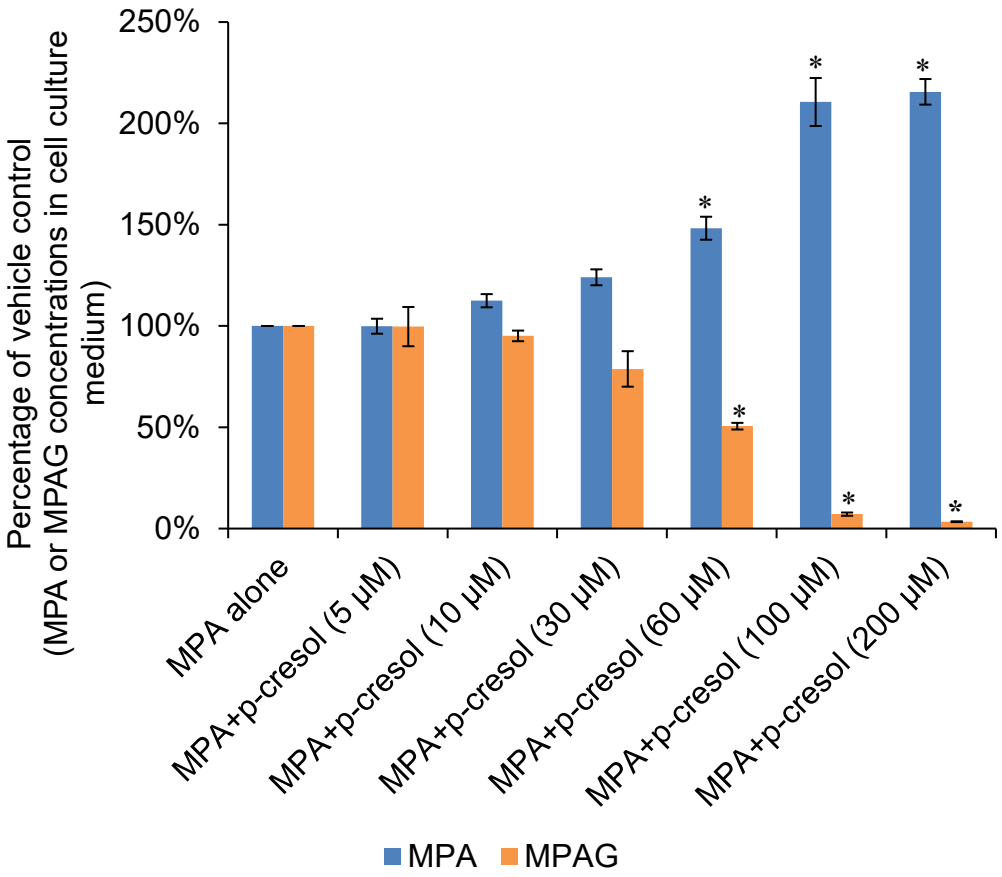

Figure V-5 Effects of p-cresol on mycophenolic acid (MPA) and mycophenolic acid glucuronide (MPAG) concentrations in HepaRG culture medium

MPA was exposed at 1.25 µM (i.e. 0.4 µg/mL), using a cell density of 0.4×10^6 cells/well, in 24-well tissue culture plates (n=3). The incubation time was 3 hours (linear kinetic conditions). *$p<0.05$ versus vehicle control (i.e. cells treated with MPA alone).

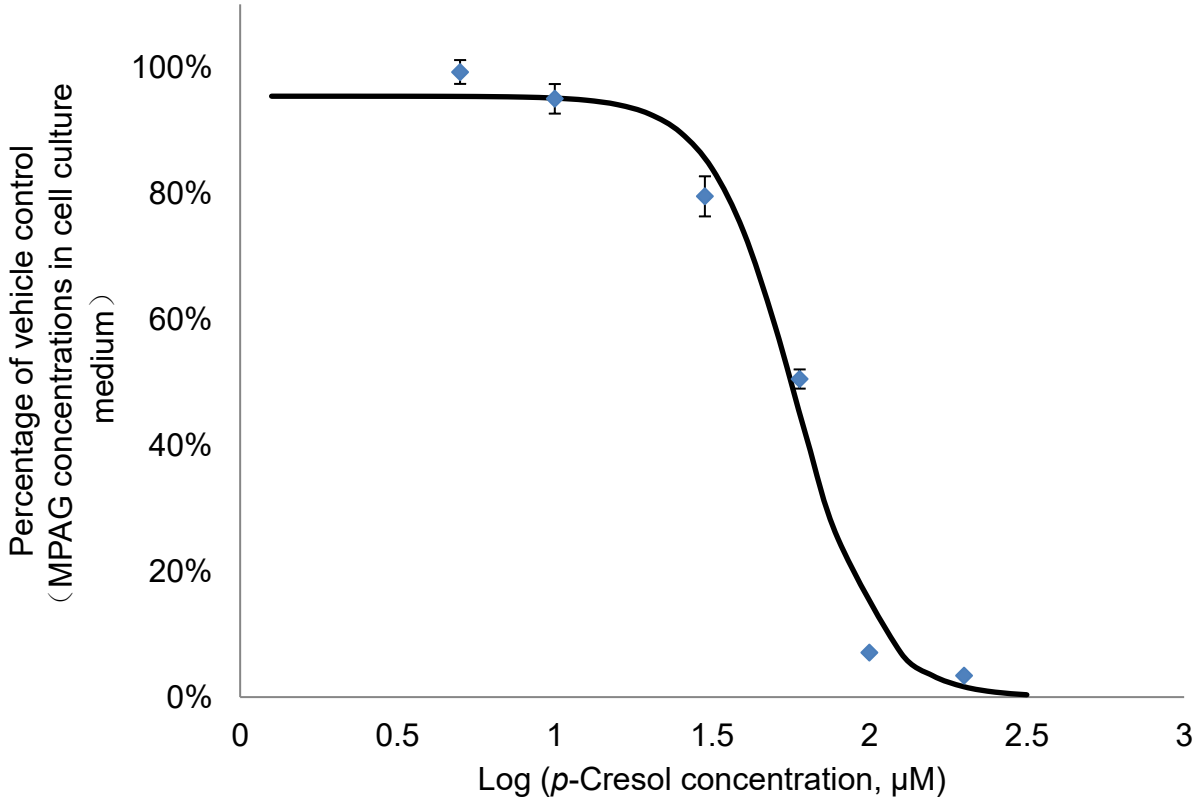

Figure V-6 Effects of varying concentrations of p-cresol on mycophenolic acid glucuronide (MPAG) formation in HepaRG culture medium

MPA was exposed at 1.25 μM (i.e. 0.4 μg/mL), using a cell density of 0.4×10^6 cells/well, in 24-well tissue culture plates (n=3). The incubation time was 3 hours (linear kinetic conditions). The IC_{50} value (~55 μM) was generated using sigmoidal–three parameter fitting in SigmaPlot14.

Chapter VI. Mechanisms of metabolism interaction between *p*-cresol and mycophenolic acid[6]

Prologue:

Having established the inhibitory effects of p-cresol toward MPA glucuronidation in HepaRG cells (Chapter V [54]), the aim of this chapter was to further characterize the mechanisms of inhibition and the effects of clinical covariates on the interaction between p-cresol and MPA. These data also allowed us to conduct in vitro – in vivo extrapolations to estimate the likely changes in MPA exposures mediated by p-cresol.

[6] This chapter is already published in a peer-reviewed journal. **Rong Y** and Kiang TKL. Mechanisms of metabolism interaction between *p*-cresol and mycophenolic acid. *Toxicological Sciences*. 2020 Feb 1;173(2):267-279. doi: 10.1093/toxsci/kfz231.

Acknowledgement: **Rong Y** and Kiang TKL. Mechanisms of metabolism interaction between *p*-cresol and mycophenolic acid. *Toxicological Sciences*. 2020;173(2):267-279. By permission of Oxford University Press, license number: 5222101173988 (for abstract), 5222110102563 (for figures and tables), 5222101438440 (for text extract).

Abstract

Mycophenolic acid (MPA) is commonly prescribed for preventing graft rejection after kidney transplantation. The primary metabolic pathways of MPA are hepatic glucuronidation through UDP-glucuronosyltransferase (UGT) enzymes in the formation of MPA-glucuronide (MPAG, major pathway) and MPA-acyl glucuronide (AcMPAG). *p*-Cresol, a potent uremic toxin known to accumulate in patients with renal dysfunction, can potentially interact with MPA via the inhibition of glucuronidation. We hypothesized that the interaction between MPA and *p*-cresol is clinically relevant and that the estimated exposure changes in the clinic are of toxicological significance. Using *in vitro* approaches (i.e., human liver microsomes and recombinant enzymes), the potency and mechanisms of inhibition by *p*-cresol towards MPA glucuronidation were characterized. Inter-individual variabilities, effects of clinical covariates, *in vitro-in vivo* prediction of likely changes in MPA exposure, and comparison to other toxins were determined for clinical relevance. *p*-Cresol inhibited MPAG formation in a potent and competitive manner (K_i=5.2 μM in pooled human liver microsomes) and the interaction was primarily mediated by UGT1A9. This interaction was estimated to increase plasma MPA exposure in patients by ~1.8-fold, which may result in MPA toxicity. The mechanism of inhibition for AcMPAG formation was noncompetitive (K_i=127.5 μM) and less likely to be clinically significant. *p*-Cresol was the most potent inhibitor of MPA-glucuronidation compared to other commonly-studied uremic toxins (e.g., indole-3-acetic acid, indoxyl sulfate, hippuric acid, kynurenic acid, 3-carboxy-4-methyl-5-propyl-2-furanpropionic acid) and its metabolites (i.e., *p*-cresol sulfate and *p*-cresol glucuronide). Our findings indicate that the interaction between *p*-cresol and MPA is of toxicological significance and warrants clinical investigation.

1. Introduction

Mycophenolic acid (MPA) is a commonly prescribed immunosuppressant for preventing graft rejection after kidney transplantation [10, 29, 51, 131, 132]. The mechanism of action is by inhibition of inosine-5'-monophosphate dehydrogenase which decreases the proliferation of T- and B- lymphocytes. MPA is highly protein bound to albumin, yielding a free fraction of 1-3% under normal physiological conditions. The metabolism of MPA is primarily mediated by uridine 5'-diphospho-glucuronosyltransferase (UGT) enzymes in the formation of MPA-glucuronide (MPAG, via UGT1A9) and MPA-acyl glucuronide (AcMPAG, via UGT2B7). MPAG formation is considered the major conjugation pathway of MPA. The glucuronides undergo extensive renal and biliary excretion that are facilitated by a variety of transporters and are subjected to extensive entero-hepatic recirculation resulting in the secondary peaks commonly observed in the plasma concentration-time profiles in humans [10, 29, 51, 131, 132]. The clearance of MPA can be affected by drugs or endogenous compounds that are capable of modulating these UGT or transporter pathways.

The therapeutic target range for MPA exposure (i.e. as area-under the concentration-time curve [AUC]) is relatively narrow and has been established to be 30-60 mg*h/L in adult kidney transplant patients [63]. However, the pharmacokinetics of MPA are associated with significant inter- and intra-individual variabilities (i.e., up to 10-fold) when using standardized, fixed dosing regimens [10], suggesting that drug concentration monitoring may help improve MPA precision dosing [51]. Furthermore, the over-exposure of MPA is associated with severe gastrointestinal, hematologic, and infectious adverse effects in kidney transplant recipients [61]; therefore, understanding clinical factors that can influence the pharmacokinetics of MPA can help minimize the variability and potentially reduce these severe toxicological complications.

Uremic toxins are known to affect drug metabolism, and the interactions can be of clinical relevance [293, 294]. *p*-Cresol, a protein-bound uremic toxin, can be accumulated in patients with chronic renal failure or with kidney transplant due to excessive production by gut microbiota and/or reduced elimination [53, 83]. The primary source of *p*-cresol is amino acid metabolism by intestinal bacteria, although environmental sources can also contribute to the overall human exposure [79]. After intestinal absorption, *p*-cresol is further conjugated to *p*-cresol sulfate (major pathway) and *p*-cresol glucuronide (relatively minor pathway), representing the predominant metabolites in the liver as part of the overall first-pass metabolism process [78, 80]. In the plasma, the primary forms of measured *p*-cresol are its conjugated, hepatically-derived metabolites. Significant plasma concentrations of total *p*-cresol (i.e. the combination of *p*-cresol, *p*-cresol sulfate, and *p*-cresol glucuronide) have been documented in humans under uremic conditions, and a free *p*-cresol concentration of ~23.9 μM has been recently reported in the liver tissues obtained from deceased hemodialysis patients [295], indicating that relatively high concentrations of *p*-cresol can be found in the enzyme active sites at one of the main origins of metabolism (i.e. liver). The toxicology of *p*-cresol and its metabolites under uremia has already been reviewed by numerous investigators (e.g. [78]). The current investigation will focus on the toxicokinetic metabolism interactions mediated by *p*-cresol.

In addition to being extensively metabolized in the liver, *p*-cresol is also an inhibitor of UGT1A9 and UGT2B7, as demonstrated *in vitro* in human liver microsomes [52], and could theoretically interact with MPA because MPA is primarily conjugated by UGT1A9 and UGT2B7 [10]. The interaction was demonstrated recently in our laboratory where the inhibitory effects of *p*-cresol toward MPA glucuronidation in HepaRG cells were first reported using concentrations attainable under uremic conditions [54]. As a follow-up to this initial observation, we hypothesized

that the interaction between MPA and *p*-cresol is mediated by UGT1A9 inhibition, is clinically relevant, and that the estimated exposure changes in the clinic are of toxicological significance. We aimed to further characterize the mechanisms of inhibition and the effects of clinical covariates on the interaction between *p*-cresol and MPA, using a variety of classical *in vitro* approaches. Inter-individual variabilities, *in vitro-in vivo* extrapolation to estimate the potential clinical/toxicological significance, and relative effects of other common uremic toxins or *p*-cresol metabolites were also determined. To our knowledge, this is the first systematic, mechanistic study characterizing the interaction between MPA and *p*-cresol. Our findings indicate potential clinically and toxicologically significant interactions that would warrant further investigations in the clinic.

2. Materials and methods

2.1. Chemicals and reagents

MPA, MPA-d_3, dimethyl sulfoxide (DMSO), Tris hydrochloride, alamethicin, uridine-5'-diphosphate-glucuronic acid (UDPGA), magnesium chloride ($MgCl_2$), bovine serum albumin (BSA), 3-carboxy-4-methyl-5-propyl-2-furanpropionic acid (CMPF), indole-3-acetic acid, 3-indoxyl sulfate potassium salt, kynurenic acid, hippuric acid, niflumic acid, and *p*-cresol were purchased from Sigma-Aldrich (Oakville, Ontario, Canada). MPAG, MPAG-d_3, AcMPAG, *p*-cresol glucuronide, and *p*-cresol sulfate potassium salt were obtained from Toronto Research Chemicals (North York, Ontario, Canada). Tris base, acetic acid, and human liver microsomes pooled from 50 individual donors (adult, mixed gender, catalog number HMMCPL, lot number PL050C-E, and PL050D-C) were purchased from Fisher Scientific (Ottawa, Ontario, Canada). Individual human liver microsomes (N=12, catalog number 452138, lot numbers HFC205,

HFC208, HFH617, HFH705, HG18, HG43, HG64, HH13-2, HH37, HH519, HH741, and HH837, representing the entire panel available from this supplier), and recombinant enzymes (UGT1A1 [catalog number 456411], UGT1A9 [catalog number 456419], UGT2B4 [catalog number 456424], UGT2B7 [catalog number 456427]) were obtained from Corning Gentest (Woburn, Massachusetts, United States).

2.2. Determination of mycophenolic acid free fraction in reaction mixtures containing microsomal protein and BSA

In consideration of potential binding effects of MPA toward proteins in the reaction mixture, the free fractions of MPA were determined in our *in vitro* experimental models containing human liver microsomal proteins or recombinant enzyme proteins and 1% BSA. The free fraction of *p*-cresol in human liver microsomes had already been determined to be ~0.7 in a concentration-independent manner (based on a BSA concentration of 2%, up to 1 mM of *p*-cresol) [52]; therefore, this value was utilized to correct for the actual free *p*-cresol concentrations in our manuscript (i.e. by multiplying the exogenously added *p*-cresol concentration by a factor of 0.7). The free fraction of MPA in each incubation mixture was determined using Amicon® ultra-centrifugal filters (MW cut-off 30 kDa, Sigma-Aldrich, Oakville, Ontario, Canada) at 14000×g at 4 ºC for 10 minutes following established protocols [54, 272]. These values were utilized to determine the actual free MPA concentrations in our experiments.

2.3. Incubation conditions

Protein concentrations and incubation times were optimized for each *in vitro* system to ensure linear enzymatic conditions for MPAG and AcMPAG formations (specific initial velocity conditions are presented in each Figure legend). MPA was dissolved in 1% methanol for all experiments as this solvent concentration has been shown to have little impact on UGT catalytic activities [296]. The compositions of the incubation medium were based on the optimized experimental parameters reported by Badee et al [297]. Briefly, enzymes were pre-treated with alamethicin (10 µg/mg protein) on ice for 30 minutes. Subsequent incubations were conducted in a reaction mixture (0.1 mL) containing 100 mM Tris buffer (pH=7.4, measured at 37 °C), 10 mM $MgCl_2$, 1% BSA, MPA, *p*-cresol, and additional uremic compounds or *p*-cresol metabolites as described below. Following a 5-minute pre-incubation at 37 ºC, reactions were initiated with 5 mM UDPGA (final concentration) in a shaking 37 ºC water bath and terminated by the addition of a cold (4 ºC) mixture consisting of 50 µL of MPA-d_3 (0.4 µg/mL), MPAG-d_3 (2 µg/mL, as internal standards), 25 µL acetonitrile, 25 µL methanol, and 2 µL 10% (v/v) acetic acid. Subsequently, the entire mixture was vortexed for 30 seconds and immediately assayed. Alternatively, samples were snap-frozen in dry ice for storage at -80 ºC. For quantification of MPA, MPAG, and AcMPAG concentrations, the mixture was centrifuged at 18600×g at 4 ºC for 4 minutes for protein precipitation. A 5 µL aliquot of the clear supernatant was injected into the liquid-chromatography tandem mass-spectrometer (LC-MS/MS) using a similar assay (slightly modified for the current incubation matrix) already published by our group [54].

2.4. Control experiments

In order to verify the general suitability of our *in vitro* experimental systems for drug interaction studies, control incubations with MPA alone or MPA with a known selective UGT1A9 inhibitor (i.e. 2.5 µM niflumic acid [298]) were conducted with different enzyme sources (i.e. pooled human liver microsomes, individual human liver microsomes, or recombinant UGT enzymes). Furthermore, enzyme kinetic constants (K_m, V_{max}) and intrinsic clearance (CL_{int}) values were determined in pooled human liver microsomes using MPA concentrations ranging from 0.25-1000 µM in order to ensure our control/baseline enzyme kinetic conditions were comparable to the reported literature values. The CL_{int} values were calculated using Equation VI-1 [299].

Equation VI-1

$$CL_{int} = \frac{V_{max}}{K_m}$$

Finally, in order to confirm the known (major) role of UGT1A9 in conjugating MPA in our systems, individual human liver microsomes with varying UGT1A9 catalytic activities (N=12, [300]) were incubated with 2.5 µM MPA (i.e. physiological free average maximum concentration in consideration of the calculated unbound fraction [54]) to verify the anticipated strong correlation between UGT1A9 activity and MPAG formation in this model.

2.5. Potency of inhibition of MPA glucuronidation by p-cresol

The potency of inhibition by *p*-cresol towards the glucuronidation of MPA was initially evaluated by determining the half-maximal inhibitory-effect concentration (IC_{50}) in pooled human liver microsomes using physiologically relevant MPA concentrations (i.e. 0.25 µM, 2.5 µM, and

25 μM; considering the ~10 folds pharmacokinetic variability typically observed for MPA [10]). Furthermore, the potency of inhibition in recombinant UGT1A9 (the major pathway for MPA glucuronidation) and additional recombinant UGT enzymes that may have sufficient activities (i.e. UGT1A1, UGT2B4, UGT2B7) were also tested [35, 173-175, 252, 253]. To complement the IC_{50} data, the inhibition-associated constants (K_i) were also determined using MPA (2.5-1000 μM) and *p*-cresol (0-60 μM) under optimized incubation conditions as described above. In order to characterize the magnitude and inter-individual variability of the interaction, individual human liver microsomes (from 12 donors, [300]) were incubated with MPA (2.5 μM) in the absence (vehicle control) or presence of *p*-cresol (i.e. 10 μM representing the IC_{50} obtained from pooled human liver microsomes or 30 μM representing ~90% inhibition).

2.6. Mechanisms of inhibition, in vitro-in vivo extrapolation, and influences of clinical covariates

In order to determine the mechanisms, the estimated clinical changes in MPA exposure, and the influences of clinical factors on the observed interaction, enzyme kinetic experiments were conducted with pooled human liver microsomes and recombinant UGT1A9 enzymes (additional recombinant enzymes did not generate MPAG or AcMPAG with our experimental conditions). K_i values were first determined as described above and the mechanisms of inhibition were further determined using data fitting (see Statistical analysis) and graphical analyses with Dixon and Cornish-Bowden plots [301, 302]. The estimated changes in human MPA exposure (i.e. AUC ratios) based on the obtained *in vitro* kinetic parameters were extrapolated using Equation VI-2 [299, 303].

Equation VI-2

$$\frac{AUC_i}{AUC} = \frac{1}{\frac{f_m}{1+\frac{[I]}{K_i}} + (1 - f_m)}$$

where [I] is the concentration of inhibitor, f_m is the fraction of MPA metabolized by the enzyme or pathway of interest, the latter is assumed to be 0.55 for UGT1A9 [35].

To determine the effects of clinical variables on the extents of the interaction, correlational analyses using individual donor data (e.g. age, sex, race, total cytochrome P450 [CYP] enzyme content, CYP1A2, CYP2A6, CYP2B6, CYP2C8, CYP2C9, CYP2C19, CYP2D6, CYP2E1, CYP3A4, CYP4A, flavin-containing monooxygenase [FMO], UGT1A1, UGT1A4, and UGT1A9 activities) [300] and inhibition data obtained from each individual human liver microsomes were conducted.

2.7. Comparative effects of other commonly-studied uremic toxins and p-cresol metabolites

In order to determine the relative inhibitory effects of other commonly-studied protein-bound uremic toxins (i.e. CMPF, indole-3-acetic acid, indoxyl sulfate, kynurenic acid, and hippuric acid [53, 75, 88]) or major *p*-cresol metabolites (i.e. *p*-cresol sulfate and *p*-cresol glucuronide [78, 80]) on MPA glucuronidation, incubations were conducted with a physiological concentration of MPA (i.e. 2.5 μM) in the presence of equi-molar concentrations of these compounds (i.e. 10 μM which represents the IC_{50} for MPAG formation by *p*-cresol) in pooled human liver microsomes. All uremic toxins and *p*-cresol metabolites were dissolved in DMSO (0.2%) and further diluted with Tris buffer.

2.8. Quantification of mycophenolic acid, mycophenolic acid glucuronide, and mycophenolic acid acyl-glucuronide

Concentrations of MPA, MPAG, and AcMPAG in the incubation medium were measured with a slightly modified LC-MS/MS assay already published by our group [54]. The assay was completely re-validated to tailor to the microsomal reaction matrices. Precision, accuracy, autosampler stability (24 hours at 4°C), and bench-top stability (6 hours at 23.5 °C) were determined based on established protocols from the US Food and Drug Administration [273].

2.9. Statistical analysis

The kinetic data were fitted to models representing the four reversible mechanisms of inhibition (i.e. competitive, noncompetitive, uncompetitive, and mixed) using SigmaPlot 14 (Systat Software, Inc., San Jose, California, United States). The best model was selected based on statistical analyses using the 95% confidence interval of K_i, the F-test, and the Akaike information criterion value, in conjunction with graphical analysis (Dixon and Cornish-Bowden plots). The K_i values were calculated with SigmaPlot 14 Parametric analyses (i.e. Student's t-test, and Pearson product correlational analysis) were only conducted if the data satisfied both normal distribution and equal variance criteria using SigmaStat version 3.5 (Systat Software Inc., San Jose, California, United States). For other data, non-parametric analyses (i.e. Kruskal-Wallis one-way analysis of variance [ANOVA] on ranks) or logarithm-transformation (i.e. for correlational analysis) were conducted. $p<0.05$ was deemed *a priori* as the level of significance. The specific statistical analyses are presented in each Figure or Table legend.

3. Results

3.1. Validation of the LC-MS/MS assay for the quantification of MPA and metabolites

The LC-MS/MS assay previously developed by our group for measuring MPA, MPAG, and AcMPAG was successfully re-validated in microsomal incubation medium per US Food and Drug Administration requirements. The lower limit of quantification (LLOQ) for MPA, MPAG, and AcMPAG was 4.67 ng/mL. The calibration curves were linear up to 3.2 μg/mL (MPA and MPAG) or 0.1 μg/mL (AcMPAG). The intra- and inter- day precision and accuracy were within 15% in high, medium, and low quality control samples (20% in LLOQ quality control samples). Autosampler and bench-top stability testing were within the accepted limits (accuracy determined to be within 15% of nominal concentrations in both high and low quality control samples). The results are summarized in Table S VI-1, Supplementary materials.

3.2. Control experiments

MPA can undergo protein binding in the incubation medium, primarily to albumin and not to microsomal proteins [33, 304]; therefore the free fractions of MPA in pooled human liver microsomes and recombinant enzymes were first characterized in order to determine the pharmacologically-active unbound concentrations in our experiments (Table S VI-2, Supplementary materials). The free fraction of MPA (0.125-1000 μM) was dependent on MPA concentration, ranging from ~50% to ~90% in both pooled human liver microsomes and recombinant UGT1A9 enzymes. The protein binding of MPA in individual human liver microsomes was assumed to be similar to that obtained in pooled human liver microsomes due to

the same albumin content and therefore were not determined. The obtained free fraction values (Table S VI-2, Supplementary materials) were used to determine the free MPA concentrations in the incubation medium. On the other hand, the free fraction of *p*-cresol in human liver microsomes was not experimentally determined and was assumed to be ~0.7 based on the findings of Barnes et al. [52] which had used comparable incubation conditions (see Discussions).

Our initial control experiments determined the optimized incubation conditions including protein concentrations and incubation times to satisfy initial velocity conditions (details specified in individual Figure legends). The suitability of our *in vitro* models for investigating metabolism-related MPA interactions was confirmed with a known selective UGT1A9 inhibitor, niflumic acid [298], which effectively reduced MPAG formation by >90% and increased MPA concentration in pooled human liver microsomes, human liver microsomes from an individual donor (lot number HFC205, with highest UGT1A9 activity, [300]), and recombinant UGT1A9 enzymes. The baseline enzyme kinetics of MPA metabolism, in the absence of inhibitors, were also assessed in pooled human liver microsomes and recombinant UGT1A9 enzymes (Table VI-1). The generated enzyme kinetic constants (K_m, V_{max}, and CL_{int}) for MPAG or AcMPAG formation in both systems were generally within or near the range reported in published literature: K_m range (77-410 µM for MPAG; 200-1710 µM for AcMPAG), V_{max} range (0.1-20.5 nmol/mg/min for MPAG; 0.14-2.73 nmol/mg/min for AcMPAG), and CL_{int} range (0.38-250 µL/mg/min for MPAG; 0.38-1.68 µL/mg/min for AcMPAG); further confirming the suitability of our *in vitro* experimental conditions [33, 35, 174, 175, 252, 253, 269, 305, 306]. Furthermore, significant correlations were observed between UGT1A9 activities in each individual human liver microsomes [300] and concentrations of MPA ($R=-0.83$, $p<0.005$) or MPAG ($R=0.89$, $p<0.0005$) in the incubation medium, consistent with the already known (major) role of UGT1A9 enzyme in the

glucuronidation of MPA [35]. In contrast, we did not have UGT2B7 activity data for our panel of individual human liver microsomes and therefore could not conduct the correlational analysis with AcMPAG.

3.3. Potency of inhibition of MPA glucuronidation by p-cresol

MPA is known to exhibit large variabilities (~10-fold) in its pharmacokinetics [10]; therefore, multiple concentrations of MPA (i.e. 0.25 μM, 2.5 μM, and 25 μM) were used to represent the MPA physiological concentration range for the purpose of determining the inhibitory effects of *p*-cresol (e.g. IC_{50} values) toward MPA glucuronidation in pooled human liver microsomes. However, when using 0.25 μM MPA, the generated MPAG concentrations were below the LLOQ in the presence of *p*-cresol, therefore the potency data could not be obtained with this specific incubation condition. The IC_{50} values representing the inhibitory effects of *p*-cresol toward MPAG formation obtained from incubations using 2.5 μM (Figure VI-1) and 25 μM MPA (i.e. 8.9 μM and 12.3 μM, respectively, Table VI-2) were below the attainable free *p*-cresol concentration in the human liver under uremic conditions (i.e. ~23.9 μM [295]), indicating a potentially clinically-significant interaction. On the other hand, the IC_{50} value corresponding to AcMPAG formation was significantly higher at 363.2 μM using an MPA concentration of 2.5 μM (Table VI-2). Furthermore, when recombinant UGT1A1, UGT1A9, UGT2B4, and UGT2B7 enzymes were incubated individually with physiological concentrations of MPA and *p*-cresol, only recombinant UGT1A9 was capable of producing MPAG at levels above the LLOQ of our analytical assay. The IC_{50} value characterizing the inhibitory effects of *p*-cresol toward the formation of MPAG by recombinant UGT1A9 was 18.2 μM (Table VI-2, Figure VI-2) which is comparable to the value generated in pooled human liver microsomes. On the other hand, no

recombinant UGT enzyme was capable of generating AcMPAG under our experimental conditions; therefore, the inhibition potency of *p*-cresol could not be obtained for this pathway.

In addition to the IC_{50} data, K_i values were also determined in pooled human liver microsomes and recombinant UGT1A9 enzymes to characterize the potency of inhibition by *p*-cresol (for MPAG formation, 5.2 μM and 23.4 μM, respectively, Table VI-2). Consistent with the IC_{50} data, the K_i value characterizing the inhibitory effects of *p*-cresol toward AcMPAG formation in pooled human liver microsomes was relatively higher than MPAG formation at 127.5 μM (an estimated value because the experimental concentration range of *p*-cresol did not span the calculated K_i values) (Table VI-2). Furthermore, the magnitudes of inhibition and the extents of inter-individual variabilities for this interaction were characterized in a panel of individual human liver microsomes (N=12, Figure VI-3, Figure VI-4) with a wide range of documented UGT1A9 catalytic activities (Table VI-3). *p*-Cresol (10 and 30 μM) increased MPA concentrations (by 122.1±13.7% and 124.5±12.2%) and decreased MPAG formation (by 35.3±10.0% and 68.2±12.1%), respectively (Figure VI-3, Figure VI-4). These effects were consistent with the average IC_{50} and IC_{90} data obtained in pooled human liver microsomes (Figure VI-1). The large standard deviation values obtained in this panel of human liver microsomes suggested that significant between-patient variability is likely to be observed in the clinic. On the other hand, *p*-cresol (10 and 30 μM) had little inhibitory effects toward AcMPAG formation in individual human liver microsomes incubated with 2.5 μM MPA (data not shown).

3.4. Mechanisms of inhibition, in vitro-in vivo extrapolation, and influences of clinical covariates

Based on data fitting using empirical models in SigmaPlot and graphical analyses with Dixon and Cornish-Bowden plots, the mechanisms of inhibition for MPAG and AcMPAG formation by *p*-cresol in pooled human liver microsomes were competitive (K_i=5.2 μM) and noncompetitive (K_i=127.5μM), respectively (Table VI-2, Figure VI-5, Figure VI-6). Consistent with these data, the mechanism of inhibition determined in recombinant UGT1A9 enzymes for MPAG formation was also competitive in nature with a comparable K_i value of 23.4 μM (Table VI-2, Figure VI-7). In order to estimate the likely changes in MPA exposure from *p*-cresol, the experimentally-generated K_i value from human liver microsomes was utilized to estimate extents of AUC increases likely observed in the clinic utilizing an already established *in vitro-in vivo* extrapolation model (Equation VI-2 [299, 303]). Considering the documented average free *p*-cresol concentration in the human liver of 23.9 μM [295], the estimated MPA exposure increase is ~1.8-fold based on the data obtained in pooled human liver microsomes. The estimated fold increase in MPA AUC is greater than the interaction threshold (i.e. >1.25 fold) deemed clinically-significant by the US Food and Drug Administration [307], further suggesting a clinically-relevant interaction between *p*-cresol and MPA.

The effects of clinical variables on the extents of *p*-cresol-mediated interactions were determined with correlational analyses in a panel of individual human liver microsomes (N=12) (Table VI-3). No variables were found to significantly correlate with the extent of MPAG reduction or MPA elevation when the incubation condition consisted of 10 μM *p*-cresol (i.e. the IC_{50} value determined in our experimental model); but, the percentage of MPA change was positively associated with UGT1A9 activity when *p*-cresol concentration was 30 μM (R=0.70,

p=0.0116, Table VI-3). These data suggest that UGT1A9 activity may be associated with the extent of *p*-cresol mediated interaction. The activities of CYP4A (R=-0.79, p=0.0024) and FMO (R=-0.69, p=0.014) were also inversely correlated with changes in MPAG concentrations with 30 μM *p*-cresol (Table VI-3).

3.5. Comparative effects of commonly-studied uremic toxins and p-cresol metabolites

The relative inhibitory effects of other common uremic toxins (i.e. CMPF, indole-3-acetic acid, 3-indoxyl sulfate, kynurenic acid, and hippuric acid) or major *p*-cresol metabolites (i.e. *p*-cresol sulfate, *p*-cresol glucuronide) toward MPA glucuronidation were investigated in pooled human liver microsomes. Compared to equi-molar concentrations (i.e. 10 μM, representing the IC_{50} value determined in our model) of uremic toxins and *p*-cresol metabolites, *p*-cresol exhibited the strongest inhibitory effects (i.e. 48.5±8.9% inhibition of MPAG formation) compared to other compounds (Figure VI-8). Trends of reduced MPAG formation in comparison to the control were associated with indole-3-acetic acid, *p*-cresol glucuronide, and *p*-cresol sulfate (78.5±3.6%, 82.2±7.8%, and 88.1±11.2%, respectively), but CMPF, indoxyl sulfate, kynurenic acid, and hippuric acid showed little inhibitory activities toward MPA glucuronidation (Figure VI-8).

4. Discussion

This study reports the following novel observations on the interaction between *p*-cresol and MPA: 1) the inhibition is potent and primarily mediated by UGT1A9; 2) the interaction is likely clinically significant, as evident by the predicted AUC changes of MPA; 3) the mechanisms of inhibition are competitive and noncompetitive for MPAG and AcMPAG formation, respectively;

4) there is significant inter-individual variability in the magnitude of the interaction; and 5) *p*-cresol is the most potent inhibitor of MPA-glucuronidation in comparison to other commonly-studied uremic toxins and its major conjugated metabolites.

These observations are consistent with and further build on the preliminary data reported in our lab using the HepaRG model [54]. The HepaRG model was limited in that the cells were derived from a single subject [172, 270] and therefore could not be representative of the population. In contrast, human liver microsomes, the primary site of the MPA and *p*-cresol interaction, are more suitable for the determination of drug interactions and the estimation of kinetic constants, because one can control the substrate/inhibitor free concentrations directly at the active site (Table S VI-2, Supplementary materials). Moreover, recombinant UGT enzymes allowed the characterization of specific UGT pathways mediating the interaction; whereas the effects of clinical covariates and inter-subject variabilities were determined using individual human liver microsomes. The utilities of our *in vitro* models were confirmed by i) similar K_m, V_{max}, and CL_{int} values for MPA in relation to published data; ii) positive inhibitory control experiments with niflumic acid, and iii) and correlational analyses demonstrating the expected strong relationships between UGT1A9 activities and MPAG formation (please see Results).

Our data illustrated that *p*-cresol is a potent and reversible inhibitor of MPA glucuronidation. The K_i values obtained for its effects on MPAG formation in pooled human liver microsomes (5.2 μM) and recombinant UGT1A9 (23.4 μM) were lower than the documented free *p*-cresol concentration (i.e. 23.9 μM) in the human liver under uremic conditions [295]. The IC_{50} values, in the same order as the apparent K_i, were generated under a physiological free concentration of MPA representing the C_{max} typically observed in humans [59], highlighting the clinical relevance of this interaction. The clinical significance is further supported by an estimated

1.8 fold increase in MPA AUC in the presence of *p*-cresol (23.9 μM [295]). However, this fold increase may very well be a conservative estimation because numerous laboratories have reported even higher (i.e. 1664 μM) concentrations of *p*-cresol sulfate in the plasma [308], suggesting that much higher concentrations of *p*-cresol, the direct precursor to *p*-cresol sulfate, can be observed in the liver. Moreover, given the significant UGT1A9 activities documented in kidney microsomes [294, 309, 310], further increases in MPA concentration as a direct result of *p*-cresol mediated inhibition in this organ may be possible. Given the relatively narrow therapeutic range of MPA (i.e. 30-60 mg*h/L) and the manifestation of MPA-induced toxicities within this target [61], a "doubling" of MPA exposure as a direct result of *p*-cresol can potentially place the patients at significantly increased risks of MPA toxicity. Our laboratory is in the process of conducting clinical experiments to verify the significance of these *in vitro* findings. However, a limitation in the current study is that the estimated free fraction for *p*-cresol of 0.7 was based on a microsomal incubation medium consisting of 2% BSA [52], which is higher than the albumin concentration (1%) used in our study. However, this does not change the estimated K_i value or the predicted MPA exposure alteration to significant degrees. Assuming a free faction of "1" for *p*-cresol, the K_i would only be slightly increased from 5.2 μM to 7.5 μM. This means that the calculated K_i is estimated to be between 5.2-7.5 μM (which is still significantly smaller than the reported free *p*-cresol concentration observed in the liver [295]) and the AUC change would be between 1.7-1.8 fold, had the free-fraction of *p*-cresol been higher due to a lower albumin concentration in our incubation medium.

Our data indicated that UGT1A9 is the primary enzyme mediating the interaction, based on the following: 1) the same mechanism of competitive inhibition was determined in both pooled human liver microsomes and recombinant UGT1A9 systems (Figure VI-5, Figure VI-7); 2)

UGT1A9 enzyme activities in individual human liver microsomes correlated with the extent of *p*-cresol mediated inhibition (Table VI-3); and 3) that the apparent IC_{50} and K_i values obtained from recombinant UGT1A9 (18.2, and 23.4 μM, respectively) were comparable to that derived from pooled human liver microsomes (8.9, and 5.2 μM, respectively). The slightly reduced IC_{50} and K_i values observed in human liver microsomes in comparison to recombinant UGT1A9 are still well within the large variabilities expected for MPA kinetics (i.e. up to 10-fold variation is considered normal [10]), but may suggest that additional UGT enzymes can also contribute to the interaction. However, in a panel of recombinant UGT enzymes tested in this study, only recombinant UGT1A9 was capable of generating sufficient levels of MPAG under our physiologically-relevant incubation conditions; therefore, the identities of these additional UGT enzymes mediating this interaction would still remain to be determined. Nevertheless, our finding of a major role of UGT1A9 in mediating the *p*-cresol/MPA interaction is consistent with the already established significant contribution of UGT1A9 in the metabolism of MPA [35] and the potent inhibitory effects of *p*-cresol toward other UGT1A9 substrates such as propofol (K_i=2.5 μM) [52]. On the other hand, the effects of *p*-cresol on UGT2B7-mediated AcMPAG formation are unlikely clinically relevant. This is based on the relatively high K_i and IC_{50} values obtained in pooled human liver microsomes (Table VI-2) and the minor contribution of this conjugation pathway to MPA metabolism [35].

The mechanism of inhibition by *p*-cresol towards MPAG formation was competitive in nature and of clinical relevance (Figure VI-5, Figure VI-7). For this type of inhibition, substrate concentration reduction (i.e. by dose-reducing mycophenolate) is unlikely to fully or efficiently mitigate the interaction; whereas minimization of *p*-cresol concentration, which may be achieved with non-pharmacological (i.e. fat lowering diet [311]) or pharmacological (i.e. synbiotics [83])

measures, could potentially alleviate some interaction. This is because patients with renal disease may experience an imbalance of bacteria (e.g. *C. difficile*) responsible for the production of *p*-cresol, potentially resulting in increased synthesis [312].This may explain the large inter-individual variability in the plasma concentrations of *p*-cresol reported in the literature (e.g. [313]). As demonstrated in this investigation, *p*-cresol is a potent and competitive inhibitor of MPA glucuronidation, hence the large variability in MPA clearance/exposure may be attributed to the fluctuation in *p*-cresol concentration as a result of microbiome imbalance. Normalizing microbiome balance through these measures can potentially mitigate the interaction between *p*-cresol and MPA. Furthermore, the competitive inhibitory nature of *p*-cresol towards UGT1A9 mediated MPAG formation may indicate that *p*-cresol is a substrate of this specific enzyme, although further reaction phenotyping studies are needed to confirm this observation. On the other hand, the observed mechanism of inhibition for MPAG formation was different than that documented for UGT1A9-mediated propofol glucuronidation (uncompetitive), indicating that the type of inhibition associated with *p*-cresol could be substrate-dependent. Similar findings have been reported by Chengcheng et al, where wogonin inhibited the glucuronidation of 4-methylumbelliferone noncompetitively, but propofol competitively, in reactions mediated by UGT1A9 [314]. On the other hand, the mechanism of inhibition toward AcMPAG formation was non-competitive in nature (Figure VI-6), but this particular pathway is unlikely to contribute significantly to the overall MPA interaction (please see discussion above). A limitation in our approach is the lack of characterization of irreversible, mechanism-based enzyme inactivation, which may be possible given that *p*-cresol can undergo oxidation in the production of reactive intermediates [315]. However, this specific bioactivation pathway is relatively minor [78, 80], and

the data reported in this manuscript and others [52] have provided support for reversible inhibitions as the primary mechanism for *p*-cresol mediated interaction.

p-Cresol mediated interaction was highly variable between subjects (Figure VI-3, Figure VI-4) and the variability did not correlate with CYP450 enzyme activities (except for CYP4A) or patient demographic factors such as sex, age, and race (Table VI-3). The lack of correlation with CYP450 enzyme activities is consistent with the known metabolism pathways of *p*-cresol, which are primarily by conjugation and not oxidation [78, 80]. Moreover, although *p*-cresol can inhibit certain CYP450 enzymes (e.g. CYP3A4), these contribute very little to the overall MPA metabolism [36]. The observed correlation with CYP4A activity (Table VI-3) may be explained by the enzyme's role in the metabolism of membrane fatty acids [316] which are known to have inhibitory effects toward UGT1A9 [317]. On the other hand, it was not clear why FMO activities correlated with the extent of MPAG formation in the presence of *p*-cresol, as this particular enzyme has not been associated, to our knowledge, with the metabolism of either *p*-cresol or MPA. Overall, the extents of interaction on MPAG formation were significantly correlated (with 30 μM *p*-cresol) with UGT1A9 activity (Table VI-3), an observation consistent with our finding that this particular enzyme is primarily responsible for mediating this interaction (please see above).

Our study found that *p*-cresol was a relatively more effective inhibitor of MPAG formation compared to other commonly-studied protein-bound uremic toxins or conjugated *p*-cresol metabolites (Figure VI-8). These results are consistent with the data reported by Barnes et al. [52] where *p*-cresol was a more potent inhibitor than benzyl alcohol, indoxyl sulfate, and hippuric acid for conjugation and oxidation marker reactions. The higher inhibitory effects of *p*-cresol compared to its conjugated metabolites were novel findings. Although various studies have attributed the pharmacological effects of *p*-cresol to the *p*-cresol sulfate metabolite [78, 82], our data suggested

that *p*-cresol itself still has toxicological relevance, especially in the context of toxicokinetic interactions.

In conclusion, *p*-cresol, at concentrations achievable under uremic conditions in humans, can significantly inhibit the glucuronidation of MPA. This interaction is of toxicological significance given the large MPA exposure changes (> 1.8-fold) expected to be observed in patients. The mechanism of inhibition provides rationales for therapeutic interventions that may mitigate this interaction. Our findings also support more focused investigations on *p*-cresol given its relatively potent effects compared to other uremic toxins and its conjugated metabolites.

Table VI-1 Summary of K_m and V_{max} values of MPA glucuronidation determined in pooled human liver microsomes and recombinant UGT1A9 enzymes

	Pooled human liver microsomes		**Recombinant UGT1A9 enzymes**	
	MPAG formation (N=2)	*AcMPAG formation (N=2)*	*MPAG formation (N=2)*	*AcMPAG formation (N=2)*
K_m, µM	154.5	271.9	74.0	ND
V_{max}, nmol/mg/min	0.35	0.06	1.21	ND
CL_{int}, µL/mg/min	2.2	0.2	16.4	ND

Pooled human liver microsomes (protein concentration=0.5 mg/mL, incubation time=5 minutes) and recombinant UGT1A9 enzyme (protein concentration=0.5 mg/mL, incubation time=15 minutes) were incubated with MPA as described in Materials and Methods (N=duplicate determinations).

Abbreviation(s): *AcMPAG*, mycophenolic acid-acyl-glucuronide; CL_{int}, intrinsic clearance; K_m, concentration of substrate at which the reaction rate is half of the maximum; *MPAG*, mycophenolic acid-glucuronide; *ND*, not detectable because the UGT1A9 enzymes did not catalyze the formation of AcMPAG; *UGT*, uridine 5'-diphospho-glucuronosyltransferase; V_{max}, maximum reaction rate.

Table VI-2 Summary of inhibition mechanism, IC_{50}, and K_i in pooled human liver microsomes and recombinant UGT1A9 enzymes

	Pooled human liver microsomes		**Recombinant UGT1A9 enzymes**
	Inhibitory effects of p-cresol toward MPAG formation (N=2)	*Inhibitory effects of p-cresol toward AcMPAG formation (N=2)*	*Inhibitory effects of p-cresol toward MPAG formation (N=2)*
Mechanism of inhibition	Competitive	Noncompetitive	Competitive
IC_{50} (µM) when MPA=0.25 µM	ND	NA	NA
IC_{50} when MPA=2.5 µM	8.9	363.2	18.2
IC_{50} when MPA=25 µM	12.3	NA	NA
K_i, µM	5.2	127.5	23.4

Pooled human liver microsomes (protein concentration=0.5 mg/mL, incubation time=5 minutes) or recombinant UGT1A9 enzymes (protein concentration=0.5 mg/mL, incubation time=15 minutes) were incubated with *p*-cresol and/or MPA as described in Materials and Methods (N=duplicate determinations).

To determine the IC_{50} values, curves of MPAG or AcMPAG vs. *p*-cresol concentrations were fitted with sigmoidal three-parameter fitting in SigmaPlot 14 (Systat Software, Inc., San Jose, California, United States). The K_i values were generated with SigmaPlot 14 software after determination of inhibition mechanism using data fitting and Dixon and Cornish-Bowden plots.

Abbreviation(s): *AcMPAG*, mycophenolic acid acyl-glucuronide; *IC_{50}*, half maximum inhibitory concentration; *K_i*, concentration of inhibitor at which under saturating substrate conditions the reaction rate is at half of the maximum rate; *MPA*, mycophenolic acid; *MPAG*, mycophenolic acid-glucuronide; *NA*, not applicable because this particular MPA concentration was not tested; *ND,* not detectable due to concentration found below the limit of quantification; *UGT*, uridine 5'-diphospho-glucuronosyltransferase.

Table VI-3 Associations between clinical factors and p-cresol mediated reduction in MPA glucuronidation in human liver microsomes (N=12 individual donors)

Enzyme activity (pmol/mg/min) [300]	*Mean ± standard deviation [Range] (N=12)[1]*	*[MPA] as % of control at [p-cresol] of 10 µM, R (p-value)*	*[MPAG] as % of control at [p-cresol] of 10 µM, R (p-value)*	*[MPA] as % of control at [p-cresol] of 30 µM, R (p-value)*	*[MPAG] as a % of control at [p-cresol] of 30 µM, R (p-value)*
UGT1A9	2735 ± 1356 [640 – 4500]	-0.10 (0.754)	0.37 (0.242)	0.70 (0.0116)*	0.33 (0.293)
Total P450c (Omura and Sato)	428 ± 273 [170 – 1200]	0.20 (0.529)	0.30 (0.345)	0.24 (0.456)	-0.19 (0.550)
CYP1A2	432 ± 276 [84 – 880]	0.39 (0.210)	0.53 (0.0781)	0.09 (0.772)	-0.17 (0.604)
CYP2A6	1084 ± 665 [250 – 2100]	0.19 (0.547)	0.35 (0.258)	0.02 (0.957)	-0.15 (0.639)
CYP2B6	63 ± 25 [21 – 110]	0.01 (0.972)	0.49 (0.128)	0.09 (0.798)	-0.12 (0.727)
CYP2C8	242 ± 240 [26 – 960]	0.21 (0.509)	0.40 (0.203)	0.32 (0.304)	-0.10 (0.755)
CYP2C9	3347 ± 1587 [560 – 5500]	0.02 (0.947)	0.31 (0.335)	0.38 (0.229)	-0.17 (0.607)
CYP2C19	67 ± 125 [0 – 450]	-0.12 (0.728)	-0.24 (0.496)	-0.02 (0.956)	-0.28 (0.399)
CYP2D6	98 ± 70 [7.3 – 250]	0.13 (0.680)	0.35 (0.268)	0.12 (0.701)	-0.26 (0.424)
CYP2E1	2055 ± 1057 [860 – 4100]	-0.09 (0.765)	0.43 (0.158)	0.10 (0.767)	0.14 (0.667)
CYP3A4	6943 ± 5243 [970 – 16000]	0.20 (0.529)	0.27 (0.404)	-0.08 (0.779)	-0.33 (0.295)
CYP4A	2053 ± 1195 [450 – 5300]	0.47 (0.120)	-0.05 (0.888)	-0.31 (0.322)	-0.79 (0.0024)*

FMO (as measured by methyl p-tolyl sulfide oxidase)	1515 ± 817 [110 – 2800]	0.45 (0.141)	0.07 (0.819)	-0.35 (0.264)	-0.69 (0.014)*
UGT1A1	1190 ± 770 [64 – 2500]	-0.25 (0.436)	-0.21 (0.520)	0.44 (0.150)	0.33 (0.301)
UGT1A4	466 ± 231 [80 – 960]	0.11 (0.741)	0.14 (0.670)	-0.37 (0.238)	-0.40 (0.193)
Donor demographics	*Categorical numbers or mean ± standard deviation [Range] (N=12)*	*[MPA] as % of control at [p-cresol] of 10 µM, R (p-value)*	*[MPAG] as % of control at [p-cresol] of 10 µM, R (p-value)*	*[MPA] as % of control at [p-cresol] of 30 µM, R (p-value)*	*[MPAG] as a % of control at [p-cresol] of 30 µM, R (p-value)*
Sex	Male 6, Female 6	NA (0.709)	NA (0.546)	NA (0.997)	NA (0.945)
Age (years)	53 ± 13 [23 – 70]	0.04 (0.901)	0.34 (0.277)	-0.01 (0.966)	0.06 (0.865)
Race	Caucasian 8, Hispanic 3, Asian 1	NA (0.284)	NA (0.579)	NA (0.489)	NA (0.149)

Individual human liver microsomes (protein concentrations=0.5 mg/mL, incubation time=10 minutes) were incubated with *p*-cresol and/or MPA as described in Materials and Methods (N=duplicate determinations).

All continuous data were logarithm-(base 10) transformed; *p-value <0.05 based on Pearson correlational analyses. Sex and race were categorized into individual groups and differences between groups determined using the Student's t-test (male vs. female) or One-Way analysis of variance (ANOVA) (Caucasian vs. Hispanic vs. Asian) in SigmaStat version 3.5.

[1]Reference data in this column were obtained from Corning Gentest [300].

Abbreviation(s): *CYP*, cytochrome P450; *FMO*, flavin-containing monooxygenase; *[MPA]*, concentrations of mycophenolic acid; *[MPAG]*, *concentrations of* mycophenolic acid-glucuronide; *NA*, not applicable; *R*, coefficient of correlation; *UGT*, uridine 5'-diphospho-glucuronosyltransferase.

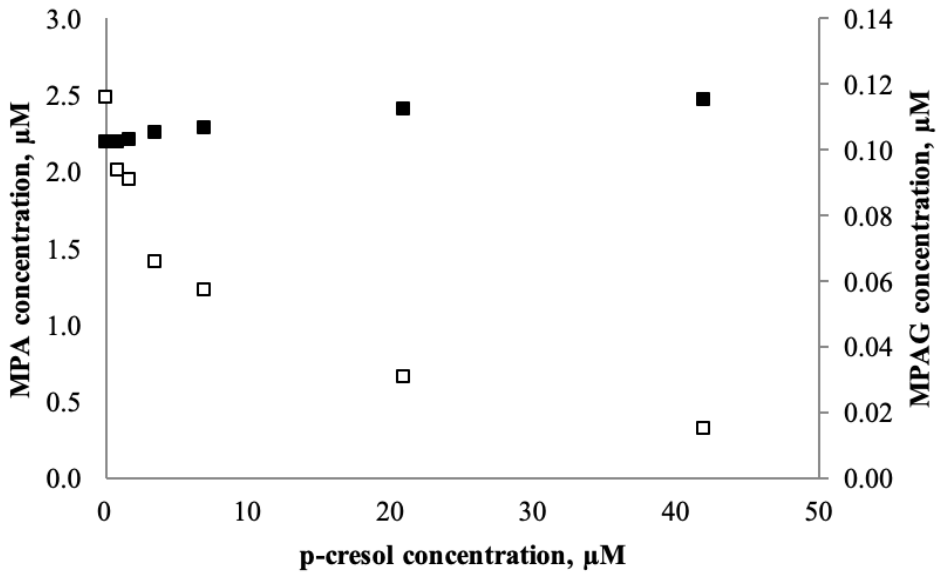

Figure VI-1 Concentration-dependent effects of p-cresol on MPA and MPAG levels in pooled human liver microsomes

Protein concentration=0.5 mg/mL, MPA=2.5 µM, and incubation time=5 minutes (N=duplicate determinations).

Abbreviation(s): *MPA*, mycophenolic acid; *MPAG*, mycophenolic acid-glucuronide. ■MPA concentration; □MPAG concentration.

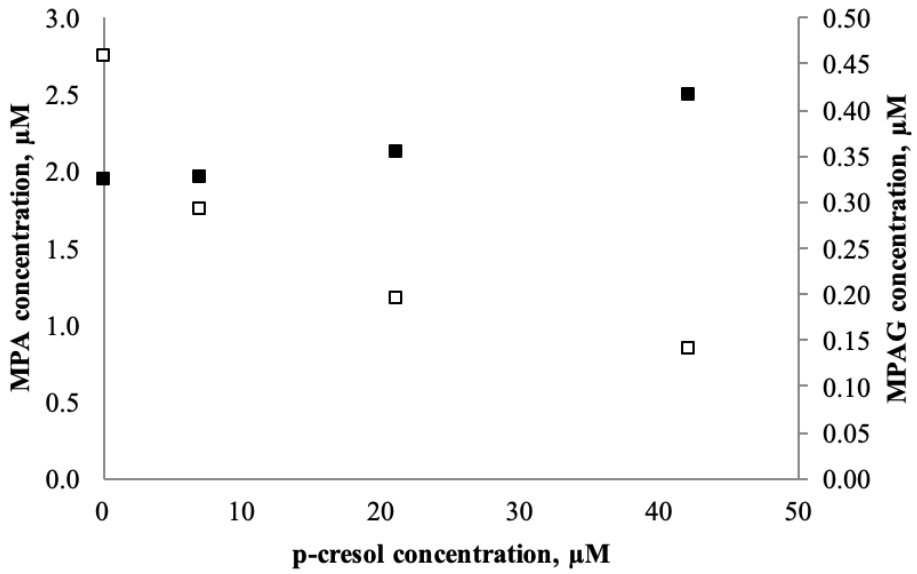

Figure VI-2 Concentration-dependent effects of p-cresol on MPA and MPAG levels in recombinant UGT1A9 enzymes

Protein concentration=0.5 mg/mL, MPA=2.5 µM, and incubation time=15 minutes (N=duplicate determinations).

Abbreviation(s): *MPA*, mycophenolic acid; *MPAG*, mycophenolic acid-glucuronide. ■MPA concentration; □MPAG concentration.

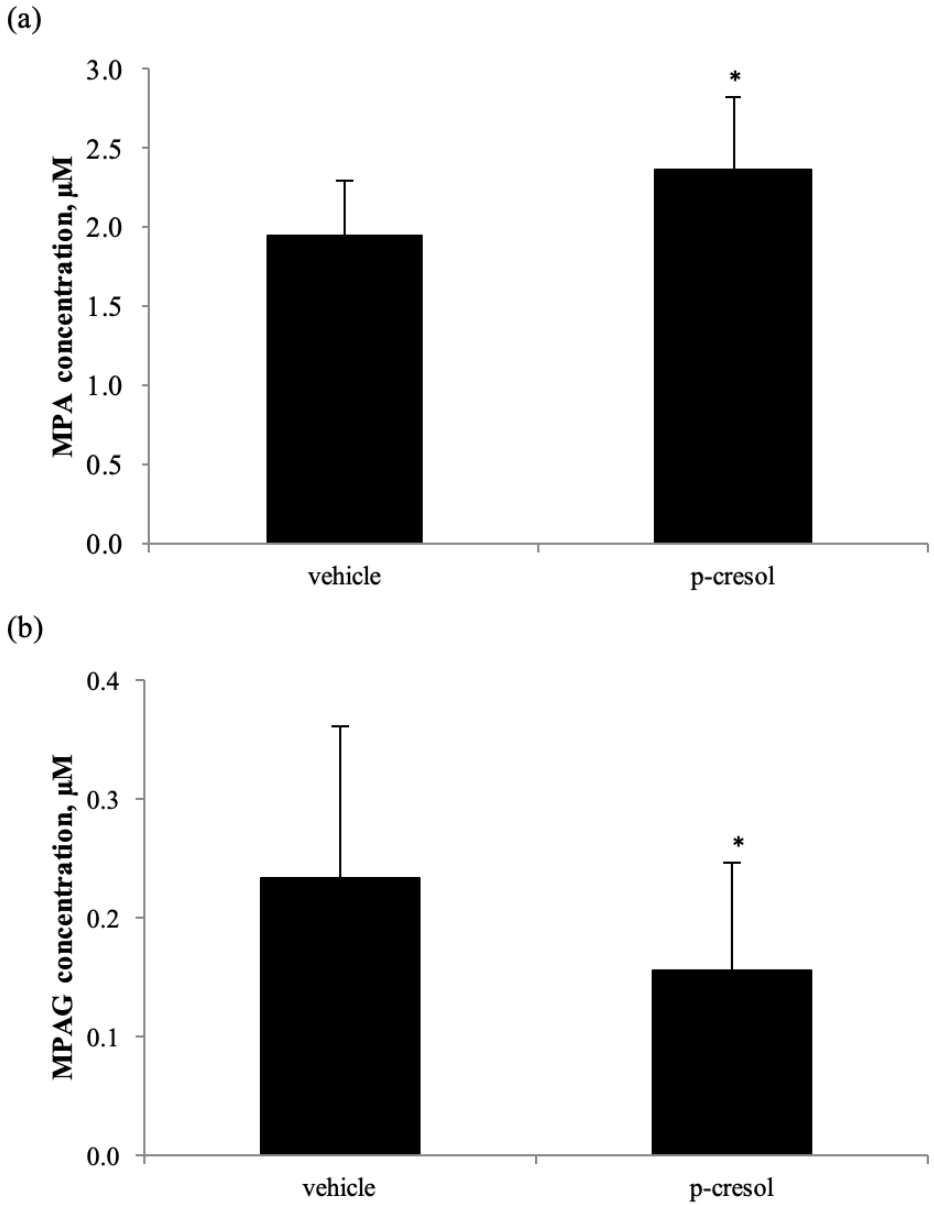
(a)
MPA concentration, µM
3.0
2.5
2.0
1.5
1.0
0.5
0.0
*
vehicle
p-cresol
(b)
MPAG concentration, µM
0.4
0.3
0.2
0.1
0.0
*
vehicle
p-cresol

Figure VI-3 Effects of 10 µM p-cresol on concentrations of (a) MPA or (b) MPAG in human liver microsomes obtained from 12 individual donors

Protein concentration=0.5 mg/mL, MPA=2.5 µM, incubation time=10 minutes

Data presented as mean ± standard deviation; *p-value <0.05 vs. the vehicle control using student's t-test.

Abbreviation(s): *MPA*, mycophenolic acid; *MPAG*, mycophenolic acid-glucuronide.

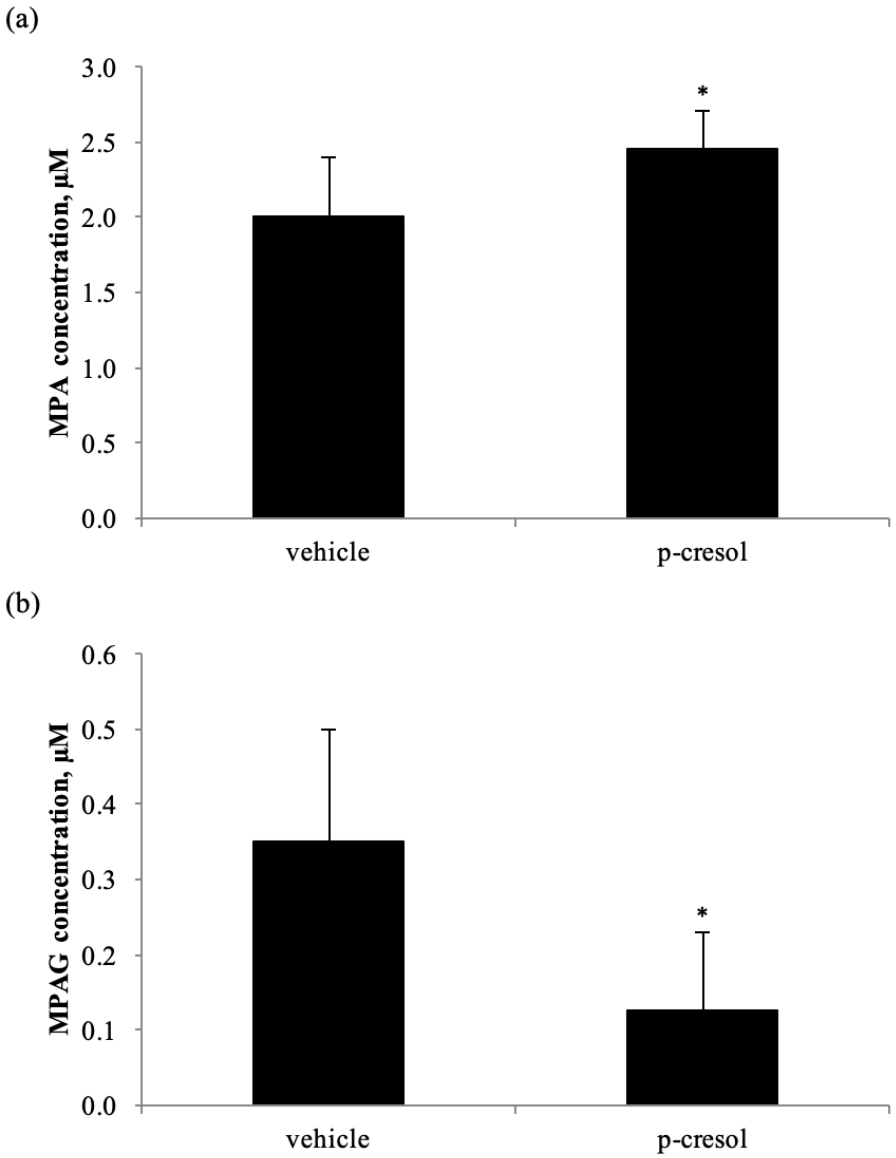
(a)
MPA concentration, µM
3.0
2.5
2.0
1.5
1.0
0.5
0.0
*
vehicle
p-cresol
(b)
MPAG concentration, µM
0.6
0.5
0.4
0.3
0.2
0.1
0.0
*
vehicle
p-cresol

Figure VI-4 Effects of 30 µM p-cresol on concentrations of (a) MPA or (b) MPAG in human liver microsomes obtained from 12 individual donors

Protein concentration=0.5 mg/mL, MPA=2.5 µM, incubation time=10 minutes

Data presented as mean ± standard deviation; *p-value <0.05 vs. the vehicle control using student's t-test.

Abbreviation(s): *MPA*, mycophenolic acid; *MPAG*, mycophenolic acid-glucuronide.

(a)

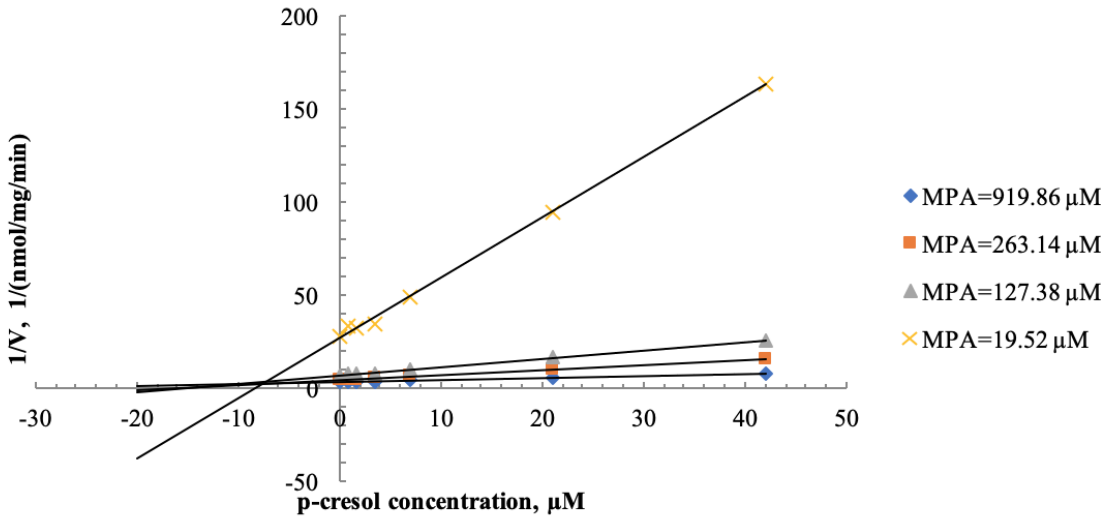
200
150
100
50
0
-50
-30
-20
-10
0
10
20
30
40
50
1/V, 1/(nmol/mg/min)
p-cresol concentration, µM
MPA=919.86 µM
MPA=263.14 µM
MPA=127.38 µM
MPA=19.52 µM

(b)

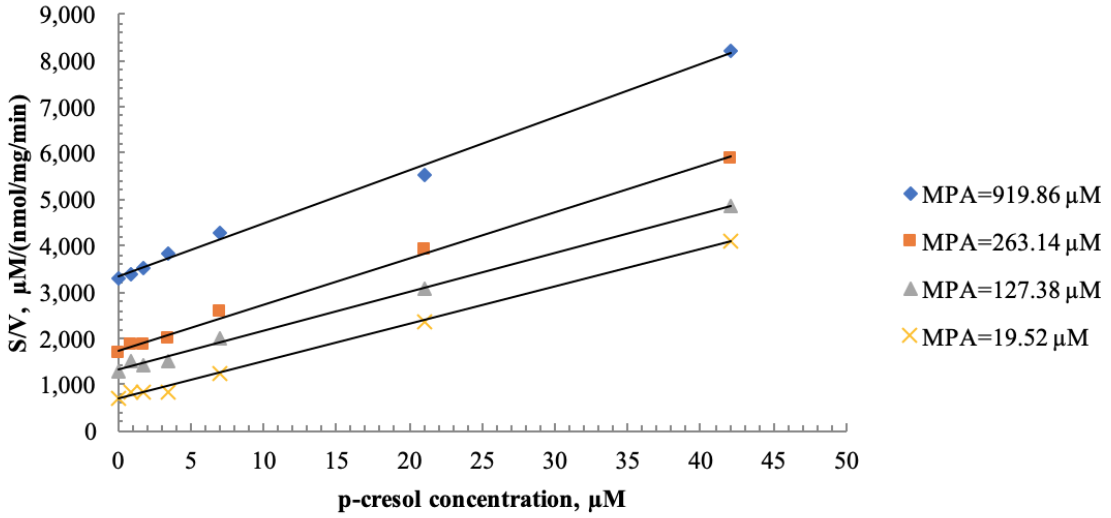
9,000
8,000
7,000
6,000
5,000
4,000
3,000
2,000
1,000
0
0
5
10
15
20
25
30
35
40
45
50
S/V, µM/(nmol/mg/min)
p-cresol concentration, µM
MPA=919.86 µM
MPA=263.14 µM
MPA=127.38 µM
MPA=19.52 µM

Figure VI-5 (a) Dixon and (b) Cornish-Bowden plots characterizing the inhibitory effects of p-cresol on MPAG formation in pooled human liver microsomes

Pooled human liver microsomes (protein concentrations=0.5 mg/mL, incubation time=5 minutes) were incubated with *p*-cresol and/or MPA as described in Materials and Methods (N=duplicate determinations).

Abbreviation(s): *MPA*, mycophenolic acid; *MPAG*, mycophenolic acid-glucuronide; *S*, substrate concentration (i.e. MPA concentration); *V*, formation rate.

(a)

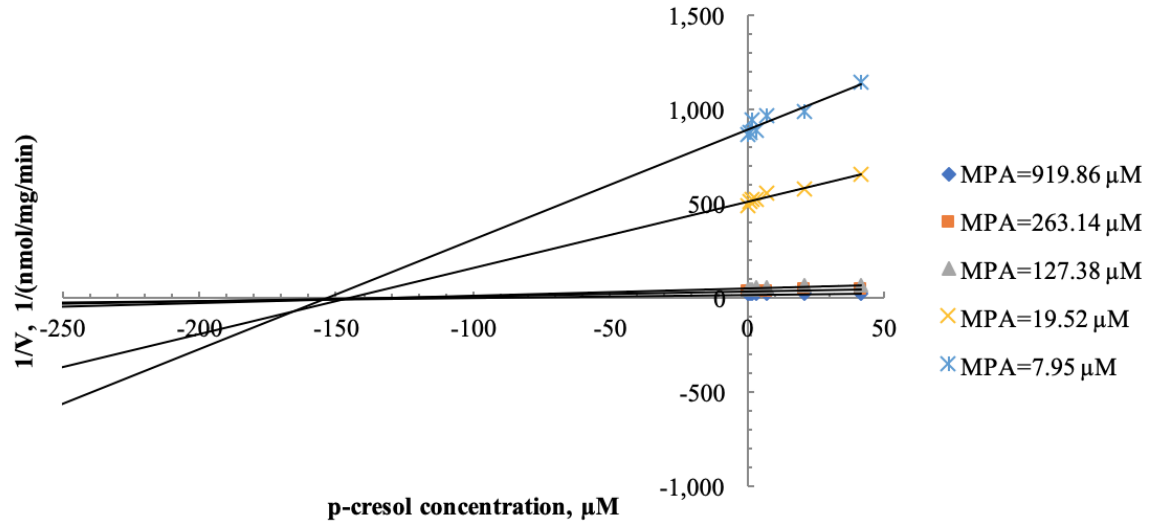
1,500
1,000
500
0
-500
-1,000
-250
-200
-150
-100
-50
0
50
1/V, 1/(nmol/mg/min)
p-cresol concentration, µM
MPA=919.86 µM
MPA=263.14 µM
MPA=127.38 µM
MPA=19.52 µM
MPA=7.95 µM

(b)

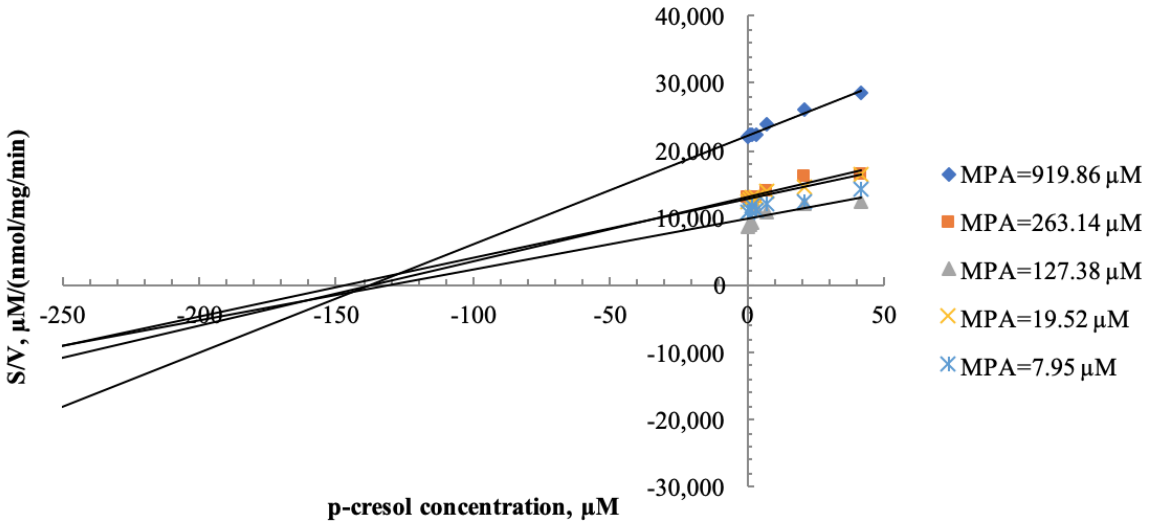
40,000
30,000
20,000
10,000
0
-10,000
-20,000
-30,000
-250
-200
-150
-100
-50
0
50
S/V, µM/(nmol/mg/min)
p-cresol concentration, µM
MPA=919.86 µM
MPA=263.14 µM
MPA=127.38 µM
MPA=19.52 µM
MPA=7.95 µM

Figure VI-6 (a) Dixon and (b) Cornish-Bowden plots characterizing the inhibitory effects of p-cresol toward AcMPAG formation in pooled human liver microsomes

Pooled human liver microsomes (protein concentrations=0.5 mg/mL, incubation time=5 minutes) were incubated with *p*-cresol and/or MPA as described in Materials and Methods (N=duplicate determinations).

Abbreviation(s): *AcMPAG*, mycophenolic acid-acyl-glucuronide; *MPA*, mycophenolic acid; *S*, substrate concentration (i.e. MPA concentration); *V*, formation rate.

(a)

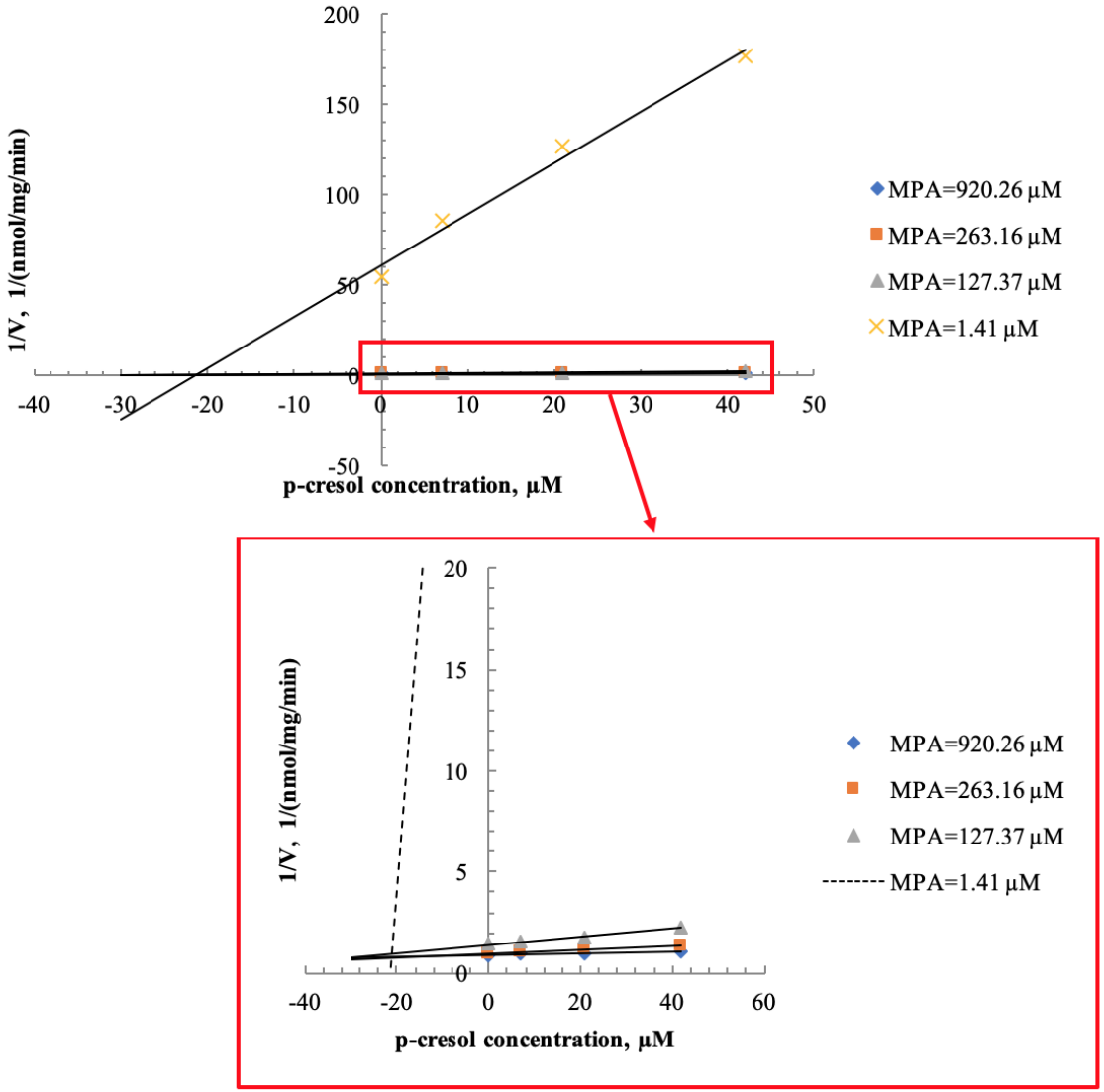
200
150
100
50
0
-50
-40
-30
-20
-10
0
10
20
30
40
50
1/V, 1/(nmol/mg/min)
p-cresol concentration, µM
MPA=920.26 µM
MPA=263.16 µM
MPA=127.37 µM
MPA=1.41 µM
20
15
10
5
0
-40
-20
0
20
40
60
1/V, 1/(nmol/mg/min)
p-cresol concentration, µM
MPA=920.26 µM
MPA=263.16 µM
MPA=127.37 µM
MPA=1.41 µM

(b)

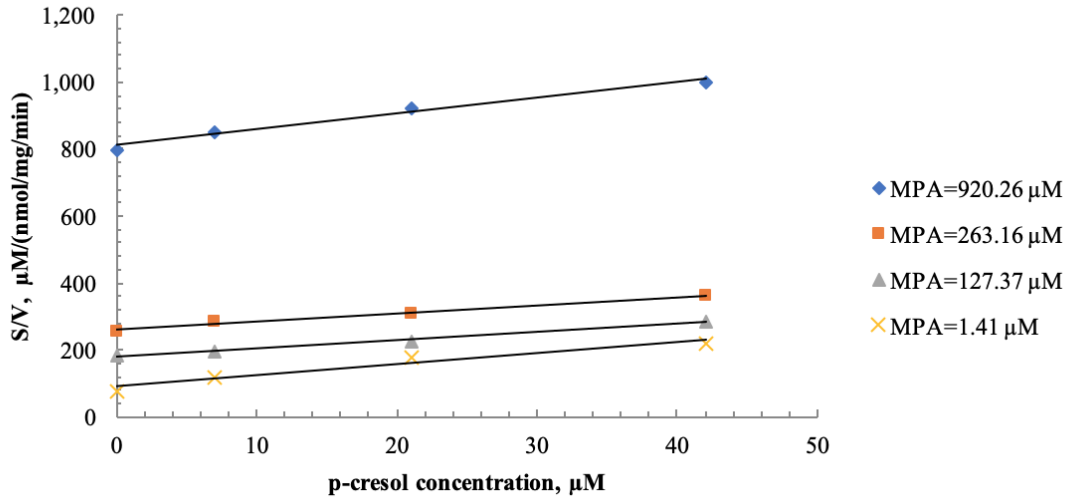

Figure VI-7 (a) Dixon and (b) Cornish-Bowden plots characterizing the inhibitory effects of p-cresol toward MPAG formation in recombinant UGT1A9 enzymes

Recombinant UGT1A9 enzymes (protein concentrations=0.5 mg/mL, incubation time=15 minutes) were incubated with *p*-cresol and/or MPA as described in Materials and Methods (N=duplicate determinations).

Abbreviation(s): *MPA*, mycophenolic acid; *MPAG*, mycophenolic acid-glucuronide; *S*, substrate concentration (i.e. MPA concentration); *V*, formation rate.

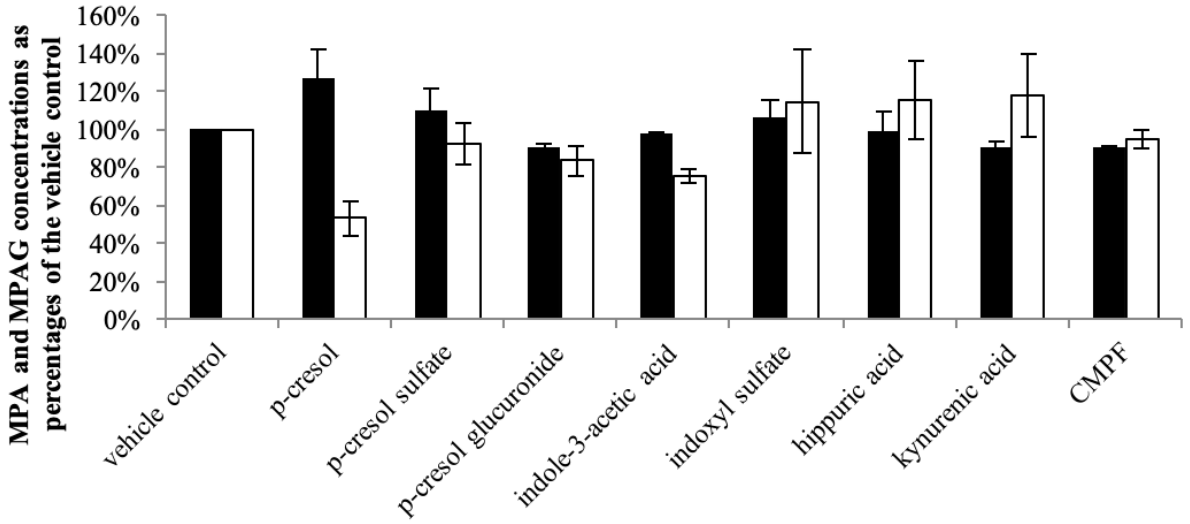

Figure VI-8 Relative effects of uremic toxins and p-cresol metabolites (equal molar concentrations, 10 µM) on MPAG formation in pooled human liver microsomes

Pooled human liver microsomes (protein concentrations=0.5 mg/mL, incubation time=5 minutes) were incubated with *p*-cresol, individual uremic toxins, or *p*-cresol metabolites with/without MPA as described in Materials and Methods (Mean±standard deviation from N=4 replicates). ■MPA concentration; □MPAG concentration.

Abbreviation(s): *CMPF*, 3-carboxy-4-methyl-5-propyl-2-furanpropionic acid; *MPA*, mycophenolic acid; *MPAG*, mycophenolic acid-glucuronide.

Supplementary materials

Table S VI-1 Validation data for the LC-MS/MS assay in microsomal incubation medium

	Nominal concentrations, ng/mL	Intra-day (1), N=5		Intra-day (2), N=5		Intra-day (3), N=5		Inter-day, N=15		Autosampler stability (4°C, 24 hours), N=5		Bench-top stability (23.5°C, 6 hours), N=5	
		Precision	Accuracy	Precision	Accuracy	Precision	Accuracy	Precision	Accuracy	Precision	Accuracy	Precision	Accuracy
MPA	1600	2.40%	-14.86%	4.54%	-3.51%	4.59%	0.16%	3.84%	-6.07%	5.13%	-3.39%	0.20%	-2.39%
	100	1.04%	-6.01%	7.07%	9.02%	8.47%	-4.48%	5.53%	-0.49%	NA	NA	NA	NA
	12.96	7.80%	9.95%	2.28%	2.79%	6.41%	-13.42%	1.22%	-0.23%	4.77%	-2.58%	1.22%	3.34%
	4.67	1.80%	1.19%	1.18%	12.21%	0.48%	-8.74%	0.83%	1.55%	NA	NA	NA	NA
MPAG	1600	0.12%	-8.49%	3.40%	-15.46%	3.46%	-4.61%	2.33%	-9.52%	1.56%	13.10%	6.40%	3.99%
	100	1.70%	-0.56%	5.98%	-10.00%	7.98%	-12.63%	5.22%	-7.73%	NA	NA	NA	NA
	12.96	4.07%	8.31%	1.93%	-12.25%	1.96%	-1.15%	1.35%	-1.69%	4.33%	-0.08%	2.01%	-2.57%
	4.67	3.96%	-7.02%	8.57%	-10.91%	1.94%	-5.90%	3.53%	-7.94%	NA	NA	NA	NA

AcMPAG	100	0.76%	-12.12%	6.65%	-4.14%	6.71%	0.22%	4.71%	-5.34%	10.31%	5.27%	11.55%	-0.82%
	36	5.80%	-7.16%	5.28%	-2.61%	5.42%	0.24%	5.50%	-3.18%	NA	NA	NA	NA
	12.96	1.71%	-0.08%	3.59%	-1.17%	3.84%	-2.69%	3.05%	-1.31%	7.83%	-10.26%	5.81%	-9.80%
	4.67	8.53%	-18.91%	6.64%	-1.33%	8.15%	-15.20%	7.77%	-11.81%	NA	NA	NA	NA

The already developed LC-MS/MS assay [54] was re-validated in the microsomal incubation medium as described in Materials and Methods, following the guidance published by the US Food and Drug Administration [273].

Abbreviation(s): *AcMPAG*, mycophenolic acid-acyl-glucuronide; *LC-MS/MS*, liquid chromatography tandem mass-spectrometry; *MPA*, mycophenolic acid; *MPAG*, mycophenolic acid-glucuronide; *NA*, not applicable because the stability results for these concentrations were not required by the US Food and Drug Administration guidance document.

Table S VI-2 Unbound fractions of MPA determined in pooled human liver microsomes and recombinant UGT1A9 enzymes (containing 1% BSA) at various MPA concentrations

MPA concentration, μM	Percentage of unbound fraction	
	Pooled human liver microsomes (N=2)	Recombinant UGT1A9 enzymes (N=2)
0.125	51.3%	ND
0.25	52.9%	ND
1.25	48.5%	ND
2.5	49.3%	56.4%
12.5	62.2%	ND
25	78.1%	ND
46.9	74.9%	ND
187.5	77.9%	67.9%
375	79.2%	70.2%
1000	91.9%	92.03%

Pooled human liver microsomes (protein concentration=0.5 mg/mL, incubation time=5 minutes) and recombinant UGT1A9 enzymes (protein concentration=0.5 mg/mL, incubation time=15 minutes) were incubated with MPA as described in Materials and Methods (N=duplicate determinations).

Unbound fractions were calculated as the ratio of measured free concentrations of MPA (i.e. MPA spiked in incubation mixture and passed through Amicon® ultra-centrifugal filters) to the measured total concentrations of MPA (i.e. MPA spiked in the incubation mixture without protein or BSA and passed though Amicon® ultra-centrifugal filters).

Abbreviation(s): *BSA*, bovine serum albumin; *MPA*, mycophenolic acid; *ND*, not determined; *UGT*, uridine 5'-diphospho-glucuronosyltransferase.

Chapter VII. Characterization of human sulfotransferases catalyzing the formation of *p*-cresol sulfate and identification of mefenamic acid as a potent metabolism inhibitor and potential therapeutic agent for detoxification[7]

Prologue:

As p-cresol was found to be a potent inhibitor of MPA metabolism (Chapter V [54] and Chapter VI [55]), it was pertinent to determine how p-cresol is further metabolized. These data were necessary to elucidate factors that could affect p-cresol disposition and hence indirectly contribute to MPA pharmacokinetic variabilities. Moreover, p-cresol is primarily found in the forms of its conjugated metabolites in the human plasma; therefore, it was also necessary to determine the enzyme kinetics of p-cresol metabolite formation to further translate our in vitro findings to the clinical experiment (Chapter V [54], Chapter VI [55], and Chapter IX [58]). Furthermore, p-cresol sulfate has been known to be toxic to various tissues, which could potentially lead to altered MPA distribution (further discussed in Chapter IX [58]); therefore, finding a targeted and potent approach for detoxifying p-cresol sulfate could also potentially lead to the reduction of MPA pharmacokinetic variabilities. The aim of this chapter was to characterize the enzyme kinetics of

[7] This chapter is already published in a peer-reviewed journal. **Rong Y** and Kiang TKL. Characterization of human sulfotransferases catalyzing the formation of *p*-cresol sulfate and identification of mefenamic acid as a potent metabolism inhibitor and potential therapeutic agent for detoxification. *Toxicology and Applied Pharmacology*. 2021 Aug 15;425:115553. doi: 10.1016/j.taap.2021.115553.

As the author of this Elsevier article, permission is not required.

SULT enzymes responsible for p-cresol sulfate formation (the primary and major metabolite of p-cresol) and to identify selective, potent inhibitors for its detoxification. As a part of this aim, various in vitro SULT models were characterized and an LC-MS/MS p-cresol sulfate assay was developed and validated.

Abstract

p-Cresol sulfate, the primary metabolite of *p*-cresol, is a uremic toxin that has been associated with toxicities and mortalities. The study objectives were to i) characterize the contributions of human sulfotransferases (SULT) catalyzing *p*-cresol sulfate formation using multiple recombinant SULT enzymes (including the polymorphic variant SULT1A1*2), pooled human liver cytosols, and pooled human kidney cytosols; and ii) determine the potencies and mechanisms of therapeutic inhibitors capable of attenuating the production of *p*-cresol sulfate. Human recombinant SULT1A1 was the primary enzyme responsible for the formation of *p*-cresol sulfate (K_m=0.19±0.02 μM [with atypical kinetic behavior at lower substrate concentrations; see text discussion], V_{max}=789.5±101.7 nmol/mg/min, K_{si}=2458.0±332.8 μM, mean±standard deviation, n=3), while SULT1A3, SULT1B1, SULT1E1, and SULT2A1 contributed negligible or minor roles at toxic *p*-cresol concentrations. Moreover, human recombinant SULT1A1*2 exhibited reduced enzyme activities (K_m=81.5±31.4 μM, V_{max}=230.6±17.7 nmol/mg/min, K_{si}=986.0±434.4 μM) compared to the wild type. The sulfonation of *p*-cresol was characterized by Michaelis-Menten kinetics in liver cytosols (K_m=14.8±3.4 μM, V_{max}=1.5±0.2 nmol/mg/min) and substrate inhibition in kidney cytosols (K_m=0.29±0.02 μM, V_{max}=0.19±0.05 nmol/mg/min, K_{si}=911.7±278.4 μM). Of the 14 investigated therapeutic inhibitors, mefenamic acid (K_i=2.4±0.1 **n**M [liver], K_i=1.2±0.3 **n**M [kidney]) was the most potent in reducing the formation of *p*-cresol sulfate, exhibiting noncompetitive inhibition in human liver cytosols and recombinant SULT1A1, and mixed inhibition in human kidney cytosols. Our novel findings indicated that SULT1A1 contributed an important role in *p*-cresol sulfonation (hence it can be considered a probe reaction) in liver and kidneys, and mefenamic acid may be utilized as a potential therapeutic agent to attenuate the generation of *p*-cresol sulfate as an approach to detoxification.

1. Introduction

p-Cresol, a phenolic compound, is a highly protein-bound uremic toxin that is mainly originated from intestinal microbial metabolism of tyrosine and phenylalanine [79]. Once formed, *p*-cresol undergoes extensive first-pass metabolism in the formation of *p*-cresol sulfate and *p*-cresol glucuronide [78]. Recently, our laboratory identified the specific UDP-glucuronosyltransferase enzymes responsible for the glucuronidation of *p*-cresol [57], but data pertaining to contributions of sulfotransferase (SULT) enzymes responsible for the sulfonation of *p*-cresol are limited [318]. As evident by the high abundance of *p*-cresol sulfate in the human serum under uremic conditions [80], sulfonation is considered the predominant pathway for the disposition of *p*-cresol. Although *p*-cresol was implicated in various toxicology papers initially (e.g. [319]), subsequent investigations have focused on *p*-cresol sulfate due to potential experimental artefacts from earlier studies [80-82].

p-Cresol sulfate exerts direct toxicity in various human *ex-vivo* or *in-vitro* models [75, 78, 87, 88]. Schepers et al. demonstrated increased oxidative-burst effects of non-stimulated human leukocytes exposed to *p*-cresol sulfate [96]. Exogenously administered *p*-cresol sulfate induced the release of endothelial microparticles in human umbilical vein endothelial cells [94] and oxidative stress in human umbilical vein endothelial or human vascular smooth muscle cells [97]. Lipogenesis was inhibited by *p*-cresol sulfate in isolated human adipocytes, suggesting an association between *p*-cresol sulfate and insulin resistance [95]. These overall effects by *p*-cresol sulfate have been linked to cardiovascular toxicity [88]. Furthermore, the nephrotoxic effects of *p*-cresol sulfate have been demonstrated with decreased cell viability [90, 91], increased reactive oxygen species production [91], and enhanced expressions of inflammatory cytokines or proteins that are associated with renal fibrosis [91] in human proximal tubular epithelial cells. In addition,

p-cresol sulfate was capable of inhibiting breast cancer resistance protein and multidrug resistance protein 4 in membrane vesicles derived from human embryonic kidney 293 cells, which could potentially result in the intracellular accumulation of *p*-cresol sulfate and other uremic toxins [78, 98]. In primary cultures of human hepatocytes, *p*-cresol sulfate (500 μM) was demonstrated to reduce cell viability, cellular ATP concentration, and mitochondrial membrane potential [92].

With respect to clinical outcomes, *p*-cresol sulfate has been associated with cardiovascular and renal toxicities [75, 78, 87, 88]. In patients at different stages of chronic kidney disease, free *p*-cresol sulfate concentrations have been identified as a significant marker of cardiovascular and overall mortalities [85, 86]. Consistent with these data, total *p*-cresol serum concentrations were positively correlated with the risk of major adverse cardiac events (including overall mortality and "rehospitalization for a cardiovascular-related illness") in coronary artery disease patients [320]. In Glorieux et al. free *p*-cresol sulfate was the only plasma marker amongst the tested uremic toxins to correlate with the primary composite outcome of fatal or non-fatal cardiovascular events in non-dialysis chronic kidney disease patients [100]. In addition, high total *p*-cresol sulfate concentrations have been associated with renal function impairment as indicated by decreased glomerular filtration rates in type 2 diabetes patients [321] and with renal dysfunction progression or overall mortality in patients in various stages of chronic kidney disease [101]. Collectively, these experimental and clinical data overwhelmingly suggested that *p*-cresol sulfate associated toxicities are of significant clinical relevance.

A growing number of therapeutic approaches (e.g. utilization of pre-/pro-/syn-biotics, adsorbents, dietary modifications, dialysis modalities) have been proposed to reduce the serum concentrations of *p*-cresol sulfate in order to alleviate the associated toxicities; however, inconsistent efficacy findings and evidence of adverse outcomes have been reported [53, 78, 322].

To our knowledge, a targeted approach that can *potently* and *selectively* modulate plasma *p*-cresol sulfate concentrations is still lacking. Therefore, we hypothesize that the sulfonation of *p*-cresol can be selectively, extensively reduced using potent therapeutic SULT inhibitors in humans. To test this hypothesis, our initial objective was to systematically characterize the sulfonation pathways of *p*-cresol using reaction phenotyping approaches with human recombinant SULT enzymes, pooled human liver cytosols, and pooled human kidney cytosols. Having characterized the SULT enzymes responsible for *p*-cresol sulfate production, we subsequently aimed to identify potent therapeutic inhibitors capable of attenuating the sulfonation of *p*-cresol, testing an extensive panel of chemicals and identifying their inhibitory mechanisms.

2. Materials and methods

2.1. Chemicals and reagents

Human recombinant SULT enzymes (SULT1A1 [catalog number 5546-ST], SULT1A3 [catalog number 5829-ST], SULT1B1 [catalog number 5959-ST], SULT1E1 [catalog number 5545-ST], and SULT2A1 [catalog number 5828-ST]) were purchased from R&D Systems (Minneapolis, MN, USA). Human recombinant SULT1A1*2 (catalog number CYP105) was purchased from Cypex (Dundee, Scotland, UK). Pooled human liver cytosols (mix of 30 males and 20 females, 47±20 years [mean±standard deviation], catalog number H0610.C, lot number 1810002) and pooled human kidney cytosols (mix of 2 males and 2 females, 57±8 years, catalog number H0610.RC, lot number 1310121) were obtained from SEKISUI XenoTech (Kansas City, KS, USA) (donor information is available in Table S VII-1, Supplementary materials [323]). 2-Mercaptoethanol (catalog number M3148), 3′-phosphoadenosine 5′-phosphosulfate lithium salt

(PAPS, catalog number A1651), diclofenac sodium salt (catalog number D6899), diflunisal (catalog number D3281), dimethyl sulfoxide (DMSO, catalog number D108), flufenamic acid (catalog number F9005), formic acid (catalog number F0507), high performance liquid chromatography (HPLC) grade methanol (catalog number 34860), HPLC grade water (catalog number 270733), ibuprofen (catalog number I4883), indomethacin (catalog number I7378), ketoprofen (catalog number K1751), ketorolac Tris salt (catalog number K1136), magnesium chloride ($MgCl_2$, catalog number M8266), meclofenamic acid sodium salt (catalog number M4531), mefenamic acid (catalog number M4267), naproxen (catalog number N8280), niflumic acid (catalog number N0630), *p*-cresol (catalog number C85751), piroxicam (catalog number P5654), potassium phosphate dibasic (catalog number P3786), potassium phosphate monobasic (catalog number P5655), salicylic acid (catalog number S7401), tolfenamic acid (catalog number T0535), and Tris hydrochloride (catalog number T3253) were purchased from Sigma Aldrich (Oakville, ON, Canada). Tris base (catalog number 15504-202) was obtained from Thermo Fisher Scientific (Ottawa, ON, Canada). Ammonium acetate (catalog number 1220-1-70) was purchased from Caledon Laboratories (Georgetown, ON, Canada). *p*-Cresol sulfate potassium salt (catalog number T536805) and *p*-cresol sulfate-d_7 potassium salt (catalog number T536802) were purchased from Toronto Research Chemicals (North York, ON, Canada). Anhydrous ethanol (catalog number 1009) was obtained from Commercial Alcohols (Tiverton, ON, Canada).

2.2. Overall incubation conditions

To ensure initial velocity conditions for the formation of *p*-cresol sulfate, protein concentrations and incubation times were optimized individually for each enzyme system (the final conditions are described in Figure and Table legends). In addition, individual components of the

incubation mixture were also optimized in human recombinant SULT1A1 (determined to be the primary catalyst responsible for the production of *p*-cresol sulfate as described in **3. Results**), pooled human liver cytosols, and pooled human kidney cytosols, including the type of buffer (i.e. 50 mM Tris vs. potassium phosphate), PAPS concentration (0-200 μM), $MgCl_2$ concentration (0-25 mM), 2-mercaptoethanol concentration (0-30 mM), and the percentage of organic solvent (i.e. 0.1% or 0.4% DMSO, ethanol, or methanol). The buffer and 2-mercaptoethanol concentrations that provided the highest catalytic activities, and concentrations of organic solvents (if required) which generated minimal inhibition were utilized. Physiological and non-saturating concentrations of PAPS and $MgCl_2$ were employed [324-326]. The incubation matrix (200 μL) consisting of the enzyme source, 50 mM Tris buffer (pH 7.5 measured at 37 °C), 1 mM $MgCl_2$, and *p*-cresol was pre-incubated in a 37 °C water bath (Precision 2864 water bath, Thermo Fisher Scientific, Ottawa, ON, Canada) for 5 minutes. Enzymatic reaction was started with the addition of 50 μL PAPS (20 μM for human recombinant SULT enzymes and pooled human liver cytosols or 5 μM for pooled human kidney cytosols [325]; prewarmed to 37 °C) with or without chemical inhibitors and maintained in the 37 °C shaking water bath until reaction termination. To stop the reaction, 90 μL ice cold methanol containing 1 μg/mL of *p*-cresol sulfate-d_7 (the internal standard, please see section *2.7* below) was added to 30 μL of the incubation sample, and the mixture was placed at room temperature (23.5 °C) for 20 minutes while being shielded from light for protein precipitation. Subsequently, the mixture was vortexed for 30 seconds (Analog vortex mixer, Thermo Fisher Scientific, Ottawa, ON, Canada) and sonicated for 30 seconds (75D ultrasonic machine, VWR, Mississauga, ON, Canada). Protein was removed by centrifugation at 4000 g for 10 minutes (4 °C, 5424R centrifuge, Eppendorf, Mississauga, ON, Canada) [57, 308]. The supernatant was collected for the determination of *p*-cresol sulfate concentration as described below in section *2.7*.

2.3. Catalytic activities of human recombinant SULT enzymes in the formation of p-cresol sulfate

The human recombinant SULT1A1, 1A3, 1B1, 1E1, and 2A1 which constituted "the major [SULT] isoforms for drug metabolism in adults" [327] were utilized in our initial experiment. Each recombinant SULT enzyme was incubated with 1, 24, and 1000 μM *p*-cresol, which corresponded to the known physiological and toxic concentrations found in the human serum/plasma [308, 328] and the human liver [295]. The catalytic activities of individual human recombinant SULT enzymes in the formation of *p*-cresol sulfate were determined under optimized incubation conditions as described in the Figure and Table legends. The kinetic behaviors of the isoforms that are capable of producing *p*-cresol sulfate were further characterized as described below in section *2.4*.

2.4. Enzyme kinetics of p-cresol sulfate formation

The enzyme kinetics describing *p*-cresol sulfate formation in human recombinant SULT1A1, 1A3, 1B1, 1E1, 1A1*2, pooled human liver cytosols, and pooled human kidney cytosols were characterized under initial velocity conditions, using the following *p*-cresol concentrations: 0-1000 μM (SULT1A1), 0-1500 μM (SULT1A3), 0-1500 μM (SULT1B1), 0-3000 μM (SULT1E1), 0-2000 μM (SULT1A1*2), 0-1000 μM (pooled human liver cytosols), and 0-1000 μM (pooled human kidney cytosols) which covered both physiological and toxic concentrations [295, 308, 328]. As SULT1A1 was determined to be the primary catalyst responsible for the production of *p*-cresol sulfate (as described in **3. Results**), its most common

loss-of-function minor allele (i.e. SULT1A1*2; Arg213His amino acid substitution, found in ~30% of the Caucasian or African American populations) was also investigated [329, 330]. The *Michaelis-Menten* (Equation VII-1), *substrate inhibition* (Equation VII-2), or *allosteric sigmoidal* (Equation VII-3) equations were used to model *p*-cresol sulfate formation in GraphPad Prism (version 9.0.0 for Windows; GraphPad Software, San Diego, CA, USA) [331],

Equation VII-1

$$v = \frac{V_{max} \times [S]}{K_m + [S]}$$

Equation VII-2

$$v = \frac{V_{max} \times [S]}{K_m + [S] \times (1 + \frac{[S]}{K_{si}})}$$

Equation VII-3

$$v = \frac{V_{max} \times [S]^h}{{K_m}^h + [S]^h}$$

where v represented the formation rate, V_{max} the maximum reaction rate, [S] the *p*-cresol concentration, K_m the concentration of *p*-cresol at half maximum reaction rate, K_{si} the dissociation constant for substrate inhibition, and h the Hill slope. The optimal model was selected based on graphical visualization and statistical testing using coefficient of determination (R^2), sum of squares, root mean square (Sy.x), root mean square error (RMSE), and Akaike information criterion (AIC). The intrinsic clearance value (CL_{int}) was calculated by V_{max}/K_m [55, 57, 332].

2.5. Relative potencies of therapeutic chemical inhibitors attenuating the formation of p-cresol sulfate

To identify therapeutic agents that can reversibly inhibit *p*-cresol sulfate formation, the inhibitory effects of selected nonsteroidal anti-inflammatory drugs (NSAIDs) were tested using human recombinant SULT1A1 enzyme (determined to be the primary catalyst responsible for the production of *p*-cresol sulfate as described in **3. Results**). The utilization of NSAIDs (please see **4. Discussion**) was based on literature review which supported their potent inhibitory effects toward SULT-mediated reactions compared to other therapeutic drugs (e.g. [333]). Diclofenac, diflunisal, flufenamic acid, ibuprofen, indomethacin, ketoprofen, ketorolac, meclofenamic acid, mefenamic acid, naproxen, niflumic acid, piroxicam, salicylic acid, and tolfenamic acid representing a variety of NSAID chemical classes were tested based on effective concentrations established in previously published papers on other SULT substrates [333-341]. The potencies of inhibitions were characterized by the half-maximum inhibitory-effect concentration (IC_{50}) values using a *p*-cresol concentration of 0.2 μM under initial velocity conditions. The IC_{50} values were determined by GraphPad Prism software [331].

2.6. Mechanisms of inhibition of selected potent chemical inhibitors attenuating the formation of p-cresol sulfate

The mechanisms and potencies (i.e. inhibition constant, K_i) of the three most potent inhibitors (i.e. based on IC_{50} values characterized in section *2.5*: mefenamic acid, tolfenamic acid, and flufenamic acid) were determined in pooled human liver and kidney cytosols using multiple *p*-cresol concentrations reflecting physiological concentrations in the presence of multiple

concentrations of each inhibitor (i.e. 0.5×IC_{50}, ~IC_{50}, 5×IC_{50} determined in section *2.5*). The inhibition data were fitted by models describing "competitive inhibition" (Equation VII-4), "noncompetitive inhibition" (Equation VII-5), "uncompetitive inhibition" (Equation VII-6), or "mixed inhibition" (Equation VII-7) in GraphPad Prism software [331],

Equation VII-4

$$v = \frac{V_{max} \times [S]}{K_m \times \left(1 + \frac{[I]}{K_i}\right) + [S]}$$

Equation VII-5

$$v = \frac{V_{max} \times [S]}{(K_m + [S]) \times \left(1 + \frac{[I]}{K_i}\right)}$$

Equation VII-6

$$v = \frac{V_{max} \times [S]}{K_m + [S] \times \left(1 + \frac{[I]}{K_i}\right)}$$

Equation VII-7

$$v = \frac{V_{max} \times [S]}{K_m \times \left(1 + \frac{[I]}{K_i}\right) + [S] \times \left(1 + \frac{[I]}{\alpha \times K_i}\right)}$$

where v represented the formation rate, V_{max} the maximum reaction rate, [S] the *p*-cresol concentration, K_m the concentration of *p*-cresol at half maximum reaction rate, [I] the inhibitor concentration, K_i the inhibition constant, and alpha (α) the constant that differentiates the specific mechanisms in the mixed inhibition model [331]. The best model was selected by statistical fitting

using R^2, sum of squares, Sy.x, RMSE, and AIC (GraphPad Prism software) [331] and further confirmed graphically using Dixon and Cornish-Bowden plots [342]. The corresponding K_i values were generated by GraphPad Prism [331] and also graphically confirmed. Furthermore, the inhibition constants and mechanisms of inhibition of mefenamic acid (i.e. the most potent inhibitor) were also determined in human recombinant SULT1A1*2 enzymes (with SULT1A1 as the control) using the same approach as described above. Only reversible inhibitions were considered because suicide inhibition is generally not considered an ideal clinical approach due to the lack of flexibility in therapeutic control.

2.7. Analytical assay for the quantification of p-cresol sulfate

Concentrations of *p*-cresol sulfate were measured using an ultra-high performance liquid chromatography with tandem mass spectrometry (LC-MS/MS, LCMS-8050, Shimadzu, Kyoto, Japan) assay developed in our laboratory. Chromatogram separation was achieved using the Raptor biphenyl analytical column (2.1×100 mm, 2.7 μm particle size, Bellefonte, PA, USA) with an isocratic flow of 90:10 methanol: water (v:v, each added 2 mM of ammonium acetate and 0.1% formic acid; flow rate 0.3 mL/minute; at 30 °C; 5 μL injection volume). The analytes were ionized using the negative electrospray ionization mode. The mass spectrum parameters were pre-optimized via both instrument software and manually to generate maximum signal counts compared to baseline noise (the individual parameters are presented in Table S VII-2, Supplementary materials). *p*-Cresol sulfate and *p*-cresol sulfate-d_7 were detected using multiple reaction monitoring with mass-to-charge ratios of 187.00→107.00 and 194.10→114.15, respectively. The assay was validated with respect to selectivity, matrix interference, carryover effects, calibration range, intra/inter-day precision and accuracy, autosampler stability, bench-top

stability, freeze-thaw stability, and one-week stability based on US Food and Drug Administration guidance on Bioanalytical Method Validation [273].

3. Results

3.1. Control experiments

All incubations were conducted using optimized protein concentrations and incubation times pertaining to initial, linear velocity conditions as described in the individual Figure and Table legends. Negative control incubations conducted in the absence of *p*-cresol or PAPS did not generate *p*-cresol sulfate (data not shown). The effects of individual components in the incubation mixture on the rate of *p*-cresol sulfate formation are summarized in the Supplementary materials [325, 326, 343]. Our control data confirmed the lack of inhibitory effects in the formation of *p*-cresol sulfate for all instances where organic solvents (kept ≤ 0.4%; [333, 344]) were utilized (data not shown).

3.2. Catalytic activities of human recombinant SULT enzymes in the formation of p-cresol sulfate

Of the five major human recombinant SULT enzymes tested (i.e. SULT1A1, 1A3, 1B1, 1E1, and 2A1 [327]) using 1, 24, 1000 μM of *p*-cresol, SULT1A1 was the predominant enzyme responsible for *p*-cresol sulfate formation under both physiological and toxic concentrations [295, 308, 328] (Figure VII-1). The catalytic activities of human recombinant SULT1A1 in the production of *p*-cresol sulfate were substrate concentration-dependent at lower *p*-cresol concentrations (i.e. 1 and 24 μM) but exhibited characteristics of substrate inhibition at higher

concentration (i.e. 1000 μM). Although *p*-cresol sulfate formation was evident in SULT1A3, SULT1B1, and SULT1E1, their activities were significantly reduced compared to SULT1A1 (Figure VII-1). On the other hand, SULT2A1 did not generate *p*-cresol sulfate formation, even at 1 mM of *p*-cresol. The enzyme kinetics for active human recombinant SULT enzymes identified in this experiment were further determined in section *3.3*. Moreover, SULT1A1 is expressed in both human liver and kidney [327] and known to be polymorphic [329, 330]; therefore, detailed enzyme kinetic characterizations were also conducted in these respective tissues and the recombinant SULT1A1*2 protein.

3.3. Enzyme kinetics of p-cresol sulfate formation

The formations of *p*-cresol sulfate in human recombinant SULT1A1 (Figure VII-2 A), SULT1A3 (Figure VII-2 B), SULT1B1 (Figure VII-2 C), and SULT1E1 (Figure VII-2 D) were detected with *p*-cresol concentrations as low as 0.3, 200, 125, and 375 μM, respectively, indicating drastic differences in enzyme affinity. Based on the relatively reduced K_m (0.19±0.02 μM, mean±standard deviation, n=3 [substrate inhibition, the model of best fit] or a more conservative estimate of (S_{50}=K_m) 5.35±0.24 μM [allosteric sigmoidal model for lower substrate concentrations]; see **Discussion**) and elevated V_{max} (789.5±101.7 μM) values of SULT1A1 compared to other tested human recombinant SULT enzymes (Figure VII-2), it was determined that SULT1A1 was likely the primary human enzyme responsible for the formation of *p*-cresol sulfate; whereas SULT1A3, SULT1B1, and SULT1E1 had minor contributions only at toxic concentrations as evident by their high K_m values at mM levels (Figure VII-2). The recombinant SULT enzymes exhibited either substrate inhibition (i.e. SULT1A1 and SULT1B1) or Michaelis-Menten kinetics (i.e. SULT1A3 and SULT1E1) (Figure VII-2). The SULT1A1*2 variant (Figure

VII-2 E) had similar kinetic behaviors compared to the wild type, but exhibited relatively lower enzyme activities as evident by higher K_m and lower V_{max} (i.e. reduced CL_{int}) (Figure S VII-5, Supplementary materials), which are consistent with the findings using other SULT1A1 substrates (e.g. [330]). Furthermore, the enzyme kinetics of *p*-cresol sulfate formation in pooled human liver and kidney cytosols can be described as Michaelis-Menten and substrate inhibition, respectively (Figure VII-2 F and Figure VII-2 G). The K_m values were slightly higher in liver cytosols and in the same order in kidney cytosols compared to human recombinant SULT1A1, but several magnitudes removed from the other tested recombinant SULT enzymes. The model fitting statistics are provided in Table S VII-3, Table S VII-4, Table S VII-5, Table S VII-6, Table S VII-7, Table S VII-8, Table S VII-9, Supplementary materials. On the other hand, the V_{max} values in recombinant (i.e. purified) enzymes are generally known to be higher compared to cytosolic preparations (e.g. [345]) as observed in our data (Figure VII-2).

3.4. Relative potencies of therapeutic chemical inhibitors attenuating the formation of p-cresol sulfate

To identify therapeutic agents that can potently reduce the formation of *p*-cresol sulfate, the inhibitory effects of 14 NSAIDs belonging to a variety of chemical classes (i.e. acetic acids, anthranilic acids, enolic acids, fenamates, propionic acids, and salicylates) were characterized using IC_{50} values in human recombinant SULT1A1 (Table VII-1 and Figure S VII-6, Supplementary materials). The IC_{50} values (indicated in Table VII-1 and Figure S VII-6, Supplementary materials) of the following drugs were calculated: mefenamic acid (maximum inhibition=94%), tolfenamic acid (maximum inhibition=90%), flufenamic acid (maximum inhibition=87%), diclofenac (maximum inhibition=51%), ketoprofen (maximum inhibition=90%),

diflunisal (maximum inhibition=88%), salicylic acid (maximum inhibition=94%), ibuprofen (maximum inhibition=67%), and naproxen (maximum inhibition=54%). On the other hand, five drugs (i.e. indomethacin, ketorolac, meclofenamic acid, niflumic acid, and piroxicam) generated less than 50% inhibition of *p*-cresol sulfate formation and therefore their IC_{50} values were not estimated.

The three most potent and effective inhibitors were mefenamic acid (IC_{50}=3.14±0.08 **n**M, n=3), tolfenamic acid (IC_{50}=0.62±0.12 μM), and flufenamic acid (IC_{50}=2.85±0.20 μM), which were anthranilic acid derivatives. Their IC_{50} values were significantly lower than the physiologically attainable concentrations observed in healthy volunteers, i.e. 15 μM peak plasma concentration following the oral administration of 250 mg mefenamic acid [346]; 11 μM peak plasma concentration following the oral administration of 200 mg tolfenamic acid [347]; and 71 μM peak plasma concentration following the oral administration of 200 mg flufenamic acid [348]; therefore they could potentially be considered as therapeutic inhibitors for *p*-cresol sulfate production (please see **4. Discussion**).

3.5. Mechanisms of inhibitions of selected potent chemical inhibitors toward the formation of p-cresol sulfate

The mechanisms of inhibition of mefenamic acid (Figure VII-3), tolfenamic acid (Figure VII-4), and flufenamic acid (Figure VII-5) towards *p*-cresol sulfate formation in pooled human liver cytosols were all noncompetitive in nature, with K_i values of 2.4±0.1 **n**M (n=3), 1.1±0.1 μM, and 14.0±0.4 μM, respectively. On the other hand, the mechanisms of inhibition for all three chemicals in pooled human kidney cytosols were of mixed inhibition, with K_i values of 1.2±0.3

nM (mefenamic acid, Figure VII-6, n=3), 0.23±0.03 μM (tolfenamic acid, Figure VII-7), and 1.3±0.1 μM (flufenamic acid, Figure VII-8); but their α values were ~1 (Figure VII-6, Figure VII-7, Figure VII-8), suggesting these mixed inhibitions weighted more heavily on the noncompetitive type (please see Equation VII-5, Equation VII-7). The relative order of inhibition potencies for the three chemical inhibitors in kidney cytosol was consistent with liver cytosols; however, the K_i values were generally lower in human kidney cytosols. In addition, the mechanisms of inhibition of the most potent inhibitor, mefenamic acid, were also characterized in both human recombinant SULT1A1 (wild type, Figure VII-9) and SULT1A1*2 enzymes (Figure VII-10). Both enzyme variants exhibited comparable K_i values (i.e. 1.1 nM for wild type vs. 0.5 nM for SULT1A1*2) and mechanism of inhibition (i.e. noncompetitive inhibition), suggesting little effects of SULT1A1*2 variant on the efficacy of inhibition by mefenamic acid. Overall, these K_i values in liver or kidney cytosols corresponded to the IC_{50} values generated in human recombinant SULT1A1 (Table VII-1 and Figure S VII-6, Supplementary materials). Moreover, the K_i values of mefenamic acid in both pooled human liver and kidney cytosols were significantly lower than the typical concentrations observed in humans (cited in section *3.4*), confirming its potential utility as a therapeutic agent for the reduction of *p*-cresol sulfate formation (please see **4. Discussion**).

3.6. Analytical assay for the quantification of p-cresol sulfate

The analytical assay for the quantification of *p*-cresol sulfate was developed in our laboratory and successfully validated based on US Food and Drug Administration guidance on Bioanalytical Method Validation [273]. The run time was 5 minutes. The assay was selective based on multiple reaction monitoring of utilized mass-to-charge ratios which had no matrix interference and no carryover effects. The linear range of *p*-cresol sulfate was 0.003 to 425 μM (Figure S VII-7,

Supplementary materials). All samples were measured within the linear range. The imprecision and bias of the high, medium, and low quality control (QC) samples were <15%, and that of lower limit of quantification (LLOQ) samples were <20% (Table S VII-10, Supplementary materials). Stability testing using bias determination with high and low QC samples in various conditions (autosampler [24 hours at 4 °C]; bench-top [6 hours at 23.5 °C]; freeze-thaw [1 cycle]; and one-week (at -80 °C)] indicated bias values between -12.52 to -2.55% (Table S VII-11, Supplementary materials). All validation parameters satisfied the US Food and Drug Administration guidance on Bioanalytical Method Validation [273].

4. Discussion

We initially characterized the sulfonation pathways of *p*-cresol using human recombinant enzymes, human liver, and kidney cytosols. To our knowledge, only limited data are available in the literature, where a possible role of recombinant SULT1A1 and perhaps SULT1A3 (at much higher substrate concentrations) have been suggested [318]; however, the activities of other SULT enzymes, contributions of specific enzymes in human cytosols, or detailed systematic enzyme kinetic analyses had not been assessed. The human liver and kidneys are the primary organs for *p*-cresol metabolism and excretion [78], and therefore they were the main tissues investigated in this study. This is supported by relatively high exposures of *p*-cresol in both organs as demonstrated in tissue biopsies obtained from deceased hemodialysis patients [295]. Of the major human recombinant SULT enzymes utilized, SULT1A1, 1B1, and 2A1 were known to be expressed (based on protein content) in the liver and kidneys, where SULT1A1 is considered the most abundant enzyme in both tissues [327]. On the other hand, SULT1E1 or SULT1A3 proteins were only expressed in the human liver or kidneys, respectively [327].

Our finding that SULT1A1 was the primary enzyme responsible for the formation of *p*-cresol sulfate in human liver and kidneys was based on the following complementary data: i) very little enzyme activities were evident in the other tested human recombinant enzymes at typical uremic concentrations of *p*-cresol (Figure VII-1); ii) the minimal substrate concentrations that generated detectable amounts of *p*-cresol sulfate in recombinant SULT1A1 were significantly lower compared to the other SULT enzymes (Figure VII-2); iii) the V_{max} value of recombinant SULT1A1 was significantly higher while K_m value lower than the other SULT enzymes (Figure VII-2); iv) the K_m value determined in pooled human kidney cytosols was similar to that obtained in recombinant SULT1A1 enzyme (Figure VII-2); v) recombinant SULT1A1 and pooled human kidney cytosols exhibited similar substrate inhibition kinetic behaviors (Figure VII-2); and vi) the inhibitory potency (i.e. K_i value) and mechanism of inhibition of mefenamic acid were overall consistent (see discussion below) between pooled human liver / kidney cytosols and recombinant SULT1A1 enzyme (Figure VII-3, Figure VII-6, Figure VII-9). With respect to kinetic fitting, the model of best fit, both statistically (Table S VII-3, in Supplementary materials) and visually (Figure VII-2 A), for our recombinant SULT1A1 data was "substrate inhibition" which generated a K_m value of 0.19±0.02 μM; however, the "allosteric sigmoidal model" generated a more accurate estimate for S_{50} (=K_m) of 5.35±0.24 μM based on visual inspection of data at lower substrate concentrations (Figure VII-2 A). To our knowledge, this is a novel observation for substrate inhibition kinetics, which typically assumes a Michaelis-Menten behavior at low substrate concentrations (please see Equation VII-1, Equation VII-2 [326, 345]). Therefore, SULT1A1-catalyzed *p*-cresol sulfonation may exhibit an "atypical substrate inhibition kinetic behavior" and the true K_m value could reside between 0.19 – 5.35 μM. Our recombinant SULT1A1 data had a similar K_m (0.19 – 5.35 μM vs. 0.5±0.1 μM) and elevated V_{max} (789.5±101.7 vs. 315±20

nmol/mg/min) compared to that reported by Brix et al. [318]. These slight discrepancies should be interpreted with caution because different incubation conditions and data fitting methods were utilized (i.e. only Michaelis-Menten model was tested in Brix et al.). Sulfonation activities are known to be dependent on compositions of the incubation matrix and methods of kinetic fitting, which have been systematically optimized/tested in our experiments (Figure S VII-1, Figure S VII-2, Figure S VII-3, Figure S VII-4, Supplementary materials). In general, our findings are consistent with the notion that SULT1A1 is the major phenolic SULT enzyme [349] as it has catalytic activities toward other compounds with the simple phenol chemical structure (e.g. *p*-nitrophenol [318, 350] and 2-aminophenol [345]). Furthermore, our data also indicated that *p*-cresol can be considered a selective probe substrate for SULT1A1 in both human liver and kidney cytosols, due to relatively high affinities (Figure VII-2), lack of (i.e. liver) or very weak (i.e. kidney) substrate inhibition characteristics (Figure VII-2), and negligible activities in other SULT enzymes (Figure VII-1) (i.e. criteria defined by Riches et al [345]).

The elevated K_m value and the different kinetic behavior (i.e. Michaelis-Menten) observed in pooled human liver cytosols (vs. substrate inhibition in human recombinant SULT1A1) might be due to additional minor contributions of SULT1B1 and SULT1E1 (which have been demonstrated to contribute ~20% of the expressed predominant SULT enzymes in the human liver [327]), both exhibiting higher K_m values and the latter also exhibiting Michaelis-Menten kinetics (Figure VII-2). Moreover, donors carrying the SULT1A1*2 allele (i.e. the slow metabolizers [330]) were likely represented in our human liver cytosol samples due to the relatively high frequency of this polymorphic allele in Caucasians, which is the major ethnicity in our liver cytosol mixture (Table S VII-1, Supplementary materials [323]) [329]. The inclusion of the kinetic effects of SULT1A1*2 carriers could also have increased the K_m value in pooled human liver cytosols. On

the other hand, the kinetic behaviors of human kidney cytosols (i.e. substrate inhibition, high K_{si} value) were generally consistent with that of human recombinant SULT1A1, suggesting the primary contribution of this specific enzyme in this tissue. Overall, the capacities of *p*-cresol sulfate formation (as indicated by V_{max} values) in pooled human kidney cytosol were lower compared to pooled human liver cytosols, which may be explained by higher active enzyme content expressed per mg of overall cytosolic protein in the liver [327]. In contrast, pooled human kidney cytosols seemed to have higher affinity over liver for *p*-cresol sulfonation (as evident by low K_m value, Figure VII-2), possibly due to additional contributions from other low affinity SULT enzymes in the liver (discussed above), but this hypothesis requires further testing due to the small mixture size (i.e. four subjects) in the utilized pooled human kidney cytosols.

Having determined human SULT1A1 as the primary enzyme responsible for *p*-cresol sulfate production, we subsequently identified potent therapeutic inhibitors capable of reducing this enzymatic reaction. Human SULT1A1 enzymes are known to be allosterically inhibited by NSAIDs [351], which are often used to reduce the sulfonation of SULT1A1 probe substrates in experimental cytosolic/tissue models [333-341]. In addition, environmental chemicals (e.g. hydroxylated polychlorobiphenyls) and natural products (e.g. quercetin) can also inhibit SULT1A1 [333, 336]; but these substances were not considered in our experiments as the quality/regulatory control with respect to source, content, and purity are much less rigorous than the approved therapeutic products used in our investigation. Furthermore, the general scarcity in knowledges on the pharmacokinetics and toxicology of natural products may potentially further hinder their development for therapeutic usage. Although NSAIDs can be associated with nephrotoxicity, these toxic effects are postulated to due to cyclooxygenase (COX) inhibition [352, 353], and it is therapeutically reasonable to utilize NSAIDs at concentrations that are inhibitory

toward SULT1A1 enzymes (for the attenuation of *p*-cresol sulfate formation) without exerting COX enzyme inhibition (or other receptors to minimize tissue toxicity), as further discussed below.

To our knowledge, our data provided the first instance where the inhibitory effects of an extensive panel of NSAIDs have been characterized in recombinant SULT1A1. The most potent inhibitor (i.e. mefenamic acid) identified (Table VII-1 and Figure S VII-6, Supplementary materials) was also reported as one of the more potent inhibitors in human cytosolic fractions or human tissues using different SULT1A1 probe substrates which may not be selective [345] toward the enzyme [333, 336-341]. Furthermore, the inhibitory effects of tolfenamic acid [337], flufenamic acid [337], diclofenac [338], ketoprofen [338], diflunisal [338], salicylic acid [334, 335, 338-341], ibuprofen [335, 338], and naproxen [335, 338] characterized using other SULT substrates were also evident with *p*-cresol in human recombinant SULT1A1 (Table VII-1 and Figure S VII-6, Supplementary materials); however, direct comparisons of potency should be cautioned because different enzyme sources have been utilized in these other studies (i.e. human tissues or cytosolic proteins), and some phenolic SULT substrates are known to be non-selective toward SULT1A1 (e.g. [345]). On the contrary, IC_{50} values could not be calculated for indomethacin, ketorolac, meclofenamic acid, niflumic acid, and piroxicam as their inhibitory effects were minimal (i.e. less than 50%, Table VII-1 and Figure S VII-6, Supplementary materials). These observations were inconsistent with the reported effects of indomethacin and ketorolac on *p*-nitrophenol sulfonation [338], possibly due to the utilization of different experimental models. Furthermore, meclofenamic acid had minimal effects on *p*-cresol sulfate formation (Table VII-1 and Figure S VII-6, Supplementary materials), in contrast to the other potent anthranilic acid derivatives (e.g. mefenamic acid, tolfenamic acid, and flufenamic acid) identified in this study. This may be explained by the two chlorine atom substitutions found in its

molecular structure [337], which may potentially hinder the binding of meclofenamic acid with SULT1A1. Likewise, the lack of inhibitory effects of niflumic acid may be due to the presence of fluorine atoms, an observation previously reported by Vietri et al. [337]. On the other hand, the null inhibitory effects of piroxicam were generally consistent with that reported in the literature [338].

In pooled human liver and kidney cytosols, mefenamic acid, tolfenamic acid, and flufenamic acid were potent inhibitors of *p*-cresol sulfate formation (Figure VII-3, Figure VII-4, Figure VII-5, Figure VII-6, Figure VII-7, Figure VII-8, Figure VII-9) with K_i values at least several folds (e.g. 6,250- and 12,500-folds for mefenamic acid in liver and kidney, respectively) lower than their documented physiological concentrations in healthy subjects [346-348]. The mechanisms of inhibition of these inhibitors in pooled human liver cytosols were noncompetitive in nature, which may be therapeutically beneficial as their inhibitory effects would not be overcame by higher *p*-cresol concentrations in the patient [351, 354]. Furthermore, slightly lower K_i values for these agents were determined in pooled human kidney cytosols (Figure VII-6, Figure VII-7, Figure VII-8), which may potentially be explained by the relatively lower amounts of SULT1A1 protein in human kidneys [327]. The mixed mechanisms of inhibition determined by these inhibitors in human kidney cytosols were associated with α values that were more consistent with a noncompetitive type of inhibition (i.e. as in human recombinant SULT1A1 discussed below and in liver cytosols; Equation VII-5, Equation VII-7), an observation confirmed with our fitting which indicated statistical values (i.e. R^2, sum of squares, Sy.x, RMSE, and AIC) favored both types of inhibition (data not shown). Both SULT1A1 and SULT1A1*2 were subjected to noncompetitive inhibition by mefenamic acid (Figure VII-9, Figure VII-10), further confirming the predominant role of SULT1A1 in the sulfonation of *p*-cresol in liver or kidney cytosols due to

similar inhibition mechanisms. The K_i value for SULT1A1*2 inhibition was similar to that of the wild type (Figure VII-9, Figure VII-10), suggesting comparable inhibitory effects in carriers of this polymorphic allele. Mefenamic acid was the only agent with K_i value in the low nM range (Figure VII-3, Figure VII-6, Figure VII-9, Figure VII-10), consistent with its inhibitory effects on *p*-nitrophenol sulfonation in recombinant SULT1A1 [351]; thus, it may be further considered as a therapeutic agent for reducing *p*-cresol sulfate formation (please see below).

NSAID-induced nephrotoxicity is mechanistically complex, and possibly due to their inhibitory effects on COX enzymes [352, 353]. Kidney injury secondary to NSAID usage are also typically associated with high doses and prolonged duration of administration [355]. Based on the IC_{50} and K_i values for *p*-cresol sulfonation inhibition determined in our experiments, we believe mefenamic acid (but not tolfenamic acid and flufenamic acid, due to their relatively high K_i values) could be used selectively to reduce *p*-cresol sulfate formation without generating nephrotoxicity. This is based on its documented IC_{50} values toward COX inhibition commonly reported in the **μ**M levels (i.e. 17-33 folds *lower potency* on human recombinant COX-1 inhibition [356], and 1250-2500 folds *lower potency* on human recombinant COX-2 inhibition [356]), compared to the highly potent K_i values of 2.4 **n**M and 1.2 **n**M for inhibition of *p*-cresol sulfate formation in pooled human liver and kidney cytosols, respectively (Figure VII-3, Figure VII-6). Moreover, although K_i values associated with COX inhibition in kidney tissues were not available to our knowledge, the IC_{50} values of mefenamic acid toward COX enzymes in other human tissues (i.e. 0.03-25 μM for COX-1 in human whole blood and U937 cell microsomes [357-359]; 0.16-2.9 μM for COX-2 in human whole blood [357, 359]) are all significantly higher than K_i values of mefenamic acid toward *p*-cresol sulfate inhibition observed in our models. These findings potentially suggest that minimal COX-associated toxicities in most tissues can be realized with the usage of low doses of

mefenamic acid for the purpose of inhibiting *p*-cresol sulfate formation. Likewise, although mefenamic acid is known to inhibit cytochrome P450 (e.g. [360]) and uridine 5'-diphospho-glucuronosyltransferase (e.g. [361]) enzymes, the IC_{50} and K_i values reported in these studies were also in the μM range, supporting the *overall selectivity* of mefenamic acid toward sulfonation inhibition. Furthermore, the clearance of mefenamic acid is through both the liver and the kidneys [362]; therefore, in patients with severely impaired renal functions (e.g. end-stage kidney disease) in whom *p*-cresol sulfate are likely elevated, mefenamic can still be cleared via non-renal routes from the body. In the treatment of pain in patients with severe kidney dysfunction on dialysis, it has also been suggested that the administration of mefenamic acid may not be strictly prohibited due to the already irreversibility of the kidney conditions [363, 364]. Overall, our data indicates that low dose, short duration of mefenamic acid administration for targeted inhibition of *p*-cresol sulfate formation could be a safe and effective potential therapeutic option. For our analyses on the lack of suitability for tolfenamic acid and flufenamic acid, please see Supplementary materials [356, 358, 359, 365, 366].

Overall, our proposed approach of utilizing mefenamic acid to mitigate *p*-cresol sulfate formation as a potent and targeted approach for detoxification is consistent with the idea of using meclofenamate as an inhibitor of indoxyl sulfate production with demonstrated nephroprotective effects in a rat model [53, 367]. In addition, curcumin was shown to significantly reduce the total plasma concentrations of *p*-cresol sulfate in hemodialysis patients [368]. Although the study authors had proposed the alteration of intestinal microbiota to be the potential mechanism, it was also possible that curcumin, being an inhibitor of SULT1A1 [369], had effectively lowered the concentration of *p*-cresol sulfate, which would also support our proposed therapeutic approach. Furthermore, although a variety of other methods have been utilized to reduce the concentration

of *p*-cresol sulfate in order to alleviate the associated toxicities (as reviewed by [53, 78, 322]), these methods have disadvantages and limitations (please see Supplementary materials for further discussion) [53, 78, 322, 370]. A targeted approach to inhibit *p*-cresol sulfonation using potent and effective SULT inhibitors [53] such as mefenamic acid could provide another therapeutic option.

A limitation in the current study is the lack of characterization of inter-subject variability and clinical covariates which are only possible using individual human cytosolic samples which were not commercially available to us. Although our findings could only represent population averages, attempts to characterize potential sources of variability (e.g. kinetic studies of the polymorphic SULT1A1*2 allele) were conducted. We also did not consider human colonic cytosols in our experiments because the liver and the kidneys [78] are, in our opinion, likely more directly involved in the generation and elimination of *p*-cresol sulfate, respectively, and hence are likely the primary organs responsible for modulating the plasma concentrations of *p*-cresol sulfate. For example, although intestinally-produced *p*-cresol sulfate could be quantitatively important, the passage of this hydrophilic compound through the enterocytes could be limited by several additional membrane barriers compared to the liver (e.g. the requirement of efflux/uptake transporters facilitating the passage of *p*-cresol sulfate from the enterocytes into the portal vein and in/out of hepatocytes). It is also likely that our findings with SULT inhibitors would be relevant to all tissues expressing SULT1A1 (including the colon), but the exact contributions of SULT1A1 in other tissues and the relative importance of each tissue in mediating plasma *p*-cresol sulfate concentrations remain to be systematically investigated. Moreover, non-specific binding was not considered for *p*-cresol (as our preliminary experiments found its unbound fractions in most tested enzymes to be >80%, consistent with the high free fraction reported in human liver microsomes [52]) or for the individual chemical inhibitors (a practically challenging endeavor requiring

analytical assays for all 14 screened inhibitors). The lack of free fraction characterizations would unlikely have affected our overall conclusion and may only potentially lead to the *under-estimation* of potency by IC_{50} and K_i values (e.g. mefenamic acid could potentially exhibit an even lower K_i value had we utilized unbound concentrations).

In conclusion, our novel findings indicated that human SULT1A1 is the primary enzyme responsible for the sulfonation of *p*-cresol (hence *p*-cresol can be used as a selective probe substrate) in both human liver and kidney cytosols, and the production of *p*-cresol sulfate can be effectively reduced by mefenamic acid at nanomolar concentrations which are unlikely to exhibit toxicity. These data may be useful for pharmacologists as the identifications of the SULT1A1 pathway and potent inhibitors can allow the effective design of mechanistic experiments for testing the cause-effect relationships of *p*-cresol sulfate induced toxicity. Our findings may also be relevant to clinicians because a potential therapeutic agent (i.e. mefenamic acid) which can selectively and potently reduce plasma *p*-cresol sulfate concentrations has been identified, adding to the currently available approaches. Further pharmacokinetic and toxicology studies are warranted.

Table VII-1 The relative potencies of selected therapeutic chemical inhibitors on the formation of p-cresol sulfate in human recombinant SULT1A1

Drug	**Potency (IC_{50} values, mean±SD)**
Mefenamic acid	3.14±0.08 nM
Tolfenamic acid	0.62±0.12 μM
Flufenamic acid	2.85±0.20 μM
Diclofenac	5.53±4.20 μM
Ketoprofen	15.62±1.90 μM
Diflunisal	16.40±10.43 μM
Salicylic acid	38.65±4.17 μM
Ibuprofen	154.61±90.87 μM
Naproxen	597.50±115.09 μM
Indomethacin	Not determined
Ketorolac	Not determined
Meclofenamic acid	Not determined
Niflumic acid	Not determined
Piroxicam	Not determined

The inhibitory effects of selected NSAIDs were tested using human recombinant SULT1A1 enzyme: mefenamic acid (in 0.1% methanol); tolfenamic acid; flufenamic acid (in 0.4% ethanol); diclofenac; ketoprofen (in 0.4% ethanol); diflunisal (in 0.4% ethanol); salicylic acid; ibuprofen (in 0.4% ethanol); naproxen (in 0.4% ethanol); indomethacin (in 0.1% methanol); ketorolac; meclofenamic acid (in 0.4% ethanol); niflumic acid; and piroxicam (in 0.4% DMSO).

The relative inhibition potencies were characterized with IC_{50} values using 0.2 μM (~K_m value) *p*-cresol concentration as described in **2. Materials and methods**. IC_{50} values were not calculated when the maximum inhibitions were < 50% of the control.

The protein concentration and incubation time representing linear, initial velocity enzymatic conditions for human recombinant SULT1A1 were 1 μg/mL and 15 minutes, respectively. If organic solvents were utilized to dissolve the inhibitors, the control also contained the same concentration of the organic solvent.

Data are presented as mean±standard deviation from 3 replicates. See Figure S VII-6, Supplementary materials for graphical data.

Curve fittings were conducted using GraphPad Prism 9.0.0 (GraphPad Software, San Diego, CA, USA).

Abbreviation(s): *DMSO*, dimethyl sulfoxide; IC_{50}, half-maximum inhibitory concentration; *NSAID*, nonsteroidal anti-inflammatory drug; *SULT*, sulfotransferase.

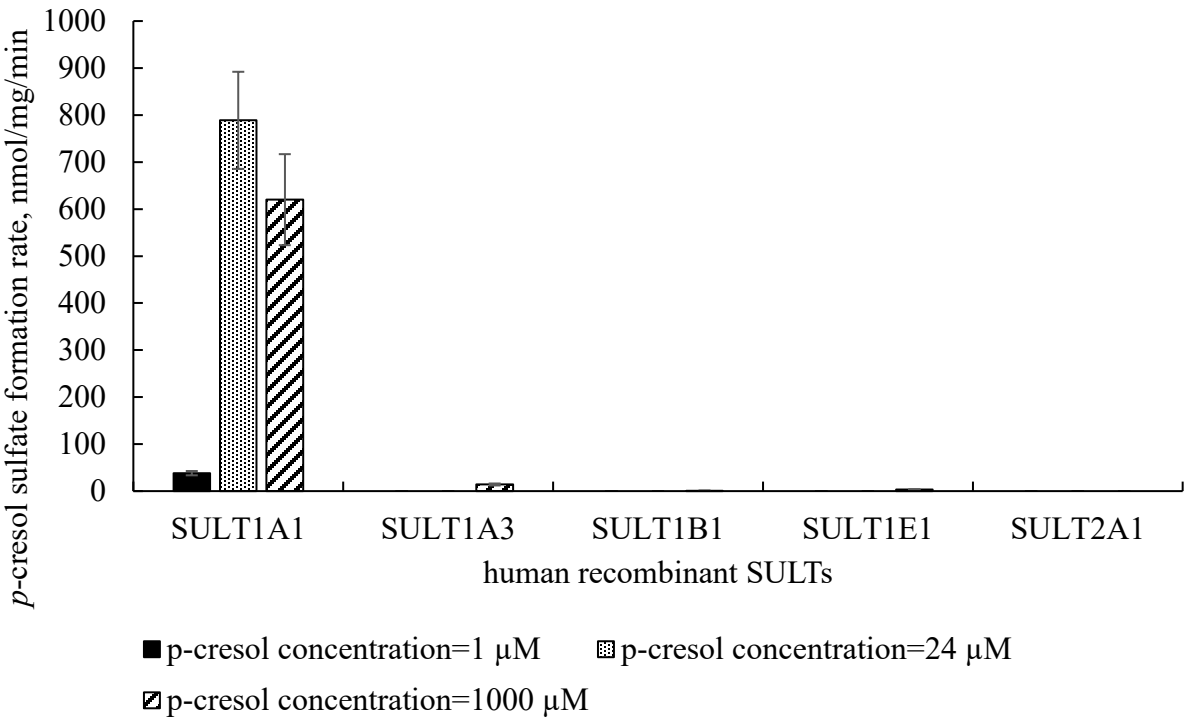

Figure VII-1 The formation of p-cresol sulfate in individual human recombinant SULT enzymes

Catalytical activities were characterized using *p*-cresol concentrations of 1, 24, and 1000 µM as described in **2. Materials and methods**.

The protein concentrations and incubation times representing linear, initial velocity enzymatic conditions were: human recombinant SULT1A1 (1 µg/mL, 15 minutes); human recombinant SULT1A3 (1 µg/mL, 20 minutes); human recombinant SULT1B1 (4 µg/mL, 20 minutes); human recombinant SULT1E1 (2 µg/mL, 20 minutes); and human recombinant SULT2A1 (4 µg/mL, 20 minutes).

Data are presented as mean±standard deviation from 3 replicates.

Abbreviation(s): *SULT*, sulfotransferase.

A

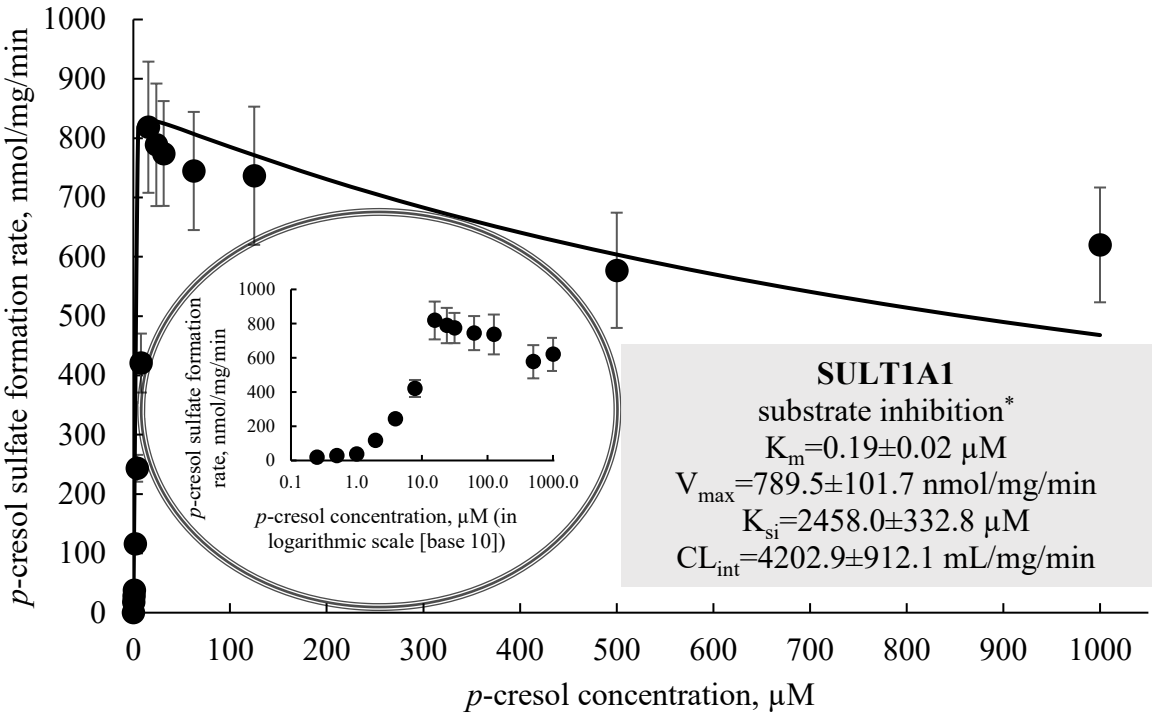
p-cresol sulfate formation rate, nmol/mg/min
p-cresol concentration, µM
p-cresol sulfate formation rate, nmol/mg/min
p-cresol concentration, µM (in logarithmic scale [base 10])
SULT1A1
substrate inhibition*
Km=0.19±0.02 µM
Vmax=789.5±101.7 nmol/mg/min
Ksi=2458.0±332.8 µM
CLint=4202.9±912.1 mL/mg/min

B

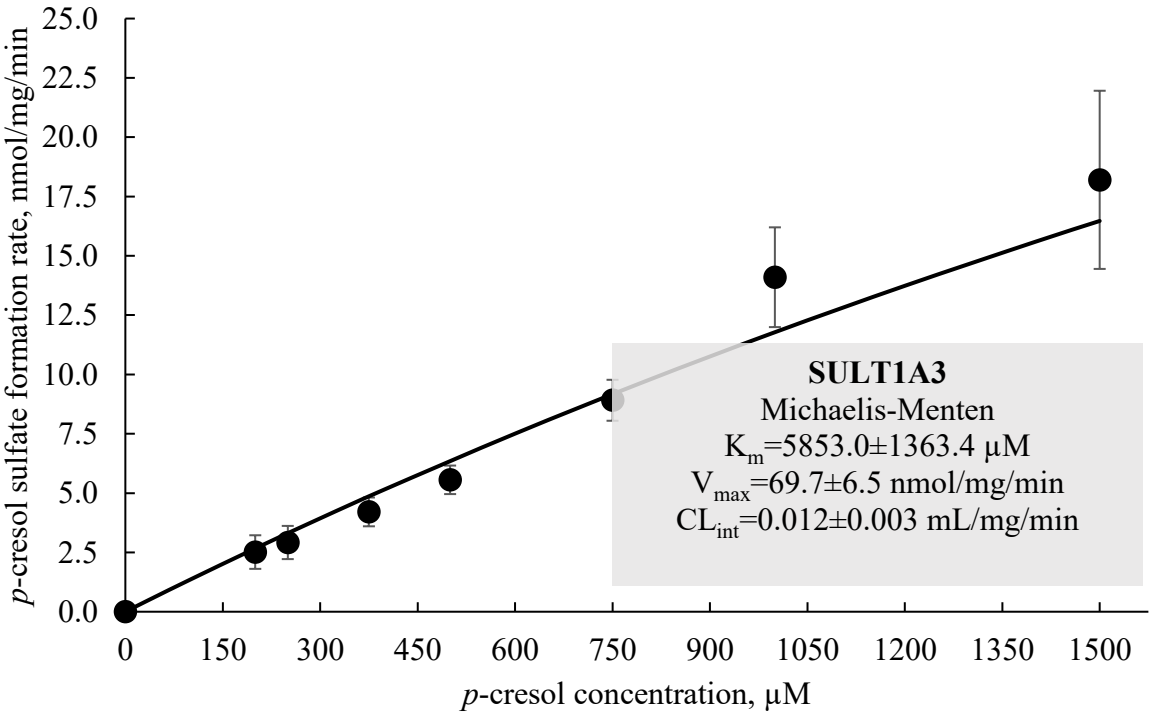
p-cresol sulfate formation rate, nmol/mg/min
p-cresol concentration, µM
SULT1A3
Michaelis-Menten
Km=5853.0±1363.4 µM
Vmax=69.7±6.5 nmol/mg/min
CLint=0.012±0.003 mL/mg/min

C

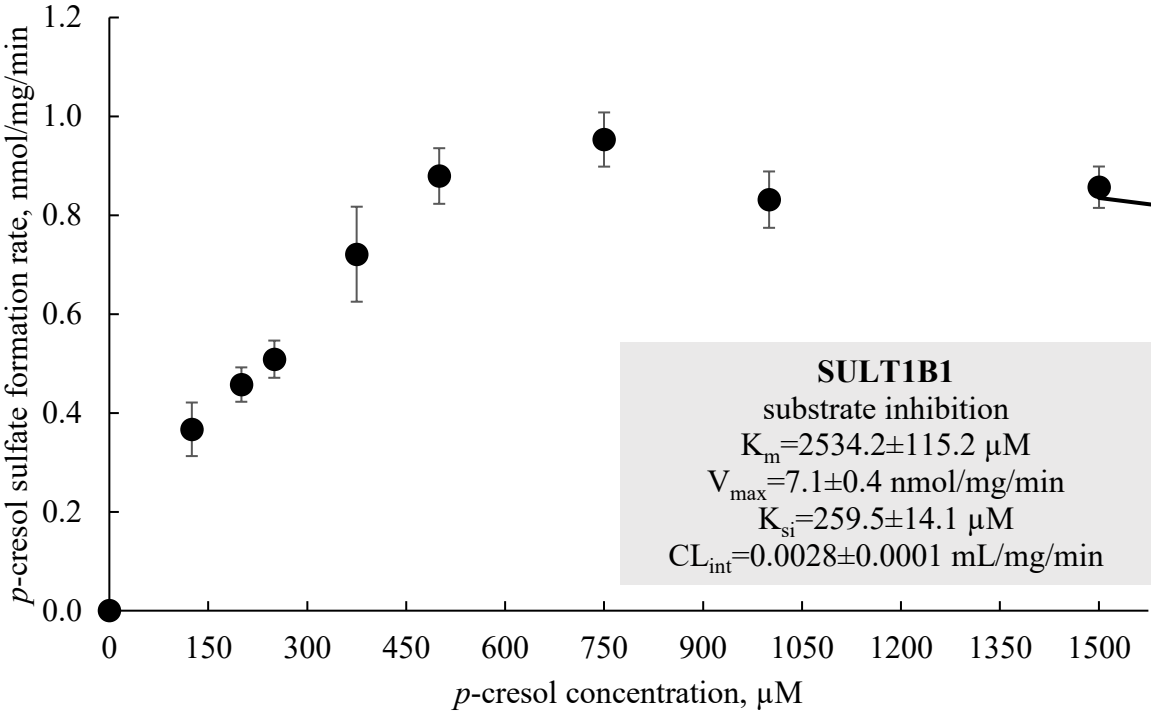
1.2
1.0
0.8
0.6
0.4
0.2
0.0
p-cresol sulfate formation rate, nmol/mg/min
0
150
300
450
600
750
900
1050
1200
1350
1500
p-cresol concentration, µM
SULT1B1
substrate inhibition
Km=2534.2±115.2 µM
Vmax=7.1±0.4 nmol/mg/min
Ksi=259.5±14.1 µM
CLint=0.0028±0.0001 mL/mg/min

D

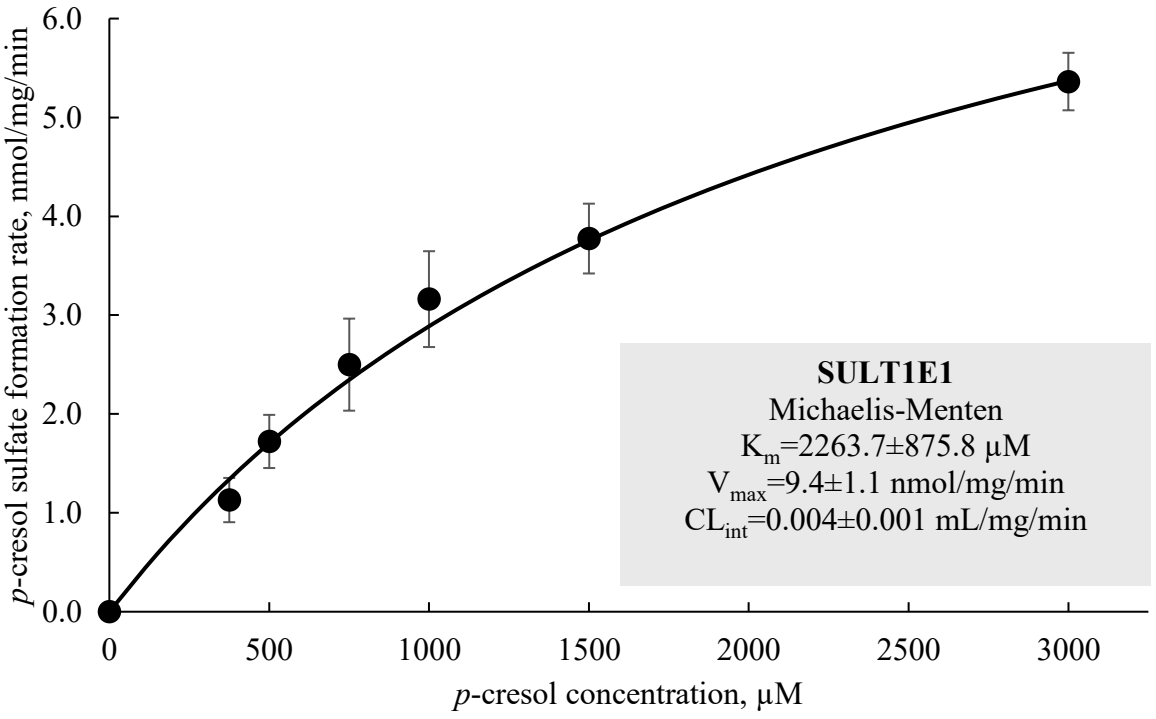
6.0
5.0
4.0
3.0
2.0
1.0
0.0
p-cresol sulfate formation rate, nmol/mg/min
0
500
1000
1500
2000
2500
3000
p-cresol concentration, µM
SULT1E1
Michaelis-Menten
Km=2263.7±875.8 µM
Vmax=9.4±1.1 nmol/mg/min
CLint=0.004±0.001 mL/mg/min

E

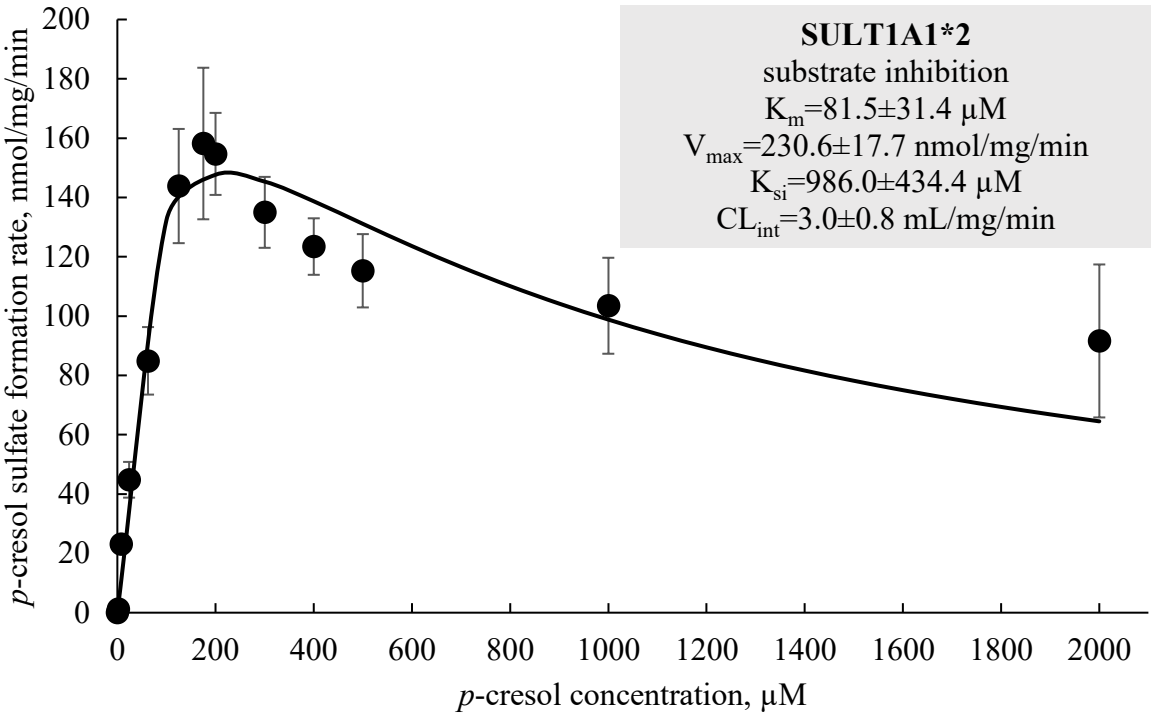
SULT1A1*2
substrate inhibition
K_m=81.5±31.4 µM
V_{max}=230.6±17.7 nmol/mg/min
K_{si}=986.0±434.4 µM
CL_{int}=3.0±0.8 mL/mg/min
p-cresol sulfate formation rate, nmol/mg/min
p-cresol concentration, µM

F

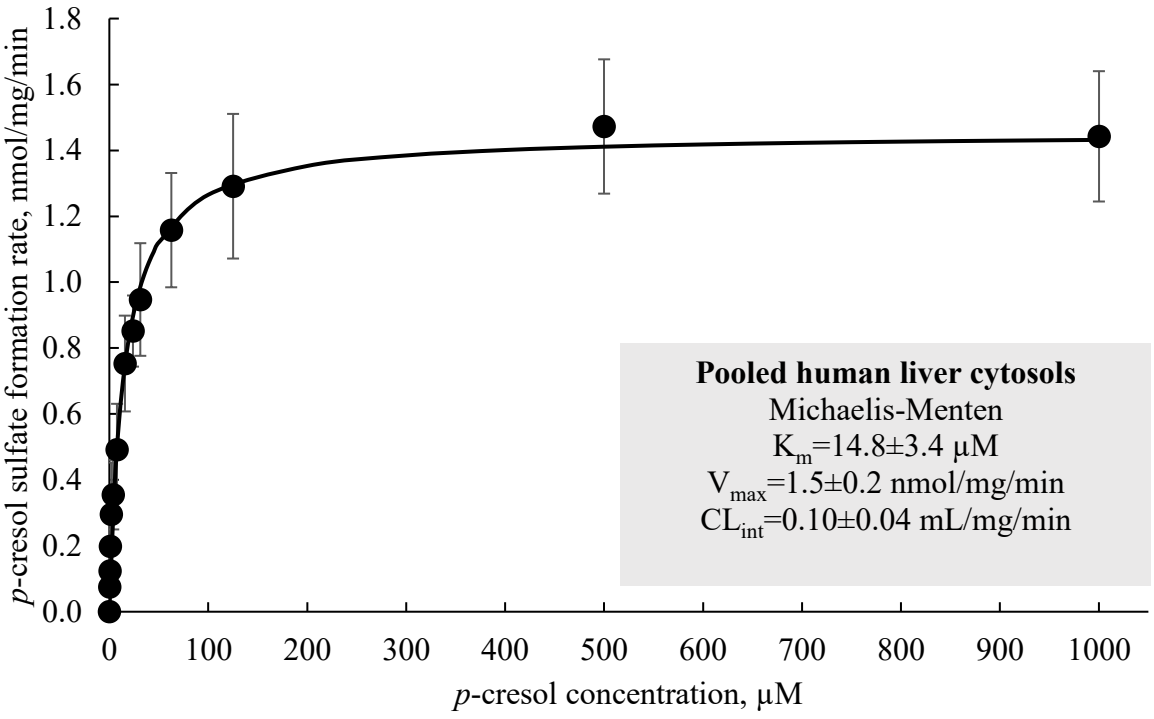
Pooled human liver cytosols
Michaelis-Menten
K_m=14.8±3.4 µM
V_{max}=1.5±0.2 nmol/mg/min
CL_{int}=0.10±0.04 mL/mg/min
p-cresol sulfate formation rate, nmol/mg/min
p-cresol concentration, µM

G

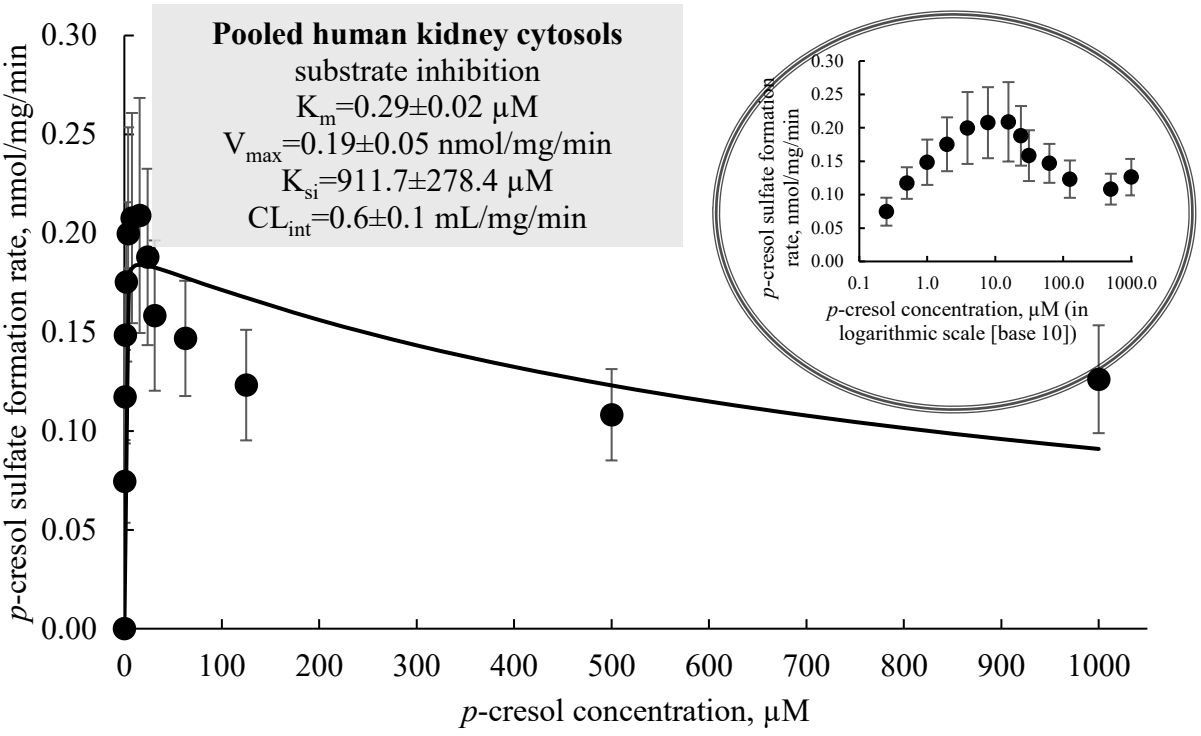

Figure VII-2 Enzyme kinetics of p-cresol sulfate formation

A. Human recombinant SULT1A1; B. human recombinant SULT1A3; C. human recombinant SULT1B1; D. human recombinant SULT1E1; E. human recombinant SULT1A1*2; F. pooled human liver cytosols; G. pooled human kidney cytosols.

The protein concentrations and incubation times representing linear, initial velocity enzymatic conditions were: human recombinant SULT1A1 (1 µg/mL, 15 minutes); human recombinant SULT1A3 (1 µg/mL, 20 minutes); human recombinant SULT1B1 (4 µg/mL, 20 minutes); human recombinant SULT1E1 (2 µg/mL, 20 minutes); human recombinant SULT1A1*2 (20 µg/mL, 15 minutes); pooled human liver cytosols (200 µg/mL, 10 minutes); and pooled human kidney cytosols (150 µg/mL, 15 minutes).

Data are presented as mean±standard deviation from 3 replicates.

Enzyme kinetic curve fittings were conducted using GraphPad Prism 9.0.0 (GraphPad Software, San Diego, CA, USA).

*Substrate inhibition was the model of best fit; however, a more conservative K_m estimate of 5.35±0.24 μM can be obtained based on the allosteric sigmoidal model (see **Discussion).**

Abbreviation(s): CL_{int}, intrinsic clearance; K_m, concentration of substrate at half maximum reaction rate; K_{si}, the dissociation constant of substrate inhibition; *SULT*, sulfotransferase; V_{max}, maximum reaction rate.

A

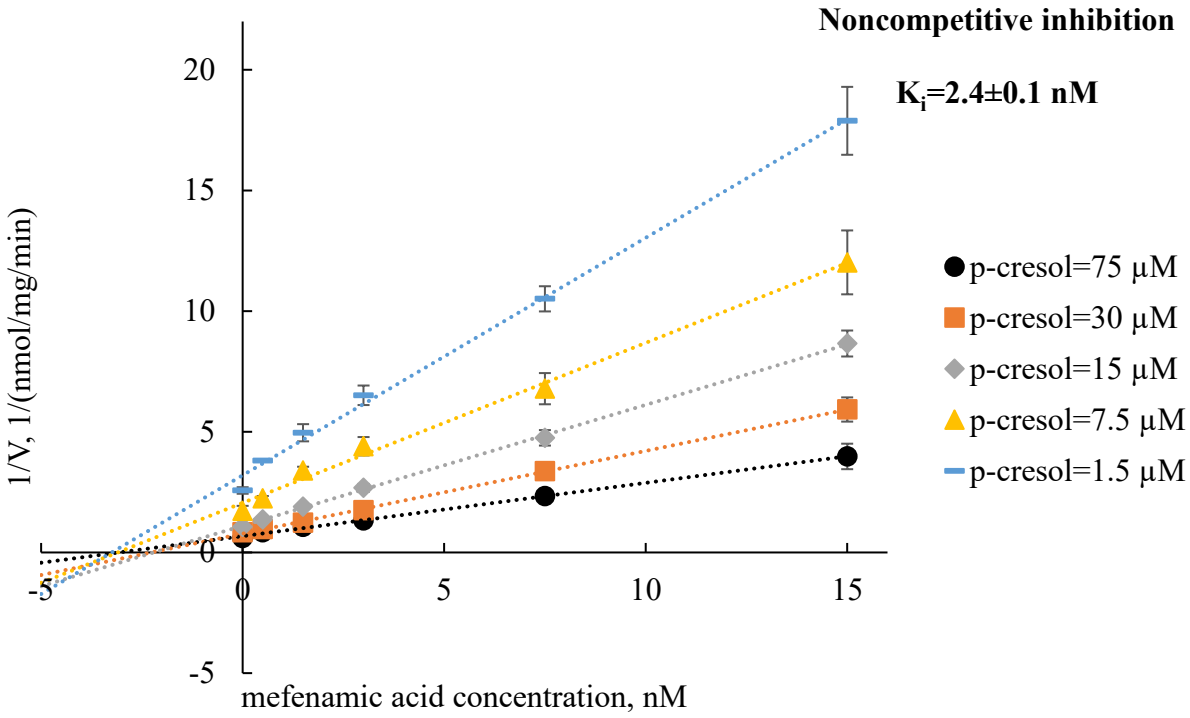
Noncompetitive inhibition
K_i=2.4±0.1 nM
1/V, 1/(nmol/mg/min)
mefenamic acid concentration, nM
p-cresol=75 µM
p-cresol=30 µM
p-cresol=15 µM
p-cresol=7.5 µM
p-cresol=1.5 µM

B

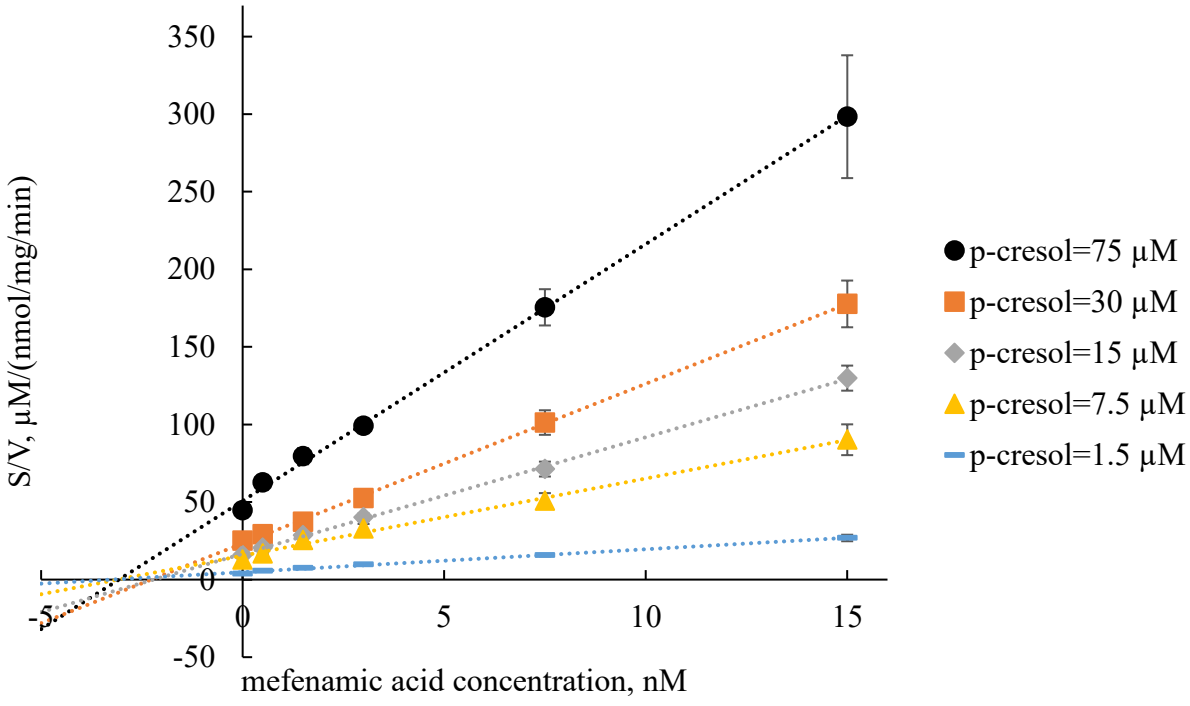
S/V, µM/(nmol/mg/min)
mefenamic acid concentration, nM
p-cresol=75 µM
p-cresol=30 µM
p-cresol=15 µM
p-cresol=7.5 µM
p-cresol=1.5 µM

Figure VII-3 Mechanism of inhibition of mefenamic acid in pooled human liver cytosols

A. Dixon plot characterizing the inhibitory effects of mefenamic acid towards *p*-cresol sulfate formation in pooled human liver cytosols; B. the corresponding Cornish-Bowden plot.

The protein concentration and incubation time representing linear, initial velocity enzymatic conditions for pooled human liver cytosols were 200 µg/mL and 10 minutes, respectively. The utilized *p*-cresol concentrations also represented non-saturating conditions (Figure VII-2).

Methanol (0.1%) was used to dissolve mefenamic acid and controls. Data are presented as mean±standard deviation from 3 replicates.

The inhibition constant was determined using GraphPad Prism 9.0.0 (GraphPad Software, San Diego, CA, USA).

Abbreviation(s): K_i, inhibition constant.

A

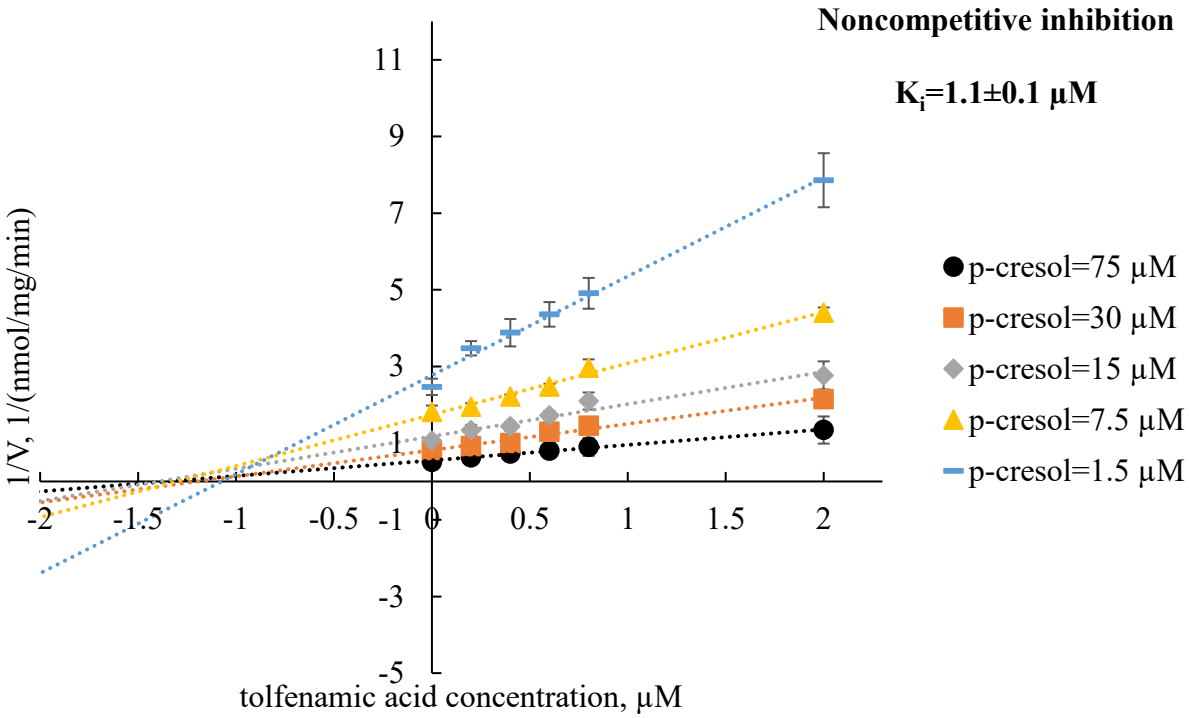
Noncompetitive inhibition
K_i=1.1±0.1 µM
1/V, 1/(nmol/mg/min)
11
9
7
5
3
1
-3
-5
-2
-1.5
-1
-0.5
0
0.5
1
1.5
2
tolfenamic acid concentration, µM
p-cresol=75 µM
p-cresol=30 µM
p-cresol=15 µM
p-cresol=7.5 µM
p-cresol=1.5 µM

B

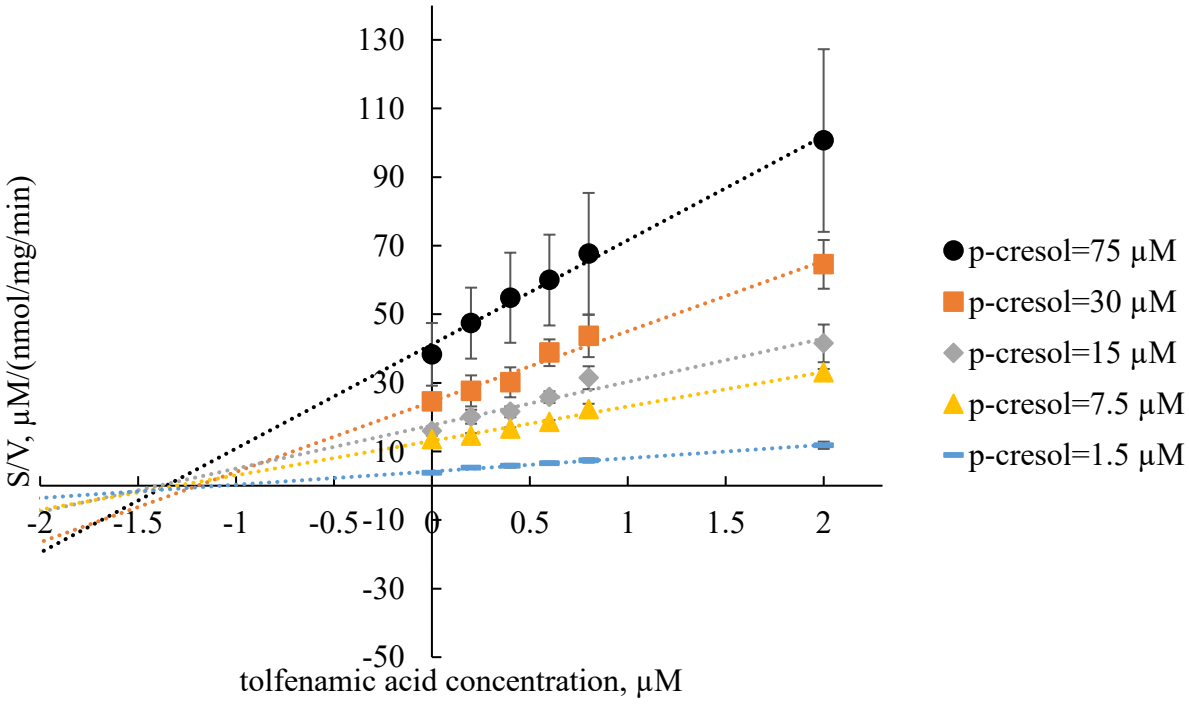
S/V, µM/(nmol/mg/min)
130
110
90
70
50
30
10
-30
-50
-2
-1.5
-1
-0.5
0
0.5
1
1.5
2
tolfenamic acid concentration, µM
p-cresol=75 µM
p-cresol=30 µM
p-cresol=15 µM
p-cresol=7.5 µM
p-cresol=1.5 µM

Figure VII-4 Mechanism of inhibition of tolfenamic acid in pooled human liver cytosols

A. Dixon plot characterizing the inhibitory effects of tolfenamic acid towards *p*-cresol sulfate formation in pooled human liver cytosols; B. the corresponding Cornish-Bowden plot.

The protein concentration and incubation time representing linear, initial velocity enzymatic conditions for pooled human liver cytosols were 200 µg/mL and 10 minutes, respectively.

The utilized *p*-cresol concentrations also represented non-saturating conditions (Figure VII-2). Data are presented as mean±standard deviation from 3 replicates.

The inhibition constant was determined using GraphPad Prism 9.0.0 (GraphPad Software, San Diego, CA, USA).

Abbreviation(s): K_i, inhibition constant.

A

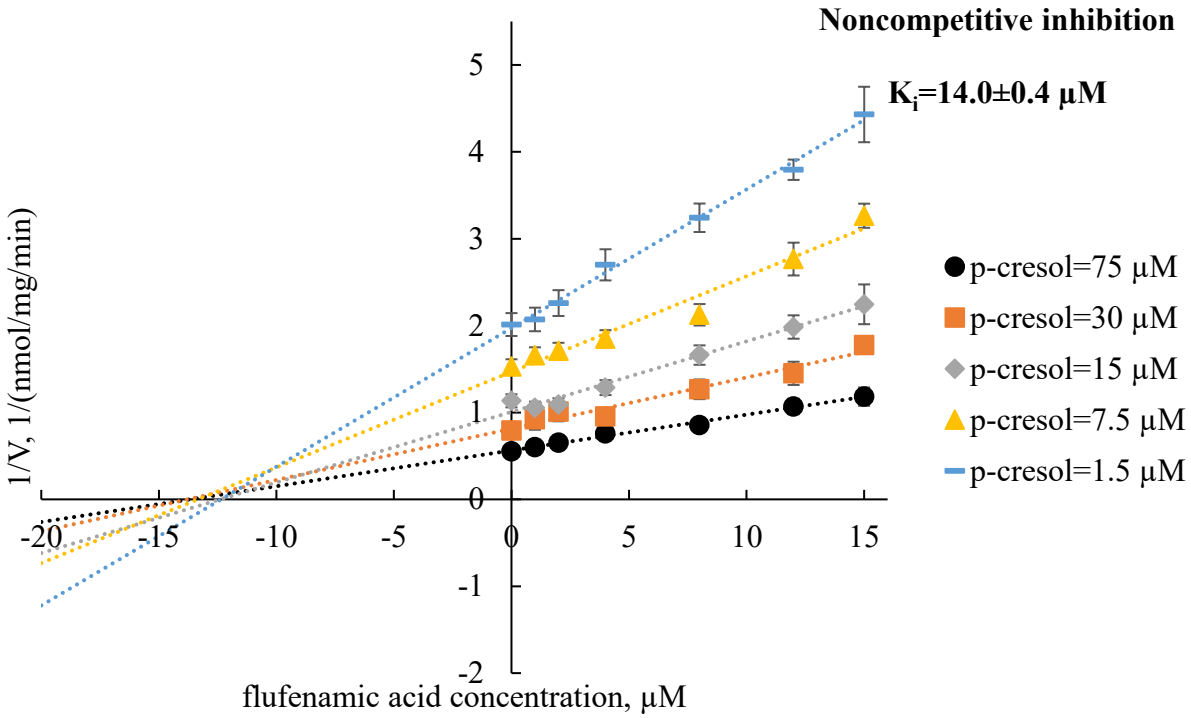
Noncompetitive inhibition
K_i=14.0±0.4 μM
1/V, 1/(nmol/mg/min)
flufenamic acid concentration, μM
p-cresol=75 μM
p-cresol=30 μM
p-cresol=15 μM
p-cresol=7.5 μM
p-cresol=1.5 μM

B

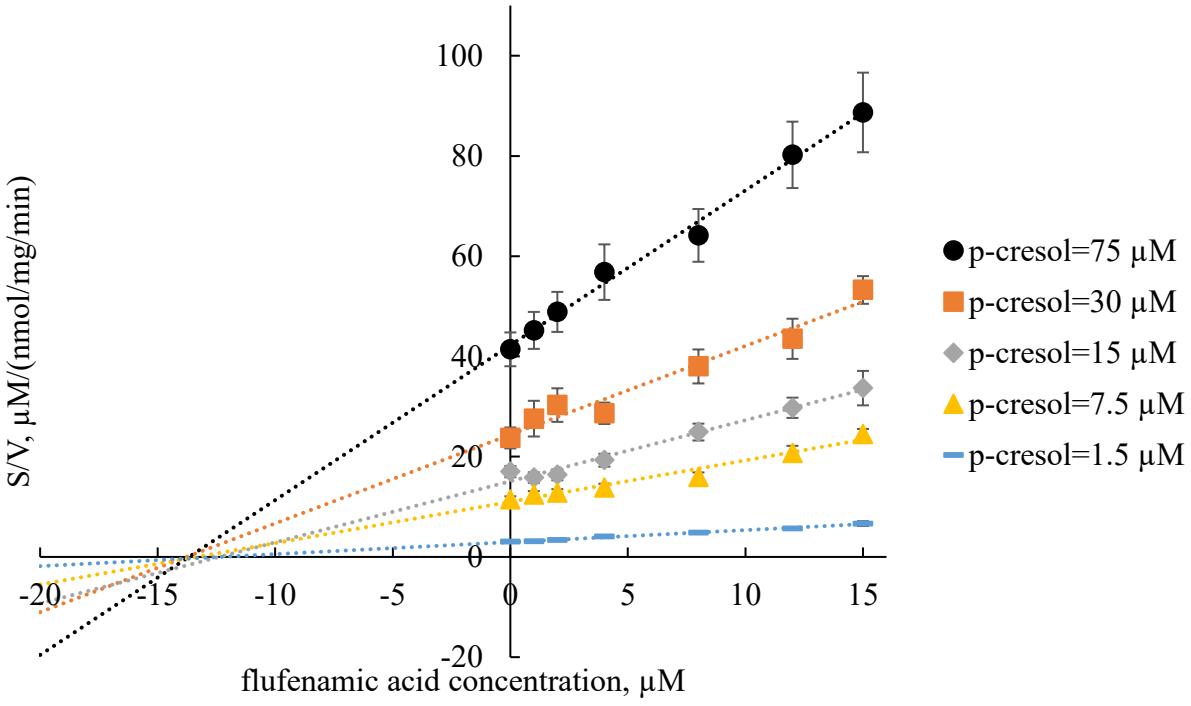
S/V, μM/(nmol/mg/min)
flufenamic acid concentration, μM
p-cresol=75 μM
p-cresol=30 μM
p-cresol=15 μM
p-cresol=7.5 μM
p-cresol=1.5 μM

Figure VII-5 Mechanism of inhibition of flufenamic acid in pooled human liver cytosols

A. Dixon plot characterizing the inhibitory effects of flufenamic acid towards *p*-cresol sulfate formation in pooled human liver cytosols; B. the corresponding Cornish-Bowden plot.

The protein concentration and incubation time representing linear, initial velocity enzymatic conditions for pooled human liver cytosols were 200 µg/mL and 10 minutes, respectively.

The utilized *p*-cresol concentrations also represented non-saturating conditions (Figure VII-2).

Ethanol (0.4%) was used to dissolve flufenamic acid and controls.

Data are presented as mean±standard deviation from 3 replicates.

The inhibition constant was determined using GraphPad Prism 9.0.0 (GraphPad Software, San Diego, CA, USA).

Abbreviation(s): K_i, inhibition constant.

A

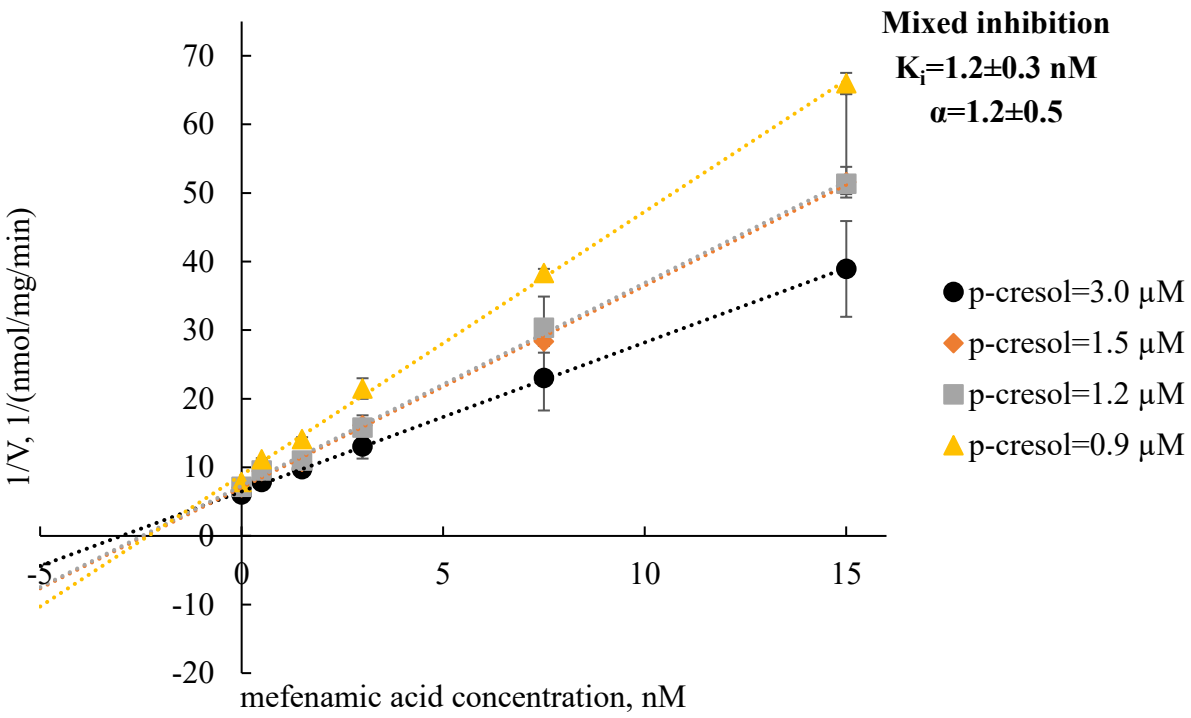
Mixed inhibition
K_i=1.2±0.3 nM
α=1.2±0.5
1/V, 1/(nmol/mg/min)
70
60
50
40
30
20
10
0
-10
-20
-5
0
5
10
15
mefenamic acid concentration, nM
p-cresol=3.0 μM
p-cresol=1.5 μM
p-cresol=1.2 μM
p-cresol=0.9 μM

B

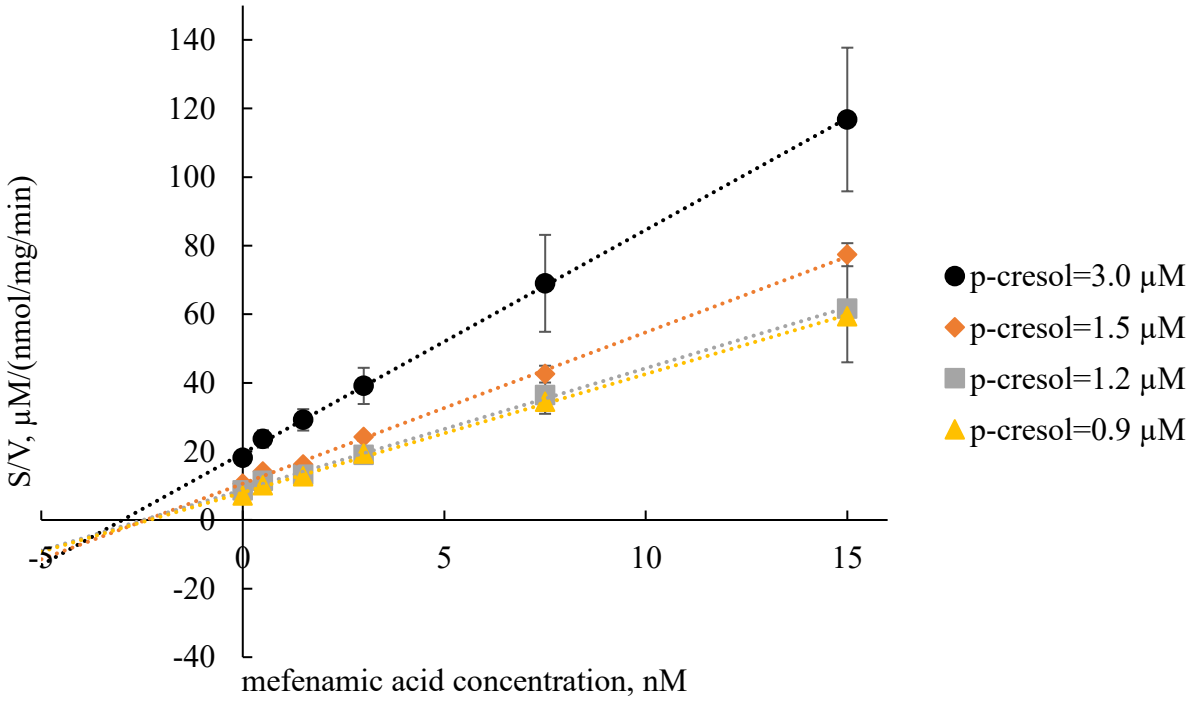
S/V, μM/(nmol/mg/min)
140
120
100
80
60
40
20
0
-20
-40
-5
0
5
10
15
mefenamic acid concentration, nM
p-cresol=3.0 μM
p-cresol=1.5 μM
p-cresol=1.2 μM
p-cresol=0.9 μM

Figure VII-6 Mechanism of inhibition of mefenamic acid in pooled human kidney cytosols

A. Dixon plot characterizing the inhibitory effects of mefenamic acid towards *p*-cresol sulfate formation in pooled human kidney cytosols; B. the corresponding Cornish-Bowden plot.

The protein concentration and incubation time representing linear, initial velocity enzymatic conditions for pooled human kidney cytosols were 150 µg/mL and 15 minutes, respectively.

The utilized *p*-cresol concentrations also represented non-saturating conditions (Figure VII-2).

Methanol (0.1%) was used to dissolve mefenamic acid and controls.

Data are presented as mean±standard deviation from 3 replicates.

The inhibition constant was determined using GraphPad Prism 9.0.0 (GraphPad Software, San Diego, CA, USA).

Abbreviation(s): α, alpha value, the constant that differentiates the specific mechanisms in the mixed inhibition model; K_i, inhibition constant.

A

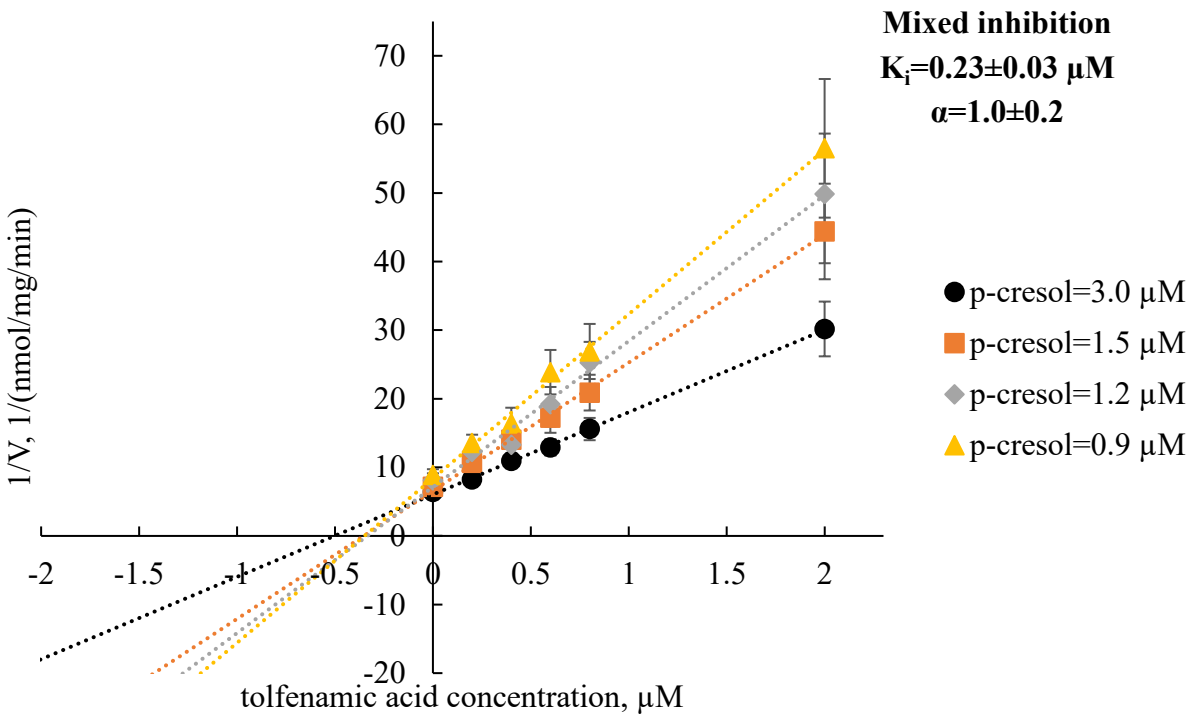
Mixed inhibition
K_i=0.23±0.03 μM
α=1.0±0.2
1/V, 1/(nmol/mg/min)
tolfenamic acid concentration, μM
p-cresol=3.0 μM
p-cresol=1.5 μM
p-cresol=1.2 μM
p-cresol=0.9 μM

B

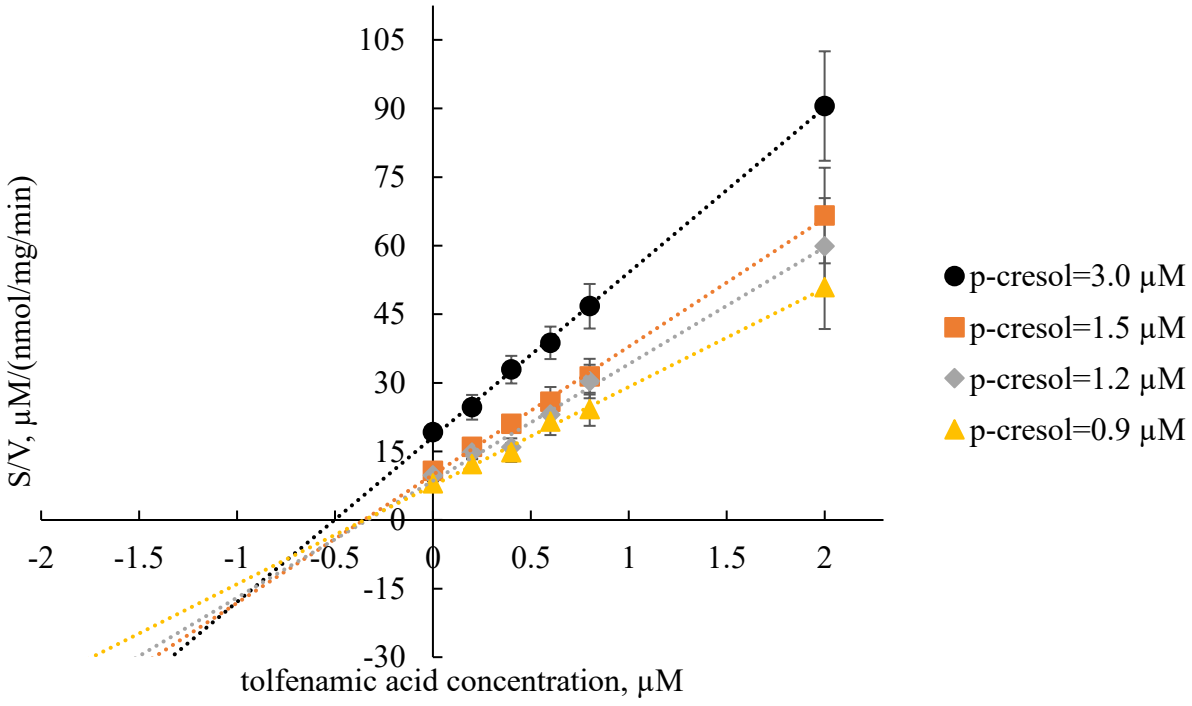
S/V, μM/(nmol/mg/min)
tolfenamic acid concentration, μM
p-cresol=3.0 μM
p-cresol=1.5 μM
p-cresol=1.2 μM
p-cresol=0.9 μM

Figure VII-7 Mechanism of inhibition of tolfenamic acid in pooled human kidney cytosols

A. Dixon plot characterizing the inhibitory effects of tolfenamic acid towards *p*-cresol sulfate formation in pooled human kidney cytosols; B. the corresponding Cornish-Bowden plot.

The protein concentration and incubation time representing linear, initial velocity enzymatic conditions for pooled human kidney cytosols were 150 µg/mL and 15 minutes, respectively.

The utilized *p*-cresol concentrations also represented non-saturating conditions (Figure VII-2).

Data are presented as mean±standard deviation from 3 replicates.

The inhibition constant was determined using GraphPad Prism 9.0.0 (GraphPad Software, San Diego, CA, USA).

Abbreviation(s): α, alpha value, the constant that differentiates the specific mechanisms in the mixed inhibition model; K_i, inhibition constant.

A

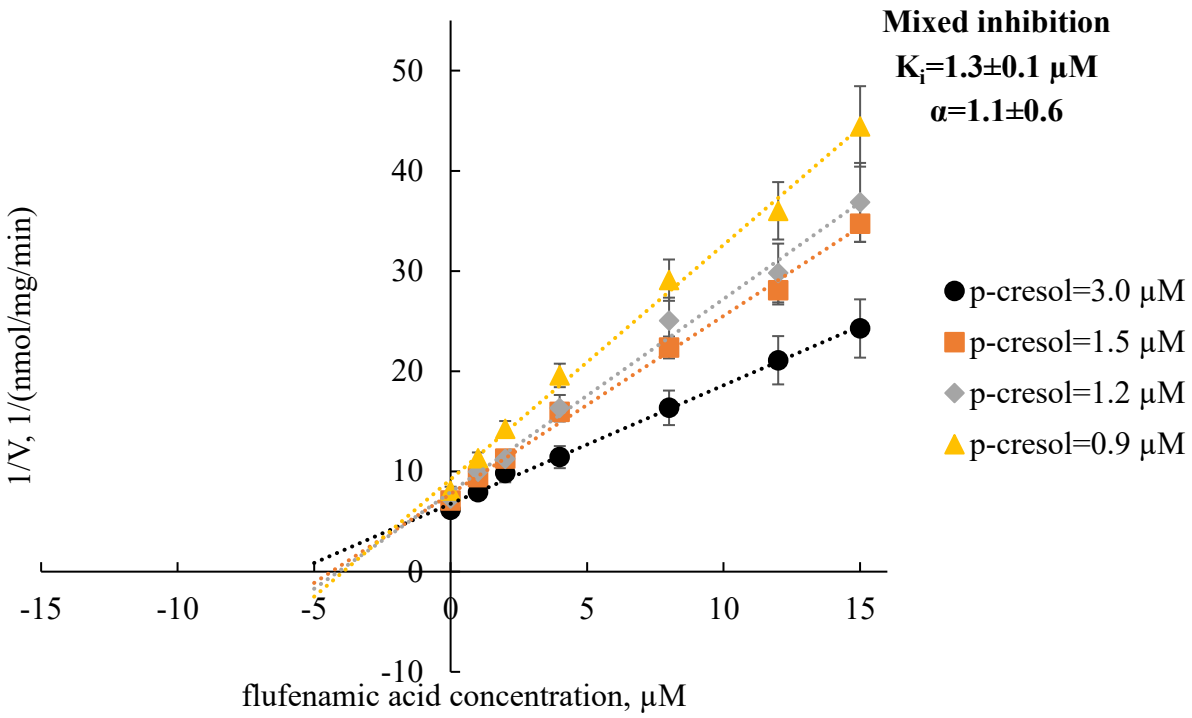
Mixed inhibition
K_i=1.3±0.1 μM
α=1.1±0.6
p-cresol=3.0 μM
p-cresol=1.5 μM
p-cresol=1.2 μM
p-cresol=0.9 μM
1/V, 1/(nmol/mg/min)
flufenamic acid concentration, μM
50
40
30
20
10
0
-10
-15
-10
-5
0
5
10
15

B

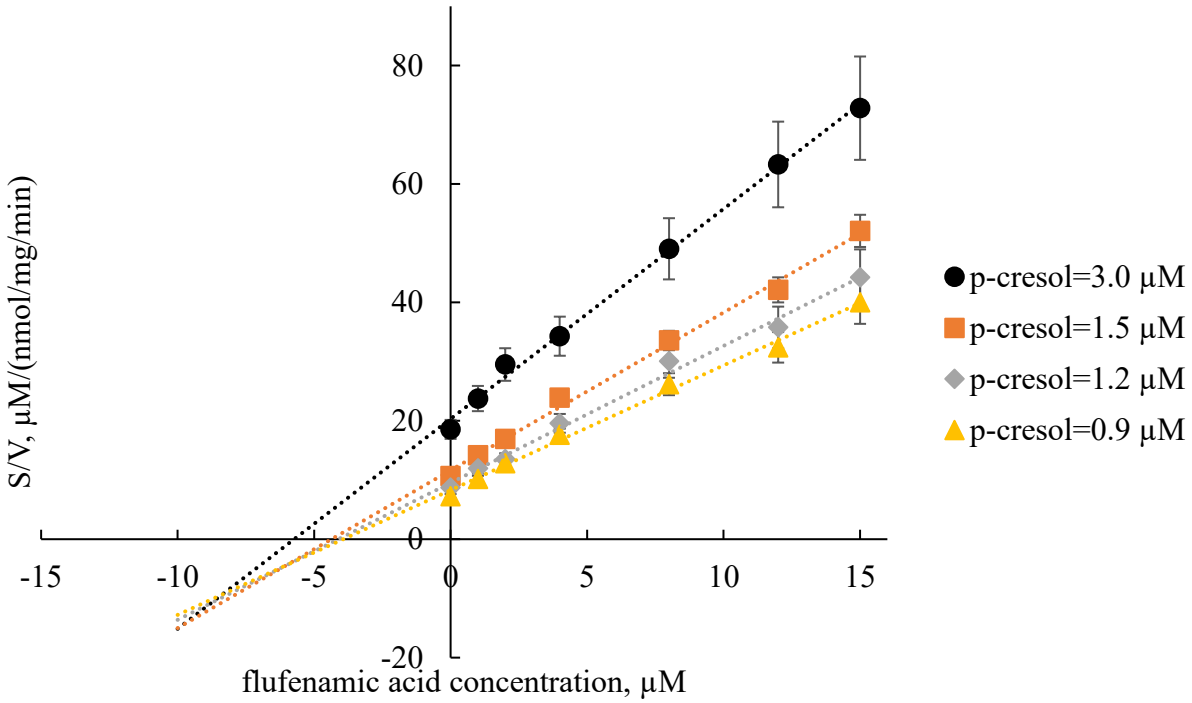
p-cresol=3.0 μM
p-cresol=1.5 μM
p-cresol=1.2 μM
p-cresol=0.9 μM
S/V, μM/(nmol/mg/min)
flufenamic acid concentration, μM
80
60
40
20
0
-20
-15
-10
-5
0
5
10
15

Figure VII-8 Mechanism of inhibition of flufenamic acid in pooled human kidney cytosols

A. Dixon plot characterizing the inhibitory effects of flufenamic acid towards *p*-cresol sulfate formation in pooled human kidney cytosols; B. the corresponding Cornish-Bowden plot.

The protein concentration and incubation time representing linear, initial velocity enzymatic conditions for pooled human kidney cytosols were 150 µg/mL and 15 minutes, respectively.

The utilized *p*-cresol concentrations also represented non-saturating conditions (Figure VII-2).

Ethanol (0.4%) was used to dissolve flufenamic acid and controls.

Data are presented as mean±standard deviation from 3 replicates.

The inhibition constant was determined using GraphPad Prism 9.0.0 (GraphPad Software, San Diego, CA, USA).

Abbreviation(s): α, alpha value, the constant that differentiates the specific mechanisms in the mixed inhibition model; K_i, inhibition constant.

A

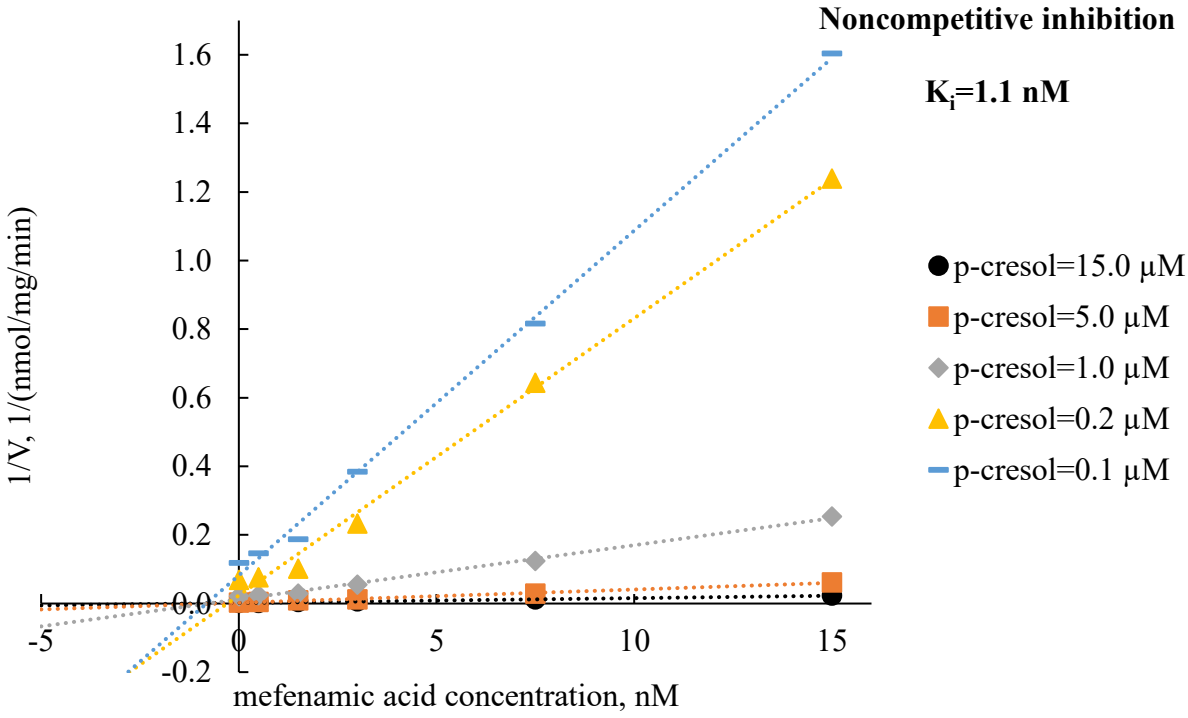
Noncompetitive inhibition
K_i=1.1 nM
1/V, 1/(nmol/mg/min)
1.6
1.4
1.2
1.0
0.8
0.6
0.4
0.2
0.0
-0.2
-5
0
5
10
15
mefenamic acid concentration, nM
p-cresol=15.0 μM
p-cresol=5.0 μM
p-cresol=1.0 μM
p-cresol=0.2 μM
p-cresol=0.1 μM

B

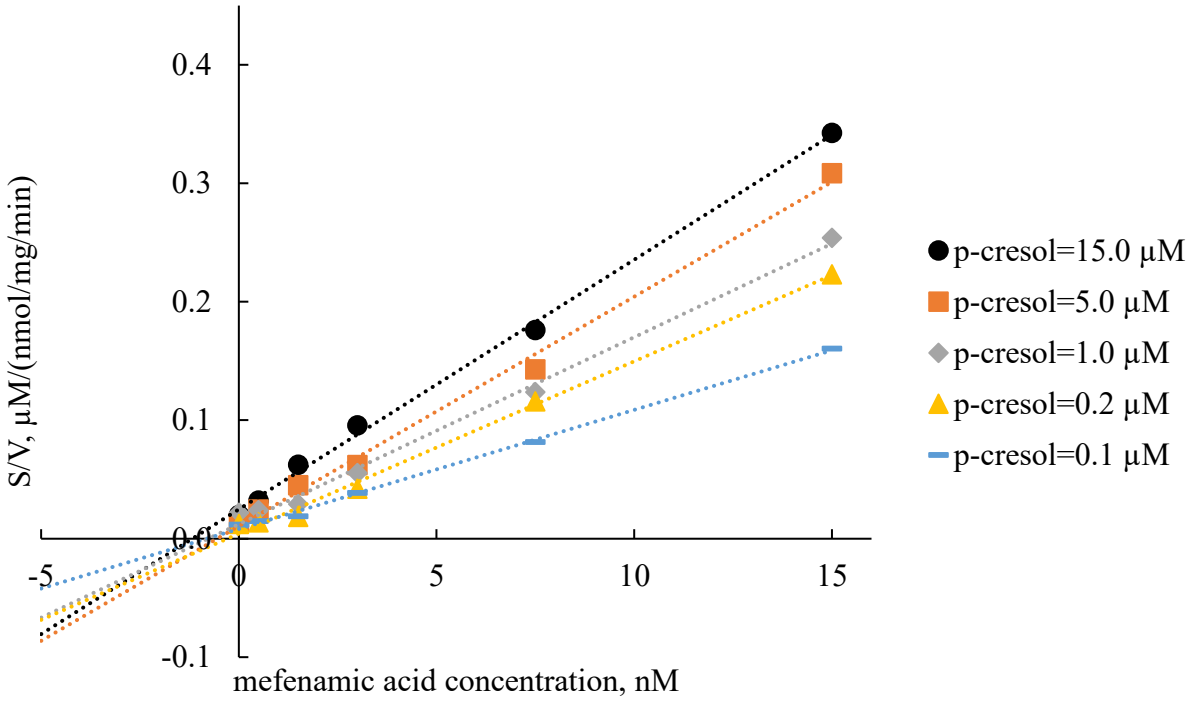
S/V, μM/(nmol/mg/min)
0.4
0.3
0.2
0.1
0.0
-0.1
-5
0
5
10
15
mefenamic acid concentration, nM
p-cresol=15.0 μM
p-cresol=5.0 μM
p-cresol=1.0 μM
p-cresol=0.2 μM
p-cresol=0.1 μM

Figure VII-9 Mechanism of inhibition of mefenamic acid in human recombinant SULT1A1

A. Dixon plot characterizing the inhibitory effects of mefenamic acid towards *p*-cresol sulfate formation in human recombinant SULT1A1; B. the corresponding Cornish-Bowden plot.

The protein concentration and incubation time representing linear, initial velocity enzymatic conditions for human recombinant SULT1A1 were 1 µg/mL and 15 minutes, respectively.

The utilized *p*-cresol concentrations also represented non-saturating conditions (Figure VII-2).

Methanol (0.1%) was used to dissolve mefenamic acid and controls. Data are presented as average values from 2 replicates.

The inhibition constant was determined using GraphPad Prism 9.0.0 (GraphPad Software, San Diego, CA, USA).

Abbreviation(s): K_i, inhibition constant; *SULT*, sulfotransferase.

A

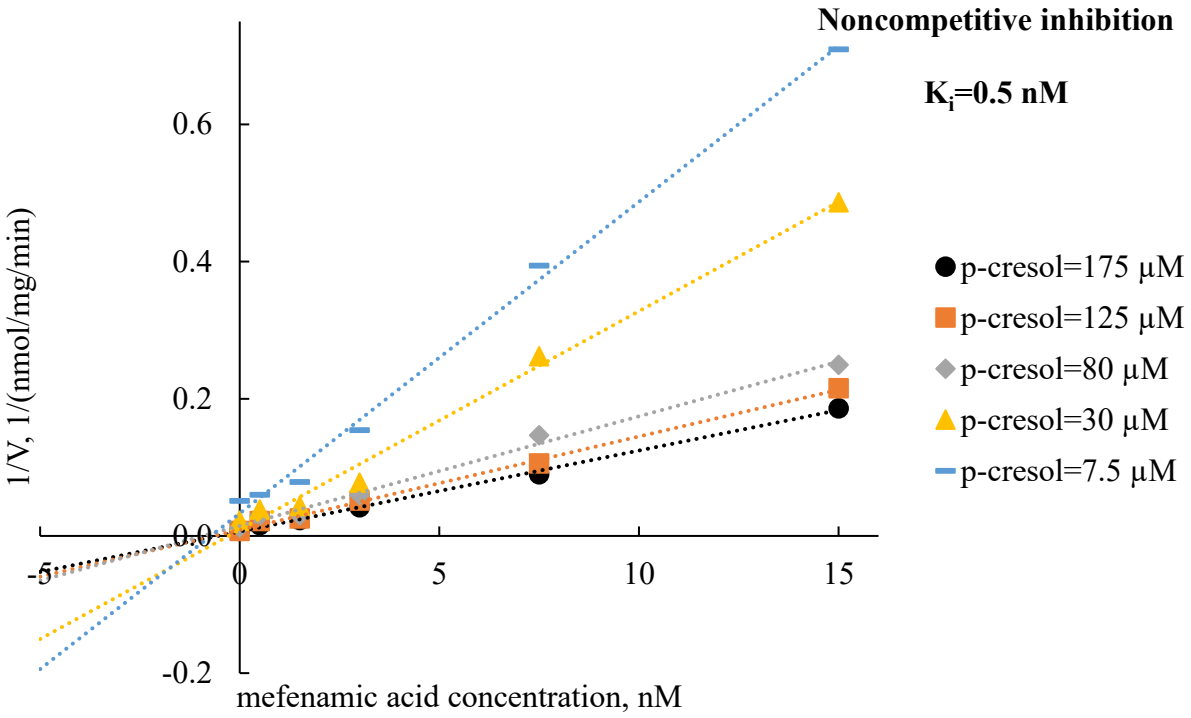
Noncompetitive inhibition
K_i=0.5 nM
1/V, 1/(nmol/mg/min)
0.6
0.4
0.2
0.0
-0.2
-5
0
5
10
15
mefenamic acid concentration, nM
p-cresol=175 μM
p-cresol=125 μM
p-cresol=80 μM
p-cresol=30 μM
p-cresol=7.5 μM

B

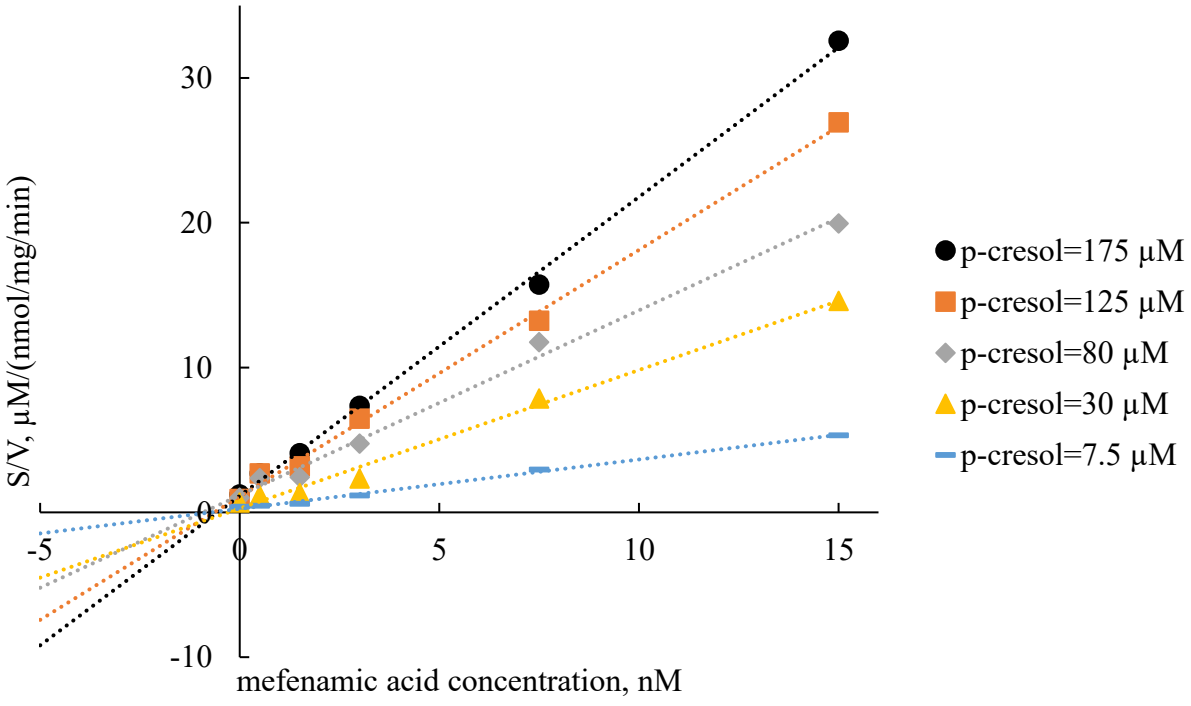
S/V, μM/(nmol/mg/min)
30
20
10
0
-10
-5
0
5
10
15
mefenamic acid concentration, nM
p-cresol=175 μM
p-cresol=125 μM
p-cresol=80 μM
p-cresol=30 μM
p-cresol=7.5 μM

Figure VII-10 Mechanism of inhibition of mefenamic acid in human recombinant SULT1A1*2

A. Dixon plot characterizing the inhibitory effects of mefenamic acid towards *p*-cresol sulfate formation in human recombinant SULT1A1*2; B. the corresponding Cornish-Bowden plot.

The protein concentration and incubation time representing linear, initial velocity enzymatic conditions for human recombinant SULT1A1*2 were 20 µg/mL and 15 minutes, respectively.

The utilized *p*-cresol concentrations also represented non-saturating conditions (Figure VII-2).

Methanol (0.1%) was used to dissolve mefenamic acid and controls.

Data are presented as average values from 2 replicates.

The inhibition constant was determined using GraphPad Prism 9.0.0 (GraphPad Software, San Diego, CA, USA).

Abbreviation(s): K_i, inhibition constant; *SULT*, sulfotransferase.

Supplementary materials

S1. Control experiments

The effects of individual components in the incubation mixture on the rate of *p*-cresol sulfate formation are illustrated in Figure S VII-1, Figure S VII-2, Figure S VII-3, Figure S VII-4. Little differences in enzyme activities were observed between the two buffers overall, but Tris buffer (50 mM, pH 7.5) was ultimately utilized owing to slightly higher rates of *p*-cresol sulfate formation in both pooled human liver and kidney cytosols (Figure S VII-1). On the other hand, varying the PAPS (co-substrate/co-factor) [326] concentration resulted in different kinetic behaviors (i.e. K_m and V_{max}) in the formation of *p*-cresol sulfate in each enzyme source (Figure S VII-2). The concentrations of PAPS were eventually fixed to 20 μM in incubations involving human recombinant SULT enzymes and pooled human liver cytosols, and 5 μM in pooled human kidney cytosols, based on known physiological concentrations in each organ [325, 326] which also generated non-saturating activities (Figure S VII-2). Likewise, varying magnesium ion concentration had differential effects on *p*-cresol sulfate formation in different enzyme sources (i.e. negative relationship in human recombinant SULT1A1, no relationship in pooled human liver cytosols, and a positive relationship in pooled human kidney cytosols; Figure S VII-3). For our experiments, $MgCl_2$ was fixed at 1 mM in all reaction mixtures as this resembled physiological condition and also provided relatively high activities in all enzyme sources [324]. A reducing agent such as 2-mercaptoethanol is added by some researchers to SULT incubations to prevent disulfide complex formation, but it was not utilized in our incubation because it did not significantly impact *p*-cresol sulfate formation in all utilized enzyme systems (Figure S VII-4), consistent with the literature (e.g. [343]).

S2. Selectivity of tolfenamic acid and flufenamic acid towards SULT1A1 inhibition versus COX inhibition

The IC_{50} values of tolfenamic acid and flufenamic acid toward COX inhibition are not sufficiently removed from its K_i values for *p*-cresol sulfate inhibition (Figure VII-4, Figure VII-5, Figure VII-7, Figure VII-8). Of the limited available data, tolfenamic acid's IC_{50} value for COX-1 inhibition in human whole blood was 2.6 μM [366]; flufenamic acid's IC_{50} values for COX-1 inhibition were in the 0.01-3 μM range in human recombinant COX-1, human whole blood, human platelets, and U937 cell microsomes [356, 358, 359, 365]; and flufenamic acid's IC_{50} values for COX-2 inhibition were in the 0.02-29.5 μM range in human recombinant COX-2 and human whole blood [356, 359, 365]. Therefore, based on the lack of selectivity towards SULT1A1 inhibition over COX inhibition, tolfenamic acid and flufenamic acid are likely not suitable to be utilized as therapeutic agents to reduce the formation of *p*-cresol sulfate.

S3. Summary of current detoxification approaches of p-cresol

A variety of other methods have been utilized to reduce the concentration of *p*-cresol sulfate in order to alleviate the associated toxicities [53, 78, 322]. Strategies have focused on *enhancing clearance* by directly reducing plasma levels of *p*-cresol sulfate using hemodialysis or peritoneal dialysis; however, the filtration efficiency is generally poor as *p*-cresol sulfate is highly protein bound in the plasma [322]. The administration of oral adsorbents such as AST-120 or sevelamer have also been investigated to reduce the uptake (hence increase the clearance) of *p*-cresol [78]; however, this approach has not always been successful (e.g. [53]) and has unwanted drug-interacting effects [78]. Moreover, interventions have attempted to *reduce the production* of *p*-

cresol. For example, dietary alteration (e.g. lowering the intake of protein while increasing carbohydrates and fibers) has been proposed to help reduce the generation of *p*-cresol from the intestinal microbiota; however, this approach might be associated with malnutrition [322]. Alternatively, the administration of probiotics, prebiotics, and synbiotics could also normalize the colonic bacteria composition and decrease *p*-cresol formation, but the efficacy may be limited [370]. Overall, the currently available methods to reduce *p*-cresol sulfate concentrations have disadvantages and limitations, and a targeted approach to inhibit *p*-cresol sulfonation using potent and effective SULT inhibitors [78] such as mefenamic acid could provide another therapeutic option.

Table S VII-1 Demographic data of donors in pooled human liver and kidney cytosols

	Pooled human liver cytosols (catalog number H0610.C; lot number 1810002; SEKISUI XenoTech)	**Pooled human kidney cytosols** (catalog number H0610.RC; lot number 1310121; SEKISUI XenoTech)
The number of donors	50	4
Gender	30 males, 20 females	2 males, 2 females
Age (years, mean±standard deviation [range])	47±20 [5-83]	57±8 [45-62]
Race	African American (1), Asian (1), Caucasian (44), Hispanic (4)	African American (1), Caucasian (3)
Cause of death	Anoxia (17), cerebrovascular accident (17), head trauma (16)	Anoxia (2), cerebrovascular accident (2)

The donor information was extracted from https://www.xenotech.com/ [323].

Table S VII-2 Compound-specific optimized MS parameters of p-cresol sulfate and p-cresol sulfate-d$_7$

Parameters	***p*-Cresol sulfate**	***p*-Cresol sulfate-d$_7$**
MRM transition (m/z)	187.00→107.00	194.10→114.15
Q_1 pre-bias (V)	21	20
Collision energy (V)	22	23
Q_3 pre-bias (V)	10	22
Interface	Electrospray ionization	
Ion mode	Negative	
Interface voltage (kV)	3	
Conversion dynode voltage (kV)	10	
Interface temperature (°C)	400	
Desolvation line temperature (°C)	100	
Heat block temperature (°C)	400	
Heating gas flow (L/min)	10	
Drying gas flow (L/min)	10	
Nebulizing gas flow (L/min)	2	
Collision-induced dissociation gas pressure (kPa)	270	

Compound specific MS parameters (including Q_1/Q_3 pre-bias and collision energy) were initially optimized with LabSolutions software using a flow injection of a mixture containing *p*-cresol sulfate and *p*-cresol sulfate-d$_7$.

The MS source parameters were further optimized manually. The final MS conditions were selected based on the highest signal counts compared to baseline noise.

Abbreviation(s): *m/z*, mass to charge ratio; *MRM*, multiple reaction monitoring; *MS*, mass spectrometry.

Table S VII-3 Statistical testing results of enzyme kinetic curve fittings for human recombinant SULT1A1

	K_m, µM	V_{max}, nmol/mg/min	K_{si}, µM	h	R^2	Adjusted R^2	Sum of Squares	Sy.x	RMSE	AIC
First replicate										
Michaelis-Menten	0.15	642.30	NA	NA	0.88	0.87	127583	103.1	99.1	136.0
Substrate inhibition	0.21	672.60	2253.0	NA	0.94	0.93	58675	73.0	67.2	129.2
Allosteric sigmoidal	5.08	611.10	NA	2.4	0.94	0.93	61757	74.9	68.9	129.9
Second replicate										
Michaelis-Menten	0.15	838.00	NA	NA	0.89	0.88	195219	127.5	122.5	142.0
Substrate inhibition	0.19	857.00	2842.0	NA	0.94	0.93	103791	97.1	89.4	137.2
Allosteric sigmoidal	5.40	793.50	NA	2.5	0.91	0.91	177386	103.9	97.2	139.1
Third replicate										
Michaelis-Menten	0.13	805.90	NA	NA	0.86	0.85	230170	138.5	133.1	144.3
Substrate inhibition	0.17	839.00	2279.0	NA	0.93	0.91	124003	106.2	97.7	139.7
Allosteric sigmoidal	5.56	765.70	NA	2.5	0.91	0.91	114637	108.1	98.9	140.6

The protein concentration and incubation time representing linear, initial velocity enzymatic conditions for human recombinant SULT1A1 were 1 µg/mL and 15 minutes, respectively.

Curve fittings were conducted using GraphPad Prism 9.0.0 (GraphPad Software, San Diego, CA, USA). The final model is based on the best of three replicates.

Abbreviation(s): *AIC*, Akaike information criterion; *h*, the Hill slope; K_m, the concentration of *p*-cresol at half maximum reaction rate; K_{si}, the dissociation constant for substrate inhibition; *NA*, not available; R^2, coefficient of determination; *RMSE*, root mean square error; *SULT*, sulfotransferase; *Sy.x*, root mean square; V_{max}, the maximum reaction rate.

Table S VII-4 Statistical testing results of enzyme kinetic curve fittings for human recombinant SULT1A3

	K_m, µM	V_{max}, nmol/mg/min	K_{si}, µM	h	R^2	Adjusted R^2	Sum of Squares	Sy.x	RMSE	AIC
First replicate										
Michaelis-Menten	6277.0	77.2	NA	NA	0.97	0.97	4.6	0.9	0.8	7.6
Substrate inhibition	Unstable	78239.0	1.6	NA	0.98	0.97	3.7	0.9	0.7	15.1
Allosteric sigmoidal	788.1	18.8	NA	1.8	0.97	0.97	5.1	1.0	1.0	8.4
Second replicate										
Michaelis-Menten	6954.0	65.0	NA	NA	0.99	0.98	4.0	0.8	0.8	6.5
Substrate inhibition	Unstable	27163017671137.0	0.0	NA	0.99	0.98	3.9	0.9	0.7	15.6
Allosteric sigmoidal	1622.0	40.4	NA	1.4	0.99	0.99	2.6	0.7	0.6	12.3
Third replicate										
Michaelis-Menten	4328.0	67.0	NA	NA	0.97	0.96	12.9	1.5	1.4	15.8
Substrate inhibition	Unstable	2989000000000000.0	Unstable	NA	0.97	0.95	12.9	1.6	1.4	25.1
Allosteric sigmoidal	Unstable	21680.0	NA	1.1	0.97	0.96	10.5	1.4	1.2	23.5

The protein concentration and incubation time representing linear, initial velocity enzymatic conditions for human recombinant SULT1A3 were 1 µg/mL and 20 minutes, respectively.

Curve fittings were conducted using GraphPad Prism 9.0.0 (GraphPad Software, San Diego, CA, USA). The final model is based on the best of three replicates (please note substrate inhibition and allosteric sigmoidal models were unstable).

Abbreviation(s): *AIC*, Akaike information criterion; *h*, the Hill slope; K_m, the concentration of *p*-cresol at half maximum reaction rate; K_{si}, the dissociation constant for substrate inhibition; *NA*, not available; R^2, coefficient of determination; *RMSE*, root mean square error; *SULT*, sulfotransferase; *Sy.x*, root mean square; V_{max}, the maximum reaction rate.

Table S VII-5 Statistical testing results of enzyme kinetic curve fittings for human recombinant SULT1B1

	K_m, µM	V_{max}, nmol/mg/min	K_{si}, µM	h	R^2	Adjusted R^2	Sum of Squares	Sy.x	RMSE	AIC
First replicate										
Michaelis-Menten	226.1	1.2	NA	NA	0.92	0.91	0.07	0.10	0.09	-33.0
Substrate inhibition	2656.0	7.6	246.9	NA	0.99	0.98	0.01	0.05	0.04	-40.4
Allosteric sigmoidal	189.7	1.0	NA	2.2	0.97	0.96	0.03	0.07	0.06	-33.4
Second replicate										
Michaelis-Menten	254.4	1.1	NA	NA	0.94	0.93	0.04	0.08	0.07	-37.2
Substrate inhibition	2427.0	6.8	274.8	NA	0.97	0.96	0.02	0.06	0.05	-38.8
Allosteric sigmoidal	203.5	0.9	NA	1.7	0.96	0.94	0.03	0.07	0.06	-32.7
Third replicate										
Michaelis-Menten	190.1	1.0	NA	NA	0.92	0.91	0.05	0.09	0.08	-35.3
Substrate inhibition	2519.5	6.9	257.9	NA	0.96	0.95	0.03	0.06	0.06	-36.9
Allosteric sigmoidal	171.7	0.9	NA	1.6	0.94	0.92	0.04	0.09	0.07	-29.7

The protein concentration and incubation time representing linear, initial velocity enzymatic conditions for human recombinant SULT1B1 were 4 µg/mL and 20 minutes, respectively.

Curve fittings were conducted using GraphPad Prism 9.0.0 (GraphPad Software, San Diego, CA, USA). The final model is based on the best of three replicates.

Abbreviation(s): *AIC*, Akaike information criterion; *h*, the Hill slope; K_m, the concentration of *p*-cresol at half maximum reaction rate; K_{si}, the dissociation constant for substrate inhibition; *NA*, not available; R^2, coefficient of determination; *RMSE*, root mean square error; *SULT*, sulfotransferase; *Sy.x*, root mean square; V_{max}, the maximum reaction rate.

Table S VII-6 Statistical testing results of enzyme kinetic curve fittings for human recombinant SULT1E1

	K_m, µM	V_{max}, nmol/mg/min	K_{si}, µM	h	R^2	Adjusted R^2	Sum of Squares	Sy.x	RMSE	AIC
First replicate										
Michaelis-Menten	3266.0	10.7	NA	NA	0.999	0.998	0.01	0.06	0.03	-20.2
Substrate inhibition	10151.0	29.2	2148.0	NA	0.998	0.997	0.03	0.09	0.07	-9.7
Allosteric sigmoidal	1775.0	7.7	NA	1.2	0.999	0.998	0.02	0.07	0.06	-12.6
Second replicate										
Michaelis-Menten	1879.0	9.2	NA	NA	0.984	0.981	0.33	0.26	0.24	-7.3
Substrate inhibition	2243.0	10.5	24352.0	NA	0.984	0.976	0.33	0.29	0.23	6.6
Allosteric sigmoidal	1167.0	7.2	NA	1.3	0.986	0.980	0.28	0.27	0.22	5.6
Third replicate										
Michaelis-Menten	1646.0	8.5	NA	NA	0.999	0.998	0.02	0.07	0.06	-13.8
Substrate inhibition	4474.0	19.0	2840.0	NA	0.997	0.996	0.06	0.12	0.10	-5.6
Allosteric sigmoidal	949.7	6.4	NA	1.4	0.993	0.992	0.13	0.16	0.15	-12.2

The protein concentration and incubation time representing linear, initial velocity enzymatic conditions for human recombinant SULT1E1 were 2 µg/mL and 20 minutes, respectively.

Curve fittings were conducted using GraphPad Prism 9.0.0 (GraphPad Software, San Diego, CA, USA). The final model is based on the best of three replicates.

Abbreviation(s): *AIC*, Akaike information criterion; *h*, the Hill slope; K_m, the concentration of *p*-cresol at half maximum reaction rate; K_{si}, the dissociation constant for substrate inhibition; *NA*, not available; R^2, coefficient of determination; *RMSE*, root mean square error; *SULT*, sulfotransferase; *Sy.x*, root mean square; V_{max}, the maximum reaction rate.

Table S VII-7 Statistical testing results of enzyme kinetic curve fittings for human recombinant SULT1A1*2

	K_m, µM	V_{max}, nmol/mg/min	K_{si}, µM	h	R^2	Adjusted R^2	Sum of Squares	Sy.x	RMSE	AIC
First replicate										
Michaelis-Menten	22.4	113.5	NA	NA	0.76	0.74	7114	25.4	24.4	90.6
Substrate inhibition	117.2	251.0	513.0	NA	0.97	0.97	832	9.1	8.3	67.1
Allosteric sigmoidal	31.9	108.9	NA	2.3	0.82	0.78	5396	23.2	21.2	91.4
Second replicate										
Michaelis-Menten	23.9	138.6	NA	NA	0.81	0.80	7564	26.2	25.1	91.4
Substrate inhibition	69.0	221.8	1078.0	NA	0.93	0.92	2664	16.3	14.9	82.2
Allosteric sigmoidal	32.2	132.1	NA	2.3	0.87	0.84	5364	23.2	21.1	91.3
Third replicate										
Michaelis-Menten	23.7	148.3	NA	NA	0.83	0.81	7998	27.0	25.8	92.2
Substrate inhibition	58.3	219.1	1367.0	NA	0.92	0.91	3563	18.9	17.2	86.0
Allosteric sigmoidal	31.5	141.2	NA	2.3	0.88	0.85	5609	23.7	21.6	91.9

The protein concentration and incubation time representing linear, initial velocity enzymatic conditions for human recombinant SULT1A1*2 were 20 µg/mL and 15 minutes, respectively.

Curve fittings were conducted using GraphPad Prism 9.0.0 (GraphPad Software, San Diego, CA, USA). The final model is based on the best of three replicates.

Abbreviation(s): *AIC*, Akaike information criterion; *h*, the Hill slope; K_m, the concentration of *p*-cresol at half maximum reaction rate; K_{si}, the dissociation constant for substrate inhibition; *NA*, not available; R^2, coefficient of determination; *RMSE*, root mean square error; *SULT*, sulfotransferase; *Sy.x*, root mean square; V_{max}, the maximum reaction rate.

Table S VII-8 Statistical testing results of enzyme kinetic curve fittings for pooled human liver cytosols

	K_m, µM	V_{max}, nmol/mg/min	K_{si}, µM	h	R^2	Adjusted R^2	Sum of Squares	Sy.x	RMSE	AIC
First replicate										
Michaelis-Menten	11.5	1.7	NA	NA	0.967	0.964	0.149	0.112	0.107	-75.2
Substrate inhibition	11.5	1.7	Unstable	NA	0.967	0.961	0.149	0.116	0.107	-51.2
Allosteric sigmoidal	16.1	1.9	NA	0.6	0.992	0.990	0.038	0.059	0.054	-70.2
Second replicate										
Michaelis-Menten	18.2	1.4	NA	NA	0.994	0.993	0.021	0.042	0.040	-82.8
Substrate inhibition	18.2	1.4	Unstable	NA	0.994	0.992	0.021	0.043	0.040	-78.8
Allosteric sigmoidal	21.6	1.4	NA	0.8	0.992	0.988	0.049	0.051	0.042	-79.0
Third replicate										
Michaelis-Menten	14.8	1.3	NA	NA	0.993	0.992	0.022	0.043	0.042	-81.7
Substrate inhibition	15.1	1.3	90051.0	NA	0.993	0.992	0.022	0.045	0.041	-77.7
Allosteric sigmoidal	16.1	1.4	NA	0.9	0.990	0.990	0.054	0.047	0.034	-73.0

The protein concentration and incubation time representing linear, initial velocity enzymatic conditions for pooled human liver cytosols were 200 µg/mL and 10 minutes, respectively.

Curve fittings were conducted using GraphPad Prism 9.0.0 (GraphPad Software, San Diego, CA, USA). The final model is based on the best of three replicates (please note the substrate inhibition model was unstable).

Abbreviation(s): *AIC*, Akaike information criterion; *h*, the Hill slope; K_m, the concentration of *p*-cresol at half maximum reaction rate; K_{si}, the dissociation constant for substrate inhibition; *NA*, not available; R^2, coefficient of determination; *RMSE*, root mean square error; *Sy.x*, root mean square; V_{max}, the maximum reaction rate.

Table S VII-9 Statistical testing results of enzyme kinetic curve fittings for pooled human kidney cytosols

	K_m, μM	V_{max}, nmol/mg/min	K_{si}, μM	h	R^2	Adjusted R^2	Sum of Squares	Sy.x	RMSE	AIC
First replicate										
Michaelis-Menten	0.18	0.14	NA	NA	0.73	0.70	0.007	0.025	0.024	-97.3
Substrate inhibition	0.26	0.15	1233.0	NA	0.86	0.84	0.004	0.018	0.017	-103.0
Allosteric sigmoidal	0.29	0.14	NA	2.4	0.78	0.74	0.006	0.023	0.021	-96.4
Second replicate										
Michaelis-Menten	0.18	0.15	NA	NA	0.63	0.60	0.013	0.033	0.032	-89.1
Substrate inhibition	0.31	0.17	744.4	NA	0.82	0.79	0.006	0.024	0.022	-95.2
Allosteric sigmoidal	Unstable	0.28	NA	0.0	0.49	0.39	0.019	0.041	0.038	-80.3
Third replicate										
Michaelis-Menten	0.18	0.21	NA	NA	0.63	0.60	0.027	0.047	0.046	-79.2
Substrate inhibition	0.31	0.24	757.6	NA	0.82	0.78	0.013	0.035	0.032	-85.1
Allosteric sigmoidal	Unstable	0.39	NA	0.0	0.48	0.39	0.038	0.058	0.054	-70.4

The protein concentration and incubation time representing linear, initial velocity enzymatic conditions for pooled human kidney cytosols were 150 μg/mL and 15 minutes, respectively.

Curve fittings were conducted using GraphPad Prism 9.0.0 (GraphPad Software, San Diego, CA, USA). The final model is based on the best of three replicates (please note the allosteric sigmoidal model was unstable).

Abbreviation(s): *AIC*, Akaike information criterion; *h*, the Hill slope; K_m, the concentration of *p*-cresol at half maximum reaction rate; K_{si}, the dissociation constant for substrate inhibition; *NA*, not available; R^2, coefficient of determination; *RMSE*, root mean square error; *Sy.x*, root mean square; V_{max}, the maximum reaction rate.

Table S VII-10 Precision and accuracy of p-cresol sulfate in the LC-MS/MS assay

Nominal concentrations, µM	**Intra-day (1), n=5**		**Intra-day (2), n=5**		**Intra-day (3), n=5**		**Inter-day, n=15**	
	CV (%)	Accuracy (%)	CV (%)	Accuracy (%)	CV (%)	Accuracy (%)	CV (%)	Accuracy (%)
319 (high QC)	2.39	91.37	1.73	90.26	4.83	101.84	6.53	94.49
213 (medium QC)	1.49	93.03	1.01	91.90	2.56	104.12	6.17	96.35
0.01 (low QC)	2.10	113.10	4.08	111.61	9.95	114.67	6.02	113.13
0.003 (LLOQ)	14.75	93.78	16.81	92.07	15.12	109.38	16.58	98.41

Abbreviation(s): *CV*, coefficient of variation; *LC-MS/MS*, liquid chromatography with tandem mass spectrometry; *LLOQ*, lower limit of quantification; *QC*, quality control.

Table S VII-11 Stability tests of p-cresol sulfate in the LC-MS/MS assay

Nominal concentrations, μM	Autosampler stability (%)	Bench-top stability (%)	Freeze-thaw stability (%)	One-week stability (%)
319 (high QC)	94.84	96.58	96.92	97.45
0.01 (low QC)	87.48	92.82	89.63	92.43

The stabilities were tested under the following conditions: i) autosampler storage (24 hours at 4 °C); ii) bench-top storage (6 hours at room temperature, i.e. 23.5 °C); iii) freeze-thaw stability (1 cycle of freezing [i.e. stored at -80 °C for 23.5 hours]-thawing [i.e. stored at room temperature for 0.5 hour]); and iv) one-week stability (stored at -80 °C for one week).

Abbreviation(s): *LC-MS/MS*, liquid chromatography with tandem mass spectrometry; *QC*, quality control.

A

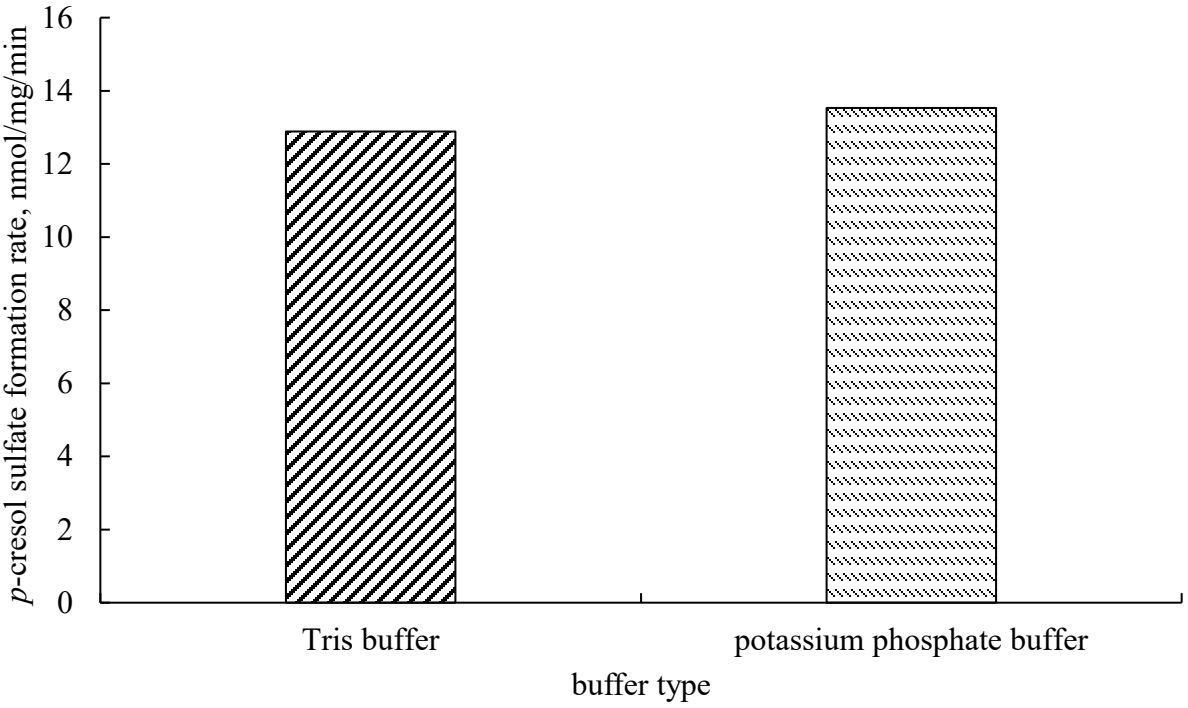
16
14
12
10
8
6
4
2
0
p-cresol sulfate formation rate, nmol/mg/min
Tris buffer
potassium phosphate buffer
buffer type

B

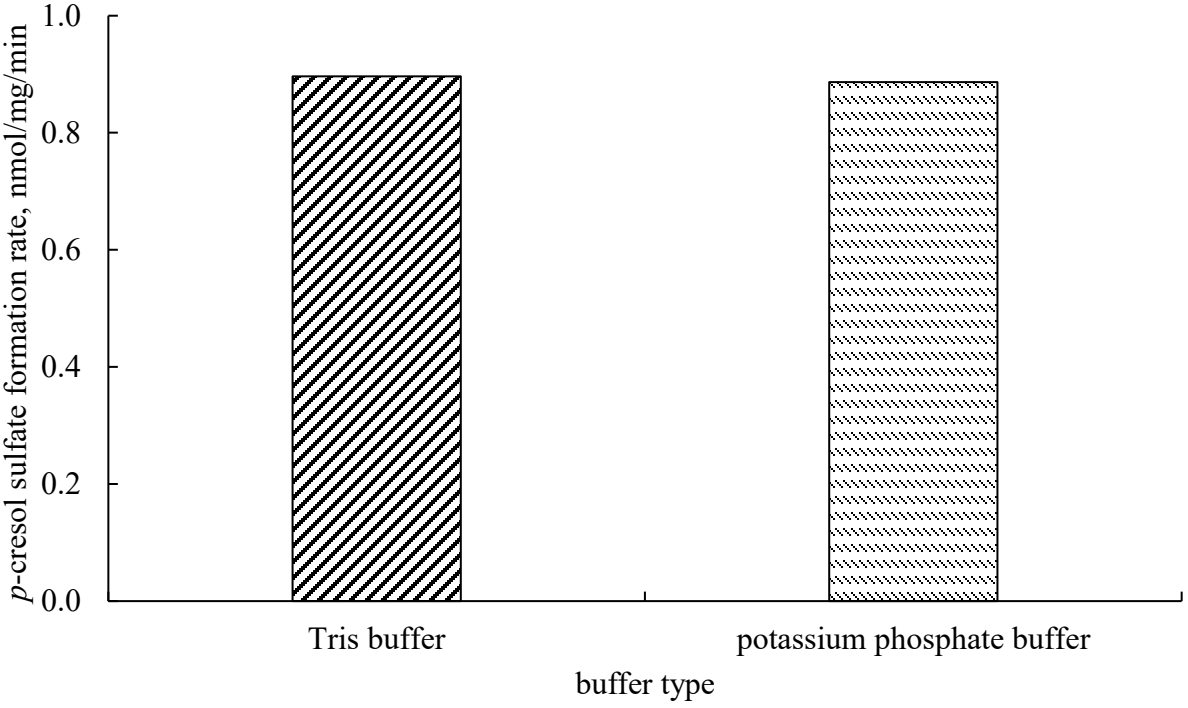
1.0
0.8
0.6
0.4
0.2
0.0
p-cresol sulfate formation rate, nmol/mg/min
Tris buffer
potassium phosphate buffer
buffer type

C

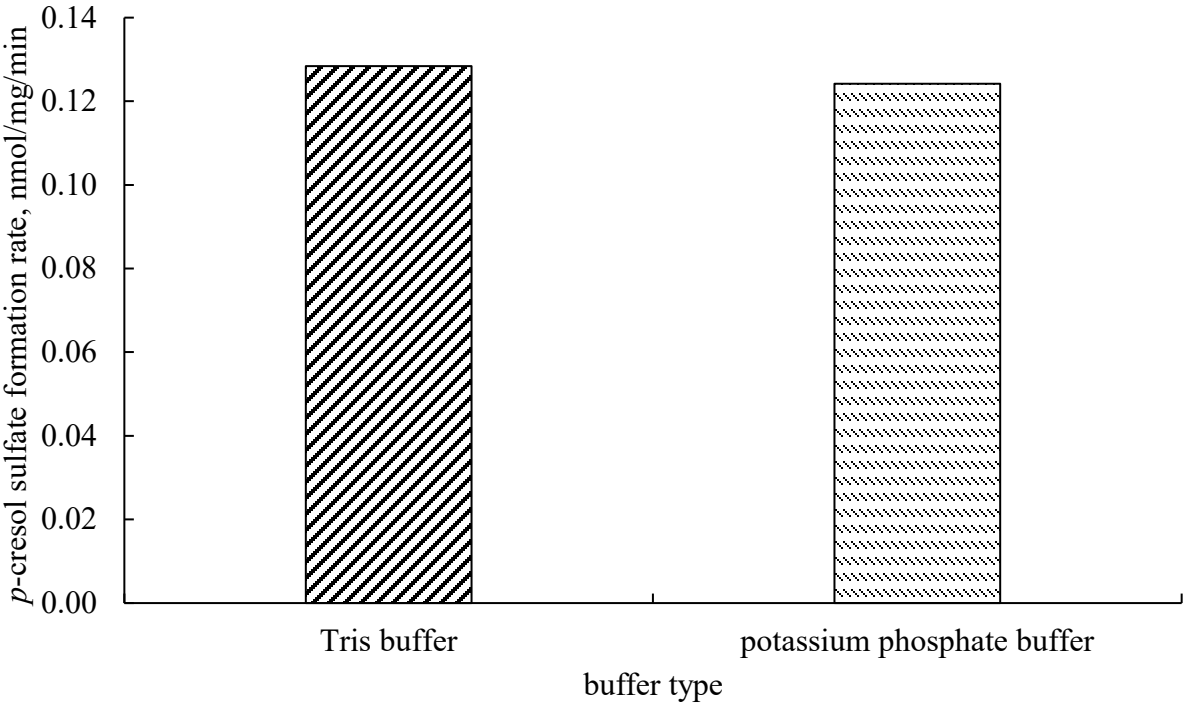

Figure S VII-1 Optimization of buffer type in the reaction mixtures

A. Human recombinant SULT1A1; B. pooled human liver cytosols; C. pooled human kidney cytosols.

The protein concentrations and incubation times representing linear, initial velocity enzymatic conditions were: human recombinant SULT1A1 (1 μg/mL, 15 minutes); pooled human liver cytosols (200 μg/mL, 10 minutes); and pooled human kidney cytosols (150 μg/mL, 15 minutes).

The *p*-cresol concentration utilized was 0.2 μM (human recombinant SULT1A1), 15 μM (pooled human liver cytosols), and 1 μM (pooled human kidney cytosols).

Data are presented as the average values from 2 replicates.

Abbreviation(s): *SULT*, sulfotransferase.

A

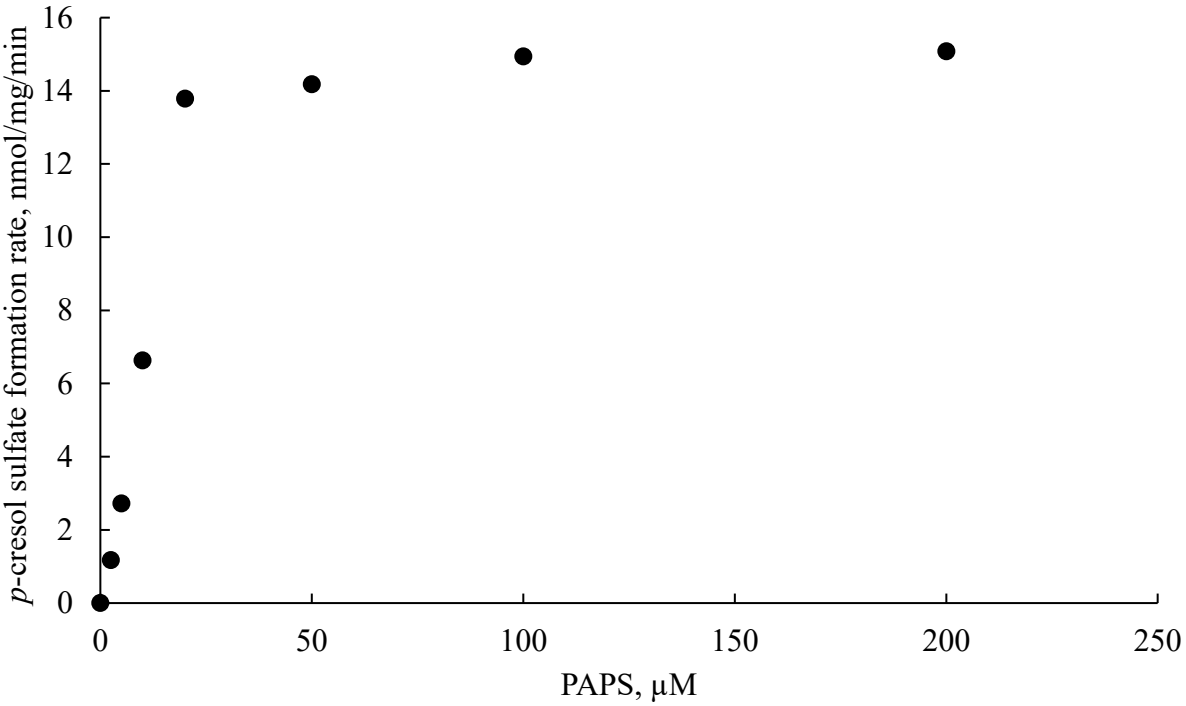
16
14
12
10
8
6
4
2
0
p-cresol sulfate formation rate, nmol/mg/min
0
50
100
150
200
250
PAPS, μM

B

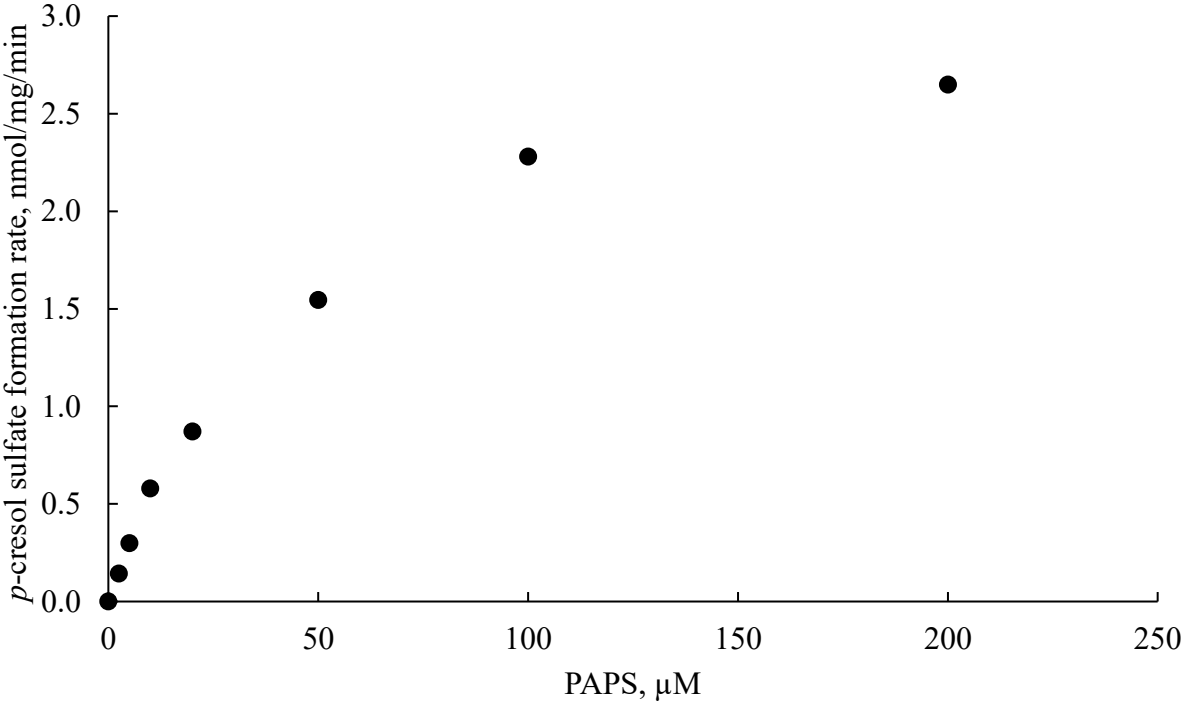
3.0
2.5
2.0
1.5
1.0
0.5
0.0
p-cresol sulfate formation rate, nmol/mg/min
0
50
100
150
200
250
PAPS, μM

C

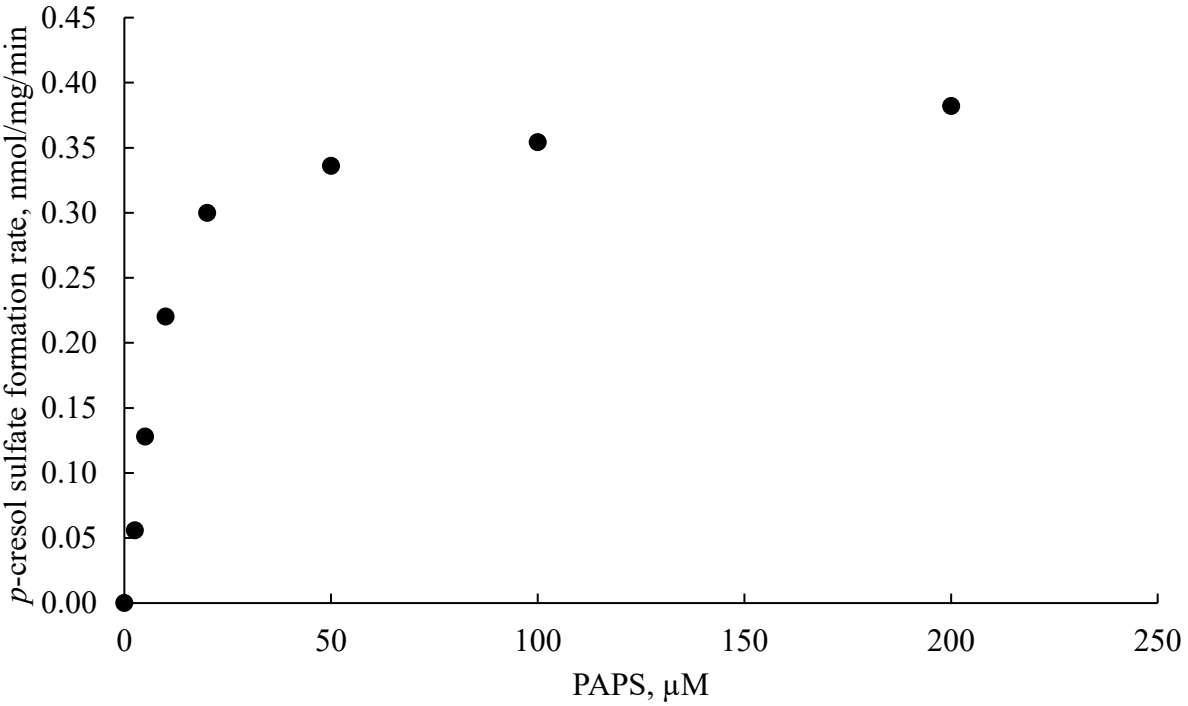

Figure S VII-2 Optimization of PAPS concentrations in the reaction mixtures

A. Human recombinant SULT1A1; B. pooled human liver cytosols; C. pooled human kidney cytosols.

The protein concentrations and incubation times representing linear, initial velocity enzymatic conditions were: human recombinant SULT1A1 (1 µg/mL, 15 minutes); pooled human liver cytosols (200 µg/mL, 10 minutes); and pooled human kidney cytosols (150 µg/mL, 15 minutes).

The *p*-cresol concentration utilized was 0.2 µM (human recombinant SULT1A1), 15 µM (pooled human liver cytosols), and 1 µM (pooled human kidney cytosols).

Data are presented as the average values from 2 replicates.

Abbreviation(s): *PAPS*, 3'-phosphoadenosine-5'-phosphosulfate; *SULT*, sulfotransferase.

A

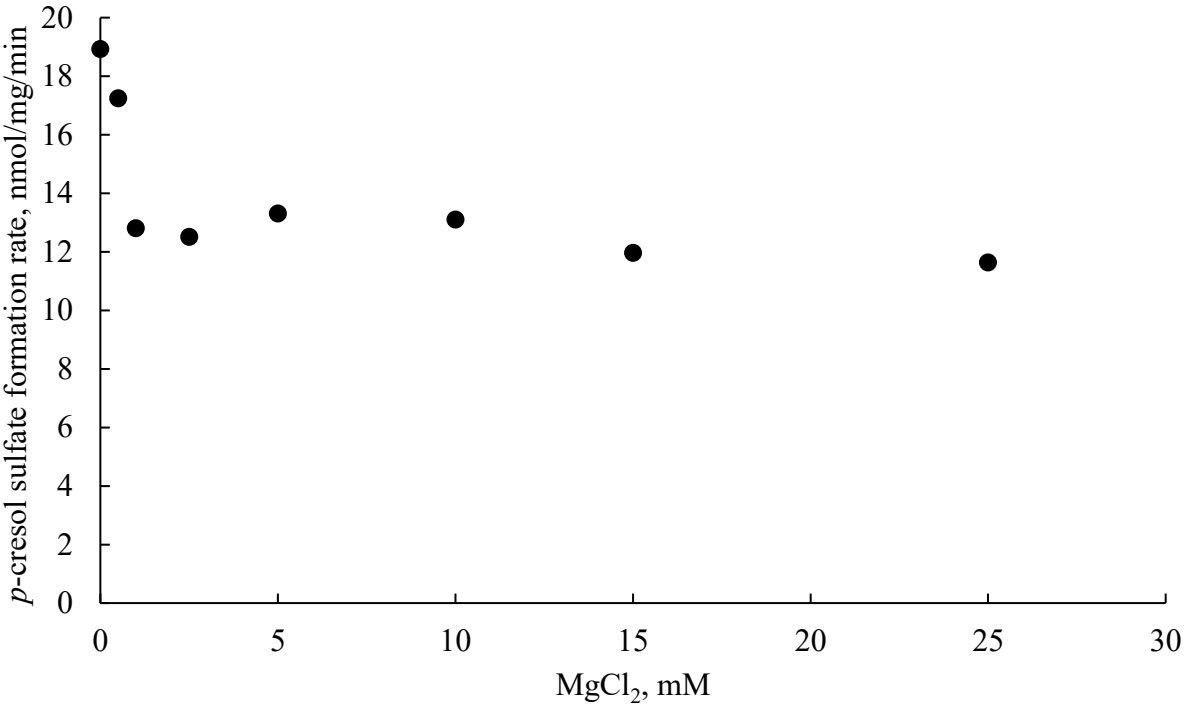
20
18
16
14
12
10
8
6
4
2
0
p-cresol sulfate formation rate, nmol/mg/min
0
5
10
15
20
25
30
MgCl2, mM

B

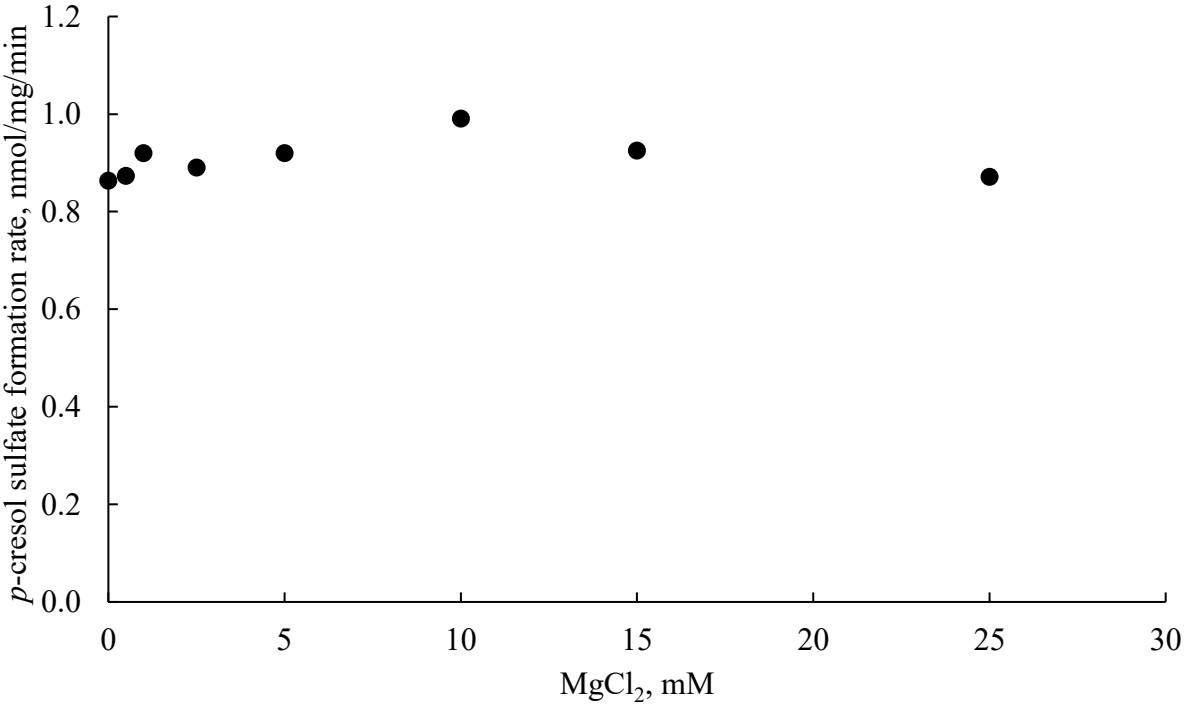
1.2
1.0
0.8
0.6
0.4
0.2
0.0
p-cresol sulfate formation rate, nmol/mg/min
0
5
10
15
20
25
30
MgCl2, mM

C

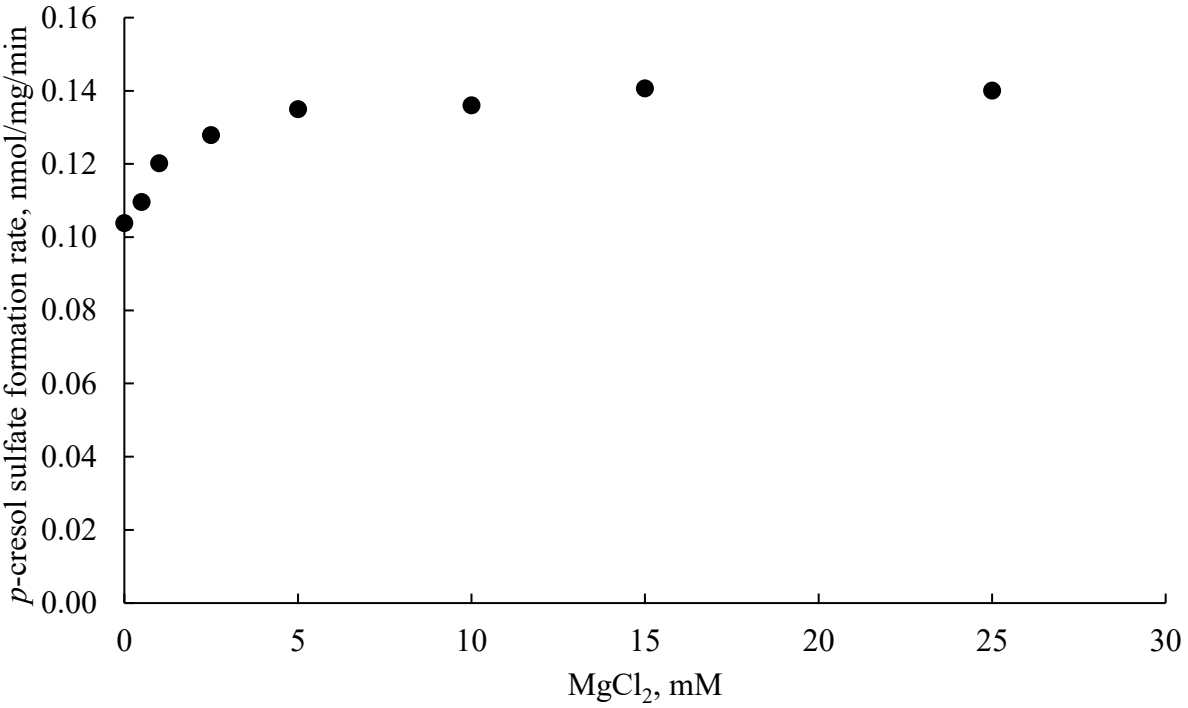

Figure S VII-3 Optimization of $MgCl_2$ concentrations in the reaction mixtures

A. Human recombinant SULT1A1; B. pooled human liver cytosols; C. pooled human kidney cytosols.

The protein concentrations and incubation times representing linear, initial velocity enzymatic conditions were: human recombinant SULT1A1 (1 µg/mL, 15 minutes); pooled human liver cytosols (200 µg/mL, 10 minutes); and pooled human kidney cytosols (150 µg/mL, 15 minutes).

The *p*-cresol concentration utilized was 0.2 µM (human recombinant SULT1A1), 15 µM (pooled human liver cytosols), and 1 µM (pooled human kidney cytosols).

Data are presented as the average values from 2 replicates.

Abbreviation(s): *SULT*, sulfotransferase.

A

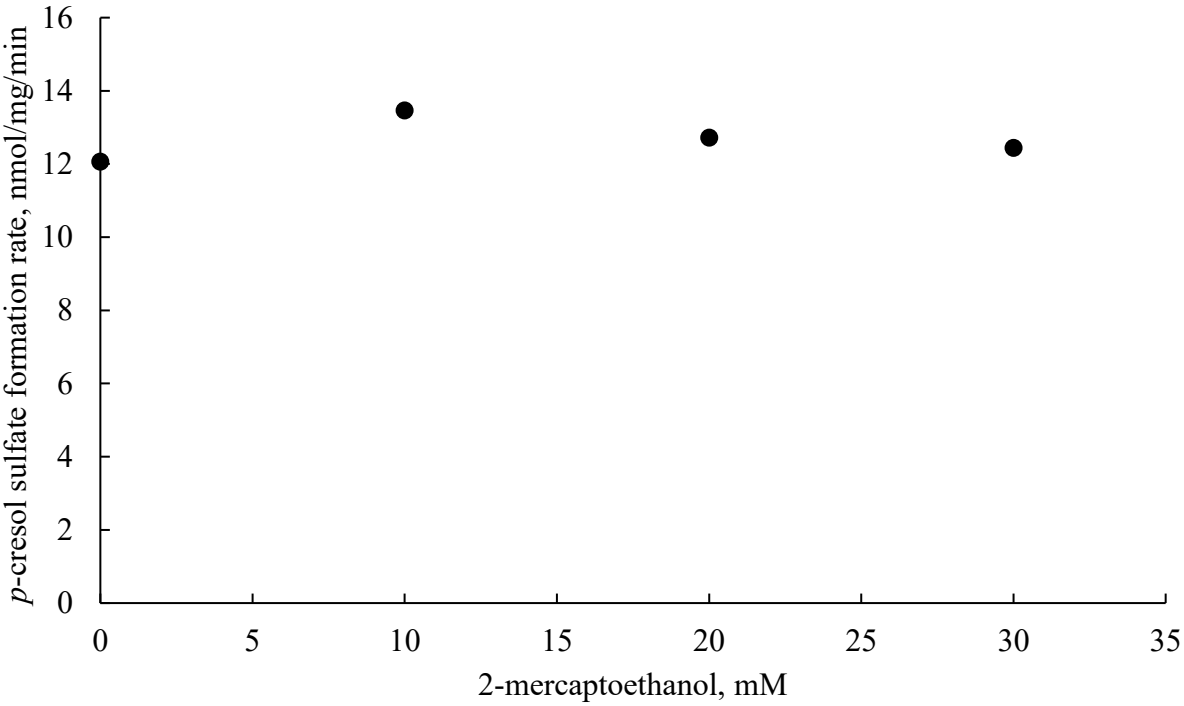
16
14
12
10
8
6
4
2
0
p-cresol sulfate formation rate, nmol/mg/min
0
5
10
15
20
25
30
35
2-mercaptoethanol, mM

B

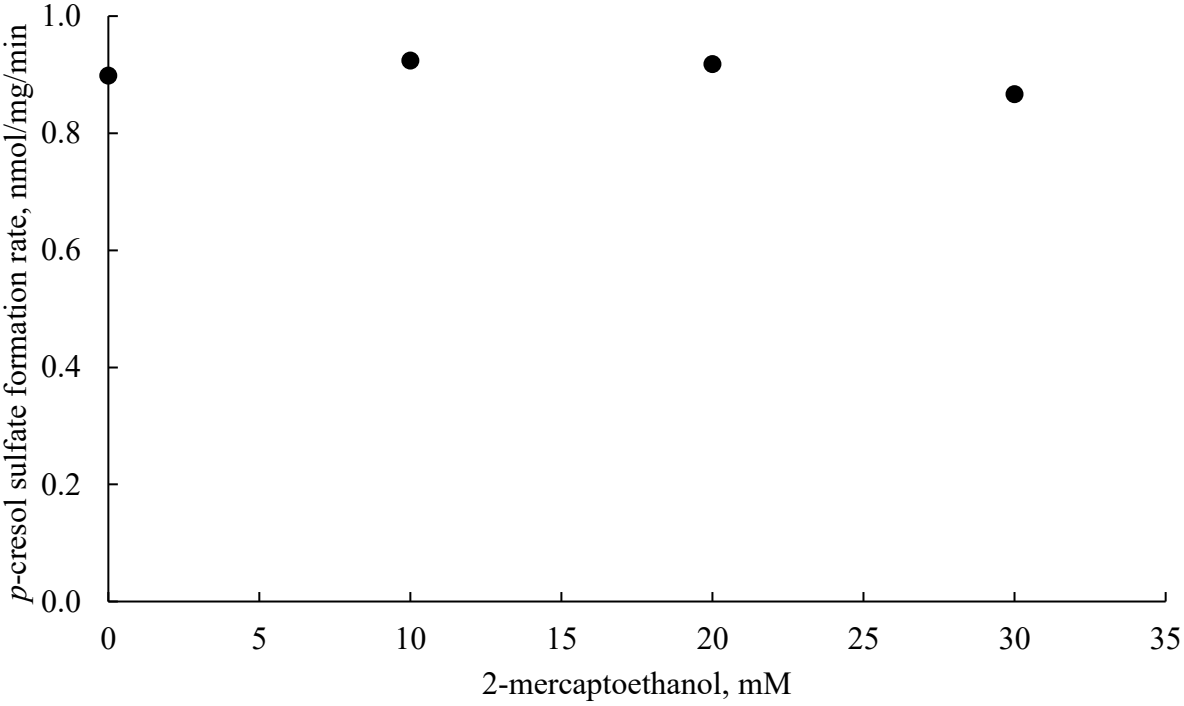
1.0
0.8
0.6
0.4
0.2
0.0
p-cresol sulfate formation rate, nmol/mg/min
0
5
10
15
20
25
30
35
2-mercaptoethanol, mM

C

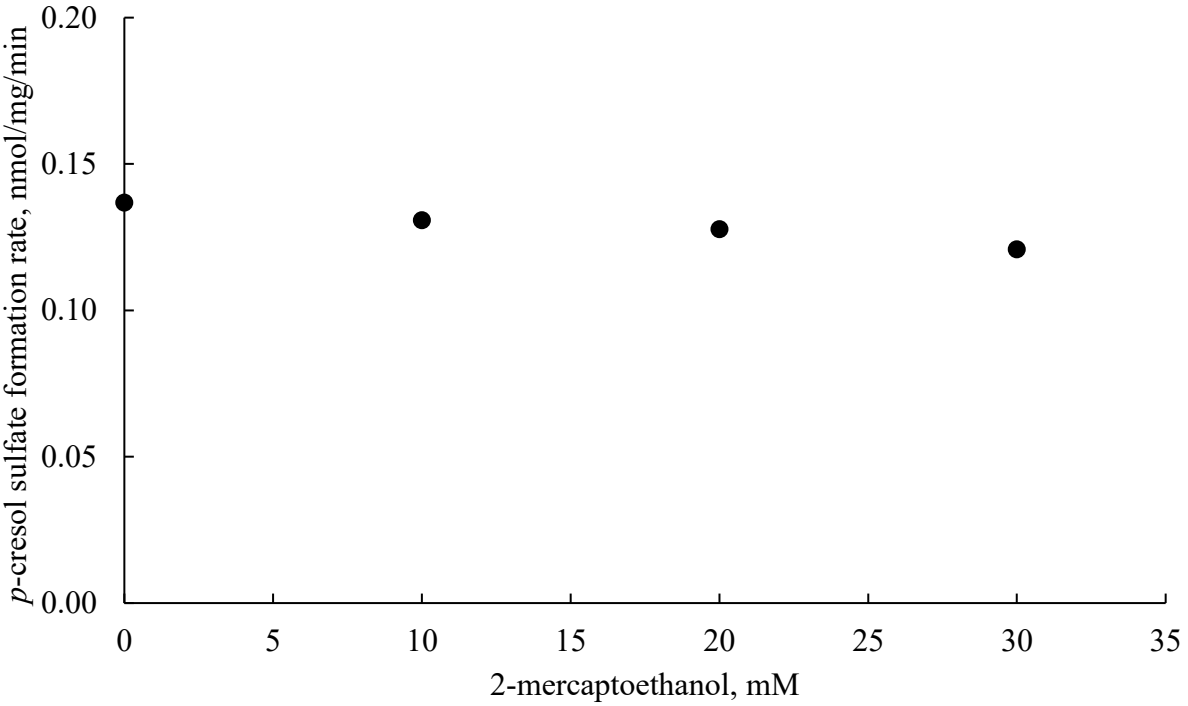

Figure S VII-4 Optimization of 2-mercaptoethanol concentrations in the reaction mixtures

A. Human recombinant SULT1A1; B. pooled human liver cytosols; C. pooled human kidney cytosols.

The protein concentrations and incubation times representing linear, initial velocity enzymatic conditions were: human recombinant SULT1A1 (1 μg/mL, 15 minutes); pooled human liver cytosols (200 μg/mL, 10 minutes); and pooled human kidney cytosols (150 μg/mL, 15 minutes).

The *p*-cresol concentration utilized was 0.2 μM (human recombinant SULT1A1), 15 μM (pooled human liver cytosols), and 1 μM (pooled human kidney cytosols).

Data are presented as the average values from 2 replicates.

Abbreviation(s): *SULT*, sulfotransferase.

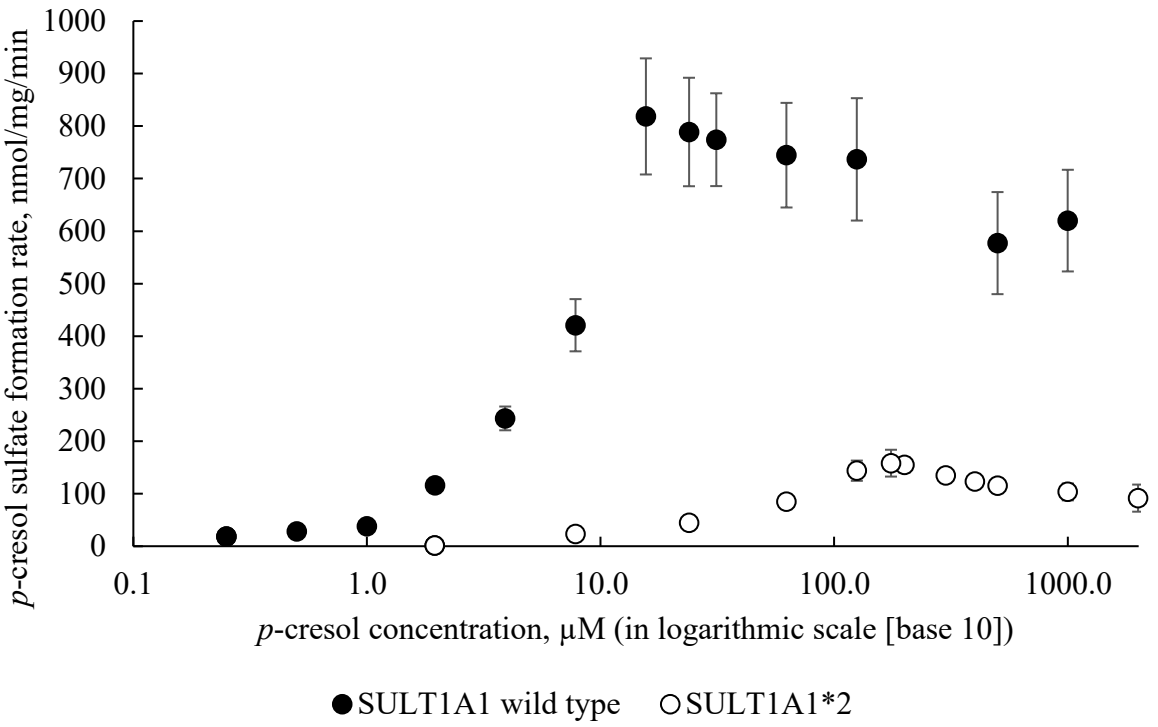

Figure S VII-5 Enzyme kinetics of p-cresol sulfate formation in human recombinant SULT1A1 (wild type) and SULT1A1*2 (in logarithmic scale [base 10])

The protein concentrations and incubation times representing linear, initial velocity enzymatic conditions were: human recombinant SULT1A1 (1 µg/mL, 15 minutes); and human recombinant SULT1A1*2 (20 µg/mL, 15 minutes).

Data are presented as mean±standard deviation from 3 replicates.

Enzyme kinetic curve fittings were conducted using GraphPad Prism 9.0.0 (GraphPad Software, San Diego, CA, USA).

Abbreviation(s): *SULT*, sulfotransferase.

A

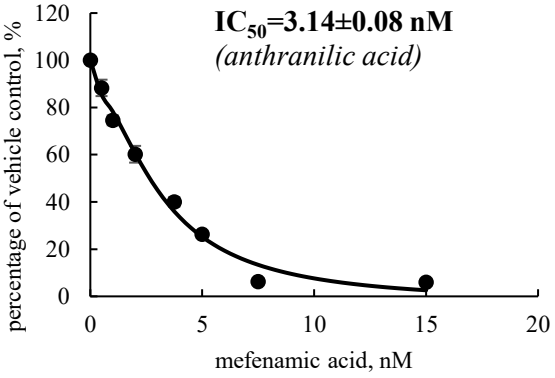
IC50=3.14±0.08 nM
(anthranilic acid)
percentage of vehicle control, %
mefenamic acid, nM

B

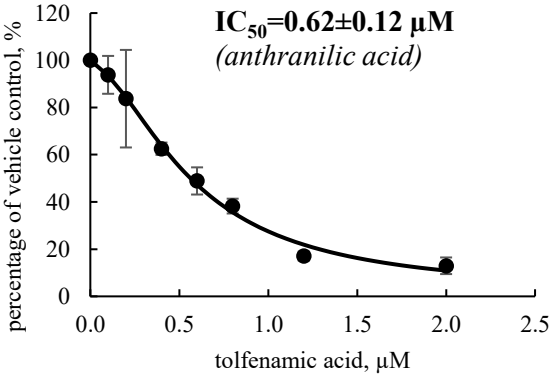
IC50=0.62±0.12 µM
(anthranilic acid)
percentage of vehicle control, %
tolfenamic acid, µM

C

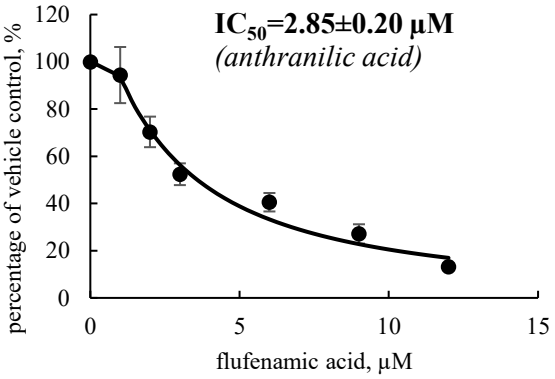
IC50=2.85±0.20 µM
(anthranilic acid)
percentage of vehicle control, %
flufenamic acid, µM

D

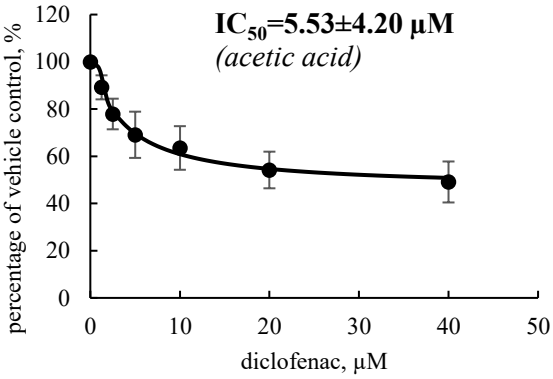
IC50=5.53±4.20 µM
(acetic acid)
percentage of vehicle control, %
diclofenac, µM

E

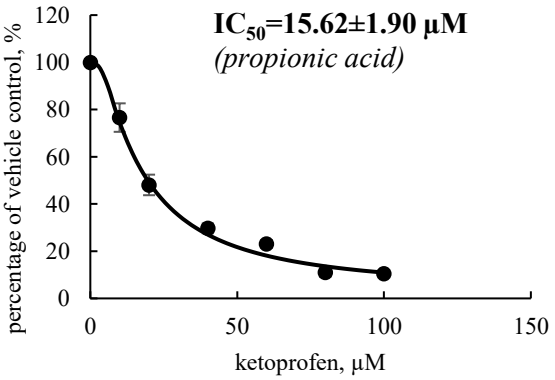
IC50=15.62±1.90 µM
(propionic acid)
percentage of vehicle control, %
ketoprofen, µM

F

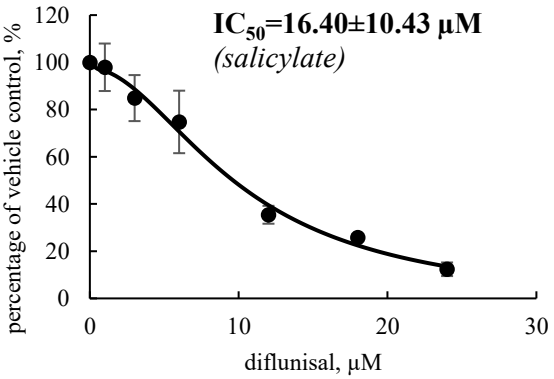
IC50=16.40±10.43 µM
(salicylate)
percentage of vehicle control, %
diflunisal, µM

G

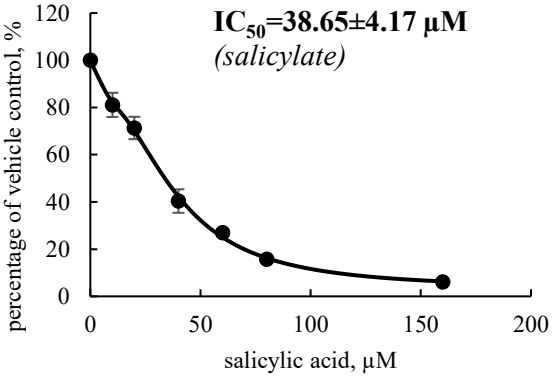
IC50=38.65±4.17 µM
(salicylate)
percentage of vehicle control, %
salicylic acid, µM

H

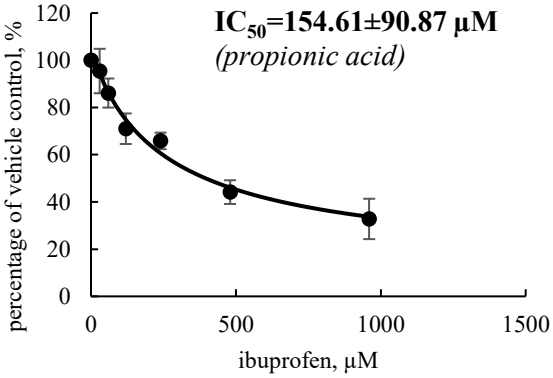
IC50=154.61±90.87 µM
(propionic acid)
percentage of vehicle control, %
ibuprofen, µM

I

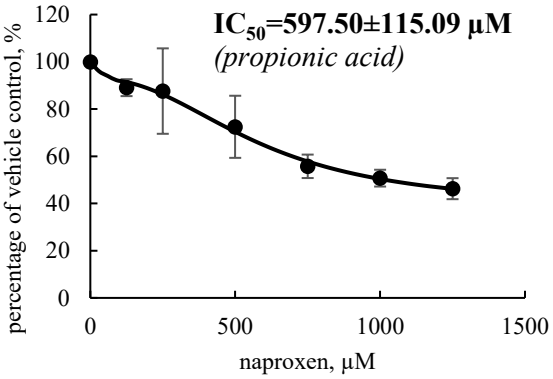
IC50=597.50±115.09 µM
(propionic acid)
percentage of vehicle control, %
naproxen, µM

J

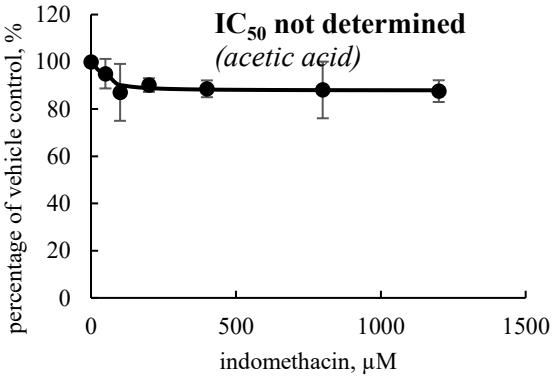
IC50 not determined
(acetic acid)
percentage of vehicle control, %
indomethacin, µM

K

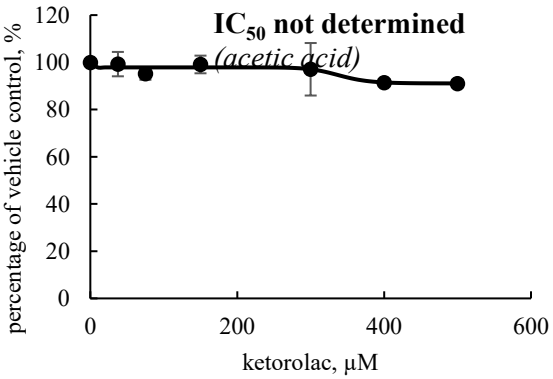
IC50 not determined
(acetic acid)
percentage of vehicle control, %
ketorolac, µM

L

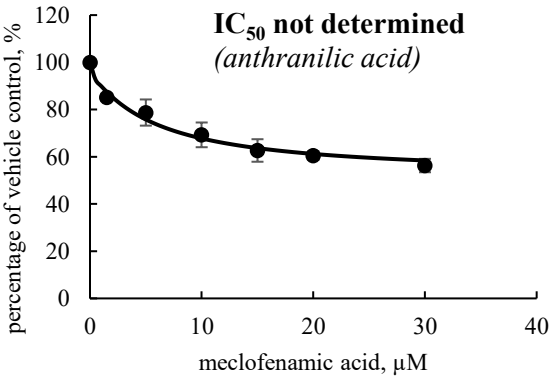
IC50 not determined
(anthranilic acid)
percentage of vehicle control, %
meclofenamic acid, µM

M **N**

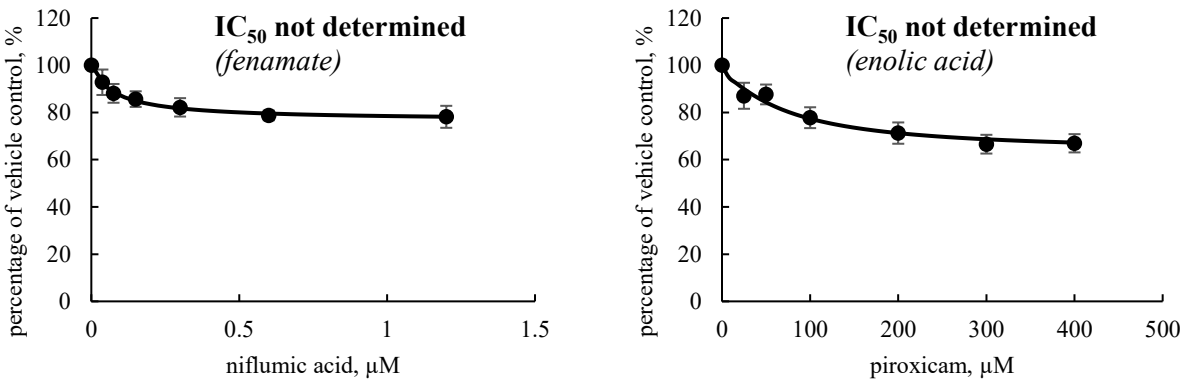

Figure S VII-6 The relative potencies of selected therapeutic chemical inhibitors in the formation of p-cresol sulfate in human recombinant SULT1A1

A. Mefenamic acid (in 0.1% methanol); B. tolfenamic acid; C. flufenamic acid (in 0.4% ethanol); D. diclofenac; E. ketoprofen (in 0.4% ethanol); F. diflunisal (in 0.4% ethanol); G. salicylic acid; H. ibuprofen (in 0.4% ethanol); I. naproxen (in 0.4% ethanol); J. indomethacin (in 0.1% methanol); K. ketorolac; L. meclofenamic acid (in 0.4% ethanol); M. niflumic acid; N. piroxicam (in 0.4% DMSO).

The relative inhibition potencies were characterized with IC_{50} values using 0.2 µM (~K_m value) *p*-cresol concentration as described in **2. Materials and methods**. IC_{50} values were not calculated when the maximum inhibitions were < 50% of the control.

The protein concentration and incubation time representing linear, initial velocity enzymatic conditions for human recombinant SULT1A1 were 1 µg/mL and 15 minutes, respectively. If organic solvents were utilized to dissolve the inhibitors, the control also contained the same concentration of the organic solvent.

Data are presented as mean±standard deviation from 3 replicates.

Curve fittings were conducted using GraphPad Prism 9.0.0 (GraphPad Software, San Diego, CA, USA).

Abbreviation(s): *DMSO*, dimethyl sulfoxide; *IC_{50}*, half-maximum inhibitory concentration; *SULT*, sulfotransferase.

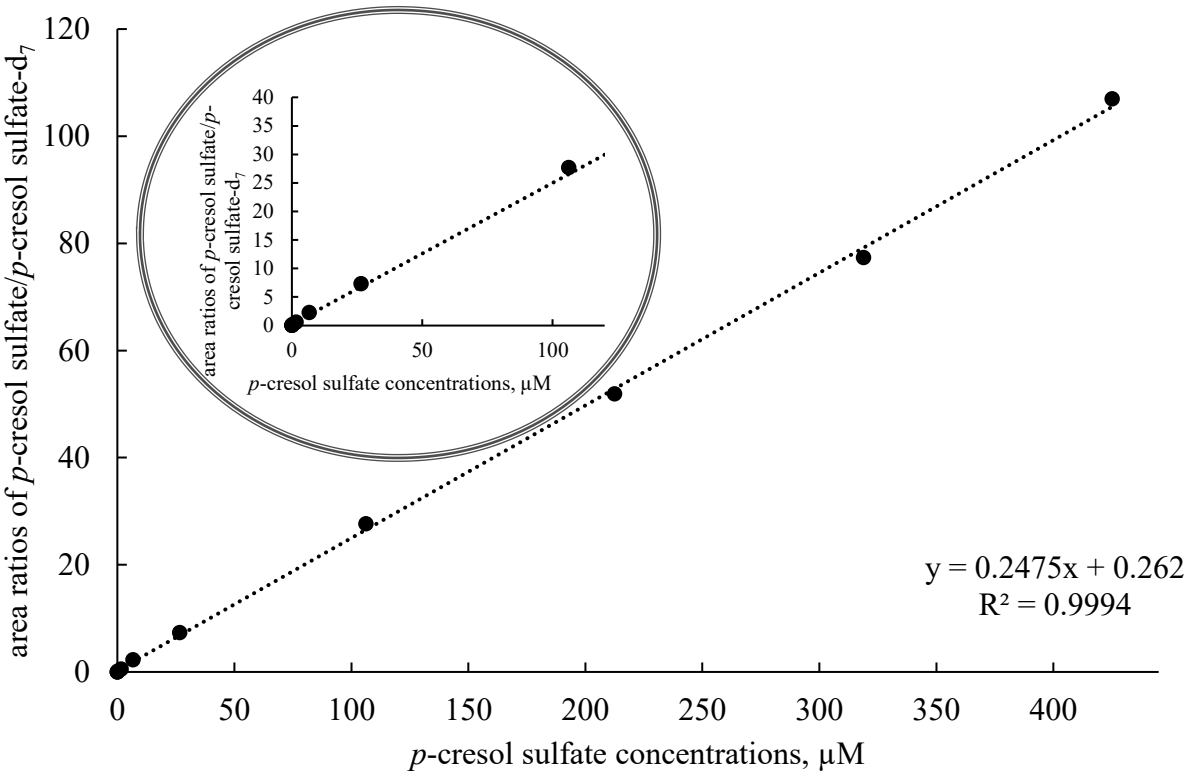

Figure S VII-7 Representative calibration curve of p-cresol sulfate from the LC-MS/MS assay

p-Cresol sulfate-d_7 was utilized as the internal standard.

The m/z transitions of *p*-cresol sulfate and *p*-cresol sulfate-d_7 were 187.00→107.00 and 194.10→114.15, respectively, as described in **2. Materials and methods**. A weighted ($1/x^2$) least - squares linear regression model was utilized.

Abbreviation(s): *LC-MS/MS*, liquid chromatography with tandem mass spectrometry; *m/z*, mass to charge ratio; R^2, coefficient of determination.

Chapter VIII. Characterizations of human UDP-glucuronosyltransferase enzymes in the conjugation of *p*-cresol[8]

Prologue:

In addition to sulfonation (Chapter VII [56]), p-cresol is also extensively conjugated by UGT enzymes in the formation of p-cresol glucuronide. As such, the enzyme kinetics of p-cresol glucuronide were characterized in order to further understand the mechanisms of its interaction with MPA (as described for Chapter VII [56] for p-cresol sulfate). The aim of this chapter was to characterize the relative contributions of UGT enzymes responsible for the formation of p-cresol glucuronide and to determine the clinical variables that could affect this conjugation reaction. As a part of this aim, various in vitro UGT models were characterized and an LC-MS/MS p-cresol glucuronide assay was developed and validated.

[8] This chapter is already published in a peer-reviewed journal. **Rong Y**, Kiang TKL. Characterizations of human UDP-glucuronosyltransferase enzymes in the conjugation of *p*-cresol. *Toxicological Sciences*. 2020 Aug 1;176(2):285-296. doi: 10.1093/toxsci/kfaa072.

Acknowledgement: **Rong Y**, Kiang TKL. Characterizations of human UDP-glucuronosyltransferase enzymes in the conjugation of *p*-cresol. *Toxicological Sciences*. 2020;176(2):285-296. By permission of Oxford University Press, license number: 5222170761912 (for abstract), 5222170957094 (for figures and tables), 5222170870358 (for text extract).

Abstract

p-Cresol is a uremic toxin that is formed by intestinal microbiota and extensively conjugated by first-pass metabolism. *p*-Cresol glucuronide exerts various forms of cellular toxicity *in vitro* and is accumulated in the plasma of subjects with kidney disease, where associations with adverse cardiovascular and renal outcomes are evident. The objective of this study was to determine the contributions of human UDP-glucuronosyltransferase (UGT) enzymes in the formation of *p*-cresol glucuronide. Utilizing commonly expressed hepatic or renal human recombinant UGTs (i.e. hrUGT-1A1, 1A3, 1A4, 1A6, 1A7, 1A8, 1A9, 1A10, 2B4, 2B7, 2B10, 2B15, and 2B17), hrUGT1A6 and hrUGT1A9 exhibited the highest catalytic activities in the generation of *p*-cresol glucuronide. The kinetics of *p*-cresol glucuronide formation in hrUGT1A6 and pooled human liver microsomes were best described by the Hill equation and in hrUGT1A9 and pooled human kidney microsomes by substrate inhibition. Using inhibitory and selective UGT inhibitors (i.e., acetaminophen or amentoflavone for UGT1A6 and niflumic acid for UGT1A9), UGT1A6 was identified the predominant enzyme responsible for *p*-cresol glucuronide production in pooled human liver (78.4-81.3% contribution) and kidney (54.3-62.9%) microsomes, whereas UGT1A9 provided minor contributions (2.8% and 35.5%, respectively). The relative contributions of UGT1A6 (72.6±11.3%, mean±SD) and UGT1A9 (5.7±4.1%) in individual human liver microsomes from 12 adult donors were highly variable, where an inverse association ($R=-0.784$, $p=0.003$) between UGT1A6 contribution and UGT1A9 probe substrate activity (i.e., mycophenolic acid) was evident. Our novel findings provide valuable tools for conducting further mechanistic studies and for designing clinical interventions to mitigate the toxicities associated with *p*-cresol glucuronide.

1. Introduction

p-Cresol and its conjugated metabolites are uremic toxins that are accumulated to relatively high concentrations in plasma/serum of patients with impaired renal function (i.e. chronic kidney disease [75] or kidney transplantation [83, 127-129]). *p*-Cresol is generated from the fermentation of tyrosine and phenylalanine by intestinal bacteria [79]. Once formed, it is subjected to extensive first-pass intestinal and hepatic metabolism in the production of *p*-cresol sulfate and *p*-cresol glucuronide [78], which have been hypothesized to be primarily responsible for mediating the toxic effects of *p*-cresol [82]. The toxic effects of *p*-cresol sulfate have been summarized by numerous investigators (e.g. [75, 78, 87, 89]) and emerging toxicity data on *p*-cresol glucuronide are also becoming evident. Based on human serum data, the free (i.e. pharmacologically active) concentrations of *p*-cresol glucuronide are similar to or higher than concentrations of *p*-cresol sulfate, suggesting an important role of the glucuronide in mediating the toxicity of *p*-cresol [86, 371, 372].

In human *in vitro* studies, Meert et al. reported the pro-inflammatory effects of *p*-cresol glucuronide as evident by increased oxidative burst activities of human leucocytes when tested in combination with *p*-cresol sulfate [371]. Exogenously administered *p*-cresol glucuronide has also been shown to reduce mitochondrial succinate dehydrogenase activities, change the epithelial cell morphology, and alter the mRNA expressions of transporters (e.g. down-regulating organic anion transporter polypeptide 4C1) in human renal proximal tubule epithelial cells [98, 99]. In primary cultures of human hepatocytes, *p*-cresol glucuronide exposure resulted in decreases in cell viability, total cellular ATP, and mitochondrial membrane potential [92]. These data indicated that *p*-cresol glucuronide can induce toxicity through a variety of mechanisms in different human cellular models.

In clinical studies, both total and free *p*-cresol glucuronide serum concentrations were directly associated with cardiovascular and overall mortality in patients at different stages of chronic kidney disease, suggesting *p*-cresol glucuronide levels may be inversely correlated with patient survival [86]. Moreover, the progression from chronic renal failure to end-stage renal disease was found to be associated with increased *p*-cresol glucuronide and decreased *p*-cresol sulfate plasma levels [98]. Similar findings were reported by Poesen et al., where increased cardiovascular events (e.g. "non-lethal myocardial infarction, myocardial ischemia, coronary intervention, ischemic stroke, or new-onset peripheral vascular disease") and mortality in chronic kidney disease patients corresponded to increased ratios of *p*-cresol glucuronide to *p*-cresol sulfate serum concentrations [84]. Similarly, in chronic kidney disease patients who were not yet symptomatic of cardiac disease, negative associations between total or free *p*-cresol glucuronide levels and cardiac function (e.g. as measured by peak cardiac output, mean arterial pressure, heart rate, and aerobic exercise capacity) were also evident [102]. Despite the correlational nature of the human clinical data, these observations consistently support an association between elevated plasma/serum *p*-cresol glucuronide levels and poor cardiovascular or renal outcomes.

While emerging data are being reported indicating the toxic effects of *p*-cresol glucuronide in various human experimental models, little is known of how this metabolite is enzymatically produced. This information is critical for understanding how *p*-cresol glucuronide mediates its toxic effects in humans. To address this important literature gap, the objective of this study was in determining the roles and contributions of individual human UGT enzymes responsible for the production of *p*-cresol glucuronide using a variety of complementary *in vitro* models. As *p*-cresol is extensively metabolized to *p*-cresol glucuronide in the liver via first-pass metabolism and can be conjugated in the kidney prior to excretion [53, 78, 84], both organs were the focus of the

current investigation. Using data obtained in human recombinant UGT enzymes (hrUGTs), human liver microsomes, and human kidney microsomes, we report novel discoveries on enzyme kinetics, relative contributions of human UGT enzymes, organ-related differences, inter-individual variabilities, and key clinical correlates of *p*-cresol glucuronide formation.

2. Materials and methods

2.1. Chemicals and reagents

p-Cresol, Tris hydrochloride, magnesium chloride ($MgCl_2$), bovine serum albumin (BSA), alamethicin from trichoderda viride, uridine 5'-diphosphate-glucuronic acid (UDPGA), acetaminophen, amentoflavone, niflumic acid, high performance liquid chromatography (HPLC)-grade methanol, HPLC-grade water, and formic acid were purchased from Sigma-Aldrich (Oakville, Ontario, Canada). Tris base was purchased from Fisher Scientific (Ottawa, Ontario, Canada). *p*-Cresol glucuronide and *p*-cresol glucuronide-d_7 (internal standard of *p*-cresol glucuronide) were purchased from Toronto Research Chemicals (North York, Ontario, Canada). Pooled human liver microsomes (pool of 150 adult donors, mixed gender, product number 452117, lot number 38293), 13 human recombinant UGT enzymes (hrUGT 1A1 [product number 456411], hrUGT1A3 [product number 456413], hrUGT1A4 [product number 456414], hrUGT1A6 [product number 456416], hrUGT1A7 [product number 456407], hrUGT1A8 [product number 456418], hrUGT1A9 [product number 456419], hrUGT1A10 [product number 456410], hrUGT2B4 [product number 456424], hrUGT2B7 [product number 456427], hrUGT2B10 [product number 453323], hrUGT2B15 [product number 456435], hrUGT2B17 [product number 456437]), and 12 individual human liver microsomes (catalog number 452138, lot numbers HFC205, HFC208,

HFH617, HFH705, HG18, HG43, HG64, HH13-2, HH37, HH519, HH741, and HH837, representing the entire panel commercially available to us at the time of procurement) were purchased from Corning Gentest (Woburn, Massachusetts, United States). Pooled human kidney microsomes (pool of 8 adult donors, mixed gender, product number H0610.R, lot number 1710160, prepared from whole kidney) were obtained from Xenotech (Kansas City, Missouri, United States).

2.2. General incubation conditions

Linear initial velocity enzymatic conditions with respect to protein concentration and incubation time were optimized for each enzyme system and described in the individual table or figure legends. Human recombinant enzymes or microsomes were pre-treated with pore-forming reagent alamethicin (10 µg/mg protein, to ensure access to UGT active sites within the endoplasmic reticulum [373]) on ice for 30 minutes [55, 297]. The reaction mixture (50 µL) consisting of enzyme, 100 mM Tris buffer (pH=7.4, measured at 37 °C), 10 mM $MgCl_2$, 2% BSA, and *p*-cresol were pre-incubated for 5 minutes in a 37 °C water bath. Enzymatic reaction was initiated by the addition of 50 µL of 5 mM UDPGA (pre-warmed in 37 °C water bath for 5 minutes). The compositions of the incubation mixture were based on optimized conditions described previously [297], with the exception that BSA concentration was modified from 1% to 2% in order for us to utilize an unbound fraction of "0.7" for *p*-cresol [52]. Incubations were terminated by adding 90 µL ice-cold deproteinization solution (containing *p*-cresol glucuonide-d_7 in methanol) to 30 µL of the incubation mixture, and the mixture was placed at room temperature for 20 minutes [308]. For protein removal, the mixture was centrifuged at 4000g for 10 minutes (4 °C) (Eppendorf 5424R centrifuge, Mississauga, Ontario, Canada) after vortex mixing (Fisher Scientific, Ottawa, Ontario, Canada) and sonication (VWR 75D ultrasonic machine, Mississauga, Ontario, Canada).

The supernatant was collected for quantification of metabolite concentrations as described below in **Quantification of *p*-cresol glucuronide using ultra-high performance liquid chromatography tandem mass spectrometry**. Negative control incubations were conducted with hrUGTs, pooled human liver microsomes, or pooled human kidney microsomes in the absence of UDPGA or *p*-cresol.

2.3. Activities of individual human recombinant UGT enzymes in the formation of p-cresol glucuronide

p-Cresol (34.1 μM and 1000 μM, which when multiplied by the unbound fraction of 0.7 [52] corresponded to 23.9 μM [free concentration reported in the human liver [295]] and 700 μM [putative toxic concentration attainable in human plasma [308]]) was incubated with 13 individual hrUGTs (1A1, 1A3, 1A4, 1A6, 1A7, 1A8, 1A9, 1A10, 2B4, 2B7, 2B10, 2B15, and 2B17) known to be expressed in hepatic and renal tissues (based on mRNA and/or protein) [310, 374-379]. The formation rates of *p*-cresol glucuronide were determined under optimized, linear enzymatic conditions. Only hrUGTs that have exhibited relatively high activities in *p*-cresol glucuronide formation were further characterized as discussed below.

2.4. Enzyme kinetics of p-cresol glucuronide formation in hrUGT1A6, hrUGT1A9, pooled human liver microsomes, and pooled human kidney microsomes

In order to characterize the kinetics of *p*-cresol glucuronide formation in each enzyme system, *p*-cresol concentrations (0-700 μM) which cover physiological and toxic concentrations were utilized [295, 308]. The rate of *p*-cresol glucuronide formation vs. the free *p*-cresol incubation

concentration plots were fitted with either “Michaelis-Menten”, “substrate inhibition”, “Hill”, or “isoenzyme (2-enzyme Michaelis-Menten)” kinetic models using SigmaPlot (version 14.0, Systat Software, Inc., San Jose, California, United States). The model of best fit was selected based on statistical testing (i.e. R^2 [coefficient of determination], F-test, and Akaike information criterion) and graphical analysis with Eadie-Hofstee plots [380]. The kinetic constants, K_m (concentration of substrate at which the reaction rate is half of the maximum), V_{max} (maximum reaction rate), and other model-specific parameters (e.g. S_{50} [equivalent to K_m], n [Hill coefficient], and K_{si} [dissociation constant for substrate inhibition]), were generated in SigmaPlot. Intrinsic clearance (CL_{int}) or maximum clearance (CL_{max}) were calculated using Equation VIII-1 for substrate inhibition and Equation VIII-2 for the Hill equation [296, 381, 382],

Equation VIII-1

$$CL_{int} = \frac{V_{max}}{K_m}$$

Equation VIII-2

$$CL_{max} = \frac{V_{max}}{S_{50}} \times \frac{n-1}{n \times (n-1)^{\frac{1}{n}}}$$

where V_{max} is the maximum reaction rate, K_m or S_{50} is the concentration of substrate at which the reaction rate is half of the maximum, and n represents the Hill coefficient.

2.5. Selectivity and potency of chemical inhibitors for reducing the formation of p-cresol glucuronide in hrUGT1A6 and hrUGT1A9

As only hrUGT1A6 and hrUGT1A9 had relatively high catalytic activities in the formation of *p*-cresol glucuronide (Figure VIII-1), the selectivity and potency of chemical inhibitors tailored to these two enzymes were characterized. hrUGT1A6 or hrUGT1A9 were incubated with 23.9 μM (free concentration) *p*-cresol and acetaminophen (0, 100, 500, 1000, and 3000 μM, as a possible inhibitor for UGT1A6 because it was demonstrated as a primary substrate) [298], amentoflavone (0, 10, 25, 50, and 100 μM, as inhibitor for UGT1A6) [383], or niflumic acid (0, 2.5, 10, 25, and 50 μM, as inhibitor for UGT1A9) [298]. The objective was to determine the concentration of each chemical inhibitor associated with maximum inhibition of target enzyme activity (e.g. niflumic acid on UGT1A9) with selectivity (i.e. no effects of niflumic acid on UGT1A6). These conditions were subsequently used to determine the relative contributions of each UGT enzyme in the formation of *p*-cresol glucuronide as described below. The concentrations of methanol for solubilizing chemical inhibitors (≤0.03%) are described in each Table and Figure legend.

2.6. Relative contributions of human UGTs in the formation of p-cresol glucuronide in human liver and kidney microsomes

In order to characterize the relative contributions of human UGT1A6 and UGT1A9 in the formation of *p*-cresol glucuronide, pooled human liver microsomes (from 150 adult donors, mixed gender), pooled human kidney microsomes (from 8 adult donors, mixed gender, prepared from whole kidney), or 12 individual human liver microsomes were incubated with 23.9 μM (free concentration) *p*-cresol and enzyme selective chemical inhibitors (i.e. 3000 μM acetaminophen for

UGT1A6, 100 μM amentoflavone for UGT1A6, or 10 μM niflumic acid for UGT1A9; see below for further discussion) using linear enzymatic conditions described in each table or figure legend. The calculated percentage of inhibition in *p*-cresol glucuronide formation in relation to the vehicle control (containing *p*-cresol dissolved in incubation medium with methanol, Figure VIII-4) was utilized to estimate the relative contribution of each enzyme in the formation of *p*-cresol glucuronide [380].

2.7. Correlations between clinical factors and the extent of inhibition by acetaminophen, amentoflavone, or niflumic acid in individual human liver microsomes

The associations between clinical factors and the relative contributions of UGT1A6 or UGT1A9 (based on the percentage of inhibitions obtained with chemical inhibitors) were characterized in 12 individual human liver microsomes [55, 300]. The assessed clinical factors were patient total cytochrome P450 (CYP) enzyme content; CYP1A2, CYP2A6, CYP2B6, CYP2C8, CYP2C9, CYP2C19, CYP2D6, CYP2E1, CYP3A4, CYP4A, flavin-containing monooxygenase (FMO), UGT1A1, UGT1A4, UGT1A9 activities; age, gender, and race [55, 300]. The inhibition data obtained from 3000 μM acetaminophen, 100 μM amentoflavone, and 10 μM niflumic acid (representing maximal inhibition of *p*-cresol glucuronide formation as described above in **Selectivity and potency of chemical inhibitors for reducing the formation of *p*-cresol glucuronide in hrUGT1A6 and hrUGT1A9**) were utilized in our correlational analyses. In addition, the inhibition data based on incubations with 1000 μM acetaminophen, representing ~half-maximal inhibitory effects (i.e. IC_{60}) were also utilized. The latter represented non-saturating conditions associated with UGT1A6 inhibition (see further discussions below). All continuous

covariates were log (base 10) transformed prior to Pearson correlational analyses using a significance threshold of $p \leq 0.003$ (based on Bonferroni's correction).

2.8. Quantification of p-cresol glucuronide using ultra-high performance liquid chromatography tandem mass spectrometry

Concentrations of *p*-cresol glucuronide in the microsomal incubation medium were quantified using an ultra-high performance liquid chromatography tandem mass spectrometry (UPLC-MS/MS) assay developed in our lab. The instrument consisted of a system controller (CBM-20A), degasser unit (DGU-20A 5R), binary pump (LC-30 AD), autosampler (SIL-30 AC), column oven (CTO-20 AC), and triple quadrupole mass spectrometry (MS) detector equipped with electrospray ionization probe (LCMS-8050, Shimadzu, Kyoto, Japan). Chromatographic separation was achieved with a Raptor^{TM} biphenyl column (2.1×100 mm, 2.7 µM, Bellefonte, Pennsylvania, United States) using isocratic elution with a mobile phase consisting of water and methanol (10:90 v/v, containing 0.1% formic acid and 2 mM ammonium acetate) at a flow rate of 0.3 mL/min. Reverse-phase chromatography is typically used in the literature for separating *p*-cresol glucuronide in other biological matrices (e.g. Itoh *et al.*, 2012 [372]). The column temperature was maintained at 30 °C, and the total run time was 5 minutes. Negative electrospray ionization with multiple reaction monitoring was utilized to detect *p*-cresol glucuronide (mass to charge ratio [*m/z*]: 282.85→106.95) and *p*-cresol glucuronide-d_7 (internal standard, *m/z*: 290.00→114.00). The utilized compound specific MS parameters, which were optimally tuned by both software and by hand for *p*-cresol glucuronide and *p*-cresol glucuronide-d_7 individually, are summarized in Table S VIII-1, Supplementary materials. Tuning, data acquisition, and integration were conducted in LabSolutions software (version 5.91, Shimadzu Corporation, Kyoto, Japan).

The assay was completely validated with respect to calibration range, selectivity, carryover, recovery, precision, accuracy, autosampler stability, and benchtop stability based on guidance provided by the US Food and Drug Administration [273].

2.9. Statistical analyses

Statistical differences were determined between two groups using Student's t test or between multiple groups using one way analysis of variance (ANOVA) followed by the Tukey test if the data were normally distributed and showed equal variance (SigmaStat, version 3.5, Systat Software, Inc., San Jose, California, United States). Alternatively, the Mann-Whitney test or Kruskal-Wallis one way ANOVA on ranks followed by the Tukey test were utilized as non-parametric equivalents. For Pearson correlational analyses, continuous covariates were log (base 10) transformed, whereas categorical covariates such as gender and race were categorized into "female vs. male" and "Caucasian vs. Hispanic vs. Asian", respectively. The specific statistical tests are described in individual table and figure legends. Curve fitting analyses for the determination of enzyme kinetics are described above in **Enzyme kinetics of *p*-cresol glucuronide formation in hrUGT1A6, hrUGT1A9, pooled human liver microsomes, and pooled human kidney microsomes**.

3. Results

3.1. Control experiments

Protein concentrations and incubation times pertaining to linear enzymatic conditions were optimized in human recombinant enzymes, pooled human liver microsomes, pooled human kidney

microsomes, and individual human liver microsomes using a free *p*-cresol concentration that has been documented in the human liver (i.e. 23.9 μM) [295]. The optimized incubation conditions are reported in individual table or figure legends. *p*-Cresol glucuronide was not detected in the negative control experiments conducted in hrUGT1A6, hrUGT1A9, pooled human liver microsomes, or pooled human kidney microsomes. Methanol, the organic solvent used to dissolve the chemical inhibitors, up to 0.1% (v/v) did not affect the formation of *p*-cresol glucuronide in all of the enzyme systems (control data not shown), consistent with the observation reported by Uchaipichat et al. using 0.5% methanol and 4-methylumbelliferone in hrUGT enzymes [296]. In our incubations, only ≤ 0.03% (v/v) of methanol was utilized.

3.2. Activities of individual human recombinant UGT enzymes in the formation of p-cresol glucuronide

Of the 13 tested hrUGTs (i.e. 1A1, 1A3, 1A4, 1A6, 1A7, 1A8, 1A9, 1A10, 2B4, 2B7, 2B10, 2B15, and 2B17) incubated with 23.9 μM *p*-cresol (free concentration reported in the human liver [295]), only hrUGT1A6 and hrUGT1A9 exhibited catalytic activities in the formation of *p*-cresol glucuronide (Figure VIII-1). In addition to hrUGT1A6 and hrUGT1A9, *p*-cresol glucuronide formation was also observed in incubations using hrUGT1A7, hrUGT2B4, and hrUGT2B7 with 700 μM *p*-cresol (putative toxic concentration attainable in human plasma [308]), but the activities were minimal compared to hrUGT1A6 and hrUGT1A9 (Figure VIII-1). Moreover, the relative activities of hrUGT1A6 and hrUGT1A9 in *p*-cresol glucuronide formation were dependent on the concentration of *p*-cresol, suggesting different kinetic characteristics between the two enzymes. Based on these observations, only hrUGT1A6 and hrUGT1A9 were selected for further kinetic characterizations. Due to the evidence of protein expressions of both enzymes in the liver and

kidney [310, 378, 379], human liver or kidney microsomes were further utilized for the determination of the relative contributions of UGT1A6 and UGT1A9 in the generation of *p*-cresol glucuronide.

3.3. Enzyme kinetics of p-cresol glucuronide formation in hrUGT1A6, hrUGT1A9, pooled human liver microsomes, and pooled human kidney microsomes

The kinetics of *p*-cresol glucuronide formation were characterized using *p*-cresol concentrations ranging from 0 to 700 μM in hrUGT1A6, hrUGT1A9, pooled human liver microsomes, and pooled human kidney microsomes (Figure VIII-2). Kinetic data from hrUGTs were compared with that generated in human liver or kidney microsomes. According to established reaction phenotyping methodologies [380], similar kinetic behaviors (e.g. K_m) between hrUGT and microsomes can be interpreted as supporting the involvement of the particular enzyme in the glucuronidation of *p*-cresol. This approach, however, has inherent limitations because kinetic constants associated with the same enzyme may not be comparable between the different enzyme sources due to differential artefactual results generated by various components (e.g. albumin) in the incubation (e.g. [380]). The Hill equation best described the kinetics of hrUGT1A6 and pooled human liver microsomes (Figure VIII-2 [A] and Figure VIII-2 [C], Equation VIII-3) [296], based on model fitting and graphical analysis. On the other hand, the kinetics of hrUGT1A9 and pooled human kidney microsomes were best characterized by substrate inhibition (Figure VIII-2 [B] and Figure VIII-2 [D], Equation VIII-4) [296, 381, 382].

Equation VIII-3

$$v = \frac{V_{max} \times [S]^n}{{S_{50}}^n + [S]^n}$$

Equation VIII-4

$$v = \frac{V_{max}}{1 + (\frac{K_m}{[S]}) + (\frac{[S]}{K_{si}})}$$

Where v is the formation rate of *p*-cresol glucuronide, [S] is the concentration of *p*-cresol, V_{max} is the maximum reaction rate, K_m or S_{50} is the concentration of substrate at which the reaction rate is half of the maximum, n is the Hill coefficient, and K_{si} is the dissociation constant for the substrate inhibition model.

The kinetic parameters (i.e. K_m [or S_{50}], V_{max}, CL_{int}, CL_{max}, n, and K_{si}) are provided in Figure VIII-2. The K_m (or S_{50}) and V_{max} values for hrUGT1A6 and hrUGT1A9 were similar despite different models of best fit, and the S_{50} values of hrUGT1A6 and pooled human liver microsomes were comparable to each other based on mean±SD values. In addition, pooled human kidney microsomes exhibited the lowest K_m values compared to all other enzyme sources, and both pooled human liver or kidney microsomes exhibited lower V_{max} and CL_{int} (or CL_{max}) values than human recombinant enzymes exhibiting the same kinetic behaviors (i.e. pooled human liver microsomes vs. hrUGT1A6 or kidney microsomes vs. hrUGT1A9).

3.4. Selectivity and potency of chemical inhibitors for reducing the formation of p-cresol glucuronide in hrUGT1A6 and hrUGT1A9

In order to determine the relative contributions of UGT1A6 and UGT1A9 in the generation of *p*-cresol glucuronide in microsomes, the definitive approach is the use of selective and potent inhibitors for both enzymes [380]. The ideal tools are UGT enzyme-specific inhibitory monoclonal antibodies, but these are not yet available to our knowledge, and therefore the chemical inhibitor

approach is still the gold standard [380]. To determine selectivity and potency in reducing *p*-cresol glucuronide formation, multiple concentrations of chemical inhibitors that could potentially affect UGT1A6 (i.e. acetaminophen [298] and amentoflavone [383]) or UGT1A9 (i.e. niflumic acid [298]) were tested in incubations containing hrUGT1A6 or hrUGT1A9 (Figure VIII-3). Acetaminophen (3000 μM) and amentoflavone (100 μM) selectively inhibited *p*-cresol glucuronide formation from hrUGT1A6 by 90.9±1.5% (mean±SD, n=3 replicates) and 95.3±1.1%, respectively ($p<0.05$), while minimally affecting hrUGT1A9 (Figure VIII-3 [A] and Figure VIII-3 [B]). Niflumic acid (10 μM) achieved maximum inhibition (90.7±7.5%) of *p*-cresol glucuronide formation from hrUGT1A9 but had little effects on hrUGT1A6 activities (Figure VIII-3 [C]). Niflumic acid as a selective and potent inhibitor toward UGT1A9 is already well-established [298], but the selectivity and inhibitory effects of acetaminophen and amentoflavone toward UGT1A6 have not been well-characterized previously. As UGT1A6 was the predominant enzyme contributing to the glucuronidation of *p*-cresol, a redundant approach (i.e. two independent selective UGT1A6 inhibitors) was utilized to ensure consistency of our findings. Having validated the potent and selective effects of UGT1A6 and UGT1A9 inhibitors (Figure VIII-3), the percentages of inhibition mediated by these chemical inhibitors were further interpreted as the relative contributions of each enzyme in human liver or kidney microsomes [380].

3.5. Relative contributions of human UGTs in the formation of p-cresol glucuronide in human liver and kidney microsomes

In pooled human liver microsomes, 3000 μM acetaminophen and 100 μM amentoflavone (selective UGT1A6 inhibitors, Figure VIII-3[A] and Figure VIII-3 [B]) reduced *p*-cresol glucuronide formation by 81.3±3.0% (mean±SD, n=3 replicates, $p<0.05$) and 78.4±3.3% ($p<0.05$),

respectively, suggesting the predominant contribution by UGT1A6 (Figure VIII-4 [A]). On the other hand, 10 μM niflumic acid (selective UGT1A9 inhibitor) only reduced the formation of *p*-cresol glucuronide by 2.8±1.5% ($p>0.05$), indicating relatively minor contributions of hepatic UGT1A9 (Figure VIII-4 [A]). In pooled human kidney microsomes prepared from whole kidney, acetaminophen, amentoflavone, and niflumic acid decreased *p*-cresol glucuronide formation by 54.3±7.8% ($p<0.05$), 62.9±6.7% ($p<0.05$), and 35.5±6.5% ($p<0.05$), respectively, indicating a reduced (yet still prominent) contribution by UGT1A6 and a greater contribution by UGT1A9 compared to human liver microsomes Figure VIII-4 [B]).

Chemical inhibition experiments were also conducted in individual human liver microsomes from 12 adult donors to characterize the inter-individual variabilities (Figure VIII-4 [C]). Similar to the observations obtained in pooled human liver microsomes (Figure VIII-4 [A]), 3000 μM acetaminophen and 100 μM amentoflavone reduced *p*-cresol glucuronide formation by 72.6±11.3% ($p<0.05$) and 71.6±12.8% ($p<0.05$), respectively, while niflumic acid only decreased *p*-cresol glucuronide formation by 5.7±4.1% (Figure VIII-4 [C]). As evident by the standard deviation values, inter-individual variabilities were significant, suggesting that individual patient factors may have affected the relative contributions of specific enzymes (please see below for further analysis). Human kidney microsomes from individual donors were not tested due to lack of available sources for testing.

3.6. Correlations between clinical factors and the extent of inhibition by acetaminophen, amentoflavone, or niflumic acid in individual human liver microsomes

In order to determine the associations between clinical factors and the relative contributions of UGT1A6 and UGT1A9 in the formation of *p*-cresol glucuronide, correlational analyses were conducted using data obtained from 12 individual human liver microsomes (Table VIII-1). The percentage inhibition of *p*-cresol glucuronide formation from 1000 μM (representing the IC_{60} value) acetaminophen was found to be negatively associated with mycophenolic acid glucuronide formation (R=-.784, p=0.003, Table VIII-1, where the mycophenolic acid glucuronidation data were obtained from Rong and Kiang [55]) which is considered a probe substrate reaction for UGT1A9 [35, 55, 380, 384]. The percentage of inhibition from 1000 μM acetaminophen in Caucasian donors (n=8) was 49.8±10.4%, whereas as that in the single Asian donor was 13.9% (no statistics were conducted due to limited sample size, and no assumptions should be made based on a single piece of data). No other significant associations were observed with other treatment conditions and donor factors (Table VIII-1).

3.7. Quantification of p-cresol glucuronide using ultra-high performance liquid chromatography tandem mass spectrometry

The UPLC-MS/MS assay for measuring *p*-cresol glucuronide in microsomal incubation medium was successfully validated based on guidance provided by the US Food and Drug Administration [273]. The run time per injection was 5 minutes, with an estimated retention factor of 4.3. The assay was linear between 0.08 to 80 μg/mL (Figure S VIII-1, Supplementary materials), and all samples were found in the linear range. Selectivity was confirmed by the absence of

interfering peaks observed at the same retention times of *p*-cresol glucuronide and *p*-cresol glucuronide-d_7 in the blank samples (i.e. noise ≤ 5% of the responses of the lower limit of quantification [LLOQ] samples) (data not shown). Carryover was less than 20% of the response in the LLOQ samples. Recoveries at low, medium, and high quality control samples were determined to be 86.3-90.1%, indicating relatively high extraction efficiency. The intra-, inter-day precision/accuracy, autosampler stability, and bench-top stability all fulfilled the requirements by the US Food and Drug Administration [273] (Table S VIII-2, Table S VIII-3, Supplementary materials). Freeze-thaw and long-term storage stabilities were not tested, because our samples were immediately processed without storage.

4. Discussion

p-Cresol glucuronide exerts toxicity in various human models, but the metabolic pathways responsible for its production remain to be elucidated. Reaction phenotyping was conducted using a systematic approach [380], where multiple complementary *in vitro* techniques (Figure VIII-1, Figure VIII-2, Figure VIII-3, Figure VIII-4, Table VIII-1) were utilized. The compositions of our incubation mixture were previously optimized [297], but the BSA concentration was slightly modified in order to utilize the unbound fraction of "0.7" for *p*-cresol [52]. Changing BSA concentration from 1% to 2% does not significantly affect the activities of hrUGT1A6 or hrUGT1A9 using 4-methylumbelliferone or propofol as substrates, respectively [297, 317]. The *p*-cresol concentration used in the current study (23.9 μM) was based on the free concentration reported in autopsied liver from hemodialysis patients [295]. It is consistent with the physiological free *p*-cresol concentrations reported in the human plasma or serum (e.g. [371, 372, 385]) and in

the human kidney (i.e. 10.7 μM [295]), and was less than the K_m values of all enzyme systems characterized in this study, ensuring linear kinetic conditions.

The 13 hrUGTs utilized in this study (Figure VIII-1) represented the majority of hepatically (i.e. UGT1A1, UGT1A3, UGT1A4, UGT1A6, UGT1A7, UGT1A8, UGT1A9, UGT1A10, UGT2B4, UGT2B7, UGT2B10, UGT2B15, and UGT2B17 [374-378]) and renally (i.e. UGT1A6, UGT1A7, UGT1A9, UGT2B4, UGT2B7, and UGT2B17 [310, 375, 377-379]) expressed isoforms (based on both mRNA and protein expression data). However, mRNA expression might not be directly correlated with protein expression, and both probe substrate activities and protein expression are considered better surrogates for enzyme catalytic activities in different tissue/organs [255, 310, 379]. Not all UGT enzymes known to be expressed in both organs were characterized in this study due to lack of availability and for the following reasons: the protein expressions of UGT1A5 are relatively minor in human liver microsomes [386]. UGT2B11 is not reactive with compounds having similar chemical structures as *p*-cresol (e.g. 4-ethyl phenol, 4-propyl phenol, or 4-nithophenol) [387], whereas the substrate specificities of UGT2A2 and UGT2A3 have only been characterized with simple polycyclic aromatic hydrocarbons [388]. Moreover, UGT3A1, UGT3A2, and UGT8A1 are demonstrated to have preferences for other co-factors such as UDP N-acetylglucosamine, UDP-glucose, UDP-xylose, and UDP-galactose rather than UDPGA [389-391].

A variety of UGTs (Figure VIII-1) were active in the generation of *p*-cresol glucuronide, consistent with overlapping substrate activities observed between human UGT isoenzymes [384]. Our findings of substantially higher hrUGT1A6 and hrUGT1A9 activities are consistent with the UGT1A subfamily being “10-20 folds” more active toward the glucuronidation of simple phenols [375]. The catalytic activities of UGT1A6 toward *p*-cresol was first reported by Harding et al. [392]

and further supported by UGT1A6 exhibiting high enzymatic activities toward alternative more complex planar phenols such as 1-naphthol or 4-methylumbelliferone [296]. The glucuronidation of *p*-cresol by UGT1A6 was best fitted using the Hill equation (Figure VIII-2 [A]), indicating a sigmoidal kinetic behavior and suggesting the presence of multiple substrate binding sites [393]. In contrast, *p*-cresol glucuronide formation by UGT1A9 can be best described by substrate inhibition (Figure VIII-2 [B]) indicating enzyme activities are reduced as *p*-cresol concentrations exceeded the K_{si} [296, 381]. Substrate inhibition is unlikely to be of consequence at the typical *p*-cresol concentration observed in the liver and plasma or serum (i.e. 8.0-23.9 μM [295, 371, 372, 385]); however, toxic concentrations of *p*-cresol (i.e. 700 μM) might lead to auto-inhibition of glucuronidation in a mechanism that may be of protective value, assuming *p*-cresol glucuronide is a toxic metabolite.

The selective inhibitory effects of acetaminophen toward UGT1A6 but not UGT1A9 (Figure VIII-3 [A]) have not been documented previously. As acetaminophen is reported to be a major substrate of UGT1A6 (with relatively high affinity) and minor substrate for UGT1A9 (with low affinity) [298], the mechanisms of inhibition and selectivity on *p*-cresol glucuronidation still remain to be characterized. The inhibition effects of niflumic acid toward UGT1A9 (Figure VIII-3 [C]) are generally consistent with previous data [298]. On the other hand, our finding of a selective inhibitory effect by amentoflavone on UGT1A6 (Figure VIII-3 [B]) was inconsistent with Lv et al., where the same concentration of amentoflavone reduced the catalytic activities of both hrUGT1A6 and hrUGT1A9 [383]. This discrepancy may be explained by the relatively higher potency of inhibition by amentoflavone toward 4-methylumbelliferone and/or completely distinctive inhibition mechanisms, which will require further confirmation. A limitation in our study is that the inhibitor concentrations utilized in our experiments were total concentrations,

without considering the effects of BSA binding; therefore, although these conditions were proven to be completely inhibitory and selective in our *in vitro* systems, the optimal conditions should be individually-tailored should they be used in other incubation systems with different BSA compositions. Using validated chemical inhibition conditions, UGT1A6 was determined the predominant enzyme responsible for the formation of *p*-cresol glucuronide in pooled human liver and kidney microsomes; whereas UGT1A9 contributed a relatively reduced role (Figure VIII-4). The enzyme kinetics of *p*-cresol glucuronide formation in pooled human liver microsomes (Figure VIII-2 [C]) were consistent with hrUGT1A6 (Figure VIII-2 [A]), supporting the major role of this enzyme. On the other hand, despite the prominent role of UGT1A6 in human kidney microsomes, the kinetic behavior was best described by substrate inhibition (Figure VIII-2 [D]) which was more relatable to that of hrUGT1A9 (Figure VIII-2 [B]). These inconsistent findings in human kidney microsomes might be due to significantly increased contribution of UGT1A9 in *p*-cresol glucuronide formation (Figure VIII-4 [B]) as a result of higher UGT1A9 protein expression in the human kidneys [294, 310, 378, 379]. Moreover, although the kinetic profile of best fit in human kidney microsomes was substrate inhibition, the relatively higher K_{si} (1643.1±543.9 μM) in comparison to that observed in hrUGT1A9 (259.1±24.9 μM) suggested a hybrid behavior reflective of contributions from both UGT1A6 and UGT1A9. Further differences in the relative contributions of UGT1A6 and UGT1A9 are also expected in cortical vs. medullary microsomes due to known variations in kinetic activities between these tubular components of the nephron [310].

The total percentage contribution of both UGT1A6 and UGT1A9 (i.e. ~81% in human liver and ~90% in kidney microsomes) did not add up to 100%, possibly due to minor contributions by UGT enzymes expressed in both organs that were not characterized (please see discussion above).

The liver is expected to be the primary organ responsible for the conjugation of *p*-cresol [55] due to extensive first-pass metabolism. In contrast, the kidneys are expected to contribute a relatively minor role in *p*-cresol glucuronidation because the majority of *p*-cresol would have already been metabolized in the liver, as evident by relatively high concentrations of conjugated *p*-cresol metabolites in the plasma in relation to *p*-cresol [53, 82]. In addition, *p*-cresol conjugation could also occur in the large intestine as part of the first-pass process [78, 394], but one might argue that the hydrophilic conjugated metabolites formed in enterocytes are unlikely to be efficiently absorbed into the portal circulation. However, due to the lack of information on the concentrations of *p*-cresol glucuronide observed on either sides of the intestinal wall and on the functional activities of intestinal *p*-cresol glucuronide transporters, further studies are required to ascertain the role of intestinal microsomes in the systemic exposure of *p*-cresol glucuronide.

Large inter-individual variability and similar patterns in relative contributions of UGT1A6 and UGT1A9 in the glucuronidation of *p*-cresol were observed in 12 individual human liver microsomes (Figure VIII-4 [C]). Correlational analyses indicated that reduced contribution from UGT1A6 (data from 1000 μM acetaminophen, corresponding to IC_{60} conditions) was associated with increased UGT1A9 probe-substrate (i.e. mycophenolic acid) activity, suggesting that UGT1A9 can contribute a more prominent role in hepatic *p*-cresol glucuronidation in individuals with elevated UGT1A9 function (e.g. genetic polymorphism [395] or enzyme induction [384]). This is consistent with the observation of higher relative UGT1A9 contribution in human kidney microsomes vs. the liver for *p*-cresol glucuronidation as a result of higher UGT1A9 protein expression (Figure VIII-4) [294, 310, 378, 379]. Given the wide inter-individual variability documented of UGT1A9 activity in human liver microsomes [297], the contribution of UGT1A9 in the glucuronidation of *p*-cresol is expected to vary several folds in the population. On the other

hand, the lack of correlation between UGT1A9 activities and the inhibition data obtained from 3000 μM acetaminophen, 100 μM amentoflavone, and 10 μM niflumic acid might be explained by already saturated inhibition responses (Figure VIII-3). It is predictable that CYP/FMO activities did not correlate with UGT contribution data as *p*-cresol is not known to be extensively oxidized. The associations between age, gender, and race were also difficult to interpret due to the limited sample size (Table VIII-1). Although we would have expected associations between inhibitory effects of acetaminophen or amentoflavone and UGT1A6 probe substrate activity (e.g. deferiprone glucuronidation), the latter information was not characterized in our individual human liver microsomes and would only have constituted, at best, supportive information [380].

The novel finding that UGT1A6 was the predominant enzyme responsible for the formation of *p*-cresol glucuronide in human liver and kidney microsomes provides valuable information for conducting further mechanistic studies (i.e. using specific UGT1A6 modulators [298, 384]) to assess the *cause-effect* relationships of *p*-cresol glucuronide-mediated toxicity. Given the strong associations between *p*-cresol glucuronide and adverse cardiovascular or renal outcomes, our findings can also be utilized to design clinical interventions (i.e. selective UGT1A6 inhibition [298, 384]) for mitigating patient morbidity.

Table VIII-1 Correlations between donor factors and the percentage of inhibition of p-cresol glucuronide formation by acetaminophen, amentoflavone, and niflumic acid in individual human liver microsomes

		R (p value) in Pearson product correlation analysis using logarithm (10) transformed data			
Activity, pmol/mg/min [55, 300]	Mean±SD (range) (n=12)[1] [55, 300]	Percentage inhibition of *p*-cresol glucuronide formation from 1000 μM acetaminophen	Percentage inhibition of *p*-cresol glucuronide formation from 3000 μM acetaminophen	Percentage inhibition of *p*-cresol glucuronide formation from 100 μM amentoflavone	Percentage inhibition of *p*-cresol glucuronide formation from 10 μM niflumic acid
Total P450c, Omura and Sato	428±273 (170-1200)	-.134 (.678)	-.375 (.230)	-.265 (.406)	-.227 (.478)
CYP1A2	432±276 (84-880)	.132 (.683)	-.330 (.295)	-.464 (.129)	-.501 (.097)
CYP2A6	1084±665 (250-2100)	-.192 (.549)	-.484 (.111)	-.203 (.526)	.030 (.926)
CYP2B6	63±25 (21-110)	-.393 (.232)	-.654 (.029)	-.302 (.367)	.123 (.719)
CYP2C8	242±240 (26-960)	-.314 (.321)	-.473 (.120)	-.222 (.487)	.039 (.904)
CYP2C9	3347±1587 (560-5500)	-.303 (.339)	-.397 (.202)	-.474 (.120)	-.324 (.305)
CYP2C19	67±125 (0-450)	.076 (.824)	-.252 (.455)	-.160 (.639)	-.539 (.089)
CYP2D6	98±70 (7-250)	-.006 (.985)	-.236 (.461)	-.415 (.183)	-.120 (.711)
CYP2E1	2055±1057 (860-4100)	-.209 (.514)	-.212 (.507)	-.525 (.079)	-.164 (.610)
CYP3A4	6943±5243 (970-16000)	.270 (.397)	-.200 (.532)	-.030 (.925)	-.002 (.995)
CYP4A	2053±1195 (450-5300)	.578 (.049)	-.099 (.760)	-.255 (.423)	-.585 (.046)
FMO (as measured by methyl p-tolyl sulfide oxidase)	1598±705 (610-2800)	.391 (.209)	-.229 (.473)	-.340 (.279)	-.501 (.097)
UGT1A1	1190±770 (64-2500)	-.168 (.601)	.310 (.327)	.024 (.941)	.005 (.987)
UGT1A4	466±231 (80-960)	.563 (.057)	.059 (.856)	-.049 (.881)	-.061 (.850)
UGT1A9 (propofol as substrate)	2735±1356 (640-4500)	-.602 (.038)	-.434 (.159)	-.223 (.487)	-.076 (.814)
UGT1A9 (mycophenolic acid as substrate) [55]	70±30 (33-129)	-.784 (.003*)	-.464 (.129)	-.071 (.826)	.297 (.349)
Demographics	Categorical numbers or mean±SD (range) (n=12)	Percentage inhibition of *p*-cresol glucuronide formation from 1000 μM acetaminophen	Percentage inhibition of *p*-cresol glucuronide formation from 3000 μM acetaminophen	Percentage inhibition of *p*-cresol glucuronide formation from 100 μM amentoflavone	Percentage inhibition of *p*-cresol glucuronide formation from 10 μM niflumic acid
Age	53±13 (23-70)	-.178 (.581)	-.244 (.444)	-.116 (.720)	.342 (.276)
Gender	Female/male, 6/6	NA (.390)	NA (.519)	NA (.863)	NA (.168)
Race	Caucasian/Hispanic/Asian, 8/3/1	NA	NA	NA	NA

Individual human liver microsomes (n=12) were incubated with *p*-cresol (23.9 μM, a free concentration reported in the human liver [295]) as described in Materials and Methods.

The utilized protein concentrations and incubation times corresponding to linear enzymatic conditions were: HG18 (0.175 mg/mL, 10 minutes), HFC205, HFH617, HFC208, HH13-2, HH837, HH741, HH37, HG43 (0.25 mg/mL, 10 minutes), and HFH705, HG64, HH519 (0.5 mg/mL, 10 minutes).

Data are presented as mean±SD from 12 individual human liver microsomes based on duplicate determinations.

All microsomal incubations contained 0.03% methanol. All continuous data were log (base 10) transformed prior to analysis.

Categorical factors such as gender and race were categorized into "female vs. male" or "Caucasian vs. Hispanic. vs. Asian" groups. Statistical analyses were conducted using the Student's t test or the Mann-Whitney test as described in Materials and Methods.

[1]Reference data in this column were obtained from Corning Gentest [300] and Rong et al. [55] which were partially presented in Table 3 in *Rong and Kiang. Toxicol Sci. 2020;173:267-279*.

[*]$p \leq 0.003$ (Bonferroni's correction) based on Pearson correlational analyses.

Abbreviation(s): CYP, cytochrome P450; FMO, flavin-containing monooxygenase; NA, not applicable; R, coefficient of correlation; UGT, UDP-glucuronosyltransferase.

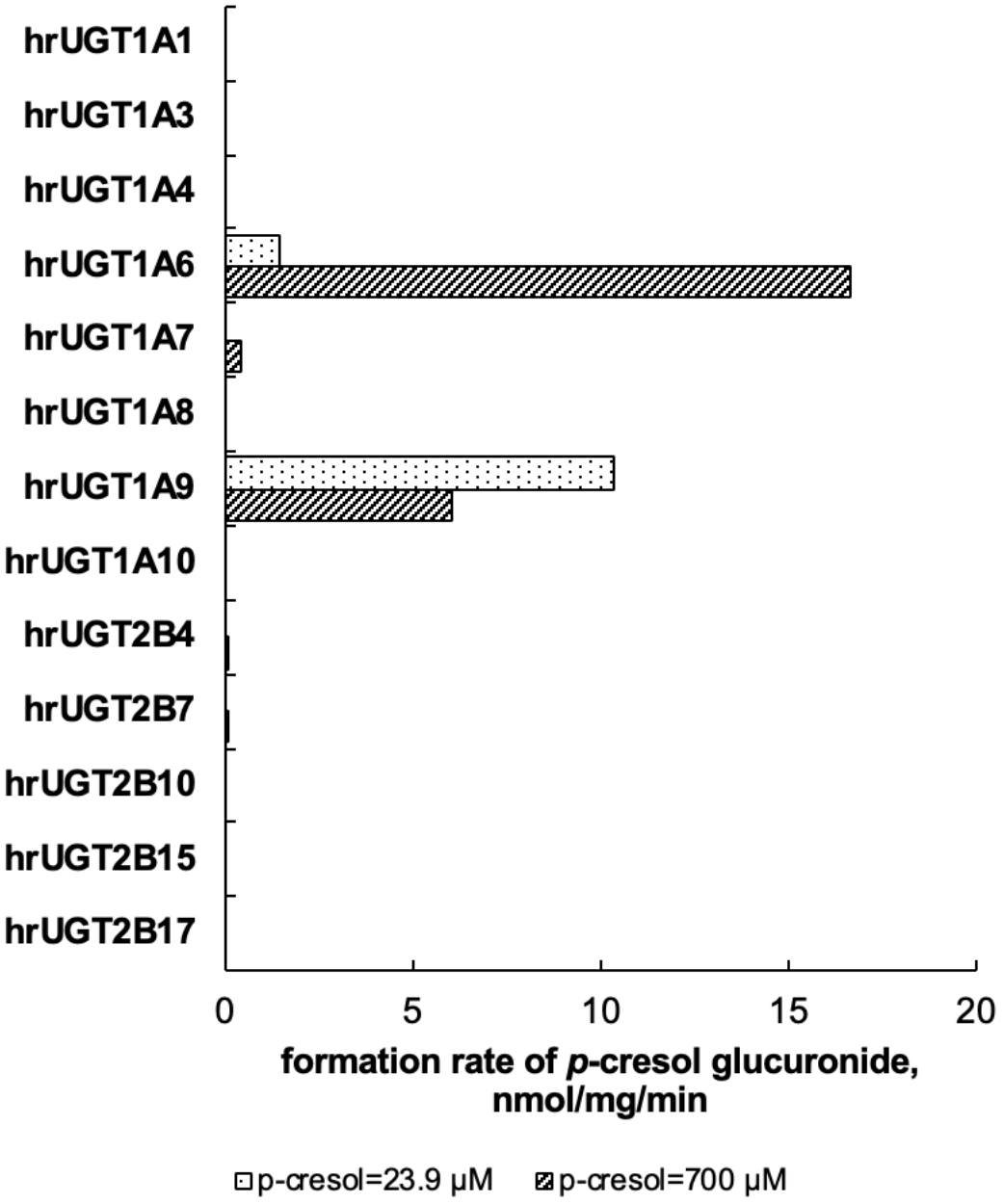

Figure VIII-1 Catalytic activities of individual human recombinant UGT isoforms in the formation of p-cresol glucuronide

Reactions were characterized using 23.9 µM *p*-cresol (free concentration reported in the human liver [295]) or 700 µM *p*-cresol (putative toxic concentration attainable in human plasma [308]) as described in Materials and Methods.

The utilized protein concentrations and incubation times corresponding to linear enzymatic conditions were: hrUGT1A1 (1 mg/mL, 30 minutes), hrUGT1A3 (1 mg/mL, 20 minutes), hrUGT1A4 (0.5 mg/mL, 30 minutes), hrUGT1A6 (0.05 mg/mL, 45 minutes), hrUGT1A7 (0.05 mg/mL, 30 minutes), hrUGT1A8 (0.5 mg/mL, 15 minutes), hrUGT1A9 (0.05 mg/mL, 45 minutes), hrUGT1A10 (0.8 mg/mL, 15 minutes), hrUGT2B4 (0.8 mg/mL, 30 minutes), hrUGT2B7 (0.5 mg/mL, 10 minutes), hrUGT2B10 (1 mg/mL, 30 minutes), hrUGT2B15 (0.5 mg/mL, 10 minutes), and hrUGT2B17 (1 mg/mL, 30 minutes).

Data are presented as average values from 2 to 3 replicates.

Abbreviation(s): hrUGT, human recombinant UGT enzyme; UGT, UDP-glucuronosyltransferase.

(A)

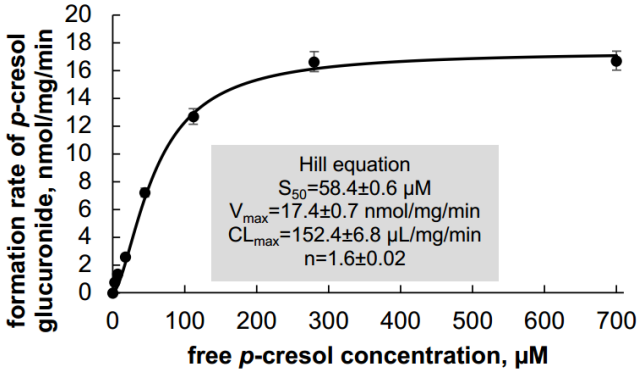
formation rate of p-cresol glucuronide, nmol/mg/min
free p-cresol concentration, μM
Hill equation
S50=58.4±0.6 μM
Vmax=17.4±0.7 nmol/mg/min
CLmax=152.4±6.8 μL/mg/min
n=1.6±0.02

(B)

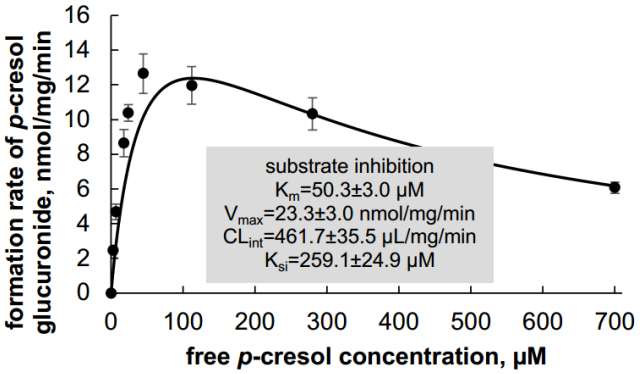
formation rate of p-cresol glucuronide, nmol/mg/min
free p-cresol concentration, μM
substrate inhibition
Km=50.3±3.0 μM
Vmax=23.3±3.0 nmol/mg/min
CLint=461.7±35.5 μL/mg/min
Ksi=259.1±24.9 μM

(C)

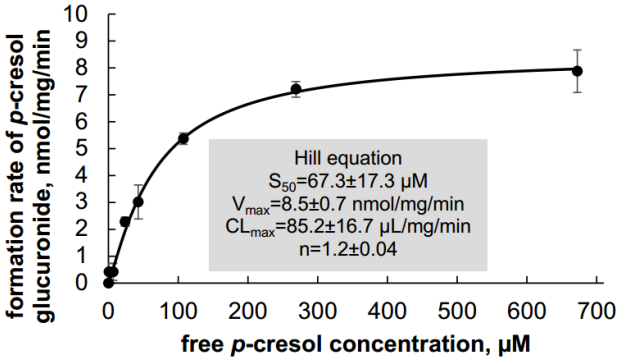
formation rate of p-cresol glucuronide, nmol/mg/min
free p-cresol concentration, μM
Hill equation
S50=67.3±17.3 μM
Vmax=8.5±0.7 nmol/mg/min
CLmax=85.2±16.7 μL/mg/min
n=1.2±0.04

(D)

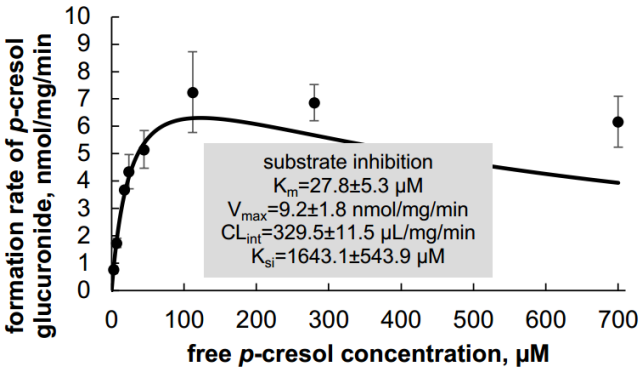
formation rate of p-cresol glucuronide, nmol/mg/min
free p-cresol concentration, μM
substrate inhibition
Km=27.8±5.3 μM
Vmax=9.2±1.8 nmol/mg/min
CLint=329.5±11.5 μL/mg/min
Ksi=1643.1±543.9 μM

Figure VIII-2 Enzyme kinetics of p-cresol glucuronide formation in (A) hrUGT1A6, (B) hrUGT1A9, (C) pooled human liver microsomes, and (D) pooled human kidney microsomes incubated with varying concentrations (0-700 µM) of p-cresol

The utilized protein concentrations and incubation times corresponding to linear enzymatic conditions were: hrUGT1A6 (0.05 mg/mL, 45 minutes), hrUGT1A9 (0.05 mg/mL, 45 minutes), pooled human liver microsomes (0.1 mg/mL, 15 minutes), and pooled human kidney microsomes (0.1 mg/mL, 10 minutes).

Data are presented as mean±SD from 3 replicates.

Kinetic parameters were determined with SigmaPlot (version 14.0).

Abbreviation(s): CL_{int}, intrinsic clearance; CL_{max}, maximum clearance; K_{si}, the dissociation constant of substrate inhibition; K_m (or S_{50}), concentration of substrate at which the reaction rate is half of the maximum; n, Hill coefficient; UGT, UDP-glucuronosyltransferase; V_{max}, maximum reaction rate.

(A)

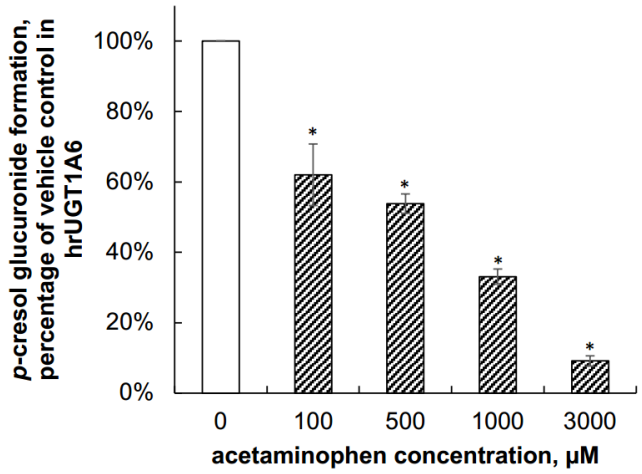
p-cresol glucuronide formation, percentage of vehicle control in hrUGT1A6
100%
80%
60%
40%
20%
0%
*
*
*
*
0
100
500
1000
3000
acetaminophen concentration, μM

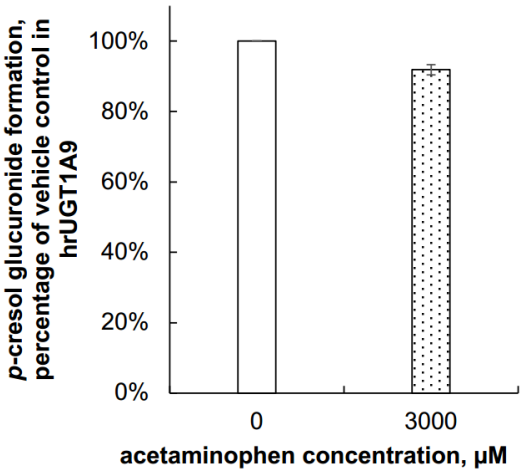
p-cresol glucuronide formation, percentage of vehicle control in hrUGT1A9
100%
80%
60%
40%
20%
0%
0
3000
acetaminophen concentration, μM

(B)

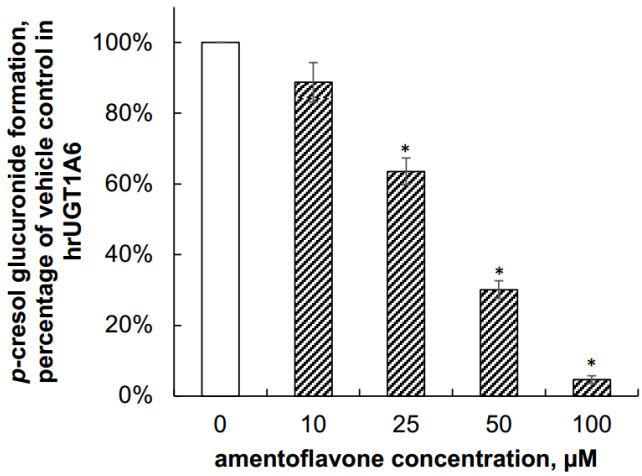
p-cresol glucuronide formation, percentage of vehicle control in hrUGT1A6
100%
80%
60%
40%
20%
0%
*
*
*
0
10
25
50
100
amentoflavone concentration, μM

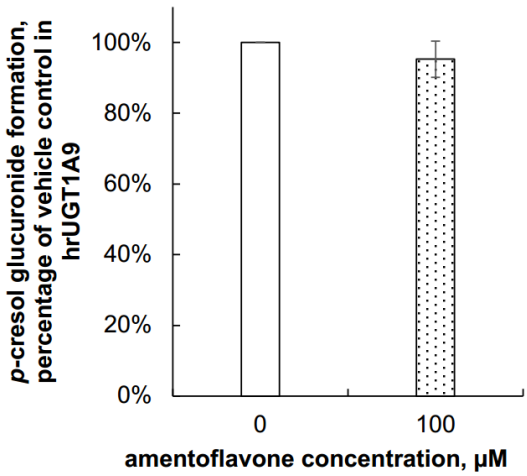
p-cresol glucuronide formation, percentage of vehicle control in hrUGT1A9
100%
80%
60%
40%
20%
0%
0
100
amentoflavone concentration, μM

(C)

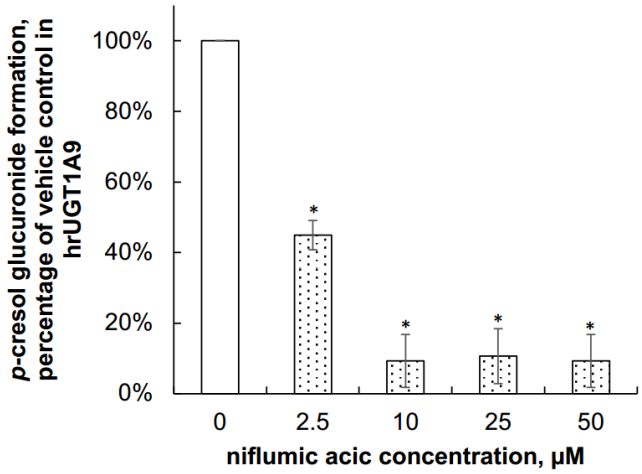
p-cresol glucuronide formation, percentage of vehicle control in hrUGT1A9
100%
80%
60%
40%
20%
0%
*
*
*
*
0
2.5
10
25
50
niflumic acic concentration, μM

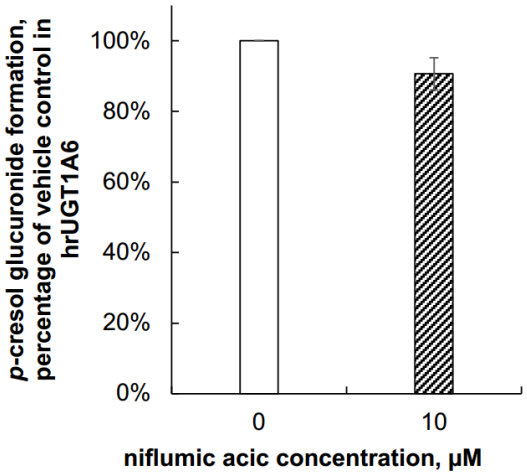
p-cresol glucuronide formation, percentage of vehicle control in hrUGT1A6
100%
80%
60%
40%
20%
0%
0
10
niflumic acic concentration, μM

Figure VIII-3 Effects of (A) acetaminophen, (B) amentoflavone, and (C) niflumic acid on p-cresol glucuronide formation in hrUGT1A6 and hrUGT1A9 enzymes incubated with p-cresol (23.9 μM, a free concentration reported in the human liver [295] which is below the characterized K_m values in the respective enzymes, Figure VIII-2)

The utilized protein concentration and incubation time corresponding to linear enzymatic conditions for both hrUGTs were 0.05 mg/mL and 45 minutes.

Data are presented as mean±SD from 3 replicates.

$^{*}p<0.05$ vs. the vehicle control (containing 0.01% or 0.03% methanol in "niflumic acid" or "amentoflavone" incubations, respectively) using one way analysis of variance with the Tukey test or Mann Whitney rank sum test.

Abbreviation(s): hrUGT, human recombinant UGT enzyme; UGT, UDP-glucuronosyltransferase.

(A)

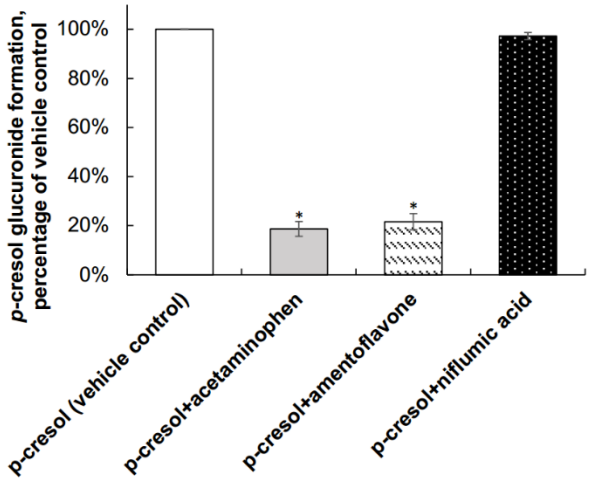
p-cresol glucuronide formation, percentage of vehicle control
100%
80%
60%
40%
20%
0%
*
*
p-cresol (vehicle control)
p-cresol+acetaminophen
p-cresol+amentoflavone
p-cresol+niflumic acid

(B)

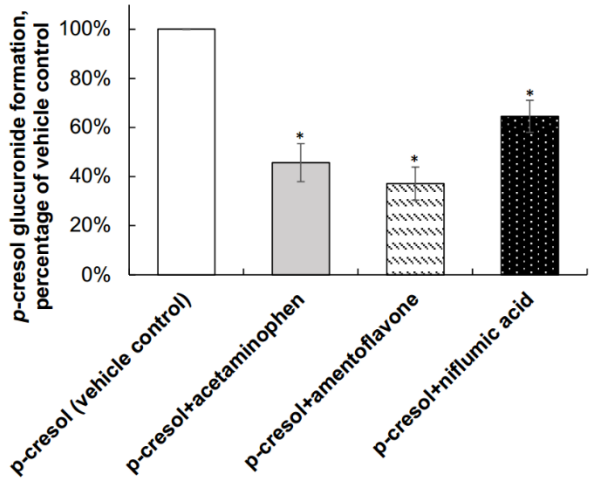
p-cresol glucuronide formation, percentage of vehicle control
100%
80%
60%
40%
20%
0%
*
*
*
p-cresol (vehicle control)
p-cresol+acetaminophen
p-cresol+amentoflavone
p-cresol+niflumic acid

(C)

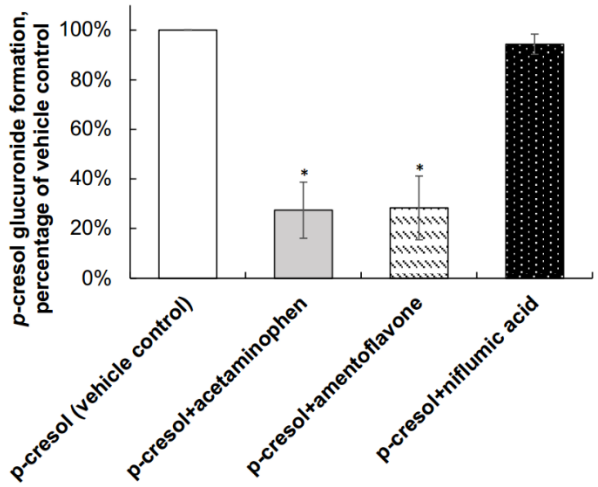
p-cresol glucuronide formation, percentage of vehicle control
100%
80%
60%
40%
20%
0%
*
*
p-cresol (vehicle control)
p-cresol+acetaminophen
p-cresol+amentoflavone
p-cresol+niflumic acid

Figure VIII-4 Effects of acetaminophen (3000 μM), amentoflavone (100 μM), and niflumic acid (10 μM) on the formation of p-cresol glucuronide in (A) pooled human liver microsomes, (B) pooled human kidney microsomes, and (C) 12 individual human liver microsomes incubated with p-cresol (23.9 μM, a free concentration reported in the human liver [295] which is below the characterized K_m values in the respective enzymes, Figure VIII-2).

The utilized protein concentrations and incubation times corresponding to linear enzymatic conditions were: pooled human liver microsomes (0.1 mg/mL, 15 minutes), pooled human kidney microsomes (0.1 mg/mL, 10 minutes), HG18 (0.175 mg/mL, 10 minutes), HFC205, HFH617, HFC208, HH13-2, HH837, HH741, HH37, HG43 (0.25 mg/mL, 10 minutes), and HFH705, HG64, HH519 (0.5 mg/mL, 10 minutes).

Data are presented as mean±SD using 3 replicates.

$^{*}p<0.05$ vs. the vehicle control (containing 0.03% methanol and 23.9 μM *p*-cresol in incubation medium) using one way analysis of variance followed by the Tukey test.

Abbreviation(s): UGT, UDP-glucuronosyltransferase.

Supplementary materials

Table S VIII-1 Compound-specific optimized MS parameters

Parameters	*p*-cresol glucuronide	*p*-cresol glucuronide-d7
Multiple reaction monitoring transition (*m/z*)	282.85→106.95	290.00→114.00
Q_1 pre-bias (V)	32	10
Collision energy (V)	35	14
Q_3 pre-bias (V)	20	21
Interface	Electrospray ionization	
Ion mode	Negative	
Collision-induced dissociation gas pressure (kPa)	270	
Conversion dynode voltage (kV)	10	
Desolvation line temperature (°C)	100	
Drying gas flow (L/min)	10	
Heat block temperature (°C)	400	
Heating gas flow (L/min)	10	
Interface temperature (°C)	400	
Interface voltage (kV)	3	
Nebulizing gas flow (L/min)	2	

Compound specific MS parameters (including Q1/Q3 pre-bias and collision energy) were initially optimized with LabSolutions software using a flow injection of a mixture containing *p*-cresol glucuronide and *p*-cresol glucuronide-d_7. The MS source parameters were further optimized manually. The final MS conditions were selected based on the highest signal counts compared to baseline noise.

Abbreviation(s): m/z, mass to charge ratio; MS, mass spectrometry.

Table S VIII-2 Validation of the UPLC-MS/MS assay for quantifying p-cresol glucuronide in microsomal incubation medium

Nominal concentrations, μg/mL	Intra-day (1), N=5		Intra-day (2), N=5		Intra-day (3), N=5		Inter-day, N=15	
	Precision	Accuracy	Precision	Accuracy	Precision	Accuracy	Precision	Accuracy
0.08 (LLOQ)	5.78%	101.81 %	6.71%	94.13%	12.83%	102.49 %	14.18%	100.29 %
0.23 (low QC)	0.91%	94.25%	9.34%	91.49%	11.49%	90.27%	6.15%	92.12%
30 (medium QC)	10.23%	92.88%	1.02%	108.48 %	8.20%	99.10%	4.93%	99.34%
60 (high QC)	4.66%	104.50 %	7.91%	110.22 %	0.37%	103.33 %	3.38%	109.49 %

Abbreviation(s): LLOQ, lower limit of quantification; QC, quality control; UPLC-MS/MS, ultra-high performance liquid chromatography tandem mass spectrometry.

Table S VIII-3 Stability testing of the UPLC-MS/MS assay for quantifying p-cresol glucuronide in microsomal incubation medium

Nominal concentrations, µg/mL	0.23 (low QC)		60 (high QC)	
	Precision	Accuracy	Precision	Accuracy
Autosampler stability	5.64%	99.20%	4.90%	90.17%
Bench-top stability	3.29%	101.35%	7.88%	92.10%

Autosampler stability (i.e. 24 hours at 4 °C) and bench-top stability (i.e. 6 hours at 23.5 °C) were determined. Freeze-thaw and long-term storage stabilities were not tested because our samples were immediately processed without storage.

Abbreviation(s): QC, quality control; UPLC-MS/MS, ultra-high performance liquid chromatography tandem mass spectrometry.

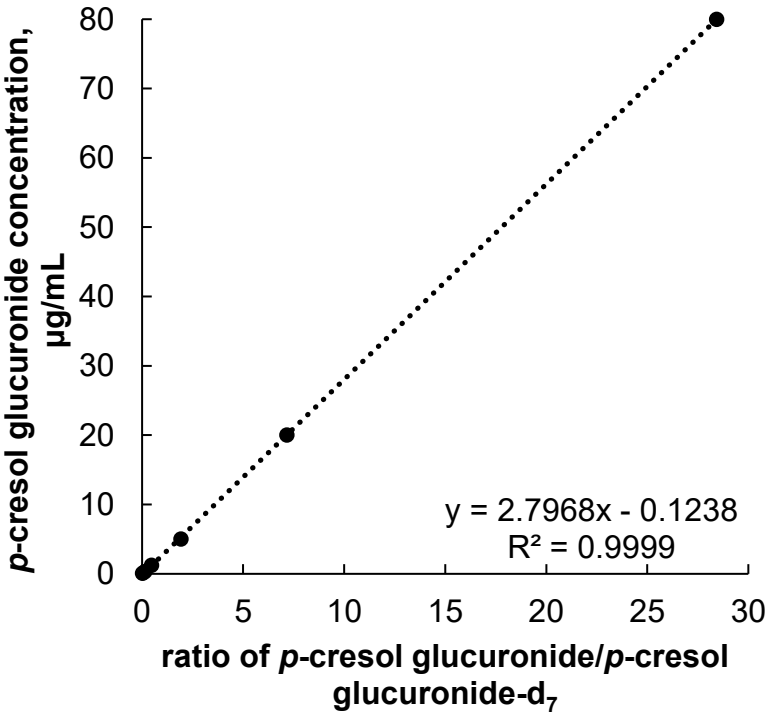

Figure S VIII-1 Representative calibration curve of p-cresol glucuronide in microsomal incubation medium

A weighted ($1/x^2$) least-squares linear regression model was utilized.

Abbreviation(s): R^2, coefficient of determination.

Chapter IX. Significant correlations between *p*-cresol sulfate and mycophenolic acid plasma concentrations in adult kidney transplant recipients[9]

Prologue:

Based on the potent inhibitory effects of p-cresol on the metabolism of MPA demonstrated in our in vitro models (Chapter V [54], Chapter VI [55]), p-cresol is predicted to increase MPA plasma exposure clinically in humans. To verify our findings in patients, the aim of this chapter was to investigate the pharmacokinetic interactions between MPA and p-cresol in de novo adult kidney transplant recipients.

[9] This chapter has been published in a peer-reviewed journal. **Rong Y**, Colbourne P, Gourishankar S, Kiang TKL. Significant correlations between *p*-cresol sulfate and mycophenolic acid plasma concentrations in adult kidney transplant recipients. *Clinical Drug investigation*. 2022 Mar;42(3):207-19. doi: 10.1007/s40261-022-01121-1.

Acknowledgement: Reprinted by permission from Springer Nature: Springer Nature, Clinical Drug investigation. Significant correlations between *p*-cresol sulfate and mycophenolic acid plasma concentrations in adult kidney transplant recipients. **Rong Y**, Colbourne P, Gourishankar S, Kiang TKL. License number: 5252850804730 (2022).

Abstract

Background and Objectives: Mycophenolic acid (MPA) is a commonly prescribed life-long immunosuppressant for kidney transplant recipients. The frequently observed large variations in MPA plasma exposure may lead to severe adverse outcomes; therefore, characterizations of contributing factors can potentially improve the precision dosing of MPA. Our group recently reported the potent inhibitory effects of *p*-cresol (a protein-bound uremic toxin that can be accumulated in kidney transplant patients) on the hepatic metabolism of MPA in human *in vitro* models. Based on these data, the hypothesis for this clinical investigation was that a direct correlation between *p*-cresol and MPA plasma exposure should be evident in adult kidney transplant recipients.

Methods: Using a prospective and observational approach, adult kidney transplant recipients within the first year post-transplant on oral mycophenolate mofetil (with tacrolimus ± prednisone) were screened for recruitment. The exclusion criteria were cold ischemia time >30 hours, malignancy, pregnancy, severe renal dysfunction (i.e., estimated glomerular filtration rate, eGFR, <10 mL/min/1.73m^2), active graft rejection, or MPA intolerance. Patients' demographic and biochemistry data were collected. Total and free plasma concentrations of MPA, MPA glucuronide (MPAG), and total *p*-cresol sulfate (i.e., the predominant, quantifiable form of *p*-cresol in the plasma) were quantified using validated assays. Correlational and categorical analyses were performed using GraphPad Prism.

Results: Forty patients (11 females) were included: donor type (living/deceased: 20/20), induction regimen (basiliximab/thymoglobulin/basiliximab followed by thymoglobulin: 35/3/2), post-transplant time (74±60 days, mean±standard deviation), age (53.7±12.4 years), body weight (79.8±18.5 kg), eGFR (51.9±18.0 mL/min/1.73m^2), serum albumin (3.6±0.5 g/dL), prednisone

dose (18.5±13.2 mg, *n*=33), and tacrolimus trough concentration (9.4±2.4 μg/L). Based on Spearman analysis, significant control correlations supporting the validity of our dataset were observed between total MPA trough concentration (C_0) and total MPAG C_0 (correlation coefficient [R]=0.39), ratio of total MPAG C_0-to-total MPA C_0 and post-transplant time (R= -0.56), total MPAG C_0 and eGFR (R= -0.35), and *p*-cresol sulfate concentration and eGFR (R= -0.70). Our primary analysis indicated the novel observation that total MPA C_0 (R=0.39), daily dose-normalized total MPA C_0 (R=0.32), and body weight-normalized total MPA C_0 (R=0.32) were significantly correlated with plasma *p*-cresol sulfate concentrations. Consistently, patients categorized with elevated *p*-cresol sulfate concentrations (i.e., ≥ median of 3.2 μg/mL) also exhibited increased total MPA C_0 (by 57% vs. those below median), daily dose-normalized total MPA C_0 (by 89%), and body weight-normalized total MPA C_0 (by 62%). Our secondary analyses with MPA metabolites, unbound concentrations, free fractions, and MPA metabolite ratios supported additional potential interacting mechanisms.

Conclusion: We have identified a novel, positive association between *p*-cresol sulfate exposure and total MPA C_0 in adult kidney transplant recipients, which is supported by published mechanistic *in vitro* data. Our findings confirm a potential role of *p*-cresol as a significant clinical variable affecting the pharmacokinetics of MPA. These data also provide the justifications for conducting subsequent full-scale pharmacokinetic-pharmacodynamic studies to further characterize the cause-effect relationships of this interaction, which could also rule out potential confounding variables not adequately controlled in this correlational study.

1. Introduction

Mycophenolic acid (MPA) is a commonly used life-long immunosuppressant in adult kidney transplant patients [2, 10, 24, 29, 31, 51]. The mycophenolate mofetil (MMF) formulation utilized in the current study is rapidly and extensively hydrolyzed to the active compound, MPA, after administration [10]. In subjects with healthy livers and kidneys, MPA binds substantially to plasma albumin, providing a free fraction of 1-3% [10]. MPA primarily undergoes conjugation in various tissues (e.g., intestines, liver, and kidneys) by uridine 5'-diphospho-glucuronosyltransferase (UGT) 1A9 and 2B7, which generate the major metabolite, MPA glucuronide (MPAG), and a relatively minor metabolite, MPA acyl glucuronide (AcMPAG), respectively [10, 35]. Being a low hepatic-extraction ratio drug, MPA's total concentrations are inversely correlated with free fraction and intrinsic clearance, whereas its free concentrations are only dependent on intrinsic clearance [10, 31]. Furthermore, the primary metabolite, MPAG, is subjected to renal excretion or entero-hepatic recirculation, the latter process yielding the occasionally observed additional plasma concentration peaks of MPA [10, 27, 30]. In the clinic, MPA is usually dosed empirically without drug concentration monitoring [51]; however, large variabilities in MPA plasma concentrations are still observed in kidney transplant patients (i.e., 10 fold variations in exposure) [10, 30, 59, 61], which could potentially lead to adverse effects due to the relatively narrow therapeutic range of MPA (i.e., 30-60 μg×h/mL) [2, 10, 61, 63]. In particular, under-exposure of MPA can lead to increased incidence of organ rejection [10, 29, 63], and over-exposure is known to be associated with hematological adverse effects [61, 133] which may further lead to severe infections, graft rejection, and even death [396-398]. Therefore, understanding the factors mediating variabilities in MPA exposure would help improve the precision dosing of MPA and mitigate its adverse effects.

A byproduct of tyrosine and phenylalanine gut bacterial metabolism [79], *p*-cresol (a protein-bound uremic toxin) is subjected to extensive first-pass metabolism in the generation of conjugated metabolites [78]. Therefore, *p*-cresol is quantifiable in the plasma in the form of its metabolites (i.e., *p*-cresol sulfate and *p*-cresol glucuronide) [80-82, 84], and the summative plasma concentrations of its conjugated metabolites are likely reflective of the free *p*-cresol concentrations available at the enzyme active sites in the liver [55]. In patients with chronic kidney disease, *p*-cresol metabolites can accumulate to high, toxic concentrations in the plasma due to compromised renal excretion [78, 84-86, 399]. Moreover, even with kidney transplantation, plasma *p*-cresol metabolite concentrations can still vary significantly based on kidney function (e.g., [127, 129, 130]). Recently, our group demonstrated a potent inhibitory effect of *p*-cresol on the hepatic metabolism of MPA in a human hepatic cell line [54] and human liver microsomes or individually-expressed UGT enzymes [55]. Based on *in vitro-in vivo* scaling conducted from these data, *p*-cresol was predicted to increase the plasma exposure of MPA by up to 1.8-fold [55] at clinically relevant concentrations observed in kidney transplant patients [83, 126-128, 130]. Therefore, significant variations in *p*-cresol concentrations (based on variabilities of its plasma metabolite levels [83, 126-130]) can potentially contribute to MPA plasma exposure variabilities in kidney transplant recipients.

In this first-in-human study, we hypothesized that *p*-cresol metabolite plasma exposure could be significantly associated with the plasma exposure of MPA in adult kidney transplant patients. Our primary objective was to characterize the correlation between plasma *p*-cresol metabolite concentrations and plasma MPA trough concentrations in patients within the 12 month post-transplant period, where the variabilities are relatively large for both MPA and *p*-cresol [126, 128, 160]. Our secondary objectives were to investigate other potential interacting mechanisms by

examining the relationships between *p*-cresol metabolites and MPA metabolites, unbound concentrations, free fractions, or MPA metabolite ratios.

2. Methods

2.1. Materials

Ammonium acetate (catalog# 1220-1-70) was purchased from Caledon Laboratories (Ontario, Canada). 2, 6-Dimethylphenol (catalog# D174904), formic acid (catalog# F0507), MPA (catalog# M5255), MPA-d_3 (catalog# M137), and *p*-cresol (catalog# C85751) were purchased from Sigma Aldrich (Ontario, Canada). *p*-Cresol glucuronide (catalog# C782005), *p*-cresol glucuronide-d_7 (catalog# C782007), *p*-cresol sulfate potassium salt (catalog# T536805), and *p*-cresol sulfate potassium salt-d_7 (catalog# T536802) were purchased from Toronto Research Chemicals (Ontario, Canada). Pooled human plasma (catalog# IPLAWBK2E, utilized as the blank human plasma) was obtained from Innovative Research (Michigan, United States). Raptor™ biphenyl column (2.7 µM particle size, 2.1 mm inner diameter, 100 mm length) was obtained from Restek Corporation (Pennsylvania, United States). Zorbax Eclipse XDB-C18 analytical column (5 µm particle size, 4.6 mm inner diameter, 250 mm length) was purchased from Agilent Technologies (Ontario, Canada).

2.2. Study design

This was a prospective and correlational study approved by the University of Alberta Research Ethics Board (Study ID: Pro00105082) with patient enrolment conducted at the University of Alberta Hospital (Edmonton, Alberta, Canada). Adult (>18 years old) kidney

transplant patients receiving oral MMF (with tacrolimus±prednisone) were screened by an independent study coordinator for recruitment between March–May, 2021. Potential participants had received kidney transplantation for less than 12 months. The exclusion criteria were cold ischemia time >30 hours, history of malignancy, active pregnancy, severely compromised renal function (i.e., estimated glomerular filtration rate [eGFR] <10 mL/min/1.73 m^2), active graft rejection, or MPA intolerance. Power analysis for multiple regression modeling was based on an anticipated effect size (f^2) of 0.35, power level of 0.8, probability level of 0.05, and assumed number of predictors of n=2 [400]. The sample size was estimated to be ~31, but 40 participants were ultimately recruited to account for potentially weaker correlations.

2.3. Clinical data collection

Demographic and biochemistry data were extracted by an independent research coordinator: age, body weight, post-transplant time, serum creatinine, eGFR (calculated by the chronic kidney disease epidemiology collaboration [CKD-EPI] equation [401]), serum albumin, total bilirubin, alanine aminotransferase, aspartate aminotransferase, gamma-glutamyl transferase, white blood count, neutrophil, sex, and donor type (deceased/living). The induction regimen (basiliximab, thymoglobulin, or basiliximab followed by thymoglobulin), concurrent immunosuppressants (i.e., dose of prednisone, dose/trough concentrations of tacrolimus, and dose of MPA), and the identities of other co-administered drugs (without dose information) were also recorded.

2.4. Sample collection, preparation, and quantification

Pre-dose (i.e., trough) patient blood samples (i.e., excess from routine care) were collected by an independent research coordinator and processed to obtain plasma (centrifugation at 2,500 g for 10 minutes at room temperature [model Storvall ST16, Thermo Scientific, Ontario, Canada]). Plasma samples were stored at -80 °C until analyses. The total (i.e., bound and unbound) concentrations of MPA, MPAG, and AcMPAG were determined by liquid chromatography-tandem mass spectrometry (LC-MS/MS): 100 µL of the internal standard solution (consisting of MPA-d_3 [0.4 µg/mL] and MPAG-d_3 [2 µg/mL] in methanol) and 52 µL of the protein precipitation solution (consisting of methanol: acetonitrile: 10% acetic acid [25 µL, 25 µL, 2 µL]) were added to 100 µL of plasma samples. The mixture was vortexed for 30 seconds (model 02215365, Fisher Scientific, Ontario, Canada) and centrifuged at 18,600 g for 4 minutes at 4 °C (model 5424R, Eppendorf, Ontario, Canada). The supernatant (5 µL) was injected into the LCMS-8050 (Shimadzu, Kyoto, Japan) [54]. The free (i.e., unbound) MPA and MPAG concentrations were quantified by an additional ultrafiltration procedure using 400 µL of plasma samples. Samples were centrifuged using Millipore Centrifree® devices (catalog# 4104, 30 KDa cut-off) for 30 minutes at 2,000 g and room temperature (model 5702R, Eppendorf, Ontario, Canada) [250, 402], and 100 µL of the filtrate was collected for processing as per protocol above. The details of the chromatographic conditions and instrument settings have already been published [54]. The only modifications for the unbound assays were the omission of 10% acetic acid (used for the stabilization of the acyl glucuronide, which was not quantified in its unbound form due to expected minimal plasma concentrations [2]) and the use of a higher injection volume of 30 µL.

p-Cresol is found in human plasma mainly in its conjugated forms (i.e., *p*-cresol sulfate and *p*-cresol glucuronide) [80-82, 84]; therefore, concentrations of *p*-cresol sulfate and *p*-cresol

glucuronide were utilized to reflect the overall plasma *p*-cresol exposure [84]. *p*-Cresol sulfate and *p*-cresol glucuronide were quantified by previously developed ultra-high-performance liquid chromatography-tandem mass spectrometry (UPLC-MS/MS) assay [56, 57]: 30 μL of human plasma sample was mixed with 90 μL of methanol containing *p*-cresol sulfate-d_7 and *p*-cresol glucuronide-d_7 (1 μg/mL each) as internal standards. Sample extraction was carried out at room temperature for 20 minutes, followed by vortex mixing (model 02215365, Fisher Scientific, Ontario, Canada) and sonication (model 75D, VWR, Ontario, Canada) for 30 seconds each. After centrifugation at 4,000 g at 4 °C for 10 minutes (model 5424R, Eppendorf, Ontario, Canada), 5 μL of the supernatant was injected into the LCMS-8050 (Shimadzu, Kyoto, Japan). The chromatographic and mass spectrum conditions have been reported previously [56, 57]. Given consistent recovery and the lack of matrix interference as compared to already validated assays [54, 56, 57], the quantification assays utilized in this research were validated in human plasma with respect to precision, accuracy, stability, and dilution integrity based on the bioanalytical method validation guidance established by the US Food and Drug Administration (FDA) [273].

2.5. Data analysis

Data are presented as mean ± standard deviation (SD). Continuous data were logarithm (base 10) transformed before processing to improve normality and equal variance. The primary analysis was to assess the correlation between plasma *p*-cresol metabolite exposure (independent variable) and the trough total plasma concentrations of MPA (raw value, normalized to daily dose, or normalized to body weight, as dependent variables) using the following 3-step approach established *a priori* (e.g., [133, 403]): i) To identify all significant individual variables affecting total MPA trough concentration using univariate regression modeling or categorical testing. ii) To

conduct multiple regression modeling combining *p*-cresol metabolite exposure and other significant clinical variables as predictors of total MPA trough concentrations. Multiple regression was not executed if *p*-cresol metabolite exposure was not a significant variable (even with other significant independent variables identified) or if *p*-cresol metabolite exposure was the only significant variable. iii) To assign subjects into distinct groups based on their *p*-cresol metabolite exposure (i.e., lesser or greater than the median) and compare the two groups with respect to total MPA concentrations using the Mann-Whitney test. For univariate models, the relationship between continuous variables were assessed by Spearman analysis, whereas the effects of categorical variables (e.g., sex, donor type, and concurrent medication) were tested using the Mann-Whitney or the Kruskal-Wallis one-way analysis of variance (ANOVA) followed by the Dunn's test. As participants may be exposed to multiple co-administered drugs, a scoring system was devised to evaluate the overall effects of potential drug interactions using the Lexicomp database [26] (Supplementary materials). Correlations between MPA (including dose) or MPA metabolite concentrations, ratios, or free fractions were not considered because these variables were not independent from each other. Furthermore, our secondary analyses determined the associations between *p*-cresol metabolite exposure and other MPA-related variables using the same approach as outlined for the primary analysis. The dependent variables included i) trough concentrations (C_0) of total MPAG, total AcMPAG, free MPA, free MPAG (as the raw value or normalized to dose or body weight); ii) ratios of total MPAG C_0-to-total MPA C_0, total AcMPAG C_0-to-total MPA C_0, total AcMPAG C_0-to-total MPAG C_0, free MPAG C_0-to-free MPA C_0; and iii) free fractions of MPA and MPAG. Statistical analyses were performed in GraphPad Prism (version 9.2.0) [404]. A p value < 0.05 was deemed significant.

3. Results

3.1. Patients and clinical data collection

Forty participants (*n*=11 females) were enrolled into the study, with a post-transplant time of 74 (± 60) days (mean [± SD]) (Table IX-1). Half of the transplantations were obtained from living donors. The age and eGFR were 53.7±12.4 years and 51.9±18.0 mL/min/1.73 m^2, respectively. The majority of other biochemistry data were within the normal limits [405] (Table IX-1). All patients received MMF (1.8±0.5 g/day) with tacrolimus (10.3±6.8 mg/day), and 33 participants (i.e., ~83% of the samples) also received prednisone (18.5±13.2 mg/day). The majority of the patients (*n*=35, i.e., ~88%) had achieved steady-state MMF administration (defined as being on at least 4 days of therapy with no dose changes, based on the population average half-life of MPA [2]). Most patients were administered basiliximab (*n*=35 / 40); therefore, induction therapy was not analyzed as a variable (Table IX-1).

3.2. Sample analyses

The plasma C_0 of MPA, MPAG, and AcMPAG were determined in 40 samples using LC-MS/MS (See **2 Methods**). Calibration ranges for total MPA and MPAG were 4.7–3200 ng/mL, and for total AcMPAG was 4.7–1600 ng/mL. Total AcMPAG concentrations were quantified un-diluted, while total MPA and MPAG required dilution (20- or 30-times) with blank plasma. Total MPA, MPAG, and AcMPAG C_0 (i.e., 2.8±2.2 µg/mL, 33.8±21.4 µg/mL, and 0.24±0.35 µg/mL, respectively [Table IX-2]) were above the lower limits of quantitation (LLOQ) and consistent with reported literature values (e.g., [10, 59, 140, 214, 234, 406]). On the other hand, the calibration range for free MPA and MPAG was 2.5–2500 ng/mL. Although sample dilution was not needed

for free MPA, a 10-fold dilution using blank plasma was required for free MPAG. Free MPA concentrations were detectable in 39 samples (0.043±0.051 µg/mL), while all free MPAG concentrations (4.9±4.5 µg/mL) were above the LLOQ. Based on these data, the corresponding free fractions (i.e., free/total concentrations) of MPA and MPAG were 1.4±0.8% (*n*=39) and 14.5±8.1 (*n*=40), respectively, which were also consistent with values reported in similar patient populations [10, 59, 250, 402]. In addition to absolute concentrations, normalized values (based on daily dose or body weight) and the MPA metabolite ratios (MPAG-to-MPA, AcMPAG-to-MPA, and/or AcMPAG-to-MPAG) were also calculated (Table IX-2). The precision, accuracy, stability, and dilution integrity of all assays were successfully validated based on guidance suggested by the FDA [273] (Table S IX-1, Table S IX-2, Table S IX-3, Table S IX-4, Supplementary materials).

Concentrations of *p*-cresol sulfate and *p*-cresol glucuronide were determined by an UPLC-MS/MS assay [56, 57] which was also validated in human plasma for this investigation (Table S IX-5, Table S IX-6, Supplementary materials). The linear calibration ranges of *p*-cresol sulfate and *p*-cresol glucuronide were 0.001–80000 ng/mL and 0.08–80000 ng/mL, respectively. *p*-Cresol sulfate was quantifiable in all 40 samples, but *p*-cresol glucuronide concentrations were all below the LLOQ despite our assay having comparable sensitivity to other published assays (e.g., [128]), an observation consistent with the literature where the sulfonated metabolite typically represented >95% of conjugated *p*-cresol [80] and very low *p*-cresol glucuronide concentrations were reported in kidney transplant populations [126, 128]. As a control experiment to rule out the instability of *p*-cresol sulfate or *p*-cresol glucuronide, *p*-cresol (would have been detected if there had been deconjugation) was also not found in these samples by an UPLC assay with a LLOQ of 0.07 µg/mL (modified based on published method [93]; data not shown). Therefore, *p*-cresol

sulfate was the only identifiable metabolite in our samples, and its plasma concentrations (3.6±2.0 μg/mL) in our population were consistent with the historical data reported in other adult kidney transplant recipients [83, 126, 128, 130] (Table IX-2). As such, *p*-cresol sulfate was used to represent the overall *p*-cresol exposure for all subsequent analyses.

3.3. Control correlations

In addition to our concentration data being comparable to literature values, control analyses were also conducted to ensure the validity of our data. A significant positive association between total MPA C_0 and total MPAG C_0 was observed in our dataset (Figure IX-1 a), which confirmed the known relationship between MPA and its direct, major metabolite [10, 51]. The ratio of total MPAG C_0 to total MPA C_0 (a marker of MPA intrinsic clearance [27, 59]) was negatively associated with post-transplant time (Figure IX-1 b), which may be consistent with the time-dependent effects of MPA clearance secondary to factors such as prednisone [10, 407]. As both MPAG and *p*-cresol sulfate are primarily excreted by the kidneys [10, 78], negative relationships between total MPAG C_0 (Figure IX-1 c) or *p*-cresol sulfate concentrations (Figure IX-1 d) and renal function were also observed (e.g., [127, 129, 130, 408]). These control correlations supported the validity of our dataset.

3.4. Primary outcome

Significant associations between *p*-cresol sulfate concentrations (representing overall *p*-cresol exposure as discussed in section 3.2) and either total MPA C_0 (coefficient of correlation [R]=0.39, p=0.013), total MPA C_0 normalized to daily dose (R=0.32, p=0.046), or total MPA C_0

normalized to body weight (R=0.32, p=0.043) were observed using univariate regression modeling (Figure IX-2; Table IX-3). Other than *p*-cresol sulfate, no other independent clinical variables in our dataset were identified affecting total MPA C_0 (Table S IX-7, Table S IX-8, Table S IX-9, Supplementary materials**)**; therefore, multiple regression modeling was not conducted per pre-established protocol (see **2 Methods**). Furthermore, patients were categorized into two groups based on the median *p*-cresol sulfate concentration. Consistent with correlational data, patients with elevated *p*-cresol sulfate concentrations (i.e., ≥ the median value of 3.2 μg/mL) exhibited increased total MPA C_0 (by 57%, p=0.007, *n*=20), total MPA C_0 normalized to daily dose (by 89%, p=0.010, *n*=20), and total MPA C_0 normalized to body weight (by 62%, p=0.006, *n*=20) compared to subjects with *p*-cresol sulfate concentrations below the median value (*n*=20) (Figure IX-3).

3.5. Secondary outcomes

The correlations between *p*-cresol sulfate and MPA metabolites (total MPAG or total AcMPAG) or free MPA or free MPAG were assessed as *secondary* outcomes. *p*-Cresol sulfate was positively correlated with daily dose-normalized free MPAG C_0 (R=0.32, p=0.043), but no other significant secondary correlations were found between *p*-cresol sulfate with any other tested dependent variables exhibiting concentration units (Table IX-3). As serum creatinine and eGFR were also significantly associated with daily dose-normalized free MPAG C_0 (Table S IX-7, Supplementary materials), multiple regression modeling was conducted incorporating *p*-cresol sulfate concentration and eGFR (instead of serum creatinine, due to collinearity) as independent variables. The outcome was the retainment of eGFR in the regression equation (p=0.021), while eliminating *p*-cresol sulfate concentration as a significant predictor. Likewise, none of the

calculated ratios or free fractions were associated with *p*-cresol sulfate concentrations (Table IX-3); therefore, multiple regression modeling was not conducted per pre-established protocol.

4. Discussion

Our primary finding was the positive association between total plasma *p*-cresol sulfate concentrations and total MPA C_0 in adult kidney transplant patients. This was the first *in vivo* observation in humans, to our knowledge, and was consistently reproduced with either regression modeling or categorical analyses, irrespective of the form of the data (i.e., raw value or normalized [Figure IX-2**,** Figure IX-3; Table IX-3]) analyzed. The observed clinical interaction is consistent with our stated hypothesis and the previously reported human *in vitro* mechanistic data [54, 55] where *p*-cresol was found a potent inhibitor of MPA glucuronidation in a human hepatic cell line [54] and human liver microsomes [55]. These novel findings were also obtained in the context of control correlations which were consistent with the literature (Figure IX-1), supporting the validity of our findings. The observation that *p*-cresol sulfate was the primary metabolite in our patient population (with relatively stable graft function and likely only minor accumulation of *p*-cresol metabolites) was also supported by the enzyme kinetics of *p*-cresol metabolism, where sulfonation is expected to be the predominant pathway given its higher efficiency (i.e., lower concentration required to achieve half-maximal catalytic activity, K_m) [56] compared to glucuronidation [57]. The concentrations of *p*-cresol sulfate observed in our sample population were also consistent with other comparable kidney transplant recipients [83, 126, 128, 130].

The correlation between *p*-cresol sulfate and total MPA C_0, although statistically significant, was, however, relatively weak (Figure IX-2; Table IX-3) (although still clinically

relevant as it potentially explained ~10-15% of MPA variability based on coefficients of determination). This was not unexpected given the multitude of other extrinsic and intrinsic variables known to affect MPA exposure [10, 27, 31], which can vary by up to 10-fold in kidney transplant recipients [10, 30, 59, 61]. The large variations in MPA concentrations were also evident in our dataset (Table IX-2, Figure IX-1**,** Figure IX-2**,** Figure IX-3). The weak correlation could also be possibly attributed to the utilization of trough MPA concentrations (ethically required for this initial first-in-human study before full exposure analysis can be conducted) which may not be the best marker for determining MPA exposure [2]. As such, full area under the concentration-time curve analysis using limited sampling strategies or population pharmacokinetic modeling [10, 31, 62] may generate even stronger associations. It may also be possible that *p*-cresol sulfate could displace the protein binding of MPA, thereby increasing the free fraction of MPA and leading to a decrease in total MPA plasma concentrations. In addition, our sample population did not exhibit substantially elevated plasma concentrations of *p*-cresol sulfate, which was expected as our participants all had successful transplantations with sufficient graft functions (i.e., eGFR values of 51.9±18.0 mL/min/1.73 m^2) to excrete *p*-cresol sulfate. The average *p*-cresol sulfate plasma concentration in our sample population was 3.6±2.0 μg/mL (or 19.1±10.6 μM), which was within or lower than the range of inhibitory constants (K_i) or half-maximal inhibitory concentration (IC_{50}) values of *p*-cresol characterized in our *in vitro* models (5.2–55 μM) [54, 55]. This indicates that we were only obtaining up to or less than 50% of inhibition in MPA metabolism in these subjects. Therefore, one might also anticipate that the correlation between *p*-cresol sulfate and total MPA C_0 would be much stronger had *p*-cresol sulfate concentrations been further elevated. For example, at the time of transplantation, serum *p*-cresol sulfate concentrations have been demonstrated to be 10-times higher than day 7 or month 3 post-transplantation [128]. Likewise, in the setting of

chronic and/or active graft rejections (not captured in our study), renal function could also be reduced significantly leading to much higher *p*-cresol accumulation; therefore, it would be worthwhile to extend the timeframe of the investigation (i.e., at later post-transplant time points) to include more patients with altered renal functions. Furthermore, *p*-cresol is primarily metabolized to *p*-cresol sulfate and *p*-cresol glucuronide by human sulfotransferase (SULT)1A1 and UGT1A6, respectively [56, 57]; and MPA is primarily conjugated by UGT1A9 to MPAG [10, 35]; therefore, individuals administrated modulators or carrying gain/loss-of-function genetic polymorphisms to these enzymes may exhibit altered *p*-cresol metabolite (no data available) and/or MPA exposure [2, 409], leading to stronger or weaker correlations. While not an objective of the current investigation, it would be worthwhile, given our positive findings, to further examine the effects of genomics on the observed interaction.

In addition to *p*-cresol inhibiting the hepatic intrinsic clearance of MPA [54, 55] as a potential mechanism explaining our primary observation, it is also possible that *p*-cresol may have inhibited the intrinsic clearance of MPA in intestines and kidneys, which also express UGT1A9 [35, 310, 376] and can also contribute to increased total MPA concentrations. Moreover, it may also be possible that impaired renal function could lead to the accumulation of total MPA C_0 through various potential mechanisms. For example, the expression levels of hepatic multidrug resistance-associated protein (MRP) 2, which can mediate the biliary excretion of MPAG [410], were reported to be increased in a rodent experimental model of chronic kidney failure [411]. This mechanism could potentially lead to an increase in the entero-hepatic recirculation of MPAG and possibly an increase in plasma MPA exposure [228]. In addition, uremic toxins have been shown to inhibit the activities of the human hepatic MRP 4 in an *in vitro* model [412], and MPAG was demonstrated to be a substrate of this efflux transporter [410, 413]; therefore, it may also be

possible that decreased MRP 4 activities from renal dysfunction/uremic toxin exposure may have led to increased entero-hepatic recirculation of MPA. Although the relationship between kidney function and MPA C_0 was not significant in our study (Table S IX-7, Supplementary materials), further characterizations are needed to rule out these potential confounding effects. Furthermore, other protein-bound uremic toxins (e.g., indoxyl sulfate and indole-3-acetic acid [e.g., [87]]) may also have impacts on the pharmacokinetics of MPA based on their potential interacting effects on drug metabolism enzymes and transporters [53], which would warrant further investigations.

On the other hand, consistent correlations between MPAG C_0 (total or free) or unbound MPA C_0 and *p*-cresol sulfate concentrations were not observed in our secondary analyses (Table IX-3), which was unexpected given the hypothesized mechanism of MPA metabolism inhibition. However, these negative findings were likely due to insufficient statistical power for these secondary, exploratory findings, or the possibilities of multiple interacting processes/mechanisms. For example, *p*-cresol may have potentially affected the entero-hepatic recirculation of MPA by inhibiting organic anion transporting polypeptides (OATP) 1B1/3, which would lead to a reduction in MPA exposure [43, 414, 415]; however, this mechanism could not be verified in the current study due to insufficient number of samples collected from each patient to adequately characterize MPA reabsorption. Furthermore, it may also be possible that *p*-cresol sulfate could have caused various forms of endothelial cellular damage [94, 97], leading to increased distribution/partitioning of unbound MPA into various tissues (peripheral compartment), thereby decreasing free MPA concentrations in the plasma (central compartment) and opposing the effects of the expected increase from UGT1A9 inhibition. Moreover, the lack of significant associations with secondary markers could also be explained by *p*-cresol sulfate potentially inhibiting the renal excretion of MPAG, therefore leading to its accumulation in the plasma that may have counteracted the effects

of decreased MPAG formation from hepatic metabolism inhibition. MPAG is primarily excreted by the kidneys [10] presumably through organic anion transporter (OAT) 3 [38], and *p*-cresol sulfate is a known inhibitor of OAT3 as established with other probe substrates [223]. Subsequent *in vitro* studies in renal tubular cellular models and *in vivo* human studies with additional plasma and urine samples (being planned) will allow the characterizations of MPA full exposure, transporter inhibition, compartmental kinetics, and renal clearance to elucidate the potential mechanisms identified from these secondary, exploratory findings.

In conclusion, we have identified a novel, positive association between *p*-cresol sulfate exposure and total MPA C_0 in adult kidney transplant recipients, which is supported by already published mechanistic *in vitro* data. Our findings confirm a role of *p*-cresol sulfate (via *p*-cresol) as a potentially significant clinical variable affecting the pharmacokinetics of MPA and suggest a potential approach for improving MPA precision dosing by targeting *p*-cresol generation. Our positive findings also provide the justifications for conducting subsequent full-scale pharmacokinetic-pharmacodynamic studies to further characterize the cause-effect relationships of this interaction and to rule out potential confounding variables which could not be adequately controlled in this correlational study.

Table IX-1 Demographic and biochemistry data in adult kidney transplant patients (n=40)

Characteristics (Normal range)	Mean ± SD	Median (minimum – maximum)
Age, years	53.7 ± 12.4	54.0 (30.0 – 72.0)
Body weight, kg	79.8 ± 18.5	78.1 (41.1 – 123.0)
Post-transplant time, day	74 ± 60	58 (7 – 216)
Serum creatinine, μM (male: 50 – 120; female: 40 – 100) [a]	137.3 ± 44.7	126.5 (72.0 – 246.0)
eGFR (CKD-EPI equation), mL/min/1.73 m^2 (> 59) [a]	51.9 ± 18.0	50.0 (23.0 – 104.0)
Serum albumin, g/dL (3.0 – 4.5) [a]	3.6 ± 0.5	3.6 (2.5 – 4.5)
Total bilirubin, mg/dL (< 1.2) [a]	0.7 ± 0.4	0.6 (0.4 – 2.4)
Alanine aminotransferase, U/L (male: < 60; female < 40) [a]	24.5 ± 15.1	20.5 (7.0 – 75.0)
Aspartate aminotransferase, U/L (*n*=39) (< 40) [a]	23.5 ± 13.2	19.0 (9.0 – 84.0)
Gamma-glutamyl transferase, U/L (*n*=39) (male: < 80; female: < 50) [a]	32.1 ± 29.1	22.0 (8.0 – 174.0)
White blood cell count, $\times 10^9$/L (4.0 – 11.0) [a]	9.2 ± 4.8	8.4 (2.1 – 22.4)
Neutrophil, $\times 10^9$/L (1.8 – 7.5) [a]	6.4 ± 4.3	5.4 (0.7 – 21.2)
Prednisone daily dose, mg (*n*=33)	18.5 ± 13.2	15.0 (5.0 – 70.0)
Tacrolimus daily dose, mg	10.3 ± 6.8	8.0 (1.0 – 30.0)
Tacrolimus total C_0, μg/L [b]	9.4 ± 2.4	9.0 (4.6 – 15.4)
MMF daily dose, g	1.8 ± 0.5	2.0 (0.5 – 2.0)
Sex		
Male, *n* (%)		29 (72.5)
Female, *n* (%)		11 (27.5)
Donor type		
Deceased, *n* (%)		20 (50.0)
Living, *n* (%)		20 (50.0)
Induction regimens		
Basiliximab, *n* (%)		35 (87.5)
Thymoglobulin, *n* (%)		3 (7.5)

Basiliximab followed by thymoglobulin, *n* (%)	2 (5.0)

[a] Normal ranges retrieved from [405] (accessed date: September 10, 2021)

[b] Common unit used in North America. Conversion factor for tacrolimus concentration: 1.0 µg/L = 1.2 nM

Abbreviation(s): C_0, trough concentration; *CKD-EPI equation,* chronic kidney disease epidemiology collaboration equation; *eGFR,* estimated glomerular filtration rate; *MMF,* mycophenolate mofetil; *SD,* standard deviation.

Table IX-2 Plasma concentrations of MPA, MPAG, AcMPAG, and p-cresol sulfate (n=40)

Parameters	Mean ± SD	Median (minimum – maximum)
Total MPA C_0, µg/mL [a]	2.8 ± 2.2	2.3 (0.2 – 10.4)
Total MPAG C_0, µg/mL [a]	33.8 ± 21.4	29.2 (2.8 – 84.3)
Total AcMPAG C_0, µg/mL [a]	0.24 ± 0.35	0.10 (0.01 – 1.42)
Daily dose-normalized total MPA C_0, µg/mL/g	1.8 ± 1.5	1.2 (0.1 – 6.3)
Daily dose-normalized total MPAG C_0, µg/mL/g	19.2 ± 12.9	15.9 (3.7 – 61.5)
Daily dose-normalized total AcMPAG C_0, µg/mL/g	0.15 ± 0.21	0.06 (0.01 – 0.88)
Body weight-normalized total MPA C_0, µg/mL/kg	0.038 ± 0.034	0.029 (0.003 – 0.152)
Body weight-normalized total MPAG C_0, µg/mL/kg	0.44 ± 0.29	0.36 (0.03 – 1.27)
Body weight-normalized total AcMPAG C_0, µg/mL/kg	0.0032 ± 0.0045	0.0014 (0.0001 – 0.0181)
Ratio of total MPAG C_0 to total MPA C_0	17.4 ± 17.2	13.9 (2.0 – 99.9)
Ratio of total AcMPAG C_0 to total MPA C_0	0.14 ± 0.26	0.04 (0.01 – 1.19)
Ratio of total AcMPAG C_0 to total MPAG C_0	0.0089 ± 0.0112	0.0045 (0.0004 – 0.0492)
Free MPA C_0, µg/mL (*n*=39)	0.043 ± 0.051	0.025 (0.004 – 0.229)
Free MPAG C_0, µg/mL	4.9 ± 4.5	4.4 (0.3 – 19.7)
Daily dose-normalized free MPA C_0, µg/mL/g (*n*=39)	0.026 ± 0.029	0.016 (0.002 – 0.115)
Daily dose-normalized free MPAG C_0, µg/mL/g	2.9 ± 2.7	2.5 (0.2-10.8)
Body weight-normalized free MPA C_0, µg/mL/kg (*n*=39)	0.00059 ± 0.00076	0.00033 (0.00005 – 0.00345)
Body weight-normalized free MPAG C_0, µg/mL/kg	0.064 ± 0.060	0.052 (0.006 – 0.296)
Ratio of free MPAG C_0 to free MPA C_0 (*n*=39)	210.8 ± 263.8	123.3 (9.6 – 1065.4)
Free fraction of MPA, % (*n*=39)	1.4 ± 0.8	1.3 (0.2 – 3.5)

Free fraction of MPAG, %	14.5 ± 8.1	12.9 (2.6 – 34.0)
Total *p*-cresol sulfate concentration, µg/mL [a]	3.6 ± 2.0	3.2 (0.4 – 8.1)

[a] Common unit used in North America. Conversion factors for MPA concentration: 1.0 µg/mL = 3.1 µM; MPAG concentration: 1.0 µg/mL = 2.0 µM; AcMPAG concentration: 1.0 µg/mL = 2.0 µM; and *p*-cresol sulfate concentration: 1.0 µg/mL = 5.3 µM

Abbreviation(s): *AcMPAG,* mycophenolic acid acyl glucuronide; *C_0,* trough concentration; *MPA,* mycophenolic acid; *MPAG,* mycophenolic acid glucuronide; *SD,* standard deviation.

Table IX-3 Spearman correlational analyses between MPA, MPAG, or AcMPAG and p-cresol sulfate

Variables	R (p value)
Total MPA C_0, μg/mL [a, b]	0.39 (0.013) *
Total MPAG C_0, μg/mL [a]	0.18 (0.263)
Total AcMPAG C_0, μg/mL [a]	0.20 (0.219)
Daily dose-normalized total MPA C_0, μg/mL/g [b]	0.32 (0.046) *
Daily dose-normalized total MPAG C_0, μg/mL/g	0.24 (0.142)
Daily dose-normalized total AcMPAG C_0, μg/mL/g	0.22 (0.176)
Body weight-normalized total MPA C_0, μg/mL/kg [b]	0.32 (0.043) *
Body weight-normalized total MPAG C_0, μg/mL/kg	0.14 (0.392)
Body weight-normalized total AcMPAG C_0, μg/mL/kg	0.17 (0.307)
Ratio of total MPAG C_0 to total MPA C_0	-0.10 (0.559)
Ratio of total AcMPAG C_0 to total MPA C_0	-0.11 (0.498)
Ratio of total AcMPAG C_0 to total MPAG C_0	0.01 (0.973)
Free MPA C_0, μg/mL	0.16 (0.316)
Free MPAG C_0, μg/mL	0.29 (0.073)
Daily dose-normalized free MPA C_0, μg/mL/g	0.14 (0.398)
Daily dose-normalized free MPAG C_0, μg/mL/g	0.32 (0.043) *
Body weight-normalized free MPA C_0, μg/mL/kg	0.11 (0.500)
Body weight-normalized free MPAG C_0, μg/mL/kg	0.24 (0.139)
Ratio of free MPAG C_0 to free MPA C_0	0.06 (0.706)
Free fraction of MPA, %	-0.06 (0.712)
Free fraction of MPAG, %	0.18 (0.259)

R and p values were obtained from Spearman correlational analyses (n=39-40)

[a] Common unit used in North America. Conversion factors for MPA concentration: 1.0 μg/mL = 3.1 μM; MPAG concentration: 1.0 μg/mL = 2.0 μM; AcMPAG concentration: 1.0 μg/mL = 2.0 μM

[b] Primary outcome analyses (please also see Figure IX-2)

[*] $p < 0.05$

Abbreviation(s): *AcMPAG,* mycophenolic acid acyl glucuronide; C_0, trough concentration; *MPA,* mycophenolic acid; *MPAG,* mycophenolic acid glucuronide; *R,* correlation coefficient.

a

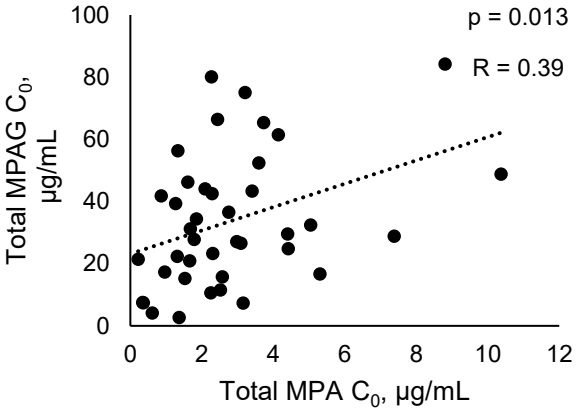
p = 0.013
R = 0.39
Total MPAG C_0, µg/mL
Total MPA C_0, µg/mL
0
20
40
60
80
100
0
2
4
6
8
10
12

b

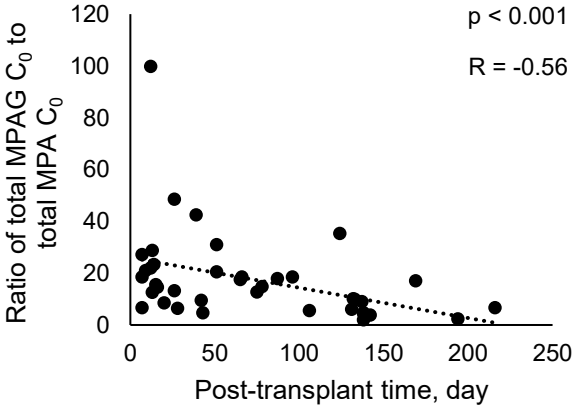
p < 0.001
R = -0.56
Ratio of total MPAG C_0 to total MPA C_0
Post-transplant time, day
0
20
40
60
80
100
120
0
50
100
150
200
250

c

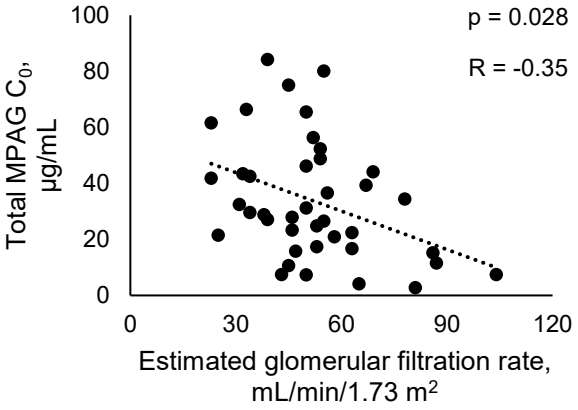
p = 0.028
R = -0.35
Total MPAG C_0, µg/mL
Estimated glomerular filtration rate, mL/min/1.73 m^2
0
20
40
60
80
100
0
30
60
90
120

d

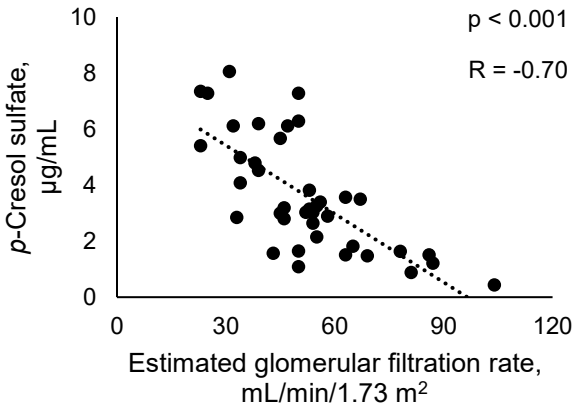

Figure IX-1 Control correlations observed between (a) total MPA C_0 and total MPAG C_0, (b) post-transplant time and the ratio of total MPAG C_0 to total MPA C_0, (c) estimated glomerular filtration rate and total MPAG C_0, and (d) estimated glomerular filtration rate and p-cresol sulfate concentrations

p and R values were obtained from Spearman correlational analyses (n=40)

Abbreviation(s): C_0, trough concentration; *MPA,* mycophenolic acid; *MPAG,* mycophenolic acid glucuronide; *R,* correlation coefficient.

a

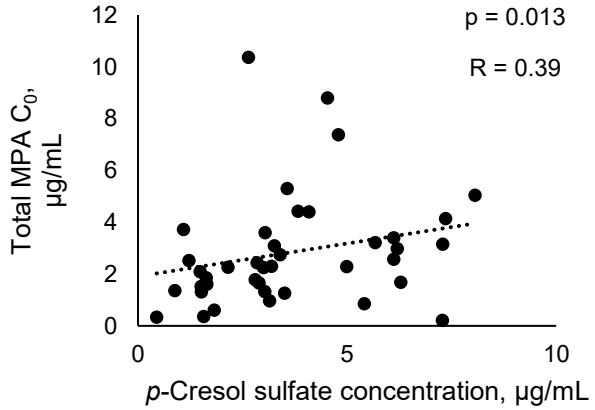
p = 0.013
R = 0.39
Total MPA C_0, µg/mL
12
10
8
6
4
2
0
0
5
10
p-Cresol sulfate concentration, µg/mL

b

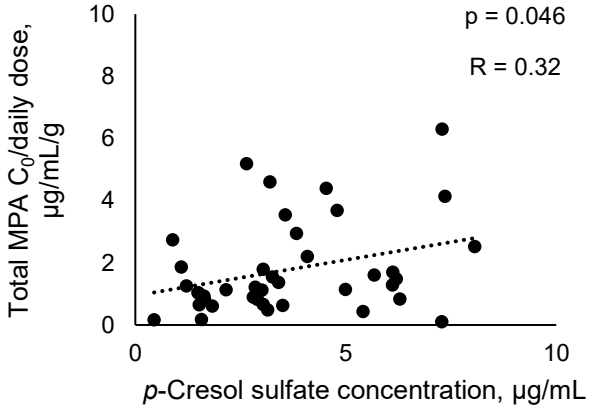
p = 0.046
R = 0.32
Total MPA C_0/daily dose, µg/mL/g
10
8
6
4
2
0
0
5
10
p-Cresol sulfate concentration, µg/mL

c

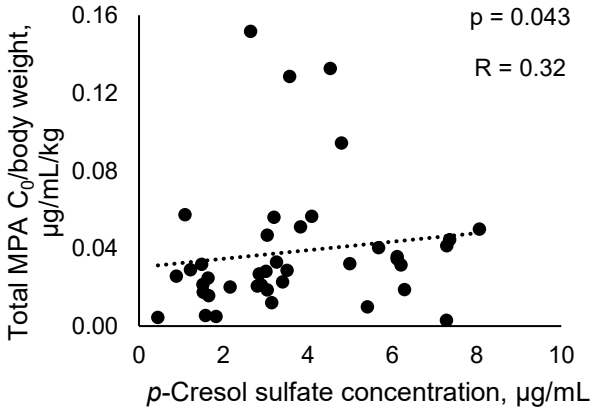
p = 0.043
R = 0.32
Total MPA C_0/body weight, µg/mL/kg
0.16
0.12
0.08
0.04
0.00
0
2
4
6
8
10
p-Cresol sulfate concentration, µg/mL

Figure IX-2 Primary outcome correlations between p-cresol sulfate concentrations and (a) total MPA C_0, (b) daily dose-normalized total MPA C_0, and (c) body weight-normalized total MPA C_0

p and R values were obtained from Spearman correlational analyses (*n*=40)

Abbreviation(s): *C_0,* trough concentration; *MPA,* mycophenolic acid; *R,* correlation coefficient.

a

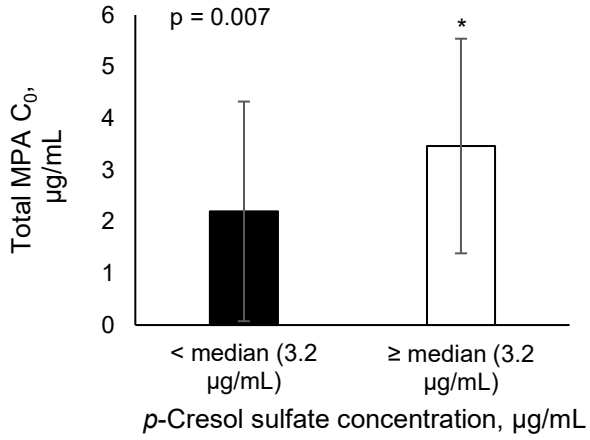
p = 0.007
*
Total MPA C_0, µg/mL
6
5
4
3
2
1
0
< median (3.2 µg/mL)
≥ median (3.2 µg/mL)
p-Cresol sulfate concentration, µg/mL

b

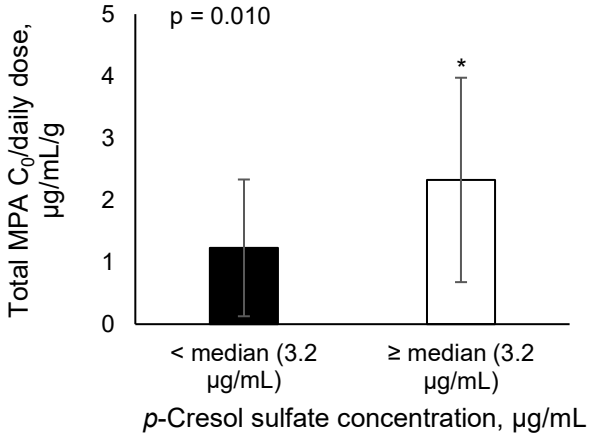
p = 0.010
*
Total MPA C_0/daily dose, µg/mL/g
5
4
3
2
1
0
< median (3.2 µg/mL)
≥ median (3.2 µg/mL)
p-Cresol sulfate concentration, µg/mL

c

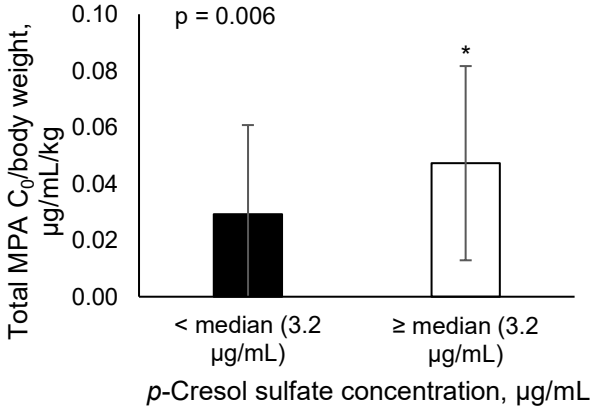
p = 0.006
*
Total MPA C_0/body weight, µg/mL/kg
0.10
0.08
0.06
0.04
0.02
0.00
< median (3.2 µg/mL)
≥ median (3.2 µg/mL)
p-Cresol sulfate concentration, µg/mL

Figure IX-3 Concentrations of (a) total MPA C_0, (b) daily dose-normalized total MPA C_0, and (c) body weight-normalized total MPA C_0 based on the median concentration value of p-cresol sulfate (n=20 in each group)

* $p < 0.05$

Abbreviation(s): *C_0,* trough concentration; *MPA,* mycophenolic acid.

Supplementary materials

S1. Scoring system for drug-drug interaction screening

As participants may be exposed to multiple co-administered drugs, a scoring system was devised to evaluate the overall effects of potential drug interactions (i.e., score 1 for drugs that are known to increase MPA exposure; score -1 for drugs that decrease MPA exposure; and score 0 for non-interacting drugs; with the sum of the interaction scores calculated for each patient) using data provided in the Lexicomp database [26].

Table S IX-1 Intra- and inter-day precision and accuracy of total MPA, MPAG, and AcMPAG assays in human plasma

Analytes	Nominal concentrations	Intra-day (1), *n*=5		Intra-day (2), *n*=5		Intra-day (3), *n*=5		Inter-day, *n*=15	
		CV (%)	Accuracy (%)	CV (%)	Accuracy (%)	CV (%)	Accuracy (%)	CV (%)	Accuracy (%)
MPA	4.67 ng/mL (LLOQ)	12.22	102.76	6.66	113.40	17.90	106.84	4.95	107.84
	12.96 ng/mL (low QC)	11.35	106.22	9.02	107.92	10.07	107.34	0.81	106.99
	100 ng/mL (medium QC)	11.21	108.15	9.19	107.09	5.45	111.25	1.99	108.83
	1600 ng/mL (high QC)	13.17	103.75	14.23	100.81	8.32	102.54	1.45	102.37
MPAG	4.67 ng/mL (LLOQ)	14.86	90.55	3.30	105.55	5.22	114.58	11.72	103.56
	12.96 ng/mL (low QC)	12.27	98.98	10.84	90.34	12.43	112.75	11.23	100.69
	100 ng/mL (medium QC)	9.27	102.60	8.55	87.37	10.17	107.90	10.73	99.29
	1600 ng/mL (high QC)	13.24	92.87	13.28	97.26	13.32	106.51	7.04	98.88
AcMPAG	4.67 ng/mL (LLOQ)	12.80	93.03	13.12	104.18	8.43	96.73	5.80	97.98
	12.96 ng/mL (low QC)	14.56	104.52	13.33	95.23	12.40	109.86	7.17	103.21
	36 ng/mL (medium QC)	11.33	104.07	12.27	101.56	9.29	86.97	9.47	97.53
	100 ng/mL (high QC)	10.34	105.40	11.96	103.75	10.72	108.44	2.24	105.86

Abbreviation(s): *AcMPAG,* mycophenolic acid acyl glucuronide; *CV,* coefficient of variation; *LLOQ,* lower limit of quantification; *MPA,* mycophenolic acid; *MPAG,* mycophenolic acid glucuronide; *QC,* quality control.

Table S IX-2 Stability tests and dilution integrity validations of total MPA, MPAG, and AcMPAG assays in human plasma

	MPA		MPAG		AcMPAG	
Nominal concentrations	12.96 ng/mL (low QC)	1600 ng/mL (high QC)	12.96 ng/mL (low QC)	1600 ng/mL (high QC)	12.96 ng/mL (low QC)	100 ng/mL (high QC)
Autosampler stability (% accuracy)	111.36	106.98	113.25	91.01	99.75	99.64
Bench-top stability (% accuracy)	92.79	104.12	105.51	99.31	105.87	94.34
Freeze-thaw stability (% accuracy)	108.00	99.13	88.92	87.99	99.38	106.54
One-month stability (% accuracy)	94.79	106.33	96.18	101.77	94.38	95.22
Dilution factor of 20 (% CV / % accuracy) [a]	3.93 / 99.55		5.86 / 96.93		NA (no dilution needed)	
Dilution factor of 30 (% CV / % accuracy) [a]	3.93 / 102.98		9.02 / 94.65		NA (no dilution needed)	

Various conditions were tested: i) autosampler stability (i.e., 24 hours at 4 °C), ii) bench-top stability (i.e., 6 hours at room temperature), iii) freeze-thaw stability (i.e., 3 cycles of freezing/thawing, where samples were frozen at -80 °C for 23.5 hours then thawed at room temperature for 0.5 hour), and iv) one-month stability (i.e., 1 month at -80 °C).

[a] Dilution stability was tested by diluting (with blank plasma) quality control samples (n=5) of which the concentrations were 20x or 30x above the upper limit of quantitation [273]. These dilution factors corresponded to the expected dilution in our samples.

Abbreviation(s): *AcMPAG,* mycophenolic acid acyl glucuronide; *CV,* coefficient of variation; *LLOQ,* lower limit of quantification; *MPA,* mycophenolic acid; *MPAG,* mycophenolic acid glucuronide; *NA,* not available; *QC,* quality control.

Table S IX-3 Intra- and inter-day precision and accuracy of free MPA and MPAG assays in human plasma

Analytes	Nominal concentrations	Intra-day (1), *n*=5		Intra-day (2), *n*=5		Intra-day (3), *n*=5		Inter-day, *n*=15	
		CV (%)	Accuracy (%)	CV (%)	Accuracy (%)	CV (%)	Accuracy (%)	CV (%)	Accuracy (%)
MPA	2.5 ng/mL (LLOQ)	11.09	82.40	10.89	97.05	5.35	106.05	13.57	95.17
	7.5 ng/mL (low QC)	11.92	104.92	11.18	102.80	8.85	110.00	10.31	105.91
	1000 ng/mL (medium QC)	5.05	106.84	6.76	99.54	6.39	95.06	7.52	100.48
	2000 ng/mL (high QC)	2.20	103.31	5.69	112.42	7.23	99.58	7.32	105.11
MPAG	2.5 ng/mL (LLOQ)	11.34	82.52	6.79	80.80	7.69	99.45	12.83	87.59
	7.5 ng/mL (low QC)	10.53	106.58	11.24	113.43	9.96	104.10	10.55	108.04
	1000 ng/mL (medium QC)	2.99	106.61	2.62	96.32	5.65	97.33	6.02	100.09
	2000 ng/mL (high QC)	1.36	101.41	3.40	111.24	3.45	111.01	5.19	107.89

Abbreviation(s): *AcMPAG,* mycophenolic acid acyl glucuronide; *CV,* coefficient of variation; *LLOQ,* lower limit of quantification; *MPA,* mycophenolic acid; *MPAG,* mycophenolic acid glucuronide; *QC,* quality control

Table S IX-4 Stability tests and dilution integrity validations of free MPA and MPAG assays in human plasma

	MPA		MPAG	
Nominal concentrations	7.5 ng/mL (low QC)	2000 ng/mL (high QC)	7.5 ng/mL (low QC)	2000 ng/mL (high QC)
Autosampler stability (% accuracy)	106.64	107.31	114.44	103.87
Bench-top stability (% accuracy)	113.07	107.42	112.91	101.51
Freeze-thaw stability (% accuracy)	102.19	111.51	108.56	98.86
One-month stability (% accuracy)	102.91	105.75	98.78	98.91
Dilution factor of 10 (% CV / % accuracy) [a]	NA (no dilution needed)		2.59 / 100.10	

Various conditions were tested: i) autosampler stability (i.e., 24 hours at 4 °C), ii) bench-top stability (i.e., 6 hours at room temperature), iii) freeze-thaw stability (i.e., 3 cycles of freezing/thawing, where samples were frozen at -80 °C for 23.5 hours then thawed at room temperature for 0.5 hour), and iv) one-month stability (i.e., 1 month at -80 °C).

[a] Dilution stability was tested by diluting (with blank plasma) quality control samples (n=5) of which the concentrations were 10x above the upper limit of quantitation [273]. These dilution factors corresponded to the expected dilution in our samples.

Abbreviation(s): *AcMPAG,* mycophenolic acid acyl glucuronide; *CV,* coefficient of variation; *LLOQ,* lower limit of quantification; *MPA,* mycophenolic acid; *MPAG,* mycophenolic acid glucuronide; *NA,* not available; *QC,* quality control.

Table S IX-5 Intra- and inter-day precision and accuracy of p-cresol sulfate and p-cresol glucuronide assays in human plasma

Analytes	Nominal concentrations	Intra-day (1), *n*=5		Intra-day (2), *n*=5		Intra-day (3), *n*=5		Inter-day, *n*=15	
		CV (%)	Accuracy (%)	CV (%)	Accuracy (%)	CV (%)	Accuracy (%)	CV (%)	Accuracy (%)
p-Cresol sulfate	0.001 ng/mL (LLOQ)	10.29	113.19	13.16	95.63	10.76	114.56	13.35	107.80
	0.004 ng/mL (low QC)	11.90	107.66	2.48	90.75	8.36	106.03	11.37	101.48
	30 µg/mL (medium QC)	6.45	109.28	2.72	100.32	6.52	111.11	6.95	106.90
	60 µg/mL (high QC)	4.64	110.85	4.31	102.88	4.98	114.29	6.26	109.34
p-Cresol glucuronide	0.08 ng/mL (LLOQ)	5.58	110.77	4.89	114.29	6.55	96.49	9.08	107.18
	0.23 ng/mL (low QC)	11.74	112.12	6.25	100.16	11.40	109.85	10.79	107.37
	30 µg/mL (medium QC)	5.00	105.76	2.46	102.12	5.04	107.93	4.69	105.27
	60 µg/mL (high QC)	3.33	110.34	2.55	110.96	3.31	113.87	3.19	111.72

Abbreviation(s): *CV,* coefficient of variation; *LLOQ,* lower limit of quantification; *QC,* quality control

Table S IX-6 Stability tests of p-cresol sulfate and p-cresol glucuronide assays in human plasma

	p-Cresol sulfate		*p*-Cresol glucuronide	
Nominal concentrations	0.004 ng/mL (low QC)	60 µg/mL (high QC)	0.23 ng/mL (low QC)	60 µg/mL (high QC)
Autosampler stability (% accuracy)	98.82	114.19	113.82	94.31
Bench-top stability (% accuracy)	98.26	114.67	112.97	94.55
Freeze-thaw stability (% accuracy)	102.87	97.62	110.55	89.65
One-month stability (% accuracy)	111.26	113.10	109.66	90.33

Various conditions were tested: i) autosampler stability (i.e., 24 hours at 4 °C), ii) bench-top stability (i.e., 6 hours at room temperature), iii) freeze-thaw stability (i.e., 3 cycles of freezing/thawing, where samples were frozen at -80 °C for 23.5 hours then thawed at room temperature for 0.5 hour), and iv) one-month stability (i.e., 1 month at -80 °C)

Abbreviation(s): *LLOQ,* lower limit of quantification; *QC,* quality control

Table S IX-7 Spearman correlational analyses of demographic and biochemistry data

R (p value)	Age, years	Body weight, kg	Post-transplant time, day	Serum creatinine, μM	eGFR, mL/min/1.73 m^2	Serum albumin, g/dL	Total bilirubin, mg/dL	ALT, U/L	AST, U/L	GGT, U/L	WBC, $\times 10^9$ /L	Neutrophil, $\times 10^9$/L	Prednisone daily dose, mg	Tacrolimus daily dose, mg	MMF daily dose, g
Total MPA C_0, μg/mL	-0.02 (0.888)	0.04 (0.799)	0.10 (0.545)	0.23 (0.157)	-0.28 (0.077)	0.11 (0.505)	-0.11 (0.507)	0.02 (0.927)	-0.24 (0.144)	-0.23 (0.156)	-0.03 (0.853)	-0.14 (0.397)	0.05 (0.797)	0.08 (0.629)	-0.06 (0.693)
Total MPAG C_0, μg/mL	0.12 (0.446)	0.12 (0.449)	-0.45 (0.003)	0.29 (0.066)	-0.35 (0.028)	-0.04 (0.810)	-0.34 (0.032)	0.06 (0.728)	-0.09 (0.581)	-0.10 (0.546)	0.24 (0.142)	0.22 (0.166)	0.27 (0.124)	0.22 (0.183)	0.41 (0.009)
Total AcMPAG C_0, μg/mL	-0.17 (0.298)	0.05 (0.781)	0.02 (0.898)	0.31 (0.054)	-0.28 (0.078)	-0.09 (0.599)	-0.02 (0.915)	-0.03 (0.870)	0.03 (0.847)	-0.08 (0.643)	-0.09 (0.585)	-0.15 (0.368)	0.003 (0.986)	0.05 (0.757)	0.11 (0.491)
Daily dose-normalized total MPA C_0, μg/mL/g	-0.06 (0.729)	-0.12 (0.452)	0.27 (0.088)	0.12 (0.464)	-0.19 (0.230)	0.01 (0.939)	-0.11 (0.497)	0.04 (0.791)	-0.10 (0.564)	-0.31 (0.058)	-0.19 (0.231)	-0.29 (0.067)	-0.11 (0.534)	0.10 (0.531)	-0.40 (0.012)
Daily dose-normalized total MPAG C_0, μg/mL/g	0.06 (0.700)	0.01 (0.960)	-0.29 (0.065)	0.25 (0.121)	-0.34 (0.031)	-0.11 (0.494)	-0.26 (0.102)	0.13 (0.440)	0.04 (0.829)	-0.19 (0.257)	0.09 (0.566)	0.08 (0.633)	0.13 (0.468)	0.22 (0.180)	0.07 (0.653)
Daily dose-normalized total AcMPAG C_0, μg/mL/g	-0.21 (0.204)	-0.04 (0.830)	0.17 (0.301)	0.27 (0.098)	-0.25 (0.127)	-0.12 (0.448)	<0.001 (0.997)	-0.03 (0.845)	0.14 (0.401)	-0.15 (0.358)	-0.21 (0.185)	-0.26 (0.101)	-0.06 (0.749)	0.02 (0.912)	-0.18 (0.274)
Body weight-normalized total MPA C_0, μg/mL/kg	-0.07 (0.646)	-0.27 (0.092)	0.17 (0.296)	0.10 (0.532)	-0.21 (0.197)	-0.02 (0.925)	-0.11 (0.515)	0.09 (0.571)	-0.19 (0.247)	-0.27 (0.101)	-0.02 (0.897)	-0.11 (0.510)	-0.07 (0.709)	0.13 (0.407)	-0.18 (0.268)
Body weight-normalized total MPAG C_0, μg/mL/kg	0.02 (0.916)	-0.18 (0.260)	-0.37 (0.020)	0.18 (0.262)	-0.28 (0.081)	-0.08 (0.611)	-0.27 (0.090)	0.08 (0.642)	-0.07 (0.660)	-0.21 (0.210)	0.29 (0.071)	0.29 (0.074)	0.11 (0.559)	0.21 (0.195)	0.31 (0.053)
Body weight-normalized total AcMPAG C_0, μg/mL/kg	-0.21 (0.193)	-0.16 (0.318)	0.03 (0.857)	0.23 (0.162)	-0.22 (0.167)	-0.06 (0.732)	0.05 (0.740)	-0.08 (0.624)	-0.04 (0.799)	-0.15 (0.355)	-0.02 (0.903)	-0.07 (0.668)	-0.04 (0.820)	0.02 (0.912)	0.04 (0.825)
Ratio of total MPAG C_0 to total MPA C_0	0.08 (0.630)	0.05 (0.750)	-0.56 (<0.001)	0.12 (0.470)	-0.13 (0.432)	-0.17 (0.309)	-0.09 (0.579)	0.04 (0.803)	0.10 (0.528)	0.22 (0.183)	0.31 (0.054)	0.40 (0.011)	0.25 (0.165)	0.07 (0.651)	0.45 (0.004)
Ratio of total AcMPAG C_0 to total MPA C_0	-0.10 (0.533)	0.02 (0.922)	-0.05 (0.775)	0.11 (0.506)	-0.06 (0.724)	-0.09 (0.573)	0.07 (0.673)	-0.03 (0.835)	0.20 (0.213)	0.12 (0.468)	-0.03 (0.877)	0.01 (0.941)	0.01 (0.935)	-0.06 (0.709)	0.14 (0.378)
Ratio of total AcMPAG C_0 to total MPAG C_0	-0.26 (0.101)	-0.06 (0.736)	0.29 (0.072)	0.08 (0.643)	-0.03 (0.867)	-0.04 (0.807)	0.16 (0.319)	-0.05 (0.745)	0.21 (0.194)	-0.04 (0.804)	-0.21 (0.192)	-0.23 (0.146)	-0.10 (0.567)	-0.08 (0.609)	-0.20 (0.226)
Free MPA C_0, μg/mL	0.16 (0.338)	-0.18 (0.280)	0.08 (0.620)	0.14 (0.392)	-0.19 (0.242)	0.14 (0.379)	-0.05 (0.774)	-0.02 (0.897)	-0.10 (0.546)	-0.14 (0.397)	-0.02 (0.924)	-0.04 (0.832)	-0.09 (0.616)	-0.04 (0.816)	-0.01 (0.960)

R (p value)	Age, years	Body weight, kg	Post-transplant time, day	Serum creatinine, μM	eGFR, mL/min/1.73 m^2	Serum albumin, g/dL	Total bilirubin, mg/dL	ALT, U/L	AST, U/L	GGT, U/L	WBC, $\times 10^9$ /L	Neutrophil, $\times 10^9$/L	Prednisone daily dose, mg	Tacrolimus daily dose, mg	MMF daily dose, g
Free MPAG C_0, μg/mL	0.13 (0.422)	0.07 (0.667)	-0.31 (0.051)	0.42 (0.007)	-0.47 (0.002)	0.11 (0.515)	0.01 (0.948)	0.08 (0.638)	-0.04 (0.805)	-0.14 (0.412)	0.12 (0.444)	0.14 (0.402)	0.18 (0.310)	0.14 (0.388)	0.20 (0.214)
Daily dose-normalized free MPA C_0, μg/mL/g	0.14 (0.383)	-0.25 (0.130)	0.26 (0.114)	0.07 (0.690)	-0.15 (0.366)	0.10 (0.529)	-0.04 (0.815)	-0.02 (0.916)	0.01 (0.945)	-0.24 (0.140)	-0.17 (0.306)	-0.17 (0.309)	-0.21 (0.239)	-0.03 (0.849)	-0.36 (0.024)
Daily dose-normalized free MPAG C_0, μg/mL/g	0.05 (0.776)	-0.02 (0.894)	-0.12 (0.467)	0.37 (0.018)	-0.43 (0.005)	0.08 (0.630)	0.10 (0.523)	0.10 (0.522)	0.08 (0.648)	-0.27 (0.101)	-0.02 (0.906)	0.002 (0.991)	0.05 (0.771)	0.10 (0.529)	-0.14 (0.406)
Body weight-normalized free MPA C_0, μg/mL/kg	0.07 (0.656)	-0.42 (0.007)	0.11 (0.523)	0.04 (0.803)	-0.13 (0.431)	0.03 (0.837)	-0.05 (0.774)	0.01 (0.971)	-0.09 (0.598)	-0.22 (0.186)	-0.01 (0.952)	-0.01 (0.965)	-0.19 (0.307)	-0.01 (0.942)	-0.09 (0.589)
Body weight-normalized free MPAG C_0, μg/mL/kg	0.06 (0.717)	-0.18 (0.273)	-0.25 (0.124)	0.30 (0.062)	-0.38 (0.015)	0.06 (0.692)	0.06 (0.716)	0.09 (0.585)	-0.03 (0.879)	-0.22 (0.177)	0.17 (0.282)	0.19 (0.236)	0.04 (0.817)	0.16 (0.330)	0.09 (0.592)
Ratio of free MPAG C_0 to free MPA C_0	-0.06 (0.731)	0.23 (0.154)	-0.36 (0.023)	0.19 (0.240)	-0.18 (0.268)	-0.03 (0.844)	0.06 (0.718)	0.07 (0.665)	0.08 (0.624)	0.08 (0.630)	0.13 (0.422)	0.16 (0.323)	0.25 (0.164)	0.10 (0.529)	0.22 (0.171)
Free fraction of MPA, %	0.24 (0.142)	-0.18 (0.261)	-0.04 (0.786)	0.05 (0.779)	-0.05 (0.742)	0.10 (0.545)	0.12 (0.479)	-0.13 (0.442)	0.08 (0.637)	0.07 (0.669)	0.04 (0.802)	0.14 (0.383)	0.03 (0.882)	-0.09 (0.574)	0.04 (0.802)
Free fraction of MPAG, %	0.08 (0.634)	-0.0001 (1.000)	0.03 (0.874)	0.26 (0.106)	-0.28 (0.085)	0.17 (0.307)	0.32 (0.043)	0.04 (0.806)	0.13 (0.432)	-0.14 (0.392)	-0.06 (0.727)	0.02 (0.894)	0.01 (0.969)	-0.01 (0.967)	-0.24 (0.130)
Total *p*-cresol sulfate concentration, μg/mL	-0.04 (0.797)	0.24 (0.128)	-0.05 (0.778)	0.67 (<0.001)	-0.70 (<0.001)	-0.17 (0.307)	0.19 (0.248)	0.08 (0.614)	-0.20 (0.220)	-0.02 (0.921)	-0.15 (0.358)	-0.14 (0.376)	0.16 (0.373)	0.15 (0.353)	-0.02 (0.882)
Total tacrolimus C_0, μg/L	0.14 (0.394)	-0.15 (0.362)	0.34 (0.033)	-0.13 (0.438)	0.10 (0.533)	0.18 (0.277)	-0.04 (0.797)	0.10 (0.546)	-0.11 (0.498)	-0.08 (0.624)	-0.32 (0.047)	-0.31 (0.048)	-0.44 (0.011)	0.03 (0.844)	0.09 (0.598)

Positive relationship	$p \leq 0.001$	$0.001 < p \leq 0.005$	$0.005 < p \leq 0.01$	$0.01 < p \leq 0.05$
Negative relationship	$p \leq 0.001$	$0.001 < p \leq 0.005$	$0.005 < p \leq 0.01$	$0.01 < p \leq 0.05$

R and p values were obtained from Spearman correlational analyses.

Abbreviation(s): *AcMPAG,* mycophenolic acid acyl glucuronide; *ALT,* alanine aminotransferase; *AST,* aspartate aminotransferase; C_0, trough concentration; *eGFR,* estimated glomerular filtration rate; *GGT,* gamma-glutamyl transferase; *MMF,* mycophenolate mofetil; *MPA,* mycophenolic acid; *MPAG,* mycophenolic acid glucuronide; *R,* correlation coefficient; *WBC,* white blood cell count.

Table S IX-8 Spearman correlational analyses of MPA, MPAG, AcMPAG, p-cresol sulfate, and tacrolimus concentrations

R (p value)	Total MPA C_0, µg/mL	Total MPAG C_0, µg/mL	Total AcMPAG C_0, µg/mL	Daily dose-normalized total MPA C_0, µg/mL/g	Daily dose-normalized total MPAG C_0, µg/mL/g	Daily dose-normalized total AcMPAG C_0, µg/mL/g	Body weight-normalized total MPA C_0, µg/mL/kg	Body weight-normalized total MPAG C_0, µg/mL/kg	Body weight-normalized total AcMPAG C_0, µg/mL/kg	Ratio of total MPAG C_0 to total MPA C_0	Ratio of total AcMPAG C_0 to total MPA C_0	Ratio of total AcMPAG C_0 to total MPAG C_0	Free MPA C_0, µg/mL	Free MPAG C_0, µg/mL	Daily dose-normalized free MPA C_0, µg/mL/g	Daily dose-normalized free MPAG C_0, µg/mL/g	Body weight-normalized free MPA C_0, µg/mL/kg	Body weight-normalized free MPAG C_0, µg/mL/kg	Ratio of free MPAG C_0 to free MPA C_0	Free fraction of MPA, %	Free fraction of MPAG, %	Total *p*-cresol sulfate concentration, µg/mL	Total tacrolimus C_0, µg/L
Total MPA C_0, µg/mL		0.39 (0.013)	0.22 (0.175)	0.90 (<0.001)	0.44 (0.005)	0.22 (0.177)	0.93 (<0.001)	0.36 (0.021)	0.25 (0.118)	-0.56 (<0.001)	-0.38 (0.016)	-0.07 (0.680)	0.72 (<0.001)	0.42 (0.006)	0.65 (<0.001)	0.43 (0.006)	0.66 (<0.001)	0.42 (0.007)	-0.29 (0.074)	-0.09 (0.567)	0.12 (0.456)	0.39 (0.013)	0.01 (0.947)
Total MPAG C_0, µg/mL	0.39 (0.013)		0.18 (0.276)	0.21 (0.201)	0.91 (<0.001)	0.02 (0.899)	0.30 (0.059)	0.93 (<0.001)	0.14 (0.405)	0.48 (0.002)	-0.15 (0.364)	-0.45 (0.003)	0.24 (0.136)	0.82 (<0.001)	0.08 (0.642)	0.64 (<0.001)	0.20 (0.217)	0.74 (<0.001)	0.41 (0.009)	-0.04 (0.799)	0.02 (0.904)	0.18 (0.263)	0.17 (0.299)
Total AcMPAG C_0, µg/mL	0.22 (0.175)	0.18 (0.276)		0.18 (0.264)	0.22 (0.174)	0.93 (<0.001)	0.27 (0.088)	0.21 (0.187)	0.96 (<0.001)	-0.03 (0.863)	0.76 (<0.001)	0.73 (<0.001)	-0.02 (0.913)	0.21 (0.191)	-0.03 (0.857)	0.20 (0.221)	0.04 (0.803)	0.25 0.123	0.17 (0.295)	-0.15 (0.378)	0.06 (0.710)	0.20 (0.219)	0.02 (0.924)
Daily dose-normalized total MPA C_0, µg/mL/g	0.90 (<0.001)	0.21 (0.201)	0.18 (0.264)		0.40 (0.010)	0.32 (0.042)	0.91 (<0.001)	0.23 (0.149)	0.23 (0.154)	-0.67 (<0.001)	-0.37 (0.019)	0.05 (0.740)	0.67 (<0.001)	0.29 (0.069)	0.77 (<0.001)	0.44 (0.004)	0.68 (<0.001)	0.34 (0.032)	-0.36 (0.023)	-0.07 (0.692)	0.17 (0.300)	0.32 (0.046)	-0.04 (0.794)
Daily dose-normalized total MPAG C_0, µg/mL/g	0.44 (0.005)	0.91 (<0.001)	0.22 (0.174)	0.40 (0.010)		0.18 (0.280)	0.42 (0.006)	0.90 (<0.001)	0.20 (0.220)	0.35 (0.025)	-0.15 (0.358)	-0.35 (0.026)	0.26 (0.114)	0.80 (<0.001)	0.24 (0.148)	0.78 (<0.001)	0.29 (0.076)	0.79 (<0.001)	0.40 (0.011)	-0.09 (0.605)	0.11 (0.488)	0.24 (0.142)	0.14 (0.400)
Daily dose-normalized total AcMPAG C_0, µg/mL/g	0.22 (0.177)	0.02 (0.899)	0.93 (<0.001)	0.32 (0.042)	0.18 (0.280)		0.31 (0.049)	0.08 (0.613)	0.91 (<0.001)	-0.19 (0.252)	0.70 (<0.001)	0.82 (<0.001)	0.01 (0.940)	0.13 (0.435)	0.13 (0.435)	0.24 (0.137)	0.11 (0.519)	0.19 (0.244)	0.07 (0.658)	-0.11 (0.512)	0.16 (0.328)	0.22 (0.176)	-0.07 (0.658)
Body weight-normalized total MPA C_0, µg/mL/kg	0.93 (<0.001)	0.30 (0.059)	0.27 (0.088)	0.91 (<0.001)	0.42 (0.006)	0.31 (0.049)		0.39 (0.012)	0.35 (0.025)	-0.58 (<0.001)	-0.29 (0.073)	0.04 (0.794)	0.72 (<0.001)	0.34 (0.033)	0.72 (<0.001)	0.40 (0.010)	0.76 (<0.001)	0.42 (0.007)	-0.38 (0.016)	-0.04 (0.803)	0.08 (0.618)	0.32 (0.043)	0.06 (0.714)
Body weight-normalized total MPAG C_0, µg/mL/kg	0.36 (0.021)	0.93 (<0.001)	0.21 (0.187)	0.23 (0.149)	0.90 (<0.001)	0.08 (0.613)	0.39 (0.012)		0.25 (0.124)	0.45 (0.003)	-0.09 (0.568)	-0.37 (0.019)	0.24 (0.143)	0.78 (<0.001)	0.12 (0.454)	0.67 (<0.001)	0.30 (0.062)	0.81 (<0.001)	0.37 (0.021)	-0.03 (0.860)	0.03 (0.839)	0.14 (0.392)	0.22 (0.171)
Body weight-normalized total AcMPAG C_0, µg/mL/kg	0.25 (0.118)	0.14 (0.405)	0.96 (<0.001)	0.23 (0.154)	0.20 (0.220)	0.91 (<0.001)	0.35 (0.025)	0.25 (0.124)		-0.08 (0.632)	0.71 (<0.001)	0.73 (<0.001)	0.08 (0.635)	0.23 (0.161)	0.08 (0.639)	0.24 (0.132)	0.18 (0.273)	0.34 (0.034)	0.09 (0.575)	-0.06 (0.714)	0.14 (0.399)	0.17 (0.307)	0.01 (0.957)
Ratio of total MPAG C_0 to total MPA C_0	-0.56 (<0.001)	0.48 (0.002)	-0.03 (0.863)	-0.67 (<0.001)	0.35 (0.025)	-0.19 (0.252)	-0.58 (<0.001)	0.45 (0.003)	-0.08 (0.632)		0.27 (0.091)	-0.33 (0.038)	-0.47 (0.003)	0.35 (0.026)	-0.59 (<0.001)	0.19 (0.241)	-0.45 (0.004)	0.31 (0.054)	0.72 (<0.001)	-0.03 (0.866)	-0.02 (0.927)	-0.10 (0.559)	0.08 (0.614)
Ratio of total AcMPAG C_0 to total MPA C_0	-0.38 (0.016)	-0.15 (0.364)	0.76 (<0.001)	-0.37 (0.019)	-0.15 (0.358)	0.70 (<0.001)	-0.29 (0.073)	-0.09 (0.568)	0.71 (<0.001)	0.27 (0.091)		0.77 (<0.001)	-0.37 (0.020)	-0.10 (0.533)	-0.33 (0.038)	-0.11 (0.519)	-0.29 (0.071)	-0.05 (0.763)	0.27 (0.091)	-0.0008 (0.996)	0.06 (0.703)	-0.11 (0.498)	-0.04 (0.794)

R (p value)	Total MPA C_0, µg/mL	Total MPAG C_0, µg/mL	Total AcMPAG C_0, µg/mL	Daily dose-normalized total MPA C_0, µg/mL/g	Daily dose-normalized total MPAG C_0, µg/mL/g	Daily dose-normalized total AcMPAG C_0, µg/mL/g	Body weight-normalized total MPA C_0, µg/mL/kg	Body weight-normalized total MPAG C_0, µg/mL/kg	Body weight-normalized total AcMPAG C_0, µg/mL/kg	Ratio of total MPAG C_0 to total MPA C_0	Ratio of total AcMPAG C_0 to total MPA C_0	Ratio of total AcMPAG C_0 to total MPAG C_0	Free MPA C_0, µg/mL	Free MPAG C_0, µg/mL	Daily dose-normalized free MPA C_0, µg/mL/g	Daily dose-normalized free MPAG C_0, µg/mL/g	Body weight-normalized free MPA C_0, µg/mL/kg	Body weight-normalized free MPAG C_0, µg/mL/kg	Ratio of free MPAG C_0 to free MPA C_0	Free fraction of MPA, %	Free fraction of MPAG, %	Total *p*-cresol sulfate concentration, µg/mL	Total tacrolimus C_0, µg/L
Ratio of total AcMPAG C_0 to total MPAG C_0	-0.07 (0.680)	-0.45 (0.003)	0.73 (<0.001)	0.05 (0.740)	-0.35 (0.026)	0.82 (<0.001)	0.04 (0.794)	-0.37 (0.019)	0.73 (<0.001)	-0.33 (0.038)	0.77 (<0.001)		-0.13 (0.443)	-0.29 (0.071)	0.003 (0.984)	-0.16 (0.314)	-0.04 (0.791)	-0.21 (0.198)	-0.11 (0.513)	0.004 (0.980)	0.13 (0.427)	0.01 (0.973)	-0.13 (0.432)
Free MPA C_0, µg/mL	0.72 (<0.001)	0.24 (0.136)	-0.02 (0.913)	0.67 (<0.001)	0.26 (0.114)	0.01 (0.940)	0.72 (<0.001)	0.24 (0.143)	0.08 (0.635)	-0.47 (0.003)	-0.37 (0.020)	-0.13 (0.443)		0.30 (0.067)	0.90 (<0.001)	0.30 (0.062)	0.95 (<0.001)	0.31 (0.056)	-0.60 (<0.001)	0.52 (0.001)	0.18 (0.281)	0.16 (0.316)	0.08 (0.623)
Free MPAG C_0, µg/mL	0.42 (0.006)	0.82 (<0.001)	0.21 (0.191)	0.29 (0.069)	0.80 (<0.001)	0.13 (0.435)	0.34 (0.033)	0.78 (<0.001)	0.23 (0.161)	0.35 (0.026)	-0.10 (0.533)	-0.29 (0.071)	0.30 (0.067)		0.19 (0.238)	0.92 (<0.001)	0.25 (0.126)	0.94 (<0.001)	0.51 (0.001)	0.08 (0.644)	0.54 (<0.001)	0.29 (0.073)	0.04 (0.810)
Daily dose-normalized free MPA C_0, µg/mL/g	0.65 (<0.001)	0.08 (0.642)	-0.03 (0.857)	0.77 (<0.001)	0.24 (0.148)	0.13 (0.435)	0.72 (<0.001)	0.12 (0.454)	0.08 (0.639)	-0.59 (<0.001)	-0.33 (0.038)	0.003 (0.984)	0.90 (<0.001)	0.19 (0.238)		0.35 (0.028)	0.91 (<0.001)	0.26 (0.117)	-0.63 (<0.001)	0.52 (0.001)	0.28 (0.079)	0.14 (0.398)	0.02 (0.900)
Daily dose-normalized free MPAG C_0, µg/mL/g	0.43 (0.006)	0.64 (<0.001)	0.20 (0.221)	0.44 (0.004)	0.78 (<0.001)	0.24 (0.137)	0.40 (0.010)	0.67 (<0.001)	0.24 (0.132)	0.19 (0.241)	-0.11 (0.519)	-0.16 (0.314)	0.30 (0.062)	0.92 (<0.001)	0.35 (0.028)		0.31 (0.052)	0.92 (<0.001)	0.43 (0.006)	0.08 (0.625)	0.66 (<0.001)	0.32 (0.043)	-0.03 (0.834)
Body weight-normalized free MPA C_0, µg/mL/kg	0.66 (<0.001)	0.20 (0.217)	0.04 (0.803)	0.68 (<0.001)	0.29 (0.076)	0.11 (0.519)	0.76 (<0.001)	0.30 (0.062)	0.18 (0.273)	-0.45 (0.004)	-0.29 (0.071)	-0.04 (0.791)	0.95 (<0.001)	0.25 (0.126)	0.91 (<0.001)	0.31 (0.052)		0.34 (0.033)	-0.60 (<0.001)	0.52 (0.001)	0.15 (0.366)	0.11 (0.500)	0.11 (0.520)
Body weight-normalized free MPAG C_0, µg/mL/kg	0.42 (0.007)	0.74 (<0.001)	0.25 (0.123)	0.34 (0.032)	0.79 (<0.001)	0.19 (0.244)	0.42 (0.007)	0.81 (<0.001)	0.34 (0.034)	0.31 (0.054)	-0.05 (0.763)	-0.21 (0.198)	0.31 (0.056)	0.94 (<0.001)	0.26 (0.117)	0.92 (<0.001)	0.34 (0.033)		0.45 (0.004)	0.09 (0.596)	0.56 (<0.001)	0.24 (0.139)	0.06 (0.702)
Ratio of free MPAG C_0 to free MPA C_0	-0.29 (0.074)	0.41 (0.009)	0.17 (0.295)	-0.36 (0.023)	0.40 (0.011)	0.07 (0.658)	-0.38 (0.016)	0.37 (0.021)	0.09 (0.575)	0.72 (<0.001)	0.27 (0.091)	-0.11 (0.513)	-0.60 (<0.001)	0.51 (0.001)	-0.63 (<0.001)	0.43 (0.006)	-0.60 (<0.001)	0.45 (0.004)		-0.42 (0.007)	0.29 (0.075)	0.06 (0.706)	-0.08 (0.647)
Free fraction of MPA, %	-0.09 (0.567)	-0.04 (0.799)	-0.15 (0.378)	-0.07 (0.692)	-0.09 (0.605)	-0.11 (0.512)	-0.04 (0.803)	-0.03 (0.860)	-0.06 (0.714)	-0.03 (0.866)	-0.0008 (0.996)	0.0004 (0.980)	0.52 (0.001)	0.08 (0.644)	0.52 (0.001)	0.08 (0.625)	0.52 (0.001)	0.09 (0.596)	-0.42 (0.007)		0.28 (0.083)	-0.06 (0.712)	-0.04 (0.825)
Free fraction of MPAG, %	0.12 (0.456)	0.02 (0.904)	0.06 (0.710)	0.17 (0.300)	0.11 (0.488)	0.16 (0.328)	0.08 (0.618)	0.03 (0.839)	0.14 (0.399)	-0.02 (0.927)	0.06 (0.703)	0.13 (0.427)	0.18 (0.281)	0.54 (<0.001)	0.28 (0.079)	0.66 (<0.001)	0.15 (0.366)	0.56 (<0.001)	0.29 (0.075)	0.28 (0.083)		0.18 (0.259)	-0.25 (0.125)
Total *p*-cresol sulfate concentration, µg/mL	0.39 (0.013)	0.18 (0.263)	0.20 (0.219)	0.32 (0.046)	0.24 (0.142)	0.22 (0.176)	0.32 (0.043)	0.14 (0.392)	0.17 (0.307)	-0.10 (0.559)	-0.11 (0.498)	0.01 (0.973)	0.16 (0.316)	0.29 (0.073)	0.14 (0.398)	0.32 (0.043)	0.11 (0.500)	0.24 (0.139)	0.06 (0.706)	-0.06 (0.712)	0.18 (0.259)		-0.11 (0.511)
Total tacrolimus C_0, µg/L	0.01 (0.947)	0.17 (0.299)	0.02 (0.924)	-0.04 (0.794)	0.14 (0.400)	-0.07 (0.658)	0.06 (0.714)	0.22 (0.171)	0.01 (0.957)	0.08 (0.614)	-0.04 (0.794)	-0.13 (0.432)	0.08 (0.623)	0.04 (0.810)	0.02 (0.900)	-0.03 (0.834)	0.11 (0.520)	0.06 (0.702)	-0.08 (0.647)	-0.04 (0.825)	-0.25 (0.125)	-0.11 (0.511)	

Positive relationship	$p \leq 0.001$	$0.001 < p \leq 0.005$	$0.005 < p \leq 0.01$	$0.01 < p \leq 0.05$
Negative relationship	$p \leq 0.001$	$0.001 < p \leq 0.005$	$0.005 < p \leq 0.01$	$0.01 < p \leq 0.05$

R and p values were obtained from Spearman correlational analyses.

Abbreviation(s): *AcMPAG,* mycophenolic acid acyl glucuronide; C_0*,* trough concentration; *MPA,* mycophenolic acid; *MPAG,* mycophenolic acid glucuronide; *R,* correlation coefficient.

Table S IX-9 Associations between categorical clinical variables and MPA, MPAG, AcMPAG, or p-cresol sulfate

Mean±SD	Sex	Donor type	Concurrent medications
	Male (*n*=29) vs. female (*n*=11)	Deceased donor (*n*=20) vs. living donor (*n*=20)	Comedications increasing (*n*=3), decreasing (*n*=20), vs. not influencing MPA exposure (*n*=15) [b,c]
Total MPA C_0, µg/mL	2.7±2.1 vs. 3.1±2.4	2.5±2.0 vs. 3.2±2.3	2.3±0.7 vs. 3.3±2.4 vs. 2.0±1.5
Total MPAG C_0, µg/mL	33.6±20.7 vs. 34.3±24.2	31.9±22.4 vs. 35.7±20.8	32.0±12.4 vs. 34.5±23.9 vs. 35.1±20.8
Total AcMPAG C_0, µg/mL	0.266±0.398 vs. 0.186±0.185	0.123±0.146 vs. 0.365±0.450*	0.241±0.188 vs. 0.166±0.206 vs. 0.269±0.418
Daily dose-normalized total MPA C_0, µg/mL/g	1.6±1.5 vs. 2.2±1.5	1.6±1.3 vs. 1.9±1.6	2.3±2.0 vs. 2.1±1.6 vs. 1.2±1.1
Daily dose-normalized total MPAG C_0, µg/mL/g	18.3±12.7 vs. 21.5±13.7	18.4±12.6 vs. 20.1±13.5	27.7±17.1 vs. 18.5±11.0 vs. 19.7±15.0
Daily dose-normalized total AcMPAG C_0, µg/mL/g	0.14±0.20 vs. 0.16±0.25	0.10±0.19 vs. 0.19±0.22*	0.34±0.47 vs. 0.09±0.10 vs. 0.14±0.21
Body weight-normalized total MPA C_0, µg/mL/kg	0.033±0.029 vs. 0.052±0.043	0.037±0.035 vs. 0.040±0.033	0.035±0.020 vs. 0.048±0.040 vs. 0.023±0.017
Body weight-normalized total MPAG C_0, µg/mL/kg	0.40±0.24 vs. 0.55±0.38	0.43±0.31 vs. 0.45±0.27	0.43±0.14 vs. 0.48±0.32 vs. 0.42±0.27
Body weight-normalized total AcMPAG C_0, µg/mL/kg	0.003±0.005 vs. 0.003±0.003	0.002±0.003 vs. 0.005±0.006*	0.005±0.005 vs. 0.002±0.003 vs. 0.003±0.005
Ratio of total MPAG C_0 to total MPA C_0	16.4±11.6 vs. 20.2±27.7	19.5±21.2 vs. 15.4±12.2	15.8±11.2 vs. 12.9±9.6 vs. 25.6±23.6
Ratio of total AcMPAG C_0 to total MPA C_0	0.13±0.22 vs. 0.17±0.35	0.11±0.26 vs. 0.17±0.26	0.10±0.08 vs. 0.06±0.06 vs. 0.25±0.39
Ratio of total AcMPAG C_0 to total MPAG C_0	0.009±0.013 vs. 0.007±0.006	0.005±0.005 vs. 0.012±0.014	0.009±0.009 vs. 0.007±0.007 vs. 0.008±0.012
Free MPA C_0, µg/mL	0.042±0.047[a] vs. 0.047±0.063	0.037±0.049[a] vs. 0.049±0.054	0.034±0.011 vs. 0.053±0.060 vs. 0.021±0.015[a,*] *p<0.05 vs. "decreasing exposure" group
Free MPAG C_0, µg/mL	4.9±4.3 vs. 4.9±5.3	4.4±4.2 vs. 5.4±4.8	4.7±0.7 vs. 4.5±4.6 vs. 5.8±5.0
Daily dose-normalized free MPA C_0, µg/mL/g	0.024±0.028[a] vs. 0.032±0.033	0.023±0.027[a] vs. 0.029±0.032	0.028±0.013 vs. 0.033±0.035 vs. 0.012±0.008[a]
Daily dose-normalized free MPAG C_0, µg/mL/g	2.8±2.6 vs. 3.2±3.0	2.6±2.4 vs. 3.2±2.9	4.3±3.0 vs. 2.5±2.4 vs. 3.3±3.2
Body weight-normalized free MPA C_0, µg/mL/kg	0.0005±0.0007[a] vs. 0.0008±0.0010	0.0005±0.0008[a] vs. 0.0006±0.0008	0.0005±0.0001 vs. 0.0008±0.0009 vs. 0.0002±0.0002[a,*] *p<0.05 vs. "decreasing exposure" group

Mean±SD	Sex	Donor type	Concurrent medications
	Male (*n*=29) vs. female (*n*=11)	Deceased donor (*n*=20) vs. living donor (*n*=20)	Comedications increasing (*n*=3), decreasing (*n*=20), vs. not influencing MPA exposure (*n*=15) [b,c]
Body weight-normalized free MPAG C_0, µg/mL/kg	0.06±0.05 vs. 0.08±0.08	0.06±0.07 vs. 0.06±0.05	0.07±0.02 vs. 0.06±0.07 vs. 0.07±0.06
Ratio of free MPAG C_0 to free MPA C_0	223.9±277.2[a] vs. 177.2±235.0	186.9±187.2[a] vs. 233.5±323.8	143.5±32.9 vs. 109.9±94.8 vs. 396.6±361.4[a, *] [*]p<0.05 vs. "decreasing exposure" group
Free fraction of MPA, %	1.5±0.8[a] vs. 1.4±0.7	1.4±0.8[a] vs. 1.5±0.8	1.6±0.9 vs. 1.4±0.7 vs. 1.3±0.9[a]
Free fraction of MPAG, %	14.6±7.7 vs. 14.2±9.5	14.0±7.5 vs. 15.0±8.9	15.5±3.7 vs. 12.8±8.7 vs. 16.9±7.7
Total *p*-cresol sulfate concentration, µg/mL	3.7±2.1 vs. 3.5±2.0	3.3±2.0 vs. 4.0±2.1	2.7±0.9 vs. 3.5±1.8 vs. 3.9±2.6

[*]$p < 0.05$ using Mann Whitney test (for 2 groups); [*]$p < 0.05$ using Kruskal-Wallis one-way analysis of variance followed by the Dunn's test (for 3 groups). Induction regimen was not analyzed as the majority of subjects (*n*=35) were on basiliximab.

[a] Lack of free MPA C_0 from one participant.

[b] Two participants were removed from concurrent medication analyses due to unclear medication history.

[c]As participants may be exposed to multiple co-administered drugs, a scoring system was devised to evaluate the overall effects of potential drug interactions (i.e., score 1 for drugs that are known to increase MPA exposure; score -1 for drugs that decrease MPA exposure; and score 0 for non-interacting drugs; with the sum of the interaction scores calculated for each patient) using data provided in the Lexicomp database [26].

Abbreviation(s): *AcMPAG,* mycophenolic acid acyl glucuronide; *C_0,* trough concentration; *MPA,* mycophenolic acid; *MPAG,* mycophenolic acid glucuronide; *SD,* standard deviation.

Chapter X. Discussion and Conclusion[10]

Being one of the first line immunosuppressants utilized after kidney transplantation, MPA is very commonly prescribed for the entire duration of the transplanted organ, despite the known variabilities in its pharmacokinetics (i.e., 10-fold variations in the plasma exposures) [10, 30]. The large pharmacokinetic variabilities of MPA could pose significant risks to patients because the therapeutic range of MPA is relatively narrow and the under- or over- exposure may lead to adverse outcomes including graft rejection, gastrointestinal side effects (e.g., constipation, diarrhea, dyspepsia, nausea, and vomiting), hematological disorders (e.g., anemia, leukopenia, neutropenia, and thrombocytopenia), and infections (e.g., cytomegalovirus infection and *pneumocystis* pneumonia) [29]. Therefore, understanding the sources of the variabilities associated with MPA pharmacokinetics may help mitigate its adverse effects and improve clinical care. The hypothesis of the current thesis was that large exposure variabilities of MPA can be attributed to extrinsic (i.e., co-administered immunosuppressants) and intrinsic (i.e., *p*-cresol species accumulated under uremic conditions) factors that alter MPA pharmacokinetics in humans. To test this hypothesis, the following main findings were obtained from the following objectives (Chapter II [59], Chapter III [25], Chapter IV [27], Chapter V [54], Chapter VI [55], Chapter VII [56], Chapter VIII [57], and Chapter IX [58]):

i) Objective 1: We were able to identify novel model building strategies in MPA population pharmacokinetic-dynamics; determine the significant interactions affecting

[10] This thesis follows the manuscript style; therefore, this conclusion chapter is intended to be generalized, focusing on the overall experimental summary, limitations, and future directions. Detailed discussions had already been provided in each data chapter (all peer-reviewed and published).

MPA clinical pharmacology; and assess the utility of these models for the precision dosing of MPA in a variety of patient (adult and pediatric) populations.

ii) Objective 2: We were able to develop and validate several analytical assays to accurately and precisely quantify MPA, MPAG, AcMPAG, *p*-cresol, *p*-cresol sulfate, and *p*-cresol glucuronide in a variety of experimental models.

iii) Objective 3: We were able to determine the biological relevance and the molecular mechanisms of the newly identified interaction between *p*-cresol and MPA (using human *in vitro* models).

iv) Objective 4: We were able to characterize the enzyme kinetics of *p*-cresol sulfate and *p*-cresol glucuronide formation, which were necessary to establish correlations with MPA exposure in patients (Objective 5). Our novel approach to detoxify *p*-cresol sulfate can also potentially mitigate the pharmacokinetic interaction between *p*-cresol sulfate and MPA.

v) Objective 5: We were able to verify our *in vitro* findings and assess the clinical relevance of the *p*-cresol and MPA interaction in adult kidney transplant recipients.

The overall discussions provided in this chapter (i.e., summary, overall limitations, and future directions) will be organized into following headings: “1. Interactions between MPA and clinical factors” and “2. Interactions between MPA and *p*-cresol”.

1. Interactions between MPA and clinical factors

1.1. Summary

Population pharmacokinetic modeling is a powerful tool to characterize the sources of MPA pharmacokinetic variabilities (reviewed in Chapter I of this thesis). The potential clinical covariates that may affect MPA exposure (*p*-cresol is discussed separately) can be classified as being extrinsic (e.g., commonly co-administered immunosuppressants) or intrinsic (e.g., patients' demographic, biochemistry, and genomic data). Using clinical data obtained from steroid-free adult kidney transplant patients, a novel population pharmacokinetic model of MPA was established and validated to examine the effects of co-administered immunosuppressants on the pharmacokinetics of MPA (Chapter II [59]). Based on our findings, the population pharmacokinetics of MPA in this population were best described by a two-compartment model with first-order absorption (lag time) and linear elimination, in line with most published MPA population pharmacokinetic models in corticosteroid-based patients [10, 27, 30, 31, 62, 71-74]. These findings suggested that corticosteroids do not considerably change the fundamental population pharmacokinetic structural model of MPA. Moreover, total AcMPAG trough concentrations, and AUC ratios of total MPAG-to-total MPA were identified as significant covariates in our final model, and their inclusion resulted in drastically reduced apparent oral clearance of MPA from ~17 L/h to ~3 L/h. The MPA clearance in steroid-free patients is markedly lower compared to that reported in similar patients on corticosteroid-based regimens, and this could potentially be explained by the enzyme induction effects of corticosteroids on the glucuronidation of MPA. As all other pharmacokinetic parameter estimates in our model were comparable to historical MPA values obtained in corticosteroid-based populations, it may also be postulated that corticosteroids had only affected the metabolism of MPA, with little effects on

other pharmacokinetic properties. The finding of considerably lowered MPA clearance in patients on corticosteroid-free regimens suggested that MPA dose adjustment or therapeutic drug monitoring may be required in the clinic to mitigate the over-exposure of MPA (e.g., when tapering the dose of corticosteroids) and prevent the manifestation of severe toxicities.

On the other hand, tacrolimus dosage, trough concentration, and exposure (i.e., AUC_{0-12}) (Chapter II [59]) were not identified as significant factors influencing the pharmacokinetics of MPA. This observation is consistent with the previously published literature in renal transplant patients using a variety of study designs and analytical approaches [108, 110, 114, 116, 119-125]. Likewise, MPA did not affect the clearance of tacrolimus in a population pharmacokinetic model of tacrolimus constructed in adult kidney transplant patients by our group (Appendix A. Population pharmacokinetic analysis of immediate-release oral tacrolimus co-administered with mycophenolate mofetil in steroid-free adult kidney transplant recipients [60]). Our collective findings indicated the lack of bi-directional interaction between tacrolimus and MPA in this patient population and suggested that dose adjustments are likely not warranted when MPA is co-administered with this specific calcineurin inhibitor, in contrast to cyclosporine (see Chapter III [25] and Chapter IV [27]).

Furthermore, from our scoping reviews of published primary literature data, potential factors causing MPA pharmacokinetic variabilities were identified in both adult and pediatric populations, in a variety of indications (Chapter III [25] and Chapter IV [27]). In the adult population, significant clinical variables affecting MPA pharmacokinetics which were consistently reported by multiple investigators were: albumin (e.g., [143, 147, 152, 158, 160, 161, 190, 192, 202, 216, 218, 220]), body weight (e.g., [139, 151, 152, 155, 188, 192, 194, 205, 217, 218]), creatinine clearance (e.g., [140, 143, 146, 151, 153, 160, 161, 184, 186, 190, 202, 204, 213, 216,

217, 220]), concurrent administration of cyclosporine (e.g., [140, 141, 146-149, 158, 160, 161, 182, 192, 193, 204, 213]), and post-transplant time (e.g., [148, 149, 152, 154, 160, 161, 204]) (Chapter III [25]). On the other hand, inconsistent effects on MPA pharmacokinetics/dynamics were reported for other clinical factors such as blood urea nitrogen (e.g., [215]), diet (e.g., [151]), physiological conditions (e.g., diabetes [213] and diarrhea [220]), genetic polymorphisms (e.g., UGT1A9 [215] and UGT2B7 [117, 139]), hemoglobin (e.g., [160]), race (e.g., [151]), sex (e.g., [161, 213]), and type of transplantation (e.g., [149]) (Chapter III [25]). Furthermore, as MPA likely exhibited age-dependent pharmacokinetics (e.g., [151, 162]), data were also summarized in pediatric patients (Chapter IV [27]). Our analysis in this population indicated that the absorption (described by k_a) and the overall elimination of MPA (described by CL/F values of total and free MPA) were generally comparable to that reported in adults (Chapter III [25] and Chapter IV [27]). In contrast, the distribution of MPA (characterized by V_c/F and/or V_p/F) were generally reduced in pediatrics than adults (Chapter IV [27]), which could potentially be explained by the significant influence of body weight [196, 210]. Moreover, consistent with the adult population, albumin [209], creatinine clearance [189], cyclosporine [210, 221], and post-transplant time [183] also affected MPA pharmacokinetics in pediatric patients (Chapter IV [27]), suggesting the potential importance of these clinical factors in explaining the variabilities of MPA pharmacokinetics, irrespective of patient chronological age.

With respect to modeling, the currently available MPA population pharmacokinetic structural models in adult and pediatric populations are generally comparable (Chapter III [25] and Chapter IV [27]). The most commonly utilized modeling software and algorithm were NONMEM and non-linear mixed-effects methods (Chapter III [25] and Chapter IV [27]). Relatively more MPA population pharmacokinetic models were identified in adults than pediatric patients, and

kidney transplantation recipients on MMF were the most studied population (Chapter III [25] and Chapter IV [27]). The majority of the MPA structural models were described by simple absorption (i.e., first order without/with lag time), one- or two- compartments, and a linear elimination process, but utilizing only total MPA concentrations (Chapter III [25] and Chapter IV [27]). In addition, few pharmacodynamic (e.g., the activities of IMPDH enzymes) and clinical outcome (e.g., rejection, leukopenia, infections) models of MPA were available in the literature (e.g., [185, 200, 207, 214, 216, 220]). Moreover, Bayesian forecasting models for predicting MPA exposure were becoming available in the pediatric population, where the optimal sampling times were identified to be a maximum of four time points within six hours post-dose ([183, 196, 198, 200, 207, 209], Chapter III [25], and Chapter IV [27]). These Bayesian models could allow the accurate and precise estimation of MPA exposure using only a limited number of sampling points, potentially optimizing patient care. However, the clinical utilities of these Bayesian predictive models in improving patient outcome would remain to be investigated.

1.2. Overall limitations and future directions

Although population pharmacokinetic modeling is a powerful approach for identifying the clinical factors associated with MPA pharmacokinetic variability, the discovered findings should be supported by additional mechanistic investigations and confirmatory data (please see discussions in Chapter II [59] and Appendix A. Population pharmacokinetic analysis of immediate-release oral tacrolimus co-administered with mycophenolate mofetil in steroid-free adult kidney transplant recipients [60]). For example, although there are already *in vitro* evidence indicating the ability of corticosteroids to induce the expressions or activities of UGT enzymes [105], direct data supporting their effects on MPA glucuronidation (or intrinsic clearance) are still

lacking. To address this gap, the metabolism interaction between steroids and MPA could be further elucidated using *in vitro* models such as primary cultures of human hepatocytes or metabolically-competent human liver cell lines (e.g., HepaRG), which have the necessary cellular machineries (e.g., nuclear receptors) for examining enzyme induction-mediated drug interactions [172, 270, 292, 416]. Moreover, to support the *in vitro* data, additional controlled clinical studies should also be considered to confirm the metabolism interaction between corticosteroids and MPA. As it is not ethical to conduct randomized, blinded, and controlled trials examining the effects of corticosteroids in transplant patients, a study design incorporating a steroid-taper group and a matched steroid-free group (matching to be based on patient demographic and biochemistry data such as age, sex, post-transplant time, albumin level, etc.) can be proposed. Using a longitudinal design, the inter-individual and intra-individual differences and variabilities in MPA clearance (based on steroid-interaction) can be determined. However, these study designs have their own inherent limitations: the *in vitro* experimental results may not be translatable to *in vivo* observations; matching subjects would not completely remove the inherent bias and demographic imbalance which are difficult to control; and the steroid-taper patients may also be confounded by other clinical variables such as post-transplant time, as discussed in Chapter III [25] and Chapter IV [27]). Therefore, a variety of complementary approaches are needed to confirm the validity and robustness of the MPA-corticosteroid interaction.

Despite the consistently reported effects of albumin, body weight, creatinine clearance, cyclosporine, and post-transplant time on MPA population pharmacokinetics (Chapter III [25] and Chapter IV [27]), the underlying mechanisms should be verified using additional experimental approaches. Although data describing MPA-albumin binding are available in the literature (e.g., [140, 143, 204, 213, 216, 218]), the optimal binding kinetic model is still unknown due to the lack

of systematic, head-to-head comparative investigations. Ideally, to determine the best binding model, both total and free MPA concentrations and the associated free fractions are required for investigating the binding and dissociation behaviors of MPA. Moreover, MPA binding characteristics can be precisely quantified mathematically using linear or non-linear binding models with single or multiple binding site(s) (e.g., as reported by our lab for other drugs such as phenytoin binding [417]). The performances of each binding model can be assessed systematically using objective function values (OFVs), Akaike information criterion (AIC), Bayesian information criterion (BIC), and relative standard errors (RSEs) [65-67, 69, 70]. Moreover, MPAG (the predominant metabolite of MPA) is also highly protein bound [10, 215], and it could potentially displace the albumin binding of MPA.; therefore, the potential interacting effects of MPAG should also be accounted for when constructing the MPA-albumin binding models. In addition, total body weight is commonly used for scaling MPA pharmacokinetic parameters [224] such as the volume of distribution or the overall clearance [185, 189, 196, 209, 210, 221]. However, the relationships between body weight and MPA V/F or CL/F (or other pharmacokinetic parameters) are often inconsistently reported in the literature (e.g., described as either linear proportional [196] vs. non-linear exponential [185, 189, 209, 210, 221] with various coefficients). As such, the optimal scaling models of MPA based on body weight should also be tested systematically using structural, covariate, and statistical modeling approaches (e.g., [25, 31, 59, 68, 166]). Finally, creatinine clearance is often utilized to represent renal function in population pharmacokinetic studies involving MPA (e.g. [140, 143, 146, 151, 153, 160, 161, 184, 186, 190, 202, 204, 213, 216, 217, 220]); however, this biological marker does not characterize secretion (i.e., transporter function) effectively [418]. To fully characterize the effects of renal function, urinary concentrations of creatinine (to represent filtration) and MPAG (to represent tubular secretion [37]) should be

incorporated in future MPA pharmacokinetic models. These data will also assist the differentiation between total vs. renal clearance values [25].

The inhibitory effects of cyclosporine on MPA entero-hepatic recirculation have been documented extensively, and the majority of studies have attributed the interaction to MRP-2 transporter inhibition (e.g., [228]). However, it may also be possible that cyclosporine could also potentially inhibit OATP1B1/3 transporters, which are responsible for mediating the hepatic uptake (and hence entero-hepatic recirculation) of MPAG [43, 229]. Further *in vitro* investigations (e.g., using sandwich cultures of human hepatocytes which can maintain a 3D cellular morphology [416]) are needed to verify this potential mechanism. Furthermore, to test the possible effects of post-transplant time on MPA pharmacokinetics, subjects with stabilized organ functions (i.e., long-term post-transplant) should be recruited in future studies, as the currently available population pharmacokinetic models have mostly only recruited patients with relatively short post-transplant times (e.g., [139-141, 183, 185, 189, 198, 210, 212-214, 216, 218, 220]). In addition, the effects of the other clinical factors (e.g., blood urea nitrogen, diet, various disease states, genetic polymorphisms, hemoglobin, race, sex, type of transplantation, etc.) which are inconsistently reported between studies whould warrant further confirmation in additional clinical investigations, but with more strategic covariate selection to minimize the confounding effects of over-parameterization in the typically under-powered population pharmacokinetic studies (see Chapter III [25]).

With respect to modeling approaches (critically reviewed in Chapter III [25] and Chapter IV [27]), the identified gaps in the literature may also warrant further investigations. Overall, very few MPA pharmacokinetic models have been identified in pediatric patients, in indications other than kidney transplantation, and in subjects administered EC-MPS (Chapter III [25] and Chapter

IV [27]). The administration of both MPA formulations in indications such as autoimmune disease, stem cell transplantation, and heart/lung/liver transplantations are expected to be increased in the future [2, 24], and more efforts on MPA pharmacokinetic modeling are warranted in these populations. Furthermore, our critique of the literature [25, 27] identified that many MPA population pharmacokinetic models are constructed with simple (i.e., non-mechanistic) structural configurations utilizing only total MPA concentrations (Chapter III [25] and Chapter IV [27]). To fully capture the complexity of MPA clinical pharmacokinetics, mechanistic models incorporating complex absorption/re-absorption, MPA metabolite concentrations, entero-hepatic recirculation, and gut and/or bile compartments are warranted in future investigations. Moreover, more emphasis should be placed on free (i.e., unbound) MPA pharmacokinetics (Chapter III [25] and Chapter IV [27]), as only the free MPA is pharmacologically active, and total MPA concentrations are not always proportional to the unbound concentrations [10, 31]. Finally, very few models in literature have included population pharmacodynamics and/or actual clinical outcomes of MPA (Chapter III [25] and Chapter IV [27]). In particular, the pharmacokinetic-rejection and pharmacokinetic-toxicity relationships should be identified, focusing on longer-term outcomes (e.g., evidence of graft failure and composite patient survival) rather than the commonly used surrogate markers (e.g., acute graft rejection, leukocyte count, and neutrophil count). To provide further guidance on the precision dosing of MPA, Bayesian estimation models should also be incorporated in an ideal model and validated against actual patient outcomes rather than the target AUC ([183, 196, 198, 200, 207, 209], Chapter III [25], and Chapter IV [27]).

2. Interactions between MPA and *p*-cresol

2.1. Summary

p-Cresol is a potent inhibitor of UGT1A9, the primary enzyme responsible for the glucuronidation of MPA [52]. To systematically characterize this interaction in multiple models, LC-MS/MS and/or UPLC analytical assays were first developed and validated to accurately and precisely quantify MPA, MPAG, AcMPAG, *p*-cresol, *p*-cresol sulfate, and *p*-cresol glucuronide in various biological matrices (Chapter V [54], Chapter VI [55], Chapter VII [56], Chapter VIII [57], and Chapter IX [58]). Although not the primary focus of this thesis, these newly developed assays all exhibited improved performances with respect to chromatography, sensitivity, or throughput efficiency compared to other methodologies in the literature. The inhibitory effects of *p*-cresol on the glucuronidation of MPA were characterized in the HepaRG whole cell model (IC_{50}~55 μM, Chapter V [54]), human liver microsomes (K_i = 5.2 μM, Chapter VI [55]), and human recombinant UGT1A9 enzymes (K_i = 23.4 μM, Chapter VI [55]). These complementary *in vitro* approaches provided robust estimations of the true range of K_i values likely observed *clinically* in humans. The mechanism of inhibition of *p*-cresol toward UGT1A9-mediated MPA glucuronidation was reversible and competitive (Chapter VI) [55], suggesting that therapeutic strategies to reduce *p*-cresol may lead to reduced pharmacokinetic variability of MPA (please see further discussion below on future directions). Based on *in vitro-in vivo* extrapolation, *p*-cresol was expected to lead to ~2 fold increase in MPA plasma exposure in patients, which indicated that fluctuations in *p*-cresol concentrations may partially explain the large pharmacokinetic variations observed for MPA (Chapter V [54] and Chapter VI [55]). Moreover, using our established *in vitro* models, it was also determined that other commonly studied protein-bound uremic toxins (e.g., indole-3-acetic acid, indoxyl sulfate, hippuric acid, kynurenic acid, and 3-carboxy-4-methyl-5-

propyl-2-furanpropionic acid) and *p*-cresol metabolites (sulfate and glucuronide) had little inhibitory effects toward MPA metabolism (Chapter VI [55]). These data collectively supported a focused investigation on *p*-cresol alone for this thesis.

As *p*-cresol was demonstrated to be a potent inhibitor of MPA metabolism, factors affecting *p*-cresol disposition are also likely to (indirectly) influence MPA pharmacokinetics. Moreover, *p*-cresol concentrations in the human plasma are negligible, as the majority of *p*-cresol is already metabolized to *p*-cresol sulfate and *p*-cresol glucuronide [78, 80-82]. Therefore, understanding the enzyme kinetics of *p*-cresol metabolite formation was necessary to interpret the correlational findings reported in our clinical experiment (Chapter IX [58]). Using human cytosols/microsomes and recombinant SULT/UGT enzymes, human SULT1A1 was identified the primary enzyme responsible for the formation of *p*-cresol sulfate (K_m = 0.19±0.02 μM, V_{max} = 789.5±101.7 nmol/mg/min, K_{si}=2458.0±332.8 μM, substrate inhibition) (Chapter VII [56]); whereas human UGT1A6 exhibited the highest catalytic activities towards the generation of *p*-cresol glucuronide (S_{50} = 58.4±0.6 μM, V_{max} = 17.4±0.7 nmol/mg/min, Hill equation) (Chapter VIII [57]). These data confirmed the high efficiency/low capacity (SULT) and low efficiency/high capacity (UGT) nature of *p*-cresol metabolism, which allowed us to focus on *p*-cresol sulfate quantification as the primary metabolite physiologically relevant in adult kidney transplant patients (Chapter IX [58]). Furthermore, based on these data, it may be hypothesized that clinical factors that could affect SULT1A1 and UGT1A6 (e.g., genetic polymorphisms and concurrent drug modulators) may also indirectly affect MPA pharmacokinetic variability. For example, as demonstrated in our experiments, the loss of function SULT1A1*2 enzyme exhibited drastically reduced catalytic activities in *p*-cresol sulfonation (Chapter VII [56]), and the high prevalence of this single nucleotide polymorphism [330] may lead to fluctuations in *p*-cresol concentrations (and

hence MPA exposure variability) in patients. Moreover, *p*-cresol sulfate causing tissue damage (e.g., [94, 97]) may be another potential mechanism which could affect (unbound) MPA distribution into the peripheral tissue, and an approach to mitigate this interaction may be to strategically reduce the sulfonation of *p*-cresol. Using our established *in vitro* models, we have further identified potent and selective inhibitors of SULT1A1 that are capable of attenuating the production of *p*-cresol sulfate (Chapter VII [56]). Of the tested drugs, mefenamic acid was the most potent therapeutic inhibitor (K_i = 2.4±0.1 nM in the human liver cytosols and K_i = 1.2±0.3 nM in the human kidney cytosols) which exhibited noncompetitive inhibition in human liver cytosols and recombinant SULT1A1 (and mixed inhibition in human kidney cytosols (Chapter VII [56]). Further characterizations of this potent SULT1A1 inhibitor are already on-going in our laboratory to determine the on-/off- target effects using *in vitro* (e.g., metabolically competent human liver [416], kidney [419], and cardiac [420] cell lines) and *in vivo* (e.g., surgically or pharmacologically-induced chronic or acute kidney animals [421-423]) models.

To translate our *in vitro* findings to the clinic, the pharmacokinetic interactions between MPA and *p*-cresol were further investigated in adult kidney transplant recipients within the first year post-transplantation (Chapter IX [58]). Significant positive correlations using Spearman rank analyses were observed between the total MPA trough concentration, daily dose-normalized total MPA trough concentration, or body weight-normalized total MPA trough concentration and the plasma *p*-cresol sulfate concentration (n=40 patients) in a prospective observational trial conducted at the University of Alberta hospital. Moreover, patients categorized with elevated *p*-cresol sulfate concentrations (i.e., ≥ median of 3.2 μg/mL) also exhibited increased total MPA trough concentrations. These clinical findings were consistent with our mechanistic *in vitro* data and further confirmed a role of *p*-cresol as a significant clinical variable affecting the

pharmacokinetics of MPA. However, additional potential interacting mechanisms between *p*-cresol and MPA (other than metabolism inhibition) have also been identified in our clinical study, and further investigations to investigate their effects are proposed below.

2.2. Overall limitations and future directions

Additional mechanisms could also possibly mediate the interaction between MPA and *p*-cresol, as discussed in our clinical study (Chapter IX [58]). Due to the hydrophobic property of MPA, its uptake into the enterocytes is likely mediated primarily via passive diffusion [30]. As *p*-cresol has been documented to increase cellular permeability (e.g., in human umbilical vein endothelial cells [424]), it may be hypothesized that *p*-cresol could also affect gastrointestinal integrity and enhance the absorption (hence the bioavailability) of MPA. To investigate this potential interaction mechanism, *in vitro* cell culture models such as fresh/cryopreserved primary human enterocytes (e.g., [425]) may be utilized, where cellular damage could be assessed directly using spectrophotometric markers (e.g., [98]), confocal microscope imaging (e.g., [424]), or by measuring the production of endothelial microparticles (e.g., [94]). In this model, the uptake kinetics of MPA could also be characterized with the measurements of intracellular/extracellular MPA concentrations, in the presence of various experimental conditions (i.e., toxic vs. non-toxic) of *p*-cresol.

On the other hand, opposing mechanisms from *p*-cresol on the absorption/re-absorption of MPA are also possible and may partially explain the relatively weak correlations observed between *p*-cresol sulfate and MPA concentrations reported in our clinical study. The entero-hepatic recirculation of MPA accounts for ~40% of the its overall exposure [10, 30] and is likely mediated

by OATP1B1/3 (i.e., facilitating the uptake of MPAG from the sinusoidal membrane into the hepatocytes [40-43]) and BCRP transporters (facilitating the efflux of MPAG into the bile at the canalicular membrane [42]). *p*-Cresol sulfate may potentially affect the entero-hepatic recirculation of MPA by inhibiting OATP1B1/3 [43, 414, 415] and/or BCRP [78, 98], which could theoretically lead to the underexposure of MPA. Similarly, other uremic retention solutes have also been reported to inhibit the transporters involved in MPA disposition [53, 75] and may contribute to variations in MPA exposure. For example, 3-carboxy-4-methyl-5-propyl-2-furanpropionic acid (CMPF) [426-428], hippuric acid [415], indole-3-acetic acid [415, 426], indoxyl sulfate [415, 426], and kynurenic acid [415] are known to inhibit OATP1B1/3, and the activities of BCRP were shown to be reduced by hippuric acid, indoxyl sulfate, and kynurenic acid [412]. To investigate the potential interacting effects of *p*-cresol (and other toxins) on the activities of hepatic transporters responsible for MPA disposition, OATP1B1/3 mediated MPA uptake could be assessed using human hepatocytes (e.g., [414]), and the BCRP-mediated MPA efflux could be determined in BCRP-overexpressed membrane vesicles (i.e., an inverted cellular membrane model with reversed transporter orientation) prepared form human hepatic cellular models (e.g., [98, 410]). However, it is worth noting that HepaRG cells may not be an ideal model to investigate OATP1B3 mediated interactions, as its function is determined as "too low to be detected" in the differentiated HepaRG cells by Kotani et al. [429]. The uptake kinetics of MPA should be determined with intracellular/extracellular concentrations, and the inhibitory effects of uremic toxins on these hepatic transporters should be characterized with K_i estimation and the assessment of inhibition mechanisms.

Furthermore, *p*-cresol sulfate could also increase the total plasma exposure of MPA by altering its distribution. Based on studies conducted in *in vitro*/*ex vivo* models, *p*-cresol sulfate has

been shown to induce cell death in human kidney proximal tubular epithelial cells [90, 91], cause morphological changes in human umbilical vein endothelial cells [94], and generate inflammation in human kidney proximal tubular epithelial cells [91]. These toxic effects of *p*-cresol sulfate may damage tight conjunctions and increase cell permeability, potentially leading to increased distribution of unbound MPA into the peripheral tissues. Based on this mechanism, the total plasma concentrations of MPA may be increased as the central volume of distribution is likely to decrease. Likewise, similar cellular damage effects were also identified for indole-3-acetic acid and indoxyl sulfate [87], which may also contribute to increased total MPA plasma exposure through this potential mechanism. To test this hypothesis, MPA distribution could be characterized in the presence/absence of *p*-cresol sulfate (or other uremic toxins) *in vivo* in rodents, where tissues and organs (e.g., blood, brain, heart, lung, liver, kidney, spleen, pancreas, etc.) can be harvested for the measurement of MPA concentrations and for histopathology examination. Compartmental distribution models (i.e., using the non-linear mixed effect modeling or physiologically-based pharmacokinetic modeling) could also be constructed to characterize the volumes of distribution in central (i.e., the plasma) and peripheral (i.e., other organs/tissues) compartments, and to determine the kinetics of MPA movement between these compartments in the presence of toxic concentrations of uremic toxins.

Another potential confounding effect is the extensive binding of *p*-cresol sulfate to plasma albumin (with a free fraction of ~8.6% [85]), which could displace MPA protein binding [10]. This interaction could lead to increased MPA free fraction and reduced total plasma MPA concentrations. Likewise, the same interacting mechanism could also be mediated by other uremic toxins that are also highly bound to plasma proteins (e.g., CMPF, hippuric acid, indole-3-acetic acid, kynurenines, phenyl acetic acid, etc. [75]). To further investigate this potential interacting

mechanism, equilibrium dialysis with plasma samples consisting of MPA could be utilized to evaluate the protein-binding displacement potency of uremic toxins under physiologically relevant conditions. In humans, the protein binding displacement effects of *p*-cresol sulfate can be assessed with population pharmacokinetic modeling, characterizing both bound and unbound concentrations of *p*-cresol sulfate, MPA, and MPAG.

In addition to inhibiting MPA hepatic metabolism, *p*-cresol may also reduce MPA conjugation in the intestines, where UGT1A9 is constitutively expressed [35, 376, 377], and further increase the total MPA plasma exposure. To test these hypotheses, microsomes prepared from human intestines and/or cryopreserved primary human enterocytes [425] can be utilized following a similar mechanistic approach demonstrated for hepatic tissues in this thesis (Chapter VI [55]). On the other hand, as both MPA and *p*-cresol undergo extensive first-pass metabolism [33], the kidneys would likely only be exposed to minimal concentrations of MPA and *p*-cresol. As well, *p*-cresol is primarily found in the forms of *p*-cresol sulfate and glucuronide in the plasma (e.g., [295]), and both metabolites exhibited little inhibitory effects on MPA metabolism based on our data (Chapter VI [55]). Therefore, the contributions of renal UGT enzymes to the MPA-*p*-cresol interaction is likely very minimal.

On the other hand, renal transporter interactions may also explain the positive associations observed between *p*-cresol sulfate and MPA. MPAG is primarily excreted by the kidneys [10, 37] presumably via the OAT-3 transporter [30, 32, 38], and *p*-cresol sulfate is a known inhibitor of OAT-3 as demonstrated in *in vitro* cell culture models [53, 223]. Therefore, *p*-cresol sulfate could potentially inhibit the renal excretion of MPAG and lead to its accumulation in the plasma. Supporting this hypothesis, a positive relationship between *p*-cresol sulfate and the daily dose-normalized free MPAG was identified in our clinical study in adult kidney transplant patients

(Chapter IX [58]). Furthermore, the OAT-3 mediated renal excretion of MPAG may also be inhibited by CMPF, hippuric acid, indole-3-acetic acid, and indoxyl sulfate [53, 430, 431]. To assess renal transporter interaction as a potential mechanism affecting MPA kinetics, experiments should be performed to investigate the inhibitory effects *p*-cresol sulfate (and other uremic toxins) on the OAT-3 mediated uptake of MPAG. Models such as the OAT-3 overexpressed HEK293 cells (e.g., [223]) and/or conditionally immortalized human proximal tubule epithelial (ciPTEC) cells (e.g., [98, 99, 432, 433]) are commonly used for this purpose. As ciPTEC cells exhibit more complete physiological functions (with the presence of a variety of metabolism enzymes, transporters, tight junction proteins, aminopeptidase N enzyme, aquaporin 1, megalin/cubilin endocytic receptors, etc. [419]) than HEK293 cells, it is the model of choice for further investigations in our laboratory (experiments already ongoing). Moreover, this potential interaction may also be studied using animal models (e.g., experimentally-induced chronic kidney disease rodents/mice [422, 423]), although the enzyme kinetics of *p*-cresol metabolism may not be directly comparable to humans (and appropriate scaling factors would need to be determined). As an example, *p*-cresol glucuronide was reported to be the predominant metabolite (more than 90%) in the Swiss mice model [422] in contrast to *p*-cresol sulfate being the major metabolite (Chapter VII [56]) in humans. Furthermore, the renal transporter-mediated MPA kinetic interactions can also be studied in human population pharmacokinetic models, utilizing plasma and urine samples to clearly differentiate filtration (e.g., serum creatinine) vs. active transport (e.g., MPAG). The potential incorporation of patients administered OAT therapeutic probe substrates may also be considered in the study design.

Lastly, the cause-effect relationships between *p*-cresol and MPA exposure variability in kidney transplant patients should be further investigated in the clinic. The hypothesis is that

attenuating *p*-cresol concentrations should lead to significantly decreased MPA plasma exposure variabilities in adult kidney transplant recipients. An initial approach is the utilization of a double-blinded crossover design (e.g., 2-week intervention followed by a 1-week washout) to assess both inter- and intra-individual variabilities of MPA. If successful, a fully randomized, controlled clinical study can be further justified. The primary objective is to assess the effects of therapeutic strategies that can decrease *p*-cresol concentrations (e.g., AST-120, synbiotics, and/or SULT inhibitors [53, 78, 322]) on MPA plasma exposure variability. MPA exposure will be determined by validated limited sampling strategies [51, 62, 434-436] using multiple regression equations or Bayesian-estimation. The model design can incorporate the ideal characteristics discussed throughout this thesis: i) adult kidney transplant recipients at various post-transplant periods on both MMF or EC-MPS should be recruited; ii) total and free plasma concentrations of MPA, MPAG, AcMPAG, *p*-cresol, *p*-cresol sulfate, and *p*-cresol glucuronide (at steady state conditions) can be quantified using already established assays (Chapter V [54], Chapter VI [55], Chapter VII [56], Chapter VIII [57], and Chapter IX [58]) at the end of each treatment period; iii) mechanistic population pharmacokinetic models incorporating entero-hepatic recirculation, protein binding, and renal clearance compartments should be established (as proposed in Chapter III [25] and Chapter IV [27]). These approaches will allow us to estimate the inter- and intra- individual variabilities and to accurately predict the MPA exposure values for each subject. If our hypothesis is correct, the inter-/intra- individual variabilities of MPA would be significantly decreased (demonstrated by reduced coefficients of variation values) after the experimental interventions to reduce *p*-cresol concentrations. Alternatively, we also anticipate the percentage of subjects exhibiting MPA $AUC_{0\text{-}12}$ within the target therapeutic range (i.e., 30-60 μg×h/mL) to be significantly increased.

In addition to the primary objective, this clinical study should also incorporate additional *exploratory* investigations to characterize other potential factors/mechanisms associated with MPA variability. The usage of EC-MPS is anticipated to be expanded in the future [2, 24], and the effects of formulation should be characterized in the covariate model. The effects of protein binding interactions by *p*-cresol sulfate can be further integrated in the structural model using aforementioned binding-dissociation constructs. Moreover, the effects of post-transplant time can be incorporated directly into the final model (i.e., by introducing a time-based scaling factor for the relevant fixed-effects variables) or indirectly using covariate modeling. As only a few published studies have differentiated total vs. renal clearance of MPA (reviewed in Chapter III [25] and Chapter IV [27]), the renal interacting effects of *p*-cresol should be quantified using appropriately collected urinary data. Ideally, subjects should be genotyped to identify key genetic polymorphisms of metabolism enzymes and transporters (e.g., UGT2B7 G211T, UGT2B7 C802T, UGT1A9 T-275A, UGT1A9 T98C, MRP2 C-24T, MRP2 G1249A, OATP1B1 A388G, and OATP1B1 C463A [133]) associated with MPA disposition. As well, pharmacodynamic or clinical outcomes of MPA such as white blood cell count, neutrophil count, and the occurrence of rejection/infection should be incorporated into the final model to establish the pharmacokinetic-dynamic relationships. As these secondary objectives are exploratory in nature, further mechanistic studies are warranted if significant observations are identified from our analyses. A potential mechanistic MPA population pharmacokinetic model that will allow us to address these objectives can be visualized in Figure X-1.

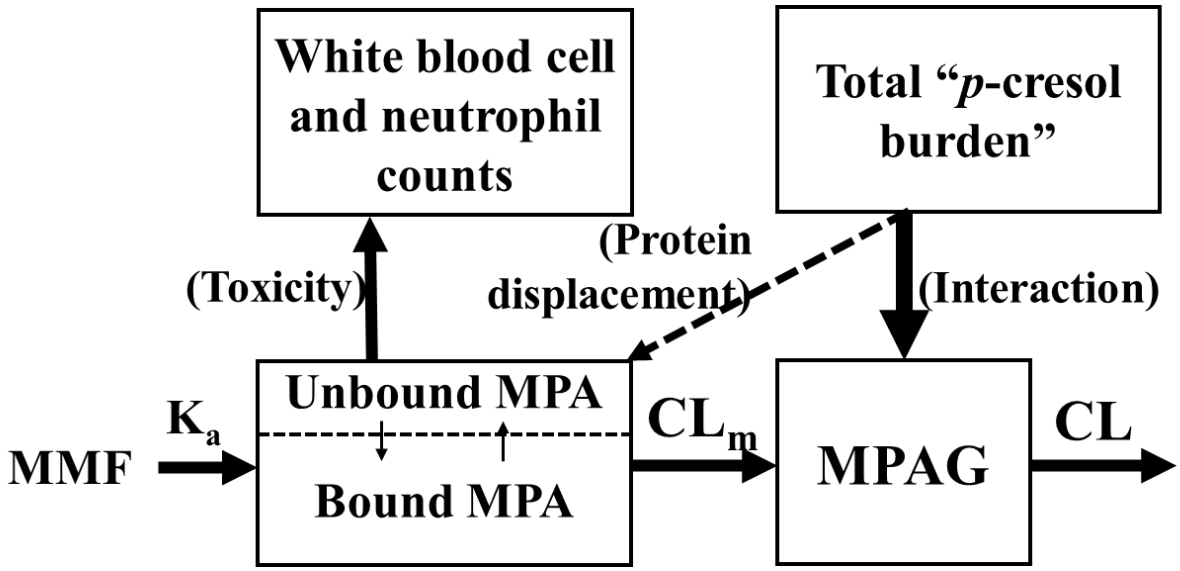

Figure X-1 Proposed population kinetic model on the interaction between p-cresol and MPA

The interaction effect may be characterized by linear ($interaction = slope \times [total\ "p-cresol\ burden"]$), exponential ($interaction = \frac{1}{e^{slope} \times [total\ "p\text{-}cresol\ burden"]}$), or E_{max} ($interaction = \frac{E_{max} \times [total\ "p\text{-}cresol\ burden"]}{EC_{50} + [total\ "p\text{-}cresol\ burden"]}$) models. The protein binding effect of MPA may be characterized by a saturable binding model ($[bound\ MPA] = \frac{B_{max} \times [unbound\ MPA]}{K_d + [unbound\ MPA]}$). The protein displacement effect may be characterized by a competitive binding model ($K_m = \frac{[MPA] \times [albumin]}{[MPA \cdot albumin]}$, $K_p = \frac{[p\text{-}cresol] \times [albumin]}{[p\text{-}cresol \cdot albumin]}$). The toxicity effect may be characterized by a direct ($E = \frac{E_{max} \times [MPA]}{EC_{50} + [MPA]}$) or effect compartment ($E = \frac{E_{max} \times [MPA]\ in\ effect\ compartment}{EC_{50} + [MPA]\ in\ effect\ compartment}$) E_{max} model. Abbreviations: B_{max}, maximal binding capacity of MPA; CL, clearance of MPAG; CL_m, clearance of MPA in the formation of MPAG; E, effect of MPA on white blood cell and neutrophil counts, EC_{50}, concentration for half-maximal effect; E_{max}, maximal effect; K_a, absorption rate constant of MPA; K_d, unbound MPA concentration for half-saturation of protein binding; K_m, dissociation constant for the binding of MPA with albumin; K_p, dissociation constant for the binding of *p*-cresol with albumin; MMF, mycophenolate mofetil; MPA, mycophenolic acid; MPAG, MPA-glucuronide; "[ ]", concentrations of specific molecule.

3. Overall conclusion

This PhD thesis has identified potential significant extrinsic (e.g., co-administration of corticosteroids) and intrinsic (e.g., body weight) factors influencing MPA pharmacokinetics. It also systematically characterized a potent metabolism interaction between *p*-cresol and MPA, using the translational approach involving *in vitro* and clinical models. For scientists, this thesis has provided the basis for conducting further mechanistic experiments and for investigating therapeutic approaches for mitigating MPA variability. For clinicians, this thesis has presented a comprehensive overview and critique of potential clinical factors that may contribute to MPA variabilities, as well as identified a novel approach for proactively managing *p*-cresol accumulation and MPA variability. For patients, this thesis may ultimately improve the clinical outcomes and their quality of lives.

Overall References

1. Bentley R. Mycophenolic acid: A one hundred year odyssey from antibiotic to immunosuppressant. Chem Rev. 2000 Oct 11;100(10):3801-26.
2. Bergan S., Brunet M., Hesselink D. A., Johnson-Davis K. L., Kunicki P. K., Lemaitre F., et al. Personalized Therapy for Mycophenolate: Consensus Report by the International Association of Therapeutic Drug Monitoring and Clinical Toxicology. Ther Drug Monit. 2021 Apr 1;43(2):150-200.
3. Franklin T. J., Cook J. M. The inhibition of nucleic acid synthesis by mycophenolic acid. Biochem J. 1969 Jul;113(3):515-24.
4. Jones E. L., Epinette W. W., Hackney V. C., Menendez L., Frost P. Treatment of psoriasis with oral mycophenolic acid. J Invest Dermatol. 1975 Dec;65(6):537-42.
5. Kirby B., Yates V. M. Mycophenolate mofetil for psoriasis. Br J Dermatol. 1998 Aug;139(2):357.
6. The Tricontinental Mycophenolate Mofetil Renal Transplantation Study Group. A blinded, randomized clinical trial of mycophenolate mofetil for the prevention of acute rejection in cadaveric renal transplantation. The Tricontinental Mycophenolate Mofetil Renal Transplantation Study Group. Transplantation. 1996 Apr 15;61(7):1029-37.
7. U.S. Food and Drug Administration. FDA approved durg - CellCept (mycophenolate mofetil). 1995 [cited 2021 November 25]; Available from: https://www.accessdata.fda.gov/scripts/cder/daf/index.cfm?event=overview.process&ApplNo=050722
8. European Medicines Agency. CellCept. 2021 [cited 2021 November 25]; Available from: https://www.ema.europa.eu/en/medicines/human/EPAR/cellcept
9. Health Canada. Product information of CellCept (mycophenolate mofetil). 2021 [cited 2021 November 25]; Available from: https://health-products.canada.ca/dpd-bdpp/info.do?lang=en&code=65823#fn1
10. Staatz C. E., Tett S. E. Clinical pharmacokinetics and pharmacodynamics of mycophenolate in solid organ transplant recipients. Clin Pharmacokinet. 2007;46(1):13-58.
11. Health Canada. Product monograph including patient medication information - Cellcept (mycophenolate mofetil). 2021 [cited 2021 November 25]; Available from: https://pdf.hres.ca/dpd_pm/00063434.PDF
12. Health Canada. Product monograph including patient medication information - Myfortic (enteric-coated mycophenolate sodium). 2018 [cited 2021 November 25]; Available from: https://pdf.hres.ca/dpd_pm/00045374.PDF
13. Lee W. A., Gu L., Miksztal A. R., Chu N., Leung K., Nelson P. H. Bioavailability improvement of mycophenolic acid through amino ester derivatization. Pharm Res. 1990 Feb;7(2):161-6.
14. Kaplan B. Enteric-coated mycophenolate sodium (myfortic®): An overview of current and future use in transplantation. Drugs. 2006;66:1-8.
15. Salvadori M., Holzer H., de Mattos A., Sollinger H., Arns W., Oppenheimer F., et al. Enteric-coated mycophenolate sodium is therapeutically equivalent to mycophenolate mofetil in de novo renal transplant patients. Am J Transplant. 2004 Feb;4(2):231-6.
16. U.S. Food and Drug Administration. CellCept - Highlights of prescribing information. 2021 [cited 2021 October 22]; Available from:

https://www.accessdata.fda.gov/drugsatfda_docs/label/2021/050722s045s046,050723s045s046,050758s042s043,050759s050s051lbl.pdf
17. Granger D. K., Group Erl B. Renal Transplant Study, Group Erl B. Renal Transplant Study. Enteric-coated mycophenolate sodium: Results of two pivotal global multicenter trials. Transplant Proc. 2001 Nov-Dec;33(7-8):3241-4.
18. Abbud-Filho M., Giron F., Hernandez E., Juarez F., Liendo C., Novoa P., et al. Stable renal transplant recipients can be safely converted from MMF to enteric-coated mycophenolate sodium tablets: Interim results of a multicenter Latin American study. Transplant Proc. 2004 Jul-Aug;36(6):1647-9.
19. Massari P., Duro-Garcia V., Giron F., Hernandez E., Juarez F., Castro C., et al. Safety assessment of the conversion from mycophenolate mofetil to enteric-coated mycophenolate sodium in stable renal transplant recipients. Transplant Proc. 2005 Mar;37(2):916-9.
20. Nashan B., Ivens K., Suwelack B., Arns W., Abbud Filho M., my Proms D. E. Study Group, et al. Conversion from mycophenolate mofetil to enteric-coated mycophenolate sodium in maintenance renal transplant patients: preliminary results from the myfortic prospective multicenter study. Transplant Proc. 2004 Mar;36(2 Suppl):521S-3S.
21. Kamar N., Garrigue V., Karras A., Mourad G., Lefrancois N., Charpentier B., et al. Impact of early or delayed cyclosporine on delayed graft function in renal transplant recipients: a randomized, multicenter study. Am J Transplant. 2006 May;6(5 Pt 1):1042-8.
22. Cibrik D., Meier-Kriesche H. U., Bresnahan B., Wu Y. M., Klintmalm G., Kew C. E., et al. Renal function with cyclosporine C2 monitoring, enteric-coated mycophenolate sodium and basiliximab: a 12-month randomized trial in renal transplant recipients. Clin Transplant. 2007 Mar-Apr;21(2):192-201.
23. Chan L., Mulgaonkar S., Walker R., Arns W., Ambuhl P., Schiavelli R. Patient-reported gastrointestinal symptom burden and health-related quality of life following conversion from mycophenolate mofetil to enteric-coated mycophenolate sodium. Transplantation. 2006 May 15;81(9):1290-7.
24. van Gelder T., Hesselink D. A. Mycophenolate revisited. Transpl Int. 2015 May;28(5):508-15.
25. Rong Y., Patel V., Kiang T. K. L. Recent lessons learned from population pharmacokinetic studies of mycophenolic acid: Physiological, genomic, and drug interactions leading to the prediction of drug effects. Expert Opinion on Drug Metabolism & Toxicology. 2022 Jan 24;17(12):1369-406.
26. Wolters Kluwer. Lexicomp database. 2021 [cited 2021 November 25]; Available from: https://online.lexi.com/lco/action/login.
27. Rong Y., Jun H., Kiang T. K. L. Population pharmacokinetics of mycophenolic acid in paediatric patients. Br J Clin Pharmacol. 2021 Apr;87(4):1730-57.
28. Allison A. C., Eugui E. M. Mechanisms of action of mycophenolate mofetil in preventing acute and chronic allograft rejection. Transplantation. 2005 Oct 15;80(2 Suppl):S181-90.
29. Staatz C. E., Tett S. E. Pharmacology and toxicology of mycophenolate in organ transplant recipients: An update. Arch Toxicol. 2014 Jul;88(7):1351-89.
30. Sherwin C. M., Fukuda T., Brunner H. I., Goebel J., Vinks A. A. The evolution of population pharmacokinetic models to describe the enterohepatic recycling of mycophenolic acid in solid organ transplantation and autoimmune disease. Clin Pharmacokinet. 2011 Jan;50(1):1-24.
31. Kiang T. K. L., Ensom M. H. H. Population pharmacokinetics of mycophenolic acid: An update. Clin Pharmacokinet. 2018 May;57(5):547-58.

32. Benjanuwattra J., Pruksakorn D., Koonrungsesomboon N. Mycophenolic acid and its pharmacokinetic drug-drug interactions in humans: Review of the evidence and clinical implications. J Clin Pharmacol. 2020 Mar;60(3):295-311.
33. Bowalgaha K., Miners J. O. The glucuronidation of mycophenolic acid by human liver, kidney and jejunum microsomes. Br J Clin Pharmacol. 2001 Nov;52(5):605-9.
34. Benet L. Z., Hoener B. A. Changes in plasma protein binding have little clinical relevance. Clin Pharmacol Ther. 2002 Mar;71(3):115-21.
35. Picard N., Ratanasavanh D., Premaud A., Le Meur Y., Marquet P. Identification of the UDP-glucuronosyltransferase isoforms involved in mycophenolic acid phase II metabolism. Drug Metab Dispos. 2005 Jan;33(1):139-46.
36. Picard N., Cresteil T., Premaud A., Marquet P. Characterization of a phase 1 metabolite of mycophenolic acid produced by CYP3A4/5. Ther Drug Monit. 2004 Dec;26(6):600-8.
37. Bullingham R. E., Nicholls A. J., Kamm B. R. Clinical pharmacokinetics of mycophenolate mofetil. Clin Pharmacokinet. 1998 Jun;34(6):429-55.
38. Uwai Y., Motohashi H., Tsuji Y., Ueo H., Katsura T., Inui K. Interaction and transport characteristics of mycophenolic acid and its glucuronide via human organic anion transporters hOAT1 and hOAT3. Biochem Pharmacol. 2007 Jun 30;74(1):161-8.
39. El-Sheikh A. A., Koenderink J. B., Wouterse A. C., van den Broek P. H., Verweij V. G., Masereeuw R., et al. Renal glucuronidation and multidrug resistance protein 2-/ multidrug resistance protein 4-mediated efflux of mycophenolic acid: interaction with cyclosporine and tacrolimus. Transl Res. 2014 Jul;164(1):46-56.
40. Geng F., Jiao Z., Dao Y. J., Qiu X. Y., Ding J. J., Shi X. J., et al. The association of the UGT1A8, SLCO1B3 and ABCC2/ABCG2 genetic polymorphisms with the pharmacokinetics of mycophenolic acid and its phenolic glucuronide metabolite in Chinese individuals. Clin Chim Acta. 2012 Apr 11;413(7-8):683-90.
41. Miura M., Satoh S., Inoue K., Kagaya H., Saito M., Inoue T., et al. Influence of SLCO1B1, 1B3, 2B1 and ABCC2 genetic polymorphisms on mycophenolic acid pharmacokinetics in Japanese renal transplant recipients. Eur J Clin Pharmacol. 2007 Dec;63(12):1161-9.
42. Miura M., Kagaya H., Satoh S., Inoue K., Saito M., Habuchi T., et al. Influence of drug transporters and UGT polymorphisms on pharmacokinetics of phenolic glucuronide metabolite of mycophenolic acid in Japanese renal transplant recipients. Ther Drug Monit. 2008 Oct;30(5):559-64.
43. Picard N., Yee S. W., Woillard J. B., Lebranchu Y., Le Meur Y., Giacomini K. M., et al. The role of organic anion-transporting polypeptides and their common genetic variants in mycophenolic acid pharmacokinetics. Clin Pharmacol Ther. 2010 Jan;87(1):100-8.
44. Fukuda T., Goebel J., Cox S., Maseck D., Zhang K., Sherbotie J. R., et al. UGT1A9, UGT2B7, and MRP2 genotypes can predict mycophenolic acid pharmacokinetic variability in pediatric kidney transplant recipients. Ther Drug Monit. 2012 Dec;34(6):671-9.
45. Hesselink D. A., van Hest R. M., Mathot R. A., Bonthuis F., Weimar W., de Bruin R. W., et al. Cyclosporine interacts with mycophenolic acid by inhibiting the multidrug resistance-associated protein 2. Am J Transplant. 2005 May;5(5):987-94.
46. Kobayashi M., Saitoh H., Kobayashi M., Tadano K., Takahashi Y., Hirano T. Cyclosporin A, but not tacrolimus, inhibits the biliary excretion of mycophenolic acid glucuronide possibly mediated by multidrug resistance-associated protein 2 in rats. J Pharmacol Exp Ther. 2004 Jun;309(3):1029-35.

47. Naesens M., Kuypers D. R., Verbeke K., Vanrenterghem Y. Multidrug resistance protein 2 genetic polymorphisms influence mycophenolic acid exposure in renal allograft recipients. Transplantation. 2006 Oct 27;82(8):1074-84.
48. van Gelder T., Klupp J., Barten M. J., Christians U., Morris R. E. Comparison of the effects of tacrolimus and cyclosporine on the pharmacokinetics of mycophenolic acid. Ther Drug Monit. 2001 Apr;23(2):119-28.
49. Westley I. S., Brogan L. R., Morris R. G., Evans A. M., Sallustio B. C. Role of Mrp2 in the hepatic disposition of mycophenolic acid and its glucuronide metabolites: Effect of cyclosporine. Drug Metab Dispos. 2006 Feb;34(2):261-6.
50. Atcheson B. A., Taylor P. J., Kirkpatrick C. M., Duffull S. B., Mudge D. W., Pillans P. I., et al. Free mycophenolic acid should be monitored in renal transplant recipients with hypoalbuminemia. Ther Drug Monit. 2004 Jun;26(3):284-6.
51. Kiang T. K., Ensom M. H. Therapeutic drug monitoring of mycophenolate in adult solid organ transplant patients: An update. Expert Opin Drug Metab Toxicol. 2016 May;12(5):545-53.
52. Barnes K. J., Rowland A., Polasek T. M., Miners J. O. Inhibition of human drug-metabolising cytochrome P450 and UDP-glucuronosyltransferase enzyme activities in vitro by uremic toxins. Eur J Clin Pharmacol. 2014 Sep;70(9):1097-106.
53. Prokopienko A. J., Nolin T. D. Microbiota-derived uremic retention solutes: perpetrators of altered nonrenal drug clearance in kidney disease. Expert Rev Clin Pharmacol. 2018 Jan;11(1):71-82.
54. Rong Y., Kiang T. K. L. Development and validation of a sensitive liquid-chromatography tandem mass spectrometry assay for mycophenolic acid and metabolites in HepaRG cell culture: Characterization of metabolism interactions between p-cresol and mycophenolic acid. Biomed Chromatogr. 2019 Aug;33(8):e4549.
55. Rong Y., Kiang T. K. L. Mechanisms of metabolism interaction between p-cresol and mycophenolic acid. Toxicol Sci. 2020 Feb 1;173(2):267-79.
56. Rong Y., Kiang T. K. L. Characterization of human sulfotransferases catalyzing the formation of p-cresol sulfate and identification of mefenamic acid as a potent metabolism inhibitor and potential therapeutic agent for detoxification. Toxicol Appl Pharmacol. 2021 Aug 15;425:115553.
57. Rong Y., Kiang T. K. L. Characterizations of human UDP-glucuronosyltransferase enzymes in the conjugation of p-cresol. Toxicol Sci. 2020 Aug 1;176(2):285-96.
58. Rong Y., Colbourne P, Gourishankar S, Kiang T. K. L. Significant correlations between p-cresol sulfate and mycophenolic acid plasma concentrations in adult kidney transplant recipients. Clinical Drug investigation. 2022 Mar;42(3):207-19.
59. Rong Y., Mayo P., Ensom M. H. H., Kiang T. K. L. Population pharmacokinetics of mycophenolic acid co-administered with tacrolimus in corticosteroid-free adult kidney transplant patients. Clin Pharmacokinet. 2019 Nov;58(11):1483-95.
60. Rong Y., Mayo P., Ensom M. H. H., Kiang T. K. L. Population pharmacokinetic analysis of immediate-release oral tacrolimus co-administered with mycophenolate mofetil in corticosteroid-free adult kidney transplant recipients. Eur J Drug Metab Pharmacokinet. 2019 Jun;44(3):409-22.
61. Kiang T. K. L., Ensom M. H. H. Exposure-toxicity relationships of mycophenolic acid in adult kidney transplant patients. Clin Pharmacokinet. 2019 Dec;58(12):1533-52.

62. Staatz C. E., Tett S. E. Maximum a posteriori Bayesian estimation of mycophenolic Acid area under the concentration-time curve: is this clinically useful for dosage prediction yet? Clin Pharmacokinet. 2011 Dec 1;50(12):759-72.
63. van Gelder T., Hilbrands L. B., Vanrenterghem Y., Weimar W., de Fijter J. W., Squifflet J. P., et al. A randomized double-blind, multicenter plasma concentration controlled study of the safety and efficacy of oral mycophenolate mofetil for the prevention of acute rejection after kidney transplantation. Transplantation. 1999 Jul 27;68(2):261-6.
64. European Medcines Agency. Cellcept, INN-mycophenolate mofetil. 2004 [cited 2020 May 18]; Available from: https://www.ema.europa.eu/en/documents/scientific-discussion/cellcept-epar-scientific-discussion_en.pdf
65. Mould D. R., Upton R. N. Basic concepts in population modeling, simulation, and model-based drug development. CPT Pharmacometrics Syst Pharmacol. 2012 Sep 26;1:e6.
66. Ette E. I., Williams P. J. Population pharmacokinetics I: Background, concepts, and models. Ann Pharmacother. 2004 Oct;38(10):1702-6.
67. Ette E. I., Williams P. J. Population pharmacokinetics II: Estimation methods. Ann Pharmacother. 2004 Nov;38(11):1907-15.
68. Kiang T. K., Sherwin C. M., Spigarelli M. G., Ensom M. H. Fundamentals of population pharmacokinetic modelling: Modelling and software. Clin Pharmacokinet. 2012 Aug;51(8):515-25.
69. Mould D. R., Upton R. N. Basic concepts in population modeling, simulation, and model-based drug development-part 2: Introduction to pharmacokinetic modeling methods. CPT Pharmacometrics Syst Pharmacol. 2013 Apr 17;2:e38.
70. Ette E. I., Williams P. J., Lane J. R. Population pharmacokinetics III: Design, analysis, and application of population pharmacokinetic studies. Ann Pharmacother. 2004 Dec;38(12):2136-44.
71. Abd Rahman A. N., Tett S. E., Staatz C. E. Clinical pharmacokinetics and pharmacodynamics of mycophenolate in patients with autoimmune disease. Clin Pharmacokinet. 2013 May;52(5):303-31.
72. Dong M., Fukuda T., Vinks A. A. Optimization of mycophenolic acid therapy using clinical pharmacometrics. Drug Metab Pharmacokinet. 2014;29(1):4-11.
73. Zhang D., Chow D. S. Clinical pharmacokinetics of mycophenolic acid in hematopoietic stem cell transplantation recipients. Eur J Drug Metab Pharmacokinet. 2017 Apr;42(2):183-9.
74. Zwart T. C., Guchelaar H. J., van der Boog P. J. M., Swen J. J., van Gelder T., de Fijter J. W., et al. Model-informed precision dosing to optimise immunosuppressive therapy in renal transplantation. Drug Discov Today. 2021. DOI: 10.1016/j.drudis.2021.06.001 Jun 10.
75. Vanholder R., Pletinck A., Schepers E., Glorieux G. Biochemical and clinical impact of organic uremic retention solutes: A comprehensive update. Toxins (Basel). 2018 Jan 8;10(1).
76. Vanholder R., De Smet R., Glorieux G., Argiles A., Baurmeister U., Brunet P., et al. Review on uremic toxins: Classification, concentration, and interindividual variability. Kidney Int. 2003 May;63(5):1934-43.
77. Graboski A. L., Redinbo M. R. Gut-derived protein-bound uremic toxins. Toxins (Basel). 2020 Sep 11;12(9).
78. Gryp T., Vanholder R., Vaneechoutte M., Glorieux G. p-Cresyl sulfate. Toxins (Basel). 2017 Jan 29;9(2).
79. Vanholder R., De Smet R., Lesaffer G. p-Cresol: A toxin revealing many neglected but relevant aspects of uraemic toxicity. Nephrol Dial Transplant. 1999 Dec;14(12):2813-5.

80. de Loor H., Bammens B., Evenepoel P., De Preter V., Verbeke K. Gas chromatographic-mass spectrometric analysis for measurement of p-cresol and its conjugated metabolites in uremic and normal serum. Clin Chem. 2005 Aug;51(8):1535-8.
81. Martinez A. W., Recht N. S., Hostetter T. H., Meyer T. W. Removal of p-cresol sulfate by hemodialysis. J Am Soc Nephrol. 2005 Nov;16(11):3430-6.
82. Vanholder R., Bammens B., de Loor H., Glorieux G., Meijers B., Schepers E., et al. Warning: The unfortunate end of p-cresol as a uraemic toxin. Nephrol Dial Transplant. 2011 May;26(5):1464-7.
83. Guida B., Cataldi M., Memoli A., Trio R., di Maro M., Grumetto L., et al. Effect of a short-course treatment with synbiotics on plasma p-cresol concentration in kidney transplant recipients. J Am Coll Nutr. 2017 Sep-Oct;36(7):586-91.
84. Poesen R., Evenepoel P., de Loor H., Kuypers D., Augustijns P., Meijers B. Metabolism, protein binding, and renal clearance of microbiota-derived p-cresol in patients with CKD. Clin J Am Soc Nephrol. 2016 Jul 7;11(7):1136-44.
85. Liabeuf S., Barreto D. V., Barreto F. C., Meert N., Glorieux G., Schepers E., et al. Free p-cresylsulphate is a predictor of mortality in patients at different stages of chronic kidney disease. Nephrol Dial Transplant. 2010 Apr;25(4):1183-91.
86. Liabeuf S., Glorieux G., Lenglet A., Diouf M., Schepers E., Desjardins L., et al. Does p-cresylglucuronide have the same impact on mortality as other protein-bound uremic toxins? PLoS One. 2013;8(6):e67168.
87. Liabeuf S., Villain C., Massy Z. A. Protein-bound toxins: Has the Cinderella of uraemic toxins turned into a princess? Clin Sci (Lond). 2016 Dec 1;130(23):2209-16.
88. Vanholder R., Schepers E., Pletinck A., Nagler E. V., Glorieux G. The uremic toxicity of indoxyl sulfate and p-cresyl sulfate: A systematic review. J Am Soc Nephrol. 2014 Sep;25(9):1897-907.
89. Meijers B. K., Evenepoel P. The gut-kidney axis: indoxyl sulfate, p-cresyl sulfate and CKD progression. Nephrol Dial Transplant. 2011 Mar;26(3):759-61.
90. Poveda J., Sanchez-Nino M. D., Glorieux G., Sanz A. B., Egido J., Vanholder R., et al. p-Cresyl sulphate has pro-inflammatory and cytotoxic actions on human proximal tubular epithelial cells. Nephrol Dial Transplant. 2014 Jan;29(1):56-64.
91. Watanabe H., Miyamoto Y., Honda D., Tanaka H., Wu Q., Endo M., et al. p-Cresyl sulfate causes renal tubular cell damage by inducing oxidative stress by activation of NADPH oxidase. Kidney Int. 2013 Apr;83(4):582-92.
92. Weigand K. M., Schirris T. J. J., Houweling M., van den Heuvel Jjmw, Koenderink J. B., Dankers A. C. A., et al. Uremic solutes modulate hepatic bile acid handling and induce mitochondrial toxicity. Toxicol In Vitro. 2019 Apr;56:52-61.
93. Zhu S., Rong Y., Kiang T. K. L. Effects of p-cresol on oxidative stress, glutathione depletion, and necrosis in HepaRG cells: Comparisons to other uremic toxins and the role of p-cresol glucuronide formation. Pharmaceutics. 2021 Jun 9;13(6).
94. Meijers B. K., Van Kerckhoven S., Verbeke K., Dehaen W., Vanrenterghem Y., Hoylaerts M. F., et al. The uremic retention solute p-cresyl sulfate and markers of endothelial damage. Am J Kidney Dis. 2009 Nov;54(5):891-901.
95. Koppe L., Pillon N. J., Vella R. E., Croze M. L., Pelletier C. C., Chambert S., et al. p-Cresyl sulfate promotes insulin resistance associated with CKD. J Am Soc Nephrol. 2013 Jan;24(1):88-99.

96. Schepers E., Meert N., Glorieux G., Goeman J., Van der Eycken J., Vanholder R. p-Cresylsulphate, the main in vivo metabolite of p-cresol, activates leucocyte free radical production. Nephrol Dial Transplant. 2007 Feb;22(2):592-6.
97. Gross P., Massy Z. A., Henaut L., Boudot C., Cagnard J., March C., et al. para-Cresyl sulfate acutely impairs vascular reactivity and induces vascular remodeling. J Cell Physiol. 2015 Dec;230(12):2927-35.
98. Mutsaers H. A., Caetano-Pinto P., Seegers A. E., Dankers A. C., van den Broek P. H., Wetzels J. F., et al. Proximal tubular efflux transporters involved in renal excretion of p-cresyl sulfate and p-cresyl glucuronide: Implications for chronic kidney disease pathophysiology. Toxicol In Vitro. 2015 Oct;29(7):1868-77.
99. Mutsaers H. A., Wilmer M. J., Reijnders D., Jansen J., van den Broek P. H., Forkink M., et al. Uremic toxins inhibit renal metabolic capacity through interference with glucuronidation and mitochondrial respiration. Biochim Biophys Acta. 2013 Jan;1832(1):142-50.
100. Glorieux G., Vanholder R., Van Biesen W., Pletinck A., Schepers E., Neirynck N., et al. Free p-cresyl sulfate shows the highest association with cardiovascular outcome in chronic kidney disease. Nephrol Dial Transplant. 2021 May 27;36(6):998-1005.
101. Wu I. W., Hsu K. H., Lee C. C., Sun C. Y., Hsu H. J., Tsai C. J., et al. p-Cresyl sulphate and indoxyl sulphate predict progression of chronic kidney disease. Nephrol Dial Transplant. 2011 Mar;26(3):938-47.
102. Chinnappa S., Tu Y. K., Yeh Y. C., Glorieux G., Vanholder R., Mooney A. Association between protein-bound uremic toxins and asymptomatic cardiac dysfunction in patients with chronic kidney disease. Toxins (Basel). 2018 Dec 5;10(12).
103. Kidney Foundation of Canada. Be an organ donor. 2021 [cited 2022 January 20]; Available from: https://kidney.ca/Get-Involved/Be-an-Organ-Donor
104. Zucker K., Tsaroucha A., Olson L., Esquenazi V., Tzakis A., Miller J. Evidence that tacrolimus augments the bioavailability of mycophenolate mofetil through the inhibition of mycophenolic acid glucuronidation. Ther Drug Monit. 1999 Feb;21(1):35-43.
105. Soars M. G., Petullo D. M., Eckstein J. A., Kasper S. C., Wrighton S. A. An assessment of UDP-glucuronosyltransferase induction using primary human hepatocytes. Drug Metab Dispos. 2004 Jan;32(1):140-8.
106. Cattaneo D., Perico N., Gaspari F., Gotti E., Remuzzi G. Glucocorticoids interfere with mycophenolate mofetil bioavailability in kidney transplantation. Kidney Int. 2002 Sep;62(3):1060-7.
107. Braun F., Schocklmann H., Ziegler E., Kunzendorf U., Armstrong V. W., Renders L. Increased mycophenolic acid exposure in stable kidney transplant recipients on tacrolimus as compared with those on sirolimus: Implications for pharmacokinetics. Clin Pharmacol Ther. 2009 Oct;86(4):411-5.
108. Alvarez-Elias A. C., Yoo E. C., Todorova E. K., Singh R. N., Filler G. A retrospective study on mycophenolic acid drug interactions: Effect of prednisone, sirolimus, and tacrolimus with MPA. Ther Drug Monit. 2017 Jun;39(3):220-8.
109. Djebli N., Picard N., Rerolle J. P., Le Meur Y., Marquet P. Influence of the UGT2B7 promoter region and exon 2 polymorphisms and comedications on Acyl-MPAG production in vitro and in adult renal transplant patients. Pharmacogenet Genomics. 2007 May;17(5):321-30.
110. Ciancio G., Burke G. W., Gaynor J. J., Mattiazzi A., Roth D., Kupin W., et al. A randomized long-term trial of tacrolimus and sirolimus versus tacrolimus and mycophenolate mofetil versus cyclosporine (NEORAL) and sirolimus in renal transplantation.

I. Drug interactions and rejection at one year. Transplantation. 2004 Jan 27;77(2):244-51.
111. Zucker K., Rosen A., Tsaroucha A., de Faria L., Roth D., Ciancio G., et al. Unexpected augmentation of mycophenolic acid pharmacokinetics in renal transplant patients receiving tacrolimus and mycophenolate mofetil in combination therapy, and analogous in vitro findings. Transpl Immunol. 1997 Sep;5(3):225-32.
112. Zucker K., Rosen A., Tsaroucha A., de Faria L., Roth D., Ciancio G., et al. Augmentation of mycophenolate mofetil pharmacokinetics in renal transplant patients receiving Prograf and CellCept in combination therapy. Transplant Proc. 1997 Feb-Mar;29(1-2):334-6.
113. Filler G., Zimmering M., Mai I. Pharmacokinetics of mycophenolate mofetil are influenced by concomitant immunosuppression. Pediatr Nephrol. 2000 Feb;14(2):100-4.
114. Cremers S., Schoemaker R., Scholten E., den Hartigh J., Konig-Quartel J., van Kan E., et al. Characterizing the role of enterohepatic recycling in the interactions between mycophenolate mofetil and calcineurin inhibitors in renal transplant patients by pharmacokinetic modelling. Br J Clin Pharmacol. 2005 Sep;60(3):249-56.
115. Hubner G. I., Eismann R., Sziegoleit W. Drug interaction between mycophenolate mofetil and tacrolimus detectable within therapeutic mycophenolic acid monitoring in renal transplant patients. Ther Drug Monit. 1999 Oct;21(5):536-9.
116. Kagaya H., Miura M., Satoh S., Inoue K., Saito M., Inoue T., et al. No pharmacokinetic interactions between mycophenolic acid and tacrolimus in renal transplant recipients. J Clin Pharm Ther. 2008 Apr;33(2):193-201.
117. Kim J. H., Han N., Kim M. G., Kim Y. W., Jang H., Yun H. Y., et al. Model based development of tacrolimus dosing algorithm considering CYP3A5 genotypes and mycophenolate mofetil drug interaction in stable kidney transplant recipients. Sci Rep. 2019 Aug 13;9(1):11740.
118. Kim J. H., Han N., Kim M. G., Yun H. Y., Lee S., Bae E., et al. Increased exposure of tacrolimus by co-administered mycophenolate mofetil: Population pharmacokinetic analysis in healthy volunteers. Sci Rep. 2018 Jan 26;8(1):1687.
119. Kuypers D. R., Claes K., Evenepoel P., Maes B., Coosemans W., Pirenne J., et al. Long-term changes in mycophenolic acid exposure in combination with tacrolimus and corticosteroids are dose dependent and not reflected by trough plasma concentration: A prospective study in 100 de novo renal allograft recipients. J Clin Pharmacol. 2003 Aug;43(8):866-80.
120. Park S. I., Felipe C. R., Pinheiro-Machado P. G., Garcia R., Fernandes F. B., Casarini D. E., et al. Tacrolimus pharmacokinetic drug interactions: Effect of prednisone, mycophenolic acid or sirolimus. Fundam Clin Pharmacol. 2009 Feb;23(1):137-45.
121. Pirsch J., Bekersky I., Vincenti F., Boswell G., Woodle E. S., Alak A., et al. Coadministration of tacrolimus and mycophenolate mofetil in stable kidney transplant patients: Pharmacokinetics and tolerability. J Clin Pharmacol. 2000 May;40(5):527-32.
122. Pou L., Brunet M., Cantarell C., Vidal E., Oppenheimer F., Monforte V., et al. Mycophenolic acid plasma concentrations: Influence of comedication. Ther Drug Monit. 2001 Feb;23(1):35-8.
123. Undre N. A., van Hooff J., Christiaans M., Vanrenterghem Y., Donck J., Heeman U., et al. Pharmacokinetics of FK 506 and mycophenolic acid after the administration of a FK 506-based regimen in combination with mycophenolate mofetil in kidney transplantation. Transplant Proc. 1998 Jun;30(4):1299-302.
124. Vidal E., Cantarell C., Capdevila L., Monforte V., Roman A., Pou L. Mycophenolate mofetil pharmacokinetics in transplant patients receiving cyclosporine or tacrolimus in combination therapy. Pharmacol Toxicol. 2000 Oct;87(4):182-4.

125. Naito T., Mino Y., Otsuka A., Ushiyama T., Ito T., Ozono S., et al. Impact of calcineurin inhibitors on urinary excretion of mycophenolic acid and its glucuronide in kidney transplant recipients. J Clin Pharmacol. 2009 Jun;49(6):710-8.
126. te Linde Elsemieke, van Roij Claudette J.M., Meijers Björn K.I., De Loor Henriette, Kessels Roy P.C., Wetzels Jack F.M. Cognitive function and uremic toxins after kidney transplantation: An exploratory study. Kidney360. 2020;1(12):1398-406.
127. Ligabue G., Damiano F., Cuoghi A., De Biasi S., Bellei E., Granito M., et al. p-Cresol and cardiovascular risk in kidney transplant recipients. Transplant Proc. 2015 Sep;47(7):2121-5.
128. Poesen R., Evenepoel P., de Loor H., Bammens B., Claes K., Sprangers B., et al. The influence of renal transplantation on retained microbial-human co-metabolites. Nephrol Dial Transplant. 2016 Oct;31(10):1721-9.
129. Huang S. T., Shu K. H., Cheng C. H., Wu M. J., Yu T. M., Chuang Y. W., et al. Serum total p-cresol and indoxyl sulfate correlated with stage of chronic kidney disease in renal transplant recipients. Transplant Proc. 2012 Apr;44(3):621-4.
130. Andre C., Choukroun G., Bennis Y., Kamel S., Lemaire-Hurtel A. S., Masmoudi K., et al. Potential interactions between uremic toxins and drugs: an application in kidney transplant recipients treated with calcineurin inhibitors. Nephrol Dial Transplant. 2021 Mar 30.
131. Kiang T. K., Ensom M. H. Anti-rejection drugs. In: Murphy JE, editor. Clinical pharmacokinetics (6th Edition): Bethesda, MD: American Society of Health-System Pharmacists; 2017. p. 205-20.
132. Kiang T. K., Ensom M. H. Immunosuppressants. In: Beringer, editor. Basic clinical pharmacokinetics: Philadelphia: Wolters Kluwer; 2017. p. 320-58.
133. Kiang T. K. L., Partovi N., Shapiro R. J., Berman J. M., Collier A. C., Ensom M. H. H. Regression and genomic analyses on the association between dose-normalized mycophenolic acid exposure and absolute neutrophil count in steroid-free, de novo kidney transplant recipients. Clin Drug Investig. 2018 Nov;38(11):1011-22.
134. Vincenti F., Schena F. P., Paraskevas S., Hauser I. A., Walker R. G., Grinyo J., et al. A randomized, multicenter study of steroid avoidance, early steroid withdrawal or standard steroid therapy in kidney transplant recipients. Am J Transplant. 2008 Feb;8(2):307-16.
135. Lemieux I., Houde I., Pascot A., Lachance J. G., Noel R., Radeau T., et al. Effects of prednisone withdrawal on the new metabolic triad in cyclosporine-treated kidney transplant patients. Kidney Int. 2002 Nov;62(5):1839-47.
136. Andrade-Sierra J., Rojas-Campos E., Cardona-Munoz E., Evangelista-Carrillo L. A., Puentes-Camacho A., Lugo-Lopez O., et al. Early steroid withdrawal in a renal transplant cohort treated with tacrolimus, mycophenolate mofetil and basiliximab. Nefrologia. 2014;34(2):216-22.
137. Qadri I., Hu L. J., Iwahashi M., Al-Zuabi S., Quattrochi L. C., Simon F. R. Interaction of hepatocyte nuclear factors in transcriptional regulation of tissue specific hormonal expression of human multidrug resistance-associated protein 2 (abcc2). Toxicol Appl Pharmacol. 2009 Feb 1;234(3):281-92.
138. Greanya E. D., Poulin E., Partovi N., Shapiro R. J., Al-Khatib M., Ensom M. H. Pharmacokinetics of tacrolimus and mycophenolate mofetil in renal transplant recipients on a corticosteroid-free regimen. Am J Health Syst Pharm. 2012 Jan 15;69(2):134-42.
139. Yu Z. C., Zhou P. J., Wang X. H., Francoise B., Xu D., Zhang W. X., et al. Population pharmacokinetics and Bayesian estimation of mycophenolic acid concentrations in Chinese adult renal transplant recipients. Acta Pharmacol Sin. 2017 Nov;38(11):1566-79.

140. Colom H., Andreu F., van Gelder T., Hesselink D. A., de Winter B. C. M., Bestard O., et al. Prediction of Free from Total Mycophenolic Acid Concentrations in Stable Renal Transplant Patients: A Population-Based Approach. Clin Pharmacokinet. 2018 Jul;57(7):877-93.
141. Chen B., Shao K., An H. M., Shi H. Q., Lu J. Q., Zhai X. H., et al. Population pharmacokinetics and Bayesian estimation of mycophenolic acid exposure in Chinese renal allograft recipients after administration of EC-MPS. J Clin Pharmacol. 2019 Apr;59(4):578-89.
142. Yau W. P., Vathsala A., Lou H. X., Zhou S., Chan E. Mechanism-based enterohepatic circulation model of mycophenolic acid and its glucuronide metabolite: Assessment of impact of cyclosporine dose in Asian renal transplant patients. J Clin Pharmacol. 2009 Jun;49(6):684-99.
143. de Winter B. C., van Gelder T., Sombogaard F., Shaw L. M., van Hest R. M., Mathot R. A. Pharmacokinetic role of protein binding of mycophenolic acid and its glucuronide metabolite in renal transplant recipients. J Pharmacokinet Pharmacodyn. 2009 Dec;36(6):541-64.
144. Musuamba F. T., Rousseau A., Bosmans J. L., Senessael J. J., Cumps J., Marquet P., et al. Limited sampling models and Bayesian estimation for mycophenolic acid area under the curve prediction in stable renal transplant patients co-medicated with ciclosporin or sirolimus. Clin Pharmacokinet. 2009;48(11):745-58.
145. Sam W. J., Akhlaghi F., Rosenbaum S. E. Population pharmacokinetics of mycophenolic acid and its 2 glucuronidated metabolites in kidney transplant recipients. J Clin Pharmacol. 2009 Feb;49(2):185-95.
146. Colom H., Lloberas N., Andreu F., Caldes A., Torras J., Oppenheimer F., et al. Pharmacokinetic modeling of enterohepatic circulation of mycophenolic acid in renal transplant recipients. Kidney Int. 2014 Jun;85(6):1434-43.
147. de Winter B. C., Mathot R. A., Sombogaard F., Neumann I., van Hest R. M., Doorduijn J. K., et al. Differences in clearance of mycophenolic acid among renal transplant recipients, hematopoietic stem cell transplant recipients, and patients with autoimmune disease. Ther Drug Monit. 2010 Oct;32(5):606-14.
148. de Winter B. C., Mathot R. A., Sombogaard F., Vulto A. G., van Gelder T. Nonlinear relationship between mycophenolate mofetil dose and mycophenolic acid exposure: Implications for therapeutic drug monitoring. Clin J Am Soc Nephrol. 2011 Mar;6(3):656-63.
149. de Winter B. C., Monchaud C., Premaud A., Pison C., Kessler R., Reynaud-Gaubert M., et al. Bayesian estimation of mycophenolate mofetil in lung transplantation, using a population pharmacokinetic model developed in kidney and lung transplant recipients. Clin Pharmacokinet. 2012 Jan 1;51(1):29-39.
150. de Winter B. C., van Gelder T., Glander P., Cattaneo D., Tedesco-Silva H., Neumann I., et al. Population pharmacokinetics of mycophenolic acid: A comparison between enteric-coated mycophenolate sodium and mycophenolate mofetil in renal transplant recipients. Clin Pharmacokinet. 2008;47(12):827-38.
151. Funaki T. Enterohepatic circulation model for population pharmacokinetic analysis. J Pharm Pharmacol. 1999 Oct;51(10):1143-8.
152. Guillet B. A., Simon N. S., Purgus R., Botta C., Morange S., Berland Y., et al. Population pharmacokinetics analysis of mycophenolic acid in adult kidney transplant patients with chronic graft dysfunction. Ther Drug Monit. 2010 Aug;32(4):427-32.
153. Han N., Yun H. Y., Kim I. W., Oh Y. J., Kim Y. S., Oh J. M. Population pharmacogenetic pharmacokinetic modeling for flip-flop phenomenon of enteric-coated mycophenolate sodium in kidney transplant recipients. Eur J Clin Pharmacol. 2014 Oct;70(10):1211-9.

154. Lamba M., Tafti B., Melcher M., Chan G., Krishnaswami S., Busque S. Population pharmacokinetic analysis of mycophenolic acid coadministered with either tasocitinib (CP-690,550) or tacrolimus in adult renal allograft recipients. Ther Drug Monit. 2010 Dec;32(6):778-81.
155. Le Guellec C., Bourgoin H., Buchler M., Le Meur Y., Lebranchu Y., Marquet P., et al. Population pharmacokinetics and Bayesian estimation of mycophenolic acid concentrations in stable renal transplant patients. Clin Pharmacokinet. 2004;43(4):253-66.
156. Musuamba F. T., Mourad M., Haufroid V., Demeyer M., Capron A., Delattre I. K., et al. A simultaneous d-optimal designed study for population pharmacokinetic analyses of mycophenolic acid and tacrolimus early after renal transplantation. J Clin Pharmacol. 2012 Dec;52(12):1833-43.
157. Shum B., Duffull S. B., Taylor P. J., Tett S. E. Population pharmacokinetic analysis of mycophenolic acid in renal transplant recipients following oral administration of mycophenolate mofetil. Br J Clin Pharmacol. 2003 Aug;56(2):188-97.
158. Staatz C. E., Duffull S. B., Kiberd B., Fraser A. D., Tett S. E. Population pharmacokinetics of mycophenolic acid during the first week after renal transplantation. Eur J Clin Pharmacol. 2005 Aug;61(7):507-16.
159. van Hest R. M., Mathot R. A., Pescovitz M. D., Gordon R., Mamelok R. D., van Gelder T. Explaining variability in mycophenolic acid exposure to optimize mycophenolate mofetil dosing: A population pharmacokinetic meta-analysis of mycophenolic acid in renal transplant recipients. J Am Soc Nephrol. 2006 Mar;17(3):871-80.
160. van Hest R. M., van Gelder T., Bouw R., Goggin T., Gordon R., Mamelok R. D., et al. Time-dependent clearance of mycophenolic acid in renal transplant recipients. Br J Clin Pharmacol. 2007 Jun;63(6):741-52.
161. van Hest R. M., van Gelder T., Vulto A. G., Mathot R. A. Population pharmacokinetics of mycophenolic acid in renal transplant recipients. Clin Pharmacokinet. 2005;44(10):1083-96.
162. Velickovic-Radovanovic R. M., Jankovic S. M., Milovanovic J. R., Catic-Dordevic A. K., Spasic A. A., Stefanovic N. Z., et al. Variability of mycophenolic acid elimination in the renal transplant recipients - population pharmacokinetic approach. Ren Fail. 2015 May;37(4):652-8.
163. Ting L. S., Decarie D., Ensom M. H. Effect of acidification on protein binding of mycophenolic acid. Ther Drug Monit. 2007 Feb;29(1):132-3.
164. Ting L. S., Partovi N., Levy R. D., Riggs K. W., Ensom M. H. Pharmacokinetics of mycophenolic acid and its phenolic-glucuronide and ACYl glucuronide metabolites in stable thoracic transplant recipients. Ther Drug Monit. 2008 Jun;30(3):282-91.
165. LIXOFT. Monolix Suite 2018. 2018 [cited 2018 June 01]; Available from: http://www.lixoft.com
166. Sherwin C. M., Kiang T. K., Spigarelli M. G., Ensom M. H. Fundamentals of population pharmacokinetic modelling: validation methods. Clin Pharmacokinet. 2012 Sep 1;51(9):573-90.
167. R Core Team. R software v3.4.2. 2018. 2018 [cited 2018 August 02]; Available from: https://www.R-project.org
168. Savic R. M., Karlsson M. O. Importance of shrinkage in empirical bayes estimates for diagnostics: Problems and solutions. AAPS J. 2009 Sep;11(3):558-69.
169. Tedesco-Silva H., Bastien M. C., Choi L., Felipe C., Campestrini J., Picard F., et al. Mycophenolic acid metabolite profile in renal transplant patients receiving enteric-coated mycophenolate sodium or mycophenolate mofetil. Transplant Proc. 2005 Mar;37(2):852-5.

170. Usui T., Kuno T., Mizutani T. Induction of human UDP-glucuronosyltransferase 1A1 by cortisol-GR. Mol Biol Rep. 2006 Jun;33(2):91-6.
171. Kanou M., Usui T., Ueyama H., Sato H., Ohkubo I., Mizutani T. Stimulation of transcriptional expression of human UDP-glucuronosyltransferase 1A1 by dexamethasone. Mol Biol Rep. 2004 Sep;31(3):151-8.
172. Ashraf M. N., Asghar M. W., Rong Y., Doschak M. R., Kiang T. K. L. Advanced in vitro HepaRG culture systems for xenobiotic metabolism and toxicity characterization. Eur J Drug Metab Pharmacokinet. 2019 Aug;44(4):437-58.
173. Mackenzie P. I. Identification of uridine diphosphate glucuronosyltransferases involved in the metabolism and clearance of mycophenolic acid. Ther Drug Monit. 2000 Feb;22(1):10-3.
174. Miles K. K., Stern S. T., Smith P. C., Kessler F. K., Ali S., Ritter J. K. An investigation of human and rat liver microsomal mycophenolic acid glucuronidation: Evidence for a principal role of UGT1A enzymes and species differences in UGT1A specificity. Drug Metab Dispos. 2005 Oct;33(10):1513-20.
175. Bernard O., Guillemette C. The main role of UGT1A9 in the hepatic metabolism of mycophenolic acid and the effects of naturally occurring variants. Drug Metab Dispos. 2004 Aug;32(8):775-8.
176. Bernard O., Tojcic J., Journault K., Perusse L., Guillemette C. Influence of nonsynonymous polymorphisms of UGT1A8 and UGT2B7 metabolizing enzymes on the formation of phenolic and acyl glucuronides of mycophenolic acid. Drug Metab Dispos. 2006 Sep;34(9):1539-45.
177. Johnson L. A., Oetting W. S., Basu S., Prausa S., Matas A., Jacobson P. A. Pharmacogenetic effect of the UGT polymorphisms on mycophenolate is modified by calcineurin inhibitors. Eur J Clin Pharmacol. 2008 Nov;64(11):1047-56.
178. Vanhove T., Bouwsma H., Hilbrands L., Swen J. J., Spriet I., Annaert P., et al. Determinants of the magnitude of interaction between tacrolimus and voriconazole/posaconazole in solid organ recipients. Am J Transplant. 2017 Sep;17(9):2372-80.
179. Li P., Shuker N., Hesselink D. A., van Schaik R. H., Zhang X., van Gelder T. Do Asian renal transplant patients need another mycophenolate mofetil dose compared with Caucasian or African American patients? Transpl Int. 2014 Oct;27(10):994-1004.
180. Allison A. C. Mechanisms of action of mycophenolate mofetil. Lupus. 2005;14 Suppl 1:s2-8.
181. Shaw L. M., Figurski M., Milone M. C., Trofe J., Bloom R. D. Therapeutic drug monitoring of mycophenolic acid. Clin J Am Soc Nephrol. 2007 Sep;2(5):1062-72.
182. Abd Rahman A. N., Tett S. E., Abdul Gafor H. A., McWhinney B. C., Staatz C. E. Development of improved dosing regimens for mycophenolate mofetil based on population pharmacokinetic analyses in adults with lupus nephritis. Eur J Drug Metab Pharmacokinet. 2017 Dec;42(6):993-1004.
183. Barau C., Furlan V., Debray D., Taburet A. M., Barrail-Tran A. Population pharmacokinetics of mycophenolic acid and dose optimization with limited sampling strategy in liver transplant children. Br J Clin Pharmacol. 2012 Sep;74(3):515-24.
184. de Winter B. C., Neumann I., van Hest R. M., van Gelder T., Mathot R. A. Limited sampling strategies for therapeutic drug monitoring of mycophenolate mofetil therapy in patients with autoimmune disease. Ther Drug Monit. 2009 Jun;31(3):382-90.

185. Dong M., Fukuda T., Cox S., de Vries M. T., Hooper D. K., Goebel J., et al. Population pharmacokinetic-pharmacodynamic modelling of mycophenolic acid in paediatric renal transplant recipients in the early post-transplant period. Br J Clin Pharmacol. 2014 Nov;78(5):1102-12.
186. Frymoyer A., Verotta D., Jacobson P., Long-Boyle J. Population pharmacokinetics of unbound mycophenolic acid in adult allogeneic haematopoietic cell transplantation: Effect of pharmacogenetic factors. Br J Clin Pharmacol. 2013 Feb;75(2):463-75.
187. Hulin A., Blanchet B., Audard V., Barau C., Furlan V., Durrbach A., et al. Comparison of 3 estimation methods of mycophenolic acid AUC based on a limited sampling strategy in renal transplant patients. Ther Drug Monit. 2009 Apr;31(2):224-32.
188. Jiao Z., Ding J. J., Shen J., Liang H. Q., Zhong L. J., Wang Y., et al. Population pharmacokinetic modelling for enterohepatic circulation of mycophenolic acid in healthy Chinese and the influence of polymorphisms in UGT1A9. Br J Clin Pharmacol. 2008 Jun;65(6):893-907.
189. Kim H., Long-Boyle J., Rydholm N., Orchard P. J., Tolar J., Smith A. R., et al. Population pharmacokinetics of unbound mycophenolic acid in pediatric and young adult patients undergoing allogeneic hematopoietic cell transplantation. J Clin Pharmacol. 2012 Nov;52(11):1665-75.
190. Langers P., Press R. R., Inderson A., Cremers S. C., den Hartigh J., Baranski A. G., et al. Limited sampling model for advanced mycophenolic acid therapeutic drug monitoring after liver transplantation. Ther Drug Monit. 2014 Apr;36(2):141-7.
191. Li H., Mager D. E., Bemer M. J., Salinger D. H., Vicini P., Sandmaier B. M., et al. A limited sampling schedule to estimate mycophenolic acid area under the concentration-time curve in hematopoietic cell transplantation recipients. J Clin Pharmacol. 2012 Nov;52(11):1654-64.
192. Li H., Mager D. E., Sandmaier B. M., Maloney D. G., Bemer M. J., McCune J. S. Population pharmacokinetics and dose optimization of mycophenolic acid in HCT recipients receiving oral mycophenolate mofetil. J Clin Pharmacol. 2013 Apr;53(4):393-402.
193. Li H., Mager D. E., Sandmaier B. M., Storer B. E., Boeckh M. J., Bemer M. J., et al. Pharmacokinetic and pharmacodynamic analysis of inosine monophosphate dehydrogenase activity in hematopoietic cell transplantation recipients treated with mycophenolate mofetil. Biol Blood Marrow Transplant. 2014 Aug;20(8):1121-9.
194. Ling J., Shi J., Jiang Q., Jiao Z. Population pharmacokinetics of mycophenolic acid and its main glucuronide metabolite: A comparison between healthy Chinese and Caucasian subjects receiving mycophenolate mofetil. Eur J Clin Pharmacol. 2015 Jan;71(1):95-106.
195. Musuamba F. T., Mourad M., Haufroid V., De Meyer M., Capron A., Delattre I. K., et al. Statistical tools for dose individualization of mycophenolic acid and tacrolimus co-administered during the first month after renal transplantation. Br J Clin Pharmacol. 2013 May;75(5):1277-88.
196. Payen S., Zhang D., Maisin A., Popon M., Bensman A., Bouissou F., et al. Population pharmacokinetics of mycophenolic acid in kidney transplant pediatric and adolescent patients. Ther Drug Monit. 2005 Jun;27(3):378-88.
197. Premaud A., Debord J., Rousseau A., Le Meur Y., Toupance O., Lebranchu Y., et al. A double absorption-phase model adequately describes mycophenolic acid plasma profiles in de novo renal transplant recipients given oral mycophenolate mofetil. Clin Pharmacokinet. 2005;44(8):837-47.
198. Premaud A., Weber L. T., Tonshoff B., Armstrong V. W., Oellerich M., Urien S., et al. Population pharmacokinetics of mycophenolic acid in pediatric renal transplant patients using parametric and nonparametric approaches. Pharmacol Res. 2011 Mar;63(3):216-24.

199. Punyawudho B., Lertdumrongluk P., Somparn P., Kittanamongkolchai W., Traitanon O., Avihingsanon Y., et al. Population pharmacokinetics of mycophenolate mofetil in Thai lupus nephritis patients. Int J Clin Pharmacol Ther. 2012 Apr;50(4):272-80.
200. Saint-Marcoux F., Guigonis V., Decramer S., Gandia P., Ranchin B., Parant F., et al. Development of a Bayesian estimator for the therapeutic drug monitoring of mycophenolate mofetil in children with idiopathic nephrotic syndrome. Pharmacol Res. 2011 May;63(5):423-31.
201. Saint-Marcoux F., Royer B., Debord J., Larosa F., Legrand F., Deconinck E., et al. Pharmacokinetic modelling and development of Bayesian estimators for therapeutic drug monitoring of mycophenolate mofetil in reduced-intensity haematopoietic stem cell transplantation. Clin Pharmacokinet. 2009;48(10):667-75.
202. Sam W. J., Joy M. S. Population pharmacokinetics of mycophenolic acid and metabolites in patients with glomerulonephritis. Ther Drug Monit. 2010 Oct;32(5):594-605.
203. Sherwin C. M., Sagcal-Gironella A. C., Fukuda T., Brunner H. I., Vinks A. A. Development of population PK model with enterohepatic circulation for mycophenolic acid in patients with childhood-onset systemic lupus erythematosus. Br J Clin Pharmacol. 2012 May;73(5):727-40.
204. van Hest R. M., van Gelder T., Vulto A. G., Shaw L. M., Mathot R. A. Pharmacokinetic modelling of the plasma protein binding of mycophenolic acid in renal transplant recipients. Clin Pharmacokinet. 2009;48(7):463-76.
205. Wang X. X., Feng M. R., Nguyen H., Smith D. E., Cibrik D. M., Park J. M. Population pharmacokinetics of mycophenolic acid in lung transplant recipients with and without cystic fibrosis. Eur J Clin Pharmacol. 2015 Jun;71(6):673-9.
206. Wang X. X., Liu W., Zheng T., Park J. M., Smith D. E., Feng M. R. Population pharmacokinetics of mycophenolic acid and its glucuronide metabolite in lung transplant recipients with and without cystic fibrosis. Xenobiotica. 2017 Aug;47(8):697-704.
207. Woillard J. B., Bader-Meunier B., Salomon R., Ranchin B., Decramer S., Fischbach M., et al. Pharmacokinetics of mycophenolate mofetil in children with lupus and clinical findings in favour of therapeutic drug monitoring. Br J Clin Pharmacol. 2014 Oct;78(4):867-76.
208. Zahr N., Amoura Z., Debord J., Hulot J. S., Saint-Marcoux F., Marquet P., et al. Pharmacokinetic study of mycophenolate mofetil in patients with systemic lupus erythematosus and design of Bayesian estimator using limited sampling strategies. Clin Pharmacokinet. 2008;47(4):277-84.
209. Zhao W., Elie V., Baudouin V., Bensman A., Andre J. L., Brochard K., et al. Population pharmacokinetics and Bayesian estimator of mycophenolic acid in children with idiopathic nephrotic syndrome. Br J Clin Pharmacol. 2010 Apr;69(4):358-66.
210. Zhao W., Fakhoury M., Deschenes G., Roussey G., Brochard K., Niaudet P., et al. Population pharmacokinetics and pharmacogenetics of mycophenolic acid following administration of mycophenolate mofetil in de novo pediatric renal-transplant patients. J Clin Pharmacol. 2010 Nov;50(11):1280-91.
211. Wang G., Ye Q., Huang Y., Lu J., Xu H., Li Z. Population pharmacokinetics of mycophenolic acid in pediatric patients with juvenile dermatomyositis and optimization of limited sampling strategy. Xenobiotica. 2021 Feb;51(2):167-76.
212. Labriffe M., Vaidie J., Monchaud C., Debord J., Turlure P., Girault S., et al. Population pharmacokinetics and Bayesian estimators for intravenous mycophenolate mofetil in haematopoietic stem cell transplant patients. Br J Clin Pharmacol. 2020 Aug;86(8):1550-9.

213. Okour M., Jacobson P. A., Ahmed M. A., Israni A. K., Brundage R. C. Mycophenolic acid and its metabolites in kidney transplant recipients: A semimechanistic enterohepatic circulation model to improve estimating exposure. J Clin Pharmacol. 2018 May;58(5):628-39.
214. Quintairos L., Colom H., Millan O., Fortuna V., Espinosa C., Guirado L., et al. Early prognostic performance of miR155-5p monitoring for the risk of rejection: Logistic regression with a population pharmacokinetic approach in adult kidney transplant patients. PLoS One. 2021;16(1):e0245880.
215. Resendiz-Galvan J. E., Romano-Aguilar M., Medellin-Garibay S. E., Milan-Segovia R. D. C., Nino-Moreno P. D. C., Jung-Cook H., et al. Population pharmacokinetics of mycophenolic acid in adult kidney transplant patients under prednisone and tacrolimus regimen. Eur J Pharm Sci. 2020 Jul 1;150:105370.
216. Riglet F., Bertrand J., Barrail-Tran A., Verstuyft C., Michelon H., Benech H., et al. Population pharmacokinetic model of plasma and cellular mycophenolic acid in kidney transplant patients from the CIMTRE study. Drugs R D. 2020 Dec;20(4):331-42.
217. Romano-Aguilar M., Resendiz-Galvan J. E., Medellin-Garibay S. E., Milan-Segovia R. D. C., Martinez-Martinez M. U., Abud-Mendoza C., et al. Population pharmacokinetics of mycophenolic acid in Mexican patients with lupus nephritis. Lupus. 2020 Aug;29(9):1067-77.
218. Sheng C., Zhao Q., Niu W., Qiu X., Zhang M., Jiao Z. Effect of protein binding on exposure of unbound and total mycophenolic acid: A population pharmacokinetic analysis in Chinese adult kidney transplant recipients. Front Pharmacol. 2020;11:340.
219. Yang C. L., Sheng C. C., Liao G. Y., Su Y., Feng L. J., Xia Q., et al. Genetic polymorphisms in metabolic enzymes and transporters have no impact on mycophenolic acid pharmacokinetics in adult kidney transplant patients co-treated with tacrolimus: A population analysis. J Clin Pharm Ther. 2021 Jul 26.
220. Yoshimura K., Yano I., Yamamoto T., Kawanishi M., Isomoto Y., Yonezawa A., et al. Population pharmacokinetics and pharmacodynamics of mycophenolic acid using the prospective data in patients undergoing hematopoietic stem cell transplantation. Bone Marrow Transplant. 2018 Jan;53(1):44-51.
221. Zeng L., Blair E. Y., Nath C. E., Shaw P. J., Earl J. W., Stephen K., et al. Population pharmacokinetics of mycophenolic acid in children and young people undergoing blood or marrow and solid organ transplantation. Br J Clin Pharmacol. 2010 Oct;70(4):567-79.
222. Hsueh C. H., Yoshida K., Zhao P., Meyer T. W., Zhang L., Huang S. M., et al. Identification and quantitative assessment of uremic solutes as inhibitors of renal organic anion transporters, OAT1 and OAT3. Mol Pharm. 2016 Sep 6;13(9):3130-40.
223. Watanabe H., Sakaguchi Y., Sugimoto R., Kaneko K., Iwata H., Kotani S., et al. Human organic anion transporters function as a high-capacity transporter for p-cresyl sulfate, a uremic toxin. Clin Exp Nephrol. 2014 Oct;18(5):814-20.
224. McLeay S. C., Morrish G. A., Kirkpatrick C. M., Green B. The relationship between drug clearance and body size: systematic review and meta-analysis of the literature published from 2000 to 2007. Clin Pharmacokinet. 2012 May 1;51(5):319-30.
225. Yang Y., Liu X. Imbalance of drug transporter-CYP450s interplay by diabetes and its clinical significance. Pharmaceutics. 2020 Apr 11;12(4).
226. Mooij M. G., Schwarz U. I., de Koning B. A., Leeder J. S., Gaedigk R., Samsom J. N., et al. Ontogeny of human hepatic and intestinal transporter gene expression during childhood: Age matters. Drug Metab Dispos. 2014 Aug;42(8):1268-74.

227. Strassburg C. P., Strassburg A., Kneip S., Barut A., Tukey R. H., Rodeck B., et al. Developmental aspects of human hepatic drug glucuronidation in young children and adults. Gut. 2002 Feb;50(2):259-65.
228. van Gelder T. How cyclosporine reduces mycophenolic acid exposure by 40% while other calcineurin inhibitors do not. Kidney Int. 2021 Dec;100(6):1185-9.
229. Picard N., Levoir L., Lamoureux F., Yee S. W., Giacomini K. M., Marquet P. Interaction of sirolimus and everolimus with hepatic and intestinal organic anion-transporting polypeptide transporters. Xenobiotica. 2011 Sep;41(9):752-7.
230. Kiang T. K., Sherwin C. M., Spigarelli M. G., Ensom M. H. Fundamentals of population pharmacokinetic modelling: modelling and software. Clin Pharmacokinet. 2012 Aug 1;51(8):515-25.
231. Grinyo J. M., Ekberg H., Mamelok R. D., Oppenheimer F., Sanchez-Plumed J., Gentil M. A., et al. The pharmacokinetics of mycophenolate mofetil in renal transplant recipients receiving standard-dose or low-dose cyclosporine, low-dose tacrolimus or low-dose sirolimus: the Symphony pharmacokinetic substudy. Nephrol Dial Transplant. 2009 Jul;24(7):2269-76.
232. Lloberas N., Torras J., Cruzado J. M., Andreu F., Oppenheimer F., Sanchez-Plumed J., et al. Influence of MRP2 on MPA pharmacokinetics in renal transplant recipients-results of the Pharmacogenomic Substudy within the Symphony Study. Nephrol Dial Transplant. 2011 Nov;26(11):3784-93.
233. Millan O., Budde K., Sommerer C., Aliart I., Rissling O., Bardaji B., et al. Urinary miR-155-5p and CXCL10 as prognostic and predictive biomarkers of rejection, graft outcome and treatment response in kidney transplantation. Br J Clin Pharmacol. 2017 Dec;83(12):2636-50.
234. Jiao Z., Zhong J. Y., Zhang M., Shi X. J., Yu Y. Q., Lu W. Y. Total and free mycophenolic acid and its 7-O-glucuronide metabolite in Chinese adult renal transplant patients: pharmacokinetics and application of limited sampling strategies. Eur J Clin Pharmacol. 2007 Jan;63(1):27-37.
235. Tonshoff B., David-Neto E., Ettenger R., Filler G., van Gelder T., Goebel J., et al. Pediatric aspects of therapeutic drug monitoring of mycophenolic acid in renal transplantation. Transplant Rev (Orlando). 2011 Apr;25(2):78-89.
236. Weber L. T., Hoecker B., Armstrong V. W., Oellerich M., Tonshoff B. Long-term pharmacokinetics of mycophenolic acid in pediatric renal transplant recipients over 3 years posttransplant. Ther Drug Monit. 2008 Oct;30(5):570-5.
237. Weber L. T., Shipkova M., Armstrong V. W., Wagner N., Schutz E., Mehls O., et al. The pharmacokinetic-pharmacodynamic relationship for total and free mycophenolic Acid in pediatric renal transplant recipients: A report of the german study group on mycophenolate mofetil therapy. J Am Soc Nephrol. 2002 Mar;13(3):759-68.
238. Official Journal of the International Society of Nephrology. KDIGO clinical practice guideline for glomerulonephritis. 2012 [cited 2018 May 18]; Available from: https://kdigo.org/wp-content/uploads/2017/02/KDIGO-2012-GN-Guideline-English.pdf
239. Bertsias G. K., Tektonidou M., Amoura Z., Aringer M., Bajema I., Berden J. H., et al. Joint European League Against Rheumatism and European Renal Association-European Dialysis and Transplant Association (EULAR/ERA-EDTA) recommendations for the management of adult and paediatric lupus nephritis. Ann Rheum Dis. 2012 Nov;71(11):1771-82.
240. Gipson D. S., Massengill S. F., Yao L., Nagaraj S., Smoyer W. E., Mahan J. D., et al. Management of childhood onset nephrotic syndrome. Pediatrics. 2009 Aug;124(2):747-57.

241. Downing H. J., Pirmohamed M., Beresford M. W., Smyth R. L. Paediatric use of mycophenolate mofetil. Br J Clin Pharmacol. 2013 Jan;75(1):45-59.
242. Sukarnjanaset W., Wattanavijitkul T., Jarurattanasirikul S. Evaluation of FOCEI and SAEM estimation methods in population pharmacokinetic analysis using NONMEM((R)) across rich, medium, and sparse sampling data. Eur J Drug Metab Pharmacokinet. 2018 Dec;43(6):729-36.
243. Fujiyama N., Miura M., Kato S., Sone T., Isobe M., Satoh S. Involvement of carboxylesterase 1 and 2 in the hydrolysis of mycophenolate mofetil. Drug Metab Dispos. 2010 Dec;38(12):2210-7.
244. Woillard J. B., Debord J., Marquet P. Comment on "Population pharmacokinetics of mycophenolic acid: An update". Clin Pharmacokinet. 2018 Sep;57(9):1211-3.
245. Ilett K. F., Tee L. B., Reeves P. T., Minchin R. F. Metabolism of drugs and other xenobiotics in the gut lumen and wall. Pharmacol Ther. 1990;46(1):67-93.
246. Guilcher G. M. Hematopoietic stem cell transplantation in children and adolescents. Pediatr Rev. 2016 Apr;37(4):135-44.
247. Bullingham R., Shah J., Goldblum R., Schiff M. Effects of food and antacid on the pharmacokinetics of single doses of mycophenolate mofetil in rheumatoid arthritis patients. Br J Clin Pharmacol. 1996 Jun;41(6):513-6.
248. Rupprecht K., Schmidt C., Raspe A., Schweda F., Shipkova M., Fischer W., et al. Bioavailability of mycophenolate mofetil and enteric-coated mycophenolate sodium is differentially affected by pantoprazole in healthy volunteers. J Clin Pharmacol. 2009 Oct;49(10):1196-201.
249. Bullingham R. E., Nicholls A., Hale M. Pharmacokinetics of mycophenolate mofetil (RS61443): A short review. Transplant Proc. 1996 Apr;28(2):925-9.
250. Nowak I., Shaw L. M. Mycophenolic acid binding to human serum albumin: Characterization and relation to pharmacodynamics. Clin Chem. 1995 Jul;41(7):1011-7.
251. Mangoni A. A., Jackson S. H. Age-related changes in pharmacokinetics and pharmacodynamics: Basic principles and practical applications. Br J Clin Pharmacol. 2004 Jan;57(1):6-14.
252. Basu N. K., Kole L., Kubota S., Owens I. S. Human UDP-glucuronosyltransferases show atypical metabolism of mycophenolic acid and inhibition by curcumin. Drug Metab Dispos. 2004 Jul;32(7):768-73.
253. Shipkova M., Strassburg C. P., Braun F., Streit F., Grone H. J., Armstrong V. W., et al. Glucuronide and glucoside conjugation of mycophenolic acid by human liver, kidney and intestinal microsomes. Br J Pharmacol. 2001 Mar;132(5):1027-34.
254. Kuypers D. R., Naesens M., Vermeire S., Vanrenterghem Y. The impact of uridine diphosphate-glucuronosyltransferase 1A9 (UGT1A9) gene promoter region single-nucleotide polymorphisms T-275A and C-2152T on early mycophenolic acid dose-interval exposure in de novo renal allograft recipients. Clin Pharmacol Ther. 2005 Oct;78(4):351-61.
255. Liu Y., Badee J., Takahashi R. H., Schmidt S., Parrott N., Fowler S., et al. Coexpression of human hepatic uridine diphosphate glucuronosyltransferase proteins: Implications for ontogenetic mechanisms and isoform coregulation. J Clin Pharmacol. 2020 Jun;60(6):722-33.
256. Filler G., Foster J., Berard R., Mai I., Lepage N. Age-dependency of mycophenolate mofetil dosing in combination with tacrolimus after pediatric renal transplantation. Transplant Proc. 2004 Jun;36(5):1327-31.

257. Parant F., Rivet C., Boulieu R., Gagnieu M. C., Dumortier J., Boillot O., et al. Age-related variability of mycophenolate mofetil exposure in stable pediatric liver transplant recipients and influences of donor characteristics. Ther Drug Monit. 2009 Dec;31(6):727-33.
258. Budde K., Sommerer C., Rissling O., Dieterlen M. T., Barten M. J. Target enzyme activity and phosphorylation of pathway molecules as specific biomarkers in transplantation. Ther Drug Monit. 2016 Apr;38 Suppl 1:S43-9.
259. Langman L. J., LeGatt D. F., Halloran P. F., Yatscoff R. W. Pharmacodynamic assessment of mycophenolic acid-induced immunosuppression in renal transplant recipients. Transplantation. 1996 Sep 15;62(5):666-72.
260. Fukuda T., Goebel J., Thogersen H., Maseck D., Cox S., Logan B., et al. Inosine monophosphate dehydrogenase (IMPDH) activity as a pharmacodynamic biomarker of mycophenolic acid effects in pediatric kidney transplant recipients. J Clin Pharmacol. 2011 Mar;51(3):309-20.
261. Rother A., Glander P., Vitt E., Czock D., von Ahsen N., Armstrong V. W., et al. Inosine monophosphate dehydrogenase activity in paediatrics: Age-related regulation and response to mycophenolic acid. Eur J Clin Pharmacol. 2012 Jun;68(6):913-22.
262. Lederer S. R., Friedrich N., Banas B., Welser G., Albert E. D., Sitter T. Effects of mycophenolate mofetil on donor-specific antibody formation in renal transplantation. Clin Transplant. 2005 Apr;19(2):168-74.
263. Sheiner L. B., Beal S. L. Some suggestions for measuring predictive performance. J Pharmacokinet Biopharm. 1981 Aug;9(4):503-12.
264. David-Neto E., Pereira Araujo L. M., Sumita N. M., Mendes M. E., Ribeiro Castro M. C., Alves C. F., et al. Mycophenolic acid pharmacokinetics in stable pediatric renal transplantation. Pediatr Nephrol. 2003 Mar;18(3):266-72.
265. Barraclough K. A., Lee K. J., Staatz C. E. Pharmacogenetic influences on mycophenolate therapy. Pharmacogenomics. 2010 Mar;11(3):369-90.
266. Picard N., Bergan S., Marquet P., van Gelder T., Wallemacq P., Hesselink D. A., et al. Pharmacogenetic biomarkers predictive of the pharmacokinetics and pharmacodynamics of immunosuppressive drugs. Ther Drug Monit. 2016 Apr;38 Suppl 1:S57-69.
267. Weber L. T., Hoecker B., Armstrong V. W., Oellerich M., Tonshoff B. Validation of an abbreviated pharmacokinetic profile for the estimation of mycophenolic acid exposure in pediatric renal transplant recipients. Ther Drug Monit. 2006 Oct;28(5):623-31.
268. Lam S., Partovi N., Ting L. S., Ensom M. H. Corticosteroid interactions with cyclosporine, tacrolimus, mycophenolate, and sirolimus: Fact or fiction? Ann Pharmacother. 2008 Jul;42(7):1037-47.
269. Vietri M., Pietrabissa A., Mosca F., Pacifici G. M. Inhibition of mycophenolic acid glucuronidation by niflumic acid in human liver microsomes. Eur J Clin Pharmacol. 2002 May;58(2):93-7.
270. Gripon P., Rumin S., Urban S., Le Seyec J., Glaise D., Cannie I., et al. Infection of a human hepatoma cell line by hepatitis B virus. Proc Natl Acad Sci U S A. 2002 Nov 26;99(24):15655-60.
271. Shimadzu Corporation. LabSolutions LCMS. 2018 [cited 2018 November 25]; Available from: https://www.shimadzu.com/an/lcms/labsol.html
272. Kawanishi M., Yano I., Yoshimura K., Yamamoto T., Hashi S., Masuda S., et al. Sensitive and validated LC-MS/MS methods to evaluate mycophenolic acid pharmacokinetics and pharmacodynamics in hematopoietic stem cell transplant patients. Biomed Chromatogr. 2015 Sep;29(9):1309-16.

273. U.S. Food and Drug Administration. Guidance for industry: Bioanalytical method validation. 2018 [cited 2018 September 15]; Available from: https://www.fda.gov/files/drugs/published/Bioanalytical-Method-Validation-Guidance-for-Industry.pdf
274. Goey A. K., Sparidans R. W., Meijerman I., Rosing H., Schellens J. H., Beijnen J. H. A sensitive LC-MS/MS method for the quantitative analysis of the Echinacea purpurea constituent undeca-2-ene-8,10-diynoic acid isobutylamide in human plasma. J Chromatogr B Analyt Technol Biomed Life Sci. 2011 Jan 1;879(1):41-8.
275. Biopredic International. HepaRG culture protocol. 2019 [cited 2018 September 15]; Available from: https://www.biopredic.com/
276. Volpe D. A., Tobin G. A., Tavakkoli F., Dowling T. C., Light P. D., Parker R. J. Effect of uremic serum and uremic toxins on drug metabolism in human microsomes. Regul Toxicol Pharmacol. 2014 Mar;68(2):297-303.
277. Roche. Cytotoxicity detection Kit PLUS (LDH). 2011 [cited 2018 September 15]; Available from: http://netdocs.roche.com/DDM/Effective/0000000000001004022000793_000_06_005_Native.pdf
278. Delavenne X., Juthier L., Pons B., Mariat C., Basset T. UPLC MS/MS method for quantification of mycophenolic acid and metabolites in human plasma: Application to pharmacokinetic study. Clin Chim Acta. 2011 Jan 14;412(1-2):59-65.
279. Figurski M. J., Korecka M., Fields L., Waligorska T., Shaw L. M. High-performance liquid chromatography-mass spectroscopy/mass spectroscopy method for simultaneous quantification of total or free fraction of mycophenolic acid and its glucuronide metabolites. Ther Drug Monit. 2009 Dec;31(6):717-26.
280. Zegarska J., Hryniewiecka E., Zochowska D., Tszyrsznic W., Jazwiec R., Borowiec A., et al. Mycophenolic acid metabolites acyl-glucuronide and glucoside affect the occurrence of infectious complications and bone marrow dysfunction in liver transplant recipients. Ann Transplant. 2015 Aug 20;20:483-92.
281. Zhang D., Chow D. S., Renbarger J. L. Simultaneous quantification of mycophenolic acid and its glucuronide metabolites in human plasma by an UPLC-MS/MS assay. Biomed Chromatogr. 2016 Oct;30(10):1648-55.
282. Benoit-Biancamano M. O., Caron P., Levesque E., Delage R., Couture F., Guillemette C. Sensitive high-performance liquid chromatography-tandem mass spectrometry method for quantitative analysis of mycophenolic acid and its glucuronide metabolites in human plasma and urine. J Chromatogr B Analyt Technol Biomed Life Sci. 2007 Oct 15;858(1-2):159-67.
283. Klepacki J., Klawitter J., Bendrick-Peart J., Schniedewind B., Heischmann S., Shokati T., et al. A high-throughput U-HPLC-MS/MS assay for the quantification of mycophenolic acid and its major metabolites mycophenolic acid glucuronide and mycophenolic acid acyl-glucuronide in human plasma and urine. J Chromatogr B Analyt Technol Biomed Life Sci. 2012 Feb 1;883-884:113-9.
284. Iboshi H., Yamaguchi H., Suzuki H., Kikuchi M., Tanaka M., Takasaki S., et al. Development of a liquid chromatography-tandem mass spectrometric method for quantification of mycophenolic acid and its glucuronides in dried blood spot samples. Ther Drug Monit. 2017 Dec;39(6):648-53.

285. Mohamed M. F., Harvey S. S., Frye R. F. Determination of mycophenolic acid glucuronide in microsomal incubations using high performance liquid chromatography-tandem mass spectrometry. J Chromatogr B Analyt Technol Biomed Life Sci. 2008 Jul 15;870(2):251-4.
286. Chhonker Y. S., Haney S. L., Bala V., Holstein S. A., Murry D. J. Simultaneous quantitation of isoprenoid pyrophosphates in plasma and cancer cells using LC-MS/MS. Molecules. 2018 Dec 11;23(12).
287. Shimadzu Corporation. LCMS 8050. 2018 [cited 2018 November 25]; Available from: https://www.shimadzu.com
288. Syed M., Srinivas N. R. A comprehensive review of the published assays for the quantitation of the immunosuppressant drug mycophenolic acid and its glucuronidated metabolites in biological fluids. Biomed Chromatogr. 2016 May;30(5):721-48.
289. McPherson R., Pincus M. Henry's clinical diagnosis and management by laboratory methods (22nd Edition): Philadelphia, PA: Elsevier/Saunders; 2011.
290. Surendradoss J., Chang T. K., Abbott F. S. Evaluation of in situ generated valproyl 1-O-beta-acyl glucuronide in valproic acid toxicity in sandwich-cultured rat hepatocytes. Drug Metab Dispos. 2014 Nov;42(11):1834-42.
291. Brandhorst G., Streit F., Goetze S., Oellerich M., Armstrong V. W. Quantification by liquid chromatography tandem mass spectrometry of mycophenolic acid and its phenol and acyl glucuronide metabolites. Clin Chem. 2006 Oct;52(10):1962-4.
292. Hart S. N., Li Y., Nakamoto K., Subileau E. A., Steen D., Zhong X. B. A comparison of whole genome gene expression profiles of HepaRG cells and HepG2 cells to primary human hepatocytes and human liver tissues. Drug Metab Dispos. 2010 Jun;38(6):988-94.
293. Yeung C. K., Shen D. D., Thummel K. E., Himmelfarb J. Effects of chronic kidney disease and uremia on hepatic drug metabolism and transport. Kidney Int. 2014 Mar;85(3):522-8.
294. Miners J. O., Yang X., Knights K. M., Zhang L. The role of the kidney in drug elimination: Transport, metabolism, and the impact of kidney disease on drug clearance. Clin Pharmacol Ther. 2017 Sep;102(3):436-49.
295. Ikematsu N., Kashiwagi M., Hara K., Waters B., Matsusue A., Takayama M., et al. Organ distribution of endogenous p-cresol in hemodialysis patients. J Med Invest. 2019;66(1.2):81-5.
296. Uchaipichat V., Mackenzie P. I., Guo X. H., Gardner-Stephen D., Galetin A., Houston J. B., et al. Human UDP-glucuronosyltransferases: Isoform selectivity and kinetics of 4-methylumbelliferone and 1-naphthol glucuronidation, effects of organic solvents, and inhibition by diclofenac and probenecid. Drug Metab Dispos. 2004 Apr;32(4):413-23.
297. Badee J., Qiu N., Parrott N., Collier A. C., Schmidt S., Fowler S. Optimization of experimental conditions of automated glucuronidation assays in human liver microsomes using a cocktail approach and ultra-high performance liquid chromatography-tandem mass spectrometry. Drug Metab Dispos. 2019 Feb;47(2):124-34.
298. Miners J. O., Bowalgaha K., Elliot D. J., Baranczewski P., Knights K. M. Characterization of niflumic acid as a selective inhibitor of human liver microsomal UDP-glucuronosyltransferase 1A9: Application to the reaction phenotyping of acetaminophen glucuronidation. Drug Metab Dispos. 2011 Apr;39(4):644-52.
299. Miners J. O., Knights K. M., Houston J. B., Mackenzie P. I. In vitro-in vivo correlation for drugs and other compounds eliminated by glucuronidation in humans: Pitfalls and promises. Biochem Pharmacol. 2006 May 28;71(11):1531-9.

300. Corning Incorporated. Corning Gentest high/low P450 single donor HLM panel. 2017 [cited 2019 March 01]; Available from: https://www.corning.com/catalog/cls/documents/donor-guides/High-Low_P450_Single_Donor_HLM_Panel_031.pdf
301. Dixon M. The determination of enzyme inhibitor constants. Biochem J. 1953 Aug;55(1):170-1.
302. Cornish-Bowden A. A simple graphical method for determining the inhibition constants of mixed, uncompetitive and non-competitive inhibitors. Biochem J. 1974 Jan;137(1):143-4.
303. Brown H. S., Ito K., Galetin A., Houston J. B. Prediction of in vivo drug-drug interactions from in vitro data: Impact of incorporating parallel pathways of drug elimination and inhibitor absorption rate constant. Br J Clin Pharmacol. 2005 Nov;60(5):508-18.
304. McLure J. A., Miners J. O., Birkett D. J. Nonspecific binding of drugs to human liver microsomes. Br J Clin Pharmacol. 2000 May;49(5):453-61.
305. Vietri M., Pietrabissa A., Mosca F., Pacifici G. M. Mycophenolic acid glucuronidation and its inhibition by non-steroidal anti-inflammatory drugs in human liver and kidney. Eur J Clin Pharmacol. 2000 Dec;56(9-10):659-64.
306. Slovak J. E., Mealey K., Court M. H. Comparative metabolism of mycophenolic acid by glucuronic acid and glucose conjugation in human, dog, and cat liver microsomes. J Vet Pharmacol Ther. 2017 Apr;40(2):123-9.
307. U.S. Food and Drug Administration. Guidance for industry: In vitro metabolism-and transporter-mediated drug-drug interaction studies 2017 [cited 2019 July 01]; Available from: https://www.fda.gov/files/drugs/published/Bioanalytical-Method-Validation-Guidance-for-Industry.pdf
308. Cuoghi A., Caiazzo M., Bellei E., Monari E., Bergamini S., Palladino G., et al. Quantification of p-cresol sulphate in human plasma by selected reaction monitoring. Anal Bioanal Chem. 2012 Oct;404(6-7):2097-104.
309. Gill K. L., Houston J. B., Galetin A. Characterization of in vitro glucuronidation clearance of a range of drugs in human kidney microsomes: comparison with liver and intestinal glucuronidation and impact of albumin. Drug Metab Dispos. 2012 Apr;40(4):825-35.
310. Knights K. M., Spencer S. M., Fallon J. K., Chau N., Smith P. C., Miners J. O. Scaling factors for the in vitro-in vivo extrapolation (IV-IVE) of renal drug and xenobiotic glucuronidation clearance. Br J Clin Pharmacol. 2016 Jun;81(6):1153-64.
311. Wan Y., Wang F., Yuan J., Li J., Jiang D., Zhang J., et al. Effects of dietary fat on gut microbiota and faecal metabolites, and their relationship with cardiometabolic risk factors: A 6-month randomised controlled-feeding trial. Gut. 2019 Aug;68(8):1417-29.
312. Wong J., Piceno Y. M., DeSantis T. Z., Pahl M., Andersen G. L., Vaziri N. D. Expansion of urease- and uricase-containing, indole- and p-cresol-forming and contraction of short-chain fatty acid-producing intestinal microbiota in ESRD. Am J Nephrol. 2014;39(3):230-7.
313. Meert N., Schepers E., De Smet R., Argiles A., Cohen G., Deppisch R., et al. Inconsistency of reported uremic toxin concentrations. Artif Organs. 2007 Aug;31(8):600-11.
314. Chengcheng G., Rui X., Tianheng M., Wei Y., Liqun P. Probe substrate and enzyme source-dependent inhibition of UDP-glucuronosyltransferase (UGT) 1A9 by wogonin. Afr Health Sci. 2013 Sep;13(3):551-5.
315. Yan Z., Zhong H. M., Maher N., Torres R., Leo G. C., Caldwell G. W., et al. Bioactivation of 4-methylphenol (p-cresol) via cytochrome P450-mediated aromatic oxidation in human liver microsomes. Drug Metab Dispos. 2005 Dec;33(12):1867-76.

316. Hardwick J. P. Cytochrome P450 omega hydroxylase (CYP4) function in fatty acid metabolism and metabolic diseases. Biochem Pharmacol. 2008 Jun 15;75(12):2263-75.
317. Rowland A., Knights K. M., Mackenzie P. I., Miners J. O. The "albumin effect" and drug glucuronidation: bovine serum albumin and fatty acid-free human serum albumin enhance the glucuronidation of UDP-glucuronosyltransferase (UGT) 1A9 substrates but not UGT1A1 and UGT1A6 activities. Drug Metab Dispos. 2008 Jun;36(6):1056-62.
318. Brix L. A., Barnett A. C., Duggleby R. G., Leggett B., McManus M. E. Analysis of the substrate specificity of human sulfotransferases SULT1A1 and SULT1A3: Site-directed mutagenesis and kinetic studies. Biochemistry. 1999 Aug 10;38(32):10474-9.
319. Vanholder R., De Smet R., Waterloos M. A., Van Landschoot N., Vogeleere P., Hoste E., et al. Mechanisms of uremic inhibition of phagocyte reactive species production: Characterization of the role of p-cresol. Kidney Int. 1995 Feb;47(2):510-7.
320. Wang C. P., Lu L. F., Yu T. H., Hung W. C., Chiu C. A., Chung F. M., et al. Associations among chronic kidney disease, high total p-cresylsulfate and major adverse cardiac events. J Nephrol. 2013 Jan-Feb;26(1):111-8.
321. Chiu C. A., Lu L. F., Yu T. H., Hung W. C., Chung F. M., Tsai I. T., et al. Increased levels of total p-cresylsulphate and indoxyl sulphate are associated with coronary artery disease in patients with diabetic nephropathy. Rev Diabet Stud. 2010 Winter;7(4):275-84.
322. Laville S. M., Massy Z. A., Kamel S., Chillon J. M., Choukroun G., Liabeuf S. Intestinal chelators, sorbants, and gut-derived uremic toxins. Toxins (Basel). 2021 Jan 26;13(2).
323. XenoTech SEKISUI. SEKISUI XenoTech. 2021 [cited 2021 February 06]; Available from: https://www.xenotech.com/
324. Al Alawi A. M., Majoni S. W., Falhammar H. Magnesium and human health: Perspectives and research directions. Int J Endocrinol. 2018;2018:9041694.
325. Cappiello M., Franchi M., Giuliani L., Pacifici G. M. Distribution of 2-naphthol sulphotransferase and its endogenous substrate adenosine 3'-phosphate 5'-phosphosulphate in human tissues. Eur J Clin Pharmacol. 1989;37(3):317-20.
326. James M. O. Enzyme kinetics of conjugating enzymes: PAPS sulfotransferase. Methods Mol Biol. 2014;1113:187-201.
327. Riches Z., Stanley E. L., Bloomer J. C., Coughtrie M. W. Quantitative evaluation of the expression and activity of five major sulfotransferases (SULTs) in human tissues: The SULT "pie". Drug Metab Dispos. 2009 Nov;37(11):2255-61.
328. Niwa T. Phenol and p-cresol accumulated in uremic serum measured by HPLC with fluorescence detection. Clin Chem. 1993 Jan;39(1):108-11.
329. Carlini E. J., Raftogianis R. B., Wood T. C., Jin F., Zheng W., Rebbeck T. R., et al. Sulfation pharmacogenetics: SULT1A1 and SULT1A2 allele frequencies in Caucasian, Chinese and African-American subjects. Pharmacogenetics. 2001 Feb;11(1):57-68.
330. Nagar S., Walther S., Blanchard R. L. Sulfotransferase (SULT) 1A1 polymorphic variants *1, *2, and *3 are associated with altered enzymatic activity, cellular phenotype, and protein degradation. Mol Pharmacol. 2006 Jun;69(6):2084-92.
331. Prism GraphPad. GraphPad Prism software. 2021 [cited 2021 February 06]; Available from: https://www.graphpad.com/scientific-software/prism/
332. Miksits M., Maier-Salamon A., Aust S., Thalhammer T., Reznicek G., Kunert O., et al. Sulfation of resveratrol in human liver: Evidence of a major role for the sulfotransferases SULT1A1 and SULT1E1. Xenobiotica. 2005 Dec;35(12):1101-19.

333. James M. O., Ambadapadi S. Interactions of cytosolic sulfotransferases with xenobiotics. Drug Metab Rev. 2013 Nov;45(4):401-14.
334. Harris R. M., Hawker R. J., Langman M. J., Singh S., Waring R. H. Inhibition of phenolsulphotransferase by salicylic acid: A possible mechanism by which aspirin may reduce carcinogenesis. Gut. 1998 Feb;42(2):272-5.
335. King R. S., Ghosh A. A., Wu J. Inhibition of human phenol and estrogen sulfotransferase by certain non-steroidal anti-inflammatory agents. Curr Drug Metab. 2006 Oct;7(7):745-53.
336. Pacifici G. M. Inhibition of human liver and duodenum sulfotransferases by drugs and dietary chemicals: a review of the literature. Int J Clin Pharmacol Ther. 2004 Sep;42(9):488-95.
337. Vietri M., De Santi C., Pietrabissa A., Mosca F., Pacifici G. M. Fenamates and the potent inhibition of human liver phenol sulphotransferase. Xenobiotica. 2000 Feb;30(2):111-6.
338. Vietri M., De Santi C., Pietrabissa A., Mosca F., Pacifici G. M. Inhibition of human liver phenol sulfotransferase by nonsteroidal anti-inflammatory drugs. Eur J Clin Pharmacol. 2000 Apr;56(1):81-7.
339. Vietri M., Pietrabissa A., Spisni R., Mosca F., Pacifici G. M. Differential inhibition of hepatic and duodenal sulfation of (-)-salbutamol and minoxidil by mefenamic acid. Eur J Clin Pharmacol. 2000 Sep;56(6-7):477-9.
340. Vietri M., Pietrabissa A., Mosca F., Rane A., Pacific G. M. Human adult and foetal liver sulphotransferases: Inhibition by mefenamic acid and salicylic acid. Xenobiotica. 2001 Mar;31(3):153-61.
341. Vietri M., Vaglini F., Pietrabissa A., Spisni R., Mosca F., Pacifici G. M. Sulfation of R(-)-apomorphine in the human liver and duodenum, and its inhibition by mefenamic acid, salicylic acid and quercetin. Xenobiotica. 2002 Jul;32(7):587-94.
342. Silverman R.B. APPENDIX I - enzyme kinetics. In: Silverman RB, editor. Organic chemistry of enzyme-catalyzed reactions (2nd Edition): San Diego: Academic Press; 2002. p. 563-96.
343. Bansal S., Lau A. J. Human liver cytosolic sulfotransferase 2A1-dependent dehydroepiandrosterone sulfation assay by ultra-high performance liquid chromatography-tandem mass spectrometry. J Pharm Biomed Anal. 2016 Feb 20;120:261-9.
344. Ma B., Shou M., Schrag M. L. Solvent effect on cDNA-expressed human sulfotransferase (SULT) activities in vitro. Drug Metab Dispos. 2003 Nov;31(11):1300-5.
345. Riches Z., Bloomer J. C., Coughtrie M. W. Comparison of 2-aminophenol and 4-nitrophenol as in vitro probe substrates for the major human hepatic sulfotransferase, SULT1A1, demonstrates improved selectivity with 2-aminophenol. Biochem Pharmacol. 2007 Jul 15;74(2):352-8.
346. Etman M. A., Farid R. M., Nada A. H., Ebian A. A. In vitro/in vivo correlation of fast release mephenamic acid microspheres in humans. Med Princ Pract. 2012;21(3):223-7.
347. Pentikainen P. J., Neuvonen P. J., Backman C. Human pharmacokinetics of tolfenamic acid, a new anti-inflammatory agent. Eur J Clin Pharmacol. 1981;19(5):359-65.
348. Lentjes E. G., van Ginneken C. A. Pharmacokinetics of flufenamic acid in man. Int J Clin Pharmacol Ther Toxicol. 1987 Apr;25(4):185-7.
349. Gamage N., Barnett A., Hempel N., Duggleby R. G., Windmill K. F., Martin J. L., et al. Human sulfotransferases and their role in chemical metabolism. Toxicol Sci. 2006 Mar;90(1):5-22.

350. Reiter C., Mwaluko G., Dunnette J., Van Loon J., Weinshilboum R. Thermolabile and thermostable human platelet phenol sulfotransferase. Substrate specificity and physical separation. Naunyn Schmiedebergs Arch Pharmacol. 1983 Sep;324(2):140-7.
351. Cook I., Wang T., Falany C. N., Leyh T. S. The allosteric binding sites of sulfotransferase 1A1. Drug Metab Dispos. 2015 Mar;43(3):418-23.
352. Horl W. H. Nonsteroidal anti-inflammatory drugs and the kidney. Pharmaceuticals (Basel). 2010 Jul 21;3(7):2291-321.
353. Osiri M., Moreland L. W. Specific cyclooxygenase 2 inhibitors: A new choice of nonsteroidal anti-inflammatory drug therapy. Arthritis Care Res. 1999 Oct;12(5):351-62.
354. Strelow J., Dewe, W., Iversen, P.W., Brooks, H.B., Radding, J.A., McGee, J., Weidner, J. Mechanism of action assays for enzymes. In: Markossian S, Sittampalam, G.S., Grossman, A., Brimacombe, K., Arkin, M., Auld, D., Xu, X. , editor. Assay guidance manual: Bethesda (MD); 2004.
355. Lucas G. N. C., Leitao A. C. C., Alencar R. L., Xavier R. M. F., Daher E. F., Silva Junior G. B. D. Pathophysiological aspects of nephropathy caused by non-steroidal anti-inflammatory drugs. J Bras Nefrol. 2019 Jan-Mar;41(1):124-30.
356. Gierse J. K., Hauser S. D., Creely D. P., Koboldt C., Rangwala S. H., Isakson P. C., et al. Expression and selective inhibition of the constitutive and inducible forms of human cyclo-oxygenase. Biochem J. 1995 Jan 15;305 (Pt 2):479-84.
357. Cryer B., Feldman M. Cyclooxygenase-1 and cyclooxygenase-2 selectivity of widely used nonsteroidal anti-inflammatory drugs. Am J Med. 1998 May;104(5):413-21.
358. Riendeau D., Charleson S., Cromlish W., Mancini J. A., Wong E., Guay J. Comparison of the cyclooxygenase-1 inhibitory properties of nonsteroidal anti-inflammatory drugs (NSAIDs) and selective COX-2 inhibitors, using sensitive microsomal and platelet assays. Can J Physiol Pharmacol. 1997 Sep;75(9):1088-95.
359. Warner T. D., Giuliano F., Vojnovic I., Bukasa A., Mitchell J. A., Vane J. R. Nonsteroid drug selectivities for cyclo-oxygenase-1 rather than cyclo-oxygenase-2 are associated with human gastrointestinal toxicity: A full in vitro analysis. Proc Natl Acad Sci U S A. 1999 Jun 22;96(13):7563-8.
360. Karjalainen M. J., Neuvonen P. J., Backman J. T. In vitro inhibition of CYP1A2 by model inhibitors, anti-inflammatory analgesics and female sex steroids: predictability of in vivo interactions. Basic Clin Pharmacol Toxicol. 2008 Aug;103(2):157-65.
361. Joo J., Kim Y. W., Wu Z., Shin J. H., Lee B., Shon J. C., et al. Screening of non-steroidal anti-inflammatory drugs for inhibitory effects on the activities of six UDP-glucuronosyltransferases (UGT1A1, 1A3, 1A4, 1A6, 1A9 and 2B7) using LC-MS/MS. Biopharm Drug Dispos. 2015 May;36(4):258-64.
362. U.S. Food and Drug Administration. PONSTEL® mefenamic acid capsules. 2008 [cited 2021 February 06]; Available from: https://www.accessdata.fda.gov/drugsatfda_docs/label/2008/015034s040lbl.pdf
363. Golper T.A., Marx, M.A., Shuler, C., Bennett, W.M. Drug dosage in dialysis patients. In: Jacobs C, Kjellstrand, C.M., Koch, K.M., Winchester, J.F., editor. Replacement of renal function by dialysis: Springer, Dordrecht; 1996. p. 750-820.
364. Launay-Vacher V., Karie S., Fau J. B., Izzedine H., Deray G. Treatment of pain in patients with renal insufficiency: The World Health Organization three-step ladder adapted. J Pain. 2005 Mar;6(3):137-48.

365. Adeniji A. O., Twenter B. M., Byrns M. C., Jin Y., Chen M., Winkler J. D., et al. Development of potent and selective inhibitors of aldo-keto reductase 1C3 (type 5 17beta-hydroxysteroid dehydrogenase) based on N-phenyl-aminobenzoates and their structure-activity relationships. J Med Chem. 2012 Mar 8;55(5):2311-23.
366. Graham G. Fenamates. In: Parnham, editor. Compendium of inflammatory diseases: Birkhauser, Basel; 2016.
367. Saigo C., Nomura Y., Yamamoto Y., Sagata M., Matsunaga R., Jono H., et al. Meclofenamate elicits a nephropreventing effect in a rat model of ischemic acute kidney injury by suppressing indoxyl sulfate production and restoring renal organic anion transporters. Drug Des Devel Ther. 2014;8:1073-82.
368. Salarolli R. T., Alvarenga L., Cardozo Lfmf, Teixeira K. T. R., de S. G. Moreira L., Lima J. D., et al. Can curcumin supplementation reduce plasma levels of gut-derived uremic toxins in hemodialysis patients? A pilot randomized, double-blind, controlled study. Int Urol Nephrol. 2021 Jun;53(6):1231-8.
369. Vietri M., Pietrabissa A., Mosca F., Spisni R., Pacifici G. M. Curcumin is a potent inhibitor of phenol sulfotransferase (SULT1A1) in human liver and extrahepatic tissues. Xenobiotica. 2003 Apr;33(4):357-63.
370. Takkavatakarn K., Wuttiputinun T., Phannajit J., Praditpornsilpa K., Eiam-Ong S., Susantitaphong P. Protein-bound uremic toxin lowering strategies in chronic kidney disease: A systematic review and meta-analysis. J Nephrol. 2021 Dec;34(6):1805-17.
371. Meert N., Schepers E., Glorieux G., Van Landschoot M., Goeman J. L., Waterloos M. A., et al. Novel method for simultaneous determination of p-cresylsulphate and p-cresylglucuronide: Clinical data and pathophysiological implications. Nephrol Dial Transplant. 2012 Jun;27(6):2388-96.
372. Itoh Y., Ezawa A., Kikuchi K., Tsuruta Y., Niwa T. Protein-bound uremic toxins in hemodialysis patients measured by liquid chromatography/tandem mass spectrometry and their effects on endothelial ROS production. Anal Bioanal Chem. 2012 Jun;403(7):1841-50.
373. Fisher M. B., Campanale K., Ackermann B. L., VandenBranden M., Wrighton S. A. In vitro glucuronidation using human liver microsomes and the pore-forming peptide alamethicin. Drug Metab Dispos. 2000 May;28(5):560-6.
374. Li X., Bratton S., Radominska-Pandya A. Human UGT1A8 and UGT1A10 mRNA are expressed in primary human hepatocytes. Drug Metab Pharmacokinet. 2007 Jun;22(3):152-61.
375. Tukey R. H., Strassburg C. P. Human UDP-glucuronosyltransferases: Metabolism, expression, and disease. Annu Rev Pharmacol Toxicol. 2000;40:581-616.
376. Rowland A., Miners J. O., Mackenzie P. I. The UDP-glucuronosyltransferases: Their role in drug metabolism and detoxification. Int J Biochem Cell Biol. 2013 Jun;45(6):1121-32.
377. Ohno S., Nakajin S. Determination of mRNA expression of human UDP-glucuronosyltransferases and application for localization in various human tissues by real-time reverse transcriptase-polymerase chain reaction. Drug Metab Dispos. 2009 Jan;37(1):32-40.
378. Fallon J. K., Neubert H., Goosen T. C., Smith P. C. Targeted precise quantification of 12 human recombinant uridine-diphosphate glucuronosyl transferase 1A and 2B isoforms using nano-ultra-high-performance liquid chromatography/tandem mass spectrometry with selected reaction monitoring. Drug Metab Dispos. 2013 Dec;41(12):2076-80.
379. Margaillan G., Rouleau M., Fallon J. K., Caron P., Villeneuve L., Turcotte V., et al. Quantitative profiling of human renal UDP-glucuronosyltransferases and glucuronidation activity: A comparison of normal and tumoral kidney tissues. Drug Metab Dispos. 2015 Apr;43(4):611-9.

380. Miners J. O., Mackenzie P. I., Knights K. M. The prediction of drug-glucuronidation parameters in humans: UDP-glucuronosyltransferase enzyme-selective substrate and inhibitor probes for reaction phenotyping and in vitro-in vivo extrapolation of drug clearance and drug-drug interaction potential. Drug Metab Rev. 2010 Feb;42(1):196-208.
381. Houston J. B., Kenworthy K. E. In vitro-in vivo scaling of CYP kinetic data not consistent with the classical Michaelis-Menten model. Drug Metab Dispos. 2000 Mar;28(3):246-54.
382. Walsky R. L., Bauman J. N., Bourcier K., Giddens G., Lapham K., Negahban A., et al. Optimized assays for human UDP-glucuronosyltransferase (UGT) activities: altered alamethicin concentration and utility to screen for UGT inhibitors. Drug Metab Dispos. 2012 May;40(5):1051-65.
383. Lv X., Zhang J. B., Wang X. X., Hu W. Z., Shi Y. S., Liu S. W., et al. Amentoflavone is a potent broad-spectrum inhibitor of human UDP-glucuronosyltransferases. Chem Biol Interact. 2018 Mar 25;284:48-55.
384. Kiang T. K., Ensom M. H., Chang T. K. UDP-glucuronosyltransferases and clinical drug-drug interactions. Pharmacol Ther. 2005 Apr;106(1):97-132.
385. De Smet R., David F., Sandra P., Van Kaer J., Lesaffer G., Dhondt A., et al. A sensitive HPLC method for the quantification of free and total p-cresol in patients with chronic renal failure. Clin Chim Acta. 1998 Nov;278(1):1-21.
386. Fallon J. K., Neubert H., Hyland R., Goosen T. C., Smith P. C. Targeted quantitative proteomics for the analysis of 14 UGT1As and -2Bs in human liver using Nano UPLC-MS/MS with selected reaction monitoring. J Proteome Res. 2013 Oct 4;12(10):4402-13.
387. Beaulieu M., Levesque E., Hum D. W., Belanger A. Isolation and characterization of a human orphan UDP-glucuronosyltransferase, UGT2B11. Biochem Biophys Res Commun. 1998 Jul 9;248(1):44-50.
388. Bushey R. T., Dluzen D. F., Lazarus P. Importance of UDP-glucuronosyltransferases 2A2 and 2A3 in tobacco carcinogen metabolism. Drug Metab Dispos. 2013 Jan;41(1):170-9.
389. Meech R., Mubarokah N., Shivasami A., Rogers A., Nair P. C., Hu D. G., et al. A novel function for UDP glycosyltransferase 8: Galactosidation of bile acids. Mol Pharmacol. 2015;87(3):442-50.
390. MacKenzie P. I., Rogers A., Elliot D. J., Chau N., Hulin J. A., Miners J. O., et al. The novel UDP glycosyltransferase 3A2: Cloning, catalytic properties, and tissue distribution. Mol Pharmacol. 2011 Mar;79(3):472-8.
391. Mackenzie P. I., Rogers A., Treloar J., Jorgensen B. R., Miners J. O., Meech R. Identification of UDP glycosyltransferase 3A1 as a UDP N-acetylglucosaminyltransferase. J Biol Chem. 2008 Dec 26;283(52):36205-10.
392. Harding D., Fournel-Gigleux S., Jackson M. R., Burchell B. Cloning and substrate specificity of a human phenol UDP-glucuronosyltransferase expressed in COS-7 cells. Proc Natl Acad Sci U S A. 1988 Nov;85(22):8381-5.
393. Shou M. Kinetic analysis for multiple substrate interaction at the active site of cytochrome P450. Methods Enzymol. 2002;357:261-76.
394. Meyer T. W., Hostetter T. H. Uremic solutes from colon microbes. Kidney Int. 2012 May;81(10):949-54.
395. Stingl J. C., Bartels H., Viviani R., Lehmann M. L., Brockmoller J. Relevance of UDP-glucuronosyltransferase polymorphisms for drug dosing: A quantitative systematic review. Pharmacol Ther. 2014 Jan;141(1):92-116.

396. Hurst F. P., Belur P., Nee R., Agodoa L. Y., Patel P., Abbott K. C., et al. Poor outcomes associated with neutropenia after kidney transplantation: Analysis of United States Renal Data System. Transplantation. 2011 Jul 15;92(1):36-40.
397. Mavrakanas T. A., Fournier M. A., Clairoux S., Amiel J. A., Tremblay M. E., Vinh D. C., et al. Neutropenia in kidney and liver transplant recipients: Risk factors and outcomes. Clin Transplant. 2017 Oct;31(10).
398. Zafrani L., Truffaut L., Kreis H., Etienne D., Rafat C., Lechaton S., et al. Incidence, risk factors and clinical consequences of neutropenia following kidney transplantation: A retrospective study. Am J Transplant. 2009 Aug;9(8):1816-25.
399. Duranton F., Cohen G., De Smet R., Rodriguez M., Jankowski J., Vanholder R., et al. Normal and pathologic concentrations of uremic toxins. J Am Soc Nephrol. 2012 Jul;23(7):1258-70.
400. Cohen J, Cohen, P, West, SG, & Aiken, LS. Applied multiple regression/correlation analysis for the behavioral sciences. 3rd ed. New York: Taylor & Francis Group; 2002.
401. Levey A. S., Stevens L. A., Schmid C. H., Zhang Y. L., Castro A. F., 3rd, Feldman H. I., et al. A new equation to estimate glomerular filtration rate. Ann Intern Med. 2009 May 5;150(9):604-12.
402. Liu Y., Liu L., Li J., Fu Q., Zhang H., Wu C., et al. Validated LC-MS/MS method for quantitation of total and free mycophenolic acid concentration and its application to a pharmacokinetic study in pediatric renal transplant recipients. Biomed Chromatogr. 2021 Feb;35(2):e4989.
403. Kiang T. K., Ng K., Ensom M. H. Multiple regression analysis of factors predicting mycophenolic acid free fraction in 91 adult organ transplant recipients. Ther Drug Monit. 2013 Dec;35(6):867-71.
404. GraphPad Prism. https://www.graphpad.com/scientific-software/prism/. Accessed 01 Jun 2021. [cited; Available from:
405. DynaLIFE Medical Labs. Reference ranges for laboratory tests. https://www.dynalife.ca/testdirectory. Accessed 10 Sep 2021. [cited; Available from:
406. Atcheson B. A., Taylor P. J., Mudge D. W., Johnson D. W., Hawley C. M., Campbell S. B., et al. Mycophenolic acid pharmacokinetics and related outcomes early after renal transplant. Br J Clin Pharmacol. 2005 Mar;59(3):271-80.
407. Shaw L. M., Korecka M., Venkataramanan R., Goldberg L., Bloom R., Brayman K. L. Mycophenolic acid pharmacodynamics and pharmacokinetics provide a basis for rational monitoring strategies. Am J Transplant. 2003 May;3(5):534-42.
408. Baczkowska T., Sadowska A., Perkowska-Ptasinska A., Lewandowski Z., Cieciura T., Pazik J., et al. Optimal mycophenolic acid and mycophenolic acid glucuronide levels at the early period after kidney transplantation are the key contributors to improving long-term outcomes. Transplant Proc. 2009 Oct;41(8):3019-23.
409. Jiang Z., Hu N. Effect of UGT polymorphisms on pharmacokinetics and adverse reactions of mycophenolic acid in kidney transplant patients. Pharmacogenomics. 2021 Oct;22(15):1019-40.
410. Matsunaga N., Wada S., Nakanishi T., Ikenaga M., Ogawa M., Tamai I. Mathematical modeling of the in vitro hepatic disposition of mycophenolic acid and its glucuronide in sandwich-cultured human hepatocytes. Mol Pharm. 2014 Feb 3;11(2):568-79.

411. Laouari D., Yang R., Veau C., Blanke I., Friedlander G. Two apical multidrug transporters, P-gp and MRP2, are differently altered in chronic renal failure. Am J Physiol Renal Physiol. 2001 Apr;280(4):F636-45.
412. Mutsaers H. A., van den Heuvel L. P., Ringens L. H., Dankers A. C., Russel F. G., Wetzels J. F., et al. Uremic toxins inhibit transport by breast cancer resistance protein and multidrug resistance protein 4 at clinically relevant concentrations. PLoS One. 2011 Apr 4;6(4):e18438.
413. Berthier J., Benmameri M., Sauvage F. L., Fabre G., Chantemargue B., Arnion H., et al. MRP4 is responsible for the efflux transport of mycophenolic acid beta-d glucuronide (MPAG) from hepatocytes to blood. Xenobiotica. 2021 Jan;51(1):105-14.
414. Reyes M., Benet L. Z. Effects of uremic toxins on transport and metabolism of different biopharmaceutics drug disposition classification system xenobiotics. J Pharm Sci. 2011 Sep;100(9):3831-42.
415. Sato T., Yamaguchi H., Kogawa T., Abe T., Mano N. Organic anion transporting polypeptides 1B1 and 1B3 play an important role in uremic toxin handling and drug-uremic toxin interactions in the liver. J Pharm Pharm Sci. 2014;17(4):475-84.
416. Guillouzo A., Corlu A., Aninat C., Glaise D., Morel F., Guguen-Guillouzo C. The human hepatoma HepaRG cells: a highly differentiated model for studies of liver metabolism and toxicity of xenobiotics. Chem Biol Interact. 2007 May 20;168(1):66-73.
417. Jun H., Rong Y., Yih C., Ho J., Cheng W., Kiang T. K. L. Comparisons of four protein-binding models characterizing the pharmacokinetics of unbound phenytoin in adult patients using non-linear mixed-effects modeling. Drugs R D. 2020 Dec;20(4):343-58.
418. Shahbaz H., Gupta M. Creatinine clearance. StatPearls. Treasure Island (FL); 2022.
419. Bajaj P., Chowdhury S. K., Yucha R., Kelly E. J., Xiao G. Emerging kidney models to investigate metabolism, transport, and toxicity of drugs and xenobiotics. Drug Metab Dispos. 2018 Nov;46(11):1692-702.
420. Lippi M., Stadiotti I., Pompilio G., Sommariva E. Human cell modeling for cardiovascular diseases. Int J Mol Sci. 2020 Sep 2;21(17).
421. Singh A. P., Junemann A., Muthuraman A., Jaggi A. S., Singh N., Grover K., et al. Animal models of acute renal failure. Pharmacol Rep. 2012;64(1):31-44.
422. Koppe L., Alix P. M., Croze M. L., Chambert S., Vanholder R., Glorieux G., et al. p-Cresyl glucuronide is a major metabolite of p-cresol in mouse: in contrast to p-cresyl sulphate, p-cresyl glucuronide fails to promote insulin resistance. Nephrol Dial Transplant. 2017 Dec 1;32(12):2000-9.
423. Sun C. Y., Li J. R., Wang Y. Y., Lin S. Y., Ou Y. C., Lin C. J., et al. p-Cresol sulfate caused behavior disorders and neurodegeneration in mice with unilateral nephrectomy involving oxidative stress and neuroinflammation. Int J Mol Sci. 2020 Sep 12;21(18).
424. Cerini C., Dou L., Anfosso F., Sabatier F., Moal V., Glorieux G., et al. p-Cresol, a uremic retention solute, alters the endothelial barrier function in vitro. Thromb Haemost. 2004 Jul;92(1):140-50.
425. Ho M. D., Ring N., Amaral K., Doshi U., Li A. P. Human enterocytes as an in vitro model for the evaluation of intestinal drug metabolism: Characterization of drug-metabolizing enzyme activities of cryopreserved human enterocytes from twenty-four donors. Drug Metab Dispos. 2017 Jun;45(6):686-91.
426. Katsube Y., Tsujimoto M., Koide H., Ochiai M., Hojyo A., Ogawa K., et al. Cooperative inhibitory effects of uremic toxins and other serum components on OATP1B1-mediated transport of SN-38. Cancer Chemother Pharmacol. 2017 Apr;79(4):783-9.

427. Fujita K., Sugiura T., Okumura H., Umeda S., Nakamichi N., Watanabe Y., et al. Direct inhibition and down-regulation by uremic plasma components of hepatic uptake transporter for SN-38, an active metabolite of irinotecan, in humans. Pharm Res. 2014 Jan;31(1):204-15.
428. Tsujimoto M., Hatozaki D., Shima D., Yokota H., Furukubo T., Izumi S., et al. Influence of serum in hemodialysis patients on the expression of intestinal and hepatic transporters for the excretion of pravastatin. Ther Apher Dial. 2012 Dec;16(6):580-7.
429. Kotani N., Maeda K., Debori Y., Camus S., Li R., Chesne C., et al. Expression and transport function of drug uptake transporters in differentiated HepaRG cells. Mol Pharm. 2012 Dec 3;9(12):3434-41.
430. Deguchi T., Kusuhara H., Takadate A., Endou H., Otagiri M., Sugiyama Y. Characterization of uremic toxin transport by organic anion transporters in the kidney. Kidney Int. 2004 Jan;65(1):162-74.
431. Kong F., Pang X., Zhong K., Guo Z., Li X., Zhong D., et al. Increased plasma exposures of conjugated metabolites of morinidazole in renal failure patients: A critical role of uremic toxins. Drug Metab Dispos. 2017 Jun;45(6):593-603.
432. Nieskens T. T. G., Peters J. G. P., Dabaghie D., Korte D., Jansen K., Van Asbeck A. H., et al. Expression of organic anion transporter 1 or 3 in human kidney proximal tubule cells reduces cisplatin sensitivity. Drug Metab Dispos. 2018 May;46(5):592-9.
433. Nieskens T. T., Peters J. G., Schreurs M. J., Smits N., Woestenenk R., Jansen K., et al. A human renal proximal tubule cell line with stable organic anion transporter 1 and 3 expression predictive for antiviral-induced toxicity. AAPS J. 2016 Mar;18(2):465-75.
434. Bruchet N. K., Ensom M. H. Limited sampling strategies for mycophenolic acid in solid organ transplantation: a systematic review. Expert Opin Drug Metab Toxicol. 2009 Sep;5(9):1079-97.
435. Poulin E., Greanya E. D., Partovi N., Shapiro R. J., Al-Khatib M., Ensom M. H. Development and validation of limited sampling strategies for tacrolimus and mycophenolate in steroid-free renal transplant regimens. Ther Drug Monit. 2011 Feb;33(1):50-5.
436. Sanchez Fructuoso A. I., Perez-Flores I., Calvo N., Valero R., Matilla E., Ortega D., et al. Limited-sampling strategy for mycophenolic acid in renal transplant recipients reciving enteric-coated mycophenolate sodium and tacrolimus. Ther Drug Monit. 2012 Jun;34(3):298-305.

Appendix A. Population pharmacokinetic analysis of immediate-release oral tacrolimus co-administered with mycophenolate mofetil in steroid-free adult kidney transplant recipients[11]

Abstract

Background and Objective: Tacrolimus is the mainstay calcineurin inhibitor frequently administered with mycophenolic acid with or without corticosteroids to prevent graft rejection in adult kidney transplant recipients. The primary objective of this study was to develop and evaluate a population pharmacokinetic model characterizing immediate-release oral tacrolimus co-administered with mycophenolate mofetil (a pro-drug of mycophenolic acid) in adult kidney transplant recipients on corticosteroid-free regimens. The secondary objective was to investigate the effects of clinical covariates on the pharmacokinetics of tacrolimus, emphasizing the interacting effects of mycophenolic acid.

[11] This section is already published. **Rong Y**, Mayo P, Ensom MHH, Kiang TKL. Population pharmacokinetic analysis of immediate-release oral tacrolimus co-administered with mycophenolate mofetil in corticosteroid-free adult kidney transplant recipients. *European Journal of Drug Metabolism and Pharmacokinetics*. 2019 Jun;44(3):409-422. doi: 10.1007/s13318-018-0525-3.

Acknowledgement: Reprinted by permission from Springer Nature: Springer Nature, European Journal of Drug Metabolism and Pharmacokinetics. Population pharmacokinetic analysis of immediate-release oral tacrolimus co-administered with mycophenolate mofetil in corticosteroid-free adult kidney transplant recipients. **Rong Y**, Mayo P, Ensom MHH, Kiang TKL. License number: 5222100438698 (2019).

Methods: Population modeling and evaluation were conducted with Monolix (Suite-2018R1) using the stochastic approximation expectation-maximization algorithm in 49 adult subjects (a total of 320 tacrolimus whole blood concentrations). Effects of clinical variables on tacrolimus pharmacokinetics were determined by population covariate modeling, regression modeling, and categorical analyses.

Results: A two-compartment, first-order absorption with lag-time, linear elimination, and constant error model best represented the population pharmacokinetics of tacrolimus. The apparent clearance value for tacrolimus was 17.9 L/h (6.95% relative standard error) in our model, which is lower compared to similar subjects on corticosteroid-based therapy. Glomerular filtration rate had significant effects on apparent clearance and central compartment volume of distribution. Conversely, mycophenolic acid did not affect the apparent clearance of tacrolimus.

Conclusion: We have developed and internally evaluated a novel population pharmacokinetic model for tacrolimus co-administered with mycophenolate mofetil in steroid-free adult kidney transplant patients. These findings are clinically important and provide further reasons for conducting therapeutic drug monitoring in this specific population.

1. Introduction

Tacrolimus is the mainstay calcineurin inhibitor widely used in conjunction with mycophenolic acid as part of a combination immunosuppressant regimen for the prevention of graft rejection in various types of solid organ transplants [1, 2]. As a result of the narrow therapeutic index and large pharmacokinetic variabilities of tacrolimus in adult kidney transplant recipients, therapeutic drug monitoring (TDM) of tacrolimus is routinely practiced [3]. Although trough concentration is often utilized for TDM, various limited-sampling strategies (LSS) for tacrolimus have been devised for the estimation of area-under the concentration-time curve (AUC), the best marker for tacrolimus exposure [4]. The pharmacokinetics of tacrolimus, however, are dependent on the nature of immunosuppressant combinations. In adult kidney transplant recipients, the practice of minimization or complete avoidance of corticosteroids is now recommended for suitable patients to mitigate the known adverse effects from corticosteroid treatment [5]. In this specific patient population, the pharmacokinetic characteristics of tacrolimus would likely differ and therefore warrant further characterization.

Oral tacrolimus undergoes extensive first-pass metabolism in humans (bioavailability <32%), is widely distributed into red blood cells (RBC, volume of distribution ~1L/kg in whole blood), and is highly bound to α-1-acid glycoprotein (free fraction ~1% under normal conditions) [1]. Both protein binding and intrinsic clearance could contribute to the overall clearance of tacrolimus. More specifically, the intrinsic clearance of tacrolimus is primarily mediated by intestinal and hepatic cytochrome P450 (CYP) 3A4/5 isoenzymes [1, 2]. Because tacrolimus is a substrate of P-glycoprotein (Pgp), it can also be subject to transporter-mediated pharmacokinetic interactions [2]. In general, corticosteroids have been shown to modulate the expressions and

activities of CYP3A4 [6] and Pgp [7], resulting in altered dose requirements or exposure values of tacrolimus in human subjects [7].

The fact that tacrolimus is almost always administered in combination with mycophenolic acid in kidney transplant recipients for the prevention of graft rejection [8] indicates that pharmacokinetic characterizations of tacrolimus must be considered in the context of mycophenolic acid. However, the effects of mycophenolic acid on tacrolimus pharmacokinetics are still under debate in the literature, as evident by inconsistent data obtained from clinical studies refuting (e.g. [9, 10]) or supporting (e.g. [11]) a mycophenolic acid-tacrolimus interaction in a variety of sample populations. Theoretically, a molecular basis for the mycophenolic acid-tacrolimus drug interaction does exist, according to *in vitro* studies characterizing the inhibitory effects of mycophenolic acid on tacrolimus oxidative metabolism [12]. However, this clinical interaction (or absence of) has not yet been proven, and thus warrants further investigation, in adult kidney transplant patients on tacrolimus and mycophenolic acid in the absence of corticosteroids.

Many population models of tacrolimus pharmacokinetics have been reported in kidney transplant patients, as reviewed recently by Brooks et al [13] and several others published since the review (e.g. [14-19]). The pharmacokinetics of tacrolimus in adult kidney transplant patients in the absence of corticosteroids have only been determined using non-compartmental pharmacokinetics analysis [20], which lacks the analytical power of non-linear mixed-effects modeling [21, 22]. To our knowledge, a population pharmacokinetic model for immediate-release tacrolimus in adult kidney transplant patients on strictly *corticosteroid-free* regimens is not yet available. Given the known mixed modulatory effects of corticosteroids on tacrolimus metabolism (i.e. inhibition/induction of CYP3A4/5 and/or transporters) [7], it was hypothesized that a unique population pharmacokinetic model of tacrolimus can be identified in this specific patient cohort.

The primary aim of this study was to develop and evaluate a novel pharmacokinetic model characterizing population mean estimates and variabilities for immediate-release tacrolimus (oral capsule) co-administered with mycophenolate mofetil (a prodrug of mycophenolic acid), in the absence of corticosteroids, in adult kidney transplant recipients. The secondary aim was to conduct a systematic investigation on the effects of clinical covariates on the pharmacokinetics of tacrolimus, with specific emphasis on the interacting effects of mycophenolic acid.

2. Patients and methods

2.1. Study population and sampling protocol

The study protocol was approved by the University of British Columbia and University of Alberta Research Ethics Boards (approval number: H17-02902, under reciprocal protocol agreement). This study was a retrospective population pharmacokinetic analyses of adult kidney transplant recipients recruited in years 2010-2018 from two open-label, non-randomized, observational clinical studies [20, 23]. *Please see supplementary material for further descriptions*.

2.2. Development and evaluation of population pharmacokinetic models

2.2.1. Software and algorithm for non-linear mixed-effects modeling

Non-linear mixed-effects pharmacokinetic modeling of tacrolimus (log-transformed data) was conducted with MonolixSuite-2018R1 software (Lixoft SAS, 8 rue de la Renaissance, Batiment D, Antony, France [25]), using the stochastic approximation expectation-maximization (SAEM) algorithm. Conditional means and standard deviations of individual population

pharmacokinetic parameters were computed with Markov chain Monte Carlo (MCMC) convergence assessment. Objective function value (OFV, expressed as minus two logarithms of the likelihood), Akaike information criterion (AIC), and Bayesian information criterion (BIC) were determined with Monte Carlo importance sampling method (Monte Carlo size N=10,000). Per convention, significant reductions in OFV (decrease by 3.84), AIC, and BIC indicated better model fitting [21, 22, 26].

2.2.2. Structural and error models

Various compartmental models for extravascularly administered tacrolimus were investigated (one-, two-, or three-compartment models; first-order absorption with/without lag-time or transit; and linear elimination) to establish the best structural model. Constant, proportional, and combined error models were investigated to characterize residual errors. Normal, lognormal, and logitnormal transformations for each error model were tested individually. The best structural/error model combination was selected systematically based on OFV, model diagnostics (discussed subsequently under 2.2.4 Model Evaluation), biologically plausible population mean estimates (with appropriate precision as measured by relative standard error [RSE]), and shrinkage values, as per standard population modeling approaches summarized by our group and others [21, 22, 26].

2.2.3. Population pharmacokinetic covariates models

Age, weight, height, albumin, serum creatinine (SCr), estimated glomerular filtration rate (eGFR), post-transplant time, oral mycophenolate mofetil study dose, and dose-normalized

mycophenolic acid AUC were utilized as continuous independent covariates. Sex was designated as a categorical covariate. For covariate modeling, all continuous variables were transformed using the following equation (Equation (1), using weight [WT] as an example):

$$\theta_i = \theta_{pop}(\frac{WT}{Median\ value\ of\ WT})^{\beta} e^{\eta_i} \quad (1)$$

where θ_i is a value of pharmacokinetic parameter θ for the ith individual, θ_{pop} is the population parameter estimate of parameter θ, $(\frac{WT}{Median\ value\ of\ WT})$ is the WT of the ith individual normalized by median value of WT in this population, β is a scaling exponent, and η^i is the deviation from the population value for the ith individual (i.e. random inter-individual variability). Pearson correlation analyses and the Wald test, using an *a priori* defined $p<0.01$ as the threshold for significance, were initially conducted to characterize potentially significant covariates. Moreover, a forward stepwise inclusion covariate identification approach in Rsmlx package (Rsmlx, version 1.1.0, Xpop Inria Team) with R software v3.4.2 (R Core Team, Vienna, Australia [27]) was also utilized as a complementary covariate identification tool. Only covariates obtained from both approaches were retained in our modeling process using backward elimination if i) the overall model OFV and/or RSE were reduced, ii) if the inclusion of the identified covariate(s) reduced inter-individual variability (ω), and iii) if the model was pharmacologically reasonable.

2.2.4. Model evaluation

Suitable models were initially verified by diagnostic plots including observation vs. population prediction (PRED), observation vs. individual prediction (IPRED), population-weighted residuals (PWRES) vs. time/predictions, and individual weighted residuals (IWRES) vs.

time/predictions, in order to assess the goodness of fit for the models. Prediction-corrected visual predictive check (VPC) was performed based on 1,000 simulated observations utilizing a 90% prediction interval in the population model. Bootstrap analysis (N=500 replicates) was conducted in Rsmlx package in R software to determine 95% confidence intervals (CI).

2.3. Secondary regression and categorical analyses on tacrolimus pharmacokinetics

Associations between independent clinical covariates and dose-normalized tacrolimus exposure (a surrogate for apparent clearance, CL/F) were initially assessed by single linear regression analyses of log-transformed data, using a significant threshold of $p<0.0056$ (Bonferroni's correction). Significant covariates (independent variables) obtained from single linear regression were further utilized in the construction of multiple regression models. Because our secondary objective was to elucidate the interaction between tacrolimus and mycophenolic acid, mycophenolic acid AUC/dose was also forced into the multiple regression model as an independent variable. Furthermore, a multiple regression model including *all* covariates (without regard to their associations in simple linear regression) was also constructed. Coefficient of determination (r^2) values from mutiple regression modeling were used to illustrate the *overall* strength of correlation between clinical covariates and dose-normalized tacrolimus exposure. Statistical analyses were performed in SigmaStat 3.5 (Systat Software Inc., San Jose, California, US [28]) where $p<0.05$ was deemed significant. To support the findings of regression modeling, categorical analyses were also utilized, where patients were sub-categorized into two mycophenolic acid AUC groups: mycophenolic acid AUC/dose <22.5 mg·h/L/g or ⩾22.5 mg·h/L/g to determine their effects on dose-normalized tacrolimus exposure. Differences between

the two groups were determined by Mann-Whitney rank sum test where $p<0.05$ was deemed significant.

3. Results

3.1. Sample population

A total of 49 (27 female) subjects were included in this retrospective population modeling study. The average (± standard deviation [SD]) age was 50 (±12) years old and the weight was 72 (±18) kg. Patient demographic and biochemistry data are summarized in Table A 1. Our sample population consisted of ~50% Caucasians and ~50% Asians. Because the exact genealogies of the patients were not systematically characterized, no further analyses on ethnicity were conducted. In total, 320 blood concentrations of tacrolimus were included, where 87.5% of the concentrations (N=280) were collected from intense sampling, and the rest (12.5%) obtained from sparse sampling (N=40).

3.2. Population pharmacokinetic structural and error models

A systematic approach to model selection (see Patients and Methods) was conducted. Table A 2 illustrates our modeling process and provides a summary of the diagnostic values (e.g. OFV). Several one compartmental models were considered initially but ultimately eliminated due to significantly higher OFV and poor fitting. Because three-compartment structural models failed to converge, they were not utilized. A two-compartment, first-order absorption with lag-time, linear elimination with constant error model (reduced OFV and acceptable RSE values) was ultimately selected as the final "base" model to describe the population pharmacokinetics of tacrolimus

(Figure A 1; Model 7, Table A 2). Six pharmacokinetic parameters were characterized in the base model: lag time in absorption (Tlag, ka), apparent clearance of tacrolimus from central compartment (CL/F), apparent inter-compartment clearance (Q/F), apparent volume of distribution of central compartment (V_1/F), and apparent volume of distribution of peripheral compartment (V_2/F). The absolute bioavailability (F) was not determined in this oral study. Because data density around the absorption phase was not adequate, initial estimates of ka were fixed to a range based on available literature data ($4.5 \pm 1.0\ h^{-1}$) [29]. A summary of the population pharmacokinetic parameter estimates is presented in Table A 3. Examples of good model fittings are shown in Figure A 2 where the observed concentrations (data dots) of individuals from intense sampling (Figure A 2 a) and sparse sampling (Figure A 2 b) are modeled with individual parameters (purple line) and population parameters including the influence of covariates (green line).

3.3. Covariate modeling

Initial analyses using Pearson correlation, the Wald test, and Rsmlx package indicated that "eGFR" was a potential covariate of CL/F and V_1/F, whereas "post-transplant time" was a potential covariate of V_1/F. Subsequently, models containing all potential covariates (i.e. eGFR on CL/F and/or V_1/F, and post-transplant time on V_1/F) were investigated by backward elimination in Monolix. The exclusion of "post-transplant time" as a covariate on V_1/F increased the OFV of the structural model from 1346.65 to 1365.89 ($p<0.05$) but decreased RSEs significantly. The exclusion of "eGFR" as a covariate of V_1/F and V_2/F further resulted in an increase in OFV by 8.44 ($p<0.05$). As the result, "post-transplant time" was removed based on software algorithm. Therefore, the final model consisted of "eGFR" on both CL/F and/or V_1/F as the only significant

covariate (Equations (2) and (3)) with improved RSE values and significantly reduced OFV (Table A 3).

$$CL_i = 17.9(\frac{eGFR}{56})^{-0.885} \times e^{\eta_{i\prime}} \quad (2)$$

$$V_{1i} = 150(\frac{eGFR}{56})^{-2.13} \times e^{\eta_{i\prime}} \quad (3)$$

See equation (1) for symbol abbreviations. The η-shrinkage for population estimate parameters were <30% (Table A 3), suggesting appropriate parameterization of this final model. In contrast, dose-normalized mycophenolic acid AUC was not determined to be a significant covariate in our model.

3.4. Model evaluation

Model evaluation was conducted per established protocols [21, 22]. Initial correlational plots of the final model (Figure A 3, Figure A 4) illustrated acceptable bias and precision based on consistent distributions of observed values vs. population/individual predictions around the line of identity (Figure A 3). There was observable positive bias both early in time (Figure A 4 a, Figure A 4 c) and at reduced concentrations (Figure A 4 b, Figure A 4 d), but the overall symmetry of scattered residuals around the y=0 line provided visual confirmation of accuracy/precision in the final structural (Figure A 4 a, Figure A 4 c) and residual error (Figure A 4 b, Figure A 4 d) models. Furthermore, the model simulated dataset (N=1000) was generally found within the area of predicted theoretical percentiles in prediction-corrected VPC (Figure A 5). There was a slight bias in the absorption phase, consistent with the findings of other diagnostic plots. However, these minor model mis-specifications did not appear to affect the overall bias and precision of key fixed effects parameters such as absorption and clearance (Table A 3). Bootstrapping analysis (500

replicates) indicated that all parameter estimates were within 95% CI (and matched the mean values generated from the final model), indicating that the final structural model was stable, and providing further evaluation of our final model (Table A 3).

3.5. Regression and categorical analyses to determine the effects of clinical covariates on dose-normalized tacrolimus exposure

Control analyses indicated that tacrolimus dose and trough concentration were strongly associated with tacrolimus AUC (i.e. the expected observation), indicating the validity of our dataset (data not shown). Using single linear regression analyses, only "SCr" and "eGFR" were significantly associated with dose-normalized tacrolimus AUC (a surrogate of CL/F), whereas "dose-normalized mycophenolic acid exposure" was not a significant predictor (Table A 4, Figure A 6). Subsequently, multiple regression models were also established to capture the effects of multiple covariates on dose-normalized tacrolimus exposure (Table A 5). Specifically, "eGFR" (not "SCr") was used due to its direct relationship with SCr. Consistent with single linear regression, multiple regression modeling also indicated "eGFR" as the only significant predictor of dose-normalized tacrolimus exposure in two multiple regression models. To further confirm the lack of drug interaction between mycophenolic acid and tacrolimus, patients sub-classified into two mycophenolic acid AUC groups (AUC/dose <22.5 mg·h/L/g or ⩾22.5 mg·h/L/g; based on the median value in our study cohort) also exhibited comparable mean dose-normalized tacrolimus AUCs (Figure A 7). These findings are consistent with the results of population pharmacokinetic covariate analysis (Table A 3).

4. Discussion

Tacrolimus is an important immunosuppressant frequently used in conjunction with mycophenolic acid, in the presence or absence of corticosteroids, in adult kidney transplant recipients [1, 2]. Corticosteroid tapering or complete avoidance has been recommended for patients with reduced graft rejection risks to minimize corticosteroid-related adverse effects [30, 31] and has gained popularity in various transplant centers. Our primary objective reported the development and evaluation of a novel tacrolimus population pharmacokinetic model in corticosteroid-free adult kidney transplant recipients. Our secondary objective reported the novel observation of lack of clinical drug-drug interaction between tacrolimus and mycophenolic acid in this specific population. To the best of our knowledge, these results represent one of the first models built with the SAEM algorithm implemented in Monolix, describing population pharmacokinetics of tacrolimus in adult kidney transplant patients.

A standardized population modeling and evaluation approach as summarized by our group [21, 22] was utilized to generate our final model (Figure A 1, Table A 2, Table A 3). Similar to our findings, many population pharmacokinetic models describing immediate-release tacrolimus in mycophenolic acid/corticosteroid-based populations have also utilized a two-compartment approach with linear elimination [13], which suggests that the absence of corticosteroids, as in our study cohort, does not alter the overall structural model of tacrolimus. On the other hand, various tacrolimus absorption models in corticosteroid-based population are available, ranging from simple first-order (with/without lag-time) (e.g. [32, 33]), multi-transit (e.g. [34]), and gamma absorptions (e.g. [35]) in adult kidney transplant recipients. Heterogeneity in tacrolimus absorption has been reported in literature [13], and the model that best described our data (first-order absorption with lag time) is consistent with the poor bioavailability and large variability observed

clinically [1]. Mechanistically, tacrolimus absorption is primarily driven by passive diffusion (hence, first-order) but can also be affected by intestinal motility and intrinsic clearance/drug transport that are primarily mediated by CYP3A4 and Pgp (hence, lag-time) [1]. As such, our absorption model is based on known tacrolimus pharmacology.

The population pharmacokinetic parameter estimates obtained for tacrolimus in this study were compared with other studies in adult renal transplant recipients on oral immediate-release tacrolimus, mycophenolate mofetil, and corticosteroids [14-19, 29, 33, 34, 36-45]. Studies in which the tacrolimus concentrations were determined using enzyme multiplied immunoassays [14-19, 29, 33, 41-45] were excluded from our comparisons due to known bias [14] in relation to data generated from liquid chromatography-mass spectrometry [34, 36-40]. In general, the population pharmacokinetic parameter estimates for drug uptake (i.e. ka [2.2 h^{-1}, 18.4% RSE] and Tlag [0.554 h, 11.1% RSE]) in our final model (Table A 3) are in agreement with published findings in subjects on corticosteroid-based therapy [34, 36-40], with estimate ranges ~0.35-4.48 h^{-1} (ka) and 0.25-0.59 h (Tlag). These results indicate that absorption of tacrolimus was not affected by the absence of corticosteroids. Likewise, the volumes of distribution obtained in our model (V_1/F=150 L [mean] and V_2/F=700 L [mean]) were in the lower end of the range values reported in literature for subjects on corticosteroid-based treatment (V_1/F=113-214 L and V_2/F= 500-3707 L), which might be explained by the fluid-retention effects of corticosteroids [2]. However, these findings were inconsistent with those reported by Bergmann et al [38] where a lower prednisolone concentration was associated with higher V_1/F. Because no specific mechanism for their observation was attributed by Bergmann et al [38], further studies should be conducted to determine the reasons for these discrepancies.

Subjects on corticosteroid-based therapy reported apparent oral clearance of tacrolimus in the range of 21.5-31.8 L/h [34, 36-40], which is higher than the clearance value obtained in our model (17.9 L/h, 6.95% RSE). The mechanism underlying this discrepancy could be explained by the absence of inductive effects of corticosteroids toward the intrinsic clearance of CYP3A4, thereby reducing the overall oral clearance of tacrolimus in our sample cohort. Furthermore, the clearance value obtained in our population pharmacokinetic model was within, but on the lower end of, the clearance range (24±14.1 L/h) reported by Greanya et al [20] which used non-compartmental analysis in a smaller subset of corticosteroid-free subjects (N=28, part of our data). However, the population-based clearance value determined in this study (Table A 3) was more precise (as evident by low RSE values) and incorporated inter-individual variability, which was not characterized in non-compartmental analysis. Ultimately, the ideal approach to determine the effects of corticosteroids on tacrolimus clearance would require the enrollment of both corticosteroid-based and corticosteroid-free patients within the same study.

The novel observation of the inverse associations between eGFR on dose-normalized tacrolimus AUC (a surrogate of apparent clearance) and eGFR on CL/F or V_1/F obtained from multiple regression and population pharmacokinetic models, respectively, may point to an underlying effect of altered *free* tacrolimus disposition. Our findings may suggest that reduced renal function (as represented by eGFR) may result in increased retention of uremic toxins which have been known to affect the disposition (i.e. decreasing the intrinsic clearance [46]) or protein binding [47] of xenobiotics. Because tacrolimus is considered a lower extraction drug, both the reduction in free drug intrinsic clearance and/or increase in free fraction will result in the enhancement of its overall clearance. Furthermore, as tacrolimus is relatively lipophilic and extensively partitioned into RBC [1], increased free fraction in the setting of reduced eGFR can

theoretically increase the transport of tacrolimus into the RBC, hence elevating both the apparent clearance and central compartment volume of distribution. These hypotheses also require further testing. The analysis of free tacrolimus concentration for this specific patient population will further provide meaningful information and insights into these potential mechanisms.

Our findings of lack of tacrolimus-mycophenolic acid drug interactions in this patient cohort are robust because they are based on multiple, complementary methodologies (i.e. population pharmacokinetic covariate modeling, multiple regression modeling, and categorical analysis). The ideal approach to population pharmacokinetics-based drug-drug interaction analysis is the utilization of an "integrated modeling" approach consisting of 2 separate population pharmacokinetic models each for tacrolimus and mycophenolic acid, with an interaction effect. This integrated modeling approach has been demonstrated by Kim et al [11] in healthy Korean male volunteers given only a single dose of the study drugs. However, it was not possible to satisfy our stringent modeling/evaluation criteria and obtain appropriate parameterizations in our *real* patient samples with *actual* (i.e. wide) variabilities using this approach. Nevertheless, our findings of lack of interaction effects by mycophenolic acid toward tacrolimus are consistent with those demonstrated by others in adult kidney transplant recipients on corticosteroid-based therapy [9, 10]. More specifically, Kagaya et al [10] found no significant effects of mycophenolic acid dose or AUC on various pharmacokinetic parameters of tacrolimus (i.e. maximum plasma concentration, trough concentration, exposure, or apparent oral clearance) in adult Japanese kidney transplant recipients. Moreover, Park et al [9] tracked adult kidney transplant patients until 6 months post-transplant and also did not find correlations between the apparent clearance values of mycophenolic acid and tacrolimus in their study cohort. On the other hand, data supporting an apparent tacrolimus-mycophenolic acid interaction have been reported in both *in vivo* [11] and *in*

vitro studies [12]. As discussed above, despite a significant interacting effect by mycophenolic acid on tacrolimus AUC and CL/F, Kim et al [11] recruited healthy adult male subjects administered only a single oral dose of tacrolimus and mycophenolate mofetil, which was not reflective of the real clinical situation. Moreover, despite evidence supporting a CYP3A4/5-mediated oxidative metabolism of mycophenolic acid and the possibility of competitive inhibition with tacrolimus via shared metabolic pathways *in vitro*, the concentration of mycophenolic acid required to inhibit tacrolimus metabolism in human liver microsomes exceeded the concentration likely attained under therapeutic dosing of mycophenolate mofetil in humans [12]. Overall, our data provided definitive evidence on the lack of influence of mycophenolic acid on tacrolimus pharmacokinetics in adult kidney transplant patients on corticosteroid-free anti-rejection therapy.

A limitation in this study was the lack of covariate analysis involving hematocrit, ethnicity, and genotype. Hematocrit was commonly identified as one of the significant covariates on tacrolimus whole blood clearance in various previous studies [29, 34, 38]. However, hematocrit data were not available in our sample cohort and should be collected and analyzed in future studies. The ethnicity composition in our cohort (which was not systemically characterized and therefore not investigated) consisted of ~50% Caucasian / 50% Asian and may not be generalizable to other transplant centers in the world. Furthermore, we did not genotype our subjects (i.e. a limitation of a retrospective analysis) with respect to CYP3A4/5 single nucleotide polymorphisms (SNP) (or other genes that have shown inconsistent findings) which have already been characterized as significant covariates for tacrolimus clearance in various models [13, 14, 17, 18]. Given the known effects of CYP3A4/5 SNPs on tacrolimus dosing requirement and the inconsistent frequencies of these SNPs observed in different ethnicities [48], an interacting effect by CYP3A4/5 and/or ethnicity on tacrolimus clearance is very likely, but remains to be determined, in corticosteroid-

free subjects. Furthermore, inclusion of a separate dataset or recruitment of an external group for model validation should be considered in the future studies.

5. Conclusion

In conclusion, we have developed and evaluated a novel population pharmacokinetic model for immediate-release tacrolimus co-administered with mycophenolate mofetil (without corticosteroids) in adult kidney transplant patients. Differences observed in key pharmacokinetic parameters (e.g. clearance, volume of distribution) of tacrolimus in our population model as compared to literature data for patients on corticosteroid-based therapy indicate that tailored tacrolimus dosing and TDM are warranted in this specific population. Moreover, the lack of apparent interacting effect by mycophenolic acid toward the pharmacokinetics of tacrolimus is reassuring, given the frequent co-administration of these two immunosuppressants in various settings.

Table A 1 Patient demographic and biochemistry data

Parameter	***Value***
Sex (Female/Male)	27/22
Age (yrs)	50 ± 12
Weight (kg)	72 ± 18
Height (cm)	166.9 ± 9.8
Albumin (g/L)	40.2 ± 4.6
SCr (μmol/L)	107.6 ± 26.1
eGFR (mL/min/1.73m^2)	57.7 ± 14.7
Post-transplant time (days)	525 ± 683
Mycophenolate mofetil dose (mg/day)	1617 ± 499
Tacrolimus dose (mg/day)	6.7 ± 4.1
Mycophenolic acid $AUC_{0\text{-}12}$ (mg·h/L)	37.4 ± 14.1
Tacrolimus $AUC_{0\text{-}12}$ (μg·h/L)	133.8 ± 37.8
Mycophenolic acid $AUC_{0\text{-}12}$/dose (mg·h/L/g)	25.3 ± 11.0
Tacrolimus $AUC_{0\text{-}12}$/dose (μg·h/L/mg)	26.1 ± 13.7

Continuous data are presented as mean ± standard deviation (SD); categorical data are presented as counts.

Abbreviation(s): *AUC*, area-under the concentration-time curve; *eGFR*, estimated glomerular filtration rate; *SCr*, serum creatinine.

Table A 2 Summary of population pharmacokinetic modeling process

Model	***Structural model description***	***Error model***	***OFV***	***AIC***	***BIC***
1	One-compartment model, first-order absorption with no delay, linear elimination	Combined 1	1618.73	1634.73	1649.87
2	One-compartment model, first-order absorption with lag time, linear elimination	Combined 1	1555.97[a]	1575.97	1594.89
3	One-compartment model, first-order transit absorption, linear elimination	Combined 1	1552.38[a]	1576.38	1599.09
4	Two-compartment model, first-order absorption with no delay, linear elimination	Combined 1	1501.33[b]	1523.33	1548.03
5	Two-compartment model, first-order absorption with lag time, linear elimination	Combined 1	1399.19[b]	1427.19	1453.68
6	Two-compartment model, first-order transit absorption, linear elimination	Combined 1	NA	NA	NA
7*	Two-compartment model, first-order absorption with lag time, linear elimination	Constant	1374.33[b]	1400.33	1424.93
8	Two-compartment model, first-order absorption with lag time, linear elimination	Proportional	NA	NA	NA
9	Two-compartment model, first-order absorption with lag time, linear elimination	Combined 2	NA	NA	NA

10	Two-compartment model, first-order transit absorption, linear elimination	Constant	NA	NA	NA

[a]Significant reduction in OFV vs. "Model 1"; [b]further significant reduction in OFV vs. the one-compartmental models.

[*]Run 7 is the final population pharmacokinetic base model (without covariate analysis).

Constant error model: $y = f + a\varepsilon$;

Proportional error model: $y = f + bf^c\varepsilon$;

Combined 1 error model: $y = f + (a + bf^c)\varepsilon$;

Combined 2 error model: $y = f + \sqrt{a^2 + b^2(f^c)^2}\varepsilon$;

Abbreviation(s): *a, b*, additive components of residual error; *c*, proportional component of residual error; ε, residual errors; *f*, function of structural models, *AIC*, Akaike information criterion; *BIC*, Bayesian information criterion; *NA*, could not reach model completion; *OFV*, objective function value.

Table A 3 Pharmacokinetic parameter estimates of the base and final model, with bootstrapping data

	Base model		***Final model***			***Bootstrap analyses***		
Parameters	Mean	RSE (%)	Mean	RSE (%)	η-shrinkage (%)	Mean	5% CI	95% CI
Fixed effects								
Tlag (h)	0.521	8.8	0.554	11.1		0.554	0.434	0.694
ka (h^{-1})	1.92	13.4	2.2	18.4		2.204	1.122	2.744
CL/F (L/h)	20.2	7.74	17.9	6.95		17.931	16.157	23.344
β^{tEGFR}CL/F			-0.885	29.5		-0.885	-1.919	-0.511
V_1/F (L)	180	17.5	150	18.1		150.179	92.033	218.631
$\beta^{tEGFR}V_1$/F			-2.13	26.2		-2.130	-3.267	-0.595
Q/F (L/h)	47.1	9.53	53.7	12.8		53.731	39.329	82.669
V_2/F (L)	486	17.1	700	21.2		700.228	316.193	1008.940
Standard deviation of the random effects								
ω_Tlag	0.427	17.5	0.519	15.5	5.19	0.519	0.261	0.745
ω_ka	0.509	37.8	0.573	36.7	2.93	0.573	0.203	0.915
ω_CL/F	0.503	10.9	0.346	13.8	-26.5	0.346	0.311	0.553
ω_V_1/F	1.1	12.5	0.808	14.1	0.519	0.808	0.141	1.184
ω_Q/F	0.441	16.4	0.558	20.5	3.95	0.558	0.235	1.045
ω_V_2/F	0.536	35.1	1.06	16.2	10.1	1.065	0.188	0.916
Error model parameter								
a	0.797	5.47	0.771	5.61		0.771	0.607	0.941
-2 log-likelihood		1374.33		1365.89*				
AIC		1400.33		1395.89				
BIC		1424.93		1424.27				

*$p<0.05$, significant reduction in OFV (final model with covariate effects vs. base model).

Abbreviation(s): *AIC*, Akaike information criterion; *BIC*, Bayesian information criterion; β^{t}-, covariate parameter estimate; *CI*, confidence interval; *CL/F*, clearance of tacrolimus from central compartment; *eGFR*, estimated glomerular filtration rate; *OFV*, objective function value; *Q/F*, inter-compartment clearance; *RSE*, relative standard error; *Tlag*, lag time of first-order absorption; V_1/F, volume of distribution of the central compartment; V_2/F, volume distribution of the peripheral compartment; ω_, inter-individual variability; all pharmacokinetic parameters are apparent values.

Table A 4 Single linear regression to determine the effects of clinical covariates on dose-normalized tacrolimus exposure

Covariates	***Tacrolimus AUC_{0-12}/dose (μg·h/L/mg) R***	***Tacrolimus AUC_{0-12}/dose (μg·h/L/mg) p-value***
Age	0.128	0.392
Weight (kg)	0	0.999
Height (cm)	-0.231	0.122
Albumin (g/L)	0.227	0.125
SCr (μmol/L)	-0.559	<0.001*
eGFR (mL/min/1.73m^2)	0.577	<0.001*
Post-transplant time (days)	0.385	0.008
Mycophenolate mofetil dose (mg/day)	0.058	0.700
Mycophenolic acid AUC_{0-12}/dose (mg·h/L/g)	-0.121	0.419

*Results were deemed significant if p<0.0056 based on Bonferroni's correction

Abbreviation(s): *AUC*, area-under the concentration-time curve; *eGFR*, estimated glomerular filtration rate; *R*, coefficient of correlation; *SCr*, serum creatinine.

Table A 5 Multiple regression models to determine the effects of multiple covariates on dose-normalized tacrolimus exposure

Dependent variables	Independent Variables	P-value in multiple linear regression	r^2 in multiple linear regression
Tacrolimus AUC/dose (μg·h/L/mg)	eGFR (mL/min/1.73m^2)	<0.001*	0.337
	Mycophenolic acid AUC/dose (mg·h/L/g)	0.591	
Tacrolimus AUC/dose (μg·h/L/mg)	Age (yrs)	0.103	0.547
	Sex (Female/Male)	0.457	
	Weight (kg)	0.511	
	Height (cm)	0.204	
	Albumin (g/L)	0.690	
	SCr (μmol/L)	0.651	
	eGFR (mL/min/1.73m^2)	0.029*	
	Post-transplant time (days)	0.492	
	Mycophenolate mofetil dose (mg/day)	0.118	
	Mycophenolic acid AUC/dose (mg·h/L/g)	0.983	

*p< 0.05

Abbreviation(s): *AUC*, area-under the concentration-time curve; *eGFR*, estimated glomerular filtration rate; r^2, coefficient of determination values; *SCr*, serum creatinine.

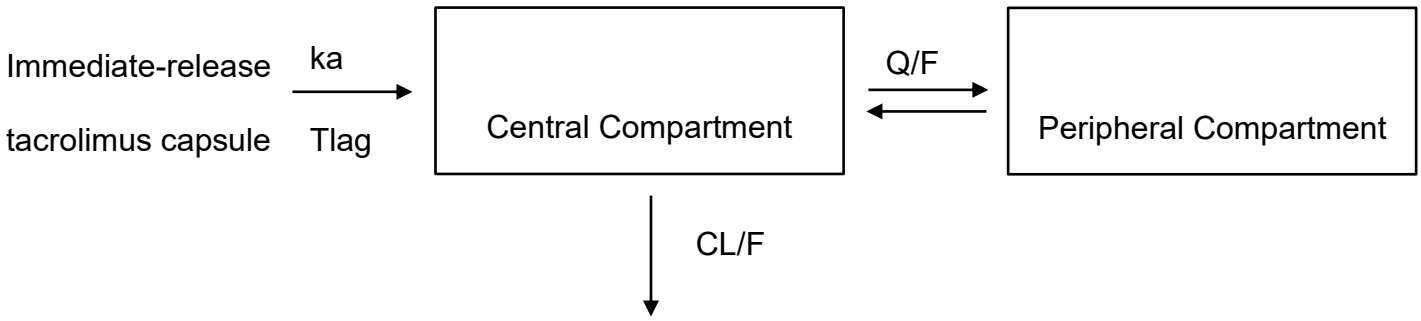

Figure A 1 Population pharmacokinetic structural model of immediate-release tacrolimus in adult, corticosteroid-free, kidney transplant patients

Abbreviation(s): *CL/F* apparent clearance; *ka* absorption rate constant; *Q/F* apparent inter-compartmental clearance; Tlag absorption lag time; V_1/F apparent central compartment volume of distribution, V_2/F apparent peripheral compartment volume of distribution.

a

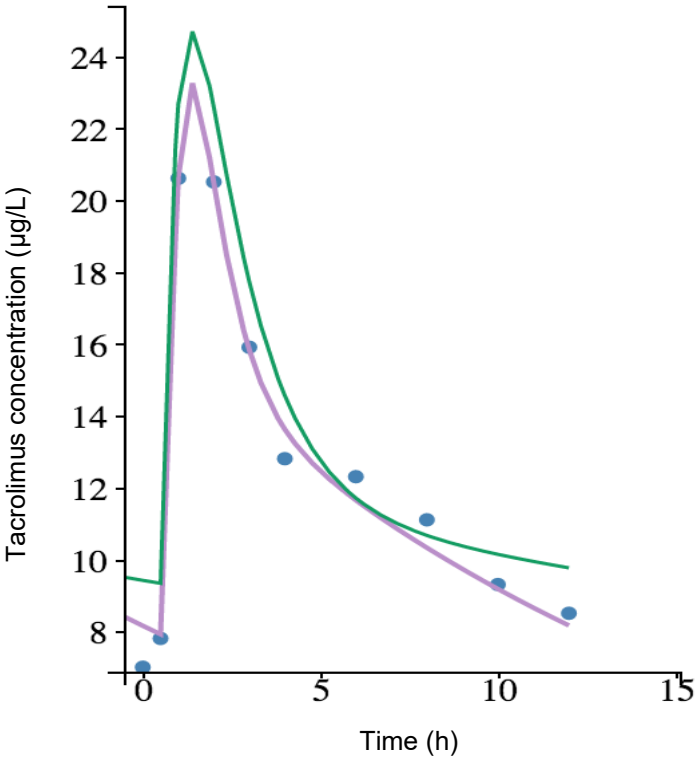
Tacrolimus concentration (µg/L)
24
22
20
18
16
14
12
10
8
0
5
10
15
Time (h)

b

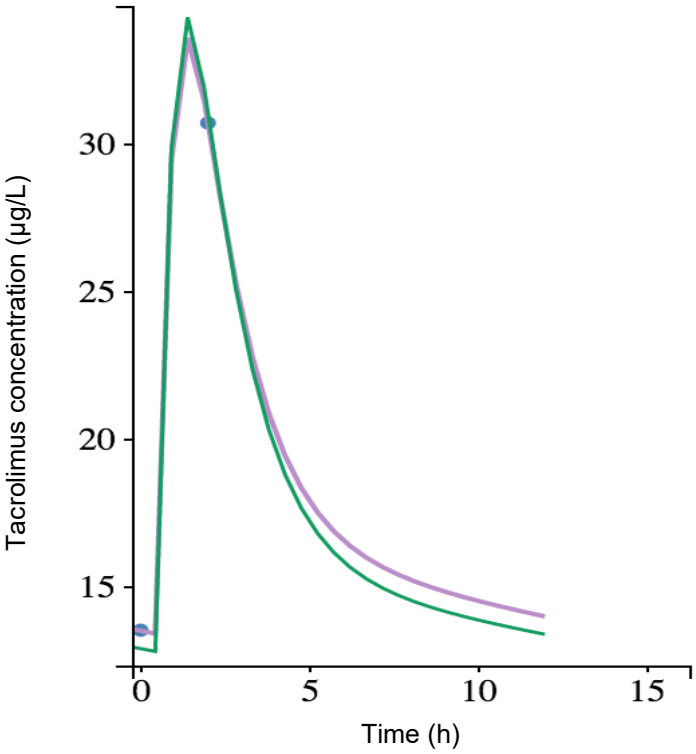

Figure A 2 (a) Sample curve fitting for an intensively sampled subject (#4); (b) sample curve fitting for a sparsely sampled subject (#39)

Blue dots: observed concentration; purple line: fitting using individual parameters; green line: population fitting including the influence of covariates.

a

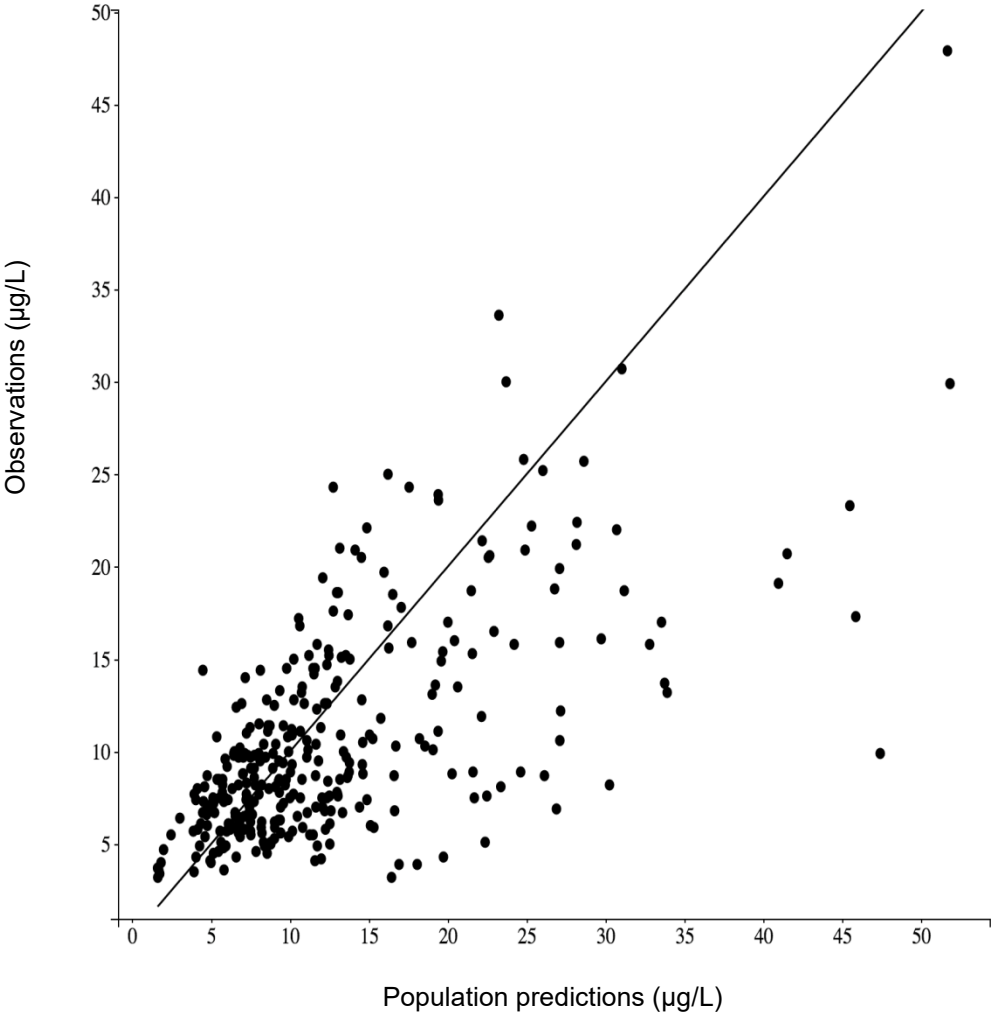
Observations (µg/L)
Population predictions (µg/L)
0
5
10
15
20
25
30
35
40
45
50

b

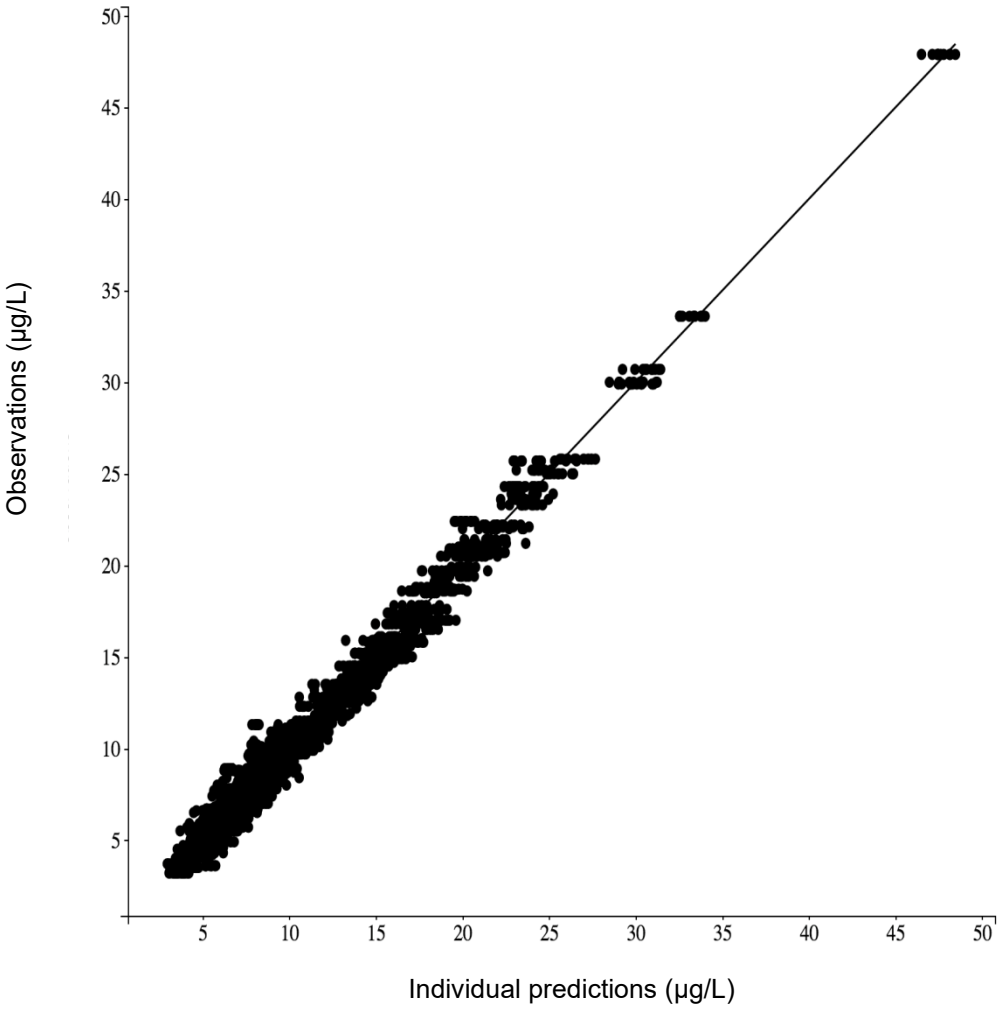

Figure A 3 (a) Observations versus population predictions (PRED); (b) observations versus individual predictions (IPRED) for the population pharmacokinetic model of tacrolimus in adult kidney transplant recipients (N=49) receiving immediate-release oral tacrolimus co-administered with mycophenolate mofetil (in the absence of corticosteroid)

a

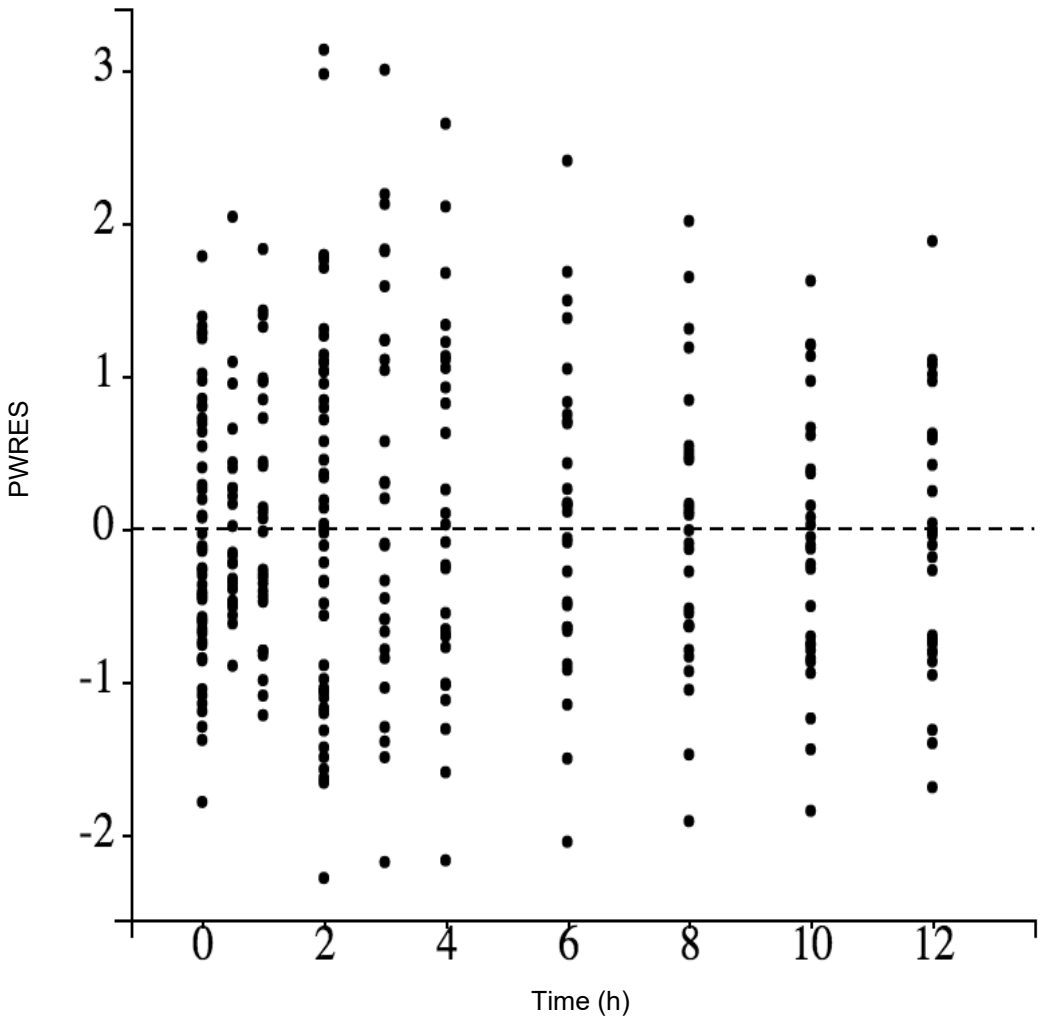

b

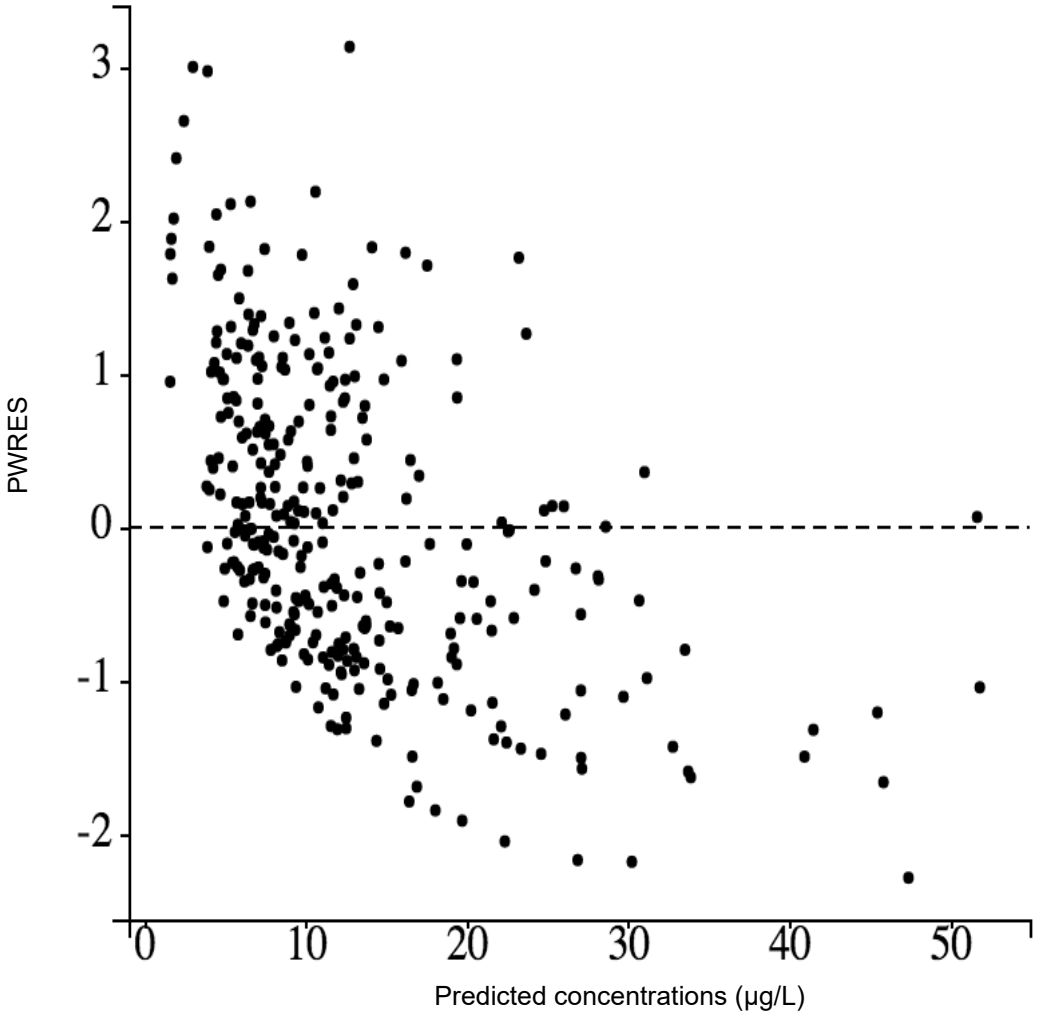

c

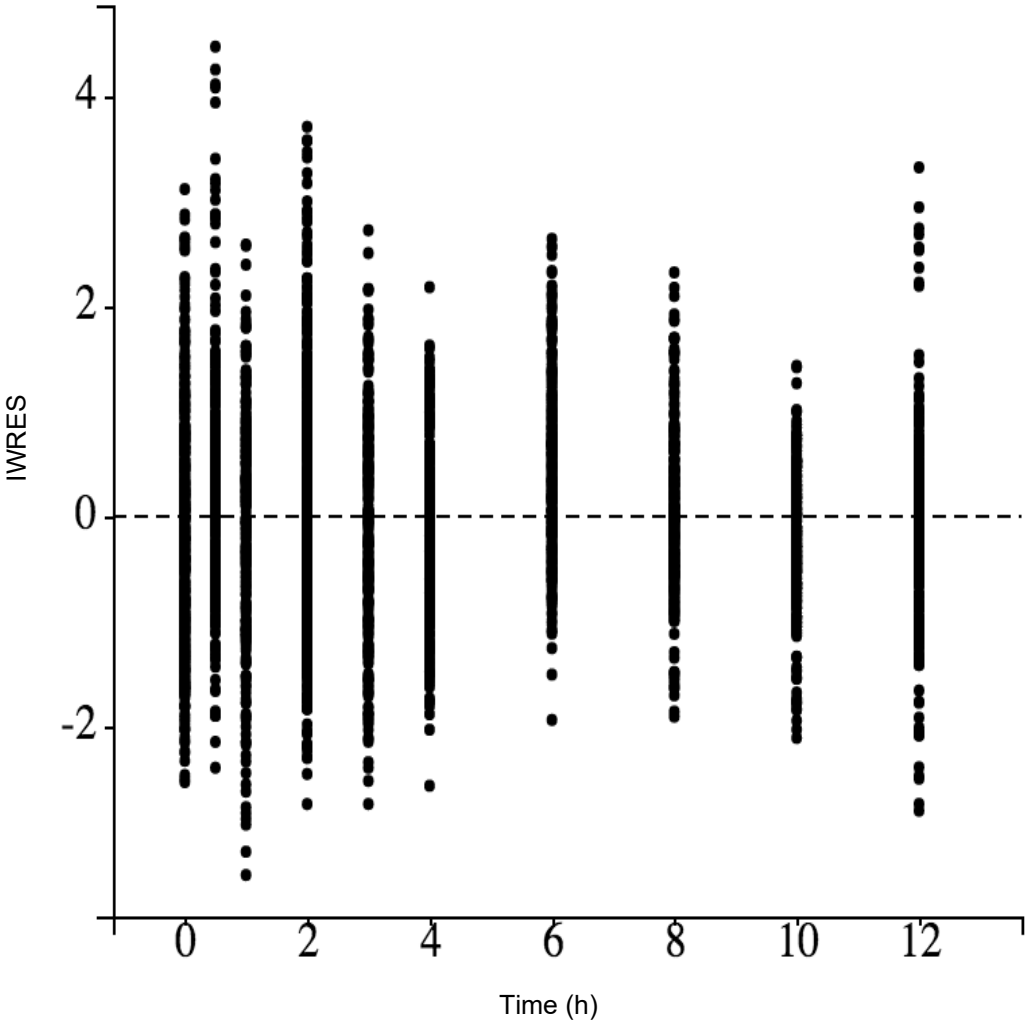

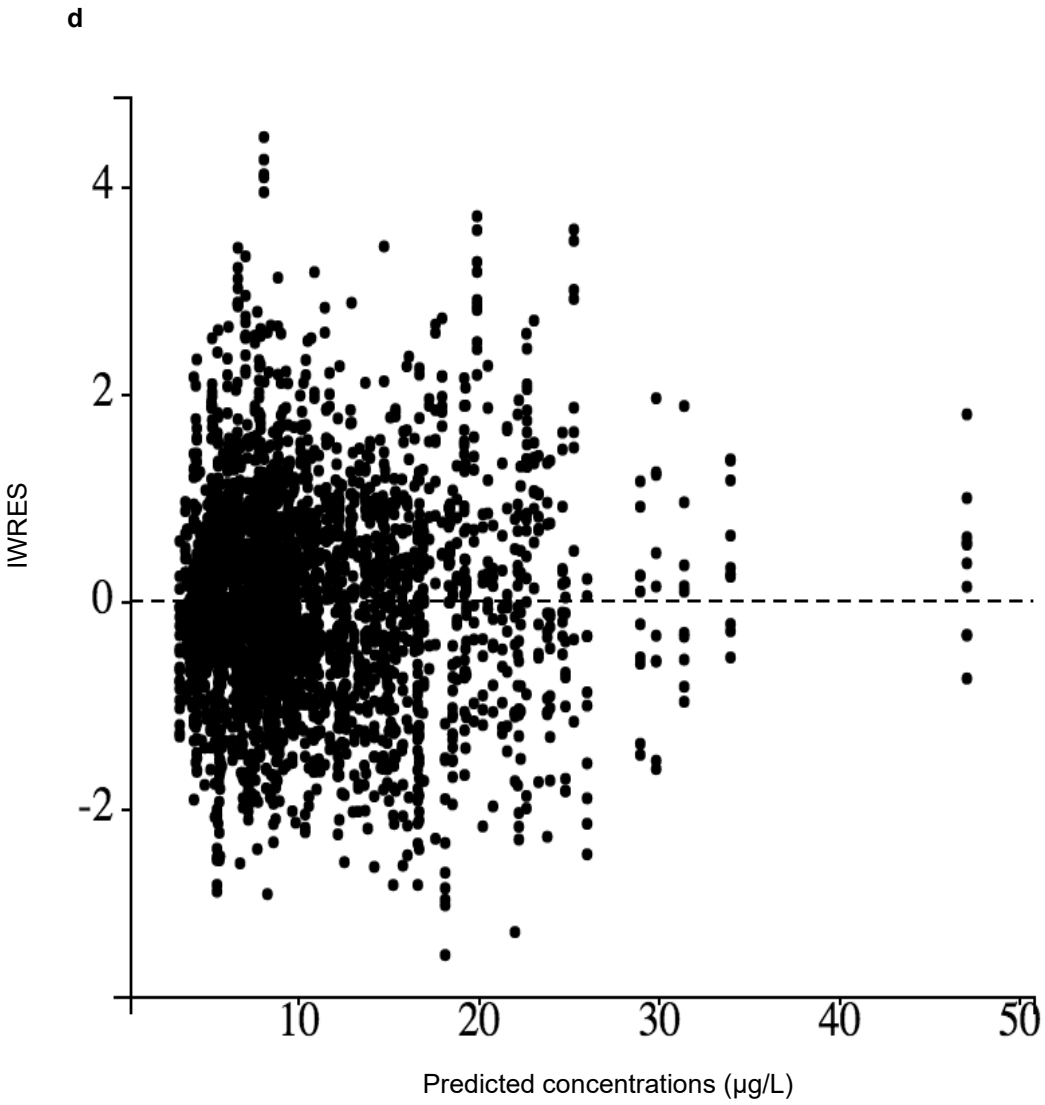

Figure A 4 (a) Population-weighted residuals versus time; (b) population-weighted residuals versus predictions; (c) individual-weighted residuals versus time; (d) individual-weighted residuals versus predictions for the population pharmacokinetic model of tacrolimus in adult kidney transplant recipients (N=49) receiving immediate-release oral tacrolimus co-administered with mycophenolate mofetil (in the absence of corticosteroid)

Abbreviation(s): *IWRES* individual-weighted residuals; *PWRES* population-weighted residuals

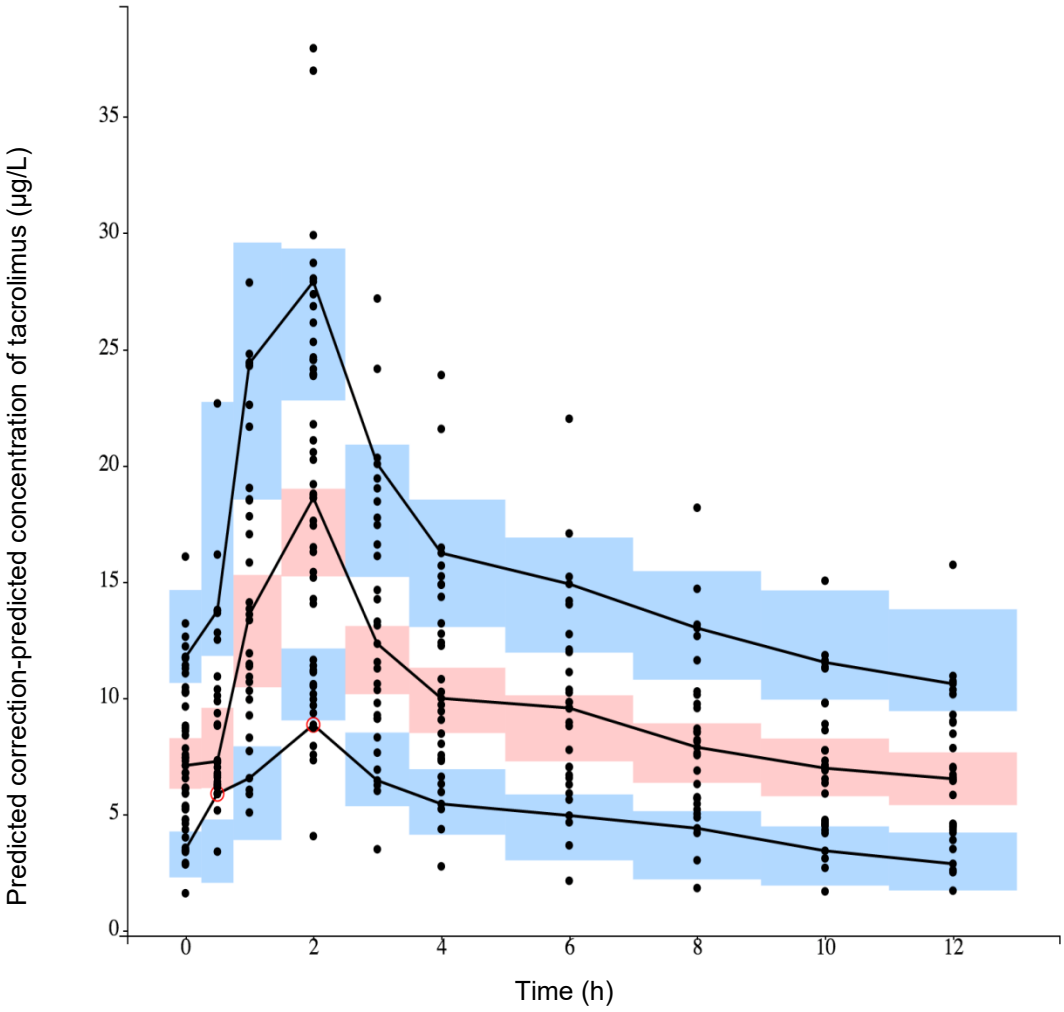

Figure A 5 Prediction-corrected visual predictive check for tacrolimus whole blood concentration-time response

Solid black lines represent the 10th, median, and 90th empirical percentiles of the observed data; blue dots represent individual observations; the theoretical percentiles of simulated data (N=1,000) were computed from the final model, where prediction intervals are displayed as colored area (blue area for 10th and 90th percentiles, and pink area for median)

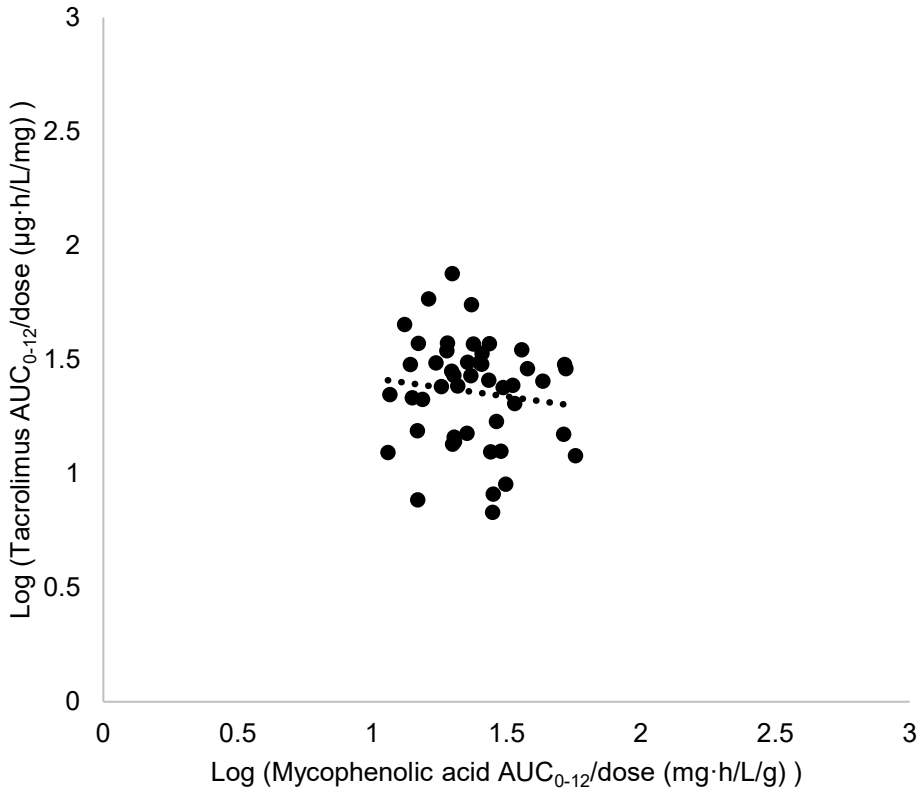

Figure A 6 Linear association between dose-normalized mycophenolic acid AUC and dose-normalized tacrolimus AUC (r^2=0.0146, p=0.419) (N=49) based on log-transformed data

Abbreviation(s): *AUC* area-under the concentration-time curve; r^2 coefficient of determination values

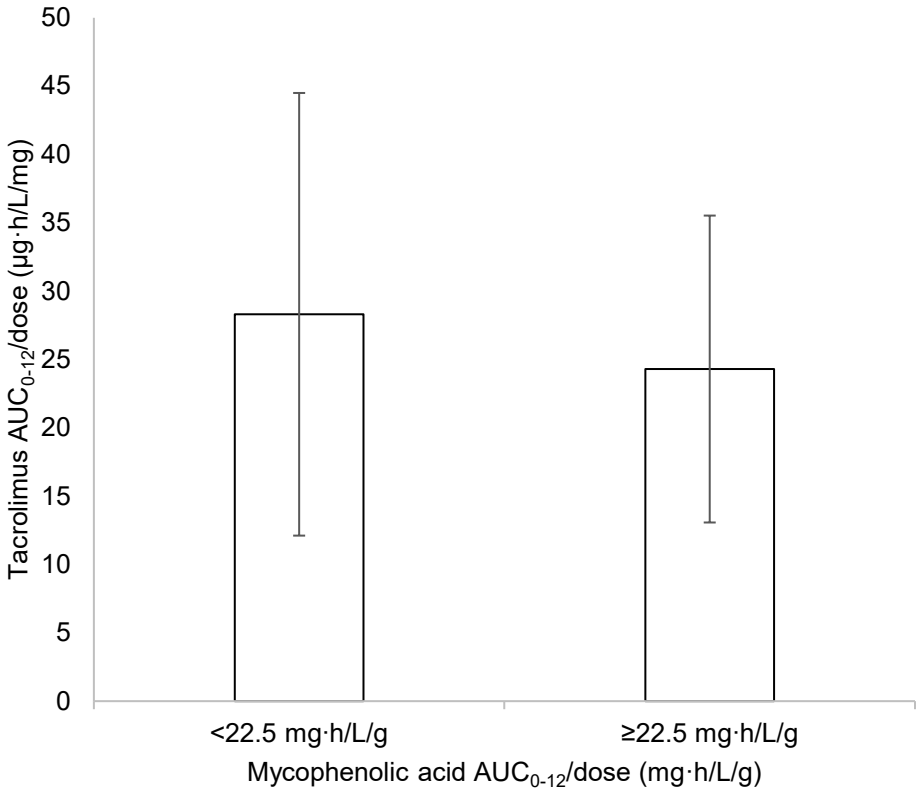

Figure A 7 Categorical analysis of the effects of dose-normalized mycophenolic acid AUC on dose-normalized tacrolimus AUC (N=49)

Data are presented as mean ± standard deviation

Abbreviation(s): *AUC* area-under the concentration-time curves

Supplementary materials

Adult (>18 years old) kidney transplant recipients (N=49) on *corticosteroid-free* pharmacotherapy including oral immediate-release tacrolimus (generic capsule, twice daily formulation) and oral mycophenolate mofetil (MMF, twice daily CellCept formulation) were recruited. The inclusion criteria included steady-state (i.e. minimum of 5 days of unaltered dosing regimen) tacrolimus and MMF, lack of corticosteroid, and stable renal function as determined by estimated glomerular filtration rate (GFR) (>40 mL/min/1.73m^2) on 2 consecutive clinic visits. *Steroid-free* and *corticosteroid-free* population were defined as patients who received no more than two doses of intravenous injection of methylprednisolone during the perioperative period and any types of oral steroids (e.g. prednisone) during the maintenance period. Subjects were excluded if they showed signs/symptoms of organ rejection and gastrointestinal disease, were classified as cytomegalovirus (CMV)-seronegative recipients receiving allograft from a CMV-seropositive donor (CMV mismatch), and were taking any known interacting drugs affecting the pharmacokinetics of tacrolimus or mycophenolic acid. The following clinical data were extracted: sex, age, weight, height, albumin, serum creatinine (SCr), estimated glomerular filtration rate (eGFR), and post-transplant time. Of the total 49 subjects, 28 had received intensive pharmacokinetic sampling of both whole blood tacrolimus and plasma mycophenolic acid concentrations, where steady-state drug concentrations were characterized in samples taken before, and at 0.5, 1, 2, 3, 4, 6, 8, 10, and 12 hours after oral doses at various periods post-transplant [20].The remaining 21 subjects received sparse blood sampling, where steady-state concentrations of tacrolimus (0 and 2 hours post-dose) and mycophenolic acid (1, 2, 4 hours post-dose) were obtained within 1 month post-transplant [23]. Drug concentrations were determined by validated analytical assays as described previously (tacrolimus by a liquid chromatography mass-

spectrometry assay and mycophenolic acid by high performance liquid chromatography with ultraviolet-light detection [20]. AUCs of tacrolimus and mycophenolic acid in sparsely-sampled patients (N=21) were calculated by validated LSSs in this specific population [24].

References

[1] Kiang T, Ensom MH. Immunosuppressants. In: Beringer P, editor. Basic Clinical Pharmacokinetics. 6th ed: Wolters Kluwer; 2017. pp. 320-358.
[2] Kiang T, Ensom MH. Anti-rejection drugs. In: Murphy J, editor. Clinical Pharmacokinetics. 6th ed: American Society of Health-System Pharmacists; 2017. pp. 205-220.
[3] Andrews LM, Li Y, De Winter BCM, Shi YY, Baan CC, Van Gelder T, Hesselink DA. Pharmacokinetic considerations related to therapeutic drug monitoring of tacrolimus in kidney transplant patients. Expert Opin Drug Metab Toxicol. 2017;13(12):1225-1236.
[4] Ting LS, Villeneuve E, Ensom MH. Beyond cyclosporine: a systematic review of limited sampling strategies for other immunosuppressants. Ther Drug Monit. 2006;28(3):419-430.
[5] Vincenti F, Schena FP, Paraskevas S, Hauser IA, Walker RG, Grinyo J, FREEDOM Study Group. A randomized, multicenter study of steroid avoidance, early steroid withdrawal or standard steroid therapy in kidney transplant recipients. Am J Transplant. 2008;8(2):307-316.
[6] Matoulkova P, Pavek P, Maly J, Vlcek J. Cytochrome P450 enzyme regulation by glucocorticoids and consequences in terms of drug interaction. Expert Opin Drug Metab Toxicol. 2014;10(3):425-435.
[7] Lam S, Partovi N, Ting LS, Ensom MH. Corticosteroid interactions with cyclosporine, tacrolimus, mycophenolate, and sirolimus: fact or fiction?. Ann Pharmacother. 2008;42(7):1037-1047.
[8] Gaston RS. Current and evolving immunosuppressive regimens in kidney transplantation. Am J Kidney Dis. 2006;47(4 Suppl 2):S3-21.
[9] Park SI, Felipe CR, Pinheiro-Machado PG, Garcia R, Fernandes FB, Casarini DE, Tedesco-Silva H,Jr, Medina-Pestana JO. Tacrolimus pharmacokinetic drug interactions: effect of prednisone, mycophenolic acid or sirolimus. Fundam Clin Pharmacol. 2009;23(1):137-145.
[10] Kagaya H, Miura M, Satoh S, Inoue K, Saito M, Inoue T, Habuchi T, Suzuki T. No pharmacokinetic interactions between mycophenolic acid and tacrolimus in renal transplant recipients. J Clin Pharm Ther. 2008;33(2):193-201.
[11] Kim JH, Han N, Kim MG, Yun HY, Lee S, Bae E, Kim YS, Kim IW, Oh JM. Increased exposure of tacrolimus by co-administered mycophenolate mofetil: population pharmacokinetic analysis in healthy volunteers. Sci Rep. 2018;8(1):1687-018-20071-3.
[12] Picard N, Cresteil T, Premaud A, Marquet P. Characterization of a phase 1 metabolite of mycophenolic acid produced by CYP3A4/5. Ther Drug Monit. 2004;26(6):600-608.
[13] Brooks E, Tett SE, Isbel NM, Staatz CE. Population pharmacokinetic modelling and bayesian estimation of tacrolimus exposure: Is this clinically useful for dosage prediction yet?. Clin Pharmacokinet. 2016;55(11):1295-1335.
[14] Zhao CY, Jiao Z, Mao JJ, Qiu XY. External evaluation of published population pharmacokinetic models of tacrolimus in adult renal transplant recipients. Br J Clin Pharmacol. 2016;81(5):891-907.
[15] Vadcharavivad S, Praisuwan S, Techawathanawanna N, Treyaprasert W, Avihingsanon Y. Population pharmacokinetics of tacrolimus in Thai kidney transplant patients: comparison with similar data from other populations. J Clin Pharm Ther. 2016;41(3):310-328.
[16] Zhang HJ, Li DY, Zhu HJ, Fang Y, Liu TS. Tacrolimus population pharmacokinetics according to CYP3A5 genotype and clinical factors in Chinese adult kidney transplant recipients. J Clin Pharm Ther. 2017;42(4):425-432.

[17] Woillard JB, Mourad M, Neely M, Capron A, van Schaik RH, van Gelder T, Lloberas N, Hesselink DA, Marquet P, Haufroid V, Elens L. Tacrolimus updated guidelines through popPK modeling: how to benefit more from CYP3A pre-emptive genotyping prior to kidney transplantation. Front Pharmacol. 2017;8:358.
[18] Hu C, Yin WJ, Li DY, Ding JJ, Zhou LY, Wang JL, Ma RR, Liu K, Zhou G, Zuo XC. Evaluating tacrolimus pharmacokinetic models in adult renal transplant recipients with different CYP3A5 genotypes. Eur J Clin Pharmacol. 2018.
[19] Campagne O, Mager DE, Brazeau D, Venuto RC, Tornatore KM. Tacrolimus population pharmacokinetics and multiple CYP3A5 genotypes in black and white renal transplant recipients. J Clin Pharmacol. 2018.
[20] Greanya ED, Poulin E, Partovi N, Shapiro RJ, Al-Khatib M, Ensom MH. Pharmacokinetics of tacrolimus and mycophenolate mofetil in renal transplant recipients on a corticosteroid-free regimen. Am J Health Syst Pharm. 2012;69(2):134-142.
[21] Kiang TK, Sherwin CM, Spigarelli MG, Ensom MH. Fundamentals of population pharmacokinetic modelling : modelling and software. Clin Pharmacokinet. 2012;51(8):515-525.
[22] Sherwin CM, Kiang TK, Spigarelli MG, Ensom MH. Fundamentals of population pharmacokinetic modelling: validation methods. Clin Pharmacokinet. 2012;51(9):573-590.
[23] Kiang T, Partovi N, Shapiro RJ, Berman JM, Collier AC, Ensom MH. Regression and genomic analyses on the association between mycophenolic acid exposure and absolute neutrophil count in steroid-free, *de novo* kidney transplant recipients. Clin Drug Investig. 2018; Accepted for publication.
[24] Poulin E, Greanya ED, Partovi N, Shapiro RJ, Al-Khatib M, Ensom MH. Development and validation of limited sampling strategies for tacrolimus and mycophenolate in steroid-free renal transplant regimens. Ther Drug Monit. 2011;33(1):50-55.
[25] LIXOFT. Monolix Suite 2018. 2018. http://www.lixoft.com. Accessed June 01 2018.
[26] Mould DR, Upton RN. Basic concepts in population modeling, simulation, and model-based drug development. CPT Pharmacometrics Syst Pharmacol. 2012;1:e6.
[27] R Core Team. R software v3.4.2. 2018. https://www.R-project.org. Accessed 02 Aug 2018.
[28] Systat Software I. SigmaStat 3.5 for Windows. 2007. https://systatsoftware.com/. Accessed 02 Jul 2018.
[29] Han N, Yun HY, Hong JY, Kim IW, Ji E, Hong SH, Kim YS, Ha J, Shin WG, Oh JM. Prediction of the tacrolimus population pharmacokinetic parameters according to CYP3A5 genotype and clinical factors using NONMEM in adult kidney transplant recipients. Eur J Clin Pharmacol. 2013;69(1):53-63.
[30] Lemieux I, Houde I, Pascot A, Lachance JG, Noel R, Radeau T, Despres JP, Bergeron J. Effects of prednisone withdrawal on the new metabolic triad in cyclosporine-treated kidney transplant patients. Kidney Int. 2002;62(5):1839-1847.
[31] Andrade-Sierra J, Rojas-Campos E, Cardona-Munoz E, Evangelista-Carrillo LA, Puentes-Camacho A, Lugo-Lopez O, Gomez B, Valdespino C, Cerrillos I, Medina-Perez M, Jalomo B, Nieves JJ, Sandoval M, Ramos-Solano F, Monteon-Ramos F, Cueto-Manzano AM. Early steroid withdrawal in a renal transplant cohort treated with tacrolimus, mycophenolate mofetil and basiliximab. Nefrologia. 2014;34(2):216-222.
[32] Antignac M, Barrou B, Farinotti R, Lechat P, Urien S. Population pharmacokinetics and bioavailability of tacrolimus in kidney transplant patients. Br J Clin Pharmacol. 2007;64(6):750-757.

[33] Scholten EM, Cremers SC, Schoemaker RC, Rowshani AT, van Kan EJ, den Hartigh J, Paul LC, de Fijter JW. AUC-guided dosing of tacrolimus prevents progressive systemic overexposure in renal transplant recipients. Kidney Int. 2005;67(6):2440-2447.
[34] Benkali K, Premaud A, Picard N, Rerolle JP, Toupance O, Hoizey G, Turcant A, Villemain F, Le Meur Y, Marquet P, Rousseau A. Tacrolimus population pharmacokinetic-pharmacogenetic analysis and Bayesian estimation in renal transplant recipients. Clin Pharmacokinet. 2009;48(12):805-816.
[35] Saint-Marcoux F, Debord J, Undre N, Rousseau A, Marquet P. Pharmacokinetic modeling and development of Bayesian estimators in kidney transplant patients receiving the tacrolimus once-daily formulation. Ther Drug Monit. 2010;32(2):129-135.
[36] Han N, Ha S, Yun HY, Kim MG, Min SI, Ha J, Lee JI, Oh JM, Kim IW. Population pharmacokinetic-pharmacogenetic model of tacrolimus in the early period after kidney transplantation. Basic Clin Pharmacol Toxicol. 2014;114(5):400-406.
[37] Asberg A, Midtvedt K, van Guilder M, Storset E, Bremer S, Bergan S, Jelliffe R, Hartmann A, Neely MN. Inclusion of CYP3A5 genotyping in a nonparametric population model improves dosing of tacrolimus early after transplantation. Transpl Int. 2013;26(12):1198-1207.
[38] Bergmann TK, Hennig S, Barraclough KA, Isbel NM, Staatz CE. Population pharmacokinetics of tacrolimus in adult kidney transplant patients: impact of CYP3A5 genotype on starting dose. Ther Drug Monit. 2014;36(1):62-70.
[39] Ogasawara K, Chitnis SD, Gohh RY, Christians U, Akhlaghi F. Multidrug resistance-associated protein 2 (MRP2/ABCC2) haplotypes significantly affect the pharmacokinetics of tacrolimus in kidney transplant recipients. Clin Pharmacokinet. 2013;52(9):751-762.
[40] Staatz CE, Willis C, Taylor PJ, Tett SE. Population pharmacokinetics of tacrolimus in adult kidney transplant recipients. Clin Pharmacol Ther. 2002;72(6):660-669.
[41] Golubovic B, Vucicevic K, Radivojevic D, Kovacevic SV, Prostran M, Miljkovic B. Total plasma protein effect on tacrolimus elimination in kidney transplant patients--population pharmacokinetic approach. Eur J Pharm Sci. 2014;52:34-40.
[42] Storset E, Holford N, Midtvedt K, Bremer S, Bergan S, Asberg A. Importance of hematocrit for a tacrolimus target concentration strategy. Eur J Clin Pharmacol. 2014;70(1):65-77.
[43] Andreu F, Colom H, Grinyo JM, Torras J, Cruzado JM, Lloberas N. Development of a population PK model of tacrolimus for adaptive dosage control in stable kidney transplant patients. Ther Drug Monit. 2015;37(2):246-255.
[44] Press RR, Ploeger BA, den Hartigh J, van der Straaten T, van Pelt J, Danhof M, de Fijter JW, Guchelaar HJ. Explaining variability in tacrolimus pharmacokinetics to optimize early exposure in adult kidney transplant recipients. Ther Drug Monit. 2009;31(2):187-197.
[45] Zuo XC, Ng CM, Barrett JS, Luo AJ, Zhang BK, Deng CH, Xi LY, Cheng K, Ming YZ, Yang GP, Pei Q, Zhu LJ, Yuan H, Liao HQ, Ding JJ, Wu D, Zhou YN, Jing NN, Huang ZJ. Effects of CYP3A4 and CYP3A5 polymorphisms on tacrolimus pharmacokinetics in Chinese adult renal transplant recipients: a population pharmacokinetic analysis. Pharmacogenet Genomics. 2013;23(5):251-261.
[46] Barnes KJ, Rowland A, Polasek TM, Miners JO. Inhibition of human drug-metabolising cytochrome P450 and UDP-glucuronosyltransferase enzyme activities in vitro by uremic toxins. Eur J Clin Pharmacol. 2014;70(9):1097-1106.
[47] Jansen J, Jankowski J, Gajjala PR, Wetzels JFM, Masereeuw R. Disposition and clinical implications of protein-bound uremic toxins. Clin Sci (Lond). 2017;131(14):1631-1647.

[48] Tang JT, Andrews LM, van Gelder T, Shi YY, van Schaik RH, Wang LL, Hesselink DA. Pharmacogenetic aspects of the use of tacrolimus in renal transplantation: recent developments and ethnic considerations. Expert Opin Drug Metab Toxicol. 2016;12(5):555-565.